frontiers | Research Topics

Targeting signalling pathways in inflammatory diseases

Edited by
Uzma Saqib, Mirza S. Baig
and Chit Laa Poh

Published in
Frontiers in Immunology

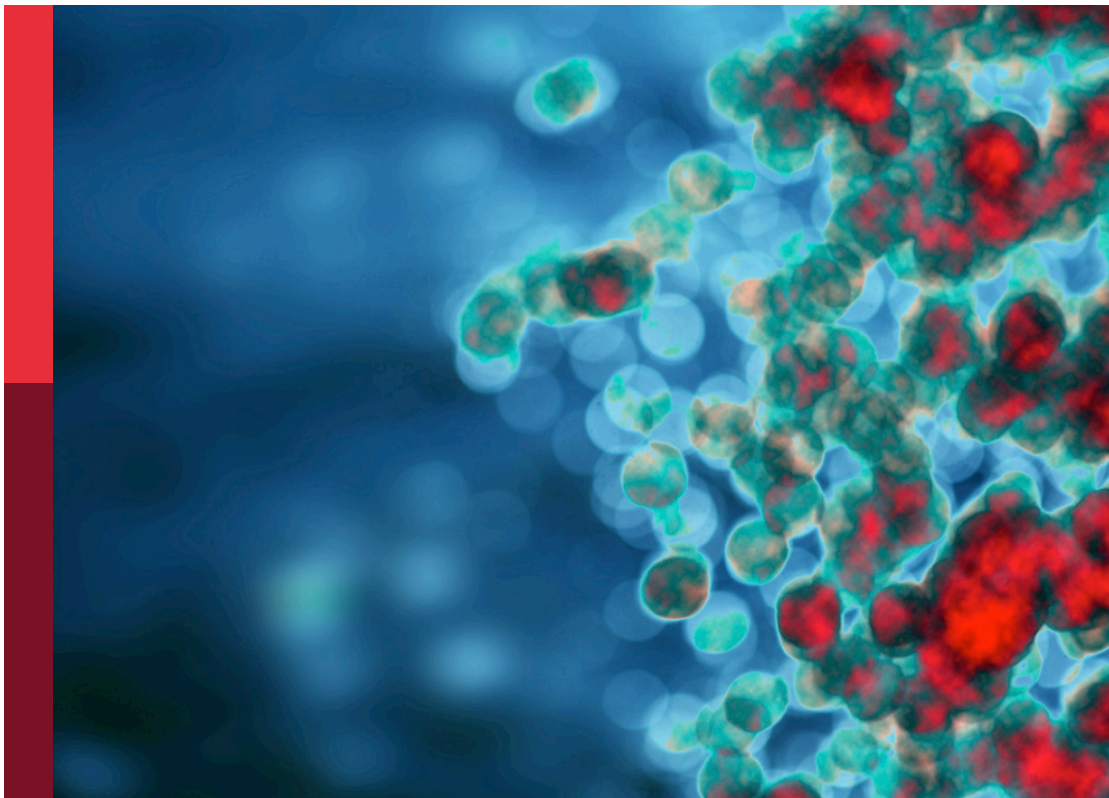

ISSN 1664-8714
ISBN 978-2-8325-3244-7
DOI 10.3389/978-2-8325-3244-7

About Frontiers

Frontiers is more than just an open access publisher of scholarly articles: it is a pioneering approach to the world of academia, radically improving the way scholarly research is managed. The grand vision of Frontiers is a world where all people have an equal opportunity to seek, share and generate knowledge. Frontiers provides immediate and permanent online open access to all its publications, but this alone is not enough to realize our grand goals.

Frontiers journal series

The Frontiers journal series is a multi-tier and interdisciplinary set of open-access, online journals, promising a paradigm shift from the current review, selection and dissemination processes in academic publishing. All Frontiers journals are driven by researchers for researchers; therefore, they constitute a service to the scholarly community. At the same time, the *Frontiers journal series* operates on a revolutionary invention, the tiered publishing system, initially addressing specific communities of scholars, and gradually climbing up to broader public understanding, thus serving the interests of the lay society, too.

Dedication to quality

Each Frontiers article is a landmark of the highest quality, thanks to genuinely collaborative interactions between authors and review editors, who include some of the world's best academicians. Research must be certified by peers before entering a stream of knowledge that may eventually reach the public - and shape society; therefore, Frontiers only applies the most rigorous and unbiased reviews. Frontiers revolutionizes research publishing by freely delivering the most outstanding research, evaluated with no bias from both the academic and social point of view. By applying the most advanced information technologies, Frontiers is catapulting scholarly publishing into a new generation.

What are Frontiers Research Topics?

Frontiers Research Topics are very popular trademarks of the *Frontiers journals series*: they are collections of at least ten articles, all centered on a particular subject. With their unique mix of varied contributions from Original Research to Review Articles, Frontiers Research Topics unify the most influential researchers, the latest key findings and historical advances in a hot research area.

Find out more on how to host your own Frontiers Research Topic or contribute to one as an author by contacting the Frontiers editorial office: frontiersin.org/about/contact

Targeting signalling pathways in inflammatory diseases

Topic editors

Uzma Saqib — Indian Institute of Technology Indore, India
Mirza S. Baig — Indian Institute of Technology Indore, India
Chit Laa Poh — Sunway University, Malaysia

Citation

Saqib, U., Baig, M. S., Poh, C. L., eds. (2023). *Targeting signalling pathways in inflammatory diseases*. Lausanne: Frontiers Media SA.
doi: 10.3389/978-2-8325-3244-7

Table of contents

frontiers | Frontiers in Immunology

TYPE Editorial
PUBLISHED 01 August 2023
DOI 10.3389/fimmu.2023.1241440

OPEN ACCESS

EDITED AND REVIEWED BY
Pietro Ghezzi,
University of Urbino Carlo Bo, Italy

*CORRESPONDENCE
Mirza S. Baig
msb.iit@iiti.ac.in

RECEIVED 16 June 2023
ACCEPTED 19 July 2023
PUBLISHED 01 August 2023

CITATION
Baig MS, Thurston TLM, Sharma R, Atre R, Saqib U, Khabiya R, Bharti S and Poh CL (2023) Editorial: Targeting signalling pathways in inflammatory diseases. *Front. Immunol.* 14:1241440. doi: 10.3389/fimmu.2023.1241440

Editorial: Targeting signalling pathways in inflammatory diseases

Mirza S. Baig[1]*, Teresa L. M. Thurston[2], Rahul Sharma[1], Rajat Atre[1], Uzma Saqib[3], Rakhi Khabiya[1], Shreya Bharti[1] and Chit L. Poh[4]

[1]Department of Biosciences and Biomedical Engineering (BSBE), Indian Institute of Technology Indore (IITI), Indore, India, [2]Centre for Bacterial Resistance Biology, Imperial College London, London, United Kingdom, [3]School of Life Sciences, Devi Ahilya Vishwavidyalaya (DAVV), Indore, India, [4]Centre for Virus and Vaccine Research, Sunway University, Bandar Sunway, Malaysia

KEYWORDS

chronic inflammation, signalling pathways, inflammatory response, macrophages, MAL (TIR domain-containing adaptor protein)

Editorial on the Research Topic
Targeting signalling pathways in inflammatory diseases

Chronic inflammation, characterized by a persistent elevation of circulating pro-inflammatory cytokines, is associated with the pathogenesis of many non-communicable diseases that cause a worldwide health burden and a reduction in quality of life (1). The identification of possible therapeutic targets implicated in the regulation of inflammation offers the opportunity to limit the dangers associated with an imbalance in the inflammatory response (2). Adaptor proteins represent key signaling molecules that regulate the host's innate immune response to infections, acting as links between receptors and other molecules in several signaling cascades (3, 4). The evident importance of these proteins in the pathophysiology of different chronic inflammatory illnesses makes them attractive therapeutic targets (4).

Here, we focus on a crucial inflammation-related adaptor of Toll-like receptors (TLR), called MyD88 adaptor-like (MAL) or Toll-interleukin-1 Receptor (TIR) domain-containing adaptor protein (TIRAP). MAL contains a TIR domain, required for mediating interactions with receptors on the membrane and with downstream signaling molecules (5). MAL represents a key mediator of TLR signaling in immune cells such as macrophages (6, 7), where activation of TLR2 and TLR4 cause persistent inflammation in a MAL-dependent fashion (7). Following receptor-mediated detection of pathogenic ligands, MAL mediates various protein-protein interactions (Figure 1A).

Tyrosine kinases, including BTK and PKCδ, have a major role in the activation of MAL, with BTK mediating phosphorylation on the four MAL residues Y86, Y106, Y159, and Y187 (5), as well as PKCδ phosphorylating Y86 and Y106 in MAL's TIR domain (8). The overlapping phosphorylation sites highlight the possible interconnected activities of these kinases with MAL, as well as pointing to possible context-dependent fine-tuning of MAL activity (8). After activation, MAL interacts with critical inflammatory proteins and eventually activates several transcriptional factors involved in the release of pro-inflammatory cytokines, which consequently leads to an inflammatory response (5). Contrary to phosphorylation, nitric oxide (NO)-mediated S-nitrosylation of

10.3389/fimmu.2023.1241440

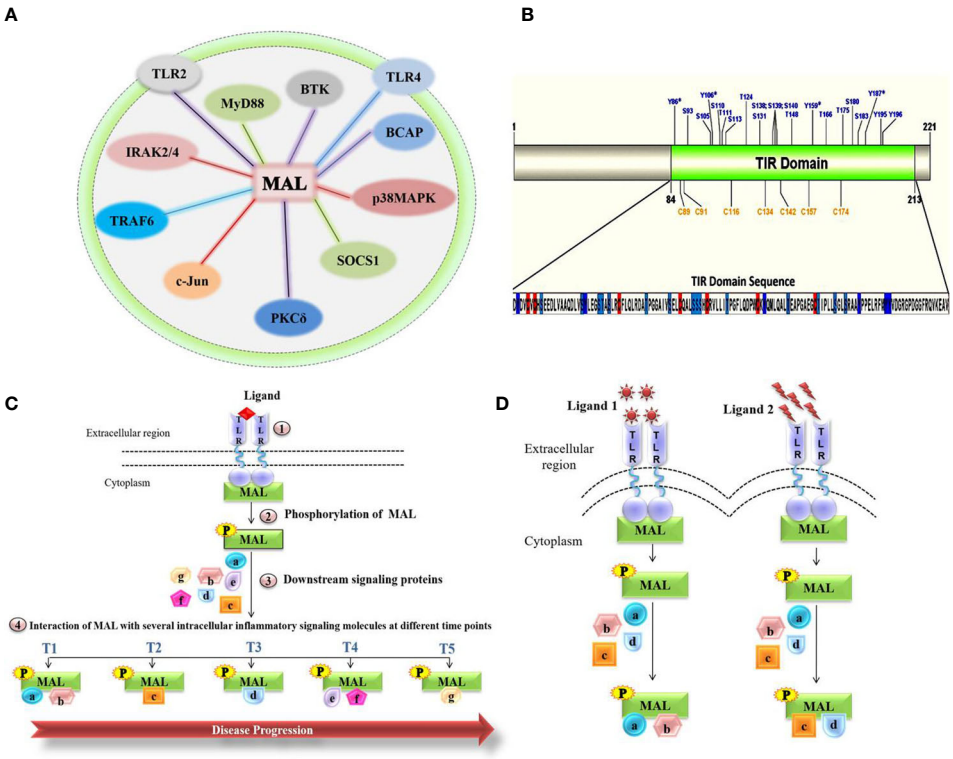

FIGURE 1
Molecular role of MAL in chronic inflammatory diseases. **(A)** Representation of the total network of TIRAP protein-protein interactions in macrophage inflammatory signaling. **(B)** Representation of the MAL-TIR domain and computational prediction of phosphorylation and S-nitrosylation (SNO) positions. **(C)** Schematic highlighting the interactions of MAL involved in disease progression. **(D)** MAL interactions under various stimulants.

cysteine residues in MAL's TIR domain attenuates the inflammatory response, which may be due to MAL interactions with downstream inflammatory signaling molecules (9).

Upon TLR4 activation, the inflammatory response involves the activation of transcription factors such as NF-kB and AP1, thereby generating pro-inflammatory cytokines. Baig et al. reported the formation of a heterotrimeric complex of p38MAPK, PKCδ, and MAL in LPS- stimulated macrophages (10). This reiterates the potential role of MAL in regulating inflammatory pathways via various protein interactions (10, 11). On the basis that the MAL-PKCδ interaction is crucial in inflammatory signaling mediated by TLR2/4 (10) and that PKCδ phosphorylates the MAL TIR domain, Rajpoot et al. conducted a virtual screen of FDA-approved drugs that would disrupt the MAL-PKCδ interaction (12). This screen revealed dorzolamide (DZD) as a novel therapeutic, where it suppressed the PKCδ-MAL-p38 MAPK signaling axis to inhibit inflammation (12). A significant (42%) increment in survival was observed in DZD-treated mice as compared to LPS alone–injected mice, validating the abrogation of inflammatory response in drug-treated mice (12). MAL also interacts with c-Jun, a subunit of the AP-1 transcription factor complex that is activated upon LPS stimulation of TLR4 (13). The interaction of MAL with c-Jun resulted in the transactivation and translocation of c-Jun, which ultimately resulted in the production of proinflammatory cytokines (13), thus making the interaction between these two proteins a potential therapeutic target. Indeed, Mansi et al. proposed a repurposed anti-inflammatory drug Gefitinib that abrogated the interaction of MAL with c-Jun, thereby inhibiting the cell's inflammatory response (13).

As post-translational modifications seem to be the major contributing factor toward MAL's variable interactions and eventual inflammatory responses, we were interested to know all the potential phosphorylation and nitrosylation sites on the TIR domain (Figure 1B). Modifications at these sites may variably impact the interactions with known and unknown interaction partners, regulators, and downstream mediators. Likely, MAL's interactions with kinases and other proteins vary temporally and spatially. Inadvertently, each of these interactions [Figure 1A and reviewed in detail by Rajpoot et al. (5)] represent potential points of therapeutic intervention. Thus, it remains crucial to understand how MAL is regulated and what interactions it forms under the influence of different stimulants acting on different TLRs. Once defined, the impact of individual interactions can then be determined during disease progression. Based on the studies published so far, we hypothesize (Figures 1C, D) that different MAL-mediated protein-protein interactions define the severity of chronic inflammation. In conclusion, unraveling the protein-protein interactions of MAL would not only lead us to a greater understanding of the underlying signaling mechanisms that occur in the progression of various life-threatening chronic inflammatory conditions, but would also direct us toward the development of important therapeutic strategies for disease treatment.

Author contributions

Conceptualization and supervision: MSB; writing and editing: MB, TT, RS, RA, US, RK, SB, and CP. All authors contributed and approved the submitted version.

Funding

This work was supported by the Cumulative Professional Development Allowance (CPDA) and the Research Development Fund (RDF) from the Indian Institute of Technology Indore (IITI) to MSB.

Acknowledgments

We thank the Indian Institute of Technology Indore (IITI) for providing facilities and other support. We thank Frontiers for giving us the opportunity to publish this Editorial for the Research Topic "*Targeting signaling pathways in inflammatory diseases*" in the reputed journal Frontiers in Immunology.

Conflict of interest

The authors declare that the research was conducted in the absence of any commercial or financial relationships that could be construed as a potential conflict of interest.

Publisher's note

References

1. Bennett JM, Reeves G, Billman GE, Sturmberg JP. Inflammation–nature's way to efficiently respond to all types of challenges: implications for understanding and managing "the epidemic" of chronic diseases. *Front Med* (2018) 5:316. doi: 10.3389/fmed.2018.00316

2. Placha D, Jampilek J. Chronic inflammatory diseases, anti-inflammatory agents and their delivery nanosystems. *Pharmaceutics* (2021) 13:64. doi: 10.3390/pharmaceutics13010064

3. Borowicz P, Chan H, Hauge A, Spurkland A. Adaptor proteins: Flexible and dynamic modulators of immune cell signalling. *Scand J Immunol* (2020) 92(5):e12951. doi: 10.1111/sji.12951

4. Atre R, Sharma R, Vadim G, Solanki K, Wadhonkar K, Singh N, et al. The indispensability of macrophage adaptor proteins in chronic inflammatory diseases. *Int Immunopharmacol* (2023) 119:110176. doi: 10.1016/j.intimp.2023.110176

5. Rajpoot S, Wary KK, Ibbott R, Liu D, Saqib U, Thurston TLM, et al. TIRAP in the mechanism of inflammation. *Front Immunol* (2021) 12:697588. doi: 10.3389/fimmu.2021.697588

6. Fitzgerald KA, Palsson-McDermott EM, Bowie AG, Jefferies CA, Mansell AS, Brady G, et al. Mal (MyD88-adapter-like) is required for Toll- like receptor-4 signal transduction. *Nature* (2001) 413:78–83. doi: 10.1038/35092578

7. Yamamoto M, Sato S, Hemmi H, Sanjo H, Uematsu S, Kaisho T, et al. Essential role for TIRAP in activation of the signalling cascade shared by TLR2 and TLR4. *Nature* (2002) 420:324–9. doi: 10.1038/nature01182

8. Rajpoot S, Srivastava G, Siddiqi MI, Saqib U, Parihar SP, HIrani N, et al. Identification of novel inhibitors targeting TIRAP interactions with BTK and PKCδ in inflammation through an in silico approach. *SAR QSAR Environ Res* (2022) 33:141–166. doi: 10.1080/1062936X.2022.2035817

9. Into T, Inomata M, Nakashima M, Shibata K, Häcker H, Matsushita K. Regulation of myD88-dependent signaling events by S nitrosylation retards toll-like receptor signal transduction and initiation of acute-phase immune responses. *Mol Cell Biol* (2008) 28:1338–47. doi: 10.1128/MCB.01412-07

10. Baig MS, Liu D, Muthu K, Roy A, Saqib U, Naim A, et al. Heterotrimeric complex of p38 MAPK, PKCδ, and TIRAP is required for AP1 mediated inflammatory response. *Int Immunopharmacol* (2017) 48:211–8. doi: 10.1016/j.intimp.2017.04.028

11. Rajpoot S, Kumar A, Zhang KYJ, Gan SH, Baig MS. TIRAP-mediated activation of p38 MAPK in inflammatory signaling. *Sci Rep* (2022) 12:5601. doi: 10.1038/s41598-022-09528-8

12. Rajpoot S, Kumar A, Gaponenko V, Thurston TL, Mehta D, Faisal SM, et al. Dorzolamide suppresses PKCδ -TIRAP-p38 MAPK signaling axis to dampen the inflammatory response. *Future Medicinal Chem* (2023) 15:533–554. doi: 10.4155/fmc-2022-0260

13. Srivastava M, Saqib U, Banerjee S, Wary K, Kizil B, Muthu K, et al. Inhibition of the TIRAP-c-Jun interaction as a therapeutic strategy for AP1-mediated inflammatory responses. *Int Immunopharmacol* (2019) 71:188–97. doi: 10.1016/j.intimp.2019.03.031

frontiers | Frontiers in Immunology

TYPE Review
PUBLISHED 28 November 2022
DOI 10.3389/fimmu.2022.1053175

OPEN ACCESS

EDITED BY
Uzma Saqib,
Indian Institute of Technology Indore, India

REVIEWED BY
Evelyn Mendoza,
Universidad Libre, Colombia
Ioannis Mitroulis,
Democritus University of Thrace, Greece

*CORRESPONDENCE
Menglong Wang
whuwangmenglong@163.com
Jun Wan
wanjun@whu.edu.cn

†These authors have contributed equally to this work

SPECIALTY SECTION
This article was submitted to Inflammation, a section of the journal Frontiers in Immunology

RECEIVED 25 September 2022
ACCEPTED 11 November 2022
PUBLISHED 28 November 2022

CITATION
Zhao M, Zheng Z, Li C, Wan J and Wang M (2022) Developmental endothelial locus-1 in cardiovascular and metabolic diseases: A promising biomarker and therapeutic target. *Front. Immunol.* 13:1053175. doi: 10.3389/fimmu.2022.1053175

Developmental endothelial locus-1 in cardiovascular and metabolic diseases: A promising biomarker and therapeutic target

Mengmeng Zhao[1,2,3†], Zihui Zheng[1,2,3†], Chenfei Li[1,23†], Jun Wan[1,2,3*] and Menglong Wang[1,2,3*]

[1]Department of Cardiology, Renmin Hospital of Wuhan University, Wuhan, China, [2]Cardiovascular Research Institute, Wuhan University, Wuhan, China, [3]Hubei Key Laboratory of Cardiology, Wuhan, China

Cardiovascular and metabolic diseases (CVMDs) are a leading cause of death worldwide and impose a major socioeconomic burden on individuals and healthcare systems, underscoring the urgent need to develop new drug therapies. Developmental endothelial locus-1 (DEL-1) is a secreted multifunctional domain protein that can bind to integrins and play an important role in the occurrence and development of various diseases. Recently, DEL-1 has attracted increased interest for its pharmacological role in the treatment and/or management of CVMDs. In this review, we present the current knowledge on the predictive and therapeutic role of DEL-1 in a variety of CVMDs, such as atherosclerosis, hypertension, cardiac remodeling, ischemic heart disease, obesity, and insulin resistance. Collectively, DEL-1 is a promising biomarker and therapeutic target for CVMDs.

KEYWORDS

DEL-1, cardiovascular diseases, metabolic diseases, inflammation resolution, anti-inflammation

Introduction

A wide range of diseases that affect the heart and blood vessels are collectively referred to as cardiovascular diseases (CVDs), including atherosclerosis (AS), myocardial infarction (MI), hypertension, cardiac hypertrophy, and heart failure. Metabolic diseases, including diabetes, obesity and nonalcoholic fatty liver disease, are closely related to the occurrence and development of CVDs (1, 2). Cardiovascular and metabolic diseases (CVMDs) are the leading causes of death worldwide and result in a major socioeconomic burden on individuals and healthcare systems (3–6). These diseases are caused by a

combination of multiple pathological factors, and their pathogenesis has not been fully elucidated. Although effective primary prevention and treatment strategies have reduced morbidity and mortality from CVMDs over the past 20 years, the prognosis of CVMDs remains unsatisfactory, and effective interventions are still lacking (7, 8).

Immune cells and inflammatory responses are involved in all stages of the occurrence and development of multiple CVMDs (9–11). The expression levels of various inflammatory mediators correlate with the clinical diagnosis and prognosis of CVMDs (12–18). Inflammation-related molecules such as interleukin-6 and growth differentiation factor 15 have been identified as biomarkers of CVDs (19). Regulation of immune function and the inflammatory response is an important strategy for the treatment of CVMDs (20–24). Increasing evidence shows that tissue-resident immune cells are involved in regulating the pathophysiological processes of CVMDs (25–28). Local tissues, such as vascular endothelium and adipose tissue, also have an important impact on the occurrence and development of CVMDs (29–32). Various local tissues in the human body are not only passive targets of immune and inflammatory responses but also active regulators of immunity (33). Local tissue signaling can regulate immune cell accumulation and functional plasticity and play a key role in immune-driven CVMDs (34, 35). Stromal and parenchymal cell-derived signals (including growth factors, cytokines, and other locally acting homeostatic factors) as well as intercellular adhesion interactions mediate local tissue-to-immune communication in CVMDs such as myocardial infarction (36–38). The compartmentalized expression of tissue signaling can facilitate optimal performance of cell-type-specific effects and spatial regulation of immune responses. Therefore, homeostatic molecules in the tissue microenvironment at different locations may be critical for CVMDs.

Developmental endothelial locus-1 (DEL-1) is a secreted multifunctional domain protein. As a local tissue signal, it exerts different regulatory functions in different expression regions (39). Endothelial cell-derived DEL-1 mainly regulates inflammation initiation by inhibiting neutrophil recruitment, while macrophage-derived DEL-1 promotes the resolution of inflammation by enhancing neutrophil apoptosis and macrophage efferocytosis (40). Increasing evidence has shown that the regulation of immune system homeostasis by DEL-1 plays an important role in CVMDs (41–43). In this article, we review the regulatory role of local tissue DEL-1 signaling in CVMDs and look forward to the future development of DEL-1 (Table 1).

Expression, structure and functions of DEL-1

Expression

DEL-1 is a 52 KD multifunctional matrix protein encoded by EDIL3 (epidermal growth factor (EGF)-like repeats and discoidin domains 3), which was cloned and characterized in angioplasty cells and early endothelial cells as early as 1998 (44). Increasing evidence shows that DEL-1 is expressed in tissues such as the brain, lung, and gums (39, 45, 46). Some tissue-resident cells, such as mesenchymal stromal cells, macrophages, neuronal cells,

TABLE 1 Roles of DEL-1 in cardiovascular and metabolic diseases.

CVMD	Animal	Animal model	Treatment	Finding	PMID
Atherosclerosis	mouse	Paigen diet for 20 weeks from the age of 24 weeks	Overall DEL-1 overexpression	Significantly reduced lipid accumulation in the aortic root; attenuated atherosclerosis	27784857
Atherosclerosis	mouse	1.Partial ligation of the left carotid artery with high fat diet for 6 weeks; 2. ApoE$^{-/-}$ mice with high fat diet for 4 or 12 weeks	Endothelial-specific overexpression of DEL-1	Endothelial DEL-1 does not protect against atherogenesis.	28796274
Hypertension	mouse	ANGII- and DOCA-salt-induced hypertension	1. Endothelial-specific overexpression of DEL-1; 2. Recombinant DEL-1	Inhibited the progression of hypertension; Attenuated hypertension-induced cardiac remodeling	35133978
Cardiac ischemia	pig	Left circumflex artery occlusions	DEL-1 overexpression	Improved cardiac function	14530019
Myocardial infarction	mouse	Permanent ligation of the left anterior descending coronary artery	DEL-1 knock out	Ameliorated adverse cardiac healing via neutrophil extracellular traps-mediated pro-inflammatory macrophage polarization.	34375400
Ischemic hindlimb	mouse	Femoral artery excision	Recombinant DEL-1 treatment	Enhanced angiogenesis in the murine ischemic hindlimb.	14981004
Ischemic stroke	mouse	Intraluminal middle cerebral artery blockade	DEL-1 overexpression	Promoted endogenous endothelial cell proliferation and angiogenesis	18534562
Insulin resistance	mouse	High fat diet for 26 weeks	Recombinant DEL-1 treatment	Attenuated HFD-induced skeletal muscle insulin resistance.	31778646

osteoclasts and some hematopoietic microenvironment cells, can also secrete DEL-1 (39, 40, 47, 48).

The mechanism regulating DEL-1 expression in tissues has not been elucidated. The reciprocal regulatory role of IL-17 and DEL-1 is now widely recognized (Figure 1). IL-17 directly inhibits endothelial DEL-1 expression, thereby promoting lymphocyte function-associated antigen 1 (LFA-1)-dependent neutrophil recruitment, while DEL-1 counteracts IL-17 production and IL-17-dependent inflammation (45, 49). Mechanistically, IL-17 reduces DEL-1 expression in a glycogen synthase kinase 3β (GSK3β)-dependent process that inhibits the binding of the key transcription factor CCAAT/enhancer-binding protein β (C/EBPβ) to the EDIL3 promoter, thereby downregulating EDIL3 transcription. This inhibitory action of IL-17 can be reversed at the GSK-3β level by PI3K/Akt signaling induced by D-resolvins. Interestingly, DEL-1 expression is reduced in aged mice, which may be related to the increased expression level of IL-17 (39, 50).

Another pro-inflammatory cytokine, TNF, can also reduce DEL-1 expression and secretion in endothelial cells by reducing C/EBPβ binding to the DEL-1 promoter, while the steroid hormone dehydroepiandrosterone (DHEA) increased DEL-1 expression and secretion in endothelial cells by activating tropomyosin receptor kinase A (TRKA) and downstream PI3K/AKT signaling to counteract the inhibitory effect of TNF and restore C/EBPβ binding to the DEL-1 promoter (51). Recently, erythromycin was reported to reverse the inhibitory effect of IL-17 on DEL-1 expression by binding to growth hormone secretagogue receptor (GHSR) and activating JAK2/MAPK p38 signaling (52). Furthermore, another independent research group found that overexpression of the p53 response element enhanced the transcriptional activity of EDIL3 (53). Primary endothelial cells isolated from p53 knockdown mice showed decreased DEL-1 mRNA expression (53). In melanoma cells, inhibition of p38/MK2 signaling reduced DEL-1 expression, suggesting that DEL-1 may be a downstream target of MK2 (54). In conclusion, the regulatory mechanism of DEL-1 expression is still unclear and needs to be further explored.

Structure and function

DEL-1 comprises three N-terminal EGF-like repeats (E1, E2 and E3) and two C-terminal discoidin I-like domains (C1 and C2) (44, 55). The RGD (Arg–Gly–Asp) motif in the second EGF-like repeat (E2) allows DEL-1 to interact with different integrins,

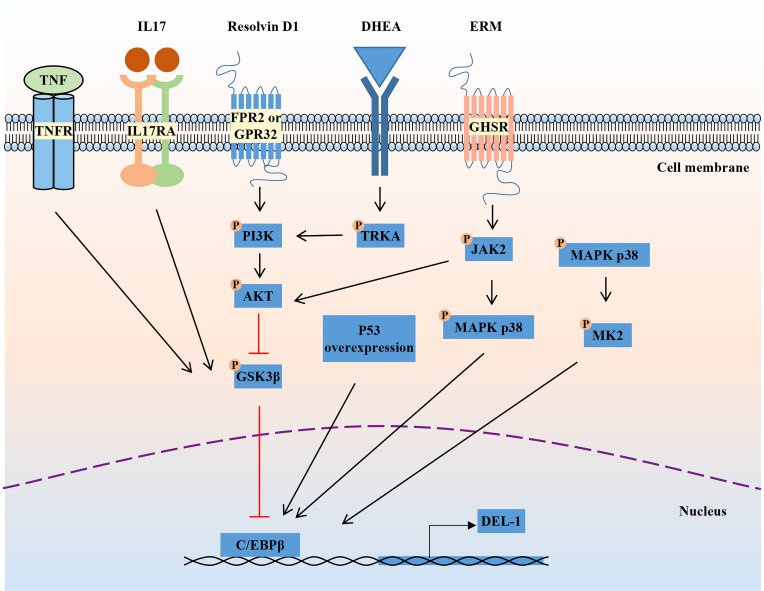

FIGURE 1
Regulation of DEL-1 expression. IL-17 and TNF reduce DEL-1 expression in a GSK3β-dependent process that inhibits the binding of the key transcription factor C/EBPβ to the EDIL3 promoter, thereby downregulating EDIL3 transcription. This inhibitory action of IL-17 can be reversed at the GSK-3β level by PI3K/AKT signaling induced by D-resolvins. Through interaction with GHSR, ERM activates JAK2 signaling, leading to DEL-1 transcription, which is MAPK p38-mediated and C/EBPβ dependent, as well as to PI3K/AKT-mediated reversal of the GSK3β-dependent inhibitory effect of IL-17 on DEL-1 expression. DHEA reduced DEL-1 expression and secretion in endothelial cells by activating TRKA and downstream PI3K/AKT signaling to restore C/EBPβ binding to the DEL-1 promoter. In addition, P53 overexpression and the activation of P38/MK2 signaling were reported to promote DEL-1 expression. DEL-1, developmental endothelial locus-1; GSK-3β, glycogen synthase kinase 3β; C/EBPβ, CCAAT/enhancer-binding protein β; PI3K, phosphoinositide 3-kinase; MAPK, mitogen-activated protein kinases; GHSR, growth hormone secretagogue receptor; ERM, erythromycin; JAK2, janus kinase 2; DHEA, dehydroepiandrosterone; TRKA, tropomyosin receptor kinase A.

including the β2 (e.g., αLβ2 and αMβ2) and β3 (e.g., αVβ3) integrins (44, 56, 57). The discoidin I-like domain and glycosaminoglycan mediate the interaction of DEL-1 with phosphatidylserine (PS) (40, 58). These interactions in turn confer important functions of DEL-1 in regulating immunity that have a major impact on the initiation and resolution of inflammation, suggesting that DEL-1 may be a promising therapeutic target (39). Specifically, the interaction of DEL-1 with αLβ2 or αMβ2 blocks the binding of the latter to its endothelial counterreceptor intercellular adhesion molecule-1 (ICAM-1), thereby inhibiting leukocyte adhesion and recruitment to sites of inflammation (46, 59). With its anti-inflammatory properties, DEL-1 can prevent a variety of inflammation-related conditions, such as multiple sclerosis and lung inflammation (45–48, 60, 61). DEL-1 can capture platelet microparticles by linking with PS and promote endothelial cell clearance of microparticles in an αVβ3 integrin-dependent manner (62). In addition, DEL-1 can act as a bridging molecule to bind PS on apoptotic cells and αVβ3 integrin on macrophages at both ends, mediating the burial of apoptotic cells and promoting inflammation resolution (40, 63). Collectively, DEL-1 exerts anti-inflammatory effects by inhibiting neutrophil recruitment and migration, promoting inflammatory resolution by accelerating macrophage reprogramming, and regulating myelopoiesis (Figure 2). These functions are discussed in detail in the review by Hajishengallis et al. (39, 64). Experiments with various deletion mutants of DEL-1 showed that fragments containing the C-terminus of C1 with a lectin-like structure were deposited directly in the ECM (58). The deposition efficiency varied according to the presence of other domains in DEL-1. The fragment containing E3 and C1 had the strongest deposition activity, while the fragment containing C2 was highly homologous to C1 and had low deposition activity (58). These data suggest that the discoidin domain of the DEL-1 protein contributes to its deposition and function in the extracellular matrix.

Genetic knockout or overexpression of DEL-1 in mice is an important tool in studying the function of DEL-1. EDIL3-/- mice have a specific phenotype characterized by increased development of spontaneous periodontitis (45). DEL-1 deficiency promoted neutrophil infiltration and inflammatory bone loss in mice with periodontitis (45). In experimental allergic encephalomyelitis (EAE), DEL-1 deficiency increased immune cell infiltration and inflammatory responses in the central nervous system, leading to increased disease severity (47). DEL-1-deficient mice exhibit increased neutrophil infiltration and inflammatory responses during lung inflammation (46). In postoperative peritoneal adhesion (PPA) mice, EDIL3-/- mice had a higher incidence of PPA and an increased inflammatory response, resulting in more severe PPA (65). Myelopoiesis in EDIL3-/- mice was suppressed in hematopoietic stem cells (HSCs) (66). The position of DEL-1 expression critically determines its regulatory function. In the future, the application of different transgenic mice with tissue- or cell-specific knockout or overexpression of DEL-1 may better help us to study its function.

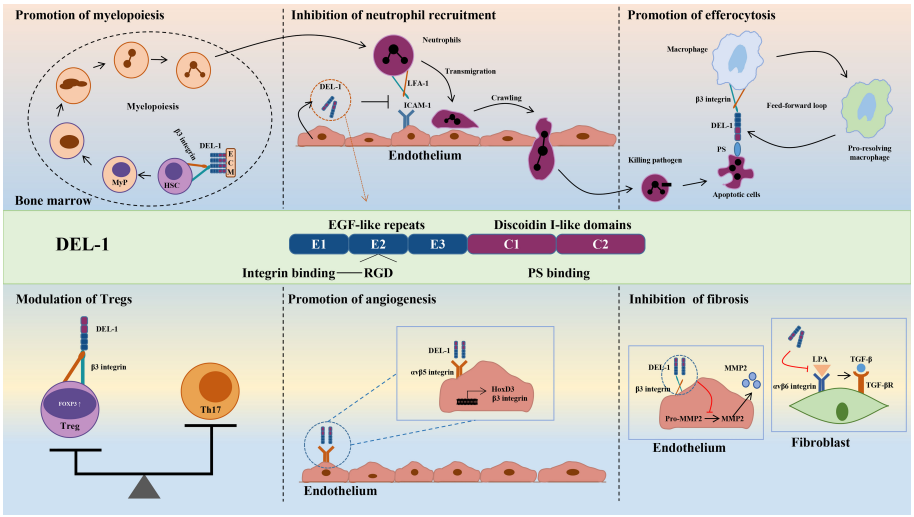

FIGURE 2
Structure and biological roles of DEL-1. The figure shows the multidomain structure of DEL-1 as well as six major regulatory activities of this protein, namely, promoting myelopoiesis, inhibiting neutrophil recruitment, promoting efferocytosis, modulating Tregs, promoting angiogenesis and inhibiting fibrosis. DEL-1, developmental endothelial locus-1; ECM, extracellular matrix; HSC, hematopoietic stem cell; MyP, myeloid progenitors; ICAM-1, intercellular adhesion molecule-1; LFA-1, lymphocyte function-associated antigen-1; PS, phosphatidyl serine; Th17, T helper 17 cell; Treg, T regulatory cell; FOXP3, forkhead box P3; HoxD3, homeobox D3; MMP2, matrix metallopeptidase 2; LPA, latency-associated peptide; TGF-β, transforming growth factor-β.

DEL-1 in CVDs

Atherosclerosis

As a lipid-driven chronic inflammatory disease that underlies various CVDs, such as ischemic heart disease (IHD) (67–69), AS is caused by the accumulation and oxidative modification of low-density lipoprotein (LDL) in the arterial intima (70). As the tissue microenvironment changes, endothelial cells release chemokines and adhesion molecules, which promote the recruitment and migration of monocytes on the endothelium; monocytes subsequently differentiate into macrophages to phagocytose oxidized low-density lipoprotein (oxLDL), while the excessive accumulation of oxLDL eventually leads to the transformation of macrophages into foam cells and initiates the secretion of inflammatory cytokines to promote the development of AS plaques; moreover, smooth muscle cells migrate to the subendothelial space to form fibrous caps and stabilize the plaques. Finn et al. found that the serum level of DEL-1 in patients with coronary heart disease (3.9 ± 0.2 pg/mg total protein) was significantly higher than that in healthy subjects (2.9 ± 0.1 pg/mg total protein) (71). However, there is still a lack of clinical evidence to prove that DEL-1 is related to the occurrence and development of AS.

In vitro evidence showed that DEL-1 can not only directly bind to oxLDL but also inhibit the uptake of oxLDL in cells transfected with multiple scavenger receptor genes in a dose-dependent manner, such as lectin-like oxidized low-density lipoprotein receptor-1 (LOX-1), scavenger receptor A (SR-A), scavenger receptor class B type I (SR-BI), and the cluster of differentiation 36 (CD36) (72). DEL-1 inhibited the uptake of oxLDL by human coronary artery endothelial cells (HCAECs) and macrophages. Furthermore, the oxLDL-induced increase in monocyte chemotactic protein-1 (MCP-1) and intercellular adhesion molecule-1 (ICAM−1) expression in HCAECs was significantly inhibited by DEL-1, which has the potential to alleviate monocyte adhesion. OxLDL-induced endothelin-1 secretion in HCAECs was also significantly inhibited by DEL-1 (72). Therefore, Del-1 not only inhibited the binding of oxLDL to the receptors but also inhibited the cellular response to oxLDL (Figure 3).

In a mouse model of AS, DEL-1 overexpression inhibited the receptor-binding activity of a modified LDL in serum, reduced the expression of adhesion molecules MCP-1 and ICAM-1 in the aorta, and reduced the oil red O-positive atherosclerotic area at the aortic roots (72). These results suggest that DEL-1 overexpression inhibits the occurrence of AS. However, in contrast to the above results, Subramanian et al. constructed an AS model by partially ligating the left carotid artery in ApoE$^{-/-}$ mice and found that endothelial cell-specific overexpression of DEL-1 had no significant effect on the development and cellular composition of AS plaques (73). These researchers fed ApoE$^{-/-}$ mice a high-fat diet for 4 or 12 weeks to study early or late lesions and found that endothelial cell-specific overexpression of DEL-1 did not affect early or late stages of AS and did not prevent AS (73). The apparent discrepancy between the results of this study and those of Kakino et al. may be due to the following: 1. The transgenic mice in Kakino et al.'s study overexpressed DEL-1 in all cell types. In addition to the mechanism mediated by endothelial cell-derived DEL-1, other mechanisms may also play a role, such as macrophages. 2. Differences in experimental methods between the two studies may also lead to conflicting results, such as differences in the background of ApoE$^{-/-}$ mice, differences in high fat diets, differences in modeling methods, and so on. In the future, transgenic mice with macrophage-specific expression may help to further elucidate the role of DEL-1 in AS.

Intercellular signaling plays a key role in AS formation, affecting the occurrence and progression of CHD, and circulating microRNAs (miRNAs) may be involved in this process (74). There were clear differences in circulating miRNA transport between CHD patients and healthy subjects, especially the reduction in miRNA enrichment in microparticles (MPs) (71,

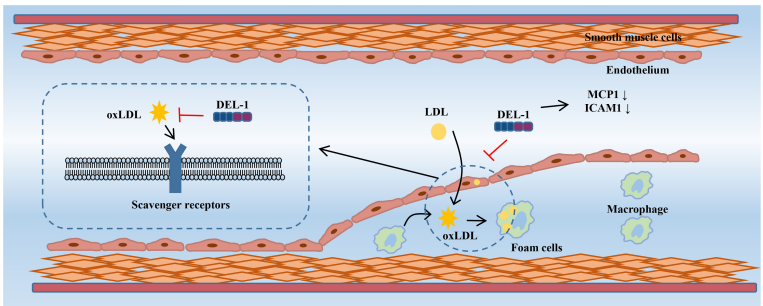

FIGURE 3
DEL-1 binds directly to oxLDL to block its binding to scavenger receptors and exert significant anti-atherogenic effects. In addition, DEL-1 reduced the expression of MCP1 and ICAM1 in the endothelial cell. DEL-1, developmental endothelial locus-1; oxLDL, oxidized low-density lipoprotein; MCP1, monocyte chemotactic protein-1; ICAM1, intercellular adhesion molecule-1.

75). Furthermore, MPs from CHD patients were less efficient at transferring miRNAs to cultured HUVECs, suggesting that MP uptake is impaired in the disease state. DEL-1 can mediate the uptake of MPs by endothelial cells by binding to PS on the external surface of MPs (62, 63). Although circulating levels of DEL-1 are increased in CHD patients, these patients have less DEL-1 binding to MPs (71). Therefore, Finn et al. suggested that DEL-1 binding to MPs was impaired in the serum of individuals with CHD, thereby altering circulating miRNA transport and affecting CHD initiation and progression. In the future, in addition to regulating the expression of DEL-1, regulating the function of DEL-1 may be an important aspect in the treatment of AS.

Hypertension

Hypertension refers to a clinical syndrome characterized by increased systemic arterial blood pressure (systolic and/or diastolic blood pressure), which may be accompanied by functional or organic damage to organs such as the heart, brain, and kidneys (76). Hypertension is the most common chronic disease and the main risk factor for cardiovascular and cerebrovascular diseases (77). Although the pathophysiological mechanisms of hypertension are not fully understood, strong evidence suggests that immune hyperactivation and chronic inflammatory responses play a crucial direct role in the development of hypertension (78). Our team's previous clinical and animal studies also proved that immune microenvironment disturbances are closely related to hypertension (79–83). Activated T lymphocytes and proinflammatory cytokines such as IL-17 are involved in the occurrence and development of angiotensin II (ANGII) and deoxycorticosterone acetate-salt (DOCA-salt)-induced hypertension (84–89). Gene knockout or neutralization with antibodies against IL-17 limited the progression of hypertension (86, 88, 90). DEL-1 can inhibit inflammation through various anti-inflammatory effects to alleviate IL-17-mediated conditions, such as inflammatory bone loss and multiple sclerosis, suggesting that DEL-1 may be a potential target for the treatment of hypertension (45, 48). Furthermore, DEL-1 promoted vascular smooth muscle cell (VSMC) adhesion, migration and proliferation in a dose-dependent manner, and this process was mediated through $\alpha V\beta_3$ integrin (91). These data suggested that DEL-1 has a paracrine role in vascular remodeling.

Recently, Failer et al. found that endothelial DEL-1-overexpressing mice had less adventitial collagen, lower medial thickness, and more elastin, suggesting that DEL-1 overexpression prevents ANGII-induced aortic remodeling (41). DEL-1 overexpression also prevented the progression of ANGII-induced hypertension, endothelial dysfunction and aortic fibrosis. DEL-1 overexpression alleviated the infiltration of CD45 leukocytes, TCR-β T cells and CD45IL-17 leukocytes in the aorta after ANGII infusion. Moreover, DEL-1 overexpression inhibited the expression of proinflammatory cytokines induced by ANGII and increased the expression level of the anti-inflammatory cytokine IL-10. In addition to inflammation, DEL-1 overexpression inhibits the activity of matrix metallopeptidase 2 (MMP2) in the aorta, whose increase critically contributes to aortic remodeling in hypertension (92, 93).

Failer et al. next investigated the preventive and therapeutic effects of recombinant DEL-1-FC on ANGII-induced hypertension. Intervention with recombinant DEL-1-FC administered before or after hypertension prevented or eliminated ANGII-induced aortic remodeling, hypertension, arterial stiffness, and inflammation (41). Recombinant DEL-1-FC also inhibited the activity of MMP2 in the aorta while promoting the infiltration of anti-inflammatory Tregs. Failer et al. also found that the mutation of the RGE part of DEL-1 abolished the protective effect of DEL-1-FC, suggesting that RGE is involved in the pathophysiological process of DEL-1 inhibiting the occurrence and development of hypertension. In a DOCA salt-induced hypertension model, recombinant DEL-1 treatment similarly attenuated aortic remodeling, hypertension, and inflammatory progression and promoted Treg infiltration (41).

A series of *in vitro* experiments further demonstrated that DEL-1 overexpression and recombinant DEL-1 treatment inhibited ANGII-induced activation of MMP2 in human and mouse vascular tissues, which was αVβ3 integrin-dependent (41, 94). Correspondingly, RGE mediates the binding of αVβ3 integrin to DEL-1, which may explain the abolition of the protective effect of DEL-1 by RGE mutation (41, 56). In conclusion, the findings of Failer et al. fully demonstrate the protective role of DEL-1 in the occurrence and development of hypertension and suggest this molecule may become a potential drug for the treatment of hypertension in the future (Figure 4).

Cardiac remodeling

Cardiac remodeling is an independent risk factor for heart failure, arrhythmias, and sudden death and is a key determinant of the clinical course and long-term prognosis of patients with CVDs (95). Pathological cardiac remodeling is characterized by cardiomyocyte hypertrophy and interstitial fibrosis under various cardiac stresses, such as hypertension and MI, resulting in increased myocardial stiffness and impaired cardiac contractility (96, 97). Cardiac remodeling is associated with fibrosis, capillary sparseness, increased production of proinflammatory cytokines, cellular dysfunction (impaired signaling, inhibition of autophagy, and abnormal cardiomyocyte/noncardiomyocyte interactions), and adverse epigenetic alterations (95). Our previous studies further shed light on the pathogenesis of cardiac remodeling, suggesting that inhibition of cardiac remodeling by pharmacological or genetic approaches significantly improves cardiac dysfunction and survival (21, 98–101).

In mice, fibroblasts constituted 27% of all cardiac cells, contributing to the maintenance of homeostasis under

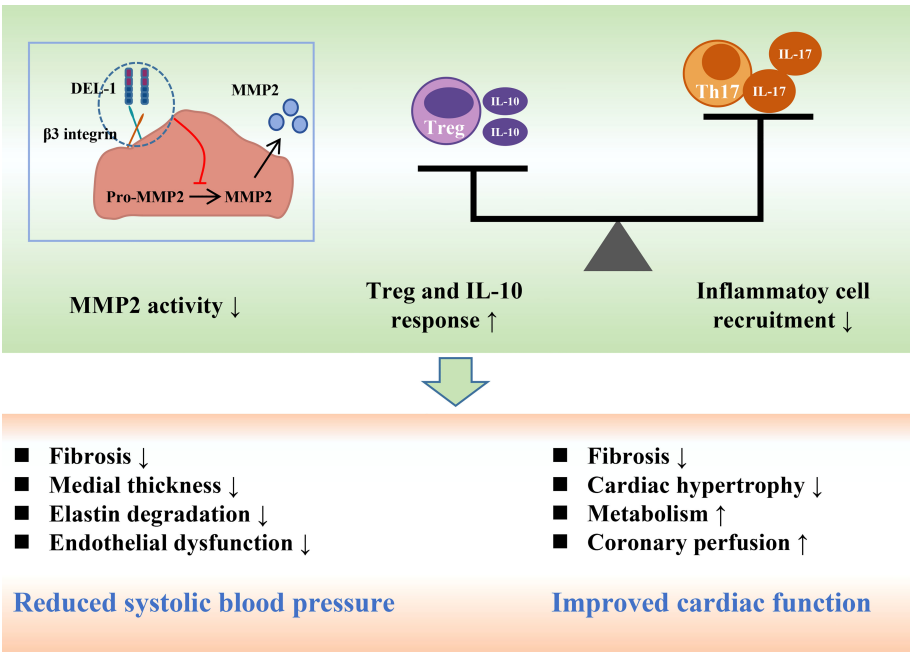

FIGURE 4
DEL-1 reduces blood pressure and maintains cardiac function by inhibiting MMP2 activity, reducing inflammatory cell infiltration and enhancing Treg and IL-10 responses. DEL-1, developmental endothelial locus-1; MMP2, matrix metallopeptidase 2; Th17, T helper 17 cell; Treg, T regulatory cell; IL, interleukin.

physiological conditions and regulating tissue remodeling in response to stress (95, 102, 103). Pathological fibrosis results from abnormal regulation of extracellular matrix (ECM) production in tissues or organs, including collagen (97). Compared with that in normal lung tissue, the expression level of DEL-1 was decreased in lung fibrous tissue, suggesting that DEL-1 may be associated with pulmonary fibrosis (60). DEL-1 deficiency promoted collagen synthesis and secretion by regulating transforming growth factor (TGF-β), thereby aggravating bleomycin-induced pulmonary fibrosis (60, 104). Yan et al. found that DEL-1-deficient mice had a higher incidence of postoperative peritoneal adhesions, accompanied by enhanced collagen production (65). In contrast, DEL-1 supplementation reduced the incidence and severity of postoperative peritoneal adhesions. *In vitro* studies have demonstrated that DEL-1 inhibits TGF-β activation in 293T cells and RAW264.7 mouse macrophages by binding to αVβ6 integrin (104). These data suggest that DEL-1 plays an important role in the initiation and progression of tissue fibrosis.

The immune system and inflammatory response mediate pathological cardiac remodeling (97). Immunomodulation may be an important strategy to alleviate cardiac remodeling. Failer et al. found that endothelial DEL-1 overexpression or recombinant DEL-1 treatment inhibited AGNII or DOCA salt-induced inflammation and MMP2 activation in the heart, thereby reducing cardiac hypertrophy, fibrosis, and dysfunction (41). However, cardiac remodeling in this study belongs to target organ damage caused by hypertension, and the regulation of DEL-1 on blood pressure may indirectly affect cardiac remodeling. Therefore, this study may have certain limitations. Future studies on cardiac remodeling may help us further understand the function of DEL-1.

Ischemic heart disease

Ischemic heart disease (IHD), mainly caused by coronary atherosclerosis and its complications, can induce congestive HF and life-threatening arrhythmias and is the leading cause of death worldwide (105, 106). Acute myocardial infarction (AMI) is the most serious IHD with the highest mortality rate (106). In a pig model of cardiac ischemia induced by left circumflex artery ligation, DEL-1 treatment improved cardiac function (107). Wei et al. found that DEL-1 levels were decreased in severe AMI patients, which is consistent with the finding thar WT mice with MI showed low levels of cardiac DEL-1 (42). Compared with WT mice, DEL-1-/- mice showed significantly improved cardiac function and alleviated cardiac remodeling post-MI. Mechanistically, the protective effect of DEL-1 deficiency in MI was associated with enhanced neutrophil recruitment and expansion of proinflammatory monocyte-derived macrophages (42). Injection of a neutrophil-specific C-X-C motif chemokine receptor 2 (CXCR2) antagonist impaired macrophage

polarization, increased cellular debris and exacerbated adverse cardiac remodeling, thereby abrogating the protective effect of DEL-1 deficiency. Inhibition of neutrophil extracellular trap (NET) formation by treatment with a neutrophil elastase inhibitor or DNase I abrogated differences in macrophage polarization and cardiac function between WT and DEL-1-/- mice after MI. Collectively, these data suggest that DEL-1 is a key regulator of neutrophil recruitment and macrophage polarization during cardiac remodeling after MI (Figure 5).

Increasing evidence has shown that healing of MI involves a series of delicately regulated inflammatory responses (108). Following MI, injured cardiomyocytes release damage-associated molecular patterns (DAMPs), cytokines, and chemokines, leading to substantial recruitment of neutrophils and monocytes/macrophages to the myocardium (109, 110). These neutrophils and monocytes contribute to the removal of debris and dead cells, as well as the activation of repair pathways. Furthermore, recruited monocytes give rise to proinflammatory or repairing macrophages. Proinflammatory macrophages produce cytokines, release MMPs to promote extracellular matrix destruction, and clear cellular debris, while repairing macrophages promotes fibroblast-to-myofibroblast transformation and enhances collagen deposition, leading to the formation of crosslinked collagen (111). A scar is formed to protect the left ventricle (LV) from rupture of the heart. Wei et al. confirmed the integral role of inflammation in the healing process (42). However, excessive inflammation may exacerbate MI-induced myocardial injury (109, 111). DEL-1 has anti-inflammatory and proresolving effects, and the lack of DEL-1 may inhibit inflammatory resolution, leading to an excessive inflammatory response and exacerbating tissue damage (40, 60, 112, 113). Therefore, the extent of the increased inflammation caused by DEL-1 deficiency in Wei et al.'s study requires further scrutiny.

The study by Wei et al. is the only report of amelioration of DEL-1 deficiency (42). In previous reports, inhibition of neutrophil recruitment improved cardiac dysfunction and cardiac remodeling after MI (114–116). Inhibition of neutrophils by DEL-1 also exerted protective effects in other diseases, which seems to contradict the study by Wei et al. (46, 48, 117). Multiple actions of DEL-1, such as anti- and proinflammatory resolution (39), coronary vasodilation (41), inhibition of MMP2 activity (41) and promotion of angiogenesis (118, 119), may protect the heart from MI-induced injury. The study by Wei et al. has certain limitations,

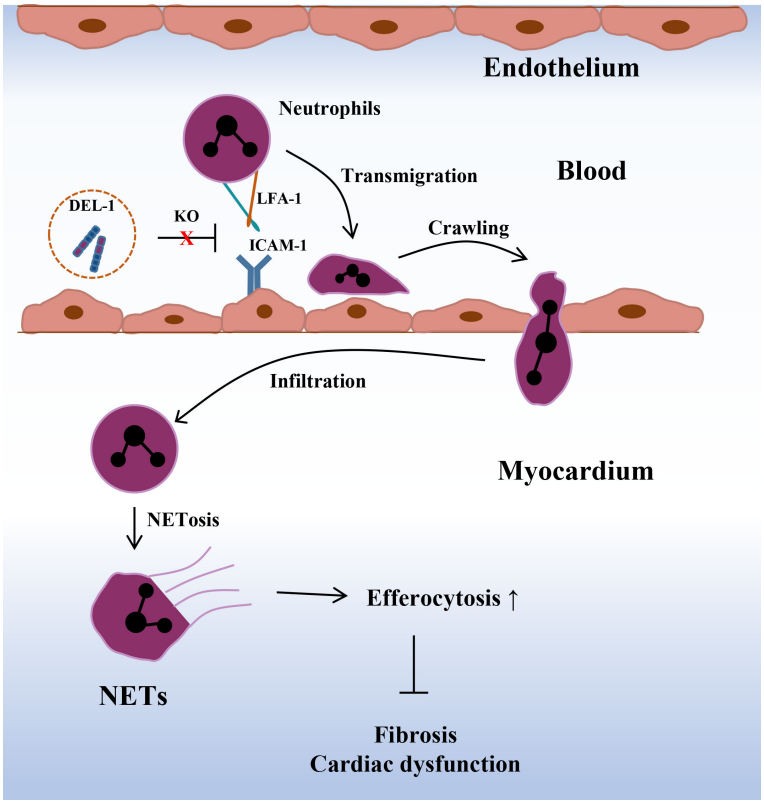

FIGURE 5
Deletion of DEL-1 promotes neutrophil infiltration and formation of NETs, thereby promoting macrophage efferocytosis and alleviating cardiac fibrosis and cardiac dysfunction after MI. DEL-1, developmental endothelial locus-1; NETs, neutrophil extracellular trap; MI, myocardial infarction.

such as the lack of cell-specific gene-edited mice and the lack of analysis of preventive or therapeutic effects of recombinant DEL-1 (42). The future use of endothelial or macrophage-specific DEL-1 transgenic mice and recombinant DEL-1 may help us further understand the role and mechanism of DEL-1 in IHD.

Other cardiovascular diseases

DEL-1 was found to regulate vascular morphogenesis or remodeling in embryonic development as early as 1998 when it was first cloned and characterized (44). DEL-1 provides a unique autocrine angiogenic pathway for the embryonic endothelium, which is mediated in part by integrin $\alpha_v\beta_3$ (120). DEL-1 mediates VSMC adhesion, migration and proliferation through interaction with integrin $\alpha_v\beta_3$, which may regulate vascular wall development and remodeling (91). Aoka et al. found that DEL-1 accelerates tumor growth by promoting enhanced angiogenesis (121). Expression of endogenous DEL-1 protein is increased in ischemic hindlimbs (122). DEL-1 binding to $\alpha_v\beta_5$ upregulated the expression of the transcription factor Hox D3 and integrin $\alpha_v\beta_3$, thereby promoting angiogenesis and functional recovery in a hindlimb ischemia model (57). Exogenous intramuscular administration of DEL-1 significantly enhanced angiogenesis in ischemic hindlimbs in mice, suggesting that DEL-1 may be a novel therapeutic agent for ischemic patients (122). A clinical study compared VLTS-589 (a plasmid encoding Del-1 conjugated to poloxamer 188) with the poloxamer 188 control in the treatment of intermittent claudication in patients with moderate to severe peripheral arterial disease (123). Intramuscular delivery of a plasmid expressing DEL-1 and the control significantly improved baseline exercise capacity at 30, 90, and 180 days, but there was no difference in outcome measures between the two groups. DEL-1-mediated angiogenesis has also been reported in many other diseases, such as ischemia models, lung adenocarcinoma, retinopathy, squamous cell carcinoma, and psoriasis (119, 124–129). Taken together, these data suggest that DEL-1-regulated angiogenesis may be a target for many diseases, but its clinical value requires further clinical trials.

Similar to MI, strokes are also caused by vascular or microvascular diseases that disrupt the blood supply to the brain, leading to brain dysfunction (130). The number of new vessels generated in ischemic brain tissue is associated with decreased morbidity and longer survival in stroke patients, suggesting that restoration of cerebral microvascular circulation is important for functional recovery after ischemic attacks (131). DEL-1 expression was increased in the ischemic cortical peri-infarct area after ischemic stroke (118). DEL-1 gene transfer induced cerebral angiogenesis and may be a novel and effective method for stimulating cerebral angiogenesis after stroke (118). Electroconvulsive seizures (ECSs) have been shown to treat major depression by modulating neurotrophy and angiogenesis (132, 133). Newton et al. found that ECS treatment increased DEL-1 expression in brain tissue and promoted angiogenesis in the adult rat hippocampus (134). In conclusion, DEL-1-mediated angiogenesis may be one of the targets for the treatment of cerebrovascular diseases.

DEL-1 in metabolic diseases

The prevalence of metabolic diseases, including diabetes, is increasing, while the westernization of dietary habits has led to an increase in obesity (135). Obesity-related chronic low-grade inflammation has been reported to cause insulin resistance in muscle, liver, and adipose tissue (136). Insulin resistance refers to the decrease in the efficiency of insulin to promote glucose uptake and utilization for various reasons, and the compensatory secretion of excessive insulin produces hyperinsulinemia to maintain the stability of serum glucose levels (137). Insulin resistance predisposes patients to metabolic syndrome and type 2 diabetes. DEL-1 ameliorates palmitate-induced endoplasmic reticulum (ER) stress and insulin resistance in the mouse skeletal muscle cell line C2C12 *via* SIRT1/SERCA2-related signaling (43). *In vivo* experiments showed that DEL-1 administration increased the expression of SIRT1 and SERCA2, thereby ameliorating insulin resistance in skeletal muscle of high fat diet (HFD)-fed mice and improving HFD-impaired glucose tolerance and insulin sensitivity (43). These results suggest that DEL-1 may be a novel therapeutic target for the management of insulin resistance and type 2 diabetes.

Regular exercise is the treatment of choice for obesity and obesity-mediated metabolic disorders such as insulin resistance, type 2 diabetes, atherosclerosis, and hypertension (138). Compared with that in healthy subjects, DEL-1 mRNA expression was decreased in the muscle of obese and diabetic patients (139). Exercise increases DEL-1 mRNA expression levels in obese/diabetic patients in a time-dependent manner (139). DEL-1 secreted by exercising skeletal muscle can affect various tissues through the bloodstream, including adipose tissue (140). *In vitro* experiments showed that DEL-1 attenuated palmitate-induced inflammation and insulin signaling impairment in adipocytes by regulating AMPK/HO-1 signaling (139). In addition, DEL-1 treatment promoted AMPK phosphorylation and enhanced adipocyte thermogenesis but did not affect intracellular lipid accumulation (139).

In another endometrial cancer (EC) cohort study, Cobb et al. found an association between patient BMI and increased DEL-1 expression in cancer tissue (141). Furthermore, HFD increased the expression of DEL-1 in tumors compared with a low-fat diet in EC model mice (141). These data suggest that DEL-1 may serve as a novel obesity-driving target that should be further explored in future research work.

Thus, DEL-1-mediated anti-inflammatory and proresolving effects provide a basis for the amelioration of metabolic diseases. DEL-1 is involved in the regulation of obesity and insulin

resistance. However, the current relevant evidence is still insufficient, and more research is needed in the future to reveal the role of DEL-1 in metabolic diseases.

Concluding remarks and future perspectives

DEL-1 has received considerable attention since it was first cloned and characterized as a factor promoting embryonic angiogenesis (44). DEL-1 is widely expressed in different tissues, such as the brain, lung and blood vessels, to maintain tissue homeostasis. As a secreted protein, the serum level of DEL-1 may be related to the diagnosis and prognosis of various diseases, such as MI, sepsis and osteoarthritis (42, 142, 143). As a local tissue signal, DEL-1 exerts anti-inflammatory and proresolving effects in different tissues and stages, thereby ameliorating a variety of inflammation-related diseases (39). Emerging studies over the past few years have convincingly demonstrated that DEL-1 has a therapeutic effect on a variety of CVMDs, including AS, hypertension, cardiac remodeling, and insulin resistance. This review summarizes the potential involvement of DEL-1 in cardiovascular and metabolic homeostasis, thereby defining DEL-1 as a promising biomarker and therapeutic target for CVMDs.

Despite our detailed understanding of the role of DEL-1 in various pathophysiological processes, several questions remain to be answered. We propose some solutions to these questions in this review. First, systemic overexpression rather than endothelial cell-specific overexpression of DEL-1 inhibited the occurrence and development of AS, and the mechanism remains unclear (72, 73). Other cells, such as macrophage-specific overexpression mice, may help us understand the role of DEL-1 in AS. Future basic research on the use of recombinant DEL-1 in the treatment of AS can provide a reference for its clinical application. Second, although Wei et al. found that DEL-1 treatment attenuated hypertension-induced cardiac remodeling, this protective effect may be attributable to reduced blood pressure (41). More direct evidence for the treatment of DEL-1 in cardiac remodeling is lacking. The application of other cardiac remodeling models could better reveal the therapeutic effect of DEL-1 on cardiac remodeling. *In vitro* experiments can also help us further understand the mechanism by which DEL-1 treatment improves cardiac remodeling. Third, DEL-1 deficiency ameliorated cardiac dysfunction and remodeling in MI by promoting inflammation (42). Although the data in this study are sufficient, we remain concerned about the extent of increased inflammation caused by DEL-1 deficiency, as excessive inflammation is damaging. Future treatment with DEL-1 overexpression or recombinant protein may help us to further understand the role and mechanism of DEL-1 in MI.

The protective effect of DEL-1 in CVMDs has important clinical value. There is currently only one phase II, multicenter, double-blind, placebo-controlled study of DEL-1 in the treatment of intermittent claudication, which combined a plasmid encoding DEL-1 with poloxamer 188 to form VLTS-589 and delivered this treatment intramuscularly (123). Although the outcomes of DEL-1 plasmid-treated patients did not change compared with the controls, this was an important attempt at clinical application of DEL-1. Some researchers have also used DEL-1 for tissue engineering to promote angiogenesis (119, 124). On the one hand, we can use gene therapy that promotes the expression of DEL-1 by constructing plasmids for clinical experiments, and on the other hand, we can also use nanomaterials and other technologies to deliver recombinant DEL-1 protein or plasmids to target tissues, such as the heart and brain. In addition, well-designed, large-scale, high-quality, and multicenter clinical trials are needed to evaluate the safety, toxicological profile, and clinical utility of DEL-1 in human patients with CVMDs.

Collectively, DEL-1 is a promising biomarker and therapeutic target for CVMDs.

Author contributions

JW and MW participated in the design of the project. MZ and CL were responsible for drafting the manuscript. ZZ was responsible for the figures of this review. All authors contributed to the article and approved the submitted version.

Funding

This work was supported by grants from the National Natural Science Foundation of China (82070436, 82100292, 82270454).

Conflict of interest

The authors declare that the research was conducted in the absence of any commercial or financial relationships that could be construed as a potential conflict of interest.

Publisher's note

References

1. Bonora E. The metabolic syndrome and cardiovascular disease. *Ann Med* (2006) 38(1):64–80. doi: 10.1080/07853890500401234

2. Kasper P, Martin A, Lang S, Kütting F, Goeser T, Demir M, et al. NAFLD and cardiovascular diseases: a clinical review. *Clin Res Cardiol* (2021) 110(7):921–37. doi: 10.1007/s00392-020-01709-7

3. Benjamin EJ, Virani SS, Callaway CW, Chamberlain AM, Chang AR, Cheng S, et al. Heart disease and stroke statistics-2018 update: A report from the American heart association. *Circulation* (2018) 137(12):e67–e492. doi: 10.1161/CIR.0000000000000558

4. Timmis A, Townsend N, Gale C, Grobbee R, Maniadakis N, Flather M, et al. European Society of cardiology: Cardiovascular disease statistics 2017. *Eur Heart J* (2018) 39(7):508–79. doi: 10.1093/eurheartj/ehx628

5. Saklayen MG. The global epidemic of the metabolic syndrome. *Curr Hypertens Rep* (2018) 20(2):12. doi: 10.1007/s11906-018-0812-z

6. Townsend N, Nichols M, Scarborough P, Rayner M. Cardiovascular disease in Europe–epidemiological update 2015. *Eur Heart J* (2015) 36(40):2696–705. doi: 10.1093/eurheartj/ehv428

7. Roth GA, Forouzanfar MH, Moran AE, Barber R, Nguyen G, Feigin VL, et al. Demographic and epidemiologic drivers of global cardiovascular mortality. *N Engl J Med* (2015) 372(14):1333–41. doi: 10.1056/NEJMoa1406656

8. Mechanick JI, Farkouh ME, Newman JD, Garvey WT. Cardiometabolic-based chronic disease, adiposity and dysglycemia drivers: JACC state-of-the-Art review. *J Am Coll Cardiol* (2020) 75(5):525–38. doi: 10.1016/j.jacc.2019.11.044

9. Hotamisligil GS. Foundations of immunometabolism and implications for metabolic health and disease. *Immunity* (2017) 47(3):406–20. doi: 10.1016/j.immuni.2017.08.009

10. Ilatovskaya DV, Halade GV, DeLeon-Pennell KY. Adaptive immunity-driven inflammation and cardiovascular disease. *Am J Physiol Heart Circ Physiol* (2019) 317(6):H1254–h1257. doi: 10.1152/ajpheart.00642.2019

11. Pedicino D, Giglio AF, Ruggio A, Massaro G, D'Aiello A, Trotta F, et al. Lymphocytes and innate-adaptive immunity crosstalk: Role in cardiovascular disease and therapeutic perspectives. *Thromb Haemost* (2018) 118(8):1352–69. doi: 10.1055/s-0038-1666860

12. Libby P. Interleukin-1 beta as a target for atherosclerosis therapy: Biological basis of CANTOS and beyond. *J Am Coll Cardiol* (2017) 70(18):2278–89. doi: 10.1016/j.jacc.2017.09.028

13. Danesh J, Kaptoge S, Mann AG, Sarwar N, Wood A, Angleman SB, et al. Long-term interleukin-6 levels and subsequent risk of coronary heart disease: two new prospective studies and a systematic review. *PloS Med* (2008) 5(4):e78. doi: 10.1371/journal.pmed.0050078

14. Ridker PM. From c-reactive protein to interleukin-6 to interleukin-1: Moving upstream to identify novel targets for atheroprotection. *Circ Res* (2016) 118(1):145–56. doi: 10.1161/CIRCRESAHA.115.306656

15. Chen YL, Qiao YC, Pan YH, Xu Y, Huang YC, Wang YH, et al. Correlation between serum interleukin-6 level and type 1 diabetes mellitus: A systematic review and meta-analysis. *Cytokine* (2017) 94:14–20. doi: 10.1016/j.cyto.2017.01.002

16. Atieh MA, Faggion CMJr., Seymour GJ. Cytokines in patients with type 2 diabetes and chronic periodontitis: A systematic review and meta-analysis. *Diabetes Res Clin Pract* (2014) 104(2):e38–45. doi: 10.1016/j.diabres.2014.02.002

17. Wang T, He C. Pro-inflammatory cytokines: The link between obesity and osteoarthritis. *Cytokine Growth Factor Rev* (2018) 44:38–50. doi: 10.1016/j.cytogfr.2018.10.002

18. Zhang J, Xu Y, Ding W, Zhao M, Liu J, Ye J, et al. Increased expression of IL-20 is associated with ischemic cardiomyopathy and acute myocardial infarction. *biomark Med* (2021) 15(17):1641–50. doi: 10.2217/bmm-2020-0529

19. Lyngbakken MN, Myhre PL, Røsjø H, Omland T. Novel biomarkers of cardiovascular disease: Applications in clinical practice. *Crit Rev Clin Lab Sci* (2019) 56(1):33–60. doi: 10.1080/10408363.2018.1525335

20. Ruscitti P, Masedu F, Alvaro S, Airò P, Battafarano N, Cantarini L, et al. Anti-interleukin-1 treatment in patients with rheumatoid arthritis and type 2 diabetes (TRACK): A multicentre, open-label, randomised controlled trial. *PloS Med* (2019) 16(9):e1002901. doi: 10.1371/journal.pmed.1002901

21. Zhao M, Zhang J, Xu Y, Liu J, Ye J, Wang Z, et al. Selective inhibition of NLRP3 inflammasome reverses pressure overload-induced pathological cardiac remodeling by attenuating hypertrophy, fibrosis, and inflammation. *Int Immunopharmacol* (2021) 99:108046. doi: 10.1016/j.intimp.2021.108046

22. Unamuno X, Gómez-Ambrosi J, Ramírez B, Rodríguez A, Becerril S, Valentí V, et al. NLRP3 inflammasome blockade reduces adipose tissue inflammation and extracellular matrix remodeling. *Cell Mol Immunol* (2021) 18(4):1045–57. doi: 10.1038/s41423-019-0296-z

23. Ridker PM, Everett BM, Pradhan A, MacFadyen JG, Solomon DH, Zaharris E, et al. Low-dose methotrexate for the prevention of atherosclerotic events. *N Engl J Med* (2019) 380(8):752–62. doi: 10.1056/NEJMoa1809798

24. Lutgens E, Atzler D, Döring Y, Duchene J, Steffens S, Weber C. Immunotherapy for cardiovascular disease. *Eur Heart J* (2019) 40(48):3937–46. doi: 10.1093/eurheartj/ehz283

25. Chen X, Wu Y, Wang L. Fat-resident tregs: an emerging guard protecting from obesity-associated metabolic disorders. *Obes Rev* (2013) 14(7):568–78. doi: 10.1111/obr.12033

26. Stolley JM, Masopust D. Tissue-resident memory T cells live off the fat of the land. *Cell Res* (2017) 27(7):847–8. doi: 10.1038/cr.2017.49

27. Zaman R, Hamidzada H, Kantores C, Wong A, Dick SA, Wang Y, et al. Selective loss of resident macrophage-derived insulin-like growth factor-1 abolishes adaptive cardiac growth to stress. *Immunity* (2021) 54(9):2057–2071.e6. doi: 10.1016/j.immuni.2021.07.006

28. Wong NR, Mohan J, Kopecky BJ, Guo S, Du L, Leid J, et al. Resident cardiac macrophages mediate adaptive myocardial remodeling. *Immunity* (2021) 54(9):2072–2088.e7. doi: 10.1016/j.immuni.2021.07.003

29. Gimbrone MAJr., García-Cardeña G. Endothelial cell dysfunction and the pathobiology of atherosclerosis. *Circ Res* (2016) 118(4):620–36. doi: 10.1161/CIRCRESAHA.115.306301

30. Tombor LS, John D, Glaser SF, Luxán G, Forte E, Furtado M, et al. Single cell sequencing reveals endothelial plasticity with transient mesenchymal activation after myocardial infarction. *Nat Commun* (2021) 12(1):681. doi: 10.1161/CIRCRESAHA.115.306301

31. Horckmans M, Bianchini M, Santovito D, Megens RTA, Springael JY, Negri I, et al. Pericardial adipose tissue regulates granulopoiesis, fibrosis, and cardiac function after myocardial infarction. *Circulation* (2018) 137(9):948–60. doi: 10.1161/CIRCULATIONAHA.117.028833

32. Burhans MS, Hagman DK, Kuzma JN, Schmidt KA, Kratz M. Contribution of adipose tissue inflammation to the development of type 2 diabetes mellitus. *Compr Physiol* (2018) 9(1):1–58. doi: 10.1002/cphy.c170040

33. Matzinger P, Kamala T. Tissue-based class control: the other side of tolerance. *Nat Rev Immunol* (2011) 11(3):221–30. doi: 10.1038/nri2940

34. Galli SJ, Borregaard N, Wynn TA. Phenotypic and functional plasticity of cells of innate immunity: macrophages, mast cells and neutrophils. *Nat Immunol* (2011) 12(11):1035–44. doi: 10.1038/ni.2109

35. Hajishengallis G, Chavakis T. Endogenous modulators of inflammatory cell recruitment. *Trends Immunol* (2013) 34(1):1–6. doi: 10.1016/j.it.2012.08.003

36. Gonçalves LM. Angiogenic growth factors: potential new treatment for acute myocardial infarction? *Cardiovasc Res* (2000) 45(2):294–302. doi: 10.1016/S0008-6363(99)00358-2

37. Frangogiannis NG. Pathophysiology of myocardial infarction. *Compr Physiol* (2015) 5(4):1841–75. doi: 10.1002/cphy.c150006

38. Daseke MJ2nd, Tenkorang MAA, Chalise U, Konfrst SR, Lindsey ML. Cardiac fibroblast activation during myocardial infarction wound healing: Fibroblast polarization after MI. *Matrix Biol* (2020) 91-92:109–16. doi: 10.1016/j.matbio.2020.03.010

39. Hajishengallis G, Chavakis T. DEL-1-Regulated immune plasticity and inflammatory disorders. *Trends Mol Med* (2019) 25(5):444–59. doi: 10.1016/j.molmed.2019.02.010

40. Kourtzelis I, Li X, Mitroulis I, Grosser D, Kajikawa T, Wang B, et al. DEL-1 promotes macrophage efferocytosis and clearance of inflammation. *Nat Immunol* (2019) 20(1):40–9. doi: 10.1038/s41590-018-0249-1

41. Failer T, Amponsah-Offeh M, Neuwirth A, Kourtzelis I, Subramanian P, Mirtschink P, et al. Developmental endothelial locus-1 protects from hypertension-induced cardiovascular remodeling *via* immunomodulation. *J Clin Invest* (2022) 132(6):e126155. doi: 10.1172/JCI126155.

42. Wei X, Zou S, Xie Z, Wang Z, Huang N, Cen Z, et al. EDIL3 deficiency ameliorates adverse cardiac remodeling by neutrophil extracellular traps (NET)-mediated macrophage polarization. *Cardiovasc Res* (2021) 118(9):2179–95. doi: 10.1093/cvr/cvab269.

43. Sun JL, Park J, Lee T, Jeong JH, Jung TW. DEL-1 ameliorates high-fat diet-induced insulin resistance in mouse skeletal muscle through SIRT1/SERCA2-mediated ER stress suppression. *Biochem Pharmacol* (2020) 171:113730. doi: 10.1016/j.bcp.2019.113730

44. Hidai C, Zupancic T, Penta K, Mikhail A, Kawana M, Quertermous EE, et al. Cloning and characterization of developmental endothelial locus-1: an embryonic endothelial cell protein that binds the alphavbeta3 integrin receptor. *Genes Dev* (1998) 12(1):21–33. doi: 10.1101/gad.12.1.21

45. Eskan MA, Jotwani R, Abe T, Chmelar J, Lim JH, Liang S, et al. The leukocyte integrin antagonist del-1 inhibits IL-17-mediated inflammatory bone loss. *Nat Immunol* (2012) 13(5):465–73. doi: 10.1038/ni.2260

46. Choi EY, Chavakis E, Czabanka MA, Langer HF, Fraemohs L, Economopoulou M, et al. Del-1, an endogenous leukocyte-endothelial adhesion inhibitor, limits inflammatory cell recruitment. *Science* (2008) 322(5904):1101–4. doi: 10.1126/science.1165218

47. Choi EY, Lim JH, Neuwirth A, Economopoulou M, Chatzigeorgiou A, Chung KJ, et al. Developmental endothelial locus-1 is a homeostatic factor in the central nervous system limiting neuroinflammation and demyelination. *Mol Psychiatry* (2015) 20(7):880–8. doi: 10.1038/mp.2014.146

48. Shin J, Maekawa T, Abe T, Hajishengallis E, Hosur K, Pyaram K, et al. DEL-1 restrains osteoclastogenesis and inhibits inflammatory bone loss in nonhuman primates. *Sci Transl Med* (2015) 7(307):307ra155. doi: 10.1126/scitranslmed.aac5380

49. Shin J, Hosur KB, Pyaram K, Jotwani R, Liang S, Chavakis T, et al. Expression and function of the homeostatic molecule del-1 in endothelial cells and the periodontal tissue. *Clin Dev Immunol* (2013) 2013:617809. doi: 10.1155/2013/617809

50. Folwaczny M, Karnesi E, Berger T, Paschos E. Clinical association between chronic periodontitis and the leukocyte extravasation inhibitors developmental endothelial locus-1 and pentraxin-3. *Eur J Oral Sci* (2017) 125(4):258–64. doi: 10.1111/eos.12357

51. Ziogas A, Maekawa T, Wiessner JR, Le TT, Sprott D, Troullinaki M, et al. DHEA inhibits leukocyte recruitment through regulation of the integrin antagonist DEL-1. *J Immunol* (2020) 204(5):1214–24. doi: 10.4049/jimmunol

52. Maekawa T, Tamura H, Domon H, Hiyoshi T, Isono T, Yonezawa D, et al. Erythromycin inhibits neutrophilic inflammation and mucosal disease by upregulating DEL-1. *JCI Insight* (2020) 5(15):e136706. doi: 10.1172/jci.insight.136706

53. Kim H, Lee SH, Lee MN, Oh GT, Choi KC, Choi EY. p53 regulates the transcription of the anti-inflammatory molecule developmental endothelial locus-1 (Del-1). *Oncotarget* (2013) 4(11):1976–85. doi: 10.18632/oncotarget.1318

54. Wenzina J, Holzner S, Puujalka E, Cheng PF, Forsthuber A, Neumüller K, et al. Inhibition of p38/MK2 signaling prevents vascular invasion of melanoma. *J Invest Dermatol* (2020) 140(4):878–890.e5. doi: 10.1016/j.jid.2019.08.451

55. Goris A, Sawcer S, Vandenbroeck K, Carton H, Billiau A, Setakis E, et al. New candidate loci for multiple sclerosis susceptibility revealed by a whole genome association screen in a Belgian population. *J Neuroimmunol* (2003) 143(1-2):65–9. doi: 10.1016/j.jneuroim.2003.08.013

56. Schürpf T, Chen Q, Liu JH, Wang R, Springer TA, Wang JH. The RGD finger of del-1 is a unique structural feature critical for integrin binding. *FASEB J* (2012) 26(8):3412–20. doi: 10.1096/fj.11-202036

57. Zhong J, Eliceiri B, Stupack D, Penta K, Sakamoto G, Quertermous T, et al. Neovascularization of ischemic tissues by gene delivery of the extracellular matrix protein del-1. *J Clin Invest* (2003) 112(1):30–41. doi: 10.1172/JCI17034

58. Hidai C, Kawana M, Kitano H, Kokubun S. Discoidin domain of Del1 protein contributes to its deposition in the extracellular matrix. *Cell Tissue Res* (2007) 330(1):83–95. doi: 10.1007/s00441-007-0456-9

59. Vestweber D. How leukocytes cross the vascular endothelium. *Nat Rev Immunol* (2015) 15(11):692–704. doi: 10.1038/nri3908

60. Kang YY, Kim DY, Lee SH, Choi EY. Deficiency of developmental endothelial locus-1 (Del-1) aggravates bleomycin-induced pulmonary fibrosis in mice. *Biochem Biophys Res Commun* (2014) 445(2):369–74. doi: 10.1016/j.bbrc.2014.02.009

61. Kourtzelis I, Kotlabova K, Lim JH, Mitroulis I, Ferreira A, Chen LS, et al. Developmental endothelial locus-1 modulates platelet-monocyte interactions and instant blood-mediated inflammatory reaction in islet transplantation. *Thromb Haemost* (2016) 115(4):781–8. doi: 10.1160/th15-05-0429

62. Dasgupta SK, Le A, Chavakis T, Rumbaut RE, Thiagarajan P. Developmental endothelial locus-1 (Del-1) mediates clearance of platelet microparticles by the endothelium. *Circulation* (2012) 125(13):1664–72. doi: 10.1161/CIRCULATIONAHA.111.068833

63. Hanayama R, Tanaka M, Miwa K, Nagata S. Expression of developmental endothelial locus-1 in a subset of macrophages for engulfment of apoptotic cells. *J Immunol* (2004) 172(6):3876–82. doi: 10.4049/jimmunol.172.6.3876

64. Hajishengallis G, Chavakis T. DEL-1: a potential therapeutic target in inflammatory and autoimmune disease? *Expert Rev Clin Immunol* (2021) 17(6):549–52. doi: 10.1080/1744666X.2021.1915771

65. Fu Y, Tsauo J, Sun Y, Wang Z, Kim KY, Lee SH, et al. Developmental endothelial locus-1 prevents development of peritoneal adhesions in mice. *Biochem Biophys Res Commun* (2018) 500(3):783–9. doi: 10.1016/j.bbrc.2018.04.158

66. Mitroulis I, Chen LS, Singh RP, Kourtzelis I, Economopoulou M, Kajikawa T, et al. Secreted protein del-1 regulates myelopoiesis in the hematopoietic stem cell niche. *J Clin Invest* (2017) 127(10):3624–39. doi: 10.1172/JCI92571

67. Geovanini GR, Libby P. Atherosclerosis and inflammation: overview and updates. *Clin Sci (Lond)* (2018) 132(12):1243–52. doi: 10.1042/CS20180306

68. Hopkins PN. Molecular biology of atherosclerosis. *Physiol Rev* (2013) 93(3):1317–542. doi: 10.1152/physrev.00004.2012

69. Libby P. The changing landscape of atherosclerosis. *Nature* (2021) 592(7855):524–33. doi: 10.1038/s41586-021-03392-8

70. Lusis AJ. Atherosclerosis. *Nature* (2000) 407(6801):233–41. doi: 10.1038/35025203

71. Finn NA, Eapen D, Manocha P, Al Kassem H, Lassegue B, Ghasemzadeh N, et al. Coronary heart disease alters intercellular communication by modifying microparticle-mediated microRNA transport. *FEBS Lett* (2013) 587(21):3456–63. doi: 10.1016/j.febslet.2013.08.034

72. Kakino A, Fujita Y, Nakano A, Horiuchi S, Sawamura T. Developmental endothelial locus-1 (Del-1) inhibits oxidized low-density lipoprotein activity by direct binding, and its overexpression attenuates atherogenesis in mice. *Circ J* (2016) 80(12):2541–9. doi: 10.1253/circj.CJ-16-0808

73. Subramanian P, Prucnal M, Gercken B, Economopoulou M, Hajishengallis G, Chavakis T. Endothelial cell-specific overexpression of developmental endothelial locus-1 does not influence atherosclerosis development in ApoE(-/-) mice. *Thromb Haemost* (2017) 117(10):2003–5. doi: 10.1160/th17-03-0160

74. Burnier L, Fontana P, Angelillo-Scherrer A, Kwak BR. Intercellular communication in atherosclerosis. *Physiol (Bethesda)* (2009) 24:36–44. doi: 10.1152/physiol.00036.2008

75. Boulanger CM, Dignat-George F. Microparticles: an introduction. *Arterioscler Thromb Vasc Biol* (2011) 31(1):2–3. doi: 10.1161/ATVBAHA.110.220095

76. Benetos A, Petrovic M, Strandberg T. Hypertension management in older and frail older patients. *Circ Res* (2019) 124(7):1045–60. doi: 10.1161/circresaha.118.313236

77. Cooper LL, Rong J, Benjamin EJ, Larson MG, Levy D, Vita JA, et al. Components of hemodynamic load and cardiovascular events: the framingham heart study. *Circulation* (2015) 131(4):354–61; discussion 361. doi: 10.1161/circulationaha.114.011357

78. Madhur MS, Elijovich F, Alexander MR, Pitzer A, Ishimwe J, Van Beusecum JP, et al. Hypertension: Do inflammation and immunity hold the key to solving this epidemic? *Circ Res* (2021) 128(7):908–33. doi: 10.1161/circresaha.121.318052

79. Ye J, Que B, Huang Y, Lin Y, Chen J, Liu L, et al. Interleukin-12p35 knockout promotes macrophage differentiation, aggravates vascular dysfunction, and elevates blood pressure in angiotensin II-infused mice. *Cardiovasc Res* (2019) 115(6):1102–13. doi: 10.1093/cvr/cvy263

80. Ye J, Wang Y, Wang Z, Ji Q, Huang Y, Zeng T, et al. Circulating Th1, Th2, Th9, Th17, Th22, and treg levels in aortic dissection patients. *Mediators Inflammation* (2018) 2018:5697149. doi: 10.1155/2018/5697149

81. Ye J, Wang Y, Wang Z, Lin Y, Liu L, Zhou Q, et al. Circulating IL-37 levels are elevated in patients with hypertension. *Exp Ther Med* (2021) 21(6):558. doi: 10.3892/etm.2021.9990

82. Ye J, Wang Y, Wang Z, Liu L, Yang Z, Wang M, et al. The expression of IL-12 family members in patients with hypertension and its association with the occurrence of carotid atherosclerosis. *Mediators Inflammation* (2020) 2020:2369279. doi: 10.1155/2020/2369279

83. Ye J, Ji Q, Liu J, Liu L, Huang Y, Shi Y, et al. Interleukin 22 promotes blood pressure elevation and endothelial dysfunction in angiotensin II-treated mice. *J Am Heart Assoc* (2017) 6(10): e005875. doi: 10.1161/JAHA.117.005875

84. Kirabo A, Fontana V, Faria AP de, Loperena R, Galindo CL, Wu J, et al. DC Isoketal-modified proteins activate T cells and promote hypertension. *J Clin Invest* (2014) 124(10):4642–56. doi: 10.1172/JCI74084

85. Itani HA, McMaster WGJr., Saleh MA, Nazarewicz RR, Mikolajczyk TP, Kaszuba AM, et al. Activation of human T cells in hypertension: Studies of humanized mice and hypertensive humans. *Hypertension* (2016) 68(1):123–32. doi: 10.1161/HYPERTENSIONAHA.116.07237

86. Saleh MA, Norlander AE, Madhur MS. Inhibition of interleukin 17-a but not interleukin-17F signaling lowers blood pressure and reduces end-organ inflammation in angiotensin II-induced hypertension. *JACC Basic Transl Sci* (2016) 1(7):606–16. doi: 10.1016/j.jacbts.2016.07.009

87. Madhur MS, Lob HE, McCann LA, Iwakura Y, Blinder Y, Guzik TJ, et al. Interleukin 17 promotes angiotensin II-induced hypertension and vascular dysfunction. *Hypertension* (2010) 55(2):500–7. doi: 10.1161/HYPERTENSIONAHA.109.145094

88. Li Y, Wu Y, Zhang C, Li P, Cui W, Hao J, et al. γδT cell-derived interleukin-17A *via* an interleukin-1β-dependent mechanism mediates cardiac injury and fibrosis in hypertension. *Hypertension* (2014) 64(2):305–14. doi: 10.1161/HYPERTENSIONAHA.113.02604

89. Basting T, Lazartigues E. DOCA-salt hypertension: an update. *Curr Hypertens Rep* (2017) 19(4):32. doi: 10.1007/s11906-017-0731-4

90. Amador CA, Barrientos V, Peña J, Herrada AA, González M, Valdés S, et al. Spironolactone decreases DOCA-salt-induced organ damage by blocking the activation of T helper 17 and the downregulation of regulatory T lymphocytes. *Hypertension* (2014) 63(4):797–803. doi: 10.1161/HYPERTENSIONAHA.113.02883

91. Rezaee M, Penta K, Quertermous T. Del1 mediates VSMC adhesion, migration, and proliferation through interaction with integrin alpha(v)beta(3). *Am J Physiol Heart Circ Physiol* (2002) 282(5):H1924–32. doi: 10.1152/ajpheart.00921.2001

92. Barhoumi T, Fraulob-Aquino JC, Mian MOR, Ouerd S, Idris-Khodja N, Huo KG, et al. Matrix metalloproteinase-2 knockout prevents angiotensin II-induced vascular injury. *Cardiovasc Res* (2017) 113(14):1753–62. doi: 10.1093/cvr/cvx115

93. Diaz-Canestro C, Puspitasari YM, Liberale L, Guzik TJ, Flammer AJ, Bonetti NR, et al. MMP-2 knockdown blunts age-dependent carotid stiffness by decreasing elastin degradation and augmenting eNOS activation. *Cardiovasc Res* (2021) 118 (10):2385–96. doi: 10.1093/cvr/cvab300.

94. Liu P, Sun M, Sader S. Matrix metalloproteinases in cardiovascular disease. *Can J Cardiol* (2006) 22 Suppl B(Suppl B):25b–30b. doi: 10.1016/s0828-282x(06)70983-7

95. Nakamura M, Sadoshima J. Mechanisms of physiological and pathological cardiac hypertrophy. *Nat Rev Cardiol* (2018) 15(7):387–407. doi: 10.1038/s41569-018-0007-y

96. Bernardo BC, Weeks KL, Pretorius L, McMullen JR. Molecular distinction between physiological and pathological cardiac hypertrophy: experimental findings and therapeutic strategies. *Pharmacol Ther* (2010) 128(1):191–227. doi: 10.1016/j.pharmthera.2010.04.005

97. Shimizu I, Minamino T. Physiological and pathological cardiac hypertrophy. *J Mol Cell Cardiol* (2016) 97:245–62. doi: 10.1016/j.yjmcc.2016.06.001

98. Wang M, Zhao M, Yu J, Xu Y, Zhang J, Liu J, et al. MCC950, a selective NLRP3 inhibitor, attenuates adverse cardiac remodeling following heart failure through improving the cardiometabolic dysfunction in obese mice. *Front Cardiovasc Med* (2022) 9:727474. doi: 10.3389/fcvm.2022.727474

99. Wang Z, Xu Y, Wang M, Ye J, Liu J, Jiang H, et al. TRPA1 inhibition ameliorates pressure overload-induced cardiac hypertrophy and fibrosis in mice. *EBioMedicine* (2018) 36:54–62. doi: 10.1016/j.ebiom.2018.08.022

100. Ye J, Liu L, Ji Q, Huang Y, Shi Y, Shi L, et al. Anti-Interleukin-22-Neutralizing antibody attenuates angiotensin II-induced cardiac hypertrophy in mice. *Mediators Inflammation* (2017) 2017:5635929. doi: 10.1155/2017/5635929

101. Wang Z, Ye D, Ye J, Wang M, Liu J, Jiang H, et al. The TRPA1 channel in the cardiovascular system: Promising features and challenges. *Front Pharmacol* (2019) 10:1253. doi: 10.3389/fphar.2019.01253

102. Pinto AR, Ilinykh A, Ivey MJ, Kuwabara JT, D'Antoni ML, Debuque R, et al. Revisiting cardiac cellular composition. *Circ Res* (2016) 118(3):400–9. doi: 10.1161/CIRCRESAHA.115.307778

103. Vliegen HW, van der Laarse A, Cornelisse CJ, Eulderink F. Myocardial changes in pressure overload-induced left ventricular hypertrophy. a study on tissue composition, polyploidization and multinucleation. *Eur Heart J* (1991) 12 (4):488–94. doi: 10.1093/oxfordjournals.eurheartj.a059928

104. Kim DY, Lee SH, Fu Y, Jing F, Kim WY, Hong SB, et al. Del-1, an endogenous inhibitor of TGF-β activation, attenuates fibrosis. *Front Immunol* (2020) 11:68. doi: 10.3389/fimmu.2020.00068

105. Heusch G. Molecular basis of cardioprotection: signal transduction in ischemic pre-, post-, and remote conditioning. *Circ Res* (2015) 116(4):674–99. doi: 10.1161/CIRCRESAHA.116.305348

106. Moran AE, Forouzanfar MH, Roth GA, Mensah GA, Ezzati M, Flaxman A, et al. The global burden of ischemic heart disease in 1990 and 2010: the global burden of disease 2010 study. *Circulation* (2014) 129(14):1493–501. doi: 10.1161/CIRCULATIONAHA.113.004046

107. Kown MH, Suzuki T, Koransky ML, Penta K, Sakamoto G, Jahncke CL, et al. Comparison of developmental endothelial locus-1 angiogenic factor with vascular endothelial growth factor in a porcine model of cardiac ischemia. *Ann Thorac Surg* (2003) 76(4):1246–51. doi: 10.1016/S0003-4975(03)00721-5

108. Nahrendorf M, Swirski FK, Aikawa E, Stangenberg L, Wurdinger T, Figueiredo JL, et al. The healing myocardium sequentially mobilizes two monocyte subsets with divergent and complementary functions. *J Exp Med* (2007) 204(12):3037–47. doi: 10.1084/jem.20070885

109. Frangogiannis NG. The inflammatory response in myocardial injury, repair, and remodelling. *Nat Rev Cardiol* (2014) 11(5):255–65. doi: 10.1038/nrcardio.2014.28

110. Frodermann V, Nahrendorf M. Neutrophil-macrophage cross-talk in acute myocardial infarction. *Eur Heart J* (2017) 38(3):198–200. doi: 10.1093/eurheartj/ehw085

111. Frangogiannis NG. Regulation of the inflammatory response in cardiac repair. *Circ Res* (2012) 110(1):159–73. doi: 10.1161/CIRCRESAHA.111.243162

112. Wang H, Li X, Kajikawa T, Shin J, Lim JH, Kourtzelis I, et al. Stromal cell-derived DEL-1 inhibits tfh cell activation and inflammatory arthritis. *J Clin Invest* (2021) 131(19): e150578. doi: 10.1172/JCI150578

113. Li X, Colamatteo A, Kalafati L, Kajikawa T, Wang H, Lim JH, et al. The DEL-1/β3 integrin axis promotes regulatory T cell responses during inflammation resolution. *J Clin Invest* (2020) 130(12):6261–77. doi: 10.1172/JCI137530

114. Deban L, Russo RC, Sironi M, Moalli F, Scanziani M, Zambelli V, et al. Regulation of leukocyte recruitment by the long pentraxin PTX3. *Nat Immunol* (2010) 11(4):328–34. doi: 10.1038/ni.1854

115. Salio M, Chimenti S, De Angelis N, Molla F, Maina V, Nebuloni M, et al. Cardioprotective function of the long pentraxin PTX3 in acute myocardial infarction. *Circulation* (2008) 117(8):1055–64. doi: 10.1161/CIRCULATIONAHA.107.749234

116. Kempf T, Zarbock A, Widera C, Butz S, Stadtmann A, Rossaint J, et al. GDF-15 is an inhibitor of leukocyte integrin activation required for survival after myocardial infarction in mice. *Nat Med* (2011) 17(5):581–8. doi: 10.1038/nm.2354

117. Li R, Zeng J, Ren T. Expression of DEL-1 in alveolar epithelial cells prevents lipopolysaccharide-induced inflammation, oxidative stress, and eosinophil recruitment in acute lung injury. *Int Immunopharmacol* (2022) 110:108961. doi: 10.1016/j.intimp.2022.108961

118. Fan Y, Zhu W, Yang M, Zhu Y, Shen F, Hao Q, et al. Del-1 gene transfer induces cerebral angiogenesis in mice. *Brain Res* (2008) 1219:1–7. doi: 10.1016/j.brainres.2008.05.003

119. Ciucurel EC, Vlahos AE, Sefton MV. Using del-1 to tip the angiogenic balance in endothelial cells in modular constructs. *Tissue Eng Part A* (2014) 20(7-8):1222–34. doi: 10.1089/ten.tea.2013.0241

120. Penta K, Varner JA, Liaw L, Hidai C, Schatzman R, Quertermous T. Del1 induces integrin signaling and angiogenesis by ligation of alphaVbeta3. *J Biol Chem* (1999) 274(16):11101–9. doi: 10.1074/jbc.274.16.11101

121. Aoka Y, Johnson FL, Penta K, Hirata Ki K, Hidai C, Schatzman R, et al. The embryonic angiogenic factor Del1 accelerates tumor growth by enhancing vascular formation. *Microvasc Res* (2002) 64(1):148–61. doi: 10.1006/mvre.2002.2414

122. Ho HK, Jang JJ, Kaji S, Spektor G, Fong A, Yang P, et al. Developmental endothelial locus-1 (Del-1), a novel angiogenic protein: its role in ischemia. *Circulation* (2004) 109(10):1314–9. doi: 10.1161/01.CIR.0000118465.36018.2D

123. Grossman PM, Mendelsohn F, Henry TD, Hermiller JB, Litt M, Saucedo JF, et al. Results from a phase II multicenter, double-blind placebo-controlled study of del-1 (VLTS-589) for intermittent claudication in subjects with peripheral arterial disease. *Am Heart J* (2007) 153(5):874–80. doi: 10.1016/j.ahj.2007.01.038

124. Ciucurel EC, Sefton MV. Del-1 overexpression in endothelial cells increases vascular density in tissue-engineered implants containing endothelial cells and adipose-derived mesenchymal stromal cells. *Tissue Eng Part A* (2014) 20 (7-8):1235–52. doi: 10.1089/ten.tea.2013.0242

125. Klotzsche-von Ameln A, Cremer S, Hoffmann J, Schuster P, Khedr S, Korovina I, et al. Endogenous developmental endothelial locus-1 limits ischaemia-related angiogenesis by blocking inflammation. *Thromb Haemost* (2017) 117 (6):1150–63. doi: 10.1160/TH16-05-0354

126. Jeong D, Ban S, Oh S, Jin Lee S, Yong Park S, Koh YW. Prognostic significance of EDIL3 expression and correlation with mesenchymal phenotype and microvessel density in lung adenocarcinoma. *Sci Rep* (2017) 7(1):8649. doi: 10.1038/s41598-017-08851-9

127. Shen W, Zhu S, Qin H, Zhong M, Wu J, Zhang R, et al. EDIL3 knockdown inhibits retinal angiogenesis through the induction of cell cycle arrest in vitro. *Mol Med Rep* (2017) 16(4):4054–60. doi: 10.3892/mmr.2017.7122

128. Niu X, Han Q, Liu Y, Li J, Hou R, Li J, et al. Psoriasis-associated angiogenesis is mediated by EDIL3. *Microvasc Res* (2020) 132:104056. doi: 10.1016/j.mvr.2020.104056

129. Kitano H, Mamiya A, Ishikawa T, Fujiwara Y, Masaoka Y, Miki T, et al. An epidermal growth factor motif of developmental endothelial locus 1 protein inhibits efficient angiogenesis in explanted squamous cell carcinoma *In vivo*. *Rev Invest Clin* (2020) 73(1):039–51. doi: 10.24875/ric.20000375

130. Kalani A, Kamat PK, Kalani K, Tyagi N. Epigenetic impact of curcumin on stroke prevention. *Metab Brain Dis* (2015) 30(2):427–35. doi: 10.1007/s11011-014-9537-0

131. Cramer SC, Nelles G, Benson RR, Kaplan JD, Parker RA, Kwong KK, et al. A functional MRI study of subjects recovered from hemiparetic stroke. *Stroke* (1997) 28(12):2518–27. doi: 10.1161/01.STR.28.12.2518

132. Altar CA, Laeng P, Jurata LW, Brockman JA, Lemire A, Bullard J, et al. Electroconvulsive seizures regulate gene expression of distinct neurotrophic signaling pathways. *J Neurosci* (2004) 24(11):2667–77. doi: 10.1523/JNEUROSCI.5377-03.2004

133. Newton SS, Collier EF, Hunsberger J, Adams D, Terwilliger R, Selvanayagam E, et al. Gene profile of electroconvulsive seizures: induction of neurotrophic and angiogenic factors. *J Neurosci* (2003) 23(34):10841–51. doi: 10.1523/JNEUROSCI.23-34-10841.2003

134. Newton SS, Girgenti MJ, Collier EF, Duman RS. Electroconvulsive seizure increases adult hippocampal angiogenesis in rats. *Eur J Neurosci* (2006) 24(3):819–28. doi: 10.1111/j.1460-9568.2006.04958.x

135. Zhou B, Lu Y, Hajifathalian K, Bentham J, Cesare M, Danaei G, et al. Worldwide trends in diabetes since 1980: a pooled analysis of 751 population-based studies with 4.4 million participants. *Lancet* (2016) 387(10027):1513–30. doi: 10.1016/S0140-6736(16)00618-8

136. Stöhr R, Federici M. Insulin resistance and atherosclerosis: convergence between metabolic pathways and inflammatory nodes. *Biochem J* (2013) 454(1):1–11. doi: 10.1042/bj20130121

137. Rohm TV, Meier DT, Olefsky JM, Donath MY. Inflammation in obesity, diabetes, and related disorders. *Immunity* (2022) 55(1):31–55. doi: 10.1016/j.immuni.2021.12.013

138. Stefani L, Galanti G. Physical exercise prescription in metabolic chronic disease. *Adv Exp Med Biol* (2017) 1005:123–41. doi: 10.1007/978-981-10-5717-5_6

139. Kwon CH, Sun JL, Kim MJ, Abd El-Aty AM, Jeong JH, Jung TW. Clinically confirmed DEL-1 as a myokine attenuates lipid-induced inflammation and insulin resistance in 3T3-L1 adipocytes *via* AMPK/HO-1- pathway. *Adipocyte* (2020) 9 (1):576–86. doi: 10.1080/21623945.2020.1823140

140. Weisberg SP, McCann D, Desai M, Rosenbaum M, Leibel RL, Ferrante AWJr. Obesity is associated with macrophage accumulation in adipose tissue. *J Clin Invest* (2003) 112(12):1796–808. doi: 10.1172/JCI200319246

141. Cobb LP, Siamakpour-Reihani S, Zhang D, Qin X, Owzar K, Zhou C, et al. Obesity and altered angiogenic-related gene expression in endometrial cancer. *Gynecol Oncol* (2021) 163(2):320–6. doi: 10.1016/j.ygyno.2021.08.010

142. Kim WY, Lee SH, Kim DY, Ryu HJ, Chon GR, Park YY, et al. Serum developmental endothelial locus-1 is associated with severity of sepsis in animals and humans. *Sci Rep* (2019) 9(1):13005. doi: 10.1038/s41598-019-49564-5

143. Christoforakis Z, Dermitzaki E, Paflioti E, Katrinaki M, Deiktakis M, Tosounidis HT, et al. Correlation of systemic metabolic inflammation with knee osteoarthritis. *Hormones (Athens)* (2022) 21(3):457–66. doi: 10.1007/s42000-022-00381-y

frontiers | Frontiers in Immunology

TYPE Original Research
PUBLISHED 01 December 2022
DOI 10.3389/fimmu.2022.1042849

OPEN ACCESS

EDITED BY
Uzma Saqib,
Indian Institute of Technology Indore, India

REVIEWED BY
Ying Wang,
University of California, Davis, United States
Sylwia Dominika Tyrkalska,
University of Murcia, Spain

*CORRESPONDENCE
Peizeng Yang
peizengycmu@126.com

SPECIALTY SECTION
This article was submitted to Inflammation, a section of the journal Frontiers in Immunology

RECEIVED 13 September 2022
ACCEPTED 18 November 2022
PUBLISHED 01 December 2022

CITATION
Xiao X, Liu Z, Su G, Liu H, Yin W, Guan Y, Jing S, Du L, Li F, Li N and Yang P (2022) A novel uveitis model induced by lipopolysaccharide in zebrafish. *Front. Immunol.* 13:1042849. doi: 10.3389/fimmu.2022.1042849

A novel uveitis model induced by lipopolysaccharide in zebrafish

Xiao Xiao[1], Zhangluxi Liu[2], Guannan Su[2], Huan Liu[1], Wenhui Yin[1], Yuxuan Guan[1], Shixiang Jing[1], Liping Du[1], Fuzhen Li[1], Na Li[1] and Peizeng Yang[1,2]*

[1]Henan International Joint Research Laboratory for Ocular Immunology and Retinal Injury Repair, Henan Province Eye Hospital, The First Affiliated Hospital of Zhengzhou University, Zhengzhou, China, [2]The First Affiliated Hospital of Chongqing Medical University, Chongqing Key Laboratory of Ophthalmology and Chongqing Eye Institute, Chongqing Branch (Municipality Division) of National Clinical Research Center for Ocular Diseases, Chongqing, China

Objective: Endotoxin-induced uveitis (EIU) is an important tool for human uveitis study. This study was designed to develop a novel EIU model in zebrafish.

Methods: An EIU model in zebrafish was induced by intravitreal lipopolysaccharide (LPS) injection and was assessed dynamically. Optical coherence tomography (OCT) was used to assess infiltrating cells in the vitreous body. The histological changes wereevaluated using HE staining and immune cells were measured by immunofluorescence. The retinal RNA Sequencing (RNA-Seq) was used to explore the transcriptional changes during inflammation. RNA-Seq data were analyzed using time-course sequencing data analysis (TCseq), ClueGO plugin in Cytoscape, and Gene Set Enrichment Analysis (GSEA) software. Flow cytometry and retinal flat mounts were used to dynamically quantify the immune cells.

Results: EIU was successfully induced in zebrafish following intravitreal LPS injection. Inflammation appeared at 4 hours post injection (hpi), reached its peak at 24 hpi, and then resolved at 72 hpi. Immunofluorescence confirmed that massive influx ofneutrophils into the iris and vitreous body, and activation of microglia as evidenced by ameboid-shaped appearance in the retina. Retinal RNA-seq during the EIU course identified four gene clusters with distinct expression characteristics related to Toll-likereceptor signaling pathway, cytokine-cytokine receptor interaction, NOD-like receptor signaling pathway, and extracellular matrix (ECM)-receptor interaction, respectively. Prednisone immersion inhibited the inflammatory response of EIU in zebrafish, whichwas confirmed by decreased neutrophils detected in flow cytometry and retinal flat mounts.

Conclusions: We developed a novel EIU model in zebrafish, which may be particularly useful for gene-editing and high-throughput screening of new drugs for the prevention and treatment of uveitis.

KEYWORDS

uveitis, zebrafish, inflammation, innate immunity, disease model

Introduction

Uveitis is one of the primary causes of visual impairment globally, accounting for 10-15% of all blindness cases in the world (1–3). Despite numerous studies conducted during the last decade, the underlying mechanisms of this disease have not yet been completely explained (4–6). Uveitis models have been successfully induced in rodents using uveitogenic antigens or LPS, which profoundly renewed our understanding about this disease (7, 8). EIU is a widely used model to simulate acute anterior uveitis (AAU), particularly human leukocyte antigen (HLA) B27 associated AAU (8–10). It has been used for the studies of pathological changes, immunological and genetic pathogenesis of uveitis (11, 12). However, the extensively used methods to study the molecular pathogenesis in mouse models, such as gene-editing, are somewhat expensive and time-consuming, and conventional methods for assessing inflammation are relatively single-dimensioned. Therefore, a superior uveitis model for multiple-dimensional study is urgently needed.

Zebrafish has become a favorable model for disease studies since it is a model organism with highly conserved genomes. In the context of immunity, zebrafish larvae develop innate immune cells within two days after fertilization, and adaptive immune system forms at approximately 3 weeks post fertilization (13, 14). Although the immune systems are relatively conserved across species, there are some differences between the mammals and zebrafish. Zebrafish is less susceptible to LPS, possibly due to the inability of the extracellular portions of zebrafish tlr4a and tlr4b to recognize LPS (15, 16). Still, it has the advantages of small body size, rapid life cycle, transparency, and simple breeding and genetic editing (17, 18). For example, in terms of gene-editing, the variant Ripk2^{Asn104Asp} in zebrafish augmented the innate immune response and NF-κB pathway in early-onset osteoarthritis by CRISPR technique (19). Pharmacologically, the morphology and locomotor behavior of zebrafish could facilitate the study on effectiveness and side-effects of medicines (20, 21).

Endotoxemia model in zebrafish has previously been described (22). However, a uveitis model in zebrafish has not been induced so far. Here, for the first time, we developed a model of EIU in zebrafish, which could be potentially applied for gene-editing and screening of novel drugs for uveitis.

Materials and methods

Animals

Zebrafish (Danio rerio) were bred and kept under conventional conditions (27.5°C, 14/10 hours of light/dark cycle, and brine shrimp twice daily feedings). The 6-month-old adult male zebrafish were used in this study. The following transgenic lines were used: (a) wild-type fish of the AB strain; (b) Tg(Mpx:GFP) zebrafish with Green fluorescent protein (GFP) expression by neutrophils; (c) Tg(coro1a:GFP;lyz:dsRed), in which microglia/macrophages express GFP only and neutrophils express both GFP and dsRed. We bought zebrafish lines from the China Zebrafish Resource Center (CZRC, China). Zebrafish experiments were approved by the Medical Ethics Committee of the First Affiliated Hospital of Zhengzhou University.

Induction of EIU

Zebrafish were anesthetized by immersion in 0.1% buffered tricaine for 5 minutes. A microinjector (PLI-100A, WARNER INSTRUMENT, USA) was inserted at the iris limbal, and 0.2μL of 0.65% saline containing 0.2mg/ml, 0.5mg/ml or 1.0mg/ml LPS (O55:B5, L6529, Sigma Aldrich, USA) were injected into the left vitreous body of the zebrafish. The corresponding dosages calculated according to the animal's body weight (0.5g/zebrafish) were 0.08μg/g, 0.2μg/g, and 0.4μg/g respectively. The opposite eye receiving an equal volume of 0.65% saline served as control. After resting for 20 seconds, zebrafish were returned into tanks with clean system water.

In vivo imaging

Following anesthesia, OCT imaging was obtained by a Micron IV retinal imaging microscope (Phoenix Research Laboratories, Pleasanton, CA) at 0 hpi (Blank control), 4 hpi, 12 hpi, 24 hpi, and 72 hpi of LPS. The parameters were set according to the manufacturer's protocol, and a full-length line scan was performed horizontally and vertically while the optic disc was focused.

H&E staining

At 0 hpi, 4 hpi, 12 hpi, 24 hpi, 72 hpi, 5 days post injection (dpi) and 7dpi of LPS, zebrafish were anesthetized in 0.1% buffered tricaine, and whole eyes were enucleated using fine forceps. The eyes were then fixed overnight in 4% PFA (Sigma-Aldrich, USA). Slide preparation was carried out in the manner previously described (23). The slides were then stained by hematoxylin-eosin for histological analysis. Stained slides were viewed at low magnification (×20) using a Leica DM4 microscope (Leica GmbH, Germany). The numbers of infiltrating cells in the anterior chamber and vitreous cavity were collected from six slides, and quantified using ImageJ software.

Immunofluorescence and quantification of inflammatory cells

At 0 hpi (Blank control), 4 hpi, 12 hpi, 24 hpi, and 72 hpi of LPS, zebrafish were anesthetized in 0.1% buffered tricaine. Cryosection was carried out in the manner previously described (23–25). Cryosections were blocked in 20% goat serum at 26°C for 30 min before being incubated with primary antibody (rabbit anti-zebrafish L-plastin (1:500, Genetex, USA), which is a leukocyte-specific form of the actin binding protein, and rabbit anti-zebrafish Mpx (1:200, Genetex, USA), which is specific for neutrophil). After washing in PBST for 30 min, the cryosections were incubated in secondary antibody Alexa-Fluor 488 (Jackson ImmunoResearch, USA) and Alexa-Fluor 594 (Jackson ImmunoResearch, USA) for 1 h, and washed in PBST for at least 30 min, then incubated in DAPI (1:1000, Sigma-Aldrich, USA), and finally covered with a cover ship. Stained slides were viewed at low magnification (×20) using a Zeiss LSM 980 confocal microscope (Carl Zeiss Meditec, Jena, Germany). The numbers of fluorescence positive cells were collected from 4 randomly selected fields, and quantified using ImageJ software.

Visualization and analysis of microglia in the retina

Tg(coro1a:GFP;lyz:dsRed) zebrafish were used for visualization of microglia and neutrophils. At 0 hpi (Blank control), 4 hpi, 12 hpi and 24 hpi of LPS, zebrafish were anesthetized in 0.1% buffered tricaine. The eyes were removed and fixed for 1 hour in 4% PFA. After cornea, lens and sclera were removed, the retina was stripped from the choroid and cut four times into four equal quadrants from the edge toward the center. The retina around the optic disc (×20 or ×63 oil objective) was scanned using a Zeiss LSM 980 confocal microscope (Carl Zeiss Meditec, Jena, Germany) with z stacks. The GFP+/dsRed- cells indicate resting microglia in blank control, which show small somas with thin and ramified cells processes. After LPS injection, GFP+/dsRed- microglia morphology changed from ramified to ameboid-shape. Outlines of individual GFP+/dsRed- cells were manually traced and measurement of morphological feature was analyzed using the "NeuronJ" tool in imageJ software.

RNA-Seq and data analysis

Retinal RNA was extracted from zebrafish at 0 hpi (Blank control), 4 hpi, 12 hpi, 24 hpi and 72 hpi of LPS, and at the aforementioned time points after saline injection. The enriched mRNA was fragmented into short fragments and reverse-transcribed into cDNA with random primers. The QiaQuick PCR extraction kit (Qiagen, Venlo, The Netherlands) was used to purify cDNA fragments, which were then end repaired, poly (A) added, and ligated to Illumina sequencing adapters. Sequencing was performed on Illumina HiSeq2500 by Gene Denovo Biotechnology Co. (Guangzhou, China).

Differentially expressed genes (DEGs, false discovery rate (FDR) ≤ 0.05 and $|\log2(\text{fold-change})| \geq 1$) were determined using limma package (version 3.48.3). TCseq (v1.16.0) in the R package was used to conduct the time-course clustering analysis of DEGs. The functional enrichment analysis was performed by Cytoscape plugin ClueGO. To image the functional correlation between paths and genes, a kappa coefficient was calculated, based on gene overlap between paths or GO terms. The kappa threshold was 0.38 by default. The same color indicated functionally similar entries. The threshold for enrichment significance was $P < 0.05$. Global mRNA expression profiles were subject to GSEA using GSEA software (http://www.gsea-msigdb.org/gsea/index.jsp). KEGG reference gene sets were downloaded from the KEGG database. The 1000 phenotype permutations were utilized in the enrichment analysis, and gene sets with nominal $P < 0.05$ and FDR < 0.25 were considered significant.

Quantitative real-time PCR

Retinal RNA of zebrafish at 0 hpi (Blank control), 4 hpi, 24 hpi and 72 hpi of LPS were extracted using TRIzol (Invitrogen, Carlsbad, CA, USA). The cDNA was generated using EasyScript® One-Step gDNA Removal and cDNA Synthesis SuperMix (Transgen, China). The QuantStudioTM3 Real-Time PCR Instrument (Thermo Fisher Scientific, USA) was used for PCR. Primers used are listed in Supplementary Table S1.

Drug treatment

Zebrafish were immersed in 50μm prednisone (T8396, Topscience, China) immediately after LPS injection

(prednisone-treated group), or immersed in 0.1% DMSO alone (vehicle-treated control).

Sample preparation and flow cytometry

At 24 hpi of LPS, four retinas at each group were dissociated using 1 ml papain vial (Papain Dissociation System Kit, Worthington, USA) at 37°C for 30 min. The digestion was terminated using 3 ml washing buffer (5 ml fetal bovine serum (Gibco, USA) into 95 ml PBS). The single-cell suspension was filtered using a 40μm cell strainer (BD Falcon, USA). Flow cytometry was performed on FACS Celesta (BD Biosciences, USA). Acquired data were analyzed using Flow Jo version 10.1.

Imaging of retinal flat mounts and quantification of fluorescent area

At 24 hpi of LPS, the Tg(Mpx:GFP) zebrafish were anesthetized in 0.1% buffered tricaine, followed by enucleating eyes. After cornea, lens and sclera were removed, the retina was stripped from the choroid and cut four times into four equal quadrants from the edge toward the center. The retina around the optic disc (×10) was scanned using a Zeiss LSM 980 confocal microscope with z series (Carl Zeiss Meditec, Jena, Germany). Percentages of the relative GFP-positive area were quantified using ImageJ software.

Statistical analysis

GraphPad Prism 8 software (GraphPad Software Inc., San Diego, CA) was used to analyze the data. Normal distribution and equality of variance of groups were examined. For normal distributions, to analyze the difference between two groups, the independent t-test was used. To compare multiple groups, the One-way ANOVA was employed, followed by Dunnett's multiple comparison test. If values did not pass the normality test, the Kruskal-Wallis test was used to compare among groups. Quantitative data are presented as mean ± SD, $P < 0.05$ was considered statistically significant.

Results

Histological and OCT imaging changes of EIU in zebrafish

Intravitreal LPS injection was performed at doses of 0.08, 0.2, and 0.4μg/g in zebrafish. There was no histological change in zebrafish receiving 0.08 or 0.2μg/g LPS, and those receiving intravitreal saline injection at 24 hpi (Figure S1). In 0.4μg/g LPS group, a mild inflammation as evidenced by sporadic infiltrating cells around iris was observed at 4 hpi. An obvious inflammation was then evidenced histologically by immune cells infiltrated the vitreous body and iris at 12 hpi, and this intraocular inflammation reached its peak at 24 hpi, showing massive influx of infiltrating cells and dilatation of iris vessels. At 72 hpi, the inflammation was alleviated and disappeared, but iris vascular dilatation still remained. The iris vascular dilatation gradually regressed at 5 and 7 dpi, leaving no signs of maladaptive structural remodeling (Figure S2). Overall, the highest number of cells infiltrating the anterior and posterior segments were seen at 24 hpi (Figure 1A). Therefore, the dosage of 0.4μg/g LPS was selected for further research. Consistent with histological observation, OCT imaging showed no obvious change in the eyes at 4 hpi of LPS compared to blank control. A large number of highly reflex dots in the vitreous body were observed at 12 hpi and followed by tremendous dots at 24 hpi. As expected, there was no highly reflex dot at 72 hpi (Figure 1B).

Immune cell infiltration of EIU in zebrafish

Immunofluorescent staining was performed to assess the influx of immune cells in the iris, vitreous body and retina during EIU process. As control, a small number of ramified L-plastin+/Mpx- cells, indicating retinal microglia, were observed in the retina of normal zebrafish. At 4 hpi, L-plastin+/Mpx+ cells appeared in the iris. The L-plastin+/Mpx- cells displayed shorter and thicker processes. More L-plastin+/Mpx+ cells infiltrated into the iris and vitreous body, accompanied by a small number of L-plastin+/Mpx- cells in and around the iris at 12 hpi. Subsequently, a tremendous influx of L-plastin+/Mpx+ cells infiltrated the vitreous body at 24 hpi, concomitanted with the L-plastin+/Mpx- cell morphology changed from ramified to ameboid-shape. At 72 hpi, the number of L-plastin+/Mpx+ cells almost declined to the normal level, while some L-plastin+/Mpx- cells still remained in the iris (Figures 2A, B). To further display the activation of microglia upon LPS challenging, we used Tg(coro1a:GFP;lyz:dsRed) zebrafish, in which neutrophils (GFP+/dsRed+) appear yellow and microglia/macrophages (GFP+/dsRed-) green. In line with the immunofluorescent staining, the GFP+/dsRed- ramified microglia only presented in the retina at 0 hpi of LPS (Figure S3 A, E). At 4 hpi of LPS, GFP+/dsRed- microglia showed enlarged cell bodies with shorter and thicker processes, accompanied by a small amount of GFP+/dsRed+ neutrophil exudation (Figure S3 B, F, I). At 12 and 24 hpi of LPS, GFP+/dsRed- microglia showed shorter and thicker processes and appeared ameboid in shape (Figure S3 G, H, I), accompanied with a massive infiltration of GFP+/dsRed+ neutrophils around the optic nerve (Figure S3 C, D).

10.3389/fimmu.2022.1042849

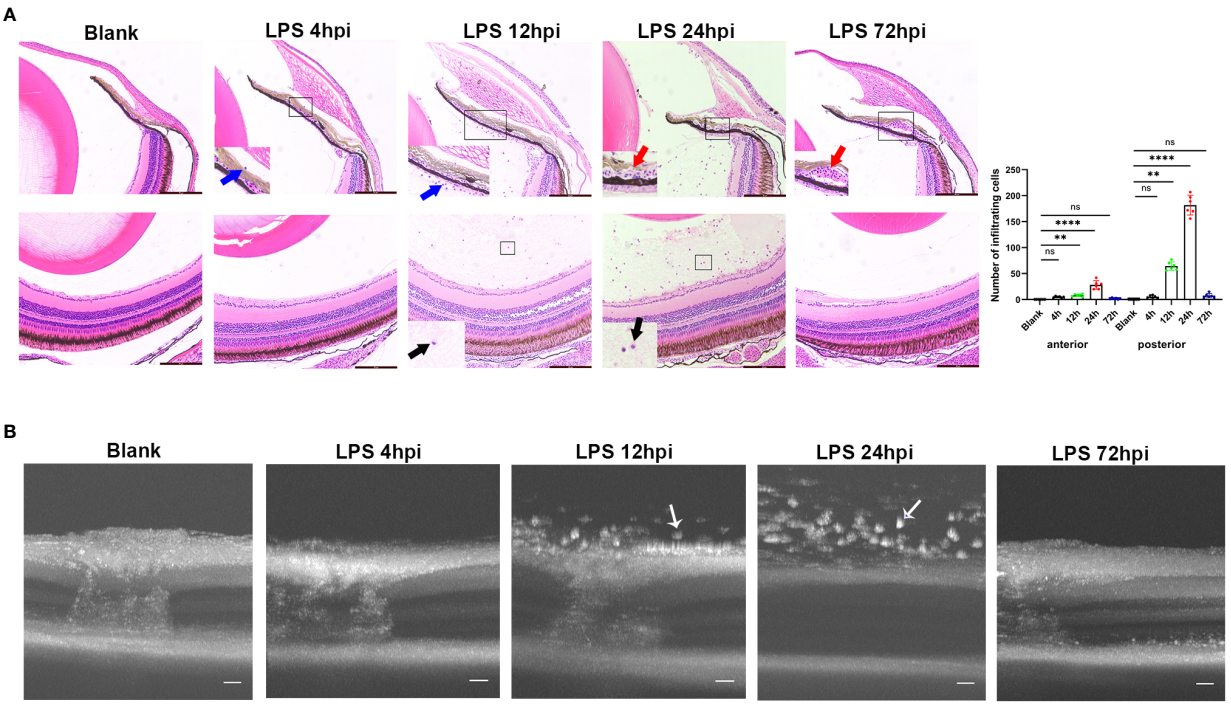

FIGURE 1
Inflammatory sign of EIU in zebrafish over time-course. **(A)** Left, H&E staining of eyes at different time points after LPS injection. Blue arrow, infiltrating cells around iris. Red arrow, vascular dilation. Black arrow, vitreous infiltration. Scale bars = 50μm. Right, quantification of inflammatory cells of anterior and posterior segments (mean ± SD; n = 6 eyes per group; $^{**}P < 0.01$, $^{****}P < 0.0001$, ns, not significant; one-way ANOVA). **(B)** Serial OCT imaging of EIU at various time points after LPS injection. White arrow, highly reflex dots. Scale bars = 20μm. hpi, hours post injection.

Transcriptomic hallmarks of EIU in zebrafish

Systematic RNA-seq experiment was performed to disclose the molecular mechanisms underlying EIU development in zebrafish. Heatmap for the Pearson's correlation coefficient was performed to provide an overview for the relationships among samples. The Pearson's correlations between the intragroup samples were all greater than 0.99, indicating that all intragroup samples were highly correlated (Figure S4). Differential expression level was set to fold change ≥ 2 (either upregulation or downregulation), and FDR should be less than 0.05. A total of 167, 540, 491 and 22 DEGs were observed respectively between LPS-injected and saline-injected groups at 4 hpi, 12 hpi, 24 hpi and 72 hpi (Figure 3A). Hierarchical clustering heatmap of DEGs showed gene expression returned to normal level at 72 hpi (Figure 3B). Time series cluster analysis by TCseq package showed four typical clusters (Figure 3C). Expression level of genes in cluster 1 peaked in 4 hpi, decreased steadily at 12 hpi and 24 hpi, and then declined to baseline at 72 hpi (Figure 3C, Cluster 1). Genes in this profile were strongly associated with Toll-like receptor signaling pathway, RIG-I like receptor signaling pathway, C-type lectin receptor signaling pathway and cytosolic DNA sensing pathway (Figure 3D, Cluster 1). Cluster 2 had a clear expression peak at 12 hpi, which then declined constantly at 24 hpi and 72 hpi (Figure 3C, Cluster 2). Genes in this profile were linked to NOD-like receptor signaling pathway, cytokine-cytokine receptor interaction, phagosome, proteasome, ABC transporters, and herpes simplex virus 1 infection (Figure 3D, Cluster 2). Expression level of genes in cluster 3 increased as the inflammation progressed, peaked at 24 hpi, and then decreased at 72 hpi (Figure 3C, Cluster 3). These genes were enriched in NOD-like receptor signaling pathway, lysosome, cytokine-cytokine receptor interaction, phagosome, C-type lectin receptor signaling pathway (Figure 3D, Cluster 3). Expression level of genes in cluster 4 decreased significantly at 12 hpi, but increased at 24 hpi, and restored to near baseline level at 72 hpi (Figure 3C, Cluster 4). Genes in this cluster were enriched in extracellular matrix (ECM)-receptor interaction, focal adhesion and intestinal immune network (Figure 3D, Cluster 4). We further performed GSEA to get insight into the biological roles of pathways involved in EIU development. The results showed that highly expressed genes were closely

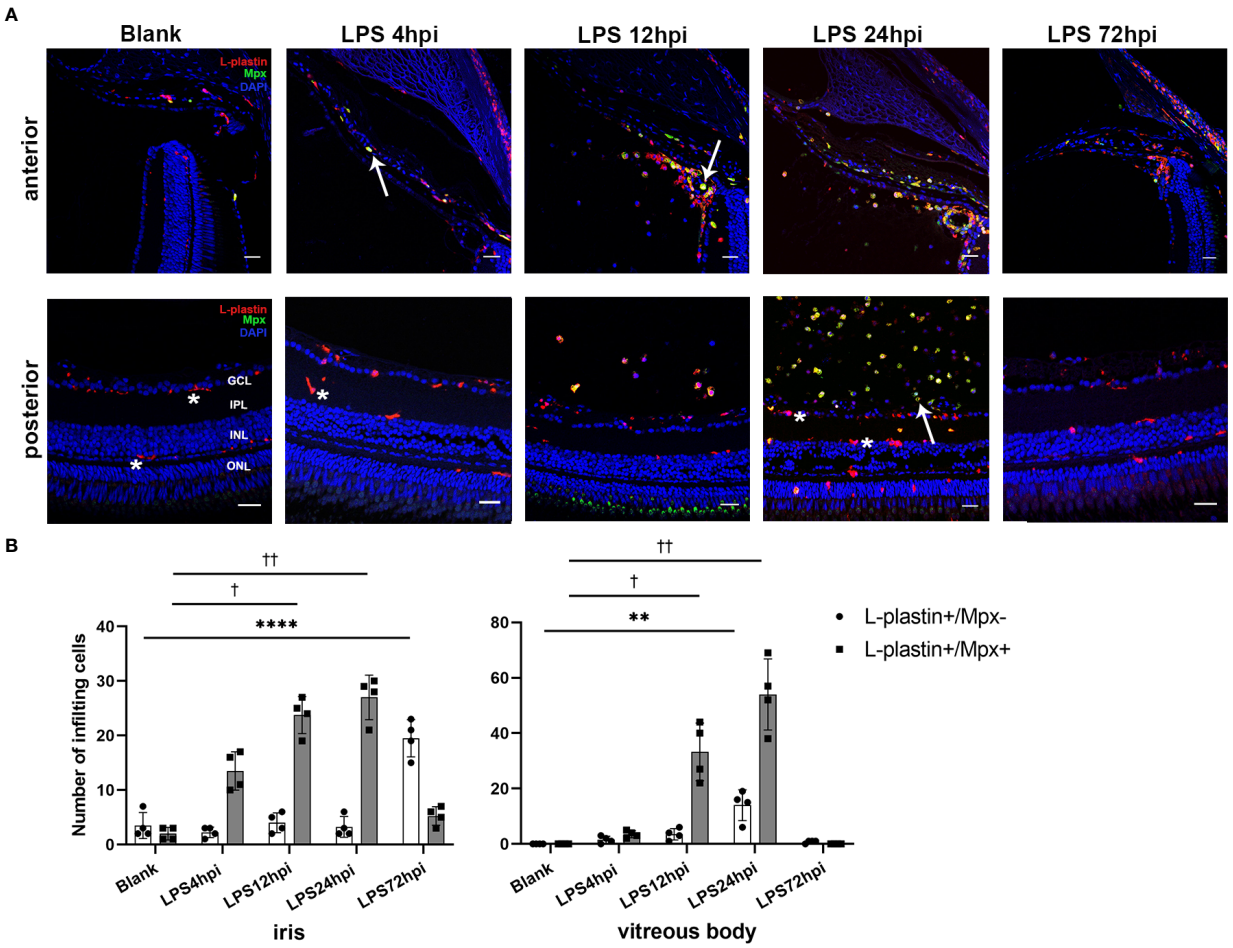

FIGURE 2
Distribution of immune cells during EIU inflammation process in zebrafish. **(A)** L-plastin (magenta), Mpx (green), and DAPI (blue) staining was seen in cryosections at 0 hpi (blank control), 4 hpi, 12 hpi, 24 hpi and 72 hpi of LPS. ONL, outer nuclear layer, INL, inner nuclear layer, IPL, inner plexiform layer, GCL, ganglion cell layer. Asterisk: L-plastin+/Mpx- cell. White arrow: L-plastin+/Mpx+ cell. Scale bar: 20μm. **(B)** Quantification of immune cells in the iris and vitreous body at each time point (mean ± SD; $^{*}P < 0.05$, $^{**}P < 0.01$, $^{****}P < 0.0001$, the number of L-plastin +/Mpx- cells were compared; $^{\dagger}P < 0.05$, $^{\dagger\dagger}P < 0.01$, number of L-plastin+/Mpx+ cells were compared, one-way ANOVA).

associated with innate immune response and NF-κB signaling pathway, whereas the low-expression genes were enriched in the ECM-receptor interaction and phototransduction (Figure S5).

Quantitative RT-PCR validation

To validate the genes from pathways with most significant *P*-values in each cluster, 23 DEGs from RNA-seq were selected for RT-PCR validation, including Toll-like receptors signaling genes (*tlr5a, tlr5b, cxcl8a*, *cd40, il1β* and *il6*) in Cluster 1 (Figure 4), proteasome pathway genes (*psme1*, *psme2*, *psma6l*, *psmb8a* and *psmb9a*) in Cluster 2, lysosome pathway genes (*ctsh*, *ctsba*, *ctsc*, *napsa* and *galns*) in Cluster 3, and ECM-receptor interaction related genes (*itga6b*, *col1a1a*, *col1a2*, *col6a3* and *col9a1b*) in Cluster 4 (Figure S6). As Tlr4 is the receptor of LPS in mammals, we also tested zebrafish *tlr4ba* and *tlr4bb* expressions using RT-PCR, although they were not found in DEGs by RNA-seq. In the Cluster 1, all the six DEGs were upregulated at 4 hpi and then returned to normal level, while *tlr4ba* and *tlr4bb* expression showed no obvious change (Figure 4), consistent with the RNA-seq results (Figure S7). Besides, the expression of *psme1*, *psma6l*, *psmb8a* and *psmb9a* from Cluster 2, *ctsh*, *ctsba* and *napsa* from Cluster 3, and *itga6b*, *col1a1a* and *col1a2* from Cluster 4 showed similar profiles between the high-throughput RNA-seq and RT-PCR data (Figure S6).

Effect of prednisone immersion on EIU in zebrafish

Prednisone immersion was used to evaluate its anti-inflammatory effect on EIU in Tg(Mpx:GFP) transgenic zebrafish

10.3389/fimmu.2022.1042849

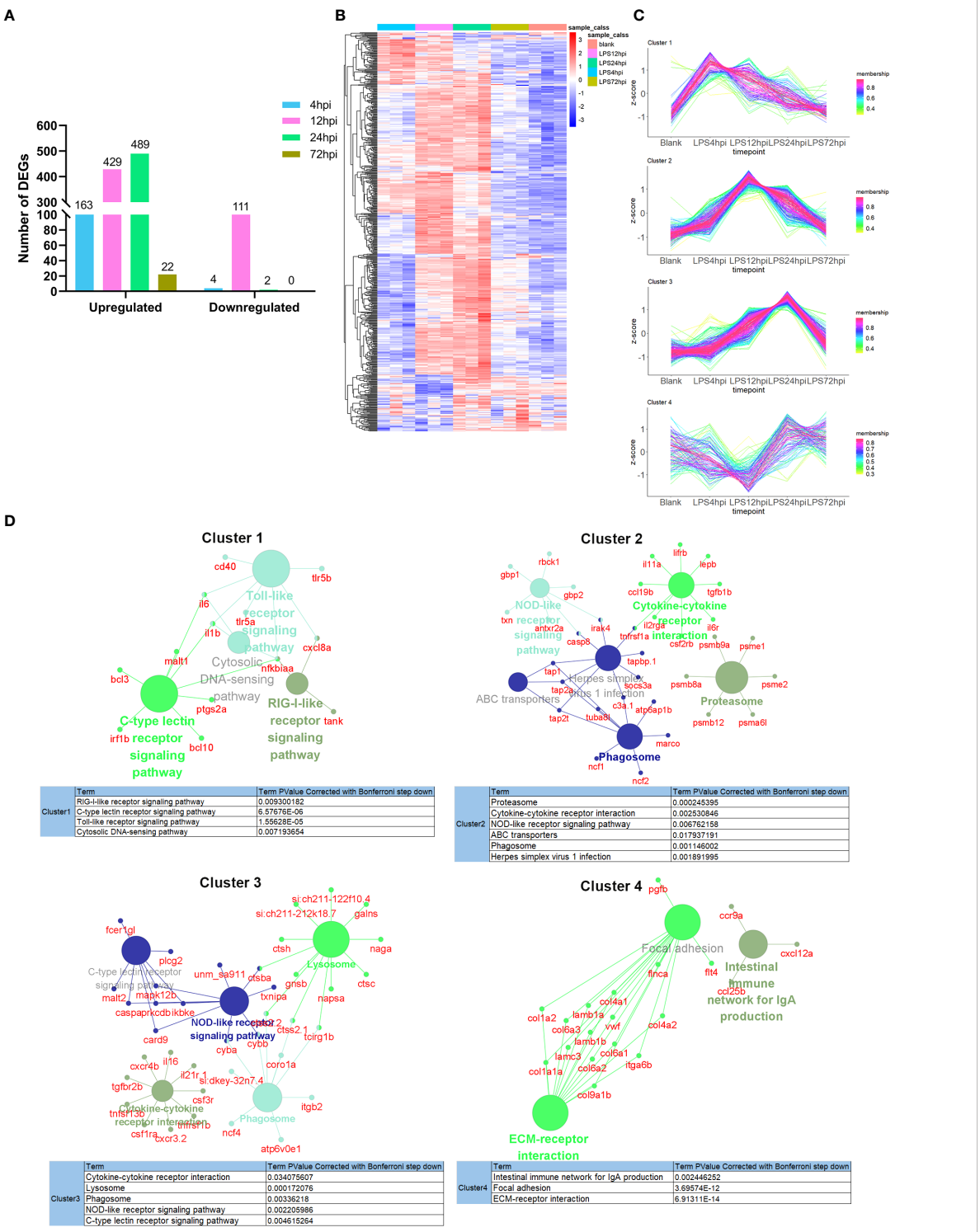

	Term	Term PValue Corrected with Bonferroni step down
Cluster1	RIG-I-like receptor signaling pathway	0.009300182
	C-type lectin receptor signaling pathway	6.57676E-06
	Toll-like receptor signaling pathway	1.55628E-05
	Cytosolic DNA-sensing pathway	0.007193654

	Term	Term PValue Corrected with Bonferroni step down
Cluster2	Proteasome	0.000245395
	Cytokine-cytokine receptor interaction	0.002530846
	NOD-like receptor signaling pathway	0.006762158
	ABC transporters	0.017937191
	Phagosome	0.001146002
	Herpes simplex virus 1 infection	0.001891995

	Term	Term PValue Corrected with Bonferroni step down
Cluster3	Cytokine-cytokine receptor interaction	0.034075607
	Lysosome	0.000172076
	Phagosome	0.00336218
	NOD-like receptor signaling pathway	0.002205986
	C-type lectin receptor signaling pathway	0.004615264

	Term	Term PValue Corrected with Bonferroni step down
Cluster4	Intestinal immune network for IgA production	0.002446252
	Focal adhesion	3.69574E-12
	ECM-receptor interaction	6.91311E-14

FIGURE 3
Transcriptomic traits of EIU in zebrafish. **(A)** Number of DEGs at 4 hpi, 12 hpi, 24 hpi and 72 hpi of LPS and saline. **(B)** Hierarchical clustering heatmap of DEGs at each time point. **(C)** The TCseq package was used to illustrate the patterns of dynamic changes in DEGs during EIU in zebrafish. **(D)** Functional enrichment analysis of DEGs in different clusters. Networks of pathways and genes in Cluster 1, Cluster 2, Cluster 3 and Cluster 4 were conducted by ClueGO and displayed by Cytoscape. Circles shown in the same color represent similar enrichment results.

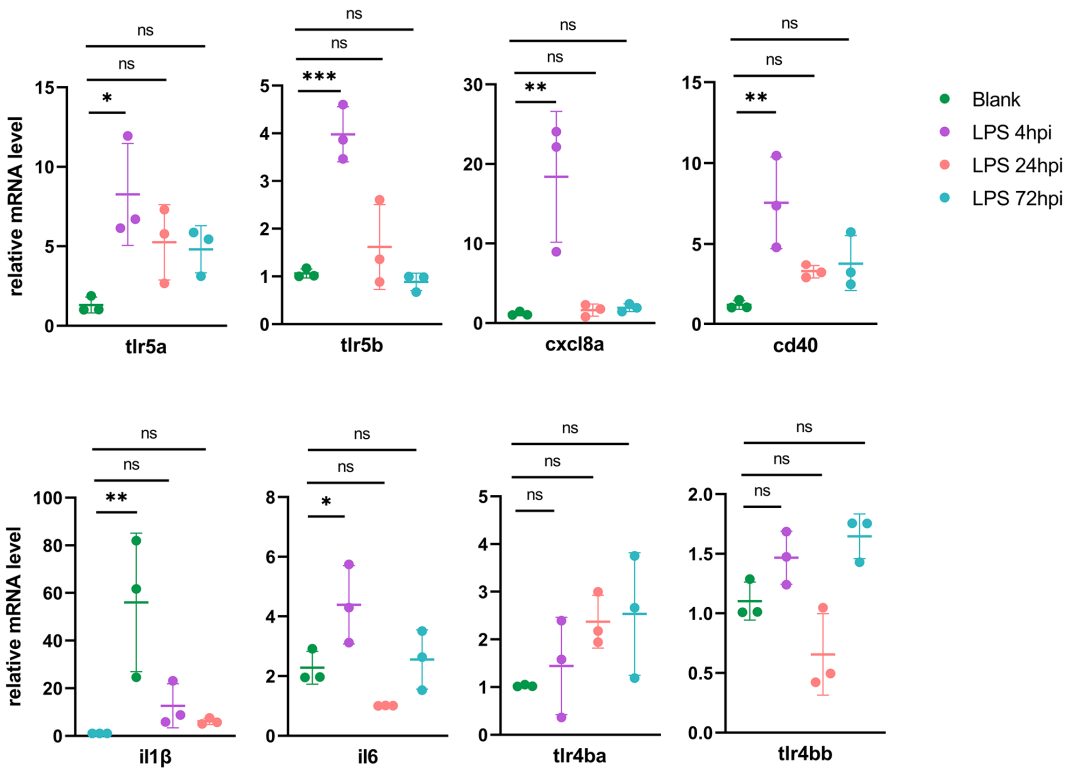

FIGURE 4
RT-PCR validation of DEGs in the initial of inflammation (mean ± SD; *$P < 0.05$, **$P < 0.01$, ***$P < 0.001$, ns, not significant; one-way ANOVA).

line. Flow cytometry result of retinal cell suspensions showed that prednisone immersion significantly inhibited EIU inflammation as evidenced by substantially decreased GFP-positive neutrophils at 24 hpi as compared with vehicle-treated control group (0.1% DMSO immersion group) (Figure 5A). Furthermore, a similar result was observed by counting the relative GFP-positive area in retinal flat mounts, showing significantly decreased GFP-positive area in prednisone-treated group (Figure 5B). Retina from prednisone immersion group also showed decreased mRNA levels of proinflammatory genes including *il1β*, *cxcl8a*, *tnfa*, *c3a* and *il16*, indicating that prednisone was not killing neutrophils directly (Figure 5C).

Discussion

In this study, we for the first time induced a zebrafish model of uveitis by intravitreal injection of LPS. In general, the intraocular inflammation of this model appeared at 4 hpi, exacerbated at 12 hpi, peaked at 24 hpi and resolved at 72 hpi, featured by distinct signaling pathways at different time points of the inflammation process. Furthermore, this intraocular inflammation was inhibited by prednisone immersion, suggesting that the EIU zebrafish model could act as a new approach to screen drugs for uveitis.

At the beginning of this study, we attempted different dosages of LPS to induce EIU in zebrafish at 0.08μg/g, 0.2μg/g and 0.4μg/g. There was no sign of intraocular inflammation according to histological analysis until the dose reached 0.4μg/g. It should be noted that this effective dose of LPS on zebrafish was 32-fold higher than that on mouse. The discrepancy of sensitivity to LPS between zebrafish and mouse might be related to the species difference between lower vertebrates and higher vertebrates (26). The studies have demonstrated that lower vertebrates, especially the fish, is tolerant to LPS stimulation due to the lack of the essential costimulatory molecular for LPS activation *via* Tlr4 (including myeloid differentiation protein 2 (MD-2) and CD14) (15, 16). Since eye is one of the first organs contacting the environment, the extracellular receptors might play an important role in resistant against bacterial infection. Despite the higher dose used in developing EIU in zebrafish, this new model has the advantage of low cost, smaller body size and rapid propagation to better satisfy experimental demands.

In the zebrafish EIU model, inflammatory cells began to infiltrated the iris at 4 hpi. A massive influx of cells was observed in the vitreous body and iris, accompanied by iris vascular

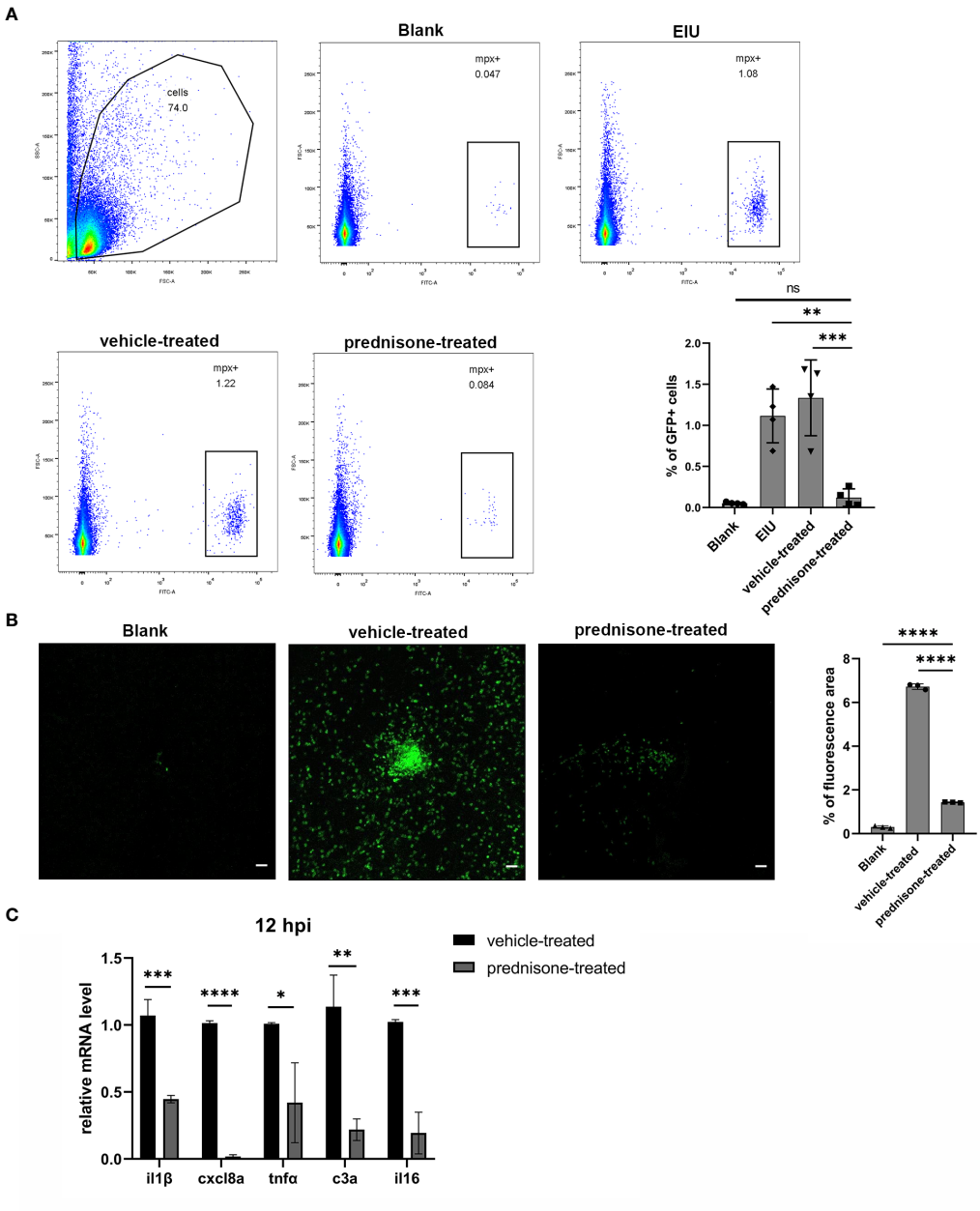

FIGURE 5
Prednisone immersion treatment inhibited EIU inflammation in zebrafish. **(A)** Live cells were separated out from the retina cell suspensions of Tg (Mpx:GFP) line. Left, Flow cytometry was used to analyze the GFP-positive neutrophils. Right, quantification of percentages of GFP-positive cells in different conditions (n = 4 per group; mean ± SD; ***$P < 0.001$; ****$P < 0.0001$; ns, not significant; one-way ANOVA). **(B)** Left, flat mounts of retina around the optic disc in Tg(Mpx:GFP) line. Scale bar, 20μm. Right, quantification of the relative GFP-positive area in retinal flat mounts in different conditions (mean ± SD; n = 3 retinas per group; ****$P < 0.0001$; one-way ANOVA). **(C)** Transcript levels of proinflammatory genes of retina in zebrafish treated with 0.1% DMSO (vehicle-treated group) or 50μm prednisone (mean ± SD; *$P < 0.05$, **$P < 0.01$, ***$P < 0.001$, ****$P < 0.0001$; unpaired t-test).

dilatation at 24 hpi, and then spontaneously resolved at 72 hpi. The characteristic of rapid inflammation resolution in zebrafish was basically consistent with EIU model in mouse (8, 27). It would be of great significance to further explore the mechanism underlying the rapid resolution and short disease course, with the hope to provide new strategies for disease control and treatment in human. However, different from mouse, zebrafish has no ciliary body (28), thus the inflammatory cells of anterior chamber were observed around the iris. Besides its power to help investigate anterior uveitis, EIU is also a compelling tool to

evaluate inflammatory responses at the posterior part of the eye. It is characterized by the breakdown of blood-retinal barrier (BRB) represented by an increment in adhesion of leukocytes to the retinal vasculature and infiltration of leukocytes into the retina/vitreous cavity (29–31). In the terms of immune cell type, myeloid cells including neutrophils and microglia/macrophages were the dominant populations of inflammatory cells in this zebrafish EIU model, consistent with mouse EIU model. Neutrophils were essential for evading infection *via* the generation of proteolytic enzymes and toxic intermediates (32). Besides, ramified L-plastin+/Mpx- microglia, the resident macrophage in the retina, morphologically transformed into ameboid-shaped during inflammation to response to inflammatory stimuli. These activated phagocytic microglial cells could facilitate the infiltration of leukocytes through the BRB and mediate adaptive inflammatory function in uveitis (33). However, it should be noted that L-plastin+/Mpx- staining is not specific to microglia, and macrophages migrated from other sites of the body might also exist.

At 4 hpi, genes related to Toll-like receptor signaling pathway mainly showed significant elevated expression. However, the Tlrs (*tlr5a and tlr5b*) expressed in zebrafish model were different from that in mammal EIU models. In mammals, *Tlr4* is the main receptor therein for LPS recognition with the participation of MD-2, LPS binding protein, and CD14 (34). Some recent studies have discovered the synergistic effect of *Tlr5* and *Tlr4* on triggering LPS-induced lung injury in mouse (35). Besides, *Tlr5* has also been proven to show potent anti-allergic effect on rodent (36). Although *tlr5* may be strongly associated with immunity or inflammation, the underlying mechanism of *tlr5*-mediated intraocular inflammation in the EIU model of zebrafish remains unclear and the exact roles of these upregulated *tlr5a* and *tlr5b* are worthy of further investigation.

At 12 hpi, upregulated genes were specifically enriched in phagosome and proteasome pathways. The phagosome is a vesicle formed by invaginating of the plasma membrane. Phagocytosis is a complex process, which could eliminate microorganisms and present them to CD4+ T cells and B cells. As previously reported, experimental autoimmune uveitis (EAU) could be alleviated by inhibiting the phagosome activation in macrophages, which prevent the activation of effector T cells and help maintaining the healthy ocular microenvironment (37). One important system closely related to the proteasome is the ubiquitin-proteasome system. Before a protein is degraded, it is first flagged for destruction by the ubiquitin conjugation system. The ubiquitin-proteasome is triggered by inflammatory stimuli and oxidative stress. In NF-κB pathway, it is necessary that the ubiquitinated IκB is degraded by proteasome to activate NF-κB. The deubiquitinase A20 has been reported to play a role in negative regulation of inflammation and immunity. In both Behcet's disease (BD) and systemic lupus erythematosus, A20 expression was lower than that in health control, and it was especially downregulated in active BD patients (38, 39). These enriched-pathways in zebrafish were similar with those in mouse EIU model (40), and the therapeutic strategy based on signaling pathway could be further investigated in the future.

The downregulated genes at 12 hpi were mainly enriched in focal adhesion and ECM-receptor interaction. These pathways have also been reported to be downregulated in EIU model in mouse (40). The focal adhesion, regulator of the vascular intracellular tight junction proteins (TJs), maintained the BRB. TJs comprise many proteins, including claudins, occludins, and zonula occludens (41). The earliest molecular sign of BRB disruption is the aberrant expression of these marker proteins. BRB impairment leads to circulating leukocytes entering the retina and activating the innate immune response. In our study, substantial cells infiltrated the eye at 12 hpi meanwhile the expression of *claudin7* was decreased obviously.

Animal models are essential tools to help develop and validate new drugs. So far, proteasome inhibitor (42), immunosuppressant-loaded nanoparticles (43), and gut microbial metabolites (6) have been applied on murine uveitis models. In this study, we successfully validated the anti-inflammatory effect of prednisone on zebrafish EIU model, suggesting this model as an effective tool for future drug screening studies.

However, our study has some limitations. First, the specific contribution of tlr5 orthologs in zebrafish uveitis model is not yet clarified due to lack of available commercial antibodies against this molecule and its downstream signaling effectors in zebrafish, which awaits further investigation. Second, whether the anti-inflammatory effect of prednisone is through alternating tlr5 orthologs and whether smalls molecules targeting the TLR-signaling pathways could impose an effective protection against EIU also remain to be answered in the future. Third, considering RNA-seq results showed changes in NOD- and TLR-pathways, Crispr-Cas9 technique could be further introduced to study the involvement of these signaling pathways in the pathogenesis. Fourth, zebrafish is less representative to human in genome if compared with rodent models. Therefore results obtained based on zebrafish model should be interpreted more cautiously. Fifth, systematic inflammation is not examined in this study and is expected to be clarified in future studies. Sixth, since estrogen has been reported to influence cytokine production in mouse EIU model (44), we only used male fish in this study. The difference of EIU in zebrafish between male and female would be explored in the future.

In summary, we developed an EIU model in zebrafish which represents the characteristics of acute intraocular inflammation. We expect that this model will provide a complementary tool for

the studies on pathogenesis and treatment of uveitis. The equations should be inserted in editable format from the equation editor.

Data availability statement

The datasets presented in this study can be found in online repositories. The names of the repository/repositories and accession number(s) can be found below: Sequence Read Archive study accession code PRJNA891767.

Ethics statement

The animal study was reviewed and approved by the Medical Ethics Committee of the First Affiliated Hospital of Zhengzhou University.

Author contributions

PY, GS, and XX conceived and designed the experiments. XX, WY, and YG performed the experiments. XX, HL, and LD analyzed the data. SJ and NL contributed reagents. XX, ZL, FL, and PY wrote the paper. All authors contributed to the article and approved the submitted version.

Funding

This work was supported by the Major Program of Medical Science and Technology Project of Health Commission of Henan Province (SBGJ202101011), the Natural Science Foundation Major International (Regional) Joint Research Project (81720108009), National Natural Science Foundation Key Program (82230032), and the National Natural Science Foundation Project (81970792), the Medical Science and Technology Project of Health Commission of Henan Province (SBGJ2020003031).

Acknowledgments

The authors thank all participants in this study.

Conflict of interest

The authors declare that the research was conducted in the absence of any commercial or financial relationships that could be construed as a potential conflict of interest.

Publisher's note

Supplementary material

The Supplementary Material for this article can be found online at: https://www.frontiersin.org/articles/10.3389/fimmu.2022.1042849/full#supplementary-material

References

1. Durrani OM, Tehrani NN, Marr JE, Moradi P, Stavrou P, Murray PI. Degree, duration, and causes of visual loss in uveitis. *Br J Ophthalmol* (2004) 88(9):1159–62. doi: 10.1136/bjo.2003.037226

2. Suttorp-Schulten MS, Rothova A. The possible impact of uveitis in blindness: A literature survey. *Br J Ophthalmol* (1996) 80(9):844–8. doi: 10.1136/bjo.80.9.844

3. Papotto PH, Marengo EB, Sardinha LR, Goldberg AC, Rizzo LV. Immunotherapeutic strategies in autoimmune uveitis. *Autoimmun Rev* (2014) 13 (9):909–16. doi: 10.1016/j.autrev.2014.05.003

4. Zhong Z, Su G, Kijlstra A, Yang P. Activation of the interleukin-23/ Interleukin-17 signalling pathway in autoinflammatory and autoimmune uveitis. *Prog Retin Eye Res* (2021) 80:100866. doi: 10.1016/j.preteyeres.2020.100866

5. Rosenbaum JT, Asquith M. The microbiome and hla-B27-Associated acute anterior uveitis. *Nat Rev Rheumatol* (2018) 14(12):704–13. doi: 10.1038/s41584-018-0097-2

6. Ye Z, Wu C, Zhang N, Du L, Cao Q, Huang X, et al. Altered gut microbiome composition in patients with vogt-Koyanagi-Harada disease. *Gut Microbes* (2020) 11(3):539–55. doi: 10.1080/19490976.2019.1700754

7. Caspi RR, Chan CC, Leake WC, Higuchi M, Wiggert B, Chader GJ. Experimental autoimmune uveoretinitis in mice. induction by a single eliciting event and dependence on quantitative parameters of immunization. *J Autoimmun* (1990) 3(3):237–46. doi: 10.1016/0896-8411(90)90143-g

8. Rosenbaum JT, McDevitt HO, Guss RB, Egbert PR. Endotoxin-induced uveitis in rats as a model for human disease. *Nature* (1980) 286(5773):611–3. doi: 10.1038/286611a0

9. Yang P, Wan W, Du L, Zhou Q, Qi J, Liang L, et al. Clinical features of hla-B27-Positive acute anterior uveitis with or without ankylosing spondylitis in a Chinese cohort. *Br J Ophthalmol* (2018) 102(2):215–9. doi: 10.1136/bjophthalmol-2016-309499

10. Zhang N, Yu S, Liu X, Lu H. Low dose of lipopolysaccharide pretreatment preventing subsequent endotoxin-induced uveitis is associated with Pi3k/Akt pathway. *J Immunol Res* (2017) 2017:1273940. doi: 10.1155/2017/1273940

11. Ildefonso CJ, Jaime H, Rahman MM, Li Q, Boye SE, Hauswirth WW, et al. Gene delivery of a viral anti-inflammatory protein to combat ocular inflammation. *Hum Gene Ther* (2015) 26(1):59–68. doi: 10.1089/hum.2014.089

12. Ohta K, Wiggert B, Taylor AW, Streilein JW. Effects of experimental ocular inflammation on ocular immune privilege. *Invest Ophthalmol Vis Sci* (1999) 40 (9):2010–8.

13. García-Moreno D, Tyrkalska SD, Valera-Pérez A, Gómez-Abenza E, Pérez-Oliva AB, Mulero V. The zebrafish: A research model to understand the evolution of vertebrate immunity. *Fish Shellfish Immunol* (2019) 90:215–22. doi: 10.1016/j.fsi.2019.04.067

14. Gomes MC, Mostowy S. The case for modeling human infection in zebrafish. *Trends Microbiol* (2020) 28(1):10–8. doi: 10.1016/j.tim.2019.08.005

15. Sullivan C, Charette J, Catchen J, Lage CR, Giasson G, Postlethwait JH, et al. The gene history of zebrafish Tlr4a and Tlr4b is predictive of their divergent functions. *J Immunol* (2009) 183(9):5896–908. doi: 10.4049/jimmunol.0803285

16. Sepulcre MP, Alcaraz-Pérez F, López-Muñoz A, Roca FJ, Meseguer J, Cayuela ML, et al. Evolution of lipopolysaccharide (Lps) recognition and signaling: Fish Tlr4 does not recognize lps and negatively regulates nf-kappab activation. *J Immunol* (2009) 182(4):1836–45. doi: 10.4049/jimmunol.0801755

17. Jurynec MJ, Sawitzke AD, Beals TC, Redd MJ, Stevens J, Otterud B, et al. A hyperactivating proinflammatory Ripk2 allele associated with early-onset osteoarthritis. *Hum Mol Genet* (2018) 27(13):2383–91. doi: 10.1093/hmg/ddy132

18. Sun Y, Zhang B, Luo L, Shi DL, Wang H, Cui Z, et al. Systematic genome editing of the genes on zebrafish chromosome 1 by Crispr/Cas9. *Genome Res* (2019) 30(1):118–26. doi: 10.1101/gr.248559.119

19. Mitchell RE, Huitema LF, Skinner RE, Brunt LH, Severn C, Schulte-Merker S, et al. New tools for studying osteoarthritis genetics in zebrafish. *Osteoarthritis Cartilage* (2013) 21(2):269–78. doi: 10.1016/j.joca.2012.11.004

20. Park KH, Kim SH. Adult zebrafish as an in vivo drug testing model for ethanol induced acute hepatic injury. *BioMed Pharmacother* (2020) 132:110836. doi: 10.1016/j.biopha.2020.110836

21. Csenki Z, Garai E, Risa A, Cserháti M, Bakos K, Márton D, et al. Biological evaluation of microbial toxin degradation by microinjected zebrafish (Danio rerio) embryos. *Chemosphere* (2019) 227:151–61. doi: 10.1016/j.chemosphere.2019.04.014

22. Hsu AY, Gurol T, Sobreira TJP, Zhang S, Moore N, Cai C, et al. Development and characterization of an endotoxemia model in zebra fish. *Front Immunol* (2018) 9:607. doi: 10.3389/fimmu.2018.00607

23. Mitchell DM, Lovel AG, Stenkamp DL. Dynamic changes in microglial and macrophage characteristics during degeneration and regeneration of the zebrafish retina. *J Neuroinflamm* (2018) 15(1):163. doi: 10.1186/s12974-018-1185-6

24. Van Dyck A, Bollaerts I, Beckers A, Vanhunsel S, Glorian N, van Houcke J, et al. Müller glia-myeloid cell crosstalk accelerates optic nerve regeneration in the adult zebrafish. *Glia* (2021) 69(6):1444–63. doi: 10.1002/glia.23972

25. Conedera FM, Pousa AMQ, Mercader N, Tschopp M, Enzmann V. Retinal microglia signaling affects müller cell behavior in the zebrafish following laser injury induction. *Glia* (2019) 67(6):1150–66. doi: 10.1002/glia.23601

26. Liu Y, Li M, Fan S, Lin Y, Lin B, Luo F, et al. A unique feature of Toll/Il-1 receptor domain-containing adaptor protein is partially responsible for lipopolysaccharide insensitivity in zebrafish with a highly conserved function of Myd88. *J Immunol* (2010) 185(6):3391–400. doi: 10.4049/jimmunol.0903147

27. Magaña-Guerrero FS, Quiroz-Mercado J, Garfias-Zenteno N, Garfias Y. Comparative analysis of inflammatory response in the Balb/C and C57bl/6 mouse strains in an endotoxin-induced uveitis model. *J Immunol Methods* (2020) 476:112677. doi: 10.1016/j.jim.2019.112677

28. Soules KA, Link BA. Morphogenesis of the anterior segment in the zebrafish eye. *BMC Dev Biol* (2005) 5:12. doi: 10.1186/1471-213x-5-12

29. Kanda A, Noda K, Oike Y, Ishida S. Angiopoietin-like protein 2 mediates endotoxin-induced acute inflammation in the eye. *Lab Invest* (2012) 92(11):1553–63. doi: 10.1038/labinvest.2012.111

30. Van Hove I, Lefevere E, De Groef L, Sergeys J, Salinas-Navarro M, Libert C, et al. Mmp-3 deficiency alleviates endotoxin-induced acute inflammation in the posterior eye segment. *Int J Mol Sci* (2016) 17(11):1825. doi: 10.3390/ijms17111825

31. Yang P, de Vos AF, Kijlstra A. Macrophages in the retina of normal Lewis rats and their dynamics after injection of lipopolysaccharide. *Invest Ophthalmol Vis Sci* (1996) 37(1):77–85.

32. Trevani AS, Andonegui G, Giordano M, Nociari M, Fontán P, Dran G, et al. Neutrophil apoptosis induced by proteolytic enzymes. *Lab Invest* (1996) 74(3):711–21.

33. Okunuki Y, Mukai R, Nakao T, Tabor SJ, Butovsky O, Dana R, et al. Retinal microglia initiate neuroinflammation in ocular autoimmunity. *Proc Natl Acad Sci U.S.A.* (2019) 116(20):9989–98. doi: 10.1073/pnas.1820387116

34. Forn-Cuní G, Varela M, Pereiro P, Novoa B, Figueras A. Conserved gene regulation during acute inflammation between zebrafish and mammals. *Sci Rep* (2017) 7:41905. doi: 10.1038/srep41905

35. Hussain S, Johnson CG, Sciurba J, Meng X, Stober VP, Liu C, et al. Tlr5 participates in the Tlr4 receptor complex and promotes Myd88-dependent signaling in environmental lung injury. *Elife* (2020) 9:e50458. doi: 10.7554/eLife.50458

36. Kirtland ME, Tsitoura DC, Durham SR, Shamji MH. Toll-like receptor agonists as adjuvants for allergen immunotherapy. *Front Immunol* (2020) 11:599083. doi: 10.3389/fimmu.2020.599083

37. Ng TF, Manhapra A, Cluckey D, Choe Y, Vajram S, Taylor AW. Melanocortin 5 receptor expression and recovery of ocular immune privilege after uveitis. *Ocul Immunol Inflammation* (2022) 30(4):876–86. doi: 10.1080/09273948.2020.1849735

38. He Y, Wang C, Su G, Deng B, Ye Z, Huang Y, et al. Decreased expression of A20 is associated with ocular behcet's disease (Bd) but not with vogt-Koyanagi-Harada (Vkh) disease. *Br J Ophthalmol* (2018) 102(8):1167–72. doi: 10.1136/bjophthalmol-2017-311707

39. Odqvist L, Jevnikar Z, Riise R, Öberg L, Rhedin M, Leonard D, et al. Genetic variations in A20 dub domain provide a genetic link to citrullination and neutrophil extracellular traps in systemic lupus erythematosus. *Ann Rheum Dis* (2019) 78(10):1363–70. doi: 10.1136/annrheumdis-2019-215434

40. Qiu Y, Yu P, Lin R, Fu X, Hao B, Lei B. Genome-wide retinal transcriptome analysis of endotoxin-induced uveitis in mice with next-generation sequencing. *Mol Vis* (2017) 23:395–406.

41. Yang X, Yu XW, Zhang DD, Fan ZG. Blood-retinal barrier as a converging pivot in understanding the initiation and development of retinal diseases. *Chin Med J (Engl)* (2020) 133(21):2586–94. doi: 10.1097/cm9.0000000000001015

42. Chen FT, Liu YC, Yang CM, Yang CH. Anti-inflammatory effect of the proteasome inhibitor bortezomib on endotoxin-induced uveitis in rats. *Invest Ophthalmol Vis Sci* (2012) 53(7):3682–94. doi: 10.1167/iovs.12-9505

43. Kasper M, Gabriel D, Möller M, Bauer D, Wildschütz L, Courthion H, et al. Cyclosporine a-loaded nanocarriers for topical treatment of murine experimental autoimmune uveoretinitis. *Mol Pharm* (2018) 15(7):2539–47. doi: 10.1021/acs.molpharmaceut.8b00014

44. Miyamoto N, Mandai M, Suzuma I, Suzuma K, Kobayashi K, Honda Y. Estrogen protects against cellular infiltration by reducing the expressions of e-selectin and il-6 in endotoxin-induced uveitis. *J Immunol* (1999) 163(1):374–9.

frontiers | Frontiers in Immunology

TYPE Original Research
PUBLISHED 08 December 2022
DOI 10.3389/fimmu.2022.1054422

OPEN ACCESS

EDITED BY
Uzma Saqib,
Indian Institute of Technology Indore, India

REVIEWED BY
Peiguang Wang,
Anhui Medical University, China
Paola Fortugno,
Università telematica San Raffaele, Italy
Hugo Chapdelaine,
Montreal Clinical Research Institute (IRCM), Canada

*CORRESPONDENCE
Xiaoming Bai
XiaomingBai@cqmu.edu.cn
Hua Wang
huawang@hospital.cqmu.edu.cn
Xiaoyan Luo
xyluo@hospital.cqmu.edu.cn

SPECIALTY SECTION
This article was submitted to Inflammation, a section of the journal Frontiers in Immunology

RECEIVED 26 September 2022
ACCEPTED 23 November 2022
PUBLISHED 08 December 2022

CITATION
Yan S, Wu X, Jiang J, Yu S, Fang X, Yang H, Bai X, Wang H and Luo X (2022) Dupilumab improves clinical symptoms in children with Netherton syndrome by suppressing Th2-mediated inflammation. *Front. Immunol.* 13:1054422. doi: 10.3389/fimmu.2022.1054422

Dupilumab improves clinical symptoms in children with Netherton syndrome by suppressing Th2-mediated inflammation

Shi Yan[1,2], Xuege Wu[1,2], Jinqiu Jiang[1,3], Shijuan Yu[1,3], Xiao Fang[1,2], Huan Yang[1,2], Xiaoming Bai[1,2]*, Hua Wang[1,2,3]* and Xiaoyan Luo[1,3]*

[1]Department of Dermatology, Children's Hospital of Chongqing Medical University Clinical Research Center for Child Health and Disorders, Ministry of Education Key Laboratory of Child Development and Disorders, Chongqing, China, [2]Chongqing Key Laboratory of Child Infection and Immunity, Children's Hospital of Chongqing Medical University, Chongqing, China, [3]Ministry of Education Key Laboratory of Child Development and Disorders, Children's Hospital of Chongqing Medical University, Chongqing, China

Background: Netherton syndrome is a rare, life-threatening autosomal recessive genetic disorder with no effective treatment yet. Skin barrier dysfunction caused by *SPINK5* gene mutations is a hallmark of the disease. Antigen penetration through the defective skin and nonspecific inflammation provide a pro-T helper 2 (Th2) immune microenvironment in the disease. Therefore, Th2 cytokines are considered to be candidate therapeutic targets.

Objective: To evaluate the clinical responses of patients with Netherton syndrome to dupilumab, an IL-4Rα antagonist, and identify changes in the Th1/2/17 pathway activity, skin barrier defect protein LEKTI expression after treatment.

Methods: Four children with severe Netherton syndrome (aged 2 y to 4 y and 6 m) who were treated with dupilumab from January to June 2022 were evaluated at baseline, and at 4, 8, 12, 16, and 20 weeks after the start of dupilumab administration. Treatment response was assessed using the Eczema Area and Severity Index (EASI), the Numerical Rating Scale (NRS), the Dermatology Life Quality Index (CDLQI), and the Dermatitis Family Impact-questionnaire (DFI). Blood eosinophil counts, serum IgE levels and inflammatory cytokines were measured. The immunotyping of Th1/2/17 cells was performed by flow cytometry and cytokine expressions in T cell subsets were analyzed by single-cell RNA sequencing. In addition, expression of the LEKTI in skin lesions was evaluated by immunohistochemical analysis.

Results: All four patients experienced clinical improvement, with significantly reduced EASI scores (by 75.0–83.9%) and NRS (by 87.5–90.0%) from baseline

to 20 weeks of treatment. Improved quality of life scores were also seen for all patients, as measured by CDLQI and DFI. Serum IgE levels also fell by 75.6–86.9%. The serum Th2 cytokines IL-4, IL-5 and IL-13 were found at low level, with no significant changes during the treatment. However, Th2 cytokines expressed by T cells, especially IL-4, decreased at single-cell level after treatment (P = 0.029). The baseline percentage of Th2 cells (among total $CD3^+CD4^+$ T cells) was significantly higher in patients than that in healthy controls (HC) ($P < 0.0001$); this percentage fell from 8.25% ± 0.75% to 4.02% ± 0.62% after 20 weeks dupilumab treatment. There was no noticeable change in LEKTI protein expression in skin lesions pre- and post-treatment. Two patients reported mild ocular adverse effects, but there were no severe adverse events.

Conclusion: Dupilumab may be an effective and safe treatment option in a subset of pediatric patients with Netherton syndrome, especially in improving itch and the quality of life. These effects were achieved in part by suppression of the Th2-mediated inflammation.

KEYWORDS

Netherton syndrome, *SPINK5* gene, LEKTI, dupilumab, treatment

Introduction

Netherton syndrome (NS; OMIM#256500), also known as Comel-Netherton syndrome, is a rare autosomal recessive disorder caused by germline loss-of-function mutations in *SPINK5* gene. The disorder is characterized by the classical triad symptoms of congenital ichthyosis, bamboo hair, and atopic diathesis with high serum IgE level (1). In most *SPINK5* mutations, premature stop codons result in a truncated Lymphoepithelial Kazal-type-related inhibitor (LEKTI) protein which leads to an unrestricted activity of kallikrein (KLK)-related peptidases (KLK5, KLK7, and KLK14). This will cause severe skin barrier breakdown and secondary inflammation (2, 3).

NS is a multisystemic disease for which a safe and effective treatment is not yet available. Several novel systematic treatments have been suggested in the recent literature, including immunoglobulins and biologicals that target specific inflammatory pathways (4). Dupilumab, a monoclonal antibody that blocks the IL-4 receptor (IL-4R), has been used to treat moderate to severe atopic dermatitis with a good safety and efficacy profile (5). A few recent case report displayed clinical effect with improving skin symptoms in patients with NS who treated with dupilumab (6–12). However, these reports have shown great heterogeneity in outcome measures and a few cases reported long-term outcomes. In addition, few reports describe the efficacy and safety of dupilumab in pediatric NS patients. In this prospective case series study, we reported four pediatric NS patients treated with dupilumab and their clinical responses, cytokine profiles change with treatment, which hopes to provide new insight into the underlying mechanisms of dupilumab therapy in NS and provide more evidence to support biologic treatment for NS patients.

Methods

Patients and control subjects

Four NS patients (median age, 3.25y; range from 2y to 4.5y) from four unrelated Chinese families were enrolled. A diagnosis of NS was made based on clinical signs, *SPINK5* mutations, and decreased/absent LEKTI expression upon immunostaining analysis. Health controls (HCs) comprised eight age-matched subjects (median age, 3 y; range from 1.5y to 5y). Patients were evaluated, and blood was collected at baseline (before therapy), and at 4, 8, 12, 16 and 20 weeks after dupilumab administration. Skin biopsies were collected at baseline and 20 weeks. All parents provided written informed consent, and the study was approved by the Ethics Committee of the Children's Hospital of Chongqing Medical University (2021-17).

Treatment

All NS patients received a loading dose of subcutaneously administered dupilumab (400 mg), followed by 200 mg every 4 weeks for 20 weeks. During dupilumab treatment, patients were

encouraged to continue the use of moisturizers, topical corticosteroids, or 1% Pimecrolimus, which were not monitored specifically.

Measures used in this study

The Children's Dermatology Life Quality Index (CDLQI) and the Dermatitis Family Impact-questionnaire (DFI) were adopted for evaluation of quality of life, the Eczema Area and Severity Index (EASI), and the Numerical Rating Scale (NRS) were used at every visit for assessing changes in symptoms. Laboratory tests, including total serum immunoglobulin (Ig) E and eosinophil (ESO) counts, were conducted at every visit. A high level of serum IgE was defined as >165.0 IU/ml, and eosinophilia was defined as a blood eosinophil count $>0.68\times10^9$ cell/L.

Assessment of serum cytokine profiles

Multiple cytokines, including IL-1 β, IL-1α, TNF- α, TNF- β, IFN-γ, IL-2, IL-4, IL-5, IL-6, IL-8, IL-9, IL-12p70, IL-13, IL-17A, IL-23, and IL-31, were measured at baseline, 4 and 20 weeks after treatment with dupilumab by Luminex 200^{TM} System (Millipore) based on manufacturer's instructions. Serum samples were diluted 2 times and incubated for 3 hours with a mix of beads coupled to antibodies specific for each measured cytokine. Then a mixed secondary streptavidin-coupled antibodies was added for 1 hour followed by phycoerythrin (PE)-conjugated biotin after several washing steps. The signal intensity was measured by PE fluorescence and a standard curve was performed to identify the absolute concentration of each cytokine in tested samples.

Assessment of cytokine profiles in T cell subsets by single-cell RNA sequencing

The PBMCs from 4 NS patients at baseline and 20 weeks after dupilumab treatment were sequenced for single cells using the 10x Genomics scRNA-seq platform. Based on the single-cell transcriptomic data, Cytokine Signaling Analyzer (CytoSig; https://cytosig.ccr.cancer.gov/) was employed in T cell subsets to evaluate the cytokine signaling activity, including IL-1A, IL-1B, IL-2, IL-4, IL-10, IL-12, IL-13, IL-15, IL-17A, IL-21, and IL-22.

Flow cytometry analysis and antibodies

Peripheral blood mononuclear cells (PBMCs) were isolated from blood samples using Ficoll-Hypaque (GE Healthcare, USA) gradient centrifugation. To obtain Th1/2/17 cells, PBMCs were incubated for 30 min in with specific antibodies (FITC-anti-CD45RA, PE-anti-CCR6, Percep-anti-CD3, PE/Cy7-anti-CD4, APC-anti-CXCR3, BV421-anti-CXCR5, BV510-anti-CCR4; all from BD Biosciences) in PBS containing 2% fetal bovine serum. Cells were examined immediately using a BD FACS-CantoII, and data were analyzed using FlowJo software (TreeStar, USA). Cells were classified as follows: Th17 cells, $CD3^+CD4^+CD45RA^-CXCR5^-CCR6^+CCR4^+$; Th2 cells, $CD3^+CD4^+CD45RA^-CXCR5^-CCR6^-CCR4^+CXCR3^-$; and TH1 cells, $CD3^+CD4^+CD45RA^-CXCR5^-CCR6^-CCR4^-CXCR3^+$.

Immunohistochemistry

After consent was obtained from the parents, skin biopsy was conducted in the ichthyosis linearis circumflexa (ILC) lesions of patients 2 and 3. Four normal skin specimens obtained from routine surgery were served as controls. Skin sections were fixed, sectioned transversely ($4\mu m$), and embedded in paraffin blocks. The slides were permeabilized with 0.5% H_2O_2, then stained with a SPINK5 polyclonal antibody (rabbit IgG; Invitrogen, PA5-52820) overnight at 4°C. A secondary biotinylated antibody (ZSGB-BIO, PV-9001, China) was performed, then reacted with diaminobenzidine (DAB) (ZSGB-BIO, ZLI-9018, China). After counterstaining with hematoxylin, images were captured under a digitalized brightfield microscope (Leica Imaging Systems Ltd., Cambridge, U.K.) and analyzed with ImageJ software (version 2.1.0). Average optical density (AOD) was used to evaluate immunofluorescence staining.

Statistical analysis

Statistical analyses were performed using GraphPad Prism software, version 8.3.1 (GraphPad Software, San Diego, CA, USA). A two-tailed unpaired t-test was used for single comparisons, and the Wilcoxon matched pairs signed rank test or the Mann-Whitney test was used to assess the statistical significance of differences between groups (****P < 0.0001; ***P < 0.001; **P < 0.01; and *P < 0.05).

Results

Demographics and genetics

The characteristics of the four NS patients (two males and two females; average age, 3.25 ± 1.041y; range, 2y–4.5y) are shown in the Table 1. All of the patients presented with ILC, Trichorrhexis Invaginata or bamboo hair (Supplement Figure S1), growth retardation, and high levels of serum IgE. Whole exome sequencing of peripheral blood DNA identified *SPINK5* mutations in all patients. (Supplement Figure S2) Two novel

10.3389/fimmu.2022.1054422

TABLE 1 Clinical and genetic characteristics of the patients with Netherton syndrome.

Patient	Age	Gender	Weight (kg)	Height (cm)	ILC	TI	Food allergy	Growth retard	IgE(IU/ml)	*SPINK5* mutation	Mutation-type
1	3y6m	F	13	86	+	+	–	+	713↑	exon26, c.2474_75delAG (p.E825Gfs*2)	Hom
2	3y	F	11	80	+	+	–	+	3330↑	exon27, c.2557C>T (p.R853X) exon1-34, lossl (73K)#	Het Het
3	2y	M	7	70	+	+	+	+	5870↑	IVS10+5G>T# exon24, c.2258_59insA (p.R753Rfs*4)#	Het Het
4	4y6m	M	12.5	94	+	+	–	+	6940↑	exon23, c.2143dupA (p.N716Kfs*11)# exon25, c.2423C>T (p.T808I)	Het Het

M, month(s); Y, year(s); F, female; M, male; ILC, Ichthyosis Linearis Circumflexa; TI, Trichorrhexis Invaginata; Hom, homozygous; Het, heterozygous; SPINK5:Serine Peptidase Inhibitor Kazal Type5; + positive; - negative; #indicates unreported SPINK5 mutation, the red ↑ represents the abnormal (elevated) level.

heterozygous mutations were found in patient 3 (IVS10+5G>T; c.2258_59insA, exon24), and patient 4 (c.2143dupA, exon23).

Dupilumab significantly improved skin lesions, itch, and quality of life

Treatment with dupilumab led to a significant improvement in clinical signs (see the images in Figures 1A–D). The affected area of skin lesions decreased to varying degrees: 75% in patients 1 and 3, and 50% in patients 2 and 4. The disease severity and pruritus were reduced markedly at 20 weeks post-dupilumab treatment, evidenced primarily by changes in the EASI and NRS (Figures 1E, F). The four patients reported at least 75.0% improvement in the EASI from baseline and an 87.5% reduction in the NRS. Accordingly, the life quality improved as CDLQI and DFI decreased by 72.1% (mean value) and 69.6% (mean value) from baseline to Week 20, respectively (Figures 1G, H). We also observed continued weight gain along the third percentile in all four patients compared to baseline. Interestingly, the height of patient 3 increased by 5 cm during treatment, after failure to thrive 1 year before treatment. Hair growth seemed to occur only in patient 1 and hair shaft nodules were not changed in any of our patients.

Dupilumab significantly decreased serum IgE in NS

All four patients had high serum IgE, and two had eosinophilia (patients 3 and 4) at baseline. During treatment, serum IgE levels fell steadily in all patients (Figure 2A): from 713 to 174 IU/ml (a decrease of 75.6%) in patient 1, from 3330 to 598 IU/ml (a decrease of 82.0%) in patient 2, from 5870 to 769 IU/ml (a decrease of 86.9%) in patient 3, and from 6940 to 988 IU/ml (a decrease of 85.8%) in patient 4. In addition, the EOS count in three patients fell slightly from the baseline value (Figure 2B). However, it is noteworthy that a transient elevation in the EOS count was observed over the course of dupilumab treatment, although the count was lower at Week 20 than at baseline.

Dupilumab suppressed Th2-type immune responses in NS

Although serum Th2 cytokines were at the normal range or low amounts (Table 2), the percentage (among total CD3+CD4+ cells) and absolute number of Th2 cells in NS patients was much higher than that in HCs ($P < 0.0001$) (Figures 3A, B). Moreover, the percentage of Th2 cells (among total CD3+CD4+ cells) fell from 8.25%± 0.75% to 4.02%±0.62% (mean ± SD), and the absolute number of Th2 cells was decreased significantly after 20 weeks of treatment ($P = 0.0021$). The numbers of Th17 and Th1 cells, however, tended to increase slightly, but the changes had no statistically significance (Supplement Figures S3A, B). Next, we examined the Th2/Th17 balance and found that the Th2/Th17 ratio was significantly lower after dupilumab therapy ($P = 0.0128$) (Supplement Figure S3C), suggesting that dupilumab might counterbalance the skew toward Th2 responses. In addition, dupilumab treatment down-regulated the expression of IL-4, a pivotal type 2 cytokines, at single cell level ($P = 0.029$). (Figures 3C, D)

No obvious changes of LEKTI expression in skin lesions

Skin samples from patient 1 and patient 4 showed diminished expression of LEKTI which displayed in HC, however, as a continuous staining of the cytoplasm in their epidermal granular layer and uppermost spinous layers (Figure 4). Furthermore, LEKTI expression in skin lesions of patient 1 and patient 4 did not change after 20 weeks of treatment, as expected.

10.3389/fimmu.2022.1054422

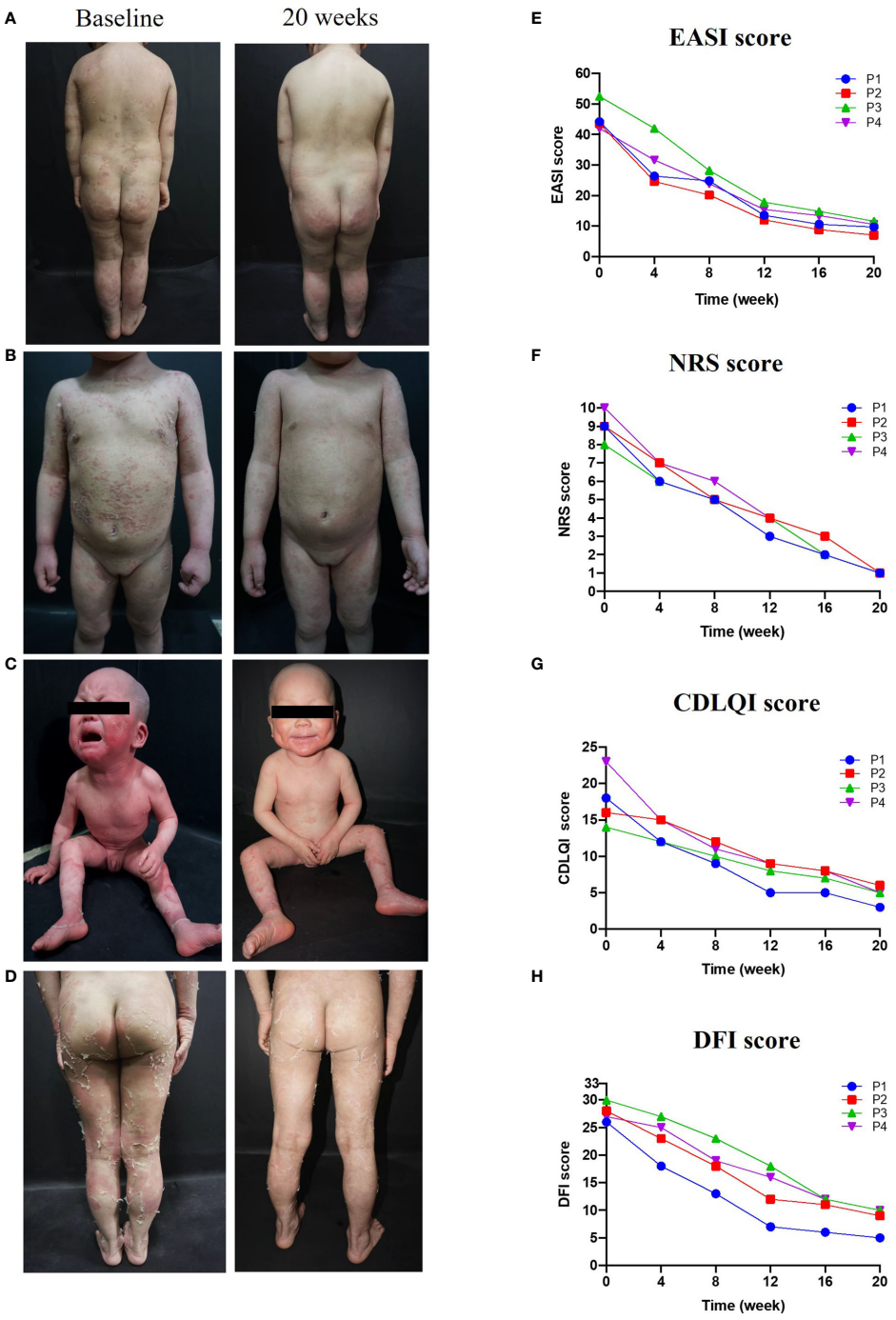

FIGURE 1
Improvements in clinical symptoms and QoL after 20 weeks of dupilumab treatment Images in **(A–C)**, and **(D)** show clinical pictures of patients 1,2,3, and 4 before and 20 weeks after treatment with dupilumab, respectively. **(E–H)** displayed changes in disease severity, pruritus, and QoL over time of treatment, **(E)** Eczema Area and Severity Index (EASI), **(F)** the Numerical Rating Scale (NRS), **(G)** the Dermatology Life Quality Index (CDLQI), and **(H)** the Dermatitis Family Impact-questionnaire (DFI).

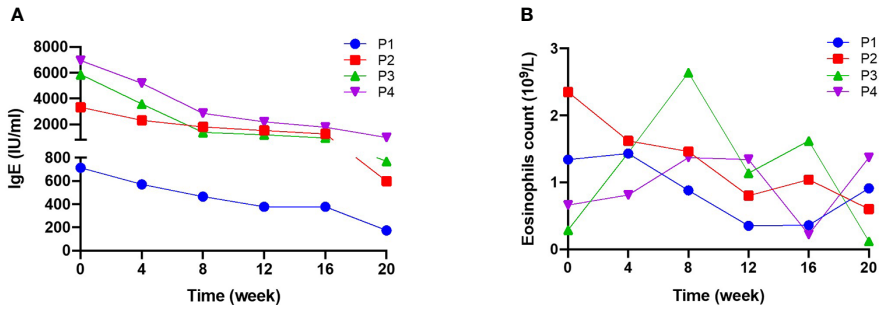

FIGURE 2
Serum IgE levels and blood eosinophil counts during 20 weeks of dupilumab treatment **(A)** serum IgE levels and **(B)** blood eosinophil (EOS) count were measured for 20 weeks. Serum IgE levels fell significantly after treatment, while there were no significant changes in EOS.

Safety

During the entire 20-week treatment period, two patients reported mild ocular symptoms presented with bilateral conjunctival hyperemia, pruritus, tearing and foreign-body sensation and alleviated by using tobramycin and dexamethasone eye drop, which did not lead to treatment discontinuation. No other commonly reported treatment-related side effects were observed.

Discussion

NS is a rare genetic disease and the existing treatment options are mostly symptomatic. Reports on the clinical effects of biologicals on NS are scarce. In the current prospective case series study, four pediatric NS patients treated with dupilumab have achieved an impressive and sustained responses, with a marked improvement in skin-related symptoms, pruritus, and quality of life. In addition, the frequency of their topical corticosteroid use was reduced, thus reducing the risk of severe local and systemic side effects, such as Cushing syndrome and growth retardation. We employed standardized measurement instruments to evaluate the treatment outcomes, therefore, avoided evidence of poor quality and heterogeneity in reporting outcomes in previous studies.

The core pathogenesis of NS is the loss of protease inhibitor LEKTI, which causes severe skin barrier impairment and triggers the expression of proinflammatory and proallergic cytokines by activating protease-activated receptor-2 (PAR-2) signaling in keratinocyte (13). Upregulated inflammatory pathways, including Th2 and Th17, and elevated TNF-α, TSLP and IgE levels in patients with NS have been observed and several biologicals targeting IL-4, IL-12/23, IgE, TNFα and IL-17 have

TABLE 2 Serum cytokine changes after 20 weeks of dupilumab treatment.

		IL-1β (pg/ml)	IL-1α (pg/ml)	TNF-α (pg/ml)	TNF-β (pg/ml)	IFN-γ (pg/ml)	IL-2 (pg/ml)	IL-4 (pg/ml)	IL-5 (pg/ml)	IL-6 (pg/ml)	IL-8 (pg/ml)	IL-9 (pg/ml)	IL-12p70 (pg/ml)	IL-13 (pg/ml)	IL-17A (pg/ml)	IL-23 (pg/ml)	IL-31 (pg/ml)
P1	Baseline	< 1.2	< 0.4	13.5	< 1.9	9.3	< 3.6	< 5.5	< 3.6	207.6↑	190.5↑	< 2.7	< 3.6	2.6	< 0.8	< 4.4	< 2.3
	4w	< 1.5	< 0.6	< 3.4	< 4.9	< 4.7	< 3.9	< 5.4	< 5	< 7.6	12.5	< 3.2	< 5.8	< 2	< 1.1	< 6.6	< 4.1
	20w	1.3	< 0.5	< 3.1	< 3	< 5.2	< 4.1	< 7.4	< 5.4	< 7.7	19.4	< 4.7	< 4.3	< 3.4	< 1.5	< 4.2	< 4.9
P2	Baseline	11.7	< 0.4	< 2.5	< 1.7	13	< 4.4	5.9	< 5.3	< 5.9	286.8↑	< 2.5	< 4.2	1.8	1	< 3.1	< 1.9
	4w	4.5	< 0.6	< 3.4	< 4.9	80	4.6	< 5.4	< 5	< 7.6	165.6↑	< 3.2	< 5.8	2.5	< 1.1	< 6.6	< 4.1
	20w	< 0.9	< 0.5	< 3.1	< 3	< 5.2	< 4.1	< 7.4	< 5.4	< 7.7	81.5↑	< 4.7	< 4.3	< 3.4	< 1.5	< 4.2	< 4.9
P3	Baseline	< 1.3	< 0.4	< 2.9	< 2.5	< 4.7	< 3.2	< 5.8	< 4.3	201.2↑	74.9↑	< 2.3	< 6	< 1	< 1.3	< 6.5	< 1.5
	4w	1.6	< 0.6	< 3.4	< 4.9	34.5	< 3.9	< 5.4	< 5	8.6	29.5	< 3.2	< 5.8	< 2	< 1.1	< 6.6	< 4.1
	20w	6.8	< 0.5	22.1	< 3	< 5.2	< 4.1	< 7.4	< 5.4	< 7.6	< 2	< 4.7	< 4.3	< 3.4	< 1.5	< 4.2	< 4.9
P4	Baseline	1.7	1.1	6.2	< 1.6	< 8.8	< 3.9	< 6	< 5.7	222.7↑	124.2↑	< 2.2	< 3.6	< 1.9	< 2.4	< 3.3	< 5.5
	4w	< 1.5	2.8	< 3.4	< 4.9	7.1	< 3.9	< 5.4	< 5	124.2↑	64.4↑	< 3.2	< 5.8	< 2	< 1.1	< 6.6	< 4.1
	20w	4.4	< 0.5	3.1	< 3	< 5.2	< 4.1	< 7.4	< 5.4	< 7.6	25.7	< 4.7	< 4.3	< 3.4	< 1.5	< 4.2	< 4.9

The values and ↑ in red represents the abnormal (elevated) level.

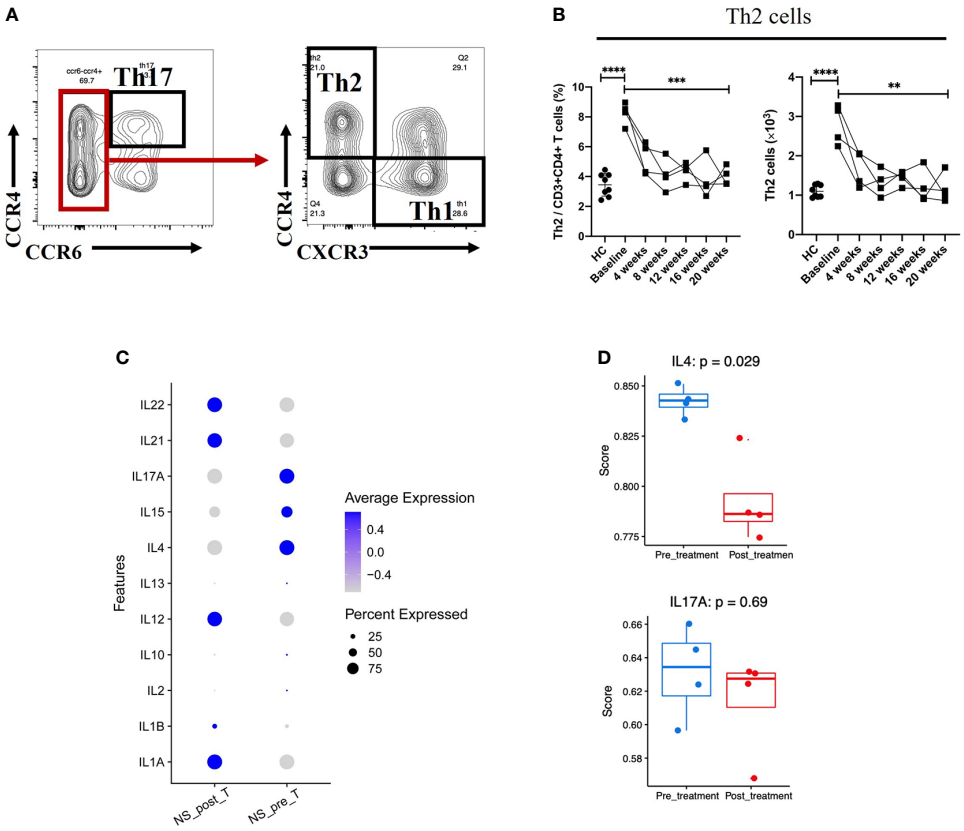

FIGURE 3
Reduction in Th2-mediated inflammation after 20 weeks of dupilumab treatment **(A)** Gating strategy used to identify Th2 and Th17 cells. **(B)** Changes in the percentages of Th2 cells among the CD3+CD4+ T cell population and in the absolute number of Th2 cells from baseline to 20 weeks of dupilumab treatment. **(C)** Dot plot illustrating (the top 11/select key) cytokine expression signatures/patterns of T cells before (pre) and 20 weeks after (post) dupilumab treatmentthe color intensity indicates the relative expression level and the size of the dots represents the percentage of cells expressing the cytokine genes across T cell subsets. **(D)** Quantitative scatter plot with a bar graph revealed the expression level of IL-4 and IL-17A in T cells across treatment conditions. The Wilcoxon matched pairs signed rank test or the Mann-Whitney U test was used to assess statistical significance: ****P < 0.0001; ***P < 0.001; **P < 0.01. Each dot represents a value for each patient.

been tried (4). The results demonstrated that both biologicals targeting Th2 and Th17 pathways appear to be effective in NS, however, the potential mechanisms are not clear (4). A recent research using transcriptomic and proteomic analysis in 13 adult NS patients revealed that IL-17/IL-36 pathways were predominantly activated axes and Th17-driven immune response was mainly involved the NS pathogenesis (14). However, the clinical benefits with using anti-IL-17A antibody for part of NS patients were reported not sustained for long (15), and most NS patients were accompanied by severe atopic diathesis with very high serum IgE levels and allergic responses to environment triggers. In addition, the molecular profiling in above mentioned multiomic study revealed a Th2 predominant signature in a subset of patients characterized by ichthyosis linearis circumflflexa (ILC) (14), suggesting that other biological pathways, including Th2 axis, may be involved in NS pathogenesis.

In present study, 4 pediatric NS patients presented with ILC phenotype, one of them displayed erythroderma at his early age. Immunophenotyping of PBMCs at the baseline revealed increased Th2 subset in all patients, but only slightly increased Th17 cell numbers. After dupilumab treatment, except for sustained symptomatic improvements, a significant decrease in both percentage (among total CD3+CD4+ cells) and absolute number of Th2 cells were observed, suggesting that the Th2 pathway activation contributed to the systemic inflammation in our cohort. This hypothesis is supported by increased IL-4 production in T cell subsets, which could in turn induces B cell proliferation, isotype switching and IgE production (16). What is evident is that after blocking the IL-4Rα by using dupilumab, the elevated serum IgE levels fell steadily in all patients. Although serum IL-4 and IL-5 were detected at normal range as the previous study (17), the serum IL-6 and IL-8 were found to be significantly elevated and followed by a

10.3389/fimmu.2022.1054422

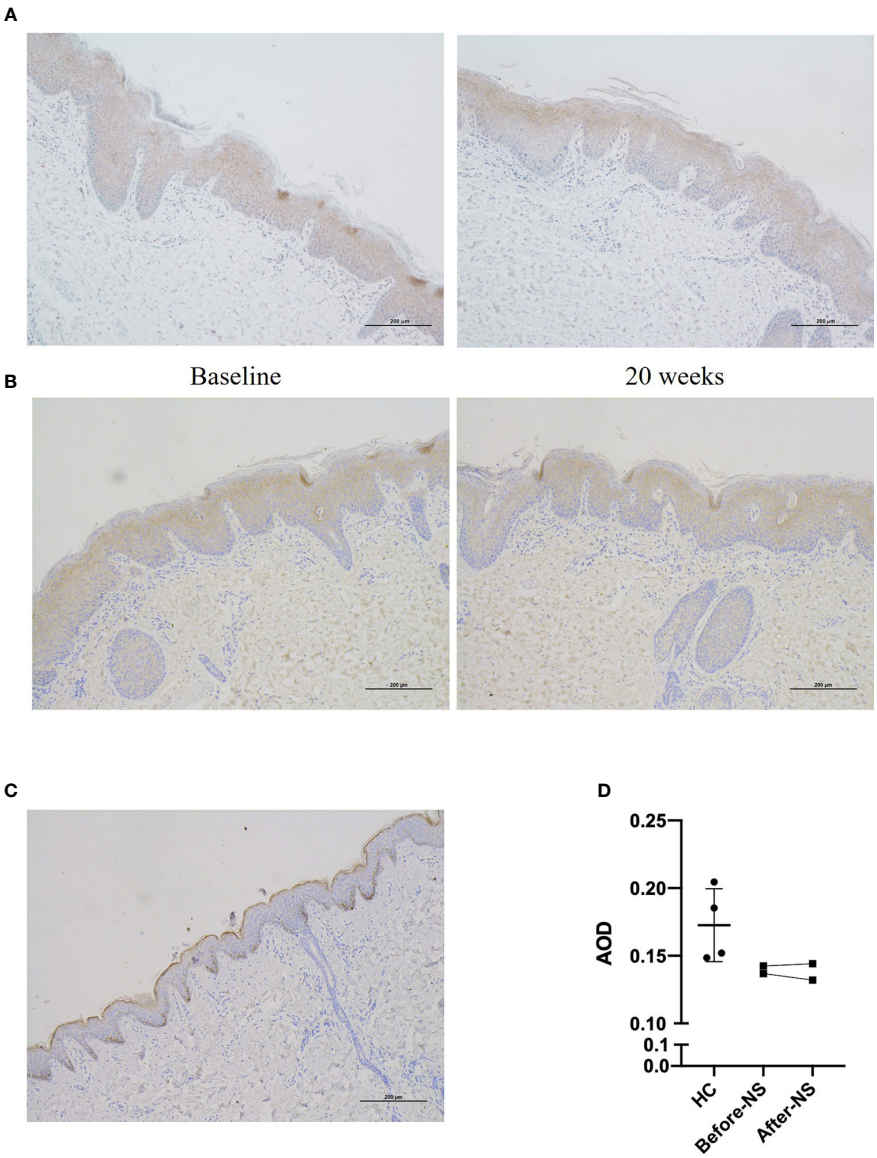

FIGURE 4
Expression of LEKTI protein in skin lesions of patients after 20 weeks of dupilumab treatment **(A, B)** show immunohistochemical staining of skin lesion for LEKTI before and after 20 weeks of dupilumab treatment in patients 1 and 4, respectively. Both patients showed a significant reduction in LEKTI expression compared with that of HCs. **(C)** LEKTI expression in HCs as a positive control: LEKTI is expressed strongly in the cytoplasm of keratinocytes in the epidermal granular and uppermost spinous layers. **(D)** Average optical density (AOD) was analyzed. The results suggest that LEKTI expression was significantly lower in the lesion skin of both patients than that of HCs and there was no obvious change after dupilumab treatment.

gradual decline during the treatment with dupilumab. Studies have shown that IL-6 plays a key role in adaptive immune response, which promotes the maturation of B cells and is considered to be one of the necessary cytokines to induce B cells to secrete IgE antibodies (18, 19), but how it is involved in mediating IgE production in NS patients is unclear. Of note, as a member of the CXC family, IL-8 is primarily responsible for chemotaxis neutrophils into inflammatory tissues (20). This is in good concordance with the recent finding that marked neutrophil skin infiltration in ILC type NS (14). However, the specific role and underlying mechanisms of IL-8 in neutrophil skin infiltration in NS remain to be studied.

We further evaluated the LEKTI protein expression in skin lesions of the NS patients in pre-and-post dupilumab therapy. Unsurprisingly, there were no obvious changes in LEKTI expression were observed, indicating that the improvements in

skin lesions by dupilumab mainly rely on suppression of downstream Th2-mediated inflammation, rather than to regulate or correct underlying LEKTI defects. In regarding to the drug safety, only two patients in this study have reported mild ocular symptoms, which similar to that in treatment of atopic dermatitis, in the entire 20-week treatment period. It goes without saying that dupilumab has accumulated a lot of experience and safety profiles in pediatric population, especially it has recently been approved for children up to 6 months of age (21). Contrarily, IL-17A biologicals Secukinumab and Ixekizumab have not approved for children under 6 years and the safety data for children and infants are scarce. When we face an infant with NS, from the perspective of drug safety, dupilumab has obvious superiority.

Taken together, our results suggest that dupilumab is a safe and effective treatment option for certain subtype of pediatric NS patients, especially with respect to in improving skin symptoms, itching and the quality of life. The possible mechanisms may involve the suppression of the Th2-mediated inflammation, but further studies with larger samples are needed.

Limitations

The study has a small number of recruited patients and the molecular features in skin lesion were not detected, which should be taken into account when drawing conclusions.

Data availability statement

The datasets presented in this study can be found in online repositories. The names of the repository/repositories and accession number(s) can be found below: GEO submission, accession number(GSE214985).

Ethics statement

The studies involving human participants were reviewed and approved by the Ethics Committee of the Children's Hospital of Chongqing Medical University. Written informed consent to participate in this study was provided by the participants' legal guardian/next of kin. Written informed consent was obtained from the individual(s), and minor(s)' legal guardian/next of kin, for the publication of any potentially identifiable images or data included in this article.

Author contributions

Concept and design: XL, HW, SYu, and XB. SYa and XL had full access to all of the data in the study and take responsibility for the integrity of the data and the accuracy of the data analysis. Drafting of the manuscript: SYa, XL, HW and XB. All authors participate in patient enrollment and follow-up.

Funding

This work was supported by grants from the National Natural Science Foundation of China (81703124 & 82173402) and the Excellent Researcher Award Program from Children's Hospital of Chongqing Medical University.

Acknowledgments

We thank the patients and their parents for participating in this study. We would also like to thank Yike Huang, MD. for contributing to the discussion of the scRNA-seq data. None of the contributors were compensated for this work.

Conflict of interest

The authors declare that the research was conducted in the absence of any commercial or financial relationships that could be construed as a potential conflict of interest.

Publisher's note

Supplementary material

The Supplementary Material for this article can be found online at: https://www.frontiersin.org/articles/10.3389/fimmu.2022.1054422/full#supplementary-material

SUPPLEMENTARY FIGURE 1
Observations of hair from the patient 1 under dermoscopy and light microscopy Hair shaft shows typical bamboo nodes under the dermoscopy **(A)** and light microscopy **(B)**.

SUPPLEMENTARY FIGURE 2
Genetic characterization of the patients. **(A)** Family pedigrees of the patients. Male subjects, squares; female subjects, circles; patient, black squares/circles; proband, arrows. **(B)** Sequence analysis of the *SPINK5* gene. The mutations are indicated by the arrow.

SUPPLEMENTARY FIGURE 3
Changes in Th1/17 cell subsets during 20 weeks of dupilumab treatment Changes in the percentage of Th17 cells **(A)** and Th1 cells **(B)** among the CD3+CD4+ T cell population and in the absolute number of Th17 cells **(A)** and Th1 cells **(B)** from baseline to 20 weeks of treatment. **(C)** Changes in the Th2/Th17 ratio from baseline to 20 weeks of treatment. The Wilcoxon matched pairs signed rank test or the Mann-Whitney U test was used to assess statistical significance: ****P < 0.0001; ***P < 0.001; **P < 0.01; and *P < 0.05. Each dot represents a value for each patient.

References

1. Petrova E, Hovnanian A. Advances in understanding of netherton syndrome and therapeutic implications. *Expert Opin Orphan Drugs* (2020) 8(11):455–87. doi: 10.1080/21678707.2020.1857724

2. Chiticariu E, Hohl D. Netherton syndrome: Insights into pathogenesis and clinical implications. *J Invest Dermatol* (2020) 140(6):1129–30. doi: 10.1016/j.jid.2019.11.007

3. Kishibe M. Physiological and pathological roles of kallikrein-related peptidases in the epidermis. *J Dermatol Sci* (2019) 95(2):50–5. doi: 10.1016/j.jdermsci.2019.06.007

4. Nouwen AEM, Schappin R, Nguyen NT, Ragamin A, Bygum A, Bodemer C, et al. Outcomes of systemic treatment in children and adults with netherton syndrome: A systematic review. *Front Immunol* (2022) 13:864449. doi: 10.3389/fimmu.2022.864449

5. Gu C, Wu Y, Luo Y, Wang S, Yin H, Gao Y, et al. Real-world efficacy and safety of dupilumab in Chinese patients with atopic dermatitis: a single-centre, prospective, open-label study. *J Eur Acad Dermatol Venereol.* (2022) 36(7):1064–73. doi: 10.1111/jdv.18109

6. Steuer AB, Cohen DE. Treatment of netherton syndrome with dupilumab. *JAMA Dermatol* (2020) 156(3):350–1. doi: 10.1001/jamadermatol.2019.4608

7. Andreasen TH, Karstensen HG, Duno M, Lei U, Zachariae C, Thyssen JP, et al. Successful treatment with dupilumab of an adult with netherton syndrome. *Clin Exp Dermatol* (2020) 45(7):915–7. doi: 10.1111/ced.14317

8. Aktas M, Salman A, Apti Sengun O, Comert Ozer E, Hosgoren Tekin S, Akin Cakici O, et al. Netherton syndrome: Temporary response to dupilumab. *Pediatr Dermatol* (2020) 37(6):1210–1. doi: 10.1111/pde.14362

9. Inaba Y, Kanazawa N, Muraoka K, Yariyama A, Kawaguchi A, Kunimoto K, et al. Dupilumab improves pruritus in netherton syndrome: A case study. *Children (Basel)* (2022) 9(3):9030310. doi: 10.3390/children9030310

10. Murase C, Takeichi T, Taki T, Yoshikawa T, Suzuki A, Ogi T, et al. Successful dupilumab treatment for ichthyotic and atopic features of netherton syndrome. *J Dermatol Sci* (2021) 102(2):126–9. doi: 10.1016/j.jdermsci.2021.03.003

11. Süßmuth K, Traupe H, Loser K, Ständer S, Kessel C, Wittkowski H, et al. Response to dupilumab in two children with netherton syndrome: Improvement of pruritus and scaling. *J Eur Acad Dermatol Venereol.* (2021) 35(2):e152–5. doi: 10.1111/jdv.16883

12. Wang J, Yu L, Zhang S, Wang C, Li Z, Li M, et al. Successful treatment of netherton syndrome with dupilumab: A case report and review of the literature. *J Dermatol* (2022) 49(1):165–7. doi: 10.1111/1346-8138.16253

13. Hovnanian A. Netherton syndrome: skin inflammation and allergy by loss of protease inhibition. *Cell Tissue Res* (2013) 351(2):289–300. doi: 10.1007/s00441-013-1558-1

14. Barbieux C, Bonnet des Claustres M, Fahrner M, Petrova E, Tsoi LC, Gouin O, et al. Netherton syndrome subtypes share IL-17/IL-36 signature with distinct IFN-α and allergic responses. *J Allergy Clin Immunol* (2022) 149(4):1358–72. doi: 10.1016/j.jaci.2021.08.024

15. Luchsinger I, Knöpfel N, Theiler M, Bonnet des Claustres M, Barbieux C, Schwieger-Briel A, et al. Secukinumab therapy for netherton syndrome. *JAMA Dermatol* (2020) 156(8):907–11. doi: 10.1001/jamadermatol.2020.1019

16. Gandhi NA, Bennett BL, Graham NM, Pirozzi G, Stahl N, Yancopoulos GD, et al. Targeting key proximal drivers of type 2 inflammation in disease. *Nat Rev Drug Discovery* (2016) 15(1):35–50. doi: 10.1038/nrd4624

17. Renner ED, Hartl D, Rylaarsdam S, Young ML, Monaco-Shawver L, Kleiner G, et al. Comèl-netherton syndrome defined as primary immunodeficiency. *J Allergy Clin Immunol* (2009) 124(3):536–43. doi: 10.1016/j.jaci.2009.06.009

18. Eto D, Lao C, DiToro D, Barnett B, Escobar TC, Kageyama R, et al. IL-21 and IL-6 are critical for different aspects of b cell immunity and redundantly induce optimal follicular helper CD4 T cell (Tfh) differentiation. *PloS One* (2011) 6(3):e17739. doi: 10.1371/journal.pone.0017739

19. Garbers C, Aparicio-Siegmund S, Rose-John S. The IL-6/gp130/STAT3 signaling axis: recent advances towards specific inhibition. *Curr Opin Immunol* (2015) 34:75–82. doi: 10.1016/j.coi.2015.02.008

20. Matsushima K, Oppenheim JJ. Interleukin-8: An evolving chemokine. *Cytokine* (2022) 153:155828. doi: 10.1016/j.cyto.2022.155828

21. Paller AS, Simpson EL, Siegfried EC, Cork MJ, Wollenberg A, Arkwright PD, et al. Dupilumab in children aged 6 months to younger than 6 years with uncontrolled atopic dermatitis: a randomised, double-blind, placebo-controlled, phase 3 trial. *Lancet* (2022) 400(10356):908–19. doi: 10.1016/S0140-6736(22)01539-2

frontiers | Frontiers in Immunology

TYPE Original Research
PUBLISHED 20 December 2022
DOI 10.3389/fimmu.2022.1064515

OPEN ACCESS

EDITED BY
Uzma Saqib,
Indian Institute of Technology Indore, India

REVIEWED BY
Hiroyuki Tanaka,
Gifu Pharmaceutical University, Japan
Seung-Hyo Lee,
Korea Advanced Institute of Science and Technology (KAIST), South Korea

*CORRESPONDENCE
Jin Ho Chung
jhchung@snu.ac.kr

†These authors have contributed equally to this work

SPECIALTY SECTION
This article was submitted to Inflammation, a section of the journal Frontiers in Immunology

RECEIVED 08 October 2022
ACCEPTED 05 December 2022
PUBLISHED 20 December 2022

CITATION
Lee Y, Oh J-H, Li N, Jang H-J, Ahn K-S, Oh S-R, Lee DH and Chung JH (2022) Topical Skullcapflavone II attenuates atopic dermatitis in a mouse model by directly inhibiting associated cytokines in different cell types. *Front. Immunol.* 13:1064515. doi: 10.3389/fimmu.2022.1064515

Topical Skullcapflavone II attenuates atopic dermatitis in a mouse model by directly inhibiting associated cytokines in different cell types

Youngae Lee[1,2,3†], Jang-Hee Oh[1,2,3†], Na Li[1,2,3,4], Hyun-Jae Jang[5], Kyung-Seop Ahn[5], Sei-Ryang Oh[5], Dong Hun Lee[1,2,3] and Jin Ho Chung[1,2,3,4*]

[1]Department of Dermatology, Seoul National University College of Medicine, Seoul, Republic of Korea, [2]Institute of Human-Environment Interface Biology, Medical Research Center, Seoul National University, Seoul, Republic of Korea, [3]Laboratory of Cutaneous Aging Research, Biomedical Research Institute, Seoul National University Hospital, Seoul, Republic of Korea, [4]Department of Biomedical Sciences, Seoul National University Graduate School, Seoul, Republic of Korea, [5]Natural Medicine Research Center, Korea Research Institute of Bioscience and Biotechnology, Cheong-ju, Chungcheongbuk-do, Republic of Korea

Skullcapflavone II (SFII), a flavonoid derived from *Scutellaria baicalensis*, is an anticancer agent. We aimed to validate SFII for atopic dermatitis (AD) therapy by demonstrating the anti-inflammatory effects of SFII in an AD mouse model produced by the topical application of the vitamin D3 analog MC903. We showed that topical treatment with SFII significantly suppressed MC903-induced serum IgE levels compared with topical hydrocortisone (HC) treatment. Topical SFII also prevents MC903-induced pruritus, skin hyperplasia, and inflammatory immune cell infiltration into lesional skin comparable to topical HC. In addition, MC903-induced immune cell chemoattractants and AD-associated cytokine production in skin lesions were effectively suppressed by topical SFII. The production of MC903-induced effector cytokines influencing T helper (Th)2 and Th17 polarization in lesioned skin is significantly inhibited by topical SFII. Furthermore, we showed that SFII can directly inhibit the production of AD-associated cytokines by human primary keratinocytes, mouse bone marrow-derived cells (BMDCs), and mouse $CD4^+$ T cells *in vitro*. Lastly, we demonstrated that topical SFII more effectively suppressed serum IgE levels, the production of IL-4 and thymic stromal lymphopoietin (TSLP), and infiltration of $CD4^+$ T cells and $Gr\text{-}1^+$ cells (neutrophils) into lesion skin compared to topical baicalein (a flavonoid derived from *Scutellaria baicalensis*), which has anti-inflammatory effects. Taken together, our findings suggest that SFII may have promising therapeutic potential for this complex disease *via* the regulation of multiple AD-associated targets.

KEYWORDS

Skullcapflavone II, atopic dermatitis, pruritus, Th2 cytokines, IgE

Introduction

Atopic dermatitis (AD) is a common chronic inflammatory skin disease characterized by complex pathogenesis and a wide spectrum of clinical phenotypes presenting with underlying skin barrier dysfunction, immune dysregulation, and pruritus (1–3). It has been reported that epidermal barrier disruption and activation of epidermal dendritic cells (DCs) lead to T helper 2 (Th2)-type immune responses (IL-4 and IL-13), which are mostly activated in patients with AD. In addition, strong activation of Th1 (IFN-γ) and Th17 (IL-17A, IL-6, and S100A8) immune responses have been reported in Asian patients with AD (4–6). A previous study has shown that common AD transcriptomes such as *S100A8/A9/A12* and *CXCL1* are increased in the lesioned skin of patients with moderate-to-severe AD by RNA-sequencing and microarray analyses (7). The secretion of chemokines (e.g., CXCL1,2,5 and CCLs) by keratinocytes is involved in the infiltration of immune cells such as T cells, mast cells, basophils, and neutrophils (8). Lesional skin infiltration by these immune cells has been shown to further promote AD-associated inflammatory cascades, and itching, as well as epidermal and dermal hyperplasia (9–11). Thus, AD is a complex and heterogeneous inflammatory skin disease (12–14). Numerous therapeutic drugs for the treatment of AD have been developed and are currently under clinical investigation to identify novel therapeutic targets for more effective long-term control of complex AD (1).

The calcipotriol (MC903)-induced AD mouse model is well established and is widely used for research on the pathophysiology of human AD (15, 16). The MC903 model is ideal for experimental approaches because of its highly reproducible phenotypes that closely resemble human AD and its ability to induce the development of lesions and itching (17). The underlying cellular and molecular mechanism of MC903-induced AD-like inflammation are well known. MC903 initially induces the secretion of an alarmin, thymic stromal lymphopoietin (TSLP), from keratinocytes through a cell autonomous event dependent on retinoid X receptor/vitamin D receptor (15), which then induces orchestrated DC-T cells-basophils-T cells cascade-derived Th2-type immune responses by stimulating IL-4 and IL-13 production by $CD4^+$ T cells in skin-draining lymph nodes (15, 18). Therefore, TSLP is considered a key initiation factor for exacerbated Th2 responses and is thought to be one of the therapeutic targets in AD. A recent study has shown that TSLP directly promotes pathogenic Th2 cell differentiation (19). TLSP also mediates the expansion of functionally distinct basophils, which promote Th2-type immune responses (20). In addition, MC903-induced neutrophil infiltration into the lesional skin causes enhanced expression of itching-associated molecules and inflammatory cytokines, leading to chronic itch and inflammation (9). Moreover, IL-4 and IL-13 are crucially involved in the direct activation of sensory neurons in humans and mice, leading to chronic itching through the activation of their neuronal receptors (21). It has also been reported that MC903 induces high concentrations of serum immunoglobulin E (IgE), as observed in extrinsic AD pathology (22, 23). IL-4 produced by activated $CD4^+$ T cells and mast cells also promotes the production of serum IgE by activating B cells and plasma cells, which mediate hypersensitivity reactions in allergic diseases such as AD and asthma (24–26).

We have previously shown that skullcapflavone II (SFII), a flavonoid derived from *Scutellaria baicalensis*, inhibits the production of thymus and activation-regulated chemokine (TARC/CCL17) and macrophage-derived chemokine (MDC) in HaCaT cells, following stimulation with TNF-α and IFN-γ (27). It has been reported that plasma levels of TARC and MDC are elevated in patients with AD, which is strongly correlated with disease severity (28, 29). The flavonoid, baicalein, is another active component derived from *Scutellaria baicalensis* and has been reported to have anti-inflammatory effects in atopic dermatitis in NC/Nga mice (30). Thus, these results prompted us to explore the novel possibility of using SFII as a safe and effective therapeutic agent against AD.

In this study, we clarified the therapeutic effects of SFII in AD using an MC903-induced AD-like mouse model. In addition, we demonstrated the direct inhibitory effects of SFII on the production of AD-associated cytokines by human primary keratinocytes and mouse immune cells *in vitro*.

Materials and methods

Antibodies and reagents

Antibodies against p-STAT1 (sc-7988) and t-STAT1 (sc-592) were purchased from Santa Cruz Biotechnology Inc. (Santa Cruz, CA, USA). Antibodies against p-p65 (CST3031S), t-p65 (CST8242S), p-ERK1/2 (CST9101S), t-ERK1/2 (CST9102S), p-JNK (CST9251S), t-JNK (CST9252S), p-p38 (CST9211S), and t-p38 (CST9212S) were purchased from Cell Signaling Technology Inc. (Danvers, MA, USA). Horseradish peroxidase-conjugated polyclonal secondary antibodies against mouse, rabbit, or goat IgG (GeneTex, Inc., Irvine, CA, USA) were also purchased. Antibodies against mouse CD4 (Clone 4SM95) and mouse Gr-1 (Clone RB6-8C5) were purchased from Invitrogen (Carlsbad, CA, USA) and R&D Systems (Minneapolis, MN, USA), respectively. The mouse eosinophil antibody (Clone BMK-13) was purchased from Novus Biologicals (Littleton, CO, USA). Inhibitors SB203580 (p38 inhibitor), SP600125 (JNK inhibitor), U0126 (MEK1 inhibitor), and MC903 were purchased from Tocris (Bristol, UK), and InSolution™ JAK inhibitor I and BAY 11-7082 (NF-κB inhibitor) were purchased from Calbiochem (San Diego, CA, USA). SFII was obtained from the Korea Research Institute of Bioscience and Biotechnology (KRIBB, Daejeon, South Korea) (31). Baicalein and hydrocortisone were purchased from

Sigma-Aldrich (St. Louis, MO, USA). Poly(I:C), peptidoglycan (PGN), and lipopolysaccharide (LPS) were purchased from *In vivo* Gen (San Diego, CA, USA).

Mice

Female BALB/c mice, 6–8 weeks old, were purchased from Koatech (Pyeongtaek, Korea), and maintained under specific pathogen-free conditions. All animal experiments were approved by the Seoul National University Hospital Institutional Animal Care and Use Committee (No. 20-0112-S1A0) and were performed in accordance with the Guidelines for the Care and Use of Laboratory Animals at Seoul National University Hospital.

MC903-induced AD-like skin inflammation in mice

In the MC903-induced AD-like model, 1.0 nmol of MC903 in 25 μl ethanol were topically applied on both ears for 7 days. After 2 h, both ears were topically treated with 25 μl of SFII, baicalein, HC, or ethanol (vehicle control). After 7 consecutive days, the ears were topically treated with SFII, baicalein, HC, or ethanol (vehicle control) daily without MC903. MC903 or compounds were dissolved in 100% ethanol. The ear thickness was measured daily using a digital caliper (Mitutoyo Corp., Tokyo, Japan). At the end of the experiment on day 13, the ear skin was snap-frozen in liquid nitrogen for RNA and protein isolation, and the ear was embedded in OCT compounds to prepare frozen sections. The number of scratch bouts were monitored and quantified for 30 min. One bout of scratching was defined as an episode in which a mouse lifted its paw and scratched continuously for any length of time, until the paw was returned to the floor (32). Scratching counts were assessed with the investigator blinded to the groups.

Histology, immunofluorescence analysis, and toluidine blue staining

Ear skin was fixed in 4% paraformaldehyde at 4°C overnight, paraffin-embedded, sectioned into 4 μm, and stained with hematoxylin and eosin (H&E). Images were acquired using a microscope. Epidermal and dermal thicknesses were measured using ImageJ software (NIH). For immunofluorescence, ear tissue sections were blocked in pre-blocking solution (GBI Labs, Bothell, WA, USA) and stained with the indicated primary antibodies at 4°C overnight. After washing, the sections were incubated with Alexa Fluor 488- or Alexa Fluor 594-conjugated secondary antibodies at 25°C for 1 h and stained with 4′-6-diamidino-2-phenylindole dihydrochloride (Thermo Fisher Scientific, Waltham, MA, USA) at 25°C for 5 min. Images were acquired using a confocal microscope (Leica STED CW; Leica Microsystems, Mannheim, Germany). For the detection of mast cells, ear sections were stained with 0.5% toluidine blue at room temperature for 15 min and then washed three times in PBS. Images were acquired using a microscope. The number of immune cells was counted every five fields (40× objective), and the average was calculated.

Quantitative PCR

Total RNA from the ear skin was isolated using RNAiso Plus (Takara Bio Inc., Shiga, Japan) according to the manufacturer's instructions. Then, 1.0 μg of total RNA was used for cDNA synthesis using the First Strand cDNA Synthesis Kit (Thermo Fisher Scientific). Quantitative RT-PCR was carried out using SYBR Premix (Bioneer, Daejeon, Korea) and quantitatively measured with an ABI Real-Time PCR instrument (ABI, Indianapolis, IN, USA). Each sample was analyzed in duplicate and the relative expression of mRNA was normalized to that of the housekeeping gene 36B4.

ELISA

Serum IgE levels were measured using ELISA according to the manufacturer's protocol (BioLegend, San Diego, CA, USA). The level of *in vivo* cytokine production in mice was measured using ELISA according to the manufacturer's protocol (BioLegend). Additionally, the level of human TSLP in the cell culture supernatants was determined by ELISA according to the manufacturer's protocol (R&D Systems).

Western blot analysis

Human primary keratinocytes were pretreated with SFII for 30 min, then stimulated with 10 μg/ml poly(I:C) for 3 h. Cells were washed with PBS, lysed with 1×TNE buffer (20 mM Tris-HCl, 150 mM NaCl, 1 mM EDTA, and 1% NP-40) containing complete mini protease inhibitor cocktails (Roche Applied Science, Indianapolis, IN, USA) and phosphatase inhibitor cocktails (Sigma-Aldrich), and heated at 95°C for 5 min. Equal amounts of cell lysate were separated on a 10% SDS-polyacrylamide gel by electrophoresis and transferred onto a nitrocellulose membrane (GE Healthcare, Chicago, IL, USA). Equal protein transfer was confirmed by Ponceau S staining (ELPIS Biotech, Daejeon, South Korea). The membranes were blocked with 5% skim milk in Tris-buffered saline with 0.1% Tween® 20 (TBS-T) and probed overnight with the indicated primary antibodies at 4°C. After washing with TBS-T, the membranes were probed with HRP-conjugated secondary

antibodies for 1 h at 25°C and visualized using WestGlow™ PICO PLUS or FEMTO chemiluminescent substrates (Biomax Co., Ltd., Seoul, Korea) using a CCD imaging system (Amersham Imager 680, GE Healthcare). Only the data with unsaturated signals were used in the analysis.

Human primary keratinocytes

Human epidermal keratinocytes were isolated as described previously (33). Human epidermal keratinocytes were cultured in a keratinocyte growth medium (KBM™ Gold™ Basal Medium; Lonza, Basel, Switzerland) supplemented with KGM™ Gold™ SingleQuots™ supplements (Lonza). Human epidermal keratinocytes were used at the third or fourth passage. Human primary keratinocytes were isolated from the epidermis of juvenile foreskin from two donors.

Generation of bone marrow cell-derived DCs

Bone marrow (BM) cells were collected from the femurs and tibias of the BALB/c mice. BM-derived dendritic cells (BMDCs) were generated by culturing BM cells from mice in complete RPMI 1640 supplemented with 20 ng/ml recombinant murine GM-CSF (PeproTech, Rocky Hill, NJ) (34, 35). Nonadherent cells were harvested on day 6 and stimulated for 24 h with TLR agonists, PGN or LPS (*In vivo*Gen), in the presence of vehicle or SFII. BMDC culture supernatants were collected and analyzed for cytokine production by ELISA.

Isolation and activation of mouse $CD4^+$ T cells

Mouse $CD4^+$ T cells from the spleen were isolated using magnetic activated cell sorting (MACS) LS columns, following the manufacturer's instructions (Miltenyi Biotec, Bergisch Gladbach, North Rhine-Westphalia, Germany). For mouse T cell proliferation assays, purified $CD4^+$ T cells were labeled with 1 mM CFSE (Invitrogen), according to the manufacturer's protocol. T cells (2×10^5) were stimulated with plate bound anti-CD3ε (5 μg/ml, clone 145-2C11) and soluble anti-CD28 (2 μg/ml, clone 37.51) antibodies for 72 h, in the presence of vehicle or SFII (36). The intensity of CFSE was analyzed using a FACSCanto II flow cytometer (BD Biosciences, San Jose, CA, USA).

Statistical analysis

Statistical analyses were performed using Prism 9.0 software (GraphPad Software, La Jolla, CA, USA). Dunnett's multiple range test was used to compare differences between two groups. Two-way ANOVA was used to compare differences between multiple groups. All graphs are presented as the mean ± standard error. The threshold for statistical significance was set at $P < 0.05$.

Results

Topical SFII attenuates MC903-induced AD-like skin inflammation

In this study, we examined the therapeutic efficacy of SFII on AD-like skin inflammation using an AD mouse model established by repeated topical application of MC903 on mouse skin. Mice ears were treated daily with MC903 for 7 days, followed by topical treatment with ethanol (100% EtOH, vehicle control), SFII, or HC (hydrocortisone, therapeutic control) for 13 days (Figure 1A). Among the vehicle-only, MC903/vehicle-, MC903/SFII-, and MC903/HC-treated groups, MC903/vehicle-treated groups developed more severe reddening and erythema of the ears compared to the other groups on days 7 and 12 (Figures 1B, C). In contrast, treatment with SFII attenuated skin inflammation and clinical score, which was comparable to that of HC, a widely used treatment for AD (Figures 1B, C). AD-like skin inflammation and ear thickening were initiated by the topical application of MC903 from day 3 (Figure 1D). However, treatment with SFII significantly suppressed MC903-induced ear thickening, as measured by a digital caliper from day 7, indicating the potential therapeutic effect of SFII on AD (Figure 1D).

Topical SFII significantly attenuates MC903-induced pruritus and serum IgE

As pruritus and elevated levels of serum IgE are the main features of AD, we examined the effects of topical application of SFII on scratching behavior and serum IgE levels in an MC903-induced AD-like mouse model. We monitored the scratching behaviors of mice on day 13 for 30 min and found that treatment with SFII significantly suppressed MC903-induced scratching bouts, which was comparable to treatment with HC (Figure 1E). Total serum IgE levels on day 13 were significantly reduced in SFII-treated ears but not in HC-treated ears, which was comparable to the vehicle-only control group (Figure 1F). To test the dose-dependent effects of SFII on MC903-induced AD-like skin inflammation, we analyzed ear thickening, inflammation, pruritus, and total IgE levels in mouse ears treated with 0.1%, 0.5%, or 1.0% SFII. Treatment with 1.0% SFII was more effective in suppressing AD-like inflammation than treatment with 0.1% or 0.5% SFII (Figures S1A–F). Therefore, we evaluated the effects of 1.0% SFII on AD-like inflammation in mice.

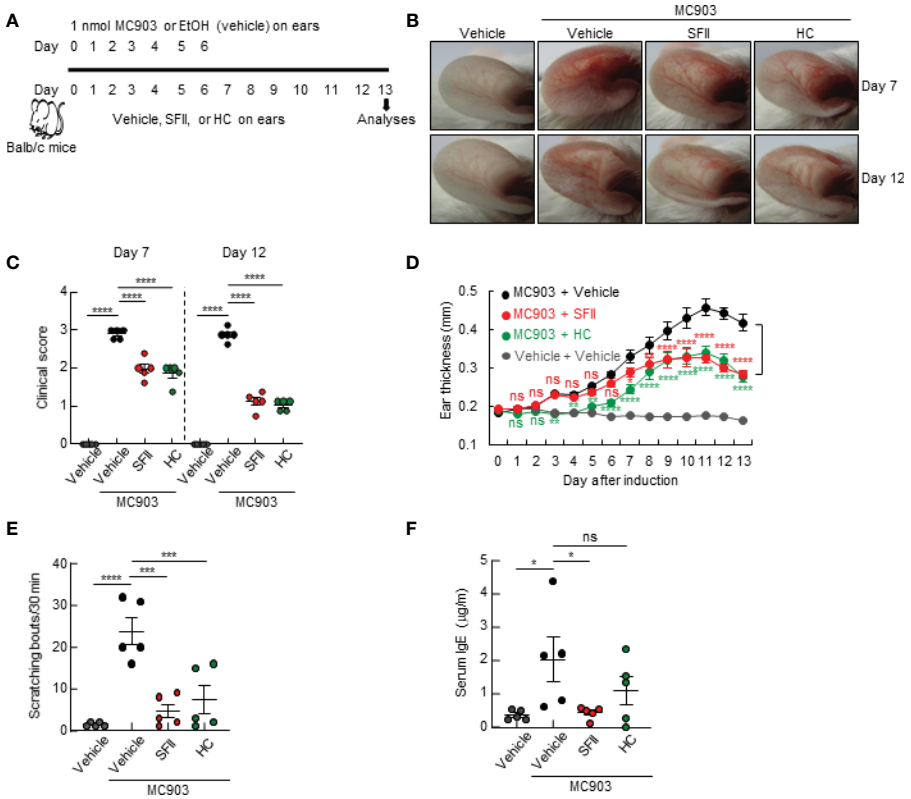

FIGURE 1
Topical SFII attenuates MC903-induced AD-like skin inflammation and pruritus **(A)** Experimental protocol of MC903-induced ear skin inflammation in BALB/c mice treated with vehicle, SFII, or HC. **(B)** MC903-induced ear skin inflammation of BALB/c mice treated with SFII, or HC on days 7 and 12. **(C)** Clinical scores of MC903-induced ear skin inflammation of BALB/c mice treated with vehicle, SFII, or HC on days 7 and 12. **(D)** Measurement of ear swelling in BALB/c mice treated with MC903 plus vehicle, SFII, or HC using a digital caliper. **(E)** Scratching bouts of BALB/c mice treated with MC903 plus vehicle, SFII, or HC on day 13. **(F)** ELISA analysis of serum IgE levels on day 13.The data are representative of the mean ± SEM of three independent experiments, with five mice per group. ns., not significant; *p < 0.05, **p < 0.01, ***p < 0.001 and ****p < 0.0001.

Topical SFII reduces MC903-induced ear thickening and immune cell infiltration

To determine the effects of the topical application of SFII on infiltration of immune cells, including $CD4^+$ T cells, neutrophils, eosinophils, and mast cells to the site of the skin lesion, we performed H&E staining, immunofluorescence analysis, and toluidine blue staining. Histological analysis revealed that MC903/SFII-treated ears had significantly reduced epidermal and dermal thickness compared to MC903/vehicle-treated ears, which was comparable to that of HC-treated ears (Figures 2A–C). Infiltration of immune cells such as $CD4^+$ T cells, Gr-1^+ cells (neutrophils), mast cells, and eosinophils into lesion skin was significantly attenuated in SFII-treated ears compared to MC903/vehicle-treated ears (Figures 2D–G, S2A, B). Moreover, topical application of SFII was comparable to treatment with HC in suppressing immune cell infiltration to the skin lesions (Figures 2D–G, S2A, B).

Topical SFII suppresses MC903-induced AD-associated cytokine production

Next, we examined the effects of topical application of SFII on AD-associated cytokine production in the skin lesions of the ears. Using ELISA, we analyzed the production of Th2 cytokines, including TSLP and IL-4, which are upregulated in AD lesions. We found that topical application of SFII significantly suppressed the production of TSLP and IL-4 in ear skin compared with MC903/vehicle-treated skin (Figures 3A, B). The production of IL-6, which is known to be required for Th17 cell polarization, was also significantly reduced in MC903/SFII-treated skin compared to that in MC903/vehicle-treated

10.3389/fimmu.2022.1064515

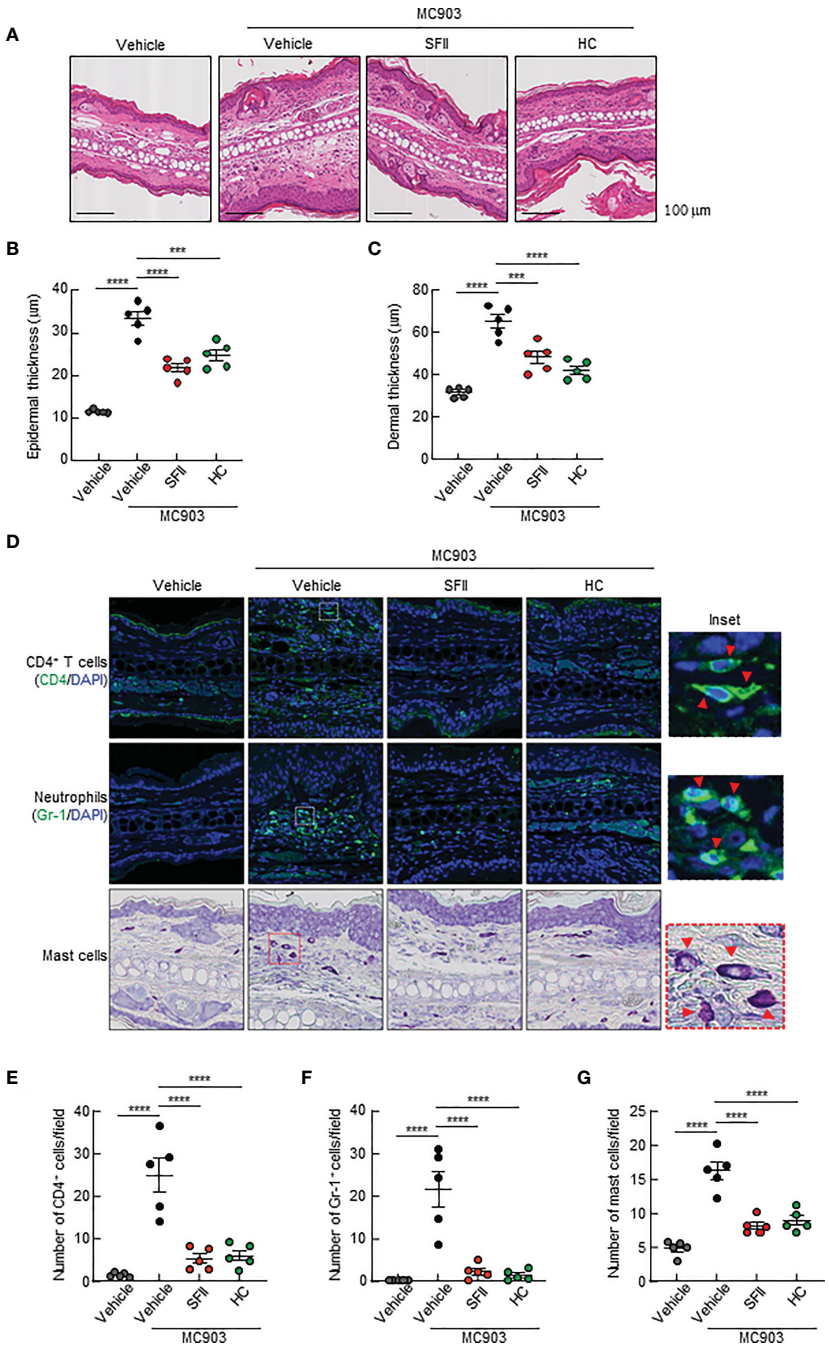

FIGURE 2
Topical SFII reduces MC903-induced ear thickening and immune cell infiltration **(A)** H&E staining of ear sections from BALB/c mice treated with vehicle, MC903 plus vehicle, SFII, or HC on day 13. **(B)** Epidermal thicknesses determined from H&E-stained ear sections. **(C)** Dermal thicknesses determined from H&E-stained ear sections. **(D)** Immunofluorescent labeling of CD4 and Gr-1, and toluidine blue staining of mast cells in ear sections on day 13. **(E)** Quantitation of $CD4^+$ T cells in immunofluorescent-labeled ear sections. **(F)** Quantitation of $Gr\text{-}1^+$ cells in immunofluorescent-labeled ear sections. **(G)** Quantitation of mast cells in toluidine blue-stained ear sections. All images represent five mice per group and all graphs represent three independent experiments with five mice in each group. ***$p < 0.001$ and ****$p < 0.0001$.

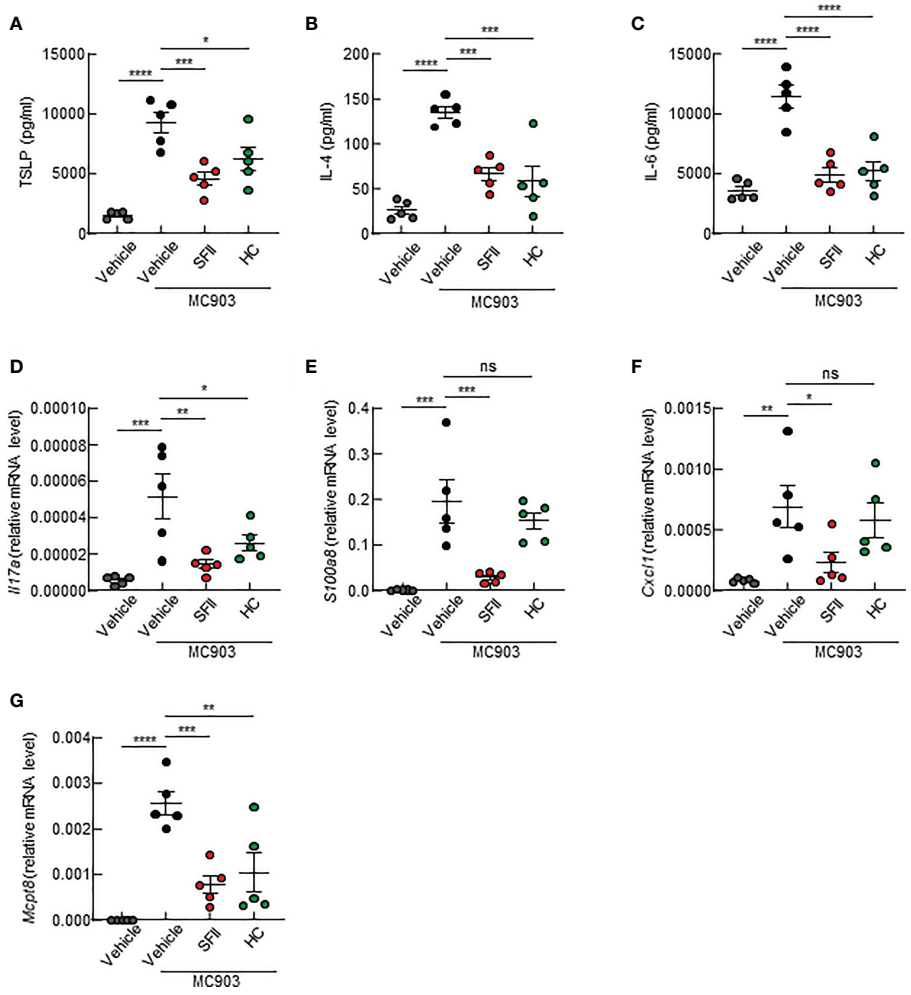

FIGURE 3
Topical SFII suppresses the production of AD-associated cytokines in ear skin induced by MC903 **(A–C)** ELISA analysis of TSLP **(A)**, IL-4 **(B)**, and IL-6 **(C)** levels in ear skin of BALB/c mice treated with MC903 plus vehicle, SFII, or HC on day 13. **(D, E)** Relative mRNA expression of *Il17a* **(D)** and *S1008a* **(E)** involved in keratinocyte proliferation on day 13. **(F)** Relative mRNA expression of *Cxcl1* involved in neutrophil recruitment on day 13. **(G)** Relative mRNA expression of *Mcpt8*, a basophil marker on day 13. All graphs represent the mean ± SEM of three independent experiments with five mice in each group. ns., not significant; *p < 0.05, **p < 0.01, ***p < 0.001 and ****p < 0.0001.

skin (Figure 3C). High levels of IL-17A (Th17 cytokine) and S100a8 (a Th17/22-related product) have also been reported in patients with AD (37, 38). Q-PCR analysis showed that the mRNA expression levels of *Il17a* and *S100a8* in MC903/SFII-treated skin were significantly lower than those in MC903/vehicle-treated skin (Figures 3D, E). Interestingly, treatment with SFII was more effective in suppressing the expression of *Il17a* and *S100a8* than treatment with HC (Figures 3D, E). Treatment with SFII also significantly suppressed the mRNA expression of *Cxcl1* (a neutrophil chemoattractant) and *Mcpt8* (a basophil marker) (Figures 3F, G). MC903-induced *Ccl7* expression (an eosinophil chemoattractant) was significantly inhibited by SFII (Figure S2E). However, treatment with MC903 had no effect on the expression of other eosinophil chemoattractants such as *Il5*, *Ccl11*, and *Ccl17* nor on the production of IL-5 in the lesioned skin (Figures S2C, D, F, G).

SFII significantly inhibits TSLP production from human primary keratinocytes *in vitro*

As we observed significantly attenuated TSLP production in topical SFII-treated mouse skin (Figure 3A), we examined the effects of SFII on poly(I:C)-induced TSLP production in human primary keratinocytes *in vitro*. TSLP levels in both the cell lysate and cell culture supernatants were determined using Q-PCR analysis and ELISA, respectively. The data showed that

treatment with SFII significantly and dose-dependently attenuated the mRNA and protein levels of TSLP induced by poly (I:C) (Figures 4A, B). To assess the molecular mechanisms by which poly(I:C) induces TSLP expression, we analyzed poly (I:C)-induced TSLP production in the presence or absence of the indicated inhibitors, including JAK inhibitor I, BAY11-7082 (a NF-κB inhibitor), U0126 (a MEK inhibitor), SB203580 (a p38 MAPK inhibitor), or SP600125 (a JNK inhibitor) (Figure 4C). The ELISA data showed that TSLP production was significantly and dose-dependently suppressed by the JAK I inhibitors, BAY11-7082, U0126, SB203580, and SP600125, indicating that TLSP production is dependent on STAT1, NF-κB, ERK1/2, p38 MAPK, and JNK signaling pathways (Figure 4C). Additionally, we identified the effect of SFII on the activation of these signaling molecules involved in Poly(I:C)-induced TSLP production and found that high doses of SFII markedly and significantly inhibited Poly(I:C)-induced phosphorylation of STAT1, ERK1/2, p38 MAPK, and JNK (Figure 4D, S3A, C–F). However, the poly (I:C)-induced phosphorylation of p65 was slightly reduced by a high dose of SFII (Figures 4D, S3B).

SFII directly inhibits AD-associated cytokine production in mouse BMDCs and CD4$^+$ T cells *in vitro*

Furthermore, we aimed to determine whether SFII could directly inhibit the activation of immune cells or whether reduced TSLP production by SFII causes attenuated activation of inflammatory immune cells *in vivo*. Because CD4$^+$ T cells are mainly involved in MC903-induced AD-like skin inflammation, we isolated CD4$^+$ T cells from the mouse spleen and stimulated them with anti-CD3/CD28 antibodies for 3 days in the presence of different concentrations of SFII. The ELISA data showed that treatment with SFII significantly and dose-dependently suppressed the production of IL-4 and IFN-γ induced by anti-CD3/CD28 antibodies (Figures 4E, F). These data suggest that SFII contributes to the attenuation of AD-like inflammation by directly blocking the production of IL-4 and IFN-γ by CD4$^+$ T cells. However, the production of IL-17Ainduced by anti-CD3/CD28 antibodies was not affected by SFII treatment (Figure 4G), suggesting that SFII-induced decline in IL-17A production in mouse skin may be caused by secondary effects. In addition, carboxyfluorescein diacetate succinimidyl ester (CFSE) cell division analysis showed that treatment with SFII significantly and dose-dependently prevented CD4$^+$ T cell proliferation (Figure 4H).

Since dendritic cells (DCs) are mainly involved in MC903-induced AD-like skin inflammation, we determined the effect of SFII on BMDC activation. We generated mouse BMDCs in the presence of GM-CSF for 6 days and then stimulated BMDCs with the TLR agonists PGN (*S. aureus*) or LPS (*K12*) in the presence of different concentrations of SFII. The ELISA data revealed that treatment with SFII significantly and dose-dependently attenuated IL-6 and IL-12 production induced by PGN or LPS in BMDCs (Figures 4I–L), indicating that treatment with SFII also directly suppresses the activation of dendritic cells.

Topical SFII is more effective at suppressing serum IgE, IL-4, and TSLP production than topical baicalein

A previous study showed that topical baicalein, a compound from *Scutellaria baicalensis*, significantly reduces immune cell infiltration and skin thickening in the AD tissues of NC/Nga mice (30). In addition, intraperitoneal or oral administration of baicalein has been shown to inhibit histamine- or compound 48/80-induced scratching behavior in mice (39, 40). We compared the therapeutic efficacy of SFII (1.0%) and baicalein (0.72%) at the same molar concentration (26.7 mM) in MC903-induced AD-like skin inflammation. Topical treatment with SFII or baicalein suppressed reddening, erythema, and swelling on day 13 (Figures 5A, B). Scratching bouts were also significantly suppressed in both SFII- and baicalein-treated mice with comparable effects (Figure 5C). However, topical treatment with SFII was more effective in suppressing serum IgE levels (Figure 5D) and production of TSLP and IL-4 (Figures 5H, I) compared to topical treatment with baicalein. Histological analysis revealed that topical treatment with SFII and baicalein reduced epidermal and dermal thickness compared to the MC903/vehicle-treated group (Figures 5E–G). However, topical treatment with SFII more effectively suppressed epidermal and dermal thickness than treatment with baicalein (Figures 5E–G). Moreover, immunofluorescence analysis and toluidine blue staining showed that infiltration of CD4$^+$ T cells, Gr-1$^+$ cells (neutrophils), and mast cells into lesion skin was significantly attenuated in SFII-, baicalein-, or HC-treated ears compared to MC903/vehicle-treated ears (Figures 6A–D). However, topical treatment with SFII more effectively suppressed infiltrating CD4$^+$ T cells, Gr-1$^+$ cells (neutrophils), and mast cells than baicalein (Figures 6A–D). The topical application of SFII was comparable to treatment with HC in suppressing immune cell infiltration into the skin lesions (Figures 6A–D).

Discussion

To date, topical glucocorticoids and the topical calcineurin inhibitor, tacrolimus, have been used as first-line therapies to treat patients with moderate-to-severe forms of AD (41, 42). However, the long-term use of immunosuppressive agents and glucocorticoids has been reported to cause multiple side effects (42–45). Therefore, the discovery of safe and effective therapeutics against AD is essential. Here, we showed that SFII, a flavonoid derived from *Scutellaria baicalensis*, is a

10.3389/fimmu.2022.1064515

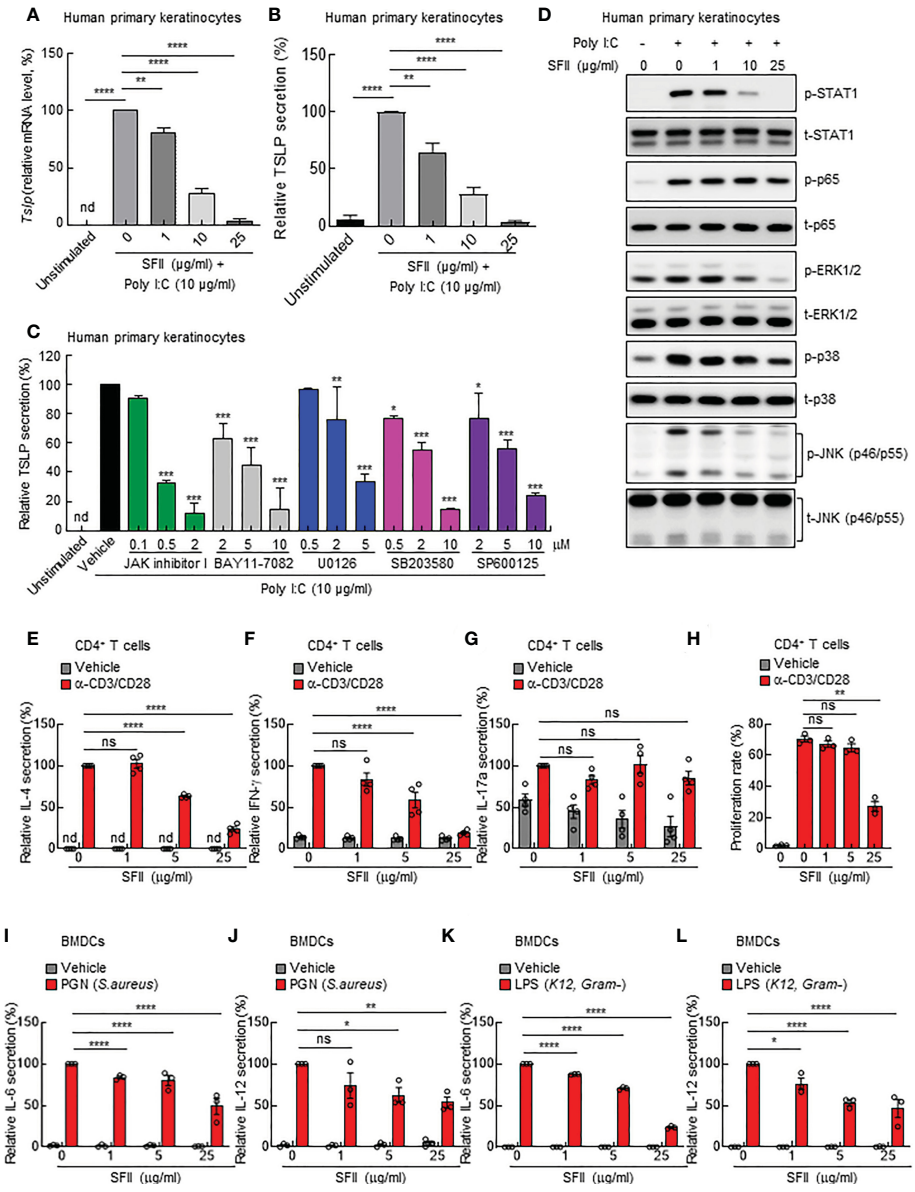

FIGURE 4
SFII directly inhibits AD-associated cytokine production from human primary keratinocytes, mouse CD4$^+$ T cells, and mouse BMDCs *in vitro* **(A)** Relative mRNA expression of TSLP in human primary keratinocytes stimulated with poly(I:C) plus vehicle or different doses of SFII for 6 h. **(B)** ELISA analysis of TSLP production in culture supernatant of human primary keratinocytes stimulated with poly(I:C) plus vehicle or different doses of SFII for 24 h. **(C)** ELISA analysis of TSLP production in culture supernatants of human primary keratinocytes stimulated with poly(I:C) plus vehicle or the indicated inhibitors at different doses. **(D)** Immunoblotting analysis of the expression levels of p-STAT1, t-STAT-1, p-p65, t-p65, p-ERK, t-ERK, p-p38, t-p38, p-JNK, and t-JNK in the total protein from human primary keratinocytes stimulated with poly(I:C) plus vehicle or different doses of SFII for 3 h. **(E–G)** ELISA analysis of IL-4 **(E)**, IFN-γ **(F)** and IL-17A **(G)** production in culture supernatants of mouse CD4$^+$ T cells stimulated with anti-CD3 (5 μg/ml) and anti-CD28 (2 μg/ml) antibodies plus vehicle or different doses of SFII for 72 h. **(H)** Quantification of CFSE analysis of mouse CD4$^+$ T cells stimulated with anti-CD3 (5 μg/ml) and anti-CD28 (2 μg/ml) antibodies plus vehicle or different doses of SFII for 72 h. **(I, J)** ELISA analysis of IL-6 **(I)** and IL-12 **(J)** production in mouse BMDC culture supernatants stimulated with PGN plus vehicle or different doses of SFII for 24 h. **(K, L)** ELISA analysis of IL-6 **(K)** and IL-12 **(L)** production in mouse BMDC culture supernatant stimulated with LPS plus vehicle or different doses of SFII for 24 h. All graphs represent the mean ± SEM from three or four independent experiments. nd., not detected; ns., not significant; *p < 0.05, **p < 0.01, ***p < 0.001 and ****p < 0.0001.

10.3389/fimmu.2022.1064515

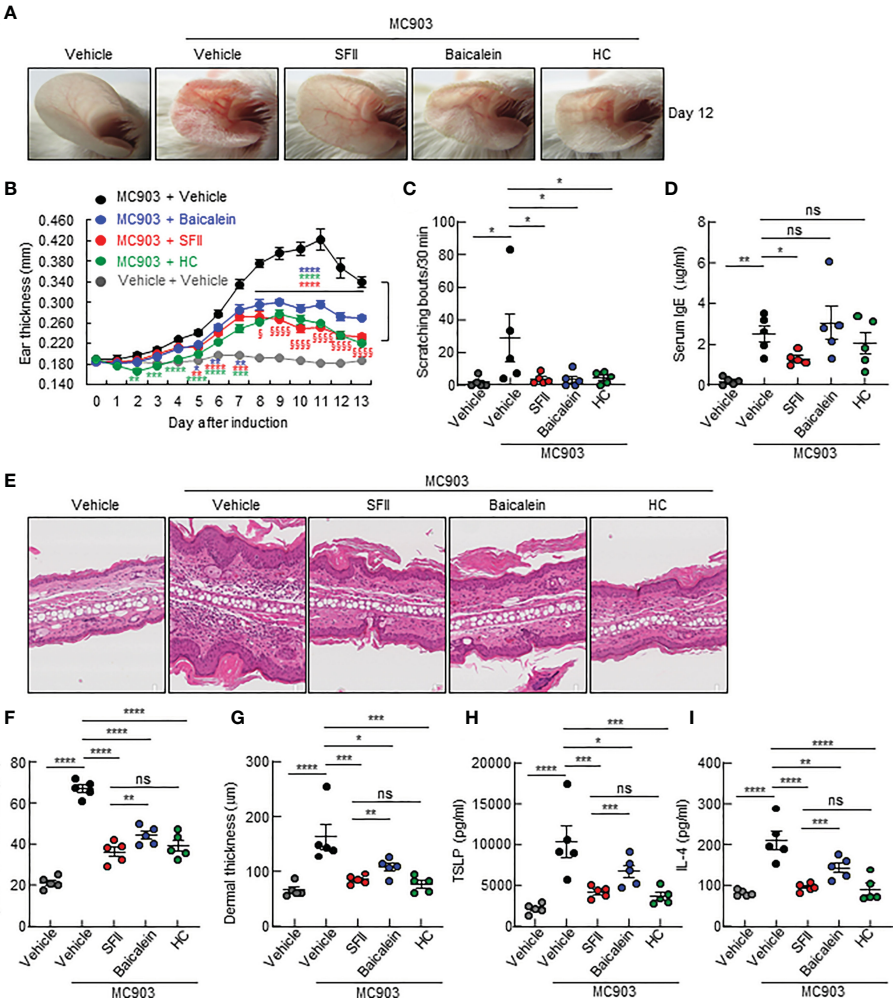

FIGURE 5
Topical SFII is more effective in MC903-induced suppression of skin thickening and the production of serum IgE, IL-4, and TSLP compared to baicalein **(A)** MC903-induced ear skin inflammation of BALB/c mice treated with vehicle, SFII, Baicalein, or HC on day 12. **(B)** Ear swelling measurements by a digital caliper of BALB/c mice treated with MC903 plus vehicle, SFII, baicalein, or HC. *p < 0.05, **p < 0.01, ***p < 0.001 and ****p < 0.0001 vs MC903/vehicle. §p < 0.05 and §§§§p < 0.0001 vs baicalein. **(C)** Scratching bouts of BALB/c mice treated with MC903 plus vehicle, SFII, baicalein, or HC on day 13. **(D)** ELISA analysis of serum IgE levels on day 13. **(E)** H&E staining of ear sections from BALB/c mice treated with MC903 plus vehicle, SFII, baicalein, or HC on day 13. **(F)** Epidermal thickness determined from H&E-stained ear sections. **(G)** Dermal thickness determined from H&E-stained ear sections. **(H, I)** ELISA analysis of TSLP **(H)** and IL-4 **(I)** in ear skin of BALB/c mice treated with MC903 plus vehicle, SFII, baicalein, or HC on day 13. All images represent five mice per group, and all graphs represent the mean ± SEM from two independent experiments, with five mice in each group. ns., not significant; *p < 0.05, **p < 0.01, ***p < 0.001 and ****p < 0.0001.

potential therapeutic target for the treatment of AD. Our findings show that topical SFII inhibits MC903-induced erythema, edema, swelling, AD-associated skin inflammation, and pruritus in mice, similar to topical HC, a corticosteroid. Natural products and flavonoids are known to exhibit powerful antioxidants and potential pharmacological effects in allergic diseases, such as asthma, AD, anaphylaxis, and food allergy, and substantial scientific evidence on their safety profile and effectiveness exists (46–49). Thus, the discovery of natural products-based drugs could be one of the approaches for the treatment of AD in humans (50).

We observed a significant reduction in MC903-induced epidermal and dermal thickening following topical SFII use, which is comparable to that observed with topical HC or tacrolimus. Concomitantly, we observed that topical SFII significantly reduced MC903-induced S100a8 expression in the skin lesions. The exact mechanism by which MC903 induces S100a8 expression is still unknown; however, induction of S100a8 expression is mediated by IL-17A through the p38 MAPK pathway (51) and MC903 also triggers IL-17A production. S100A8 is known to promote keratinocyte proliferation (52) and its expression is markedly increased in

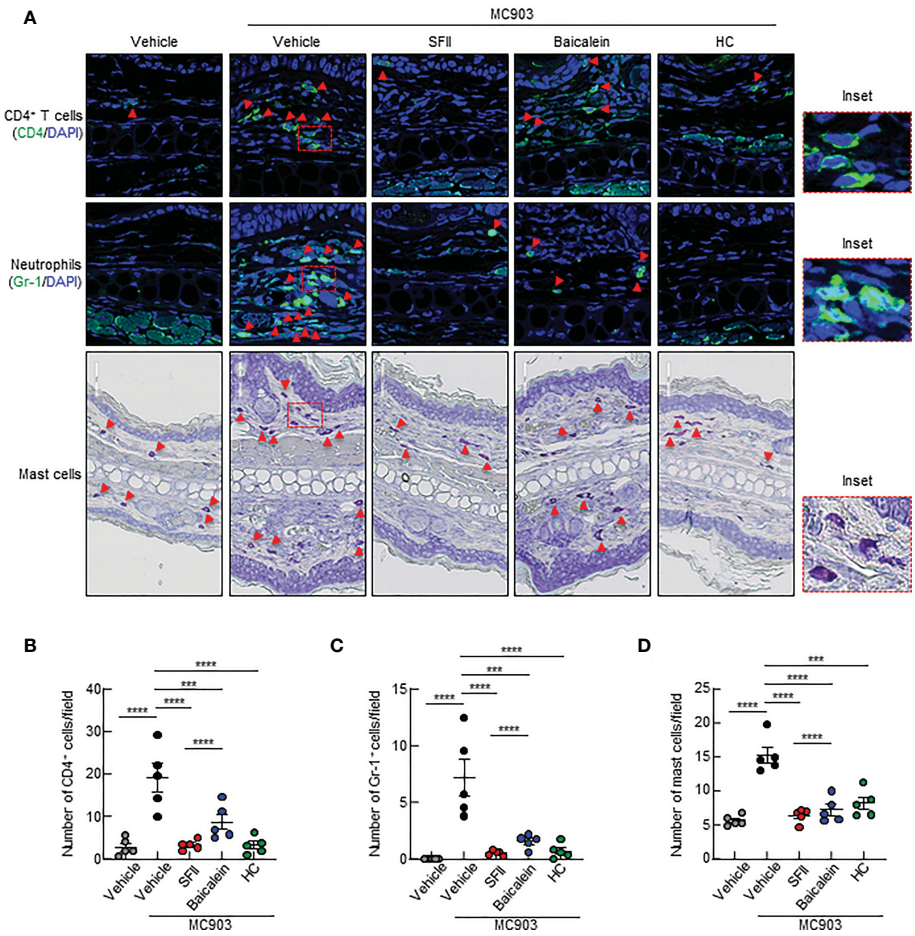

FIGURE 6
Topical SFII is more effective at suppressing MC903-induced infiltration of CD4$^+$ T cells and neutrophils into skin compared to baicalein **(A)** Immunofluorescent labeling of CD4 and Gr-1, and toluidine blue staining of mast cells in ear sections on day 13. **(B)** Quantitation of CD4$^+$ T cells in immunofluorescent-labeled ear sections. **(C)** Quantitation of Gr-1$^+$ cells in immunofluorescent-labeled ear sections. **(D)** Quantitation of mast cells in toluidine blue-stained ear sections. All images represent five mice per group, and all graphs are representative of the mean ± SEM from two independent experiments, with five mice in each group. ns., not significant; ***p < 0.001 and ****p < 0.0001.

acute and chronic AD skin (53). Our data suggest that reduced S100a8 expression by SFII may contribute to decreased epidermal thickening. Skin dermal thickening and allergic inflammation are promoted by immune cell infiltration. Of these, effector CD4$^+$ T cells and mast cells are crucial for the pathogenesis of AD by producing Th2 cytokines, such as IL-4 and IL-13 (53). Here, we revealed that topical SFII significantly inhibited the infiltration of CD4$^+$ T cells and mast cells, as well as IL-4 production in skin lesions induced by MC903, which was comparable to that induced by topical HC. Skin-infiltrating neutrophils and basophils also promote AD inflammation and itch (9, 54). Epithelial cell-derived CXCL1 is crucial in recruiting and activating neutrophils (9, 55). We further showed that topical SFII significantly suppressed the expression of the neutrophil chemoattractant, *Cxcl1*, and neutrophil infiltration in skin lesions. The mechanism by which CXCL1 expression is induced by MC903 remains unclear. However, protease-activated receptor agonists or IL-17A increases CXCL1 production in keratinocytes (9, 56) and CXCL1 expression is unaffected by the loss of TSLPR or neutrophil depletion (9). In addition, we observed that topical SFII reduced *Mcpt8* expression, a specific marker for murine basophils, suggesting reduced infiltration of basophils in the lesioned skin. We also showed that topical SFII reduced eosinophil recruitment and *Ccl7* expression in the lesioned skin. Eosinophils are associated with disease severity in patients with AD (57) and involved in itch, dermal thickening, and water loss in AD-like mouse models (58, 59). Although our data showed that the expression of eosinophil-associated factors (IL-5, *Ccl11*, and *Ccl17*) did not change following MC903 treatment for 7 consecutive days

(additional 6 days without MC903), other studies have shown that the expression of IL-5 and CCL24 (eotaxin-2) are significantly increased from day 9 or on day 14 after MC903 treatment (58, 60). These findings suggest that the expression of eosinophil-associated factors in lesioned skin appears to be a late immune response. Thus, our findings suggest that reduced skin-infiltrating $CD4^+$ T cells, mast cells, neutrophils, basophils, and eosinophils may cause decreased dermal thickening and ameliorate allergic inflammatory responses.

A recent study has shown that systemic depletion of neutrophils using an anti-Gr-1 antibody dramatically inhibits scratching behavior in an MC903-induced AD model, suggesting that neutrophils mediate itching (9). In parallel, we showed that topical SFII significantly suppressed MC903-induced scratching bouts, which were comparable to that of topical HC. Moreover, CXCL1 and IL-4 have been shown to directly stimulate itch-sensory neurons, leading to chronic itching (21) (61, 62). Thus, our data suggest that reduced IL-4 and CXCL1 production and reduced neutrophil infiltration following SFII administration may contribute to the inhibition of the itch response.

Epithelial cell-derived TSLP has been shown to trigger Th2 immune responses and skin-infiltrating immune cells, including dendritic cells, basophils, $CD4^+$ T cells, and mast cells (18). TSLP is also a pruritogen that activates neurons to induce itch (63). We observed that topical SFII significantly inhibited MC903-induced TSLP production in the skin lesions. Moreover, our *in vitro* studies showed that SFII directly suppressed TSLP production by human primary keratinocytes *via* inhibition of STAT1, ERK1/2, p38 MAPK, and JNK signaling pathways, indicating that decreased TSLP by SFII may result in reduced Th2 inflammation and infiltrated immune cells as well as the suppression of itching.

Furthermore, our *in vitro* studies of BMDCs revealed that SFII significantly suppressed the production of IL-6 and IL-12 induced by the TLR ligands PGN or LPS. In addition, we showed that SFII significantly suppressed the production of IL-4 and IFN-γ in anti-CD3/CD28-stimulated $CD4^+$ T cells from the mouse spleen and T cell proliferation, indicating that SFII directly suppresses immune cell activation. Overall, our findings suggest that reduced TSLP production in keratinocytes by SFII may result in reduced Th2 inflammatory responses and that SFII could directly regulate the activation of immune cells, including DCs, Th2, and Th1 cells. *In vitro* IL-17A production in anti-CD3/CD28-stimulated $CD4^+$ T cells was not affected by SFII, whereas topical SFII significantly inhibited IL-17A expression in MC903-induced skin lesions *in vivo*, suggesting that SFII may indirectly suppress IL-17A production in mouse skin. Thus, one possible explanation is that reduced IL-6 and IL-12 production by SFII, which is involved in Th17 polarization (64, 65), may result in reduced IL-17A production *in vivo*.

Lastly, we showed that topical SFII and baicalein significantly suppressed MC903-induced skin thickening, pruritus, and AD-related cytokine production compared to the MC903/vehicle-treated group. However, topical SFII is more effective in suppressing MC903-induced skin thickening and IL-4 and TSLP production in lesioned skin compared to topical baicalein. Interestingly, we observed that MC903-induced serum IgE levels were significantly suppressed by topical SFII alone, but not by topical baicalein or HC. A previous study has shown that intraperitoneal injection of baicalein reduces OVA-induced serum IgE levels in a mouse model of airway inflammation (66). Thus, these contrasting findings are likely due to differences in disease models, drug administration methods, and duration of treatment. Enhanced total IgE levels by HC have been reported previously (67, 68), and consistent with this, we confirmed that topical HC does not significantly reduce serum IgE levels in the MC903-induced AD-like mouse model. Further studies are required to understand the mechanism by which SFII effectively suppresses IgE production. Furthermore, we showed that MC903-induced infiltration of immune cells, including $CD4^+$ T cells, neutrophils, and mast cells, was significantly reduced in skin treated with topical SFII, baicalein, and HC-treated skin. However, topical SFII was more effective than baicalein at suppressing the infiltration of immune cells, including $CD4^+$ T cells and neutrophils, but not mast cells. Overall, our findings suggest that topical SFII has a more beneficial effect on AD treatment than topical baicalein.

In conclusion, we show that topical SFII can ameliorate AD-like pathology by regulating multiple targets in the MC903 mouse model. Moreover, we revealed that topical SFII has a beneficial effect on the suppression of IgE production compared to topical baicalein or HC. Therefore, our findings suggest the effectiveness of SFII in the pharmacological management and treatment of complex AD and pruritus as a single agent therapy or combination therapy with corticosteroids. Further studies are needed to determine the specific targets of SFII in cells, and clinical studies are warranted to determine the effects of SFII in patients with AD.

Data availability statement

The original contributions presented in the study are included in the article/Supplementary Material. Further inquiries can be directed to the corresponding author.

Ethics statement

The animal study was reviewed and approved by Seoul National University Hospital Institutional Animal Care and Use Committee.

Author contributions

YL and J-HO designed and performed experiments, analyzed the data, and prepared the figures. NL and H-JJ performed experiments and prepared research reagents. K-SA, S-RO, DL, and JC conceived the project and supervised this research. YL and JC wrote this original draft. All authors contributed to the article and approved the submitted version.

Funding

This research was supported by the Bio & Medical Technology Development Program of the National Research Foundation (NRF) funded by the Ministry of Science and ICT (2019M3A9I3091696) and by grants from the YANGYOUNG FOUNDATION.

Conflict of interest

The authors declare that the research was conducted in the absence of any commercial or financial relationships that could be construed as a potential conflict of interest.

Publisher's note

All claims expressed in this article are solely those of the authors and do not necessarily represent those of their affiliated organizations, or those of the publisher, the editors and the reviewers. Any product that may be evaluated in this article, or claim that may be made by its manufacturer, is not guaranteed or endorsed by the publisher.

Supplementary material

The Supplementary Material for this article can be found online at: https://www.frontiersin.org/articles/10.3389/fimmu.2022.1064515/full#supplementary-material

SUPPLEMENTARY FIGURE 1
Topical 1.0% SFII is more effective at attenuating MC903-induced AD-like skin inflammation and pruritus compared to 0.1% and 0.5% SFII **(A)** MC903-induced ear skin inflammation of BALB/c mice treated with 0.1%, 0.5%, or 1.0% SFII, tacrolimus, or HC on day 12. **(B)** Measurement of ear swelling in BALB/c mice treated with MC903 plus vehicle, 0.1%, 0.5%, or 1.0% SFII, tacrolimus, or HC using a digital caliper. **(C)** Scratching bouts of BALB/c mice treated with MC903 plus vehicle, 0.1%, 0.5%, or 1.0% SFII, tacrolimus, or HC on day 13. **(D)** ELISA analysis of serum IgE levels on day 13. **(E)** H&E staining of ear sections from BALB/c mice treated with vehicle, MC903 plus vehicle, 0.1%, 0.5%, or 1.0% SFII, tacrolimus, or HC on day 13. **(F)** Epidermal and dermal thickness determined from H&E-stained ear sections. The data are representative of the mean ± SEM of two independent experiments, with five mice per group. ns., not significant; * $p < 0.05$, ** $p < 0.01$, *** $p < 0.001$ and **** $p < 0.0001$.

SUPPLEMENTARY FIGURE 2
Topical SFII reduces MC903-induced eosinophil infiltration and Ccl7 expression **(A)** Immunofluorescent labeling of eosinophils in ear sections on day 13. **(B)** Quantitation of eosinophils in immunofluorescent-labeled ear sections. **(C)** ELISA analysis of IL-5 levels in ear skin of BALB/c mice treated with MC903 plus vehicle, SFII, or HC on day 13. **(D–G)** Relative mRNA expression of *Il5* **(D)**, *Ccl7* **(E)**, *Ccl11* **(F)**, and *Ccl17* **(G)** involved in eosinophil-associated factors on day 13. All images represent five mice per group, and all graphs are representative of the mean ± SEM from three independent experiments, with five mice in each group. ns., not significant; ** $p < 0.01$, *** $p < 0.001$ and **** $p < 0.0001$.

SUPPLEMENTARY FIGURE 3
SFII markedly and significantly inhibits Poly(I:C)-induced phosphorylation of STAT1, ERK1/2, p38 MAPK, and JNK **(A)** Quantitation of p-STAT-1/t-STAT-1 in western blot data. **(B)** Quantitation of p-p65/t-p65 in western blot data. **(C)** Quantitation of p-ERK1/2/t-ERK1/2 in western blot data. **(D)** Quantitation of p-p38/t-p38 in western blot data. **(E, F)** Quantitation of p-JNK/t-JNK (55 kDa) **(E)** and p-JNK/t-JNK (46 kDa) **(F)** in western blot data. All graphs represent the mean ± SEM from four independent experiments. ns., not significant; * $p < 0.05$, ** $p < 0.01$ and *** $p < 0.001$.

References

1. Bieber T. Atopic dermatitis: an expanding therapeutic pipeline for a complex disease. *Nat Rev Drug Discovery* (2022) 21:21–40. doi: 10.1038/s41573-021-00266-6

2. Odhiambo JA, Williams HC, Clayton TO, Robertson CF, Asher MI, Group IPTS. Global variations in prevalence of eczema symptoms in children from ISAAC phase three. *J Allergy Clin Immunol* (2009) 124:1251–1258.e1223. doi: 10.1016/j.jaci.2009.10.009

3. Langan SM, Irvine AD, Weidinger S. Atopic dermatitis. *Lancet* (2020) 396:345–60. doi: 10.1016/S0140-6736(20)31286-1

4. Noda S, Suarez-Farinas M, Ungar B, Kim SJ, de Guzman Strong C, Xu H, et al. The Asian atopic dermatitis phenotype combines features of atopic dermatitis and psoriasis with increased TH17 polarization. *J Allergy Clin Immunol* (2015) 136:1254–64. doi: 10.1016/j.jaci.2015.08.015

5. Brunner PM, Guttman-Yassky E. Racial differences in atopic dermatitis. *Ann Allergy Asthma Immunol* (2019) 122:449–55. doi: 10.1016/j.anai.2018.11.015

6. Suaini NHA, Tan CPT, Loo EXL, Tham EH. Global differences in atopic dermatitis. *Pediatr Allergy Immunol* (2021) 32:23–33. doi: 10.1111/pai.13335

7. Suarez-Farinas M, Ungar B, Correa da Rosa J, Ewald DA, Rozenblit M, Gonzalez J, et al. RNA Sequencing atopic dermatitis transcriptome profiling provides insights into novel disease mechanisms with potential therapeutic implications. *J Allergy Clin Immunol* (2015) 135:1218–27. doi: 10.1016/j.jaci.2015.03.003

8. Chieosilapatham P, Kiatsurayanon C, Umehara Y, Trujillo-Paez JV, Peng G, Yue H, et al. Keratinocytes: innate immune cells in atopic dermatitis. *Clin Exp Immunol* (2021) 204:296–309. doi: 10.1111/cei.13575

9. Walsh CM, Hill RZ, Schwendinger-Schreck J, Deguine J, Brock EC, Kucirek N, et al. Neutrophils promote CXCR3-dependent itch in the development of atopic dermatitis. *Elife* (2019) 8:e48448. doi: 10.7554/eLife.48448

10. Yang TB, Kim BS. Pruritus in allergy and immunology. *J Allergy Clin Immunol* (2019) 144:353–60. doi: 10.1016/j.jaci.2019.06.016

11. Wang F, Trier AM, Li F, Kim S, Chen Z, Chai JN, et al. A basophil-neuronal axis promotes itch. *Cell* (2021) 184:422–440.e417. doi: 10.1016/j.cell.2020.12.033

12. Tokura Y. Extrinsic and intrinsic types of atopic dermatitis. *J Dermatol Sci* (2010) 58:1–7. doi: 10.1016/j.jdermsci.2010.02.008

13. Suarez-Farinas M, Dhingra N, Gittler J, Shemer A, Cardinale I, de Guzman Strong C, et al. Intrinsic atopic dermatitis shows similar TH2 and higher TH17 immune activation compared with extrinsic atopic dermatitis. *J Allergy Clin Immunol* (2013) 132:361–70. doi: 10.1016/j.jaci.2013.04.046

14. Sims JT, Chang CY, Higgs RE, Engle SM, Liu Y, Sissons SE, et al. Insights into adult atopic dermatitis heterogeneity derived from circulating biomarker profiling in patients with moderate-to-severe disease. *Exp Dermatol* (2021) 30:1650–61. doi: 10.1111/exd.14389

15. Li M, Hener P, Zhang Z, Kato S, Metzger D, Chambon P. Topical vitamin D3 and low-calcemic analogs induce thymic stromal lymphopoietin in mouse keratinocytes and trigger an atopic dermatitis. *Proc Natl Acad Sci U.S.A.* (2006) 103:11736–41. doi: 10.1073/pnas.0604575103

16. Moosbrugger-Martinz V, Schmuth M. & dubrac, s. a mouse model for atopic dermatitis using topical application of vitamin D3 or of its analog MC903. *Methods Mol Biol* (2017) 1559:91–106. doi: 10.1007/978-1-4939-6786-5_8

17. Kim D, Kobayashi T, Nagao K. Research techniques made simple: Mouse models of atopic dermatitis. *J Invest Dermatol* (2019) 139:984–990.e981. doi: 10.1016/j.jid.2019.02.014

18. Leyva-Castillo JM, Hener P, Michea P, Karasuyama H, Chan S, Soumelis V, et al. Skin thymic stromal lymphopoietin initiates Th2 responses through an orchestrated immune cascade. *Nat Commun* (2013) 4:2847. doi: 10.1038/ncomms3847

19. Rochman Y, Dienger-Stambaugh K, Richgels PK, Lewkowich IP, Kartashov AV, Barski A, et al. TSLP signaling in CD4(+) T cells programs a pathogenic T helper 2 cell state. *Sci Signal* (2018) 11:eaam8858. doi: 10.1126/scisignal.aam8858

20. Siracusa MC, Saenz SA, Hill DA, Kim BS, Headley MB, Doering TA, et al. TSLP promotes interleukin-3-independent basophil haematopoiesis and type 2 inflammation. *Nature* (2011) 477:229–33. doi: 10.1038/nature10329

21. Oetjen LK, Mack MR, Feng J, Whelan TM, Niu H, Guo CJ, et al. Sensory neurons Co-opt classical immune signaling pathways to mediate chronic itch. *Cell* (2017) 171:217–228.e213. doi: 10.1016/j.cell.2017.08.006

22. Elentner A, Finke D, Schmuth M, Chappaz S, Ebner S, Malissen B, et al. Langerhans cells are critical in the development of atopic dermatitis-like inflammation and symptoms in mice. *J Cell Mol Med* (2009) 13:2658–72. doi: 10.1111/j.1582-4934.2009.00797.x

23. Nakajima S, Igyarto BZ, Honda T, Egawa G, Otsuka A, Hara-Chikuma M, et al. Langerhans cells are critical in epicutaneous sensitization with protein antigen *via* thymic stromal lymphopoietin receptor signaling. *J Allergy Clin Immunol* (2012) 129:1048–1055.e1046. doi: 10.1016/j.jaci.2012.01.063

24. Ring J. Terminology of allergic phenomena. *Chem Immunol Allergy* (2014) 100:46–52. doi: 10.1159/000358500

25. Punnonen J, Yssel H, de Vries JE. The relative contribution of IL-4 and IL-13 to human IgE synthesis induced by activated CD4+ or CD8+ T cells. *J Allergy Clin Immunol* (1997) 100:792–801. doi: 10.1016/S0091-6749(97)70276-8

26. Kashiwada M, Levy DM, McKeag L, Murray K, Schroder AJ, Canfield SM, et al. IL-4-induced transcription factor NFIL3/E4BP4 controls IgE class switching. *Proc Natl Acad Sci U.S.A.* (2010) 107:821–6. doi: 10.1073/pnas.0909235107

27. Lee H, Lee DH, Oh JH, Chung JH. Skullcapflavone II suppresses TNF-alpha/IFN-gamma-Induced TARC, MDC, and CTSS production in HaCaT cells. *Int J Mol Sci 22* (2021). doi: 10.3390/ijms22126428

28. Horikawa T, Nakayama T, Hikita I, Yamada H, Fujisawa R, Bito T, et al. IFN-gamma-inducible expression of thymus and activation-regulated chemokine/CCL17 and macrophage-derived chemokine/CCL22 in epidermal keratinocytes and their roles in atopic dermatitis. *Int Immunol* (2002) 14:767–73. doi: 10.1093/intimm/dxf044

29. Shimada Y, Takehara K, Sato S. Both Th2 and Th1 chemokines (TARC/CCL17, MDC/CCL22, and Mig/CXCL9) are elevated in sera from patients with atopic dermatitis. *J Dermatol Sci* (2004) 34:201–8. doi: 10.1016/j.jdermsci.2004.01.001

30. Yun MY, Yang JH, Kim DK, Cheong KJ, Song HH, Kim DH, et al. Therapeutic effects of baicalein on atopic dermatitis-like skin lesions of NC/Nga mice induced by dermatophagoides pteronyssinus. *Int Immunopharmacol* (2010) 10:1142–8. doi: 10.1016/j.intimp.2010.06.020

31. Jang HY, Ahn KS, Park MJ, Kwon OK, Lee HK, Oh SR. Skullcapflavone II inhibits ovalbumin-induced airway inflammation in a mouse model of asthma. *Int Immunopharmacol* (2012) 12:666–74. doi: 10.1016/j.intimp.2012.01.010

32. Wilson SR, Gerhold KA, Bifolck-Fisher A, Liu Q, Patel KN, Dong X, et al. TRPA1 is required for histamine-independent, mas-related G protein-coupled receptor-mediated itch. *Nat Neurosci* (2011) 14:595–602. doi: 10.1038/nn.2789

33. Gilchrest BA. *In vitro* assessment of keratinocyte aging. *J Invest Dermatol* (1983) 81:184s–9s. doi: 10.1111/1523-1747.ep12541084

34. Inaba K, Inaba M, Romani N, Aya H, Deguchi M, Ikehara S, et al. Generation of large numbers of dendritic cells from mouse bone marrow cultures supplemented with granulocyte/macrophage colony-stimulating factor. *J Exp Med* (1992) 176:1693–702. doi: 10.1084/jem.176.6.1693

35. Lutz MB, Kukutsch N, Ogilvie AL, Rossner S, Koch F, Romani N, et al. An advanced culture method for generating large quantities of highly pure dendritic cells from mouse bone marrow. *J Immunol Methods* (1999) 223:77–92. doi: 10.1016/S0022-1759(98)00204-X

36. Boise LH, Minn AJ, Noel PJ, June CH, Accavitti MA, Lindsten T, et al. CD28 costimulation can promote T cell survival by enhancing the expression of bcl-XL. *Immunity* (1995) 3:87–98. doi: 10.1016/1074-7613(95)90161-2

37. Jin S, Park CO, Shin JU, Noh JY, Lee YS, Lee NR, et al. DAMP molecules S100A9 and S100A8 activated by IL-17A and house-dust mites are increased in atopic dermatitis. *Exp Dermatol* (2014) 23:938–41. doi: 10.1111/exd.12563

38. Esaki H, Brunner PM, Renert-Yuval Y, Czarnowicki T, Huynh T, Tran G, et al. Early-onset pediatric atopic dermatitis is TH2 but also TH17 polarized in skin. *J Allergy Clin Immunol* (2016) 138:1639–51. doi: 10.1016/j.jaci.2016.07.013

39. Trinh HT, Joh EH, Kwak HY, Baek NI, Kim DH. Anti-pruritic effect of baicalin and its metabolites, baicalein and oroxylin a, in mice. *Acta Pharmacol Sin* (2010) 31:718–24. doi: 10.1038/aps.2010.42

40. Inagaki N, Igeta K, Kim JF, Nagao M, Shiraishi N, Nakamura N, et al. Involvement of unique mechanisms in the induction of scratching behavior in BALB/c mice by compound 48/80. *Eur J Pharmacol* (2002) 448:175–83. doi: 10.1016/S0014-2999(02)01933-7

41. Boguniewicz M. Topical treatment of atopic dermatitis. *Immunol Allergy Clin North Am* (2004) 24:631–644,vi-vii. doi: 10.1016/j.iac.2004.06.011

42. Alomar A, Berth-Jones J, Bos JD, Giannetti A, Reitamo S, Ruzicka T, et al. The role of topical calcineurin inhibitors in atopic dermatitis. *Br J Dermatol* (2004) 151(Suppl 70):3–27. doi: 10.1111/j.1365-2133.2004.06269.x

43. Siegfried EC, Jaworski JC, Kaiser JD, Hebert AA. Systematic review of published trials: long-term safety of topical corticosteroids and topical calcineurin inhibitors in pediatric patients with atopic dermatitis. *BMC Pediatr* (2016) 16:75. doi: 10.1186/s12887-016-0607-9

44. Schoepe S, Schacke H, May E, Asadullah K. Glucocorticoid therapy-induced skin atrophy. *Exp Dermatol* (2006) 15:406–20. doi: 10.1111/j.0906-6705.2006.00435.x

45. Shlivko IL, Kamensky VA, Donchenko EV, Agrba P. Morphological changes in skin of different phototypes under the action of topical corticosteroid therapy and tacrolimus. *Skin Res Technol* (2014) 20:136–40. doi: 10.1111/srt.12095

46. Wu S, Pang Y, He Y, Zhang X, Peng L, Guo J, et al. A comprehensive review of natural products against atopic dermatitis: Flavonoids, alkaloids, terpenes, glycosides and other compounds. *BioMed Pharmacother* (2021) 140:111741. doi: 10.1016/j.biopha.2021.111741

47. Tanaka T, Takahashi R. Flavonoids and asthma. *Nutrients* (2013) 5:2128–43. doi: 10.3390/nu5062128

48. Kumazawa Y, Takimoto H, Matsumoto T, Kawaguchi K. Potential use of dietary natural products, especially polyphenols, for improving type-1 allergic symptoms. *Curr Pharm Des* (2014) 20:857–63. doi: 10.2174/13816128006140220120344

49. Castell M, Perez-Cano FJ, Abril-Gil M, Franch A. Flavonoids on allergy. *Curr Pharm Des* (2014) 20:973–87. doi: 10.2174/13816128113199990041

50. Atanasov AG, Zotchev SB, Dirsch VMInternational Natural Product Sciences, T, , Supuran CT. Natural products in drug discovery: advances and opportunities. *Nat Rev Drug Discovery* (2021) 20:200–16. doi: 10.1038/s41573-020-00114-z

51. Mose M, Kang Z, Raaby L, Iversen L, Johansen C. TNFalpha- and IL-17A-mediated S100A8 expression is regulated by p38 MAPK. *Exp Dermatol* (2013) 22:476–81. doi: 10.1111/exd.12187

52. Iotzova-Weiss G, Dziunycz PJ, Freiberger SN, Lauchli S, Hafner J, Vogl T, et al. S100A8/A9 stimulates keratinocyte proliferation in the development of squamous cell carcinoma of the skin *via* the receptor for advanced glycation-end products. *PloS One* (2015) 10:e0120971. doi: 10.1371/journal.pone.0120971

53. Gittler JK, Shemer A, Suarez-Farinas M, Fuentes-Duculan J, Gulewicz KJ, Wang CQ, et al. Progressive activation of T(H)2/T(H)22 cytokines and selective epidermal proteins characterizes acute and chronic atopic dermatitis. *J Allergy Clin Immunol* (2012) 130:1344–54. doi: 10.1016/j.jaci.2012.07.012

54. Mali SS, Bautista DM. Basophils add fuel to the flame of eczema itch. *Cell* (2021) 184:294–6. doi: 10.1016/j.cell.2020.12.035

55. Dhingra N, Suarez-Farinas M, Fuentes-Duculan J, Gittler JK, Shemer A, Raz A, et al. Attenuated neutrophil axis in atopic dermatitis compared to psoriasis reflects TH17 pathway differences between these diseases. *J Allergy Clin Immunol* (2013) 132:498–501.e493. doi: 10.1016/j.jaci.2013.04.043

56. Kim MH, Jin SP, Jang S, Choi JY, Chung DH, Lee DH, et al. IL-17A-Producing innate lymphoid cells promote skin inflammation by inducing IL-33-Driven type 2 immune responses. *J Invest Dermatol* (2020) 140:827–837.e829. doi: 10.1016/j.jid.2019.08.447

57. Kiehl P, Falkenberg K, Vogelbruch M, Kapp A. Tissue eosinophilia in acute and chronic atopic dermatitis: a morphometric approach using quantitative image

analysis of immunostaining. *Br J Dermatol* (2001) 145:720–9. doi: 10.1046/j.1365-2133.2001.04456.x

58. Naidoo K, Jagot F, van den Elsen L, Pellefigues C, Jones A, Luo H, et al. Eosinophils determine dermal thickening and water loss in an MC903 model of atopic dermatitis. *J Invest Dermatol* (2018) 138:2606–16. doi: 10.1016/j.jid.2018.06.168

59. Lee JJ, Protheroe CA, Luo H, Ochkur SI, Scott GD, Zellner KR, et al. Eosinophil-dependent skin innervation and itching following contact toxicant exposure in mice. *J Allergy Clin Immunol* (2015) 135:477–87. doi: 10.1016/j.jaci.2014.07.003

60. Li C, Maillet I, Mackowiak C, Viala C, Di Padova F, Li M, et al. Experimental atopic dermatitis depends on IL-33R signaling *via* MyD88 in dendritic cells. *Cell Death Dis* (2017) 8:e2735. doi: 10.1038/cddis.2017.90

61. Deftu AF, Filippi A, Shibsaki K, Gheorghe RO, Chiritoiu M, Ristoiu V. Chemokine (C-X-C motif) ligand 1 (CXCL1) and chemokine (C-X-C motif) ligand 2 (CXCL2) modulate the activity of TRPV1+/IB4+ cultured rat dorsal root ganglia neurons upon short-term and acute application. *J Physiol Pharmacol* (2017) 68:385–95.

62. Deftu AF, Filippi A, Gheorghe RO, Ristoiu V. CXCL1 activates TRPV1 *via* gi/o protein and actin filaments. *Life Sci* (2018) 193:282–91. doi: 10.1016/j.lfs.2017.09.041

63. Wilson SR, The L, Batia LM, Beattie K, Katibah GE, McClain SP, et al. The epithelial cell-derived atopic dermatitis cytokine TSLP activates neurons to induce itch. *Cell* (2013) 155:285–95. doi: 10.1016/j.cell.2013.08.057

64. Navarini AA, French LE, Hofbauer GF. Interrupting IL-6-receptor signaling improves atopic dermatitis but associates with bacterial superinfection. *J Allergy Clin Immunol* (2011) 128:1128–30. doi: 10.1016/j.jaci.2011.09.009

65. Cesare AD, Meglio PD, Nestle FO. A role for Th17 cells in the immunopathogenesis of atopic dermatitis? *J Invest Dermatol* (2008) 128:2569–71. doi: 10.1038/jid.2008.283

66. Xu T, Ge X, Lu C, Dai W, Chen H, Xiao Z, et al. Baicalein attenuates OVA-induced allergic airway inflammation through the inhibition of the NF-kappaB signaling pathway. *Aging (Albany NY)* (2019) 11:9310–27. doi: 10.18632/aging.102371

67. Bohle B, Willheim M, Baier K, Stadler B, Spitzauer S, Scheiner O, et al. Hydrocortisone enhances total IgE levels–but not the synthesis of allergen-specific IgE–in a monocyte-dependent manner. *Clin Exp Immunol* (1995) 101:474–9. doi: 10.1111/j.1365-2249.1995.tb03137.x

68. Wu CY, Sarfati M, Heusser C, Fournier S, Rubio-Trujillo M, Peleman R , et al. Glucocorticoids increase the synthesis of immunoglobulin e by interleukin 4-stimulated human lymphocytes. *J Clin Invest* (1991) 87:870–7. doi: 10.1172/JCI115092

frontiers | Frontiers in Immunology

TYPE Correction
PUBLISHED 07 February 2023
DOI 10.3389/fimmu.2023.1150830

OPEN ACCESS

APPROVED BY
Frontiers Editorial Office, Frontiers Media SA, Switzerland

*CORRESPONDENCE
Jin Ho Chung
jhchung@snu.ac.kr

†These authors have contributed equally to this work

SPECIALTY SECTION
This article was submitted to Inflammation, a section of the journal Frontiers in Immunology

RECEIVED 25 January 2023
ACCEPTED 27 January 2023
PUBLISHED 07 February 2023

CITATION
Lee Y, Oh J-H, Li N, Jang H-J, Ahn K-S, Oh S-R, Lee DH and Chung JH (2023) Corrigendum: Topical Skullcapflavone II attenuates atopic dermatitis in a mouse model by directly inhibiting associated cytokines in different cell types. *Front. Immunol.* 14:1150830. doi: 10.3389/fimmu.2023.1150830

Corrigendum: Topical Skullcapflavone II attenuates atopic dermatitis in a mouse model by directly inhibiting associated cytokines in different cell types

Youngae Lee[1,2,3†], Jang-Hee Oh[1,2,3†], Na Li[1,2,3,4], Hyun-Jae Jang[5], Kyung-Seop Ahn[5], Sei-Ryang Oh[5], Dong Hun Lee[1,2,3] and Jin Ho Chung[1,2,3,4*]

[1]Department of Dermatology, Seoul National University College of Medicine, Seoul, Republic of Korea, [2]Institute of Human-Environment Interface Biology, Medical Research Center, Seoul National University, Seoul, Republic of Korea, [3]Laboratory of Cutaneous Aging Research, Biomedical Research Institute, Seoul National University Hospital, Seoul, Republic of Korea, [4]Department of Biomedical Sciences, Seoul National University Graduate School, Seoul, Republic of Korea, [5]Natural Medicine Research Center, Korea Research Institute of Bioscience and Biotechnology, Cheong-ju, Chungcheongbuk-do, Republic of Korea

KEYWORDS

Skullcapflavone II, atopic dermatitis, pruritus, Th2 cytokines, IgE

A Corrigendum on

Topical Skullcapflavone II attenuates atopic dermatitis in a mouse model by directly inhibiting associated cytokines in different cell types

by Lee Y, Oh J-H, Li N, Jang H-J, Ahn K-S, Oh S-R, Lee DH, and Chung JH (2022) *Front. Immunol.* 13:1064515. doi: 10.3389/fimmu.2022.1064515

In the published article, there was an error in the author list, and authors Youngae Lee and Jang-Hee Oh were erroneously not annotated as co-first authors. The corrected author list appears below.

Youngae Lee[1,2,3†], Jang-Hee Oh[1,2,3†], Na Li[1,2,3,4], Hyun-Jae Jang[5], Kyung-Seop Ahn[5], Sei-Ryang Oh[5], Dong Hun Lee[1,2,3] and Jin Ho Chung[1,2,3,4*]

[†] *These authors have contributed equally to this work.*

The authors apologize for this error and state that this does not change the scientific conclusions of the article in any way. The original article has been updated.

Publisher's note

All claims expressed in this article are solely those of the authors and do not necessarily represent those of their affiliated organizations, or those of the publisher, the editors and the reviewers. Any product that may be evaluated in this article, or claim that may be made by its manufacturer, is not guaranteed or endorsed by the publisher.

frontiers | Frontiers in Immunology

TYPE Original Research
PUBLISHED 23 December 2022
DOI 10.3389/fimmu.2022.1039009

OPEN ACCESS

EDITED BY
Uzma Saqib,
Indian Institute of Technology Indore, India

REVIEWED BY
Robert W. Sobol,
Brown University, United States
Deborah Croteau,
National Institute on Aging, United States

*CORRESPONDENCE
Dawit Kidane
dawit.kidane@austin.utexas.edu

SPECIALTY SECTION
This article was submitted to Inflammation, a section of the journal Frontiers in Immunology

RECEIVED 07 September 2022
ACCEPTED 05 December 2022
PUBLISHED 23 December 2022

CITATION
Zhao S, Goewey Ruiz JA, Sebastian M and Kidane D (2022) Defective DNA polymerase beta invoke a cytosolic DNA mediated inflammatory response. *Front. Immunol.* 13:1039009. doi: 10.3389/fimmu.2022.1039009

Defective DNA polymerase beta invoke a cytosolic DNA mediated inflammatory response

Shengyuan Zhao[1], Julia A. Goewey Ruiz[1], Manu Sebastian[2,3] and Dawit Kidane[1]*

[1]Division of Pharmacology and Toxicology, College of Pharmacy, The University of Texas at Austin, Dell Pediatric Research Institute, Austin, TX, United States, [2]Dept. of Veterinary Medicine & Surgery, University of Texas (UT) MD Anderson Cancer Center, Houston, TX, United States, [3]Dept. of Translational Molecular Pathology, University of Texas (UT) MD Anderson Cancer Center, Houston, TX, United States

Base excision repair (BER) has evolved to maintain the genomic integrity of DNA following endogenous and exogenous agent induced DNA base damage. In contrast, aberrant BER induces genomic instability, promotes malignant transformation and can even trigger cancer development. Previously, we have shown that deoxyribo-5′-phosphate (dRP) lyase deficient DNA polymerase beta (POLB) causes replication associated genomic instability and sensitivity to both endogenous and exogenous DNA damaging agents. Specifically, it has been established that this loss of dRP lyase function promotes inflammation associated gastric cancer. However, the way that aberrant POLB impacts the immune signaling and inflammatory responses is still unknown. Here we show that a dRP lyase deficient variant of POLB (Leu22Pro, or L22P) increases mitotic dysfunction associated genomic instability, which eventually leads to a cytosolic DNA mediated inflammatory response. Furthermore, poly(ADP-ribose) polymerase 1 inhibition exacerbates chromosomal instability and enhances the cytosolic DNA mediated inflammatory response. Our results suggest that POLB plays a significant role in modulating inflammatory signaling, and they provide a mechanistic basis for future potential cancer immunotherapies.

KEYWORDS

DNA polymerase beta, base excision repair, cytosolic DNA mediated inflammatory signaling, PARP inhibitor, interferon type I cytokines

Introduction

DNA damage is a biological process that negatively impacts host cells' genomic integrity and human health (1–4). Cells accrue DNA damage as a result of endogenous metabolic activities or environmental exposures, such as ultraviolet light and chemical mutagens that can promote cancer (5). To ensure genomic integrity, cells have evolved

sophisticated mechanisms to repair DNA damage, including base excision repair (BER), which is the predominant repair pathway to process oxidative and alkylating agent derived DNA base lesions (6–10). Further, multiple studies have shown that BER modulates the inflammatory response (11, 12). Mammalian cells harbor two sub-BER pathways that are dependent on the number of oxidized DNA bases to process and the key enzyme involved in the repair process (13). The two sub-pathways are known as short-patch BER (SP-BER) and long-patch BER (LP-BER) (14, 15). SP-BER engages in repairing one nucleotide gaps (16, 17), while the LP-BER involves processing and repairing 2 to 12 nucleotide gaps. Both BER pathways begin as DNA glycosylase recognizes and removes the DNA base lesion. In both pathways, AP-endonuclease 1 (APE1) cleaves the DNA backbone to generate a 3'-OH terminus at the site of damage followed by DNA polymerase beta (POLB), which possesses DNA polymerase and deoxyribo-5′-phosphate (dRP) lyase activities, both of which are known to be important for efficient BER. The dRP lyase activity resides within the 8kDa amino terminal domain of POLB and is responsible for the removal of the 5'-phosphate group (5'-dRP), and subsequently the polymerase domain of POLB adds one nucleotide, leaving a nick which is sealed by DNA ligase I or III (18). While POLB is a major player in SP-BER, LP-BER, involved in processing 2 to 12 nucleotide bases, allows different DNA polymerases such as DNA Pol δ and DNA Pol ε, and other main DNA replication enzymes to conduct strand-displacement DNA synthesis. The displaced single stranded DNA structure or 5'-DNA flap is removed by flap endonuclease I (FEN1) (19) followed by the resulting DNA nicks being sealed by Ligase I or Ligase III (20).

When BER is unable to continue the repair process, there is an accumulation of DNA base damage, single-strand breaks (SSBs) and apurinic/apyrimidinic (AP) sites (21–25). SSBs are converted into double-strand breaks (DSBs) during the S- phase of DNA repalication (26, 27). The BER intermediates such as SSBs and 5'-dRP groups provide the opportunity for poly(ADP-ribose) polymerase 1 (PARP1) to bind and activate poly(ADP-ribose) (PAR) synthesis to facilitate the recruitment of downstream proteins, such as POLB, which fill the gap and XRCC1-Ligase III complex which seals the nick (28, 29). It is possible then that an accumulation of DNA base damage in BER deficient cells could lead to activation of the DNA damage response and modulate an inflammatory response (30, 31). Multiple studies have suggested that DNA repair factors play a role in modulating an inflammatory response (32, 33). Once nuclear DNA integrity is compromised through a deficient DNA repair system or exogenous DNA damaging agents, cells will likely release the DNA into the cytosolic compartment and possibly activate STING signaling and engage an inflammatory response. It is well documented that chronic stimulation of the immune system is critical for tumor promotion and progression (34, 35). One of the key interfaces between defective DNA repair and immunogenicity is the cyclic GMP-AMP synthase/stimulator of IFN genes (cGAS/STING) pathway (33, 36). The cGAS-STING pathway, which senses cytosolic DNA, has been linked to an anti-tumor inflammatory response (37). In this pathway, STING, an endoplasmic reticulum localized protein, is a critical adaptor for the cytosolic DNA sensing pathway (38, 39). Cytosolic double-stranded DNA is sensed by cGAS, leading to activation of the transmembrane protein STING and activation of the transcription factors interferon regulatory factor 3 (mainly IRF3) and nuclear factor kappa B (NF-κB) followed by an upregulation of interferon beta (IFN-β) related genes (40, 41).

Previously, we demonstrated that the human gastric cancer-associated variant of POLB (Leu22Pro or L22P) lacks dRP lyase function *in vitro* and induces replication associated genomic instability and cellular transformation (42). The L22P mutation of POLB lacks dRP lyase activity, which leads to inefficient BER and an accumulation of BER intermediates (21). These intermediates can further block replication fork progression and exacerbate genomic instability (42, 43). Therefore, L22P can serve as a good model to study the interplay between aberrant BER and inflammation in gastric cancer (44). In the present work, we hypothesize that loss of dRP lyase function of POLB enhances cytosolic DNA mediated inflammatory immune signaling through the cGAS/STING pathway. Results from this work show that a novel role of POLB in modulating inflammatory response. We discovered that loss of the dRP lyase function of POLB leads to chromosomal instability and spontaneous upregulation of cytosolic DNA mediated inflammatory response. We also show that targeting PARP1 in dRP lyase deficient cells (L22P variant) exacerbates the release of cytosolic DNA, activates STING signaling, and promotes an inflammatory response. Our study reveals a previously unidentified role of POLB in regulating the cellular inflammatory response thus providing a potential target in a defective BER pathway to enhance an immune based therapy response in the future.

Material and methods

Cell lines and materials

We constructed a POLB L22P conditional knock-in mouse model as described previously (21). C57BL/6 Mouse Embryonic Fibroblasts (MEFs) were isolated from embryonic tissue at embryonic day 14.5 (21). Two MEF cell lines isolated from WT and L22P mice were characterized. All animal studies were conducted according to protocols approved by the Institutional Animal Care and Usage Committee of The University of Texas at Austin (protocol # AUP202-00070). Embryos from WT and L22P transgenic mice were isolated at embryonic day 14.5. After the heads, tails, limbs, and most of the internal organs were removed, the embryos were minced and typsinized for 20 min,

and then seeded into T-75 cell culture dishes in 10 mL DMEM supplemented with 10% fetal bovine serum (FBS), 1% penicillin/streptomycin, and 1% L-glutamine at 37°C with 5% CO_2. The cells were split at 1:2 ratios when freshly confluent, passaged two or three times to obtain a morphologically homogenous culture, and then frozen or expanded for further studies.

Chemicals

To determine whether MEFs are sensitive to exogenous alkylating and oxidative DNA damaging agents, 1-methyl-1-nitrosourea (MNU, Cat. N2939, Spectrum Chemical, New Brunswick, NJ) and H_2O_2 (Cat. H1009, Sigma-Aldrich, St. Louis, MO) were dissolved or diluted in water and stored at -20°C before use. Olaparib was purchased from Selleck Chemicals and prepared according to the manufacturer's protocol (Cat. S1060, Selleck Chemicals).

Cytoplasmic and whole-cell DNA isolation

Cells were trypsinized and washed with PBS two times before DNA isolation. Whole-cell DNA was isolated using QIAamp DNA Mini Kit (Cat. 51304, Qiagen) according to the manufacturer's protocol. For cytoplasmic DNA, cells were lysed in hypotonic lysis buffer (10mM HEPES pH 7.4,10mM KCl, 1.5mM $MgCl_2$, 0.34M sucrose, 10% glycerol, 0.1% Triton X-100) on ice for 5 mins before centrifuging at 1700g for 5 mins. The supernatant containing the cytoplasmic fraction was collected and centrifuged at 13000g for 10 mins to remove other organelles and incompletely lysed cells. Extraction was validated by Western blot with α-tubulin as the cytoplasmic marker and histone 3 as the nuclear marker. DNA concentration was later quantified using PicoGreen dsDNA assay kit (Cat. P7589, Thermo Fisher) according to the manufacturer's protocol.

Alkali comet assay

Alkali comet assay was performed using Comet Assay Single Cell Gel Electrophoresis Assay Kit (Cat. 4250-050-K, Trevigen) according to the manufacturer's protocol. Cells were mixed with low-melting agarose before plating on comet assay slides for overnight lysis. The next day, chromosomal DNA was denatured under alkali unwinding buffer (pH>13) and underwent electrophoresis (20V) for one hour at 4°C. After drying the slides, DNA was stained with SYBR Gold (Cat. S11494, ThermoFisher) and images were taken with a FITC filter using a Zeiss fluorescence microscope (Zeiss, San Diego, CA, USA) then analyzed by Open Comet Assay using Image J application as described previously (45).

Abasic site quantification

Genomic DNA was extracted using DNAzol® Reagent (Cat. 10503027, Thermo Fisher) to minimize base loss during sample preparations. DNA was diluted in TE buffer to reach 100ng/µl, and AP sites were measured using AP Sites Quantitation Kit (Cat. STA-324, Cell Biolabs) according to manufacturers' protocol. Briefly, AP sites were labeled with aldehyde reactive probe (ARP). The probe contains biotin which can be further conjugated with streptavidin-enzyme before performing colorimetric quantification. The standard samples provided in the kit were used to plot a standard curve.

DNA-PARP-1 crosslinks measurement

Cells were plated and allowed to grow until 70% confluent before Olaparib treatment for 24 hours. Then cells were isolated and lysed with DNAzol. DNA was sheared by passing through a 21-gauge needle and then through a 25-gauge needle, three times each. NaCl was added to reach a final concentration of 4M and incubated at 37°C in a shaking water bath for 20 mins. Urea was then added to reach a final concentration of 4M, and the mixture was incubated for 20 mins in a 37°C shaking water bath. To precipitate DNA-protein crosslinks (DPCs), an equal volume of 100% ethanol was added. The solution was then mixed by inversion followed by the addition of a QIAEX II silica slurry (Cat # 20021, Qiagen). Samples were rocked for 40 mins at room temperature to allow DNA to bind to silica. Silica particles were collected by centrifugation and washed 4 times with 50% ethanol. DPC was eluted from silica by adding 2ml of 8mM NaOH and was incubated at 65°C for 5 mins. The elution process was repeated and the supernatant fractions combined. DPC samples were verified by measuring the DNA concentration. To digest DNA, samples were mixed with digestion buffer (10mM $MgCl_2$, 10mM $ZnCl_2$, 0.1M NaAc pH=5, 5 units of DNase I, and 5 units of S1 nuclease). The mixture was incubated at 37°C for one hour then at 65°C for 10 mins to stop the digestion. Next, ice-cold trichloroacetic acid (TCA) was added to reach a final concentration of 15% and samples were incubated on ice for one hour to precipitate out DPC proteins. Proteins were pelleted by centrifugation and then washed with 15% ice-cold TCA followed by ice-cold acetone, 2 times each. The pellet was allowed to air-dry and dissolve in RIPA buffer before Western blot.

Real-Time q-PCR

RNA was extracted using the Trizol/chloroform method and washed with 75% ethanol. cDNA was then immediately synthesized from RNA using High-Capacity cDNA Reverse

Transcription Kit (Cat. 4368814, Applied Biosystems). To determine gene expression levels, synthesized cDNA was used as a template for real-time q-PCR using iTaq Universal SYBR Green Supermix (Cat. 1725121, Biorad). Primers are listed in the Supplementary Table 1. PCR results were analyzed using $2^{-\Delta\Delta}$Ct method.

Western blotting

Cells were lysed with radioimmunoprecipitation assay (RIPA) buffer supplemented with a protease inhibitor (Cat. 25765800, Sigma Aldrich) and a phosphatase inhibitor (Cat. P5726, Sigma Aldrich). After denaturing the samples at 95°C for 5 minutes, 30µg of each protein sample was separated using SDS-PAGE and transferred onto nitrocellulose membranes (Cat. 1620112, Bio-Rad, Hercules, CA). Next, the membranes were blocked with 5% BSA for 1 hour, and then incubated with primary antibodies against STING (Cat. 13647S, Cell Signaling), IRF3 (Cat. 4302S, Cell Signaling), p-IRF3 (Cat. 4947S, Cell Signaling), TBK1 (Cat. 3013S, Cell Signaling), p-TBK1 (Cat. 5483S, Cell Signaling), β-actin (Cat. 3700S, Cell Signaling), and Vinculin (Cat. 13901S, Cell Signaling) overnight at 4°C. The following day, the membranes were washed with PBST and incubated with anti-mouse (Cat. NXA931, GE Healthcare, Chicago, IL) or anti-rabbit (Cat. NA934V, GE Healthcare) secondary antibody for 2 hours before developing with ECL substrates (Cat. 170506, BioRad). The gel images were captured using Chem-DocXRS image acquisition machine (Bio-Rad).

Immunofluorescence and micronuclei scoring

WT and L22P MEF cells were cultured in four well chamber slides (Cat # 154453, Thermo Fisher) with complete media. When cell confluency reached 70%, cells were fixed with 3.7% paraformaldehyde (PFA) for 15 mins, followed by permeabilization with 0.5% Triton X-100 for 10 mins. Slides were then blocked with 3% BSA for one hour at room temperature followed by primary antibody incubation overnight at 4°C. Primary antibodies applied include γH_2AX (1:1000, Cat. 07-164, Millipore), 53BP1 (1:400Cat. Sc-22760, Santa Cruz), α-tubulin (1:400, Cat. 2144S, Cell Signaling), ssDNA (Cat. MAB3299, Sigma), and dsDNA (Cat. ab27156, Abcam). The next day, slides were washed with PBS three times and incubated with secondary antibody for one hour at room temperature. Secondary antibodies applied include Alexa Fluor 488 anti-mouse antibody (Cat. 715-095-150, Jackson immunoResearch Labs) and Texas Red anti-rabbit antibody (Cat. 711-025-152, Jackson ImmunoResearch Labs). Slides were then washed with PBS three times and mounted with mounting media containing DAPI (Cat. H-1200-10, Vector Laboratories) and covered with coverslips. Images were captured using a Zeiss microscope under a 63X objective. The co-localization of γH2AX/53BP1 greater than five foci per per nucleus is considered as the average cut value to identify the difference between different genotypes as well as treated versus untreated group. Micronuclei were identified and quantified as DAPI positive nucleus-shaped particles with diameter smaller than 1/3 of the primary nucleus located nearby.

Measurement of DNA concentration using PicoGreen

To determine the concentration of DNA isolated from cytoplasm, we applied PicoGreen dsDNA assay kit (Cat. P7589, Thermo Fisher) due to its high sensitivity and accuracy. Cytoplasmic DNA was diluted to 1:10 in 1X TE buffer. The standard curve was prepared using Lambda DNA standard ranging from 10 pg/µL to 1 ng/µL. The standard DNA (100 µL) or DNA samples were mixed with 1X PicoGreen solution of the volume in the dark. The sample mixture was shaken for 5 mins before measuring the fluorescence intensity in a microplate reader at 480nm/520nm (Ex/Em).

Immunohistology

Gastric tissues from WT and L22P mice were collected and fixed in 3.7% PFA overnight before paraffin embedding. Tissues were then sectioned along the longitudinal axis for immune-histological staining using ImmunoCruz rabbit ABC Staining System (Santa Cruz, sc-2018). Primary antibodies applied include STING (1:200, Cat. 13647S, Cell Signaling), IRF3 (1:200, Cat. 4302S, Cell Signaling), and p-IRF3 (1:100, Cat. 4947S, Cell Signaling). Stained slides were then scanned using Scanscope (Leica Biosystem). For each slide, 5 fields were randomly selected, and the number of positively stained nuclei and total nuclei were counted.

Statistical analysis

Three independent experiments were performed for immunofluorescence, comet assay, AP site measurement and qRT-PCR. Data were statistically analyzed using Student t-test. Data from more than two study groups were analyzed using two way of ANOVA statstical analysis. Furthermore, the expression of PARP1 and interferon gene correlation was calculated using spearman coefficient with Graph Pad Prism software. Results were considered significant at $P< 0.05$.

Results

dRP lyase deficient POLB cells accumulate genomic instability

To determine whether cells with dRP lyase deficient POLB are susceptible to spontaneous and DNA damaging agent induced genomic instability, we characterized two independent MEFs cells (MEF #3 and MEF 2) from each genotype (WT and L22P). First, we examined whether dRP lyase proficient and deficient mouse embryonic fibroblasts (MEFs) cells accumulate base excision repair intermediates including abasic sites (AP sites). AP sites were measured using an AP site assay kit (Colorimetric; Cat. STA-324, Cell Biolabs, USA) that utilizes an aldehyde reactive probe (ARP) reagent that reacts specifically with an aldehyde group, which is the open ring form of an AP site. We observed a significant increase in the enhancement of AP sites in L22P cells versus WT cells (Figure 1A; P<0.001). In addition, L22P fibroblast cells significantly harbored spontaneous and exogenous induced single strand breaks (SSBs) compared with WT cells as shown by the formation of longer comet tail moments using an alkali comet assay (Figure 1B, C). We then considered whether BER intermediates (AP sites and SSBs) contributed to double strand break (DSB) formation with and without DNA damaging agents. We treated WT and L22P cells with MNU or H_2O_2 treatment for one hour and examined the colocalization of γH2AX and 53BP1 foci formation (Figure 1D). We found that spontaneously and exogenously induced DSBs increased significantly in dRP lyase deficient (L22P) cells versus WT cells (Figure 1E; P<0.001). To determine whether or not the presence of L22P variant altered the protein expression of other BER proteins linked to genomic instability, we performed Western blot assay analysis on POLB, PARP1, and XRCC1 and saw no observable difference in protein expression levels between WT and L22P (Figure 1F).

Loss of dRP lyase function increases mitotic dysfunction and accumulation of cytosolic DNA

Previously we have shown that L22P induces chromosomal instability and cytokinesis failure (21). In this study, we examined whether L22P cells enter into mitosis with DNA damage caused by micronuclei formation. We further

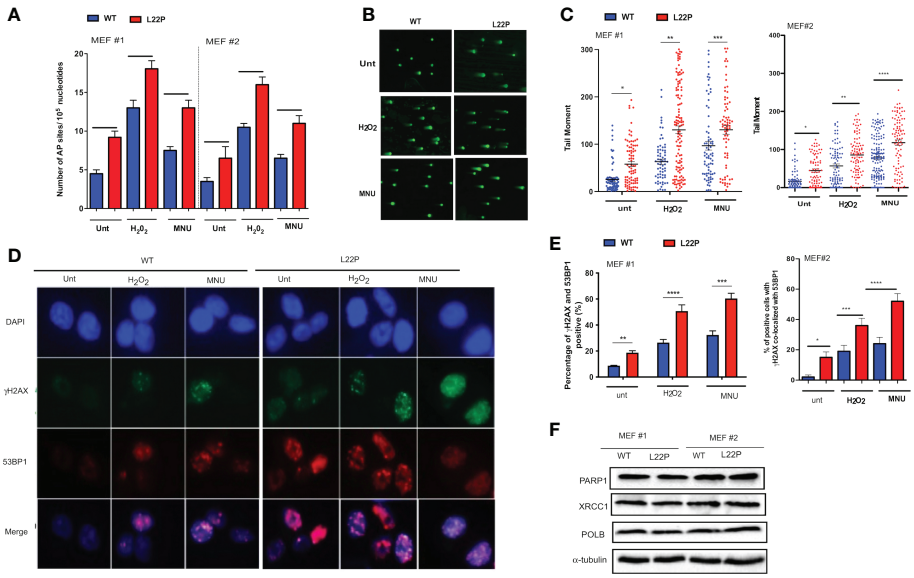

FIGURE 1
Loss of dRP lyase function causes mitotic dysfunction and telomere crisis. **(A)** Estimated AP sites with and without MNU and/or H_2O_2 treatment in WT and L22P cells; The number of AP sites was measured and calculated based upon a standard curve generated using ARP standard DNA solutions as described previously (DNA Damage AP sites assay kit, Colorimetric, Abcam). **(B)** Representative image of single stranded breaks (SSBs) from Comet assay with and without alkylating agent (MNU) and hydrogen peroxide (H_2O_2) induced in dRP lyase deficient (L22P) versus proficient (WT) cells; **(C)** Percentage of cells with SSBs in WT versus L22P cells from Comet assay. The data were analyzed based on the paired t-test using GraphPad Prism software. (n=3 independent experiments with at least 100 comets from each groups included for analysis); **(D)** Representative image of co-localization of gH2AX (green) and 53BP1 (red), which represents DSBs; **(E)** Percentage of cells positive for co-localization of H2AX/53BP1 proteins shows DSBs in WT and L22P cells. All images were taken 63x Zeiss microscope from three independent experiments and any cells with >5 foci of γH2AX/53BP1 co-localization per cell were categorized as positive. **(F)** Western bot analysis of BER proteins (PARP1, XRCC1 and POLB) from MEF#1 and MEF#2 cells. Two MEF cell lines (labeled as MEF #1 and MEF #2) were used to generate the data. Two-way ANOVA followed test or student's test were performed to analyze the data from three independent experiments. P*<0.05, **P<0.01, ***P<0.001, ****P<0.0001.

examined whether the formation of micronuclei could be initiated by errors in chromosome segregation or damaged DNA (Figure 2A). The percentage of L22P cells harboring micronuclei was significantly increased versus WT cells (35% versus 13%, P**<0.01; Figure 2B). Next, we generated stable MEF cell lines expressing C-terminally HA-tagged POLB-WT or L22P at equal levels to the endogenous WT protein and characterized the micronuclei from each of these lines. We also generated clonal MEF cell lines expressing exogenous HA-tagged human POLB (WT and L22P) at approximately equal levels to endogenous POLB in a tetracycline-repressible manner as described in Supplement Material and Methods. Supplement Figure 2 shows that MEF cells expressing L22P had increased amounts of micronuclei compared to cells expressing the WT POLB.

Furthermore, Supplement Figure 2 shows that MEF cells expressing L22P had a significantly higher percentage of cells with DSBs (Supplement Figure 2B). Furthermore, the percentage of cells with micronuclei significantly increased in MEF cells expressing HA-Tag L22P-POLB compared to cells expressing

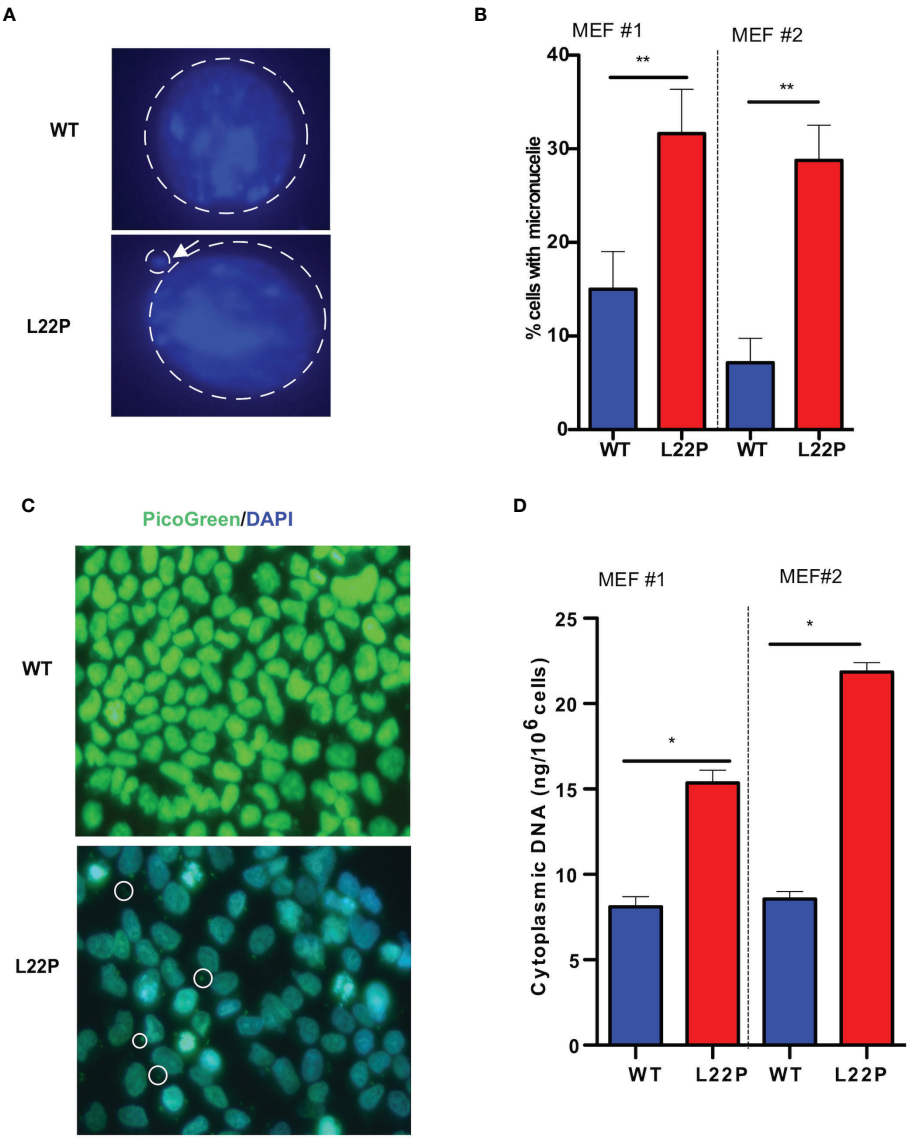

FIGURE 2
Excessive DNA accumulates in the cytosol of POLB defective cells. **(A)** Representative image of micronuclei formation in dRP lyase proficient and deficient cells; **(B)** Percentage of cells positive for micronuclei; **(C)** Representative image of subcellular localization of cytosolic DNA (bold circle shows the cytosolic DNA, green represents Picogreen stained DNA, and blue represents nuclear DNA stained with DAPI); **(D)** Quantification of cytosolic double-strand DNA (dsDNA) in L22P versus WT cells. Two MEF cell lines (labeled as MEF #1 and MEF #2) were used to generate the data. Data were analyzed using a paired t-test in GraphPad Prism; P*<0.05, **P<0.01.

10.3389/fimmu.2022.1039009

the HA- tag WT POLB (Supplement Figures 2C, D). To further determine whether BER deficient cells accumulate cytosolic DNA, we examined the localization of cytosolic DNA using PicoGreen immunofluorescence assay using L22P and WT cells. We found that a majority of the L22P cells harbored cytosolic DNA (Figure 2C; white arrow). To determine whether the aberrant dRP lyase function of L22P leads to an elevated amount of cytosolic DNA, we isolated cytosolic DNA from cytosolic fraction and total DNA from total cell extracts using the Cell Fraction Kit (Cat # ab109719, Abcam) protocol. We performed nuclear and cytoplasmic fractionation of cell lysates followed by DNA precipitation and quantified double-stranded DNA (dsDNA) in the cytoplasmic fractions of L22P and WT cells. The amount of cytosolic dsDNA was significantly higher in L22P cells (16± 3 ng/10^6 cells) as compared to WT cells (6 ± 0.2 ng/10^6 cells) (Figure 2D; data presented from two MEFs cells; MEF1 and MEF2). These results clearly demonstrate that aberrant POLB leads to elevated levels of cytosolic DNA.

Aberrant dRP lyase function of POLB cells activates the cGAS/STING pathway

Micronuclei arise following the mis-segregation of broken chromosomes during mitosis (46–48) and have recently been described as platforms for cGAS/STING-mediated immunity activation following DNA damage (47–49). We found that unrepaired DSBs trigger mitotic dysfunction (micronuclei formation) (Figures 2A, B). In addition, to determine whether cGAS localization in micronuclei is a general phenomenon in L22P cells, we transfected WT and L22P MEFs cells with pMSCVpuro-GFP-cGAS or stably expressing GFP-cGAS plasmids (generous gift from Dr. Andrew P. Jackson & Dr. Martin A. Reijns, MRC, UK) and examined the colocalization of cGAS at the micronuclei. As seen in Figure 3A, we found that cGAS strongly colocalized with micronuclei in L22P cells. In addition, the percentage of DNA sensor (cGAS) positive micronuclei was significantly increased in cells with the dRP lyase deficient POLB (27%) (Figure 3B), suggesting that nuclear DNA (nDNA) released from micronuclei may be an important danger signal to elicit an inflammatory response, functioning in an immune-stimulatory role triggering downstream factors of the STING-TANK binding kinase 1 (TBK1)-IRF3 inflammatory signaling axis. To determine whether L22P induced micronuclei trigger STING signaling activation, we examined which downstream cGAS/STING pathway proteins were activated by Western blot analysis. We found that STING-TBK1-IRF3 signaling pathways was activated in dRP lyase deficient cells [as seen by phosphorylation of STING at Ser366 (pSTING); p-TBK1 (Ser172) and p-IRF3 (Ser385)] (Figure 3C; from MEF1 and MEF2 cell lines). Moreover, to examine whether micronuclei

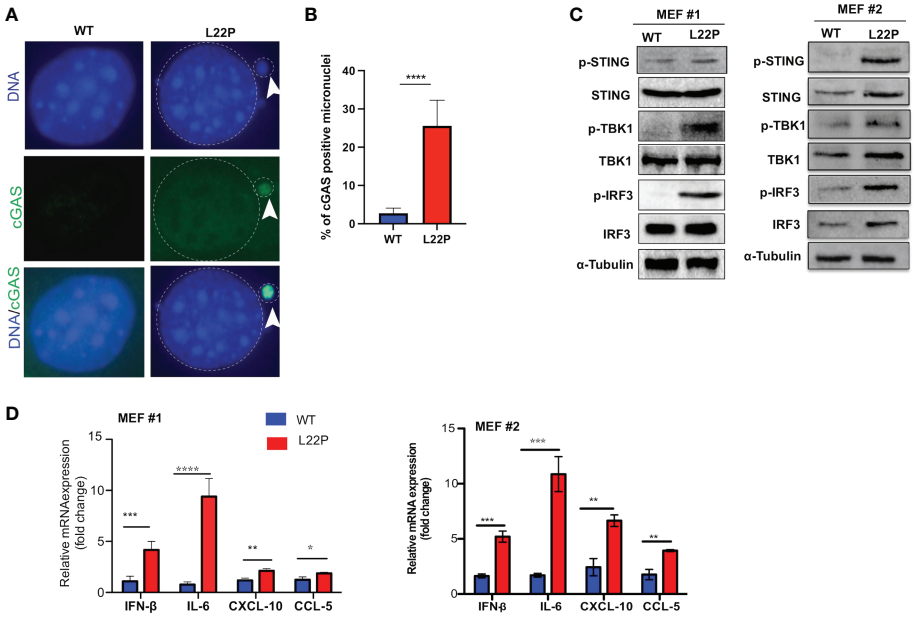

FIGURE 3
POLB defective cells exhibit cytosolic mediated cGAS-STING activation. **(A)** Representative image localization of cGAS at micronuclei; **(B)** Quantification of positive cGAS localization at micronuclei; **(C)** STING/TBK1/IRF-3 signaling pathway activation detected with Western blot of protein extract from WT and L22P cells. Anti-STING/anti-Phospho-STING (Ser366); IRF3/p-IRF3 (ser385); TBK1/P-TBK-1 (Ser172) antibodies were used to detect the activation of cGAS/STING dependent pathway. Two MEF cell lines (labeled as MEF #1 and MEF #2) were used to generate the data; **(D)** Fold change in mRNA expression of type I interferon cytokines measured using RT-qPCR in dRP lyase deficient (L22P) versus proficient cells (WT). Data were analyzed using a paired t-test in GraphPad Prism; P*<0.05, **P<0.01, ***P<0.001, ****P<0.0001.

formation induced in L22P cells might stimulate a cytokine response, we measured the levels of mRNA expression of type I interferon cytokines in WT versus L22P cells and found that interferon beta 1 (IFNβ), C-X-C motif chemokine ligand 10 (CXCL10), C-C motif chemokine ligand 5 (CCL5) and interleukin 6 (IL-6) were significantly increased in L22P cells versus WT (Figure 3D; P***<0.001; P***<0.001). Overall, this data suggested that a normally functioning POLB is required to prevent a spontaneous immune response.

Targeting PARP1 exacerbates mitotic dysfunction and enhances cytosolic DNA mediated inflammatory signaling in dRP lyase deficient cells

PARP1 is known to be activated in response to DNA damage and is responsible for the synthesis of the majority of poly(ADP-ribose) (PAR) following genotoxic stress (50, 51). In addition, PARP1 modulates different DNA repair pathways, mitosis, gene expression and cell death (51–61). Previously, we have shown that PARP1 inhibitor exacerbates genomic instability in dRP lyase deficient cells (42). PARP1 inhibitor-mediated trapping of PARP1 on DNA lesions appears to be influential for the DNA-STING immune response, as the extent of PARP1 trapping correlates with the magnitude of immune signaling (62). To determine whether blocking PARP1 enhances a DNA sensor mediated inflammatory response in dRP lyase deficient cells, L22P MEF cells were treated with the PARP1 inhibitor Olaparib (1μM). We then examined any resulting mitotic dysfunction and cGAS/STING downstream signaling cytokines. We found that 80% of L22P expressing cells harbored micronuclei versus WT cells (20%) after Olaparib treatment (Figure 4A; P****<0.001). Moreover, Olaparib treatment significantly induced cytosolic DNA in L22P cells (30ng/10^6 cells) versus WT (10ng/10^6 cells) (Figure 4B; P*** <0.001) and Olaparib treatment in dRP lyase deficient cells enhanced the cytoplasmic DNA localization (Figure 4C). Furthermore, we examined whether Olaparib treatment increased chromatin association of PARP1 in L22P cells as compared with treated WT and untreated L22P. We found that Olaparib treatment did induce chromatin associated PARP1 in dRP lyase deficient cells (Figure 4D). We also measured PARP1 trapping in dRP lyase deficient cells using a DNA silica assay (see Materials & Methods section) and found that PARP1 trapping significantly increased 3.7 fold in dRP lyase deficient cells (Figure 4E). In support of this observation, we stained dRP lyase deficient and WT cells with a primary antibody against p-IRF3 (at Ser385) and detected that the translocation of p-IRF3 to the nucleus significantly increased in L22P cells treated with Olaparib versus WT (Figures 4F, G; P**<0.01). Furthermore, the mRNA expression of type I interferon response cytokines/chemokines (IFNβ, CXCL10 and CXCL5) significantly increased in Olaparib treated L22P cells versus WT (Figure 4H; P<0.001). Next, we considered the relationship among PARP1 and

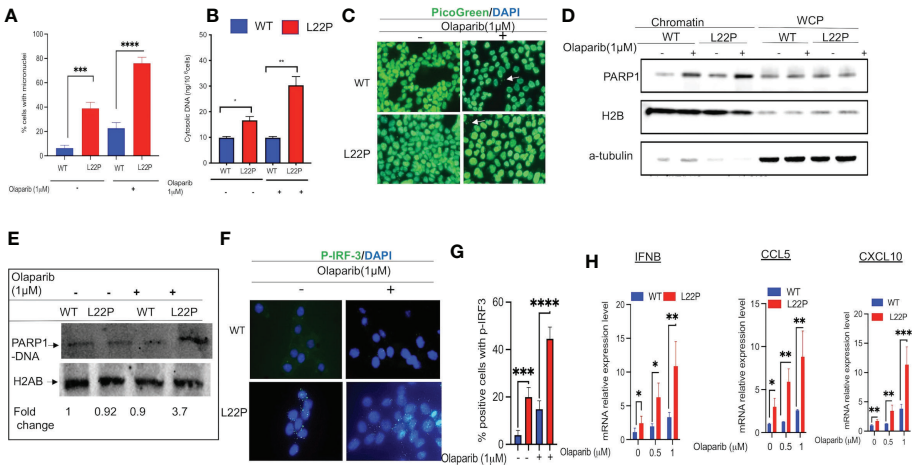

FIGURE 4
Targeting PARP1 [Olaparib (PARPi)] increases a defect in chromosomal segregation and promotes an inflammatory response. **(A)** Percent of positive cells with micronuclei after Olaparib treatment for 24 hours in L22P versus WT; **(B)** Quantification of cytoplasmic DNA from dRP lyase proficient and deficient cells; **(C)** Representative image of cells stained with Picogreen and DAPI to show cytoplasmic DNA with Olaparib and without in dRP lyase proficient and deficient cells (white arrow); **(D)** Chromatin association of PARP1 in Olaparib treated and untreated dRP lyase proficient and deficient cells; **(E)** PARP1-DNA complex analysis using dRP lyase proficient and deficient cells with and without Olaparib treatment; **(F)** Subcellular localization of p-IRF3 in dRP lyase proficient versus deficient cells with and without Olaparib treatment; **(G)** Quantification of P-IR3 positive nuclei with Olaparib treated and untreated dRP lyase proficient and deficient cells; **(H)** mRNA expression of type I interferon genes using RT-qPCR (IFNB, CCL5 and CXCL10) from WT and L22P cells with and without Olaparib treatment. Data were analyzed using a paired t-test in GraphPad Prism; P*<0.05, P**<0.01, P***<0.001, P****<0.0001.

interferon-stimulated genes (ISGs) at the transcriptional level in cancer patients by analyzing the transcriptome profiles in The Cancer Genome Atlas (TCGA) database. Our analysis indicated that PARP1 expression was negatively correlated with the expression of ISGs (IRF7 and ISG15) in human stomach cancer (n = 407 samples, $P < 0.01$), which is consistent with our *in vitro* study observations (Supplement Figure 2).

dRP lyase deficient POLB triggers cytosolic DNA mediated chronic inflammation in L22P mice

STING has recently been identified as one of the critical adaptors for sensing cytosolic DNA, followed by the phosphorylation of IRF3 and subsequent production of type-I IFN and IL-6 (63). Previously, we have found that L22P induces an accumulation of DSBs and inflammation in mice (21). To gain further insight into how spontaneous DNA damage in L22P mice drives cytosolic mediated inflammatory response, we studied the stomach of L22P and age-matched WT littermate control mice. We observed that the stomach tissue from L22P mice stained with an antibody against H2AX showed a significant percentage of positively stained cells as compared with stomach tissue derived from WT mice, which indicates an increased level of genomic instability in the L22P mice (Figures 5A, B). We then explored the expression levels of cGAS-STING pathway proteins using immunochemistry and found that the L22P mice stomach tissue had significant changes in both STING (Figures 5C, D) and p-IRF3 protein levels as well as subcellular localization (Figures 5E, F). Furthermore, the mRNA expression of interferon type-I cytokines including IFNβ, CXCL10, and CCL5 significantly increased in the stomach tissues of dRP lyase deficient mice versus WT mice (Figure 5G; P***<0.001).

Discussion

We report in this paper that POLB with a defective dRP lyase function plays a major role in cellular mitotic dysfunction and increased genomic instability. In particular, our data show that dRP lyase deficient cells harbor unrepaired BER intermediates such as apurinic/apyrimidinic (AP) sites and single-stranded DNA breaks (SSBs) that are potentially converted into DSBs. AP sites are among the most frequent spontaneous lesions in DNA. AP sites are replication-blocking lesions that could result in the accumulation of DSBs, leading to chromosomal fragmentation and genomic instability if not repaired in an accurate and timely manner (64, 65). In addition, cleavage of AP sites by AP endonucleases or AP lyases generates DNA single-strand breaks (SSBs) with 5'- or 3'-blocked ends (65). It has been previously reported that an accumulation of oxidative stress related DNA damage eventually causes replication stress in BER deficient cells (66). Our study supports that finding and shows that exposure to oxidative and alkylating DNA damaging agents exacerbates DNA damage and aberrant mitotic features in dRP

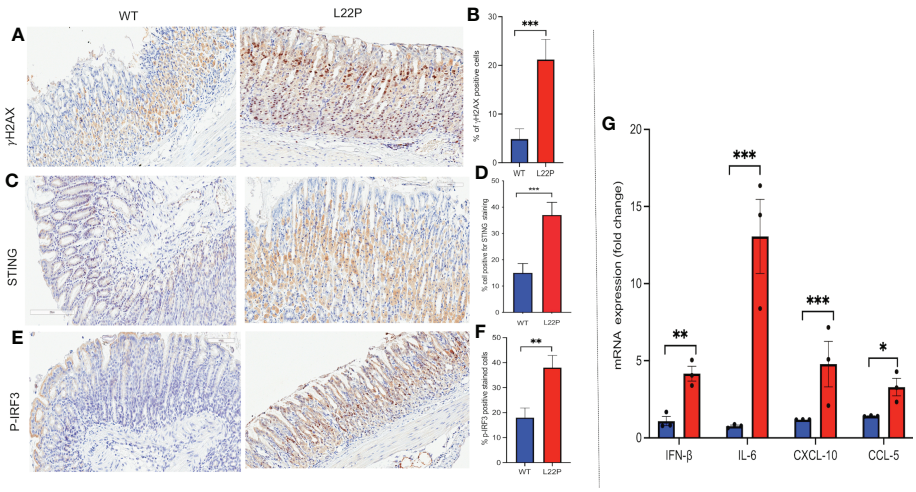

FIGURE 5
cGAS/STING activation in dRP lyase deficient mice. **(A)** Immunohistochemistry staining of stomach tissue section with DSB marker (gH2AX) in dRP lyase deficient (L22P) and WT mice; **(B)** Percentage of cells positive for gH2AX; **(C)** Immunohistochemistry staining of STING on stomach tissue of dRP lyase deficient versus proficient WT mice; **(D)** Percent of cells positive for STING **(E)** Immunohistochemistry stain of Ph-IRF3 localization in stomach tissue section of L22P versus WT mice **(F)** Percent of cells positive for ph-IRF3 **(G)** Quantification of mRNA cytosolic DNA-STING signaling mediated cytokines expression using qRT-PCR from stomach tissues derived from dRP lyase deficient and proficient WT mice. Data were analyzed using student t-test in GraphPad Prism; P*<0.05, P**<0.01, P***<0.001.

lyase deficient cells. This observation aligns with our previous results demonstrating that POLB dRP lyase deficiency increases replication associated DSBs (42). Furthermore, an elevation of micronuclei formation is commonly observed in dRP lyase deficient cells, a sign of spontaneous genomic instability. Our previously published data have shown that POLB dRP lyase deficient cells harbor mis-chromosomal segregation phenotypes and cytokinesis failure that derives from unrepaired DSBs progressing through mitosis (21). In line with this result, deficiency in several DNA repair pathways is associated with an increased frequency of micronuclei (67, 68). Importantly, other studies have demonstrated the molecular mechanism of micronuclei formation in cells following unrepaired DNA damage progressing through mitosis (48, 69).

Micronuclei formation is a consequence of irreversible nuclear envelope collapse, which arises frequently in cells due to defective nuclear lamina organization (70). It is well documented that micronuclear DNA is particularly susceptible to DNA damage, leading to chromothripsis (46, 71). We wanted to better understand how dRP lyase deficient cells with micronuclei may contribute to a release of cytosolic DNA that may play a predominant role in triggering cGAS/STING signaling. As shown in Figure 2, we analyzed the cytosolic subcellular localization of dsDNA and cytosolic DNA concentration measurements from cell extracts and found that POLB dRP lyase deficient cells accumulate cytosolic DNA which potentially serves as a danger associated molecular pattern. Our results show that a loss of nuclear genomic integrity in POLB dRP lyase deficient cells enables the cells to accrue cytosolic DNA. Similarly, other studies have shown that homologous recombination repair genes such as RPA and RAD51, which support genome stability during replication, were shown to prevent the accumulation of cytosolic DNA (72). In addition, several DNA damage response genes (e.g. ATM and DNA sensor MRE11) were found to prevent an accumulation of cytosolic DNA (32, 73). It is possible that micronuclei rupture results in immunostimulatory cytosolic DNA being recognized by cGAS, thus activating immune surveillance (48), and possibly leading to an inflammatory immune response that is known to be triggered by cytosolic DNA (74). The localization experiment as shown in Figure 3 demonstrated that a cGAS significantly localized to micronuclei in POLB dRP lyase deficient cells. In support of this observation, Mackenzie KJ, et al. have reported that cytosolic DNA accumulation is a result of genomic instability and triggers a cGAS/STING-dependent interferon response (48), which our observation support. Another study has shown that inactivation of the DNA repair genes BRCA2 results in cGAS-positive micronuclei which also triggered a cGAS-STING dependent interferon response (75). Moreover, defects in cellular DNA damage response can induce cytosolic DNA which also has been linked to a cGAS-STING mediated immune response (39, 76). Additionally, DNA structure-specific endonuclease MUS81, which cleaves DNA structures at stalled replication forks, also mediates a STING-dependent activation of immune signaling (77). Similarly, our findings highlight the involvement of DNA polymerase beta in cytosolic DNA mediated inflammatory response.

Targeting BER factors may increase cytosolic DNA and enhance cGAS-STING signaling which could increase the immunogenicity of a tumor's microenvironment. A recent publication has shown that POLB deficiency triggers cytosolic DNA mediated cGAS-STING signaling pathway activation in immune cells with autoimmune disease (78). Previously, we have shown that treatment with PARP inhibitor increases replication associated DSBs in dRP lyase deficient cells during S-phase of the cell cycle (79), which suggests that dRP lyase deficient cells accumulate 5'-dRP groups, which are critical for interaction with PARP1. Mechanistically, PARP inhibitor engages PARP1 to form a covalent bond with 5'-dRP groups and blocks BER (79) or hinders the BER process (80). Results from our study demonstrate that treatment of dRP lyase-defective cells with PARP1 inhibitor (Olaparib) increased mitotic defects and resulted in an elevated number of micronuclei. Those dRP lyase deficient cells with unrepaired DSBs will likely progress into mitosis, leading to mis-segregation of a chromosome resulting in micronuclei formation. Our data are in agreement with similar findings on the impact of PARP inhibitor causing mitotic defects such as chromosome misalignment, anaphase DNA bridges, lagging chromosomes, and micronuclei formation (81). Further, in this work we report that PARP1 inhibitor treated dRP lyase deficient cells accumulate cytosolic DNA and exhibit a significant increase in the amount of PARP-DNA complexes as well as chromatin associated PARP1 (Figure 4). As a consequence, targeting PARP leads to elevated levels of cytosolic DNA mediated cGAS-STING signaling. Our results support another previously published finding that PARP-trapping is critical for the induction of immune signaling (62). In addition, our *in vivo* data show that there is an increase in the protein expression of STING and p-IRF3 in the stomach tissue of POLB dRP lyase deficient mice. From our histological analysis, it seems that the parietal cells, which are found in the gastric glands of the stomach fundus and body, are the major target of DNA damage and IRF3 phosphorylation. Further, we show that cytokine mRNA expression significantly increased in dRP lyase deficient mice stomach tissues versus WT mice stomach tissue. These results suggest that the normal function of POLB is required for maintenance of immune homoeostasis.

Overall, our results suggest that normal function of POLB is critical to suppress cytosolic DNA mediated cGAS-STING activation. Further, PARP inhibitor treatment exacerbates cGAS-STING signaling in POLB defective cells. Our data demonstrate that PARP inhibition could be used to further increase micronuclei formation and thereby force activation of the subsequent cGAS-STING-mediated inflammatory response. It is possible that other potential cytosolic nucleic acid receptor pathways are likely activated and trigger multiple signaling cascades in dRP lyase deficient cells to trigger type I interferons and activation of TBK1, IRF3. Many studies have shown that Type I IFNs,TBK1 and IRF3 are activated by toll-like receptors (TLRs) and cytosolic nucleic acids

(RNA and DNA) sensors such as RIG-I-like receptors (RLRs) (82–85). We hope that our observations may open up new opportunities to build on this existing work and lead to an understanding of how the various cytosolic nucleic acid receptors enable dRP lyase deficient cells to induce type I interferons and pro-inflammatory cytokines. Furthermore, our study lays a foundation for future exploration into whether PARP1 inhibitor treatment might provoke inflammatory signaling and enhance immune checkpoint inhibitor treatment in BER deficient cancer patients.

Data availability statement

The original contributions presented in the study are included in the article/Supplementary Material. Further inquiries can be directed to the corresponding author.

Ethics statement

The animal study was reviewed and approved by The University of Texas at Austin, IACUC.

Author contributions

JG performed *in vitro* experiments and participated in data analysis; SZ performed data analysis, data interpretation, and manuscript writing; MS provided pathological analysis of the data and provide pathological interpretation. DK performed data analysis, interpretation, and manuscript writing. All authors contributed to the article and approved the submitted version.

Funding

The author(s) disclose receipt of the following financial support for the research, authorship, and/or publication of this article: DK was supported by NIH/NCI (R21 CA249346-01A1) and American Gastroenterology Association Robert & Sally Funderburg funds.

Acknowledgments

We thank Dr. Martin A. Reijns and Dr. Andrew P. Jackson (MRC Human Genetics Unit, MRC Institute of Genetics and Molecular Medicine, The University of Edinburgh, Edinburgh, UK) for providing the GFP-cGAS plasmid. We sincerely appreciate the researchers who worked on this experiment. We also thank Stephanie D. Scott for editing the manauscript. MS provided pathological analysis of the data and provide pathological. DK was supported by NIH/NCI (R21 CA249346-01A1) and American Gastroenterology Association Robert & Sally Funderburg funds.

Conflict of interest

The authors declare that the research was conducted in the absence of any commercial or financial relationships that could be construed as a potential conflict of interest.

Publisher's note

Supplementary material

The Supplementary Material for this article can be found online at: https://www.frontiersin.org/articles/10.3389/fimmu.2022.1039009/full#supplementary-material

References

1. Yousefzadeh M, Henpita C, Vyas R, Soto-Palma C, Robbins P, Niedernhofer L. DNA Damage-how and why we age? *Elife* (2021) 10:e62852. doi: 10.7554/eLife.62852

2. Mussali-Galante P, Avila-Costa MR, Pinon-Zarate G, Martinez-Levy G, Rodriguez-Lara V, Rojas-Lemus M, et al. DNA Damage as an early biomarker of effect in human health. *Toxicol Ind Health* (2005) 21(7-8):155–66. doi: 10.1191/0748233705th224oa

3. Sharma P, Sampath H. Mitochondrial DNA integrity: Role in health and disease. *Cells* (2019) 8(2):100. doi: 10.3390/cells8020100

4. Yu Y, Cui Y, Niedernhofer LJ, Wang Y. Occurrence, biological consequences, and human health relevance of oxidative stress-induced DNA damage. *Chem Res Toxicol* (2016) 29(12):2008–39. doi: 10.1021/acs.chemrestox.6b00265

5. Friedberg EC. A brief history of the DNA repair field. *Cell Res* (2008) 18(1):3–7. doi: 10.1038/cr.2007.113

6. Ames BN. Dietary carcinogens and anticarcinogens. oxygen radicals and degenerative diseases. *Science* (1983) 221(4617):1256–64. doi: 10.1126/science.6351251

7. Barnes DE, Lindahl T. Repair and genetic consequences of endogenous DNA base damage in mammalian cells. *Annu Rev Genet* (2004) 38:445–76. doi: 10.1146/annurev.genet.38.072902.092448

8. Lindahl T. Instability and decay of the primary structure of DNA. *Nature* (1993) 362(6422):709–15. doi: 10.1038/362709a0

9. Krokan HE, Nilsen H, Skorpen F, Otterlei M, Slupphaug G. Base excision repair of DNA in mammalian cells. *FEBS Lett* (2000) 476(1-2):73–7. doi: 10.1016/S0014-5793(00)01674-4

10. Dianov GL, Souza-Pinto N, Nyaga SG, Thybo T, Stevnsner T, Bohr VA. Base excision repair in nuclear and mitochondrial DNA. *Prog Nucleic Acid Res Mol Biol* (2001) 68:285–97. doi: 10.1016/S0079-6603(01)68107-8

11. Seifermann M, Ulges A, Bopp T, Melcea S, Schafer A, Oka S, et al. Role of the DNA repair glycosylase OGG1 in the activation of murine splenocytes. *DNA Repair (Amst)* (2017) 58:13–20. doi: 10.1016/j.dnarep.2017.08.005

12. Senejani AG, Liu Y, Kidane D, Maher SE, Zeiss CJ, Park HJ, et al. Mutation of POLB causes lupus in mice. *Cell Rep* (2014) 6(1):1–8. doi: 10.1016/j.celrep.2013.12.017

13. Wilson SH. Mammalian base excision repair and DNA polymerase beta. *Mutat Res* (1998) 407(3):203–15. doi: 10.1016/S0921-8777(98)00002-0

14. Beard WA, Horton JK, Prasad R, Wilson SH. Eukaryotic base excision repair: New approaches shine light on mechanism. *Annu Rev Biochem* (2019) 88 (1):137–62. doi: 10.1146/annurev-biochem-013118-111315

15. Fortini P, Dogliotti E. Base damage and single-strand break repair: Mechanisms and functional significance of short- and long-patch repair subpathways. *DNA Repair* (2007) 6(4):398–409. doi: 10.1016/j.dnarep.2006.10.008

16. Kubota Y, Nash RA, Klungland A, Schar P, Barnes DE, Lindahl T. Reconstitution of DNA base excision-repair with purified human proteins: Interaction between DNA polymerase beta and the XRCC1 protein. *EMBO J* (1996) 15(23):6662–70. doi: 10.1002/j.1460-2075.1996.tb01056.x

17. Wei YF, Robins P, Carter K, Caldecott K, Pappin DJ, Yu GL, et al. Molecular cloning and expression of human cDNAs encoding a novel DNA ligase IV and DNA ligase III, an enzyme active in DNA repair and recombination. *Mol Cell Biol* (1995) 15(6):3206–16. doi: 10.1128/MCB.15.6.3206

18. Tomkinson AE, Chen L, Dong Z, Leppard JB, Levin DS, Mackey ZB, et al. Completion of base excision repair by mammalian DNA ligases. *Prog Nucleic Acid Res Mol Biol* (2001) 68:151–64. doi: 10.1016/S0079-6603(01)68097-8

19. Miller AS, Balakrishnan L, Buncher NA, Opresko PL, Bambara RA. Telomere proteins POT1, TRF1 and TRF2 augment long-patch base excision repair in vitro. *Cell Cycle (Georgetown Tex)* (2012) 11(5):998–1007. doi: 10.4161/cc.11.5.19483

20. Kim Y-J, Wilson DM3rd. Overview of base excision repair biochemistry. *Curr Mol Pharmacol* (2012) 5(1):3–13. doi: 10.2174/1874467211205010003

21. Zhao S, Klattenhoff AW, Thakur M, Sebastian M, Kidane D. Mutation in DNA polymerase beta causes spontaneous chromosomal instability and inflammation-associated carcinogenesis in mice. *Cancers (Basel)* (2019) 11 (8):1160. doi: 10.3390/cancers11081160

22. David SS, O'Shea VL, Kundu S. Base-excision repair of oxidative DNA damage. *Nature* (2007) 447(7147):941–50. doi: 10.1038/nature05978

23. Hegde ML, Hazra TK, Mitra S. Early steps in the DNA base excision/single-strand interruption repair pathway in mammalian cells. *Cell Res* (2008) 18(1):27–47. doi: 10.1038/cr.2008.8

24. Yang N, Chaudhry MA, Wallace SS. Base excision repair by hNTH1 and hOGG1: A two edged sword in the processing of DNA damage in gamma-irradiated human cells. *DNA Repair (Amst)* (2006) 5(1):43–51. doi: 10.1016/j.dnarep.2005.07.003

25. Klattenhoff AW, Thakur M, Chu CS, Ray D, Habib SL, Kidane D. Loss of NEIL3 DNA glycosylase markedly increases replication associated double strand breaks and enhances sensitivity to ATR inhibitor in glioblastoma cells. *Oncotarget* (2017) 8(68):112942–58. doi: 10.18632/oncotarget.22896

26. Eccles LJ, O'Neill P, Lomax ME. Delayed repair of radiation induced clustered DNA damage: Friend or foe? *Mutat Res* (2011) 711(1-2):134–41. doi: 10.1016/j.mrfmmm.2010.11.003

27. Sage E, Harrison L. Clustered DNA lesion repair in eukaryotes: Relevance to mutagenesis and cell survival. *Mutat Res* (2011) 711(1-2):123–33. doi: 10.1016/j.mrfmmm.2010.12.010

28. Schreiber V, Dantzer F, Ame JC, de Murcia G. Poly(ADP-ribose): Novel functions for an old molecule. *Nat Rev Mol Cell Biol* (2006) 7(7):517–28. doi: 10.1038/nrm1963

29. Srivastava DK, Berg BJ, Prasad R, Molina JT, Beard WA, Tomkinson AE, et al. Mammalian abasic site base excision repair. identification of the reaction sequence and rate-determining steps. *J Biol Chem* (1998) 273(33):21203–9. doi: 10.1074/jbc.273.33.21203

30. Fontes FL, Pinheiro DML, Oliveira A, Oliveira R, Lajus TBP, Agnez-Lima LF. Role of DNA repair in host immune response and inflammation. *Mutat Research-Reviews Mutat Res* (2015) 763:246–57. doi: 10.1016/j.mrrev.2014.11.004

31. Kay J, Thadhani E, Samson L, Engelward B. Inflammation-induced DNA damage, mutations and cancer. *DNA Repair* (2019) 83:102673. doi: 10.1016/j.dnarep.2019.102673

32. Kondo T, Kobayashi J, Saitoh T, Maruyama K, Ishii KJ, Barber GN, et al. DNA Damage sensor MRE11 recognizes cytosolic double-stranded DNA and induces type I interferon by regulating STING trafficking. *Proc Natl Acad Sci USA* (2013) 110(8):2969–74. doi: 10.1073/pnas.1222694110

33. Reislander T, Lombardi EP, Groelly FJ, Miar A, Porru M, Di Vito S, et al. BRCA2 abrogation triggers innate immune responses potentiated by treatment with PARP inhibitors. *Nat Commun* (2019) 10(1):3143. doi: 10.1038/s41467-019-11048-5

34. Nowarski R, Gagliani N, Huber S, Flavell RA. Innate immune cells in inflammation and cancer. *Cancer Immunol Res* (2013) 1(2):77–84. doi: 10.1158/2326-6066.CIR-13-0081

35. Goldszmid RS, Trinchieri G. The price of immunity. *Nat Immunol* (2012) 13 (10):932–8. doi: 10.1038/ni.2422

36. Mukherjee S, Abdisalaam S, Bhattacharya S, Srinivasan K, Sinha D, Asaithamby A. Mechanistic link between DNA damage sensing, repairing and signaling factors and immune signaling. *Adv Protein Chem Struct Biol* (2019) 115:297–324. doi: 10.1016/bs.apcsb.2018.11.004

37. Ahn J, Xia T, Konno H, Konno K, Ruiz P, Barber GN. Inflammation-driven carcinogenesis is mediated through STING. *Nat Commun* (2014) 5:5166. doi: 10.1038/ncomms6166

38. Xiao TS, Fitzgerald KA. The cGAS-STING pathway for DNA sensing. *Mol Cell* (2013) 51(2):135–9. doi: 10.1016/j.molcel.2013.07.004

39. Chen Q, Sun L, Chen ZJ. Regulation and function of the cGAS-STING pathway of cytosolic DNA sensing. *Nat Immunol* (2016) 17(10):1142–9. doi: 10.1038/ni.3558

40. Liu X, Wang C. The emerging roles of the STING adaptor protein in immunity and diseases. *Immunology* (2016) 147(3):285–91. doi: 10.1111/imm.12561

41. Wu J, Sun L, Chen X, Du F, Shi H, Chen C, et al. Cyclic GMP-AMP is an endogenous second messenger in innate immune signaling by cytosolic DNA. *Science* (2013) 339(6121):826–30. doi: 10.1126/science.1229963

42. Rozacky J, Nemec AA, Sweasy JB, Kidane D. Gastric cancer associated variant of DNA polymerase beta (Leu22Pro) promotes DNA replication associated double strand breaks. *Oncotarget* (2015) 6(27):24474–87. doi: 10.18632/oncotarget.4426

43. Dalal S, Chikova A, Jaeger J, Sweasy JB. The Leu22Pro tumor-associated variant of DNA polymerase beta is dRP lyase deficient. *Nucleic Acids Res* (2008) 36 (2):411–22. doi: 10.1093/nar/gkm1053

44. Prasad R, Shock DD, Beard WA, Wilson SH. Substrate channeling in mammalian base excision repair pathways: Passing the baton. *J Biol Chem* (2010) 285(52):40479–88. doi: 10.1074/jbc.M110.155267

45. Gyori BM, Venkatachalam G, Thiagarajan PS, Hsu D, Clement MV. OpenComet: An automated tool for comet assay image analysis. *Redox Biol* (2014) 2:457–65. doi: 10.1016/j.redox.2013.12.020

46. Crasta K, Ganem NJ, Dagher R, Lantermann AB, Ivanova EV, Pan Y, et al. DNA Breaks and chromosome pulverization from errors in mitosis. *Nature* (2012) 482(7383):53–8. doi: 10.1038/nature10802

47. Gekara NO. DNA Damage-induced immune response: Micronuclei provide key platform. *J Cell Biol* (2017) 216(10):2999–3001. doi: 10.1083/jcb.201708069

48. Mackenzie KJ, Carroll P, Martin CA, Murina O, Fluteau A, Simpson DJ, et al. cGAS surveillance of micronuclei links genome instability to innate immunity. *Nature* (2017) 548(7668):461–5. doi: 10.1038/nature23449

49. Bartsch K, Knittler K, Borowski C, Rudnik S, Damme M, Aden K, et al. Absence of RNase H2 triggers generation of immunogenic micronuclei removed by autophagy. *Hum Mol Genet* (2017) 26(20):3960–72. doi: 10.1093/hmg/ddx283

50. Ray Chaudhuri A, Nussenzweig A. The multifaceted roles of PARP1 in DNA repair and chromatin remodelling. *Nat Rev Mol Cell Biol* (2017) 18(10):610–21. doi: 10.1038/nrm.2017.53

51. De Vos M, Schreiber V, Dantzer F. The diverse roles and clinical relevance of PARPs in DNA damage repair: Current state of the art. *Biochem Pharmacol* (2012) 84(2):137–46. doi: 10.1016/j.bcp.2012.03.018

52. Weaver AN, Yang ES. Beyond DNA repair: Additional functions of PARP-1 in cancer. *Front Oncol* (2013) 3:290. doi: 10.3389/fonc.2013.00290

53. Bryant HE, Petermann E, Schultz N, Jemth AS, Loseva O, Issaeva N, et al. PARP is activated at stalled forks to mediate Mre11-dependent replication restart and recombination. *EMBO J* (2009) 28(17):2601–15. doi: 10.1038/emboj.2009.206

54. Yang YG, Cortes U, Patnaik S, Jasin M, Wang ZQ. Ablation of PARP-1 does not interfere with the repair of DNA double-strand breaks, but compromises the reactivation of stalled replication forks. *Oncogene* (2004) 23(21):3872–82. doi: 10.1038/sj.onc.1207491

55. Berti M, Ray Chaudhuri A, Thangavel S, Gomathinayagam S, Kenig S, Vujanovic M, et al. Human RECQ1 promotes restart of replication forks reversed by DNA topoisomerase I inhibition. *Nat Struct Mol Biol* (2013) 20(3):347–54. doi: 10.1038/nsmb.2501

56. Ray Chaudhuri A, Hashimoto Y, Herrador R, Neelsen KJ, Fachinetti D, Bermejo R, et al. Topoisomerase I poisoning results in PARP-mediated replication fork reversal. *Nat Struct Mol Biol* (2012) 19(4):417–23. doi: 10.1038/nsmb.2258

57. Halappanavar SS, Shah GM. Defective control of mitotic and post-mitotic checkpoints in poly(ADP-ribose) polymerase-1(-/-) fibroblasts after mitotic spindle disruption. *Cell Cycle* (2004) 3(3):335–42. doi: 10.4161/cc.3.3.670

58. Kanai M, Tong WM, Sugihara E, Wang ZQ, Fukasawa K, Miwa M. Involvement of poly(ADP-ribose) polymerase 1 and poly(ADP-ribosyl)ation in regulation of centrosome function. *Mol Cell Biol* (2003) 23(7):2451–62. doi: 10.1128/MCB.23.7.2451-2462.2003

59. Tong WM, Yang YG, Cao WH, Galendo D, Frappart L, Shen Y, et al. Poly (ADP-ribose) polymerase-1 plays a role in suppressing mammary tumourigenesis in mice. *Oncogene* (2007) 26(26):3857–67. doi: 10.1038/sj.onc.1210156

60. Maya-Mendoza A, Moudry P, Merchut-Maya JM, Lee M, Strauss R, Bartek J. High speed of fork progression induces DNA replication stress and genomic instability. *Nature* (2018) 559(7713):279–84. doi: 10.1038/s41586-018-0261-5

61. Sugimura K, Takebayashi S, Taguchi H, Takeda S, Okumura K. PARP-1 ensures regulation of replication fork progression by homologous recombination on damaged DNA. *J Cell Biol* (2008) 183(7):1203–12. doi: 10.1083/jcb.200806068

62. Kim C, Wang XD, Yu Y. PARP1 inhibitors trigger innate immunity *via* PARP1 trapping-induced DNA damage response. *Elife* (2020) 9:e60637. doi: 10.7554/eLife.60637

63. Wang Y, Lian Q, Yang B, Yan S, Zhou H, He L, et al. TRIM30alpha is a negative-feedback regulator of the intracellular DNA and DNA virus-triggered response by targeting STING. *PloS Pathog* (2015) 11(6):e1005012. doi: 10.1371/journal.ppat.1005012

64. Rogakou EP, Boon C, Redon C, Bonner WM. Megabase chromatin domains involved in DNA double-strand breaks in vivo. *J Cell Biol* (1999) 146(5):905–16. doi: 10.1083/jcb.146.5.905

65. Boiteux S, Guillet M. Abasic sites in DNA: Repair and biological consequences in saccharomyces cerevisiae. *DNA Repair (Amst)* (2004) 3(1):1–12. doi: 10.1016/j.dnarep.2003.10.002

66. Fouquerel E, Barnes RP, Uttam S, Watkins SC, Bruchez MP, Opresko PL. Targeted and persistent 8-oxoguanine base damage at telomeres promotes telomere loss and crisis. *Mol Cell* (2019) 75(1):117–30 e6. doi: 10.1016/j.molcel.2019.04.024

67. Rosin MP, German J. Evidence for chromosome instability *in vivo* in bloom syndrome: Increased numbers of micronuclei in exfoliated cells. *Hum Genet* (1985) 71(3):187–91. doi: 10.1007/BF00284570

68. Shima N, Hartford SA, Duffy T, Wilson LA, Schimenti KJ, Schimenti JC. Phenotype-based identification of mouse chromosome instability mutants. *Genetics* (2003) 163(3):1031–40. doi: 10.1093/genetics/163.3.1031

69. Harding SM, Benci JL, Irianto J, Discher DE, Minn AJ, Greenberg RA. Mitotic progression following DNA damage enables pattern recognition within micronuclei. *Nature* (2017) 548(7668):466–70. doi: 10.1038/nature23470

70. Hatch EM, Fischer AH, Deerinck TJ, Hetzer MW. Catastrophic nuclear envelope collapse in cancer cell micronuclei. *Cell* (2013) 154(1):47–60. doi: 10.1016/j.cell.2013.06.007

71. Zhang CZ, Spektor A, Cornils H, Francis JM, Jackson EK, Liu S, et al. Chromothripsis from DNA damage in micronuclei. *Nature* (2015) 522(7555):179–84. doi: 10.1038/nature14493

72. Wolf C, Rapp A, Berndt N, Staroske W, Schuster M, Dobrick-Mattheuer M, et al. RPA and Rad51 constitute a cell intrinsic mechanism to protect the cytosol from self DNA. *Nat Commun* (2016) 7:11752. doi: 10.1038/ncomms11752

73. Hartlova A, Erttmann SF, Raffi FA, Schmalz AM, Resch U, Anugula S, et al. DNA Damage primes the type I interferon system *via* the cytosolic DNA sensor STING to promote anti-microbial innate immunity. *Immunity* (2015) 42(2):332–43. doi: 10.1016/j.immuni.2015.01.012

74. Deng L, Liang H, Xu M, Yang X, Burnette B, Arina A, et al. STING-dependent cytosolic DNA sensing promotes radiation-induced type I interferon-dependent antitumor immunity in immunogenic tumors. *Immunity* (2014) 41(5):843–52. doi: 10.1016/j.immuni.2014.10.019

75. Heijink AM, Talens F, Jae LT, van Gijn SE, Fehrmann RSN, Brummelkamp TR, et al. BRCA2 deficiency instigates cGAS-mediated inflammatory signaling and confers sensitivity to tumor necrosis factor-alpha-mediated cytotoxicity. *Nat Commun* (2019) 10(1):100. doi: 10.1038/s41467-018-07927-y

76. Parkes EE, Walker SM, Taggart LE, McCabe N, Knight LA, Wilkinson R, et al. Activation of STING-dependent innate immune signaling by s-Phase-Specific DNA damage in breast cancer. *J Natl Cancer Inst* (2017) 109(1):djw199. doi: 10.1093/jnci/djw199

77. Ho SS, Zhang WY, Tan NY, Khatoo M, Suter MA, Tripathi S, et al. The DNA structure-specific endonuclease MUS81 mediates DNA sensor STING-dependent host rejection of prostate cancer cells. *Immunity* (2016) 44(5):1177–89. doi: 10.1016/j.immuni.2016.04.010

78. Gu L, Sun Y, Wu T, Chen G, Tang X, Zhao L, et al. A novel mechanism for macrophage pyroptosis in rheumatoid arthritis induced by pol beta deficiency. *Cell Death Dis* (2022) 13(7):583. doi: 10.1038/s41419-022-05047-6

79. Strom CE, Johansson F, Uhlen M, Szigyarto CA, Erixon K, Helleday T. Poly (ADP-ribose) polymerase (PARP) is not involved in base excision repair but PARP inhibition traps a single-strand intermediate. *Nucleic Acids Res* (2011) 39(8):3166–75. doi: 10.1093/nar/gkq1241

80. Murai J, Huang SY, Das BB, Renaud A, Zhang Y, Doroshow JH, et al. Trapping of PARP1 and PARP2 by clinical PARP inhibitors. *Cancer Res* (2012) 72(21):5588–99. doi: 10.1158/0008-5472.CAN-12-2753

81. Slade D. Mitotic functions of poly(ADP-ribose) polymerases. *Biochem Pharmacol* (2019) 167:33–43. doi: 10.1016/j.bcp.2019.03.028

82. Liu S, Cai X, Wu J, Cong Q, Chen X, Li T, et al. Phosphorylation of innate immune adaptor proteins MAVS, STING, and TRIF induces IRF3 activation. *Science* (2015) 347(6227):aaa2630. doi: 10.1126/science.aaa2630

83. Ablasser A, Hur S. Regulation of cGAS- and RLR-mediated immunity to nucleic acids. *Nat Immunol* (2020) 21(1):17–29. doi: 10.1038/s41590-019-0556-1

84. McNab F, Mayer-Barber K, Sher A, Wack A, O'Garra A. Type I interferons in infectious disease. *Nat Rev Immunol* (2015) 15(2):87–103. doi: 10.1038/nri3787

85. Akira S, Takeda K. Toll-like receptor signalling. *Nat Rev Immunol* (2004) 4(7):499–511. doi: 10.1038/nri1391

frontiers | Frontiers in Immunology

TYPE Original Research
PUBLISHED 09 January 2023
DOI 10.3389/fimmu.2022.1090056

OPEN ACCESS

EDITED BY
Chit Laa Poh,
Sunway University, Malaysia

REVIEWED BY
Kasturi Mahadik,
Centre for Cellular & Molecular Biology (CCMB), India
Liang Bai,
Xi'an Jiaotong University, China

*CORRESPONDENCE
Haitao Lv
lvhaitao@suda.edu.cn
Lei Gu
Lei.Gu@mpi-bn.mpg.de

†These authors have contributed equally to this work

SPECIALTY SECTION
This article was submitted to Inflammation, a section of the journal Frontiers in Immunology

RECEIVED 04 November 2022
ACCEPTED 19 December 2022
PUBLISHED 09 January 2023

CITATION
Huang H, Dong J, Jiang J, Yang F, Zheng Y, Wang S, Wang N, Ma J, Hou M, Ding Y, Meng L, Zhuo W, Yang D, Qian W, Chen Q, You G, Qian G, Gu L and Lv H (2023) The role of FOXO4/NFAT2 signaling pathway in dysfunction of human coronary endothelial cells and inflammatory infiltration of vasculitis in Kawasaki disease.
Front. Immunol. 13:1090056.
doi: 10.3389/fimmu.2022.1090056

The role of FOXO4/NFAT2 signaling pathway in dysfunction of human coronary endothelial cells and inflammatory infiltration of vasculitis in Kawasaki disease

Hongbiao Huang[1,2,3†], Jinfeng Dong[4†], Jiaqi Jiang[1†], Fang Yang[2†], Yiming Zheng[1], Shuhui Wang[1], Nana Wang[1], Jin Ma[1], Miao Hou[1], Yueyue Ding[1], Lijun Meng[5], Wenyu Zhuo[1], Daoping Yang[1], Weiguo Qian[1], Qiaobin Chen[2], Guoping You[6], Guanghui Qian[1], Lei Gu[3,7*] and Haitao Lv[1*]

[1]Department of Pediatrics, Institute of Pediatric Research, Children's Hospital of Soochow University, Suzhou, Jiangsu, China, [2]Department of Pediatrics, Fujian Provincial Hospital, Fujian Provincial Clinical College of Fujian Medical University, Fuzhou, Fujian, China, [3]Epigenetics Laboratory, Max Planck Institute for Heart and Lung Research, Bad Nauheim, Germany, [4]Department of Hematology, the First Affiliated Hospital of Fujian Medical University, Fuzhou, Fujian, China, [5]Department of Hematology, Children's Hospital of Soochow University, Suzhou, China, [6]Department of Emergency, Fujian Provincial Hospital, Fujian Provincial Clinical College of Fujian Medical University, Fuzhou, Fujian, China, [7]Cardiopulmonary Institute (CPI), Bad Nauheim, Germany

Aims: The Ca+/NFAT (Nuclear factor of activated T cells) signaling pathway activation is implicated in the pathogenesis of Kawasaki disease (KD); however, we lack detailed information regarding the regulatory network involved in the human coronary endothelial cell dysfunction and cardiovascular lesion development. Herein, we aimed to use mouse and endothelial cell models of KD vasculitis *in vivo* and *in vitro* to characterize the regulatory network of NFAT pathway in KD.

Methods and Results: Among the NFAT gene family, *NFAT2* showed the strongest transcriptional activity in peripheral blood mononuclear cells (PBMCs) from patients with KD. Then, *NFAT2* overexpression and knockdown experiments in Human coronary artery endothelial cells (HCAECs) indicated that *NFAT2* overexpression disrupted endothelial cell homeostasis by regulation of adherens junctions, whereas its knockdown protected HCAECs from such dysfunction. Combined analysis using RNA-sequencing and transcription factor (TF) binding site analysis in the *NFAT2* promoter region predicted regulation by Forkhead box O4 (FOXO4). Western blotting, chromatin immunoprecipitation, and luciferase assays validated that *FOXO4* binds to the promoter and transcriptionally represses *NFAT2*. Moreover, *Foxo4* knockout increased the extent of inflamed vascular tissues in a mouse model of

KD vasculitis. Functional experiments showed that inhibition NFAT2 relieved *Foxo4* knockout exaggerated vasculitis *in vivo*.

Conclusions: Our findings revealed the FOXO4/NFAT2 axis as a vital pathway in the progression of KD that is associated with endothelial cell homeostasis and cardiovascular inflammation development.

KEYWORDS

Kawasaki disease, FOXO4, Ca+/NFAT pathway, transcription factor, vasculitis

1 Introduction

Kawasaki disease (KD) is an acute vasculitis that is self –limiting and affects children. In developed countries, KD represents the most common cause of childhood acquired heart disease (1). Serious complications include coronary artery disease, which is closely related to the incidence of cardiovascular disease, especially coronary heart disease in adulthood (2), thus, a deeper mechanistic understanding of KD is required.

The incidence of KD differs among ethnicities, thus research linking genetic background to disease susceptibility has led to improved clinical trials (3). The only signaling pathway mentioned in the Genetics section of 2017 AHA guidelines as being related to clinical treatment is the Nuclear factor of activated T cells (NFAT) pathway (3). NFAT signaling affects immune cells and endothelial cells. The reasons for these phenotypes are the expression of downstream cytokines and adhesion proteins (4, 5). Although our understanding of the relationship between NFAT signaling and KD has developed in recent decades, the detailed mechanisms of NFAT activation in KD remain unknown.

NFAT was first identified as a member of an inducible nuclear protein complex involving interleukin-2 (IL-2) in T cells (6). The NFAT transcription factor family includes five members. NFAT1 (NFATc2 or NFATp) was first identified in 1993 (7). Phosphatase calcineurin regulates NFAT2 (NFATc1 or NFATc) (8), and NFAT3~5 were also identified recently (9). Research showed that NFAT acts as a transcriptional activator in the nucleus during the development of KD. Recent research showed that NFAT signaling activation disturbs the homeostasis of human coronary artery endothelial cells (HCAECs) (4). However, the function of the NFAT pathway in HCAECs, particularly in causing KD-related vasculitis, has not been determined.

In the present study, to identify the NFAT family member with the strongest transcriptional activation in KD, their relative expression in peripheral blood mononuclear cells (PBMCs) from patients with KD and dual luciferase experiments were carried out. NFAT2 had the strongest transcriptional activation in the NFAT family, and overexpression and knockdown of *NFAT2* in HCAECs demonstrated its important role in HCAEC homeostasis *in vitro*. We also predicted that the upstream transcription factor of *NFAT2* is Forkhead box O4 (FOXO4), which binds to the *NFAT2* promoter region, as verified using chromatin immunoprecipitation-quantitative polymerase chain reaction (ChIP-qPCR).

Next, we developed a *Candida albicans* water-soluble fraction (CAWS)-induced KD vasculitis mouse model, allowing us to detect NFAT2 and FOXO4 expression in PBMCs and heart tissues. The specific NFAT inhibitory peptide (11arginine (R)-VIVIT) has been used to observe the pathological changes after suppressing NFAT signaling (10). Moreover, by generating *Foxo4* knockout mice combined with (11R)-VIVIT, we demonstrated that FOXO4 is a negative regulator in CAWS-induced KD vasculitis and NFAT2 is a positive regulator. Blocking NFAT signaling reduced the severity of KD vasculitis-associated vascular inflammation in wild-type (WT) mice and *Foxo4* knockout mice. Therefore, we identified that NFAT2 promotes KD and FOXO4 transcriptionally represses *NFAT2* during the progression of KD vasculitis.

2 Methods

2.1 Sampling of human blood

The study was carried out following the tenets of the Declaration of Helsinki and the Ethics Committee of Soochow University Affiliated Children's Hospital approved the study (Suzhou, China; approval no. 2020CS075). The Ethics Committee informed all the participants and their parents about the study details, who then provided written informed consent. Details about Sampling human blood are provided in the Supplemental material.

2.2 Genetically engineered mice

Details about genetically engineered mice are provided in the Supplemental material.

2.3 Preparation of CAWS

The CAWS was prepared from *Candida albicans* strain NBRC1385 using previously described methods (11, 12) and the details are provided in the Supplemental material.

2.4 CAWS-induced vasculitis in mouse model

All animal experiments were carried out following the Guide for the Care and Use of Laboratory Animals of the China National Institutes of Health, and the Animal Care and Use Committee of Soochow University approved the experiments (approval number: SUDA20220906A01). Details about the preparation of the genetically engineered mice are provided in the Supplemental material.

2.5 Histology and immunohistochemical staining

The sections were stained using hematoxylin and eosin (HE) and elastic van Gieson (EVG) staining as described previously (13). The severity of inflammatory infiltration was evaluated using heart vessel inflammation scores (14). The immunohistochemical quantification usied modified H-scores (15) and details are provided in the Supplemental material.

2.6 Immunofluorescence staining

More detailed descriptions about the experiments are provided in the Supplemental material.

2.7 Cell culture

Detailed descriptions of the cell culture conditions for HCAECs cells are provided in the Supplemental Information.

2.8 FOXO4 knockdown, FOXO4 overexpression, NFAT2 knockdown and NFAT2 overexpression in HCAEC cells

We packaged the lentiviruses according to a previously described method (16) and the details are provided in the Supplemental material.

2.9 Stimulation of cultured HCAECs with tumor necrosis factor-α

Details about these experiments are provided in the Supplemental material.

2.10 RNA extraction and quantitative real-time reverse transcription PCR

Experimental and primer details are provided in the Supplemental material. The $2^{-\Delta\Delta Ct}$ method (17) was used to analyze the qRT-PCR data.

2.11 Western blotting

The details about the western blotting analysis are provided in Supplemental material.

2.12 Luciferase assay

The details about the Luciferase assay are provided in the Supplemental material.

2.13 Chromatin immunoprecipitation assay

The ChIP assay was carried out according to a previously described method (18) and is detailed in the Supplemental material.

2.14 RNA sequencing

The details about the RNA-seq experiment are provided in the Supplemental material.

2.15 Cell proliferation assays

The details about cell proliferation assays are provided in the Supplemental material.

2.16 Statistical analysis

The details about the statistical analysis are provided in the Supplemental material.

3 Results

3.1 NFAT2 was significantly elevated in PBMCs from patients with KD and in the TNFα-stimulated HCAEC model

qRT-PCR analysis of PBMCs revealed that compared with other members of the NFAT family, *NFAT2* mRNA levels were significantly upregulated in patients diagnosed with KD compared with that in the healthy controls (Figure 1A). The luciferase reporter assays showed that *NFAT2* had the strongest transcriptional activity among the NFAT family (Figure 1B). To further determine the critical roles of NFAT2 in KD, 40 ng/ml TNFα was used to stimulate HCAECs to mimic vasculitis *in vitro*. The dose of TNFα was determined by the expression of NFAT2 after HCAECs were stimulated by different doses (Supplementary Figure 1A). Over 0–8 hours of stimulation, *NFAT2* mRNA showed the highest upregulation compared with other members of the NFAT family (Figure 1C). Similarly, the RNA-seq results at different timepoints also showed that *NFAT2* expression increased most significantly compared with the TNFα stimulation group at zero hour (Supplementary Figure 1B). These findings clearly demonstrated upregulated *NFAT2* mRNA expression in patients and in vasculitis *in vitro*, suggesting that NFAT2 has an important function in the development of KD.

3.2 NFAT2 disrupted the homeostasis of endothelial cells by regulating adherens junctions

To investigate the function of NFAT2 in HCAECs, *NFAT2* overexpression (OE) and knockdown (KnD) lentiviruses were transfected into HCAECs and empty lentiviral vectors for overexpression (OE-CON) and knockdown (KnD-CON) were employed as the appropriate controls. *NFAT2* overexpression and knockdown in HCAECs were verified using western blotting and qRT-PCR (Figures 2A–D).

Next, we used RNA-Seq to investigate the mechanism of NFAT2 in HCAECs. Differentially expressed genes (DEGs) in the RNA-Seq data were identified using mRNA clustering and map plotting, with criteria of an absolute value log2 FoldChange > 0 and an adjusted $p < 0.05$. Overexpression of *NFAT2* resulted in the upregulation of 2100 genes and the downregulation of 2541 genes (Figure 2E). Knockdown of *NFAT2* resulted in the

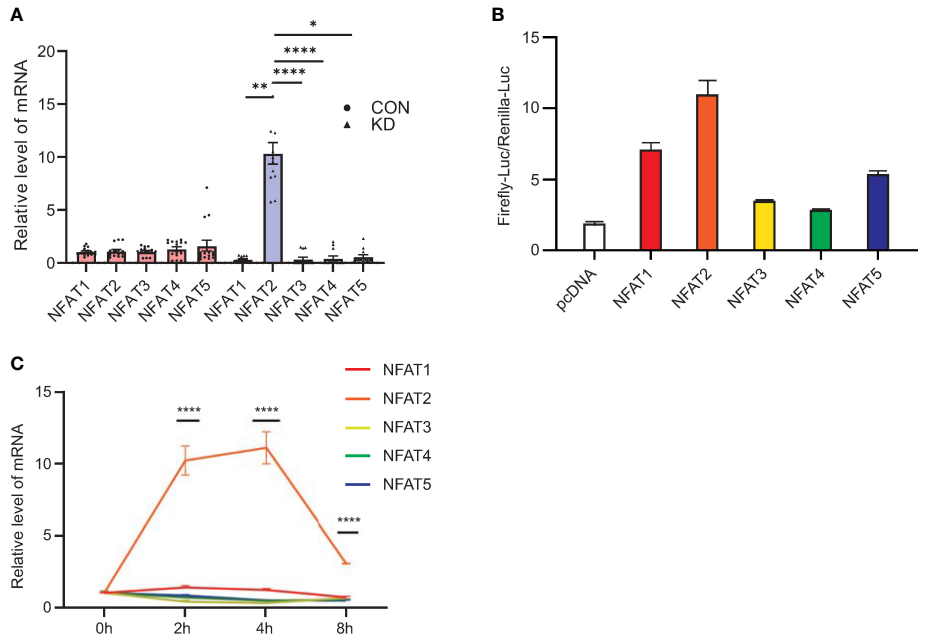

FIGURE 1
Levels of *NFAT2* mRNA increase during Kawasaki Disease progression. **(A)** qRT-PCR results for peripheral blood mononuclear cells (PBMCs) in blood samples from patients with Kawasaki Disease (n = 12) and healthy controls (n = 15). **(B)** 293T cells were transfected with control plasmid or *NFAT1~NFAT5*, together with NFAT_Luc and Renilla plasmids respectively. The cells were harvested 72 hours after transfection. The relative activity of NFAT-driven firefly luciferase activity was normalized to that of Renilla luciferase activity (Firefly-luc/Renilla-luc). **(C)** qRT-PCR results of NFAT family members in HCAEC that were stimulated by TNFα (40 ng/ml) at different timepoints (n = 3). Data are presented as the mean ± SEM. Quantitative data were analyzed using the Kruskal–Wallis test **(A)** and one-way ANOVA **(C)**, *P < 0.05, **P < 0.01, ****P < 0.0001. CON, control group; KD, Kawasaki Disease; NFAT, nuclear factor of activated T cells; HCAEC, Human coronary artery endothelial cells; ANOVA, analysis of variance.

upregulation of 808 genes and the downregulation of 846 genes in HCAECs (Figure 2F). Gene ontology (GO) analysis was then used to functionally annotate the DEGs. The GO results indicated that the genes regulated by NFAT2 were involved in the regulation of adherens junctions, such as cell adhesion molecule binding and cell-substrate junction (Figures 2G, H).

To confirm the GO results, we chose the classical molecule Cadherin 5 (CDH5) to carry out an adherens junction

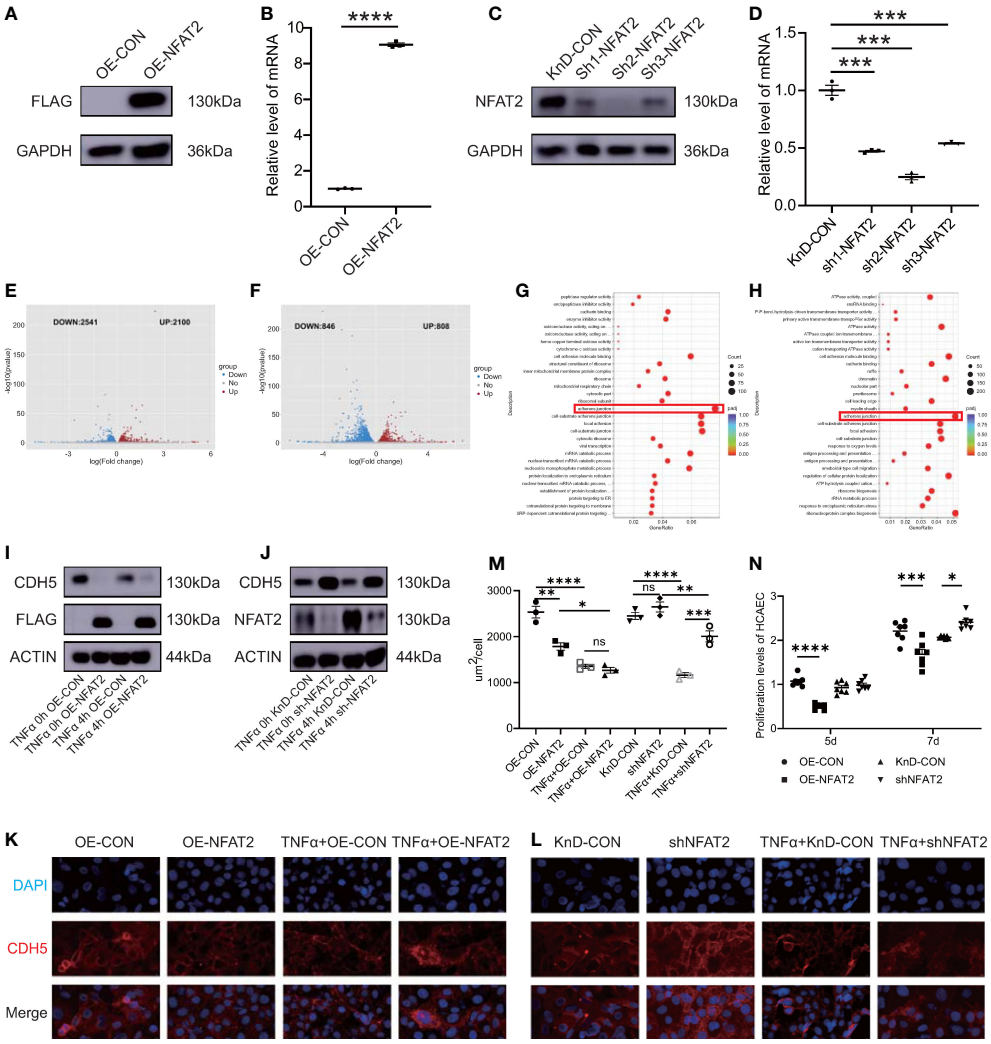

FIGURE 2
NFAT2 disrupted endothelial cell homeostasis. **(A, B)** At 7 days after transfection of *NFAT2* overexpressing lentiviruses ((OE-NFAT2) and their corresponding control (OE-CON), **(A)** NFAT2 protein levels were assayed using western blotting, with a loading control comprising GAPDH, and **(B)** *NFAT2* mRNA expression was assessed using qRT-PCR (n = 3). **(C, D)** At 7 days after transfection of lentiviruses for the knockdown *NFAT2* (sh1~sh3) and its corresponding controls (KnD-CON), **(C)** western blotting was used to assess NFAT2 protein levels, with a loading control comprising GAPDH, and **(D)** *NFAT2* mRNA expression was assessed using qRT-PCR (n = 3). **(E, F)** Volcano plot showing differentially expressed genes (DEGs) in response to *NFAT2* overexpression **(E)** or *NFAT2* knockdown **(F)**. Red dots represent upregulated genes; and blue dots represent downregulated genes. Gene Ontology (GO) functional enrichment analysis of DEGs related to *NFAT2* overexpression **(G)** and *NFAT2* knockdown **(H)**. **(I)** HCAECs transfected with *NFAT2* overexpressing lentiviruses (OE-NFAT2) and their corresponding control (OE-CON) were stimulated with/without TNFα (40 ng/ml) for 4 hours. CDH5 and NFAT2 protein levels were analyzed. β-Actin served as a loading control. **(J)** HCAECs transfected with *NFAT2* knockdown lentiviruses (shNFAT2) and their corresponding control (KnD-CON) were stimulated with/without TNFα (40 ng/ml) for 4 hours. CDH5 and NFAT2 protein levels were analyzed as described. β-Actin served as a loading control. **(K–M)** The expression of CDH5 was detected by immunofluorescence. *NFAT2* overexpression **(K)** and knockdown **(L)** vectors and their corresponding controls were transfected into HCAECs, respectively. After 7 days, cells were stimulated with/without TNFα (40 ng/ml) for 4 hours. The cells were immunostained with rabbit anti-CDH5, followed by staining with 594 goat anti-rabbit IgG (red). Cell nuclei were stained with DAPI (blue). The fluorescent images were captured **(K)**. The immunofluorescence area per cell in the different groups is shown **(M)** (n = 3). **(N)** HCAECs were transfected with *NFAT2* overexpression and knockdown vectors and their corresponding controls. After 5 days and 7 days, the proliferation of HCAECs were detected using a CCK8 assay (n = 7). Data are presented as the mean ± SEM. Quantitative data were analyzed using an unpaired t test (two-tailed) **(B, D)** and one-way ANOVA **(M, N)**, *P < 0.05, **P < 0.01, ***P < 0.001, ****P < 0.0001.

experiment in HCAECs (19, 20). NFAT2 negatively regulated CDH5 expression in both the overexpression and knockdown group. The protein level of CDH5 decreased after TNFα stimulation, regardless of whether NFAT2 was overexpressed or not (Figures 2I, J). Consistently, immunofluorescence staining for CDH5 showed that overexpression of *NFAT2* notably disrupted CDH5 formation. Conversely, knockdown of *NFAT2* promoted the formation of CDH5. Regardless of the expression level of NFAT2, CDH5 levels were decreased in TNFα-stimulated cells compared with that in TNFα non-treated HCAECs (Figures 2K–M).

We also evaluated HCAEC proliferation using Counting Kit-8(CCK8) assays (4). The results showed that the proliferation of HCAECs in the OE-NFAT2 group at 5 and 7 days was significantly lower than that in the OE-CON group. In the KnD-NFAT2 group, HCAEC proliferation was not statistically significant at 5 days, but was significantly higher than that in the KnD-CON group at 7 days (Figure 2N). Collectively, the data indicated that NFAT2 has a vital function in the homeostasis of HCAECs.

3.3 FOXO4 negatively regulates NFAT2 in HCAECs

Next, we investigated the regulation of NFAT2 *in vitro*. We identified genes with variable expression in the *in vitro* vasculitis model that could interact with the *NFAT2* promoter region as possible NFAT2 regulators. The RNA-seq analysis was carried out between HCAECs stimulated with TNFα for 4 h and unstimulated cells to identify DEGs (Figure 3A). The LASAGNA-Search 2.0 database was used to predict proteins that can interact with the promoter region of *NFAT2* (21) (Supplementary Figure 1C). Among the DEGs that were altered in the *in vitro* vasculitis model, four encoded proteins that might bind to the *NFAT2* promoter (Figures 3B, C). Among them, FOXO4 had highest prediction score. In addition, during TNFα stimulation of HCAECs for different times, *FOXO4* mRNA expression decreased significantly after 4 h (Supplementary Figures 1B, D).

To observe the expression of *FOXO4* in immune cells, we detected the mRNA expression of *FOXO4* in PBMCs from the healthy control group and patients with KD. Compared with that in the control group, the KD group had lower *FOXO4* expression in PBMCs (Figure 3D).

To identify the relationship between FOXO4 and NFAT2, several experiments were carried out *in vitro*. First, increasing amounts of the *FOXO4* overexpression plasmid were transfected into 293T cells. The immunoblotting results showed that *FOXO4* overexpression decreased the endogenous NFAT2 protein level in 293T cells. The increased amounts of transfected *FOXO4* led to a dose-dependent decrease in the levels of NFAT (Figure 3E). Consistent with protein level, *NFAT2* mRNA expression decreased gradually in cells overexpressing *FOXO4* (Figures 3F, G), suggesting that *FOXO4* regulates *NFAT2* at the mRNA level. We then showed that *FOXO4* overexpression decreased the protein level of NFAT2, whereas *FOXO4* knockdown increased it in HCAECs (Figures 3H, I). It is very difficult to transfect multiple plasmids into HCAECs at the same time; therefore, we used 293T cells for the luciferase assays, similar to previous research (22). Luciferase reporter assays showed that *FOXO4* overexpression inhibited the activation of the *NFAT2* reporter (Figure 3J), suggesting that FOXO4 regulates the transcription of *NFAT2*.

To further determine whether FOXO4 directly regulates *NFAT2* in HCAECs, we carried out a ChIP assay in HCAECs transfected with FLAG-tagged FOXO4 lentivirus to identify the binding regions. Primers were designed to amplify various genomic fragments upstream of the transcription start site of *NFAT2*. Real-time PCR assays of the immunoprecipitated DNA revealed that the P3~5 (−2331/−1049 bp) fragments had the highest enrichment (Figure 3K). Other fragments were not enriched compared with the immunoglobulin G control (Figure 3K). According to the luciferase activities, FOXO4 repressed both the basal *NFAT2* transcription and that driven by the −2300/−1000 fragment in a dose-dependent manner (Figure 3L). Thus, these results identified FOXO4 as a transcriptional repressor of *NFAT2* that physically binds to the −2300/−1000 region of its promoter.

3.4 FOXO4 stabilized the homeostasis of endothelial cells

Next, we investigated if FOXO4 has opposite functions to those of NFAT2. *FOXO4* overexpression (OE) and knockdown (KnD) lentiviruses were transfected into HCAECs. The protein level of CDH5 decreased after TNFα stimulation regardless of *FOXO4* overexpression (Figures 4A, B). Immunofluorescence staining for CDH5 indicated that *FOXO4* overexpression promoted CDH5 formation at intercellular borders, which was consistent with the western blotting results. TNFα-stimulated HCAECs showed lower CDH5 levels than TNFα non-treated HCAECs (Figures 4C–E).

The proliferation of HCAECs in the OE-FOXO4 group was significantly higher than that in the OE-CON group and proliferation in the KnD-FOXO4 group was significantly lower than that in the KnD-CON group at 7 days (Figure 4F). These data strongly suggested that FOXO4 has the opposite function to NFAT2 in maintaining endothelial cell homeostasis.

10.3389/fimmu.2022.1090056

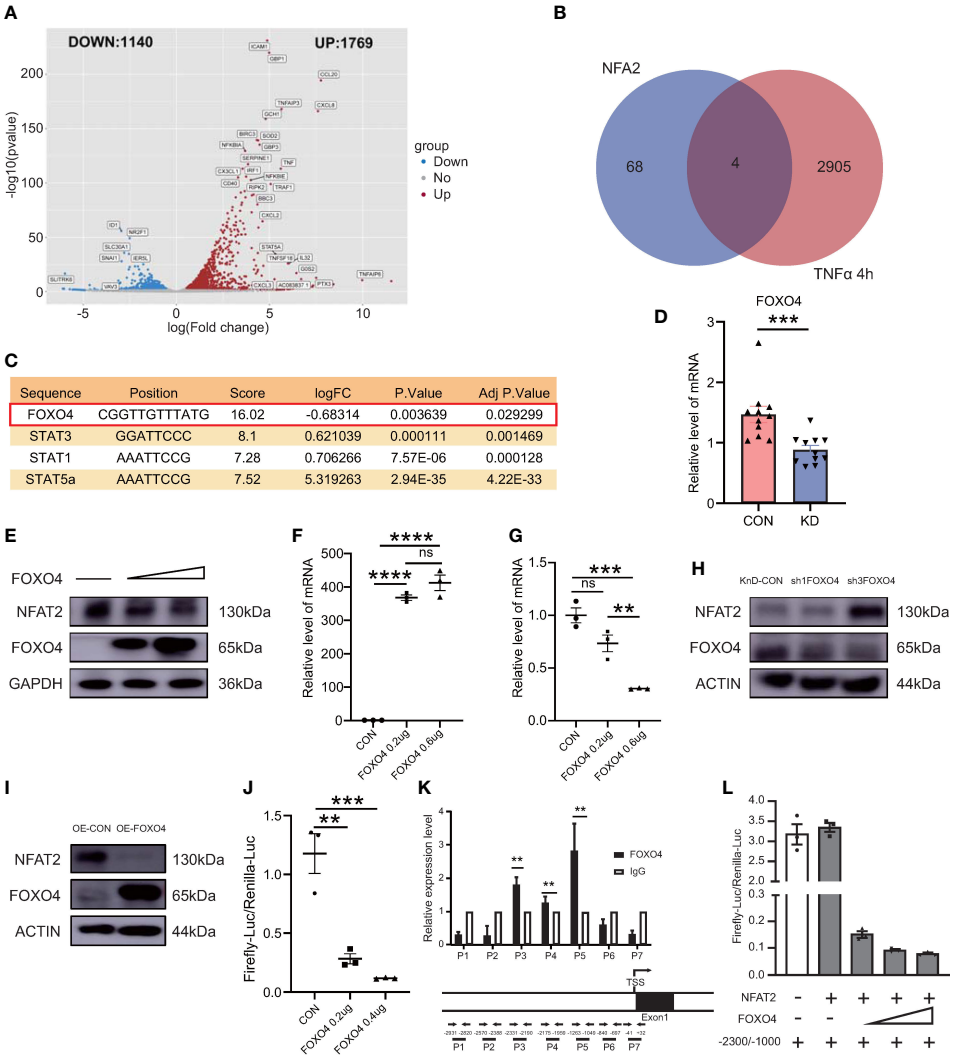

FIGURE 3
FOXO4 negatively regulates *NFAT2* by inhibiting its transcription binding to its promoter *in vitro*. **(A)** Volcano plot map of differentially expressed genes (DEGs) in HCAECs stimulated by TNFα (40ng/ml) for 4 hours. Red dots, upregulated genes; blue dots, downregulated genes. **(B)** Venn diagram displaying the overlapping genes between the DEGs in **(B)** and target genes predicted to have NFAT2 binding sites in their promoter or transcription start site according to the LASAGNA-Search 2.0 database. **(C)** Detailed information for the four overlapping genes. **(D)** *FOXO4* mRNA expression in peripheral blood mononuclear cells (PBMCs) in blood samples from patients with Kawasaki Disease (n = 11) and healthy controls (n = 11). **(E)** Immunoblotting analysis of NFAT2 levels in 293T cells transfected with the empty vector or an increasing amount of FOXO4 plasmid. **(F, G)** qRT-PCR results of 293T cells transfected with empty vector or an increasing amount of FOXO4 plasmid. mRNA expression of *FOXO4* **(F)** and *NFAT2* **(G)**. **(H–I)** HCAECs were transfected with *FOXO4* overexpression (OE-FOXO4) **(H)** and knockdown (shFOXO4) **(I)** lentiviruses and their corresponding controls for 7 days. FOXO4 and NFAT2 levels were analyzed. The loading control was β-Actin. **(J)** 293T cells were transfected with the control plasmid or increasing amounts of the FOXO4 plasmid, together with NFAT_Luc and Renilla plasmids, respectively. The cells were harvested at 72 hours after transfection. The relative NFAT-driven firefly luciferase activity was normalized to that of Renilla luciferase (Firefly-luc/Renilla-luc). **(K)** HCAECs transfected with *FOXO4* overexpressing lentiviruses were subjected to a ChIP assay. Real-time PCR with the indicated primers was used to assess the abundance of gene fragments in the input and immunoprecipitates. The upper image shows the *NFAT2* gene expression and the lower image shows the locations of primers for the ChIP assay. **(L)** The Firefly-luc/Renilla-luc in 293T cells transfected with the indicated plasmids. The location of the transcription start site in *NFAT2* was set as 0. Therefore, –2300 and –1000 indicate the upstream 1000~2300 bp fragments, respectively. IgG, immunoglobulin **(G)** Data are presented as the mean ± SEM. Quantitative data were analyzed using the Mann–Whitney test (two-tailed) **(D)** and one-way ANOVA **(F, G, J)**, **P < 0.01, ***P < 0.001, ****P < 0.0001.

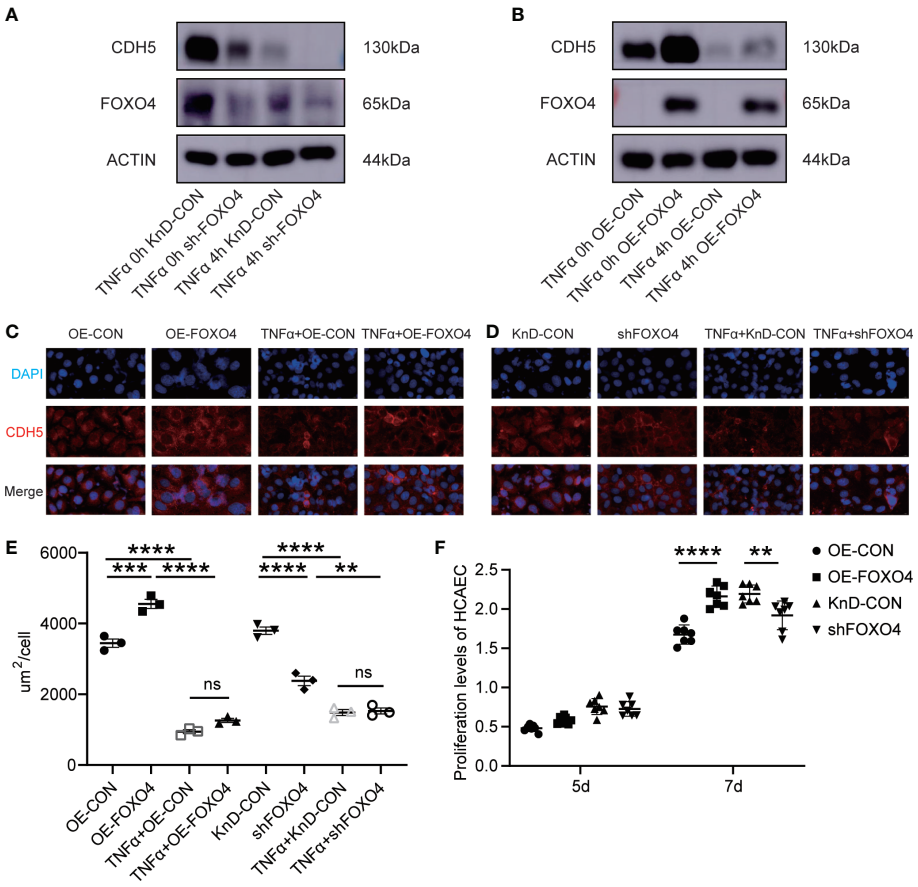

FIGURE 4
FOXO4 stabilized endothelial cell homeostasis *in vitro*. **(A)** HCAECs transfected with lentiviruses to knockdown *FOXO4* lentiviral (shFOXO4) and their corresponding controls (KnD-CON) were stimulated with/without TNFα (40 ng/ml) for 4 hours. CDH5 and FOXO4 levels were analyzed. The loading control was β-Actin. **(B)** HCAECs transfected with lentiviruses overexpressing *FOXO4* (OE-FOXO4) and their corresponding controls (OE-CON) were stimulated with/without TNFα (40 ng/ml) for 4 hours. CDH5 and NFAT2 protein level were analyzed. The loading control was β-Actin. **(C-E)** CDH5 expression was detected using immunofluorescence. *FOXO4* overexpression **(C)** and knockdown **(D)** vectors and their corresponding controls were transfected into HCAECs, respectively. After 7 days, cells were stimulated with/without TNFα (40 ng/ml) for 4 hours. The cells were then immunostained with rabbit anti-CDH5, followed by staining with 594 goat anti-rabbit IgG (red). Cell nuclei were stained with DAPI (blue) and the fluorescent images were captured. The immunofluorescence area per cell in the different groups (n = 3) **(E)**. **(F)** FOXO4 overexpression and knockdown vectors and their corresponding controls were transfected into HCAECs, respectively. After 5 days and 7 days, CCKL8 assays were used to detect HCAEC proliferation (n = 7). Data are presented as the mean ± SEM. Quantitative data were analyzed using one-way ANOVA **(E, F)**, **P < 0.01, ***P < 0.001, ****P < 0.0001.

3.5 The expression of NFAT2 is upregulated in CAWS-induced vasculitis

We further investigated the *in vivo* expression of NFAT2 and FOXO4. CAWS-induced vasculitis is widely used to study KD because the coronary artery lesions induced by CAWS are similar those of human KD (23). We tested different timepoints after CAWS injection to identify the most appropriate timepoint (Figure 5A). The weight of mice decreased slightly after the injection of CAWS, with the most obvious difference between the weight of the CAWS and control groups being observed at 14 days after CAWS injection (Figure 5B, Supplementary Figure 2D). HE and EVG staining indicated that perivascular inflammation began 14 days after CAWS injection, and the inflammatory infiltration was more obvious and the fibrous tissue damage was more serious at 28 days after CAWS injection (Figures 5C–E, Supplementary Figure 2A–C).

In PBMCs of CAWS injected mice, *Nfat2* expression increased significantly at 14 days after CAWS injection (Figure 5F) and *Foxo4* expression decreased (Figure 5G). Interestingly, the expression of *Foxo4* increased at 28 days (Figure 5G and Supplementary Figure 2F–H). In the heart tissue of the CAWS injected mice, the protein level of NFAT2 showed a similar phenomenon (Figure 5H). Therefore, we used 14 days after CAWS injection as the timepoint in the vasculitis model for follow-up studies. FOXO4 was downregulated at both

10.3389/fimmu.2022.1090056

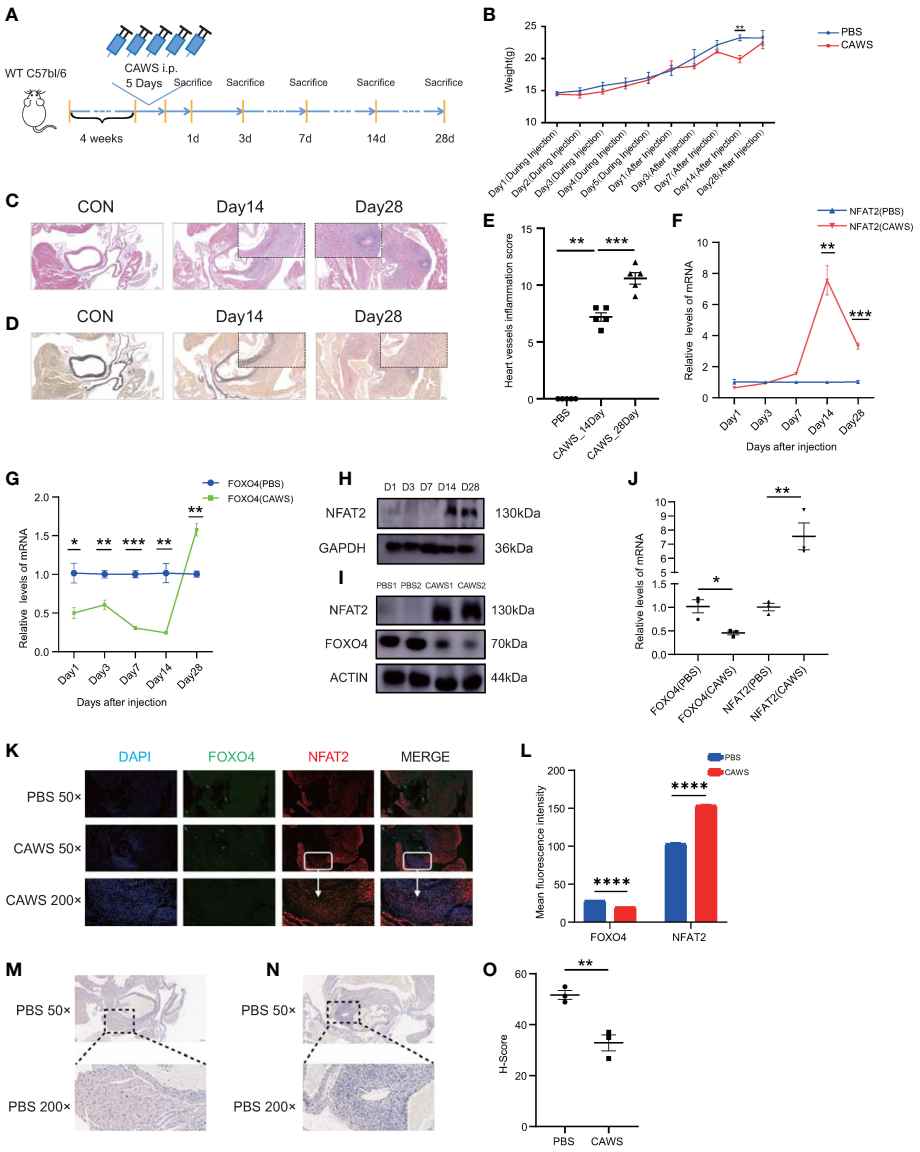

FIGURE 5
NFAT2 expression levels are upregulated during the progression of CAWS-induced vasculitis. **(A)** The protocol for constructing the CAWS-induced mouse model. **(B)** The change of weight during (n = 5) and after (n = 5) PBS/CAWS injection in mice. **(C, D)** At different timepoints the mouse were sacrificed, heart tissues were harvested, made into sections, and subjected to hematoxylin and eosin **(HE)** staining **(C)** and elastic van Gieson (EVG) staining **(D)**. Scale bars, 200 μm (50×) (Large) and 10 μm (200×) (Small). **(E)** Scores of heart vessel inflammation for WT mice injected with CAWS (n = 5). **(F–H)** NFAT expression was significantly upregulated at 14–28 days after CAWS injection, at the mRNA level in PBMCs (n = 3) **(F)** and at the protein level in heart tissues **(H)**, especially after 14 days. **(G)** The mRNA expression of *Foxo4* was almost opposite to that of *Nfat2* in PBMCs (n = 3). **(I, J)** NFAT expression was upregulated and that of FOXO4 was downregulated in heart tissues at 14 days after CAWS injection at both protein (n = 3) **(I)** and mRNA **(J)** levels. **(K)** Immunofluorescence imaging of FOXO4 (green) and NFAT2 (red) in heart sections from PBS/CAWS-injected 14 days WT group mice. Scale bars, 200 μm (50×) and 10 μm (200×). All images show DAPI staining of nuclei. **(L)** Mean fluorescence intensity of FOXO4 and NFAT2 in heart sections from PBS/CAWS-injected 14 days WT group mice. **(M–O)** Immunohistochemical staining for CDH5 in heart sections from PBS-injected **(M)** and CAWS-injected **(N)** WT group mice. CDH5 protein levels quantified using the H-score **(O)** (n = 3). Data are presented as the mean ± SEM. Quantitative data were analyzed using unpaired t tests (two-tailed) **(B, F, G, J, L, O)** and the Mann–Whitney test (two-tailed) **(E)** *P < 0.05, **P < 0.01, ***P < 0.001, ****P < 0.0001.

the mRNA and protein level at 14 days after CAWS injection (Figure 5I, J). The LASAGNA-Search 2.0 database also predicted target proteins that bind the promoter of *Nfat2* in the mouse, including FOXO4 (Supplementary Figure 2E).

Next, we sought to determine whether the increase of NFAT2 was associated with the inflamed region from CAWS-injected heart tissue. Consequently, immunofluorescence was used to detect NFAT2 and FOXO4 expression in heart tissue sections

from CAWS-injected mice. NFAT2 expression increased and FOXO4 decreased in the inflamed region of the heart tissue at 14 and 28 days after CAWS injection (Figures 5K, L and Supplementary Figure 2F–H). CDH5 expression decreased in the inflamed area, which was verified by western blotting (Figures 5M–O). Taken together, these data demonstrated that NFAT2 was upregulated and FOXO4 was downregulated in CAWS-induced heart tissues, especially in the inflamed region.

For better understand the phenotypic changes in inflamed region, we also performed immunofluorescence to detect classic immune cell infiltration. The results showed that macrophages (F4/80) and monocytes (CD14) infiltrated in the areas of high inflammation, which has been verified infiltrated in a KD-like mouse model abdominal aorta using single cell RNA-Seq (24) (Supplement Figure 3 A–D).

3.6 NFAT2 pharmacological blockade alleviates CAWS-induced KD vasculitis

NFAT2 expression increased in the inflammatory regions and the Ca+/NFAT pathway plays an important role in KD (3); therefore, we used an NFAT2 inhibitor to determine whether it could inhibit inflammation in CAWS-induced KD vasculitis. The peptide 11R-VIVIT was used because it is a highly specific inhibitor of the NFAT signaling pathway. To observe the effect of 11R-VIVIT on the NFAT family, we detect the mRNA level of NFAT members in CAWS and 11R-VIVIT injected heart tissue. The results demonstrated the expression of *Nfat2* was downregulated most significantly among NFAT family members (Figure 6A). Compared with that in the CAWS +DMSO-injected control group, the NFAT2 protein level was significantly downregulated after 5 days of continuous 11R-VIVIT injection (Figures 6B, C).

To ascertain whether blocking NFAT2 directly would reduce CAWS-induced KD vasculitis, mice were administered with 11R-VIVIT for 5 consecutive days starting 1 h before CAWS injection. We found that 11R-VIVIT treatment significantly reduced CAWS-induced vasculitis (Figures 6D–F). NFAT2 expression also decreased in the inflamed region of the heart tissue at 14 days after 11E-VIVIT injection (Figures 6G, J). Treatment with 11R-VIVIT also increased CDH5 expression in the inflamed region of CAWS-injected heart tissue (Figures 6H–J). Taken together, our results showed that inhibition of NFAT2 using 11R-VIVIT partly prevented the development of CAWS-induced heart inflammation in mice.

3.7 NFAT2 acts as the downstream molecule of FOXO4 in CAWS-induced vasculitis

To determine FOXO4's *in vivo* functions, we bought the *Foxo4*-KO mouse from Cyagen Biosciences (designated as Foxo4^{em1cyagen}). The *Foxo4* gene (NM_018789) is located on mouse chromosome X and comprises three exons. To produce the KO mouse, all three exons were targeted by Cas9/gRNA co-injection into fertilized eggs (Figure 7A). Loss of *Foxo4* in the *Foxo4*-KO mice was verified by DNA electrophoresis (Supplementary Figure 4A). Wild-type (WT) mice and Foxo4^{em1cyagen} mice were injected with PBS or CAWS, respectively. After 14 days of injection, heart tissue was processed for HE and EVG-staining for histological examination (Supplementary Figure 4B). Compared with that in the WT group, the Foxo4^{em1cyagen} group showed increased heart artery inflammation after CAWS-induced KD vasculitis. There were no significant differences after PBS injection in both the WT and Foxo4^{em1cyagen} groups (Figures 7B–D). NFAT2 expression increased in the CAWS-injected Foxo4^{em1cyagen} group compared with that in the PBS-injected Foxo4^{em1cyagen} group and the CAWS-injected WT group (Figures 7E, H, Supplementary Figure 4C). In contrast, CDH5 expression decreased significantly in the CAWS-injected Foxo4^{em1cyagen} group compared with that in PBS injection group (Figures 7F–H).

These results encouraged us to assess whether FOXO4 modulates CAWS-induced vasculitis through NFAT2. We carried out rescue experiments in the Foxo4^{em1cyagen} group by simultaneously injecting CAWS and inhibiting NFAT2 using 11R-VIVIT (Supplementary Figure 4D). We observed that injection of 11R-VIVIT in the CAWS-injected Foxo4^{em1cyagen} group partly alleviated heart artery inflammation and the heart vessel inflammation scores also decreased (Figures 7I–K). Furthermore, 11R-VIVIT partially increased the expression of CDH5 and decreased the expression of NFAT2 in the inflamed region of CAWS-induced heart tissue (Figures 7L–O, Supplementary Figure 4E). As a result, we concluded that knockout of *Foxo4* promotes inflammation in CAWS-induced KD vasculitis, at least in part, by activating the transcription of *Nfat2*.

4 Discussion

Initially, this study was prompted by the observation that transcription factor (TF) NFAT2 is upregulated in immune cells and stromal cells through NFAT signaling, a pathway associated with KD. Recent studies on KD showed that the formation of vasculitis is highly related to the infiltration of immune cells into stromal cells (24). To better understand the role of the NFAT signaling pathway, especially that of NFAT2, in KD progression, we conducted our research from three different aspects. First, we identified that NFAT2 has the strongest transcriptional activation among NFAT family member. Second, we used TNFα-stimulated HCAECs to simulate the infiltration of stromal cells in vasculitis. Third, we used a CAWS-induced mouse model of KD vasculitis to study the overall changes in

10.3389/fimmu.2022.1090056

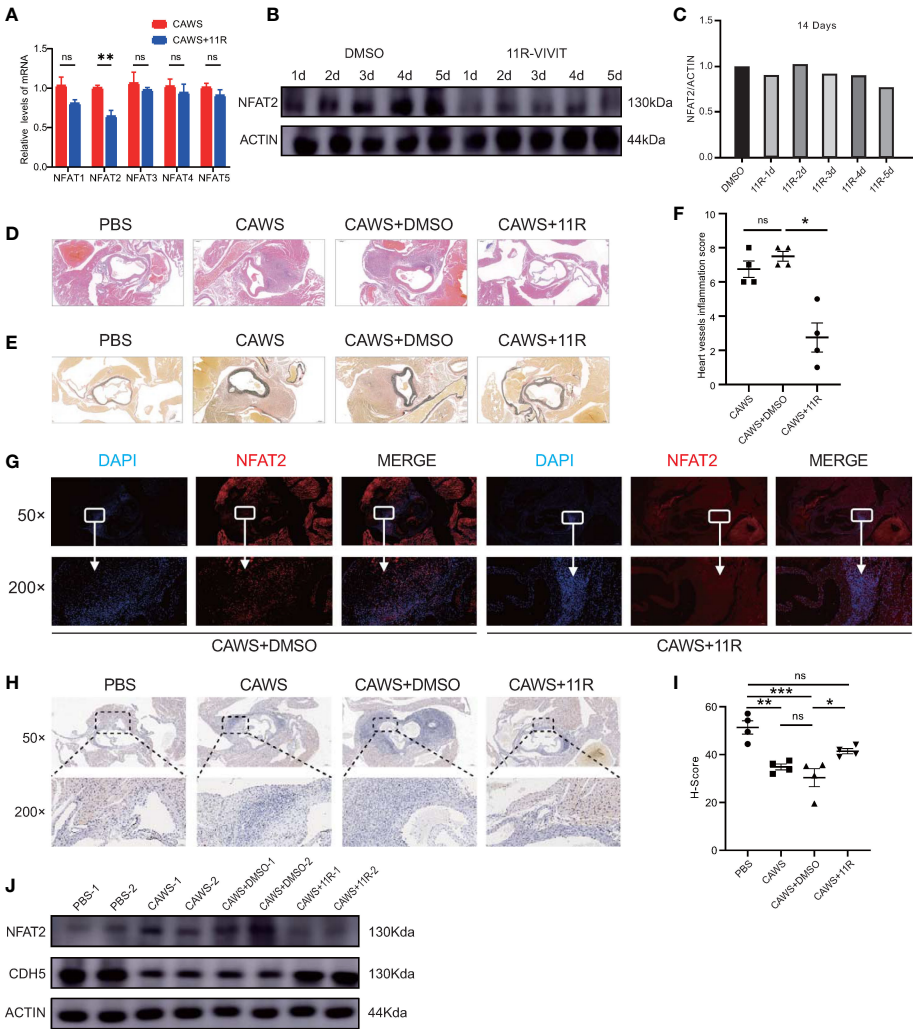

FIGURE 6
11R-VIVIT alleviated CAWS-induced KD vasculitis. **(A)** qRT-PCR results for NFAT family members in CAWS+11R-VIVIT injected heart tissue (n = 3). **(B, C)** Immunoblotting analysis of NFAT2 levels in mouse heart tissues from CAWS groups and mouse models injected with an increasing amount of 11R-VIVIT. The loading control comprised β-Actin **(B)**. NFAT2 levels in different groups quantified using ImageJ **(C)**. **(D–F)** Different groups the mouse were sacrificed and heart tissues were harvested, made into sections, and then subjected to hematoxylin and eosin (HE) staining **(D)** and elastic van Gieson (EVG) staining **(F)**. Heart vessel inflammation scores of WT mice in different groups was analyzed **(F)** (n = 4). **(G)** Immunofluorescent staining for NFAT2 (red) in heart sections from CAWS+DMSO/CAWS+11R-injected WT mice. All images show DAPI staining of nuclei. **(H)** immunohistochemical staining for CDH5 in heart sections from different groups. **(I)** CDH5 protein levels quantified by the H-score (n = 4). **(J)** Western blotting assessment of NFAT2 and CDH5 levels in different groups. The loading control comprised β-Actin. Scale bars, 200 μm (50×) and 10 μm (200×). Data are presented as the mean ± SEM. Quantitative data were analyzed using Kruskal–Wallis tests **(F)** and one-way ANOVA **(I)**, *P < 0.05, **P < 0.01, ***P < 0.001.

heart tissue, including both immune cells and stromal cells. In this study, we identified a novel pathway comprising FOXO4/NFAT2. This pathway affects endothelial cell homeostasis *in vitro* and formation of CAWS-induced vasculitis *in vivo*. Our results showed that the downregulation of FOXO4 promoted NFAT2 expression, causing an imbalance in endothelial cell homeostasis and worsening of vascular inflammatory infiltration. Inhibition of *Nfat2* in *Foxo4*-KO mice reduced the level of inflammatory infiltration.

We found the NFAT2 expression was significantly elevated in immune cells (PBMCs) from patients with KD, similar to a previous study (25). Previous research also reported that NFAT inhibitors, such as cyclosporine, can prevent progression of inflammation in the arterial wall by blocking cytotoxic CD8+T cells infiltration into the arterial wall (26). This might represent the important impact of NFAT inhibitors KD patients' PBMCs. This could be explained by the fact that the Ca+/NFAT signaling pathway is activated in the acute stage of KD, and NFAT2 is an

10.3389/fimmu.2022.1090056

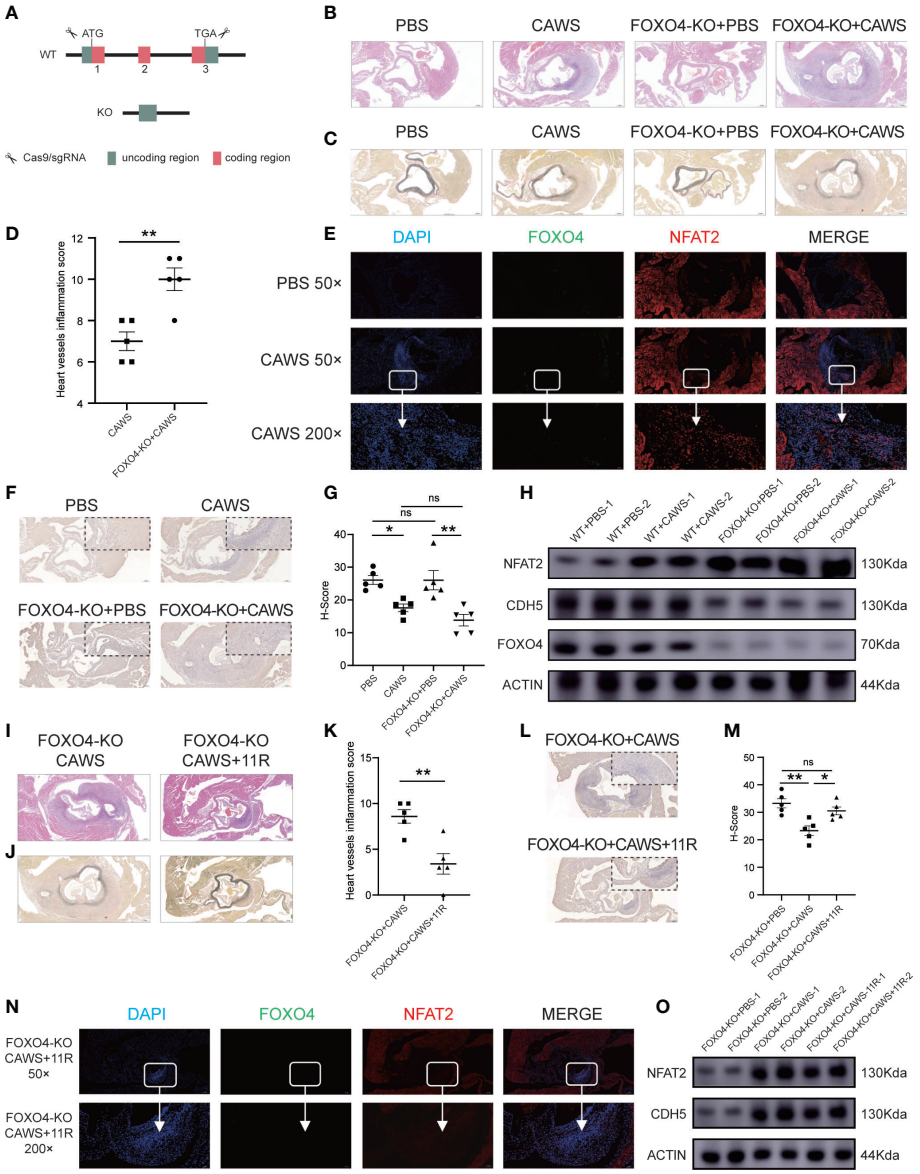

FIGURE 7
FOXO4-KO mice could exacerbate the vasculitis induced by CAWS, but the inflammation was relieved after blocking NFAT2. **(A)** The Cas9/gRNA method generated the FOXO4-KO mice. **(B–D)** Different groups of mice were sacrificed and heart tissues were harvested, made into section sections, and subjected to hematoxylin and eosin (HE)-staining **(B)** and elastic van Gieson (EVG) staining **(C)**. Heart vessel inflammation scores of FOXO4-KO and WT mice in different groups were analyzed **(D)** (n = 5). **(E)** Immunofluorescence staining for FOXO4 (green) and NFAT2 (red) in heart sections of the PBS/CAWS-injected FOXO4-KO group mice. All images show DAPI staining of nuclei. **(F)** Immunohistochemical staining for CDH5 in heart sections from four different groups. **(G)** The CDH5 protein level quantified by the H-score (n = 5). **(H)** Western blotting determination of NFAT2, FOXO4, and CDH5 protein levels in different groups. The loading control comprised β-Actin. Different groups of FOXO4-KO mouse were sacrificed, and heart tissues were harvested and made into sections, which were subjected to HE staining **(I)** and EVG staining **(J)** sections. **(K)** Heart vessel inflammation scores of FOXO4-KO+CAWS, and FOXO4-KO+CAWS+11R mice were analyzed (n = 5). **(L)** Immunohistochemical staining for CDH5 in heart sections from different FOXO4-KO groups. **(M)** CDH5 protein levels quantified by the H-score (n = 5). **(N)** Immunofluorescence staining for FOXO4 (green) and NFAT2 (red) in heart sections from FOXO4-KO+CAWS+11R-injected group mice. All images show DAPI staining of nuclei. **(O)** Western blotting analysis of NFAT2 and CDH5 levels in different FOXO4-KO mouse groups. The loading control comprised β-Actin. Scale bars, 200 μm (50×) and 10 μm (200×). Data are presented as the mean ± SEM. Quantitative data were analyzed using unpaired t tests (two-tailed) **(D, K)** and one-way ANOVA **(E, M)**, *P < 0.05, **P < 0.01.

important TF in this pathway. In addition, NFAT2 was upregulated in PBMCs from CAWS-induced mice. To date, there has been no report about CAWS directly activating the NFAT signaling pathway; however, higher production of proinflammatory cytokines, including TNFα and interleukin (IL)-1β, has been observed in the serum of CAWS-injected mice (27, 28). This might be the reasons why the NFAT pathway is activated and NFAT2 is upregulated.

As important stromal cells in heart tissue, HCAECs also have an important relationship with intravascular thrombosis (29), which is considered one of the most serious complications of KD (3). We selected HCAECs to study the mechanism of KD from the perspective of stromal cells. TNFα plays an importance role in KD, and was significantly elevated in patients' plasma; therefore, anti-TNF-α therapy has been a common treatment option for patients with intravenous immunoglobulin (IVIG) resistant KD (30–32). Consequently, we used TNFα to stimulate HCAECs to simulate the effect of inflammatory factors on stromal cells *in vitro*. Similar to previous research, NFAT2 expression increased significantly after TNFα stimulation (4). To better understand the changes in NFAT2 expression *in vivo*, we observed the expression of NFAT2 in heart tissue, especially in the inflamed areas, after CAWS-induced vasculitis. Those observations were similar to those made in previous research, in which stimulation by proinflammatory cytokines, such as TNFα, upregulated NFAT2 in both PBMCs and endothelial cells (4, 33). We also found that inhibiting NFAT2 expression using 11R-VIVIT could alleviate vascular inflammation. 11R-VIVIT is not a specific inhibitor of NFAT2. However, no specific inhibitor of NFAT2 is currently available. *NFAT2* shows the strongest transcriptional activity, thus most 11R-VIVIT studies have focused on NFAT2 rather than other members of NFAT family, as did our design (34, 35). 11R-VIVIT selectively interferes with the calcineurin-NFAT2 interaction without altering the calcineurin phosphatase activity *in vivo* and *in vitro* (36–38).

We also found that an increase of NFAT2 in endothelial cells decreased the function of intercellular junctions *via* CDH5. *In vitro*, similar to previous experiments using human umbilical vein endothelial cells, CDH5 expression decreased significantly after being stimulated by proinflammatory factors (39). *In vivo*, cardiac ischemic injury, cardiac fibrosis, and even occlusion formation were also observed in *Cdh5*-KO mice (39, 40). These changes are similar to the cardiovascular manifestations of KD. Moreover, in acute KD, dysregulation of endothelial cell homeostasis probably affects aneurysm formation and vascular wall injury (4). These might be one of reasons why suppressing the Ca+/NFAT signaling pathway can reduce coronary artery lesions in KD.

Mammals have four FOXO TFs: FOXO1, FOXO3a, FOXO4, and FOXO6 (41). FOXO4 is mainly involved in cell cycle arrest, apoptosis, and muscle homeostasis (42). To date, there has been no research on the role or mechanism of FOXO4 in KD. However, previous studies provided several possibilities: 1) Inflammatory cytokine expression. A previous study reported that FOXO4 represses the expression of inflammatory cytokines, such as TNFα and IL-1β, which have vital functions in the mechanism of KD (43). 2) Preventing aortic aneurysm formation. Blocking the nuclear translocation of FOXO4 stimulated aortic aneurysm formation (44). Coronary or aortic aneurysms are important complications of KD; therefore; FOXO4 might have a protective role in the progress of KD.

At day 28 after CAWS injection, we found the mRNA and protein levels of FOXO4 were upregulated, for which there are two possible reasons. Firstly, it might suggest that the heart tissue is entering the subacute phase/recovery phase. Acute arteritis mainly involves immune cell infiltration, and subacute chronic arteritis in KD involves luminal myofibroblast proliferation (23). In our mouse model, at day 14, arteries are mainly infiltrated by immune cells, and their shape is normal. However, at day 28, luminal myofibroblasts obviously proliferate and vessels lose their original shape (Figure 5D), which indicated that vasculitis has entered the subacute phase. We found that FOXO4 might be a protector in the process of KD-like vasculitis, such that the level of FOXO4 could increase in the subacute or recovery phase. Secondly, FOXO4 might be uncoupled from *NFAT2* when the disease enters the subacute phage; but the mechanism of this phenotype needs to be further studied in the future. At day 28, the CAWS mice tended to regain the weight lost by day 14, perhaps for the same reason. When the mice entered into the subacute phase, their weight recovered gradually.

Interestingly, *in vivo*, the level of inflammation in CAWS-injected heart tissue in the *Foxo4*-KO group was more serious than that in the WT group. Previous studies using *Foxo4*-KO mice reported that the *Foxo4*-KO group produced more severe inflammatory infiltration (43, 45). *Foxo4*-KO immune cells would increase resident smooth muscle cell proliferation and endothelial cell dysfunction, which would further enhance inflammation and the formation of coronary/aorta vasculitis (45). Consistently, we demonstrated that the NFAT inhibitor, 11R-VIVIT, attenuated CAWS-induced inflammatory responses in *Foxo4*-KO heart tissue. This indicated that the FOXO4/NFAT2 signaling pathway functions not only in HCAECs, but also in mouse heart tissue.

There are several limitations of this study. First, we only examined PBMCs from patients with KD and health controls, and further study should focus on patients with KD with and without coronary artery lesions. Second, the mechanism by which FOXO4 is downregulated in different cells or tissues remains unknown. Third, although we demonstrated that FOXO4 inhibits *NFAT2* transcription by physically binding to a region of its promoter, the exact mechanism of this inhibition remains to be determined. For example, does FOXO4 represses *NFAT2* transcription by competitive inhibition of its activator and why does FOXO4 appear to be uncoupled from *Nfat2* when the mice entered the subacute phage. Fourth, 11R-VIVIT might

affect other NFAT family members; therefore, we need a specific inhibitor of NFAT2 to improve our experiments in the future. These aspects will be examined in future studies.

In this study, NFAT2 was identified to have an important role in the Ca+/NFAT pathway. Moreover, partly through its negative regulation of NFAT2, FOXO4 functions as a transcriptional repressor to suppress vasculitis and maintain endothelial cell homeostasis, thereby controlling vasculitis in KD. The FOXO4/NFAT2 signaling pathway could be developed as a novel therapeutic target, and exploiting its related intrinsic inhibitory mechanisms could lead to novel therapies to prevent and treat KD.

Data availability statement

The original contributions presented in the study are publicly available. This data can be found here: GEO, GSE210094.

Ethics statement

The studies involving human participants were reviewed and approved by the Ethics Committee of Soochow University Affiliated Children's Hospital (approval no. 2020CS075). Written informed consent to participate in this study was provided by the participants' legal guardian/next of kin. The animal study was reviewed and approved by Animal Care and Use Committee of Soochow University.

Author contributions

HH conceived and coordinated the project, analyzed the data, and wrote the paper. HH, JD, and JJ performed the majority of the experiments. YZ performed the qRT-PCR experiments. JD and SW carried out the transfection of lentivirus targeting FOXO4 and NFAT2 experiments. JD and JJ supported the ChIP-qPCR experiments. HH, JJ, YZ, and NW performed the animal experiments. YD, JM and MH help with the *in vivo* experiments. WZ, FY, LM, DY, GY, and QC provided critical ideas and comments for the NFAT2 and FOXO4 study, HL, HH, JD, DY, WQ and GQ discussed the results. HL and LG critically discussed the data and read and revised the manuscript. All authors contributed to the article and approved the submitted version.

Funding

This work was supported by the National Natural Science Foundation of China [grant numbers 81870365, 81970436, 82270512, and 82070529] and the Project of Education and Scientific Research for Young and Middle aged Teachers in Fujian Province, China [grant number JAT200124] HH received support from the China Scholarship Council for 1 year study at the Max-Planck Institute for Heart and Lung Research. LG was supported by the Deutsche Forschungsgemeinschaft (DFG, German Research Foundation), EXC 2026, Cardio-Pulmonary Institute (CPI), Project ID 390649896..

Acknowledgments

The authors are grateful to the Institute of Pediatric Research, Children's Hospital of Soochow University, for their provision of the equipment necessary to carry out the study.

Conflict of interest

The authors declare that the research was conducted in the absence of any commercial or financial relationships that could be construed as a potential conflict of interest.

Publisher's note

Supplementary material

The Supplementary Material for this article can be found online at: https://www.frontiersin.org/articles/10.3389/fimmu.2022.1090056/full#supplementary-material

References

1. Huang H, Xu L, Ding Y, Qin J, Huang C, Li X, et al. Bioinformatics identification of hub genes and signaling pathways regulated by intravenous immunoglobulin treatment in acute Kawasaki disease. *Exp Ther Med* (2021) 22 (1):784. doi: 10.3892/etm.2021.10216

2. Fukazawa R, Kobayashi J, Ayusawa M, Hamada H, Miura M, Mitani Y, et al. Jcs/Jscs 2020 guideline on diagnosis and management of cardiovascular sequelae in Kawasaki disease. *Circ J* (2020) 84(8):1348–407. doi: 10.1253/circj.CJ-19-1094

3. McCrindle BW, Rowley AH, Newburger JW, Burns JC, Bolger AF, Gewitz M, et al. Diagnosis, treatment, and long-term management of Kawasaki disease: A scientific statement for health professionals from the American heart association. *Circulation* (2017) 135(17):e927–99. doi: 10.1161/CIR.0000000000000484

4. Wang Y, Hu J, Liu J, Geng Z, Tao Y, Zheng F, et al. The role of Ca(2+)/Nfat in dysfunction and inflammation of human coronary endothelial cells induced by sera from patients with Kawasaki disease. *Sci Rep* (2020) 10(1):4706. doi: 10.1038/s41598-020-61667-y

5. Onouchi Y, Gunji T, Burns JC, Shimizu C, Newburger JW, Yashiro M, et al. Itpkc functional polymorphism associated with Kawasaki disease susceptibility and formation of coronary artery aneurysms. *Nat Genet* (2008) 40(1):35–42. doi: 10.1038/ng.2007.59

6. Serfling E, Barthelmäs R, Pfeuffer I, Schenk B, Zarius S, Swoboda R, et al. Ubiquitous and lymphocyte-specific factors are involved in the induction of the mouse interleukin 2 gene in T lymphocytes. *EMBO J* (1989) 8(2):465–73. doi: 10.1002/j.1460-2075.1989.tb03399.x

7. McCaffrey PG, Luo C, Kerppola TK, Jain J, Badalian TM, Ho AM, et al. Isolation of the cyclosporin-sensitive T cell transcription factor nfatp. *Science* (1993) 262(5134):750–4. doi: 10.1126/science.8235597

8. Northrop JP, Ho SN, Chen L, Thomas DJ, Timmerman LA, Nolan GP, et al. Nf-at components define a family of transcription factors targeted in T-cell activation. *Nature* (1994) 369(6480):497–502. doi: 10.1038/369497a0

9. Vaeth M, Feske S. Nfat control of immune function: New frontiers for an abiding trooper. *F1000Research* (2018) 7:260. doi: 10.12688/f1000research.13426.1

10. Aramburu J, Yaffe MB, López-Rodríguez C, Cantley LC, Hogan PG, Rao A. Affinity-driven peptide selection of an nfat inhibitor more selective than cyclosporin a. *Science* (1999) 285(5436):2129–33. doi: 10.1126/science.285.5436.2129

11. Stock AT, Hansen JA, Sleeman MA, McKenzie BS, Wicks IP. Gm-csf primes cardiac inflammation in a mouse model of Kawasaki diseasegm-csf triggers cardiac inflammation. *J Exp Med* (2016) 213(10):1983–98. doi: 10.1084/jem.20151853

12. Jia C, Zhang J, Chen H, Zhuge Y, Chen H, Qian F, et al. Endothelial cell pyroptosis plays an important role in Kawasaki disease *Via* Hmgb1/Rage/Cathespin b signaling pathway and Nlrp3 inflammasome activation. *Cell Death Dis* (2019) 10(10):778. doi: 10.1038/s41419-019-2021-3

13. Hamaoka-Okamoto A, Suzuki C, Yahata T, Ikeda K, Nagi-Miura N, Ohno N, et al. The involvement of the vasa vasorum in the development of vasculitis in animal model of Kawasaki disease. *Pediatr Rheumatol* (2014) 12(1):1–9. doi: 10.1186/1546-0096-12-12

14. Lee Y, Schulte DJ, Shimada K, Chen S, Crother TR, Chiba N, et al. Interleukin-1beta is crucial for the induction of coronary artery inflammation in a mouse model of Kawasaki disease. *Circulation* (2012) 125(12):1542–50. doi: 10.1161/CIRCULATIONAHA.111.072769

15. Paschalis A, Sheehan B, Riisnaes R, Rodrigues DN, Gurel B, Bertan C, et al. Prostate-specific membrane antigen heterogeneity and DNA repair defects in prostate cancer. *Eur Urol* (2019) 76(4):469–78. doi: 10.1016/j.eururo.2019.06.030

16. La Madrid AM, Campbell N, Smith S, Cohn SL, Salgia R. Targeting alk: A promising strategy for the treatment of non-small cell lung cancer, non-hodgkin's lymphoma, and neuroblastoma. *Targ Oncol* (2012) 7(3):199–210. doi: 10.1007/s11523-012-0227-8

17. Livak KJ, Schmittgen TD. Analysis of relative gene expression data using real-time quantitative pcr and the 2– Δδct method. *Methods* (2001) 25(4):402–8. doi: 10.1006/meth.2001.1262

18. Chen Y-L, Li X-L, Li G, Tao Y-F, Zhuo R, Cao H-B, et al. Brd4 inhibitor Gne987 exerts anti-cancer effects by targeting super-enhancers in neuroblastoma. *Cell Biosci* (2022) 12(1):1–20. doi: 10.1186/s13578-022-00769-8

19. Skaria T, Bachli E, Schoedon G. Wif1 prevents Wnt5a mediated Limk/Cfl phosphorylation and adherens junction disruption in human vascular endothelial cells. *J Inflammation (Lond)* (2017) 14:10. doi: 10.1186/s12950-017-0157-4

20. Bai S, Wei Y, Hou W, Yao Y, Zhu J, Hu X, et al. Orai-Igfbp3 signaling complex regulates high-glucose exposure-induced increased proliferation, permeability, and migration of human coronary artery endothelial cells. *BMJ Open Diabetes Res Care* (2020) 8(1):e001400. doi: 10.1136/bmjdrc-2020-001400

21. Lee C, Huang C-H. Lasagna-search 2.0: Integrated transcription factor binding site search and visualization in a browser. *Bioinformatics* (2014) 30(13):1923–5. doi: 10.1093/bioinformatics/btu115

22. Fang J, Ji Y-X, Zhang P, Cheng L, Chen Y, Chen J, et al. Hepatic Irf2bp2 mitigates nonalcoholic fatty liver disease by directly repressing the transcription of Atf3. *Hepatology* (2020) 71(5):1592–608. doi: 10.1002/hep.30950

23. Noval Rivas M, Arditi M. Kawasaki Disease: Pathophysiology and insights from mouse models. *Nat Rev Rheumatol* (2020) 16(7):391–405. doi: 10.1038/s41584-020-0426-0

24. Porritt RA, Zemmour D, Abe M, Lee Y, Narayanan M, Carvalho TT, et al. Nlrp3 inflammasome mediates immune-stromal interactions in vasculitis. *Circ Res* (2021) 129(9):e183–200. doi: 10.1161/CIRCRESAHA.121.319153

25. Lv YW, Chen Y, Lv HT, Li X, Tang YJ, Qian WG, et al. Kawasaki Disease Ox40-Ox40l axis acts as an upstream regulator of nfat signaling pathway. *Pediatr Res* (2019) 85(6):835–40. doi: 10.1038/s41390-019-0312-0

26. Burns JC. Cyclosporine and coronary outcomes in Kawasaki disease. *J Pediatr* (2019) 210:239–42. doi: 10.1016/j.jpeds.2019.04.044

27. Nakamura J, Watanabe S, Kimura H, Kobayashi M, Karasawa T, Kamata R, et al. Adeno-associated virus vector-mediated interleukin-10 induction prevents vascular inflammation in a murine model of Kawasaki disease. *Sci Rep* (2018) 8(1):7601. doi: 10.1038/s41598-018-25856-0

28. Zhang J, Zhuge Y, Rong X, Ni C, Niu C, Wen Z, et al. Protective roles of xijiao dihuang tang on coronary artery injury in Kawasaki disease. *Cardiovasc Drugs Ther* (2021). doi: 10.1007/s10557-021-07277-w

29. Chin-Quee SL, Hsu SH, Nguyen-Ehrenreich KL, Tai JT, Abraham GM, Pacetti SD, et al. Endothelial cell recovery, acute thrombogenicity, and monocyte adhesion and activation on fluorinated copolymer and phosphorylcholine polymer stent coatings. *Biomaterials* (2010) 31(4):648–57. doi: 10.1016/j.biomaterials.2009.09.079

30. Burns JC, Mason WH, Hauger SB, Janai H, Bastian JF, Wohrley JD, et al. Infliximab treatment for refractory Kawasaki syndrome. *J Pediatr* (2005) 146(5):662–7. doi: 10.1016/j.jpeds.2004.12.022

31. Shimizu M, Mizuta M, Usami M, Inoue N, Sakakibara Y, Yamada K, et al. Clinical significance of serum soluble tnf receptor ii level and soluble tnf receptor Ii/I ratio as indicators of coronary artery lesion development in Kawasaki disease. *Cytokine* (2018) 108:168–72. doi: 10.1016/j.cyto.2018.03.037

32. Yamaji N, da Silva Lopes K, Shoda T, Ishitsuka K, Kobayashi T, Ota E, et al. Tnf-alpha blockers for the treatment of Kawasaki disease in children. *Cochrane Database Syst Rev* (2019) 8:CD012448. doi: 10.1002/14651858.CD012448.pub2

33. Yokota K, Sato K, Miyazaki T, Aizaki Y, Tanaka S, Sekikawa M, et al. Characterization and function of tumor necrosis factor and Interleukin-6–induced osteoclasts in rheumatoid arthritis. *Arthritis Rheumatol* (2021) 73(7):1145–54. doi: 10.1002/art.41666

34. Xie Z-Y, Dong W, Zhang L, Wang M-J, Xiao Z-M, Zhang Y-H, et al. Nfat inhibitor 11r-vivit ameliorates mouse renal fibrosis after ischemia-Reperfusion-Induced acute kidney injury. *Acta Pharmacol Sin* (2022) 43(8):2081–93. doi: 10.1038/s41401-021-00833-y

35. Liu F, Zhu Z, Mao Y, Liu M, Tang T, Qiu S. Inhibition of titanium particle-induced osteoclastogenesis through inactivation of Nfatc1 by vivit peptide. *Biomaterials* (2009) 30(9):1756–62. doi: 10.1016/j.biomaterials.2008.12.018

36. Dou C, Zhang H, Ke G, Zhang L, Lian Z, Chen X, et al. The kruppel-like factor 15-Nfatc1 axis ameliorates podocyte injury: A novel rationale for using glucocorticoids in proteinuria diseases. *Clin Sci (Lond)* (2020) 134(12):1305–18. doi: 10.1042/CS20200075

37. Noguchi H, Sugimoto K, Miyagi-Shiohira C, Nakashima Y, Kobayashi N, Saitoh I, et al. Rcan-11r peptide provides immunosuppression for fully mismatched islet allografts in mice. *Sci Rep* (2017) 7(1):3043. doi: 10.1038/s41598-017-02934-3

38. Zhang L, Li R, Shi W, Liang X, Liu S, Ye Z, et al. Nfat2 inhibitor ameliorates diabetic nephropathy and podocyte injury in Db/Db mice. *Br J Pharmacol* (2013) 170(2):426–39. doi: 10.1111/bph.12292

39. Jordan NP, Tingle SJ, Shuttleworth VG, Cooke K, Redgrave RE, Singh E, et al. Mir-126-3p is dynamically regulated in endothelial-to-Mesenchymal transition during fibrosis. *Int J Mol Sci* (2021) 22(16):8629. doi: 10.3390/ijms22168629

40. Patel J, Baz B, Wong HY, Lee JS, Khosrotehrani K. Accelerated endothelial to mesenchymal transition increased fibrosis *Via* deleting notch signaling in wound vasculature. *J Invest Dermatol* (2018) 138(5):1166–75. doi: 10.1016/j.jid.2017.12.004

41. Link W. Introduction to foxo biology. *Methods Mol Biol* (2019) 1890:1–9. doi: 10.1007/978-1-4939-8900-3_1

42. Liu W, Li Y, Luo B. Current perspective on the regulation of Foxo4 and its role in disease progression. *Cell Mol Life Sci* (2020) 77(4):651–63. doi: 10.1007/s00018-019-03297-w

43. Zhou W, Cao Q, Peng Y, Zhang QJ, Castrillon DH, DePinho RA, et al. Foxo4 inhibits nf-kappab and protects mice against colonic injury and inflammation. *Gastroenterology* (2009) 137(4):1403–14. doi: 10.1053/j.gastro.2009.06.049

44. Zhao G, Fu Y, Cai Z, Yu F, Gong Z, Dai R, et al. Unspliced Xbp1 confers vsmc homeostasis and prevents aortic aneurysm formation *Via* Foxo4 interaction. *Circ Res* (2017) 121(12):1331–45. doi: 10.1161/CIRCRESAHA.117.311450

45. Zhu M, Zhang QJ, Wang L, Li H, Liu ZP. Foxo4 inhibits atherosclerosis through its function in bone marrow derived cells. *Atherosclerosis* (2011) 219(2):492–8. doi: 10.1016/j.atherosclerosis.2011.09.038

frontiers | Frontiers in Immunology

TYPE Review
PUBLISHED 09 January 2023
DOI 10.3389/fimmu.2022.1093985

OPEN ACCESS

EDITED BY
Uzma Saqib,
Indian Institute of Technology Indore, India

REVIEWED BY
Yuanyuan Zhao,
Huazhong University of Science and Technology, China
Lei Gu,
Max Planck Institute for Heart and Lung Research, Germany

*CORRESPONDENCE
Baofeng Yang
yangbf@ems.hrbmu.edu.cn

SPECIALTY SECTION
This article was submitted to Inflammation, a section of the journal Frontiers in Immunology

RECEIVED 09 November 2022
ACCEPTED 19 December 2022
PUBLISHED 09 January 2023

CITATION
Ju J, Liu Y, Liang H and Yang B (2023) The role of pyroptosis in endothelial dysfunction induced by diseases. *Front. Immunol.* 13:1093985. doi: 10.3389/fimmu.2022.1093985

The role of pyroptosis in endothelial dysfunction induced by diseases

Jin Ju[1], Yanyan Liu[2], Haihai Liang[3,4] and Baofeng Yang[3,4]*

[1]Guangdong Key Laboratory for Biomedical Measurements and Ultrasound Imaging, National-Regional Key Technology Engineering Laboratory for Medical Ultrasound, School of Biomedical Engineering, Shenzhen University Medical School, Shenzhen, China, [2]Guangdong Provincial Key Laboratory of Tumor Interventional Diagnosis and Treatment, Zhuhai People's Hospital, Zhuhai Hospital Affiliated with Jinan University, Jinan University, Zhuhai, Guangdong, China, [3]Key Laboratory of Cardiovascular Research, State-Province Key Laboratories of Biomedicine-Pharmaceutics of China, Ministry of Education, Department of Pharmacology, College of Pharmacy, Harbin Medical University, Harbin, Heilongjiang, China, [4]Research Unit of Noninfectious Chronic Diseases in Frigid Zone (2019RU070), Chinese Academy of Medical Sciences, Harbin, Heilongjiang, China

Most organs in the body rely on blood flow, and vesicular damage is the leading cause of injury in multiple organs. The endothelium, as the barriers of vessels, play a critical role in ensuring vascular homeostasis and angiogenesis. The rapid development of risk factors in endothelial injuries has been seen in the past decade, such as smoking, infectious, and diabetes mellites. Pyroptotic endothelium is an inflammatory mode of governed endothelial cell death that depend on the metabolic disorder and severe infectious such as atherosclerosis, and sepsis-related acute lung injury, respectively. Pyroptotic endothelial cells need GSDMD cleaved into N- and C-terminal by caspase1, and the cytokines are released by a pore constructed by the N-terminal of GSDMD in the membrane of ECs, finally resulting in severe inflammation and pyroptotic cell death. This review will focus on the patho-physiological and pharmacological pathways of pyroptotic endothelial metabolism in diseases. Overall, this review indicates that pyroptosis is a significant risk factor in diseases and a potential drug target in related diseases.

KEYWORDS

pyroptosis, endothelial dysfuction, organ injury, NLRP3, caspase1, cell signaling, drug treatment, protein protein interaction

1 Introduction

Pathological conditions could cause cell death, and cells could actively participate in the process of cell death (1). These regulated cell death (RCD) modes have contributed to the influence of human patho-physiological conditions such as embryonic development, homeostatic maintenance, and disease pathology (2). Adult organs are made up of more

than thirty trillion cells, and millions of cells are vanished by programmed cell death (PCD) daily and replaced by freshly same cells to ensure the functions of organs. PCD is a kind of cell death due to incidents in cells, such as apoptosis (3). But dissimilar to apoptosis, the latest finding of RCD, pyroptosis, displays a preliminary disturbance of the integrity of the plasma membrane, leading to extracellular spillage of intracellular contents (4). Epigenetic modifications, such as carbon 5 methylation and m^6A methylation, are involved in the onset and progression of cell death (5, 6). dysregulation of the epigenome drives aberrant transcriptional programmes that promote multitude of different diseases, including cancer, chronic pulmonary disease and obesity (7, 8).

The endothelium, as the barrier of the vascular arterial, venous, and lymphatic vessels, is vital for multiorgan health. Endothelial cells (ECs), a continuous cells monolayer lining the blood vessel wall, are a significant element of maintaining vascular homeostasis, anti-inflammatory, and antithrombosis (9). Endothelial cells are differentiated from endothelial progenitor cells and regulated by epigenetics (10, 11). Vascular endothelium dysfunction could induce multiple phenomena such as vasospasm, increasing oxidation stress, inflammation, leukocyte, macrophage adhesion, and so on (12). There are studies that many fatal diseases are related to endothelium dysfunction, like atherosclerosis, sepsis, diabetes mellitus, and stroke.

In the last few years, experimental and clinical research has displayed a new clue on endothelium dysfunctions. This paper aims to review related articles that have progressed in this field.

2 Functions of endothelial cells

Blood vessels have various functions in different organs. For example, blood vessels provide organs with oxygen and nourishment, and lymphatic vessels absorb and filter tissue fluid from organs (13, 14). Although blood vessels mostly remain inert for the whole of adulthood, they can also form new vessels rapidly when injured or in pathological situations. The ECs of the blood vessel lining play a crucial role in the development of a vessel. As a critical aspect of neovascularization, capillary sprouting is established by interactions among three EC subtypes, such as tip cells, stalk cells, and quiescent phalanx cells, and every type of ECs has a special role in this process (15).

The endothelium, the largest organ and may be one of the most various organs in the body, play multiple physiological roles, including the provision of a non-thrombogenic, nonadherent, and permeability surface, formation and secretion of molecules and cytokines such as nitric oxide (NO), maintenance of the basement membrane collagen and proteoglycans upon which they rest (9). ECs in different places (arterial, microvascular, venous, etc.) show multiple functions in multiple conditions; thus, their activated mechanisms are different (16). For example, pulmonary microvascular ECs are more sensitive to oxidative phosphorylation and ATP levels than arterial ECs (17). Brain ECs have more mitochondria and are more dependent on oxidative metabolism than peripheral blood vessels (18). Pathological conditions are also associated with EC heterogeneity and metabolic consequences. Growing evidence indicates that pyroptosis can work as an effective defense against pathological conditions, but excessive endothelial pyroptosis is the pathogenesis in many diseases, such as stroke, atherosclerosis, and acute lung injury.

3 Pyroptosis

Pyroptosis is a proinflammatory mode of RCD that depends on the synthetic action of inflammatory proteases named cysteine-dependent aspartate-specific protease (caspase) (19). Pyroptosis was first called (‘pyro’ means fire or fever, ‘ptosis’ means denote a falling) to imply a fire-like inflammatory of this mode RCD in 2001 (20). Interestingly, pyroptotic cells undergo early plasma membrane permeabilization, like necroptosis and accidental necrosis. The process of pyroptosis nonetheless shares some characteristics with apoptosis, even though it does not result in cell death and is generally considered immunologically silent (21). Pyroptosis is crucial to protect against foreign microbe, however, it can also lead to damage while unrestrained. It is reported excessive inflammasome promote multiple acute diseased (including sepsis, disseminated intravascular coagulation, cytokine release syndrome etc.) and chronic diseases (including atherosclerosis, diabetes, ischemic stroke etc.) (22).

The pyroptotic pathway is an important target for drugs because it plays a pivotal role in various diseases, such as infectious, stroke, sepsis, and diabetes mellites (21, 23, 24). Currently, several compounds, such as VX-765, are being tested for the treatment of pyroptosis-related diseases (25–27). The STRING database made those compounds a protein-protein interaction (PPI) network in this review (Figure 1), and the Gene Ontology (GO) and Kyoto Encyclopedia of Genes and Genomes (KEGG) enrichment analyses demonstrated those compounds might relieve endothelial dysfunction in atherosclerosis or infections respond to inflammation (Figure 2) (28–34). Some danger signals (e.g., cytokines, etc.) are released while cells have died; perhaps some are even released in primary pyroptosis (35). These signaling molecules cause the enlargement of blood vessels in a concentrated place, resulting in a high blood flow. This enlargement can bring on more features of inflammation, such as

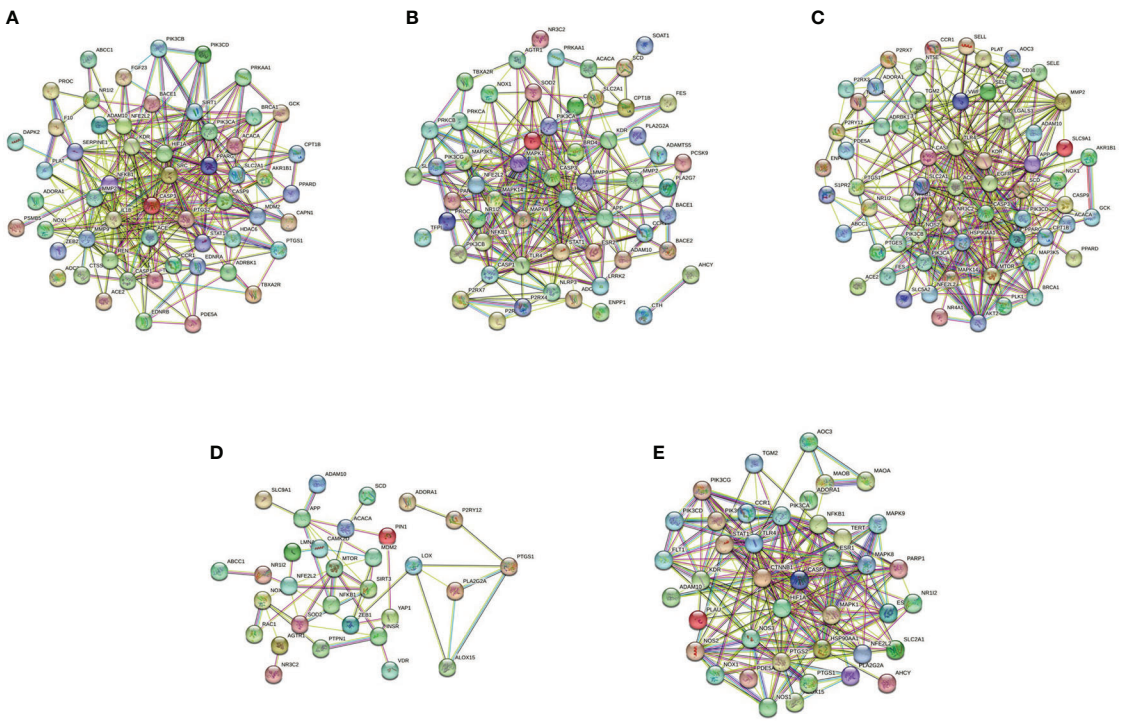

FIGURE 1
PPI network of five compounds targets in endothelial dysfunction diseases. **(A)**, Z-VAD-FMK; **(B)**, MCC950; **(C)**, VX-765; **(D)**, Disulfiram; **(E)**, Dimethyl fumarate. Database of SEA (https://sea.bkslab.org), Super-PRED (https://prediction.charite.de), PharmMapper (http://www.lilab-ecust.cn/pharmmapper/), and SwissTargetPrediction (http://www.swisstargetprediction.ch) was used to predict therapeutic targets of compounds and used a database of DisGeNET (https://www.disgenet.org/) to predict the pathogenic target of endothelial dysfunction in diseases. Then shared regulatory network was determined using Venny2.1 (https://bioinfogp.cnb.csic.es/tools/venny/) and made the PPI network by the STRING database (https://string-db.org/).

fever and swelling in the inflammation area. Overall, inflammation can protect against bacterial invasion. But it can also promote pathological inflammation, which can lead to the development of disorders such as abnormal blood clotting and sepsis (36–38).

Metabolic disorder and severe infectious increase the risk of pyroptosis in ECs, and promote several diseases, such as atherosclerosis, and sepsis-related acute lung injury, respectively (39, 40). In metabolic disorders or infectious conditions, caspase1 can promote lipids or inflammasome to aggregate and induce inflammatory factor release in ECs. In the canonical pathway, NLRP3 was stimulated by intracellular signaling molecule and assembled with pro-caspase1 and ASC, resulting in activated caspase1. Activated caspase1 stimulates pyroptosis, a caspase1-dependent inflammatory cell death described by a broken cellular membrane and released inflammatory mediators. Recently studies showed that gasdermin D (GSDMD) was cleaved by the inflammatory caspases1, 4, and 5 in humans and then separated GSDMD N-terminal (GSDMD-N)), which forms the transmembrane pore and functions as the executor of pyroptosis (19, 41, 42).

4 Endothelial dysfunction and pyroptosis in pathological

4.1 CVD

Cardiovascular disease (CVD) is a major public health problem and the reason for death globally. Atherosclerosis is a lipid metabolism syndrome that leads to the development of heart damage (such as myocardial infarction) and stroke by creating lipid-rich plaques that obstruct blood vessels inducing blood flow restriction and increasing the potential for plaque disruption (43). Once the plaques rupture and block the arterial lumen, tissues or organs supplied by the artery will show the parent's organ irreversible injury and death. ECs protect cardiovascular homeostasis in normal conditions, even though lipid-rich plaques restrict blood flow. But in the terminal stage of the disease, endothelial dysfunction contributes to developing vulnerable plaques and impairs vascular homeostasis. As the main reason for the progression of atherosclerosis, pyroptosis may play a crucial role in endothelial dysfunction. Pyroptosis

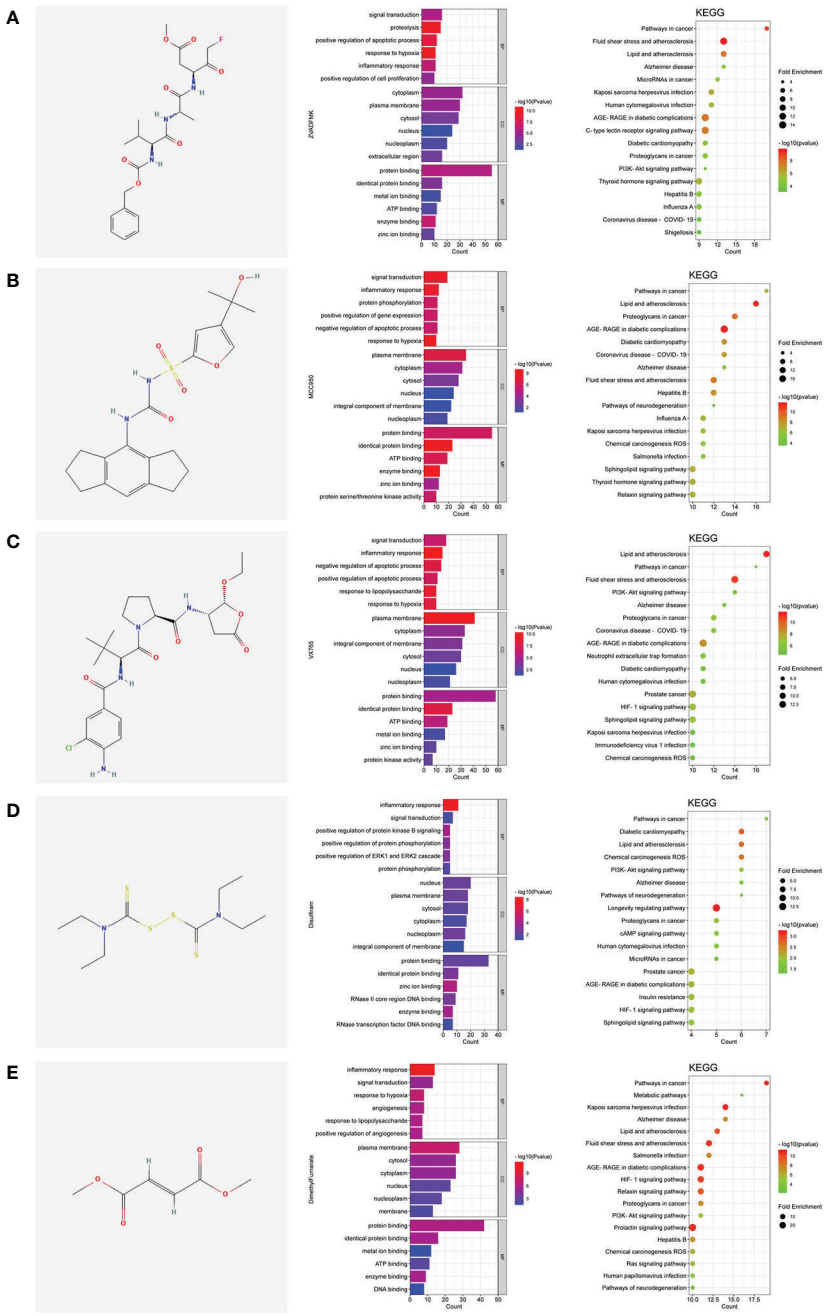

FIGURE 2
The shared regulatory targets of the GO and KEGG enrichment analyses. **(A)**, Z-VAD-FMK; **(B)**, MCC950; **(C)**, VX-765; **(D)**, Disulfiram; **(E)**, Dimethyl fumarate. The analyses of GO and KEGG were carried out by DAVID Knowledgebase (https://david.ncifcrf.gov). The images were made by bioinformatics (http://www.bioinformatics.com.cn).

promotes inflammation, plaque disruption, and angiemphraxis by the release of inflammatory mediators such as interleukin 1β (IL1β) and interleukin 18 (IL18), and induces cell death, which hence develops CVD events (44).

Present evidence shows that the reasons for atherogenesis, such as cigarette smoking, and metabolic syndrome, are significant contributors to endothelial dysfunction (Figure 3 left). Nicotine is a main avertible risk factor for atherosclerosis and CVDs. It promotes atherosclerosis in vulnerable areas, including the aorta, coronary arteries, carotid and cerebral arteries, and the large arteries in the peripheral circulation (45). In ECs, nicotine promotes the production of reactive

oxygen species (ROS), which activates NOD-like receptor thermal protein domain associated protein 3 (NLRP3) inflammasome, leading to the activation of caspase1 (46). A study displayed that nicotine aggravated atherosclerosis in ApoE−/− mice fed with a high-fat diet (HFD), indicated by the more sizeable plaques and more lipids measured by oil red O. In normal diet mice, nicotine also promotes atherosclerotic plaques size and lipid aggregation; even so, the effect of nicotine was not more effective in HFD-fed mice. In addition, nicotine promotes endothelial damage and dysfunction by inducing pyroptotic macrophages (47).

Just as mentioned in the context, investigators have examined the effects of cholesterol on CVDs. In vessels, lipids accumulate under endothelium and impaired ECs directly. While endothelial damage, low-density lipoprotein (LDL) is remodeled to oxidized LDL (oxLDL) and adheres to intimal vessel forming interlayers (48, 49). OxLDL contributes to synthesizing adhesion molecules and releasing inflammatory mediators in impaired ECs (50, 51). OxLDL induces caspase1 activation by ROS, and NLRP3 levels rise in ECs (52, 53), and mixed lineage kinase domain-like (MLKL) aggravates oxLDL-induced pyroptosis by NLRP3-mediated inflammasome in human umbilical vein endothelial cells (HUVECs) (54). OxLDL also impaired mitochondrial structure and function, producing excess ROS in ECs. Proprotein convertase subtilisin/kexin type 9 (PCSK9)and trimethylamine N-oxide (TMAO) inhibited the function of mitochondrial by downregulating ubiquinol-cytochrome c reductase core protein 1 (UQCRC1) (55) and upregulating succinate dehydrogenase complex subunit B (SDHB) (56) expression, respectively, leading to ROS elevation and promotes the pyroptosis of ECs and the subsequent release of proinflammation cytokines. MicroRNA is also involved in pyroptotic endothelial dysfunction. miR-125a-5p, overexpression in oxLDL treatment ECs, directly targeted tet methylcytosine dioxygenase 2 (TET2) 3'-UTR and decreased protein expression, resulting in abnormal mitochondrial DNA (mtDNA) methylation levels and mitochondrial dysfunction promotes the production of ROS, which stimulated nuclear factor-κB (NF-κB) and subsequent induced NLRP3 inflammation and activated caspase1 (57).

There are several risk factors promoting pyroptosis in ECs and contributing to atherogenesis. Hyperhomocysteinemia (HHcy) induced high mobility group box 1 (HMGB1) overexpression because of produced NLRP3 inflammasome and caspase1 across the membrane, thereby cleaved GSDMD and induced pyroptosis (58, 59). Low shear stress decreased the levels of TET2, which recruited less histone deacetylase 2 (HDAC2) to increase the levels of SDHB. The high level of SDHB leads to mitochondria dysfunction and the production of ROS, which stimulates ECs pyroptosis (60); low shear stress also inhibits the levels of miR-181b-5p, resulting in an upregulation in signal transducer and activator of transcription 3 (STAT3) expression, which induced the synthesis of NLRP3 *via* histone acetylation in high levels. Moreover, NLRP3 induced caspase1 activation and activated caspase1 promote proinflammation factors pro-IL1β and pro-IL18 into mature. Eventually, GSDMD-N formation is cleaved by caspase1, leading to perforate cellular membranes, fragmented DNA, and release IL1β and IL18 from ECs, finally promoting pyroptosis ECs progression in atherosclerosis (61).

Many studies focus on therapeutic effects and potential drug targets (Figure 3 right). Melatonin (N-acetyl-5-methoxytryptamine) is a neuroendocrine hormone synthesized in the pineal gland and many other organs (62, 63). In HFD-fed ApoE−/− mice, OxLDL stimulates pyroptotic cell death factors, including activation of MEG3 and inhibition of miR-223, resulting in NLRP3-ASC-procaspase1-assemble and activated caspase1, furthermore melatonin protected pyroptotic endothelium in ECs and improved atherosclerosis in mice models (64). Melatonin also protects against pyroptotic endothelial dysfunction by improving mitochondrial function and reducing ROS production (65). In addition, Melatonin alleviates nicotine-induced EC pyroptosis *via* suppressing ROS/NLRP3 pathway (66). Estrogen can promote autophagy by activation of estrogen receptor α, resulting in averts atherosclerosis by weakened EC pyroptosis (67). Fibroblast growth factor 21 (FGF21), an endocrine cytokine, protect mitochondrial structure and function by regulating the TET2-UQCRC1 pathway and results in reducing ROS production and inhibiting EC pyroptosis (68, 69). Chemical substances extracted in some plants were identified anti-pyroptosis effects in ECs, such as Chochicine, Dihydromyricetin, Ecklonia cava extract, hydroxytyrosol acetate by regulating AMPK, NRF2, NLRP3, HDAC11 respectively (70–74). miR-223 and miR-103 were reported to attenuate oxLDL/H2O2-induced pyroptotic cell death in ECs, demonstrating that non-coding RNA is a potential target in therapeutic atherosclerosis (75, 76). Interestingly, a report shows that bone marrow–derived mesenchymal stem cells conditioned medium attenuated the pyroptosis of vascular ECs induced by LPS and ATP, indicating a new therapy about biomedicine (77).

4.2 Infectious disease

The infectious disease also can induce ECs pyroptosis. Sepsis, critical organ damage induced by a metabolic disorder response to infections, is the primary means of ECs pyroptosis (78). The clinical feature of sepsis is volatile, relying on the preliminary area of infection, the pathogenic microbe, the type of organ damage, the body conditions of the patient, and the initial treatment (40). Symptoms of infectious and organ damage are complex and may have gone unnoticed, so the international consensus guidelines display a long list of sepsis warning signs. In this review, the summary pathway diagram that pyroptotic ECs induced multiple organ injury in infectious patients was created and shown in Figure 4.

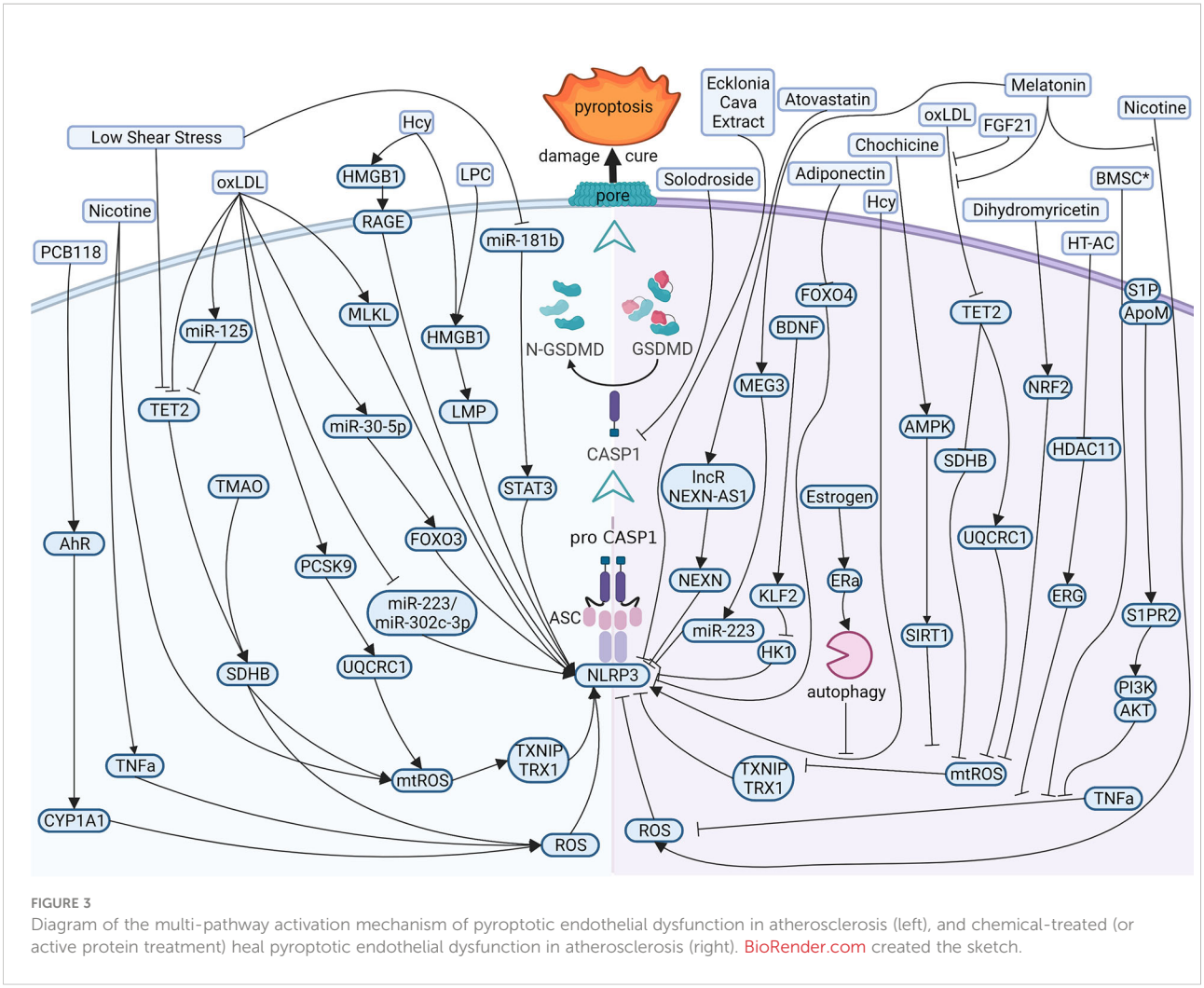

FIGURE 3
Diagram of the multi-pathway activation mechanism of pyroptotic endothelial dysfunction in atherosclerosis (left), and chemical-treated (or active protein treatment) heal pyroptotic endothelial dysfunction in atherosclerosis (right). BioRender.com created the sketch.

ECs, which make up 50% of lung cells, are a part of the respiratory circulatory system and supply venous blood to the pulmonary parenchyma to carry out oxygen exchange (79). Pulmonary endothelium is tolerated stretching while breathing and always stays in the external environment, which increase the risk of being invaded by microbe from the air or peripheric pathogens. So, lung ECs are vulnerable to inflammatory damage in numerous clinical conditions, including sepsis, chronic obstructive pulmonary disease, Hemorrhagic shock, acute respiratory distress syndrome, and others (80–82). Several research focuses on the influence of pyroptosis on ECs in lung injury.

The lipopolysaccharide (LPS) inducing pyroptosis is the leading cause of dysfunction effects on the endothelium. LPS is the main component of the outer membrane of Gram-negative bacteria. It is sensed by the plasma-membrane-located toll like receptor 4 (TLR4) co-receptor MD2 complex in conjunction with co-receptor CD14, which specifically recognizes the lipid A structure of LPS and induces GSDMD-dependent pathway of pyroptosis by acting caspase11, caspase4, caspase5 (83, 84).

LPS promotes acute pulmonary vascular ECs injury in experimental animals and vitro (85, 86). LPS could inhibit endothelial nitric oxide synthase (eNOS) phosphorylation in ECs, and this phenomenon was diminished by reticulocalbin 2 (RCN2) silencing; overexpression of RCN2 in LPS-treated HUVECs could inhibit eNOS phosphorylation and induce HUVECs pyroptosis, NAC abolished this effect (87). Interestingly, a paper showed a new mechanism for LPS that induces the GSDMD pathway involving mitochondria (88). The mitochondrial membrane was combined with the GSDMD-N fragment induced by LPS, resulting in severe mitochondrial damage. Mitochondrial damage reduced mitochondrial membrane potential and promoted mtDNA release into endothelial cytoplasm, which was identified by cyclic GMP-AMP synthase (cGAS) and promoted reproduction of cyclic GMP-AMP (cGAMP) to stimulating inflammatory stimulator of interferon genes (STING) pathway. There is a new report about an auxiliary function of the perforating GSDMD in mtDNA in the cytoplasm and activating DNA-sensing cGAS/STING pathway, finally inducing EC pyroptosis and vessel disorder

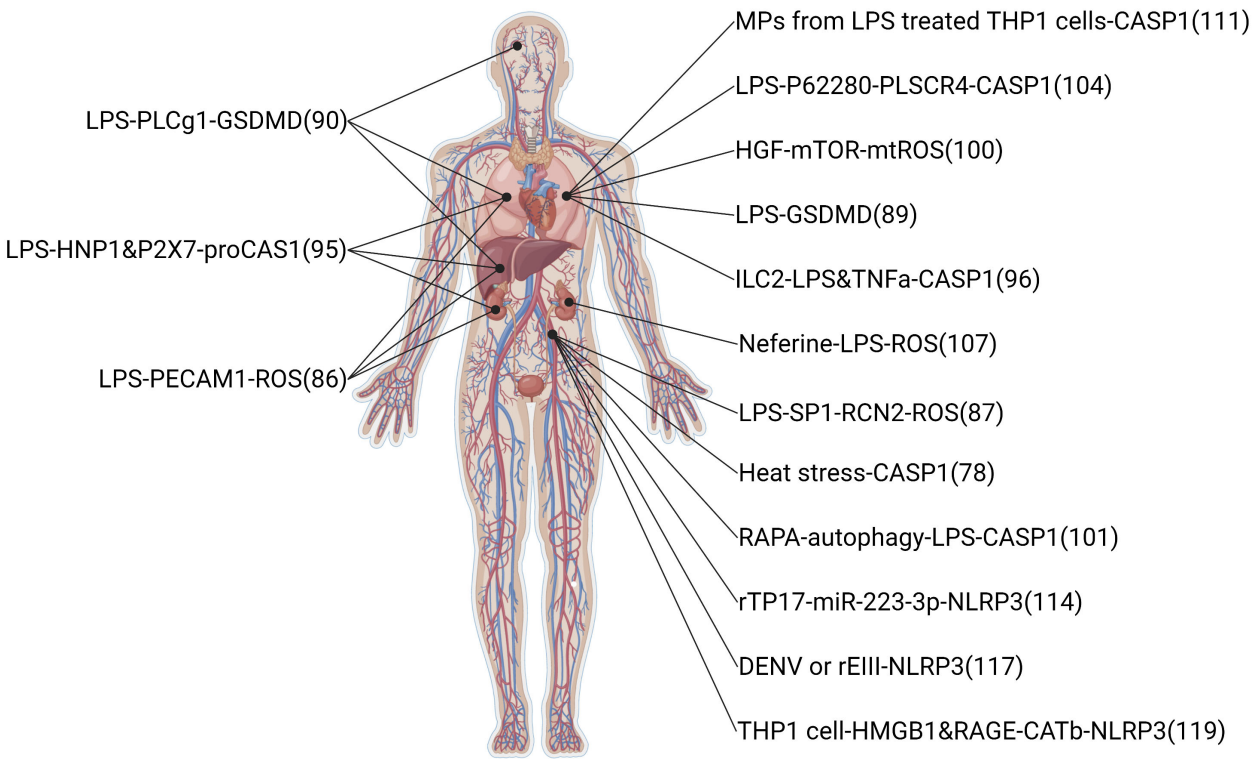

FIGURE 4
Related signaling pathway in infectious-induced pyroptotic endothelial dysfunction in multiple organs. The highest point indicates brain endothelium, the two second-highest points indicate lung endothelium, the middle point indicates liver endothelium, the two second-lowest points indicate kidney endothelium, and the lowest point indicates vessel endothelium. The original material was created by FIGdraw (https://www.figdraw.com/) and the sketch was made by BioRender.com.

(88). cGAS/STING pathway could inhibit the process of dephosphorylation and nuclear translocation of the transcription factor Yes1 associated transcriptional regulator (YAP1) and induce cyclin D-mediated cell cycle arrest. In addition, the deletion of cGAS in mice brought back endothelial vitality in the damaged lung. Furthermore, GSDMD-dependent pyroptosis induced multiple organ injuries in sepsis mice, such as lung, kidney, and liver (89). Liu et al. have reported a paper suggesting that PhospholipaseCγ1-calcium promotes GSDMD-N translocation to the plasma membrane and increases LPS-induced EC pyroptosis and multi-organ damage, such as liver, lung and brain (90). A sturdy showed compared with H1N1 and control groups, more expression levels of caspase1 in endothelial tissue of the COVID-19 group, and this phenomenon might indicate that pyroptosis is happening in lung microvascular ECs of the COVID-19 patients (91).

Leukocytes participated in sepsis-induced pyroptosis endothelium dysfunction widely. Human neutrophil peptides 1-3(HNPs), the most generous neutrophil granule proteins, are abundantly expressed in neutrophils. The difference between HNPs is only an N-terminal amino acid sequence: the N-terminal amino acid is alanine in HNP1 and aspartic in HNP3. This amino acid is absent in HNP2, which is thought to be a proteolytic product of HNP1 and HNP3 (92, 93). A study showed that the overexpression of HNP1-3 (DEFA1/DEFA3) remarkably damaged the clinical characteristics of sepsis, making patients in China displayed a high gene copy number of DEFA1/DEFA3 means more easily affected by severe sepsis (94). In another paper, mice with high HCN of DEFA1/DEFA3 genes displayed graver pulmonary, hepatic, and renal injury and a dangerous consequence during infectious, suggesting a genotype-restricted function in phenotype development (95). In this study, the protein levels of vascular cell adhesion molecule 1 (VCAM1) and intercellular adhesion molecule 1 (ICAM1) in the lung tissue of DEFA1/DEFA3-HCN mice were significantly higher than those of DEFA1/DEFA3-LCN mice and WT mice 24 hours after the onset of disease septicemia. The figures showed that in mice bearing DEFA1/DEFA3 HCN, the activation state of vascular ECs in vital organs was more pronounced after the onset of sepsis. Furthermore, HNP1 activates caspase1 inflammasome by interaction with P2X7

and induces pyroptosis cell death in ECs. Group 2 innate lymphoid cells (ILC2) can protect lung ECs from pyroptosis in sepsis (96). ILC2, one of three subtypes of innate lymphoid cells (ILC1, ILC2, and ILC3), was detected in the lungs as a significant ILC population. ILC2 cells in the lungs and peritoneal cavity following CLP-induced sepsis showed IL33/suppression of tumorigenicity 2 (ST2), signaling overexpression and expansion of ILC2 in the lungs and provides ILC2-derived IL9, which alleviates sepsis-induced EC pyroptosis through controlling caspase1 activation. Furthermore, monocyte promotes human pulmonary microvascular endothelial cell (HPMEC) pyroptosis in hypoxia/reperfusion(H/R) injuries. In H/R injuries, the NLRP3 inflammasome and IL1β expression are increased, caspase1 is activated in monocytes, and eventually, IL1β and IL1R compomer of HPMECs induces pyroptosis through IL1R/NF-κB/NLRP3 signaling pathway (97).

Several potential drugs have been reported to protect against organ injury in sepsis *via* a pyroptosis-dependent pathway. Hepatocyte growth factor (HGF) is a pleiotropic cytokine involved in various cellular and biological processes, including attenuating cellular damage and reducing inflammation. Previous studies have demonstrated LPS-induced organ damage and elevated plasma HGF levels in rodents with systemic inflammatory response syndrome and early sepsis (98, 99). Recently, a paper showed that HGF improves the pyroptotic state of ECs by protecting mitochondrial physiology from releasing mitochondrial damage-related molecules and activating the mechanistic target of rapamycin kinase (mTOR) signaling. Intravenous injection of recombinant HGF into mice can alleviate mice's lung endothelial pyroptosis caused by sepsis of various microorganisms and improve lung endothelial injury and acute lung injury (100). HGF will be a promising adjuvant therapy strategy for treating sepsis and acute lung injury. Furthermore, Rapamycin, a specific MTOR inhibitor, inhibited pyroptosis and protected ECs from excessive inflammation in the septic response (101). Phospholipid supersucrases (PLSCRs) translocate membranes in a Ca^{2+}-dependent manner and perform nonspecific, bidirectional, and phospholipid-independent transduction in lipid bilayers, increasing their exposure to cell membranes (102, 103). A group of single-pass plasma membrane proteins that mediate layer migration. When HPMECs were stimulated with LPS, PLSCR4 expression, inflammatory cytokines IL1β, and IL18 levels increased EC permeability. While the PLSCR4 was silenced, human pulmonary microvascular endothelial cell (HPMEC) pyroptosis was remarkably risen, indicating the protective function of PLSCR4 in ECs (104). Neferine has various biological and pharmacological properties such as antitumor, antiinflammatory, antioxidative, antifibrosis, and antiarrhythmic (105, 106). Neferine is an alkaloid ingredient from the lotus seed embryo of Nelumbo nucifera. A paper by Tang et al. showed that neferine could inhibit LPS-ATP-induced oxidative stress and NLRP3 inflammasome signaling, increasing SOD production and improving EC viability (107).

Microparticles (MPs), a single membrane structure produced by apoptotic cells, have been detected in the site of disturbed blood flow in some pathological states, such as sepsis (108–110). Mitra showed that p30 GSDMD was found in MPs of septic patients (111). Furthermore, authors indicated that GSDMD was modified in MPs combined with activated caspase1 and released by LPS-stimulated Tohoku Hospital Pediatrics 1 cells, and these MPs with GSDMD and caspase1 promoted HPMEC pyroptosis. They demonstrated that GSDMD microencapsulation in MPs combined with caspase1 could be necessary for monocytes released MPs to vascular cells, resulting in caspase1-mediated pyroptotic HPMEC death.

Several clinical infectious conditions also can induce endothelium pyroptosis. Syphilis is a kind of multi-stage and chronic disease; the primary reason is infection by treponema pallidum subsp pallidum (T pallidum), which can influence various organs and has a high morbidity rate. The infections of syphilis are increasing rapidly worldwide (112, 113). A paper showed that miR-223-3p was remarkably decreased in syphilis patients compared with control groups, the levels of NLRP3 and caspase1 were increased in syphilis patients, and miR-223-3p inhibited T pallidum-induced caspase1 activation, IL1β production, and Lactate dehydrogenase (LDH) release in HUVECs, the mechanism is miR-223-3p targets NLRP3 directly (114). This paper highlighting demonstrated that miR-223-3p could become a drug target for treating infectious syphilis. Dengue virus (DENV) infection is a kind of the fastest growing mosquito-borne infections (115, 116). In a present study, Lien et al. found that the virion-associated envelope protein domain III (EIII) overexpression increases endothelial ROS production, induces tumor necrosis factor a (TNFa) and IL1β release, and promotes caspase1 activation, EC pyroptosis, and NLRP3 inflammasome inhibitor treatment significantly attenuates rEIII-induced ECs injury and significantly decreased bleeding in a dual-targeted rEIII autoantibody model (117). Kawasaki disease (KD), an acute vasculitis syndrome, is the primary reason for acquired heart disease in pediatric populations of developed countries (118). In a study by Jia et al., activation of pyroptosis is induced by HMGB1, resulting in increased levels of receptor for advanced glycation end-products (RAGE) and cathepsin B, which bring out NLRP3-caspase1 mediated inflammation-induced pyroptosis in ECs (119).

4.3 Diabetes mellitus

Diabetes is a global health problem and microvascular dysfunction is a major complication, leading to a series of diseases, such as retinopathy, nephropathy, neuropathy, and

atherosclerotic diseases. The harmful effect of high glucose (HG) intrinsically is well-established on the endothelium. ECs of large vessels and the microvasculature were damaged by HG and had differences in autoregulation of glucose uptake in different organs (120, 121). For example, when exposed to high concentrations of extracellular glucose, retinal microvascular ECs did not reduce glucose uptake, whereas brain and cardiac ECs did. HG-induced diabetic retinopathy (DR) pyroptosis has attracted a lot of attention at present.

DR is a common retinal microvascular complication and a major reason for blindness in adults (122). In HG conditions, human retinal microvascular endothelial cell (HRMEC) dysfunction is a multifactorial pathogenesis, responsible for pathogenesis that is closely related to cell migration and apoptosis when cells are exposed to advanced glycation end products (AGEs). It is regulated by various inflammatory and apoptotic factors (123, 124). A paper showed HRMECs were pyroptotic by HG treatment (125). HRMECs HG-treated showed lower cell viability, and higher Caspase1 activity, indicating HG can induce HRMECs pyroptosis. Furthermore, HG treatment decreased miR-590-3p levels and increased NADPH oxidase 4 (NOX4) and NLRP1 expression in HRMECs. NOX4 and NLRP1 are direct targets to miR-590-3p and are the main intracellular regulator of the pyroptotic process, highlighting the significance of miR-590-3p in pyroptosis in DR. Another paper by Yang et al. showed AGEs induces ECs pyroptosis by active GSDMD and cleaved caspase1 in HRMECs (126). Moreover, authors indicate H3 relaxin, a multipotent peptide hormone of the insulin superfamily, remarkably inhibited migration, apoptosis, and pyroptosis in endothelium and relieved diabetic nephropathy *via* P2X7R-NLRP3 inflammation in HRMECs.

The corneal endothelium is the deepest monolayer of the cornea and keeps the stroma dehydrated by pumping fluid from the cornea into the anterior chamber. Intraocular pro-inflammatory cytokines can activate the activation of caspase1 and GSDMD (127). Corneal confocal microscopy showed that the density of corneal ECs was abnormally decreased and increased, suggesting that ECs are atypical in patients with diabetes (128). Corneal endothelium of donors indicated that the levels of NLRP3, caspase1, and IL1β were remarkably increased in the corneal endothelium of diabetic donors. Expression of lncRNA KCNQ1 opposite strand/antisense transcript 1 (KCNQ1OT1), a participant in multiple (physio) pathological processes of diabetic complications wildly, is upregulated, and miR-214, a downstream target of KCNQ1OT1, is downregulated in HG treatment corneal ECs. Caspase1 was reported to be a target gene of miR-214 and decreased expression by miR-214 directly, and result in providing a pyroptotic process in diabetic corneal endothelial dysfunction. Moreover, a paper showed metastasis-associated lung adenocarcinoma transcript 1 (MALAT1) stimulated pyroptosis by binding to miR-22 directly and inhibiting NLRP3 expression in EA.hy926 cells (129). A novel deep learning algorithm was used in corneal diseases to identify specific characteristics of the corneal sagittal plane, that may be helpful for diagnoses of corneal diseases (130).

Diabetic nephropathy (DN) also is a kind of diabetes complication. HG stimulated the caspase1-GSDMD-mediated pyroptotic pathway in glomerular endothelial cells (GECs) (131). Butyric acid, a short-chain fatty acid produced by the intestinal flora in the gut lumen, decreased the levels of GSDMD-N by suppressing caspase1-GSDMD pyroptotic process in HG conditions, thus providing GECs damage and inhibiting the releasing of pro-inflammatory factors (131). Butyric acid is a potential drug for endothelium dysfunction.

4.4 Stroke

Stroke is a kind of cerebrovascular disease that results from vascular rupture or blockage and the treatment of ischemic stroke according to the repair of blood flow in the ischemic zone. However, in some ischemic brain tissue, reperfusion may exacerbate injury or dysfunction and induce cerebral ischemia-reperfusion injury (CIRI). During CIRI, pro-inflammatory factors (for example oxygen free radicals); stimulate inflammatory cytokines, and increase the expression of adhesion molecules in leukocytes and vascular ECs, while neutrophils migrate and attach to microvascular ECs, resulting in neutrophils damage caused by aggression in ischemic tissue (132).

In experiments, oxygen-glucose deprivation (OGD) was used to mimic the condition of ischemia in cells. A paper showed bEnd.3 cells, a kind of mouse brain microvascular ECs, encourage the level of GSDMD-N at the membrane of bEnd.3 cells and produce pyroptosis-associated proteins under OGD condition, suggesting that the process of pyroptosis and inflammasome in brain microvascular ECs is happening in ischemic stroke (133). Furthermore, Mediresinol (MDN) activates PGC1α, promotes the interaction of PGC1α and PPARα in brain microvascular endothelial cells (BMECs), increases the expression of GOT1 and PAH, and ischemia-induced phenylalanine improves accumulation, thereby reducing mitochondrial ROS (mtROS). There are few studies on its pharmacological effects, and only the effect against Candida albicans infection has been reported (134). MDN is a potential drug for the treatment of blood-brain barrier (BBB) disruption and ischemic brain injury by inhibiting the pyroptosis of BMECs.

A paper used the OGD model or TNFα treated (mimic inflammation in reperfusion conditions) to show OGD-induced occludin degeneration and the lack of occludin could encourage BMECs death in both apoptotic and pyroptotic process during reoxygenation or TNFα treatment in cells (135). In this paper, OGD/reoxygenation (OGD/R) and TNFα activated pyroptosis

in bEnd.3 cells and cleaved caspase1 and GSDMD-N expression significantly rose in OGD/R (or TNFα) treatment cells compared with normal cells, indicating the pyroptotic process of OGD (ischemia) and TNFα treatment EC in the stage of reoxygenation (reperfusion). Furthermore, overexpression of occludin inhibits both OGD/R and TNFα treated bEnd.3 cell pyroptosis indicates a potential occludin target in BBB disturbance in ischemic stroke.

Post-stroke cognitive impairment (PSCI) is a kind of long-term injury. A study used middle cerebral artery occlusion (MCAO)/1, 3, 7, 28 days reperfusion model to mimic PSCI (136). In this paper, hippocampus and cortex 1, 3, or 7 days after 45 min MCAO/reperfusion was measured by immunofluorescence staining and absent in melanoma 2 (AIM2), caspase1 and GSDMD were remarkably increased in the PSCI group, indicating pyroptosis happened. Furthermore, the immunofluorescence of AIM2 in PSCI mice was primarily co-localized with CD31 (EC marker) rather than NeuN (neuronal marker) and GFAP (astrocyte marker), indicating AIM2 production was generated in EC by PSCI pathogenesis. Moreover, AIM2 also mediated traumatic brain injury (TBI)-induced BMVECs pyroptosis (137).

4.5 Others

Hemorrhagic shock (HS) also could induce ECs pyroptosis in the lung. A study by Yang et al. showed the relationship between HS and ECs pyroptosis. They found that cold-inducible RNA-binding protein (CIRP), a protein of the cold shock protein family, promotes vascular damage and leads to pulmonary injury (138); Releasing of CIRP activates ECs pyroptosis by regulating adhesion molecules to promote intrusion of polymorphonuclear leukocytes and generate proinflammatory cytokines and ROS in hemorrhagic or septic shock conditions. CIRP also increased the level of NLRP3 inflammasome and promoted caspase1-mediated EC pyroptosis. Yang also reports another finding about the mechanism of EC pyroptosis induced by HS in the same year. In this paper, researchers listed two factors that induced caspase1 activation in ECs: HS stimulated the production of HMGB1 which assembled inflammasome and activated caspase1 *via* the RAGE pathway and induced the endocytosis of HMGB1 in ECs; otherwise, caspase1 was activated by LPS through TLR4-NLRP3 signaling pathway in ECs (139). Significantly, this study highlights the activated caspase1 in pyroptotic ECs in HS conditions. Lung transplantation is considered the only effective treatment for end-stage lung disease and there are numerous risk factors that can stimulate ischemia/reperfusion in the lung transplant (140). A study showed monocyte promote HPMEC pyroptosis in hypoxia/reoxygenation (H/R) conditions, the mechanism is both NLRP3 inflammasome and caspase1 are activated in monocytes, which stimulate IL1β secretion and bind to IL1R, leading to HPMECs pyroptosis through IL1R/NF-κB/NLRP3 signaling pathway (97).

5 Summary and perspectives

Many conditions can induce endothelium pyroptosis, and endothelium pyroptosis is a leading cause of organ injury, such as atherosclerosis, acute lung injury, diabetic retinopathy, and so on. The endothelium is not made up of just one fundamental EC but rather a large group of EC subtypes dissimilar in phenotype, function, and location. There is much less information about the mechanism by which this heterogeneity drives EC metabolism or how it is steered by EC metabolism in physiologically, and how different types of ECs respond to pathological conditions through the metabolic pathways according to their biosynthetic requirements. It is important for precision medicine.

Pyroptosis is an important potential target in diseases. Several compounds are pyroptotic inhibitors and being developed for pyroptosis-related diseases (25). In this review, we collected the potential targets of those compounds and pathogenic target of endothelial dysfunction by database. The shared regulatory networks of potential targets were recreated by Venny2.1 bioinformation tool and used in recreated PPI networks and KEGG and GO enrichment analyses. GO biological process suggested those compounds may have a role of inflammatory response in endothelial dysfunction (Figure 2). PPI networks and KEGG enrichment analysis showed those shared regulatory interactions belong to atherosclerosis, infectious and diabetes related pathway (Figures 1, 2). Overall, the compounds, such as Z-VAD-FMK, have great therapeutic potential for pyroptotic endothelial dysfunction in diseases.

In CVDs, atherosclerosis is the main disease in pyroptotic endothelial dysfunction. Clinically, patients are asked to quit smoking, exercise and maintain their weight, blood pressure and blood lipids through a controlled diet, and adherence to this advice is help for lower cardiovascular mortality (141, 142). OxLDL is a major method to induce pyroptosis in ECs. OxLDL is a kind of oxidation of natural LDL and the most critical factor in atherosclerosis. OxLDL can influence multiple proteins (or non-encoding RNAs) to regulate the NLRP3-caspase1 pathway and induce EC pyroptosis. Pyroptosis attack ECs according to ROS (or mtROS)-NLRP3-caspase1 pathway mostly. Therefore, most drug targets (such as melatonin, dihydromyricetin, etc.) are chosen by inhibited ROS (or mtROS) to reverse endothelial damage.

Sepsis, as a systemic inflammatory response to infection, is the leading cause of pyroptotic endothelial dysfunctions in infection. Mechanisms of organ failure and death in patients with sepsis are little known, and autopsy studies do not show widespread necrosis (143). Therefore, endothelial homeostasis may be key in revealing the mechanisms of sepsis-induced organ injury. LPS, a kind of endotoxin released from Gram-negative bacteria into blood, is a major factor to induce pyroptotic endothelial dysfunction in infections. LPS-induced pyroptotic endothelial dysfunction damages multiple organs, such as the

lung, brain, liver, and kidney. Furthermore, the lung is the most vulnerable to LPS-induced organ injury, the reason may be pulmonary ECs are the most cell in the lung and initial exposure to LPS in blood. In clinical, supportive care (including rapid recognition of sepsis and delivery of effective antibiotics, resuscitation with fluid therapy in early septic shock, lung protective ventilation, more judicious use of fluid therapy once shock has resolved, better guidelines for blood product transfusion, and enhanced methods to reduce secondary nosocomial infections) should be given more attention to ensure organs conditions in septic patients (144).

Vasculitis is a group of inflammatory autoimmune diseases induced by genetics, infection, and abnormalities of the innate and acquired immune systems. Autoantibodies, especially antineutrophil cytoplasmic antibody (ANCA) and anti-endothelial cell antibody (AECA), play an important role in the pathogenesis of vasculitis. In clinical, ANCA and AECA is used as a marker for vasculitis measured by indirect immunofluorescence and ELISA. However, there is a notable leak of empirical research focusing specifically on the relationship between pyroptosis and ANCA, exploring those relationship may contribute to revealing the pathogenesis of vasculitis.

Endothelial dysfunction is a major complication occurring in diabetes and induces organs of patients with diabetes injury, such as DR, DN, etc. Clinically, diabetic patients with a disease duration of more than 10 years often have a combination of retinopathy, which is one of the main causes of blindness. HG conditions and AGEs promote pyroptosis in retinal and corneal endothelial dysfunctions *via* an NLRP3-caspase1-GSDMD pathway and result in blindness. HG also promotes GEC pyroptosis *via* a caspase1-GSDMD pathway, and this effect is inhibited by butyric acid. Another complication of diabetes is cardiac dysfunction, which is defined as a microvascular disease and contribution to heart failure, cardiac shock, and sudden death in diabetic patients. It is still unclear how diabetes influences cardiac dysfunction. Endothelial dysfunction may be a key risk factor. However, there is no study about pyroptotic endothelial dysfunction in diabetic cardiomyopathy, and much uncertainty still exists about the relationship between those. Revealing the role of pyroptotic ECs in diabetic cardiomyopathy may contribute to ascertaining the mechanism of diabetic cardiomyopathy.

Endothelial barriers comprise BBB at the inner coating and endothelial homeostasis is important for brain health. During cerebral ischemia, oxidative stress and immune-inflammatory response promote endothelial dysfunction. In clinical, the treatment of ischemic stroke depends on the restoration of blood flow in the ischemic area, so reperfusion injury is also an important mode of injury in stroke patients. The present studies reported that OGD, a method to mimic the condition of ischemia in cells, could induce brain endothelial cell pyroptosis *via* mtROS or caspase1-GSDMD pathway. *In vivo*, MCAO/reperfusion was used to mimic long-term brain injury and indicated that brain ECs could secrete AIM2 and promote the caspase1-GSDMD pathway in the PSCI brain.

We have reviewed recent work on pyroptotic ECs in multiple diseases and discussed the lack in present studies. We have also analyzed several compounds, which are reported to test the effect in pyroptosis-associated diseases, using network pharmacology and the analysis of the GO and KEGG showing those compounds have tremendous potential for regulated pyroptosis-related endothelial dysfunction in diseases. This review hopes to provide new insight into how classic and emerging risk factors promote pyroptotic endothelium and how to develop a therapeutic strategy for organ injury treatment through the regulation of EC pyroptosis.

Author contributions

JJ contributions to the design and writing of this manuscript. HL and BY reviewed the review. YL designed the figure. All authors contributed to the article and approved the submitted version.

Funding

This work was supported by the National Natural Science Foundation of China (U21A20339), and the CAMS Innovation Fund for Medical Sciences (CIFMS, 2019-I2M-5-078)

Conflict of interest

The authors declare that the research was conducted in the absence of any commercial or financial relationships that could be construed as a potential conflict of interest.

Publisher's note

References

1. Elmore S. Apoptosis: a review of programmed cell death. *Toxicol Pathol* (2007) 35(4):495–516. doi: 10.1080/01926230701320337

2. Danial NN, Korsmeyer SJ. Cell death: critical control points. *Cell* (2004) 116 (2):205–19. doi: 10.1016/S0092-8674(04)00046-7

3. Engelberg-Kulka H, Amitai S, Kolodkin-Gal I, Hazan R. Bacterial programmed cell death and multicellular behavior in bacteria. *PloS Genet* (2006) 2(10):e135. doi: 10.1371/journal.pgen.0020135

4. Zheng X, Chen W, Gong F, Chen Y, Chen E. The role and mechanism of pyroptosis and potential therapeutic targets in sepsis: A review. *Front Immunol* (2021) 12:711939. doi: 10.3389/fimmu.2021.711939

5. Wang Q, Gu L, Adey A, Radlwimmer B, Wang W, Hovestadt V, et al. Tagmentation-based whole-genome bisulfite sequencing. *Nat Protoc* (2013) 8 (10):2022–32. doi: 10.1038/nprot.2013.118

6. Gu L, Wang L, Chen H, Hong J, Shen Z, Dhall A, et al. CG14906 (mettl4) mediates m(6)A methylation of U2 snRNA in drosophila. *Cell Discovery* (2020) 6:44. doi: 10.1038/s41421-020-0178-7

7. Chu Z, Gu L, Hu Y, Zhang X, Li M, Chen J, et al. STAG2 regulates interferon signaling in melanoma *via* enhancer loop reprogramming. *Nat Commun* (2022) 13 (1):1859. doi: 10.1038/s41467-022-29541-9

8. Bauer T, Trump S, Ishaque N, Thurmann L, Gu L, Bauer M, et al. Environment-induced epigenetic reprogramming in genomic regulatory elements in smoking mothers and their children. *Mol Syst Biol* (2016) 12(3):861. doi: 10.15252/msb.20156520

9. Ross R. The pathogenesis of atherosclerosis: a perspective for the 1990s. *Nature* (1993) 362(6423):801–9. doi: 10.1038/362801a0

10. Hill JM, Zalos G, Halcox JP, Schenke WH, Waclawiw MA, Quyyumi AA, et al. Circulating endothelial progenitor cells, vascular function, and cardiovascular risk. *N Engl J Med* (2003) 348(7):593–600. doi: 10.1056/NEJMoa022287

11. Blanco MA, Sykes DB, Gu L, Wu M, Petroni R, Karnik R, et al. Chromatin-state barriers enforce an irreversible mammalian cell fate decision. *Cell Rep* (2021) 37(6):109967. doi: 10.1016/j.celrep.2021.109967

12. Badimon L, Pena E, Arderiu G, Padro T, Slevin M, Vilahur G, et al. C-reactive protein in atherothrombosis and angiogenesis. *Front Immunol* (2018) 9:430. doi: 10.3389/fimmu.2018.00430

13. Carmeliet P, Jain RK. Molecular mechanisms and clinical applications of angiogenesis. *Nature* (2011) 473(7347):298–307. doi: 10.1038/nature10144

14. Tammela T, Alitalo K. Lymphangiogenesis: Molecular mechanisms and future promise. *Cell* (2010) 140(4):460–76. doi: 10.1016/j.cell.2010.01.045

15. Potente M, Gerhardt H, Carmeliet P. Basic and therapeutic aspects of angiogenesis. *Cell* (2011) 146(6):873–87. doi: 10.1016/j.cell.2011.08.039

16. Ricard N, Bailly S, Guignabert C, Simons M. The quiescent endothelium: signalling pathways regulating organ-specific endothelial normalcy. *Nat Rev Cardiol* (2021) 18(8):565–80. doi: 10.1038/s41569-021-00517-4

17. Parra-Bonilla G, Alvarez DF, Al-Mehdi AB, Alexeyev M, Stevens T. Critical role for lactate dehydrogenase a in aerobic glycolysis that sustains pulmonary microvascular endothelial cell proliferation. *Am J Physiol Lung Cell Mol Physiol* (2010) 299(4):L513–22. doi: 10.1152/ajplung.00274.2009

18. Tang X, Luo YX, Chen HZ, Liu DP. Mitochondria, endothelial cell function, and vascular diseases. *Front Physiol* (2014) 5:175. doi: 10.3389/fphys.2014.00175

19. Shi J, Zhao Y, Wang K, Shi X, Wang Y, Huang H, et al. Cleavage of GSDMD by inflammatory caspases determines pyroptotic cell death. *Nature* (2015) 526 (7575):660–5. doi: 10.1038/nature15514

20. Cookson BT, Brennan MA. Pro-inflammatory programmed cell death. *Trends Microbiol* (2001) 9(3):113–4. doi: 10.1016/S0966-842X(00)01936-3

21. Fink SL, Cookson BT. Apoptosis, pyroptosis, and necrosis: mechanistic description of dead and dying eukaryotic cells. *Infect Immun* (2005) 73(4):1907–16. doi: 10.1128/IAI.73.4.1907-1916.2005

22. Ryder CB, Kondolf HC, O'Keefe ME, Zhou B, Abbott DW. Chemical modulation of gasdermin-mediated pyroptosis and therapeutic potential. *J Mol Biol* (2022) 434(4):167183. doi: 10.1016/j.jmb.2021.167183

23. Franchi L, Eigenbrod T, Munoz-Planillo R, Nunez G. The inflammasome: a caspase-1-activation platform that regulates immune responses and disease pathogenesis. *Nat Immunol* (2009) 10(3):241–7. doi: 10.1038/ni.1703

24. Lamkanfi M, Dixit VM. Inflammasomes and their roles in health and disease. *Annu Rev Cell Dev Biol* (2012) 28:137–61. doi: 10.1146/annurev-cellbio-101011-155745

25. Burdette BE, Esparza AN, Zhu H, Wang S. Gasdermin d in pyroptosis. *Acta Pharm Sin B* (2021) 11(9):2768–82. doi: 10.1016/j.apsb.2021.02.006

26. Li Q, Dai Z, Cao Y, Wang L. Caspase-1 inhibition mediates neuroprotection in experimental stroke by polarizing M2 microglia/macrophage and suppressing NF-kappaB activation. *Biochem Biophys Res Commun* (2019) 513(2):479–85. doi: 10.1016/j.bbrc.2019.03.202

27. Do Carmo H, Arjun S, Petrucci O, Yellon DM, Davidson SM. The caspase 1 inhibitor VX-765 protects the isolated rat heart *via* the RISK pathway. *Cardiovasc Drugs Ther* (2018) 32(2):165–8. doi: 10.1007/s10557-018-6781-2

28. Szklarczyk D, Gable AL, Nastou KC, Lyon D, Kirsch R, Pyysalo S, et al. The STRING database in 2021: customizable protein-protein networks, and functional characterization of user-uploaded gene/measurement sets. *Nucleic Acids Res* (2021) 49(D1):D605–D12. doi: 10.1093/nar/gkab835

29. Sherman BT, Hao M, Qiu J, Jiao X, Baseler MW, Lane HC, et al. DAVID: a web server for functional enrichment analysis and functional annotation of gene lists (2021 update). *Nucleic Acids Res* (2022) 50(W1):W216–21. doi: 10.1093/nar/gkac194

30. Keiser MJ, Roth BL, Armbruster BN, Ernsberger P, Irwin JJ, Shoichet BK. Relating protein pharmacology by ligand chemistry. *Nat Biotechnol* (2007) 25 (2):197–206. doi: 10.1038/nbt1284

31. Wang X, Shen Y, Wang S, Li S, Zhang W, Liu X, et al. PharmMapper 2017 update: a web server for potential drug target identification with a comprehensive target pharmacophore database. *Nucleic Acids Res* (2017) 45(W1):W356–W60. doi: 10.1093/nar/gkx374

32. Nickel J, Gohlke BO, Erehman J, Banerjee P, Rong WW, Goede A, et al. SuperPred: update on drug classification and target prediction. *Nucleic Acids Res* (2014) 42(Web Server issue):W26–31. doi: 10.1093/nar/gku477

33. Daina A, Michielin O, Zoete V. SwissTargetPrediction: updated data and new features for efficient prediction of protein targets of small molecules. *Nucleic Acids Res* (2019) 47(W1):W357–W64. doi: 10.1093/nar/gkz382

34. Pinero J, Ramirez-Anguita JM, Sauch-Pitarch J, Ronzano F, Centeno E, Sanz F, et al. The DisGeNET knowledge platform for disease genomics: 2019 update. *Nucleic Acids Res* (2020) 48(D1):D845–D55. doi: 10.1093/nar/gkz1021

35. Conos SA, Lawlor KE, Vaux DL, Vince JE, Lindqvist LM. Cell death is not essential for caspase-1-mediated interleukin-1beta activation and secretion. *Cell Death Differ* (2016) 23(11):1827–38. doi: 10.1038/cdd.2016.69

36. Wu C, Lu W, Zhang Y, Zhang G, Shi X, Hisada Y, et al. Inflammasome activation triggers blood clotting and host death through pyroptosis. *Immunity* (2019) 50(6):1401–11.e4. doi: 10.1016/j.immuni.2019.04.003

37. Broz P, Dixit VM. Inflammasomes: mechanism of assembly, regulation and signalling. *Nat Rev Immunol* (2016) 16(7):407–20. doi: 10.1038/nri.2016.58

38. Rathinam VAK, Zhao Y, Shao F. Innate immunity to intracellular LPS. *Nat Immunol* (2019) 20(5):527–33. doi: 10.1038/s41590-019-0368-3

39. Qian Z, Zhao Y, Wan C, Deng Y, Zhuang Y, Xu Y, et al. Pyroptosis in the initiation and progression of atherosclerosis. *Front Pharmacol* (2021) 12:652963. doi: 10.3389/fphar.2021.652963

40. Angus DC, van der Poll T. Severe sepsis and septic shock. *N Engl J Med* (2013) 369(9):840–51. doi: 10.1056/NEJMra1208623

41. Kayagaki N, Stowe IB, Lee BL, O'Rourke K, Anderson K, Warming S, et al. Caspase-11 cleaves gasdermin d for non-canonical inflammasome signalling. *Nature* (2015) 526(7575):666–71. doi: 10.1038/nature15541

42. Liu X, Zhang Z, Ruan J, Pan Y, Magupalli VG, Wu H, et al. Inflammasome-activated gasdermin d causes pyroptosis by forming membrane pores. *Nature* (2016) 535(7610):153–8. doi: 10.1038/nature18629

43. Ross R. Atherosclerosis–an inflammatory disease. *N Engl J Med* (1999) 340 (2):115–26. doi: 10.1056/NEJM199901143400207

44. Xu YJ, Zheng L, Hu YW, Wang Q. Pyroptosis and its relationship to atherosclerosis. *Clin Chim Acta* (2018) 476:28–37. doi: 10.1016/j.cca.2017.11.005

45. Wilhelmsen L. Coronary heart disease: epidemiology of smoking and intervention studies of smoking. *Am Heart J* (1988) 115(1 Pt 2):242–9. doi: 10.1016/0002-8703(88)90644-8

46. Wu X, Zhang H, Qi W, Zhang Y, Li J, Li Z, et al. Nicotine promotes atherosclerosis *via* ROS-NLRP3-mediated endothelial cell pyroptosis. *Cell Death Dis* (2018) 9(2):171. doi: 10.1038/s41419-017-0257-3

47. Mao C, Li D, Zhou E, Zhang J, Wang C, Xue C. Nicotine exacerbates atherosclerosis through a macrophage-mediated endothelial injury pathway. *Aging (Albany NY)* (2021) 13(5):7627–43. doi: 10.18632/aging.202660

48. Suciu CF, Prete M, Ruscitti P, Favoino E, Giacomelli R, Perosa F. Oxidized low density lipoproteins: The bridge between atherosclerosis and autoimmunity. possible implications in accelerated atherosclerosis and for immune intervention in autoimmune rheumatic disorders. *Autoimmun Rev* (2018) 17(4):366–75. doi: 10.1016/j.autrev.2017.11.028

49. Fernandez-Friera L, Fuster V, Lopez-Melgar B, Oliva B, Garcia-Ruiz JM, Mendiguren J, et al. Normal LDL-cholesterol levels are associated with subclinical

atherosclerosis in the absence of risk factors. *J Am Coll Cardiol* (2017) 70(24):2979–91. doi: 10.1016/j.jacc.2017.10.024

50. Weissberg PL, Bennett MR. Atherosclerosis - an inflammatory disease. *New Engl J Med* (1999) 340(24):1928–9.

51. Tousoulis D, Oikonomou E, Economou EK, Crea F, Kaski JC. Inflammatory cytokines in atherosclerosis: current therapeutic approaches. *Eur Heart J* (2016) 37 (22):1723–+. doi: 10.1093/eurheartj/ehv759

52. Yin Y, Li XY, Sha XJ, Xi H, Li YF, Shao Y, et al. Early hyperlipidemia promotes endothelial activation *via* a caspase-1-Sirtuin 1 pathway. *Arterioscl Throm Vas* (2015) 35(4):804–16. doi: 10.1161/ATVBAHA.115.305282

53. Zhang Y, Li X, Pitzer AL, Chen Y, Wang L, Li PL. Coronary endothelial dysfunction induced by nucleotide oligomerization domain-like receptor protein with pyrin domain containing 3 inflammasome activation during hypercholesterolemia: Beyond inflammation. *Antioxid Redox Sign* (2015) 22 (13):1084–96. doi: 10.1089/ars.2014.5978

54. Wu Q, He X, Wu LM, Zhang RY, Li LM, Wu CM, et al. MLKL aggravates ox-LDL-Induced cell pyroptosis *via* activation of NLRP3 inflammasome in human umbilical vein endothelial cells. *Inflammation* (2020) 43(6):2222–31. doi: 10.1007/s10753-020-01289-8

55. Zeng JF, Tao J, Xi LZ, Wang Z, Liu LS. PCSK9 mediates the oxidative low-density lipoprotein-induced pyroptosis of vascular endothelial cells via the UQCRC1/ROS pathway. *Int J Mol Med* (2021) 47(4). doi: 10.3892/ijmm.2021.4886

56. Wu P, Chen JN, Chen JJ, Tao J, Wu SY, Xu GS, et al. Trimethylamine n-oxide promotes apoE(-/-) mice atherosclerosis by inducing vascular endothelial cell pyroptosis *via* the SDHB/ROS pathway. *J Cell Physiol* (2020) 235(10):6582–91. doi: 10.1002/jcp.29518

57. Zeng ZL, Chen JJ, Wu P, Liu YM, Zhang TT, Tao J, et al. OxLDL induces vascular endothelial cell pyroptosis through miR-125a-5p/TET2 pathway. *J Cell Physiol* (2019) 234(5):7475–91. doi: 10.1002/jcp.27509

58. Leng YP, Chen RF, Chen RT, He S, Shi XL, Zhou XY, et al. HMGB1 mediates homocysteine-induced endothelial cells pyroptosis *via* cathepsin V-dependent pathway. *Biochem Bioph Res Co* (2020) 532(4):640–6. doi: 10.1016/j.bbrc.2020.08.091

59. Xi H, Zhang YL, Xu YJ, Yang WY, Jiang XH, Sha XJ, et al. Caspase-1 inflammasome activation mediates homocysteine-induced pyrop-apoptosis in endothelial cells. *Circ Res* (2016) 118(10):1525–U174. doi: 10.1161/CIRCRESAHA.116.308501

60. Chen JN, Zhang JW, Wu JX, Zhang SL, Liang YM, Zhou B, et al. Low shear stress induced vascular endothelial cell pyroptosis by TET2/SDHB/ROS pathway. *Free Radical Bio Med* (2021) 162:582–91. doi: 10.1016/j.freeradbiomed.2020.11.017

61. Xu XS, Yang Y, Wang GF, Yin Y, Han S, Zheng DH, et al. Low shear stress regulates vascular endothelial cell pyroptosis through miR-181b-5p/STAT-3 axis. *J Cell Physiol* (2021) 236(1):318–27. doi: 10.1002/jcp.29844

62. Stehle JH, Saade A, Rawashdeh O, Ackermann K, Jilg A, Sebesteny T, et al. A survey of molecular details in the human pineal gland in the light of phylogeny, structure, function and chronobiological diseases. *J Pineal Res* (2011) 51(1):17–43. doi: 10.1111/j.1600-079X.2011.00856.x

63. Acuna-Castroviejo D, Escames G, Venegas C, Diaz-Casado ME, Lima-Cabello E, Lopez LC, et al. Extrapineal melatonin: sources, regulation, and potential functions. *Cell Mol Life Sci* (2014) 71(16):2997–3025. doi: 10.1007/s00018-014-1579-2

64. Zhang Y, Liu X, Bai X, Lin Y, Li ZE, Fu JB, et al. Melatonin prevents endothelial cell pyroptosis via regulation of long noncoding RNA MEG3/miR-223/NLRP3 axis. *J Pineal Res* (2018) 64(2). doi: 10.1111/jpi.12449

65. Zeng JF, Tao J, Xia LZ, Zeng ZL, Chen JJ, Wang Z, et al. Melatonin inhibits vascular endothelial cell pyroptosis by improving mitochondrial function *via* up-regulation and demethylation of UQCRC1. *Biochem Cell Biol* (2021) 99(3):339–47. doi: 10.1139/bcb-2020-0279

66. Wang XB, Bian Y, Zhang R, Liu XD, Ni L, Ma BT, et al. Melatonin alleviates cigarette smoke-induced endothelial cell pyroptosis through inhibiting ROS/NLRP3 axis. *Biochem Bioph Res Co* (2019) 519(2):402–8. doi: 10.1016/j.bbrc.2019.09.005

67. Meng QH, Li Y, Ji TT, Chao Y, Li J, Fu Y, et al. Estrogen prevent atherosclerosis by attenuating endothelial cell pyroptosis *via* activation of estrogen receptor alpha-mediated autophagy. *J Adv Res* (2021) 28:149–64. doi: 10.1016/j.jare.2020.08.010

68. Zeng ZL, Zheng QP, Chen JJ, Tan XH, Li Q, Ding LX, et al. FGF21 mitigates atherosclerosis via inhibition of NLRP3 inflammasome-mediated vascular endothelial cells pyroptosis. *Exp Cell Res* (2020) 393(2). doi: 10.1016/j.yexcr.2020.112108

69. Chen JJ, Tao J, Zhang XL, Xia LZ, Zeng JF, Zhang H, et al. Inhibition of the ox-LDL-Induced pyroptosis by FGF21 of human umbilical vein endothelial cells through the TET2-UQCRC1-ROS pathway. *DNA Cell Biol* (2020) 39(4):661–70. doi: 10.1089/dna.2019.5151

70. Oh S, Son M, Park CH, Jang JT, Son KH, Byun K. The reducing effects of pyrogallol-Phloroglucinol-6,6-Bieckol on high-fat diet-induced pyroptosis in endothelial and vascular smooth muscle cells of mice aortas. *Mar Drugs* (2020) 18(12). doi: 10.3390/md18120648

71. Yang MY, Lv H, Liu Q, Zhang L, Zhang RX, Huang XT, et al. Colchicine alleviates cholesterol crystal-induced endothelial cell pyroptosis through activating AMPK/SIRT1 pathway. *Oxid Med Cell Longev* (2020) 2020. doi: 10.1155/2020/9173530

72. Hu Q, Zhang T, Yi L, Zhou X, Mi MT. Dihydromyricetin inhibits NLRP3 inflammasome-dependent pyroptosis by activating the Nrf2 signaling pathway in vascular endothelial cells. *Biofactors* (2018) 44(2):123–36. doi: 10.1002/biof.1395

73. Yao F, Jin Z, Lv XH, Zheng ZH, Gao HQ, Deng Y, et al. Hydroxytyrosol acetate inhibits vascular endothelial cell pyroptosis via the HDAC11 signaling pathway in atherosclerosis. *Front Pharmacol* (2021) 12. doi: 10.3389/fphar.2021.656272

74. Yao F, Jin Z, Zheng Z, Lv X, Ren L, Yang J, et al. HDAC11 promotes both NLRP3/caspase-1/GSDMD and caspase-3/GSDME pathways causing pyroptosis *via* ERG in vascular endothelial cells. *Cell Death Discovery* (2022) 8(1):112. doi: 10.1038/s41420-022-00906-9

75. Wang XM, Li XW, Wu YH, Song Y. Upregulation of miR-223 abrogates NLRP3 inflammasome-mediated pyroptosis to attenuate oxidized low-density lipoprotein (ox-LDL)-induced cell death in human vascular endothelial cells (ECs). *In Vitro Cell Dev-An* (2020) 56(8):670–9. doi: 10.1007/s11626-020-00496-9

76. Wang YR, Song XJ, Li ZB, Liu N, Yan YY, Li TY, et al. MicroRNA-103 protects coronary artery endothelial cells against H2O2-induced oxidative stress *via* BNIP3-mediated end-stage autophagy and antipyroptosis pathways. *Oxid Med Cell Longev* (2020) 2020. doi: 10.1155/2020/8351342

77. Liu Y, Li PY, Qiao CH, Wu TJ, Sun XK, Wen M, et al. Chitosan hydrogel enhances the therapeutic efficacy of bone marrow-derived mesenchymal stem cells for myocardial infarction by alleviating vascular endothelial cell pyroptosis. *J Cardiovasc Pharm* (2020) 75(1):75–83. doi: 10.1097/FJC.0000000000000760

78. Pei Y, Geng Y, Su L. Pyroptosis of HUVECs can be induced by heat stroke. *Biochem Biophys Res Commun* (2018) 506(3):626–31. doi: 10.1016/j.bbrc.2018.10.051

79. Katz AM. Knowledge of the circulation before William Harvey. *Circulation* (1957) 15(5):726–34. doi: 10.1161/01.CIR.15.5.726

80. Vita JA. Endothelial function. *Circulation* (2011) 124(25):e906–12. doi: 10.1161/CIRCULATIONAHA.111.078824

81. Deanfield JE, Halcox JP, Rabelink TJ. Endothelial function and dysfunction: testing and clinical relevance. *Circulation* (2007) 115(10):1285–95. doi: 10.1161/CIRCULATIONAHA.106.652859

82. Eelen G, de Zeeuw P, Simons M, Carmeliet P. Endothelial cell metabolism in normal and diseased vasculature. *Circ Res* (2015) 116(7):1231–44. doi: 10.1161/CIRCRESAHA.116.302855

83. Park BS, Song DH, Kim HM, Choi BS, Lee H, Lee JO. The structural basis of lipopolysaccharide recognition by the TLR4-MD-2 complex. *Nature* (2009) 458 (7242):1191–5. doi: 10.1038/nature07830

84. Shi J, Gao W, Shao F. Pyroptosis: Gasdermin-mediated programmed necrotic cell death. *Trends Biochem Sci* (2017) 42(4):245–54. doi: 10.1016/j.tibs.2016.10.004

85. Brigham KL, Meyrick B. Endotoxin and lung injury. *Am Rev Respir Dis* (1986) 133(5):913–27.

86. Luo L, Xu M, Liao D, Deng J, Mei H, Hu Y. PECAM-1 protects against DIC by dampening inflammatory responses *via* inhibiting macrophage pyroptosis and restoring vascular barrier integrity. *Transl Res* (2020) 222:1–16. doi: 10.1016/j.trsl.2020.04.005

87. Zhao J, Liu Z, Chang Z. Lipopolysaccharide induces vascular endothelial cell pyroptosis *via* the SP1/RCN2/ROS signaling pathway. *Eur J Cell Biol* (2021) 100 (4):151164. doi: 10.1016/j.ejcb.2021.151164

88. Huang LS, Hong Z, Wu W, Xiong S, Zhong M, Gao X, et al. mtDNA activates cGAS signaling and suppresses the YAP-mediated endothelial cell proliferation program to promote inflammatory injury. *Immunity* (2020) 52 (3):475–86.e5. doi: 10.1016/j.immuni.2020.02.002

89. Chen H, Li Y, Wu J, Li G, Tao X, Lai K, et al. RIPK3 collaborates with GSDMD to drive tissue injury in lethal polymicrobial sepsis. *Cell Death Differ* (2020) 27(9):2568–85. doi: 10.1038/s41418-020-0524-1

90. Liu H, Tang D, Zhou X, Yang X, Chen AF. PhospholipaseCgamma1/calcium-dependent membranous localization of gsdmd-n drives endothelial pyroptosis, contributing to lipopolysaccharide-induced fatal outcome. *Am J Physiol Heart Circ Physiol* (2020) 319(6):H1482–H95. doi: 10.1152/ajpheart.00731.2019

91. Nagashima S, Mendes MC, Camargo Martins AP, Borges NH, Godoy TM, Miggiolaro A, et al. Endothelial dysfunction and thrombosis in patients with

COVID-19-Brief report. *Arterioscler Thromb Vasc Biol* (2020) 40(10):2404–7. doi: 10.1161/ATVBAHA.120.314860

92. Oppenheim JJ, Biragyn A, Kwak LW, Yang D. Roles of antimicrobial peptides such as defensins in innate and adaptive immunity. *Ann Rheum Dis* (2003) 62 Suppl 2:ii17–21. doi: 10.1136/ard.62.suppl_2.ii17

93. Lehrer RI, Lu W. Alpha-defensins in human innate immunity. *Immunol Rev* (2012) 245(1):84–112. doi: 10.1111/j.1600-065X.2011.01082.x

94. Chen Q, Hakimi M, Wu S, Jin Y, Cheng B, Wang H, et al. Increased genomic copy number of DEFA1/DEFA3 is associated with susceptibility to severe sepsis in Chinese han population. *Anesthesiology* (2010) 112(6):1428–34. doi: 10.1097/ALN.0b013e3181d968eb

95. Chen Q, Yang Y, Hou J, Shu Q, Yin Y, Fu W, et al. Increased gene copy number of DEFA1/DEFA3 worsens sepsis by inducing endothelial pyroptosis. *Proc Natl Acad Sci U S A* (2019) 116(8):3161–70. doi: 10.1073/pnas.1812947116

96. Lai D, Tang J, Chen L, Fan EK, Scott MJ, Li Y, et al. Group 2 innate lymphoid cells protect lung endothelial cells from pyroptosis in sepsis. *Cell Death Dis* (2018) 9(3):369. doi: 10.1038/s41419-018-0412-5

97. Zhou P, Guo H, Li Y, Liu Q, Qiao X, Lu Y, et al. Monocytes promote pyroptosis of endothelial cells during lung ischemia-reperfusion *via* IL-1R/NF-kappaB/NLRP3 signaling. *Life Sci* (2021) 276:119402. doi: 10.1016/j.lfs.2021.119402

98. Sakon M, Kita Y, Yoshida T, Umeshita K, Gotoh M, Kanai T, et al. Plasma hepatocyte growth factor levels are increased in systemic inflammatory response syndrome. *Surg Today* (1996) 26(4):236–41. doi: 10.1007/BF00311581

99. Sekine K, Fujishima S, Aikawa N. Plasma hepatocyte growth factor is increased in early-phase sepsis. *J Infect Chemother* (2004) 10(2):110–4. doi: 10.1007/s10156-004-0301-Y

100. Peng F, Chang W, Sun Q, Xu X, Xie J, Qiu H, et al. HGF alleviates septic endothelial injury by inhibiting pyroptosis *via* the mTOR signalling pathway. *Respir Res* (2020) 21(1):215. doi: 10.1186/s12931-020-01480-3

101. Zhuo L, Chen X, Sun Y, Wang Y, Shi Y, Bu L, et al. Rapamycin inhibited pyroptosis and reduced the release of IL-1beta and IL-18 in the septic response. *BioMed Res Int* (2020) 2020:5960375. doi: 10.1155/2020/5960375

102. Wiedmer T, Zhou Q, Kwoh DY, Sims PJ. Identification of three new members of the phospholipid scramblase gene family. *Biochim Biophys Acta* (2000) 1467(1):244–53. doi: 10.1016/S0005-2736(00)00236-4

103. Basse F, Stout JG, Sims PJ, Wiedmer T. Isolation of an erythrocyte membrane protein that mediates Ca2+-dependent transbilayer movement of phospholipid. *J Biol Chem* (1996) 271(29):17205–10. doi: 10.1074/jbc.271.29.17205

104. Liu X, Wang D, Zhang X, Lv M, Liu G, Gu C, et al. Effect and mechanism of phospholipid scramblase 4 (PLSCR4) on lipopolysaccharide (LPS)-induced injury to human pulmonary microvascular endothelial cells. *Ann Transl Med* (2021) 9(2):159. doi: 10.21037/atm-20-7983

105. Kadioglu O, Law BYK, Mok SWF, Xu SW, Efferth T, Wong VKW. Mode of action analyses of neferine, a bisbenzylisoquinoline alkaloid of lotus (Nelumbo nucifera) against multidrug-resistant tumor cells. *Front Pharmacol* (2017) 8:238. doi: 10.3389/fphar.2017.00238

106. Marthandam Asokan S, Mariappan R, Muthusamy S, Velmurugan BK. Pharmacological benefits of neferine - a comprehensive review. *Life Sci* (2018) 199:60–70. doi: 10.1016/j.lfs.2018.02.032

107. Tang YS, Zhao YH, Zhong Y, Li XZ, Pu JX, Luo YC, et al. Neferine inhibits LPS-ATP-induced endothelial cell pyroptosis *via* regulation of ROS/NLRP3/Caspase-1 signaling pathway. *Inflammation Res* (2019) 68(9):727–38. doi: 10.1007/s00011-019-01256-6

108. Martinez MC, Tesse A, Zobairi F, Andriantsitohaina R. Shed membrane microparticles from circulating and vascular cells in regulating vascular function. *Am J Physiol Heart Circ Physiol* (2005) 288(3):H1004–9. doi: 10.1152/ajpheart.00842.2004

109. Diamant M, Tushuizen ME, Sturk A, Nieuwland R. Cellular microparticles: new players in the field of vascular disease? *Eur J Clin Invest* (2004) 34(6):392–401. doi: 10.1111/j.1365-2362.2004.01355.x

110. Martin S, Tesse A, Hugel B, Martinez MC, Morel O, Freyssinet JM, et al. Shed membrane particles from T lymphocytes impair endothelial function and regulate endothelial protein expression. *Circulation* (2004) 109(13):1653–9. doi: 10.1161/01.CIR.0000124065.31211.6E

111. Mitra S, Exline M, Habyarimana F, Gavrilin MA, Baker PJ, Masters SL, et al. Microparticulate caspase 1 regulates gasdermin d and pulmonary vascular endothelial cell injury. *Am J Respir Cell Mol Biol* (2018) 59(1):56–64. doi: 10.1165/rcmb.2017-0393OC

112. Morshed MG, Singh AE. Recent trends in the serologic diagnosis of syphilis. *Clin Vaccine Immunol* (2015) 22(2):137–47. doi: 10.1128/CVI.00681-14

113. Zhang X, Zhang T, Pei J, Liu Y, Li X, Medrano-Gracia P. Time series modelling of syphilis incidence in China from 2005 to 2012. *PloS One* (2016) 11(2):e0149401. doi: 10.1371/journal.pone.0149401

114. Long FQ, Kou CX, Li K, Wu J, Wang QQ. MiR-223-3p inhibits rTp17-induced inflammasome activation and pyroptosis by targeting NLRP3. *J Cell Mol Med* (2020) 24(24):14405–14. doi: 10.1111/jcmm.16061

115. Pang T, Mak TK, Gubler DJ. Prevention and control of dengue-the light at the end of the tunnel. *Lancet Infect Dis* (2017) 17(3):e79–87. doi: 10.1016/S1473-3099(16)30471-6

116. Gubler DJ. Dengue and dengue hemorrhagic fever. *Clin Microbiol Rev* (1998) 11(3):480–96. doi: 10.1128/CMR.11.3.480

117. Lien TS, Sun DS, Wu CY, Chang HH. Exposure to dengue envelope protein domain III induces Nlrp3 inflammasome-dependent endothelial dysfunction and hemorrhage in mice. *Front Immunol* (2021) 12:617251. doi: 10.3389/fimmu.2021.617251

118. Uehara R, Belay ED. Epidemiology of Kawasaki disease in Asia, Europe, and the united states. *J Epidemiol* (2012) 22(2):79–85. doi: 10.2188/jea.JE20110131

119. Jia C, Zhang J, Chen H, Zhuge Y, Chen H, Qian F, et al. Endothelial cell pyroptosis plays an important role in Kawasaki disease *via* HMGB1/RAGE/cathespin b signaling pathway and NLRP3 inflammasome activation. *Cell Death Dis* (2019) 10(10):778. doi: 10.1038/s41419-019-2021-3

120. Rajah TT, Olson AL, Grammas P. Differential glucose uptake in retina- and brain-derived endothelial cells. *Microvasc Res* (2001) 62(3):236–42. doi: 10.1006/mvre.2001.2337

121. Alpert E, Gruzman A, Riahi Y, Blejter R, Aharoni P, Weisinger G, et al. Delayed autoregulation of glucose transport in vascular endothelial cells. *Diabetologia* (2005) 48(4):752–5. doi: 10.1007/s00125-005-1681-y

122. Lim RR, Wieser ME, Ganga RR, Barathi VA, Lakshminarayanan R, Mohan RR, et al. NOD-like receptors in the eye: Uncovering its role in diabetic retinopathy. *Int J Mol Sci* (2020) 21(3). doi: 10.3390/ijms21030899

123. Mizutani M, Kern TS, Lorenzi M. Accelerated death of retinal microvascular cells in human and experimental diabetic retinopathy. *J Clin Invest* (1996) 97(12):2883–90. doi: 10.1172/JCI118746

124. Samways DS, Li Z, Egan TM. Principles and properties of ion flow in P2X receptors. *Front Cell Neurosci* (2014) 8:6. doi: 10.3389/fncel.2014.00006

125. Gu C, Draga D, Zhou C, Su T, Zou C, Gu Q, et al. miR-590-3p inhibits pyroptosis in diabetic retinopathy by targeting NLRP1 and inactivating the NOX4 signaling pathway. *Invest Ophthalmol Vis Sci* (2019) 60(13):4215–23. doi: 10.1167/iovs.19-27825

126. Yang K, Liu J, Zhang X, Ren Z, Gao L, Wang Y, et al. H3 relaxin alleviates migration, apoptosis and pyroptosis through P2X7R-mediated nucleotide binding oligomerization domain-like receptor protein 3 inflammasome activation in retinopathy induced by hyperglycemia. *Front Pharmacol* (2020) 11:603689. doi: 10.3389/fphar.2020.603689

127. Gomez A, Serrano A, Salero E, Tovar A, Amescua G, Galor A, et al. Tumor necrosis factor-alpha and interferon-gamma induce inflammasome-mediated corneal endothelial cell death. *Exp Eye Res* (2021) 207:108574. doi: 10.1016/j.exer.2021.108574

128. Zhang Y, Song Z, Li X, Xu S, Zhou S, Jin X, et al. Long noncoding RNA KCNQ1OT1 induces pyroptosis in diabetic corneal endothelial keratopathy. *Am J Physiol Cell Physiol* (2020) 318(2):C346–C59. doi: 10.1152/ajpcell.00053.2019

129. Song Y, Yang L, Guo R, Lu N, Shi Y, Wang X. Long noncoding RNA MALAT1 promotes high glucose-induced human endothelial cells pyroptosis by affecting NLRP3 expression through competitively binding miR-22. *Biochem Biophys Res Commun* (2019) 509(2):359–66. doi: 10.1016/j.bbrc.2018.12.139

130. Gu H, Guo Y, Gu L, Wei A, Xie S, Ye Z, et al. Deep learning for identifying corneal diseases from ocular surface slit-lamp photographs. *Sci Rep* (2020) 10(1):17851. doi: 10.1038/s41598-020-75027-3

131. Gu J, Huang W, Zhang W, Zhao T, Gao C, Gan W, et al. Sodium butyrate alleviates high-glucose-induced renal glomerular endothelial cells damage *via* inhibiting pyroptosis. *Int Immunopharmacol* (2019) 75:105832. doi: 10.1016/j.intimp.2019.105832

132. Vidale S, Consoli A, Arnaboldi M, Consoli D. Postischemic inflammation in acute stroke. *J Clin Neurol* (2017) 13(1):1–9. doi: 10.3988/jcn.2017.13.1.1

133. Wang Y, Guan X, Gao CL, Ruan W, Zhao S, Kai G, et al. Medioresinol as a novel PGC-1alpha activator prevents pyroptosis of endothelial cells in ischemic stroke through PPARalpha-GOT1 axis. *Pharmacol Res* (2021) 169:105640. doi: 10.1016/j.phrs.2021.105640

134. Hwang JH, Hwang IS, Liu QH, Woo ER, Lee DG. (+)-medioresinol leads to intracellular ROS accumulation and mitochondria-mediated apoptotic cell death in candida albicans. *Biochimie* (2012) 94(8):1784–93. doi: 10.1016/j.biochi.2012.04.010

135. Zhang Y, Li X, Qiao S, Yang D, Li Z, Xu J, et al. Occludin degradation makes brain microvascular endothelial cells more vulnerable to reperfusion injury in vitro. *J Neurochem* (2021) 156(3):352–66. doi: 10.1111/jnc.15102

136. Kim H, Seo JS, Lee SY, Ha KT, Choi BT, Shin YI, et al. AIM2 inflammasome contributes to brain injury and chronic post-stroke cognitive

impairment in mice. *Brain Behav Immun* (2020) 87:765–76. doi: 10.1016/j.bbi.2020.03.011

137. Ge X, Li W, Huang S, Yin Z, Xu X, Chen F, et al. The pathological role of NLRs and AIM2 inflammasome-mediated pyroptosis in damaged blood-brain barrier after traumatic brain injury. *Brain Res* (2018) 1697:10–20. doi: 10.1016/j.brainres.2018.06.008

138. Yang WL, Sharma A, Wang Z, Li Z, Fan J, Wang P. Cold-inducible RNA-binding protein causes endothelial dysfunction *via* activation of Nlrp3 inflammasome. *Sci Rep* (2016) 6:26571. doi: 10.1038/srep26571

139. Yang J, Zhao Y, Zhang P, Li Y, Yang Y, Yang Y, et al. Hemorrhagic shock primes for lung vascular endothelial cell pyroptosis: role in pulmonary inflammation following LPS. *Cell Death Dis* (2016) 7(9):e2363. doi: 10.1038/cddis.2016.274

140. Laubach VE, Sharma AK. Mechanisms of lung ischemia-reperfusion injury. *Curr Opin Organ Transplant* (2016) 21(3):246–52. doi: 10.1097/MOT.0000000000000304

141. Benjamin EJ, Virani SS, Callaway CW, Chamberlain AM, Chang AR, Cheng S, et al. Heart disease and stroke statistics-2018 update: A report from the American heart association. *Circulation* (2018) 137(12):e67–e492. doi: 10.1161/CIR.0000000000000558

142. American Heart Association Nutrition C, Lichtenstein AH, Appel LJ, Brands M, Carnethon M, Daniels S, et al. Diet and lifestyle recommendations revision 2006: a scientific statement from the American heart association nutrition committee. *Circulation* (2006) 114(1):82–96. doi: 10.1161/CIRCULATIONAHA.106.176158

143. Hotchkiss RS, Karl IE. The pathophysiology and treatment of sepsis. *N Engl J Med* (2003) 348(2):138–50. doi: 10.1056/NEJMra021333

144. Gotts JE, Matthay MA. Sepsis: pathophysiology and clinical management. *BMJ* (2016) 353:i1585. doi: 10.1136/bmj.i1585

10.3389/fimmu.2022.1093985

Glossary

AGEs	Advanced glycation end products
AIM2	Absent in melanoma 2
BMEC	Brain microvascular endothelial cell
cGAMP	Cyclic GMP–AMP
cGAS	Cyclic GMP-AMP synthase
CIRI	Cerebral ischemia-reperfusion injury
CIRP	Cold-inducible RNA-binding protein
CVD	Cardiovascular disease
DENV	Dengue virus
DN	Diabetic nephropathy
DR	Diabetic retinopathy
EC	Endothelial cell
EIII	Virion-associated envelope protein domain III
eNOS	Endothelia nitric oxide synthase
FGF21	Fibroblast growth factor 21
GECs	Glomerular endothelial cells
GO	Gene ontology
GSDMD	Gasdermin D
GSDMD-N	N-terminal GSDMD
H/R	Hypoxia/reoxygenation
HDAC2	Histone deacetylase 2
HFD	High fat diet
HG	High glucose
HGF	Hepatocyte growth factor
HHcy	Hyperhomocysteinemia
HMGB1	High mobility group box 1
HNPs	Human neutrophil peptides
HPMEC	Human pulmonary microvascular endothelial cell
HS	Hemorrhagic shock
HUVEC	Human umbilical vein endothelial cell
ICAM1	Intercellular adhesion molecule 1
ILC2	Group 2 innate lymphoid cells
KD	Kawasaki disease
KEGG	Kyoto Encyclopedia of Genes and Genomes
LDL	Low-density lipoprotein
LPS	Lipopolysaccharide
MCAO	Middle cerebral artery occlusion
MDN	Mediresinol
MLKL	Mixed lineage kinase domain-like
MPs	Microparticles
mtDNA	Mitochondrial DNA
mTOR	Mechanistic target of rapamycin kinase
mtROS	Mitochondrial ROS
NF-κB	Nuclear factor-κB
NLRP3	NOD-like receptor thermal protein domain associated protein 3
OGD	Oxygen glucose deprivation
OGD/R	OGD/reoxygenation
oxLDL	Oxidized LDL
PCD	Programmed cell death
PCSK9	Proprotein convertase subtilisin/kexin type 9
PLSCRs	Phospholipid scramblases
PSCI	Post-stroke cognitive impairment
RCD	Regulated cell death
RCN2	Reticulocalbin 2
RMEC	Retinal microvascular endothelial cell
ROS	Reactive oxygen species
STAT3	Signal transducer and activator of transcription 3
STING	Stimulator of interferon genes
T pallidum	Treponema pallidum subsp pallidum
TBI	Traumatic brain injury
TET2	Targeted tet methylcytosine dioxygenase 2
TLR4	Toll like receptor 4
TMAO	Trimethylamine N-oxide
UQCRC1	Ubiquinol-cytochrome c reductase core protein 1
VCAM1	Vascular cell adhesion molecule 1
YAP1	Yes1 associated transcriptional regulator

frontiers | Frontiers in Immunology

TYPE Original Research
PUBLISHED 09 January 2023
DOI 10.3389/fimmu.2022.1050743

OPEN ACCESS

EDITED BY
Mirza S. Baig,
Indian Institute of Technology Indore, India

REVIEWED BY
Zihui Zheng,
Nanjing University of Chinese Medicine, China
Lei Zhao,
University of Wisconsin-Madison, United States

*CORRESPONDENCE
Gen Wen
wengen2006@126.com
Shuo Wang
shuowang97@126.com

†These authors have contributed equally to this work

SPECIALTY SECTION
This article was submitted to Inflammation, a section of the journal Frontiers in Immunology

RECEIVED 22 September 2022
ACCEPTED 05 December 2022
PUBLISHED 09 January 2023

CITATION
Liu X, Xiao H, Peng X, Chai Y, Wang S and Wen G (2023) Identification and comprehensive analysis of circRNA–miRNA–mRNA regulatory networks in osteoarthritis.
Front. Immunol. 13:1050743.
doi: 10.3389/fimmu.2022.1050743

Identification and comprehensive analysis of circRNA–miRNA–mRNA regulatory networks in osteoarthritis

Xuanzhe Liu[1†], Huimin Xiao[2†], Xiaotong Peng[3†], Yimin Chai[1], Shuo Wang[1*] and Gen Wen[1*]

[1]Department of Orthopedic Surgery, Shanghai Sixth People's Hospital Affiliated to Shanghai Jiao Tong University School of Medicine, Shanghai, China, [2]College of Fisheries and Life Science, Shanghai Ocean University, Shanghai, China, [3]Department of Gynecology, Shanghai First Maternity and Infant Hospital, School of Medicine, Tongji University, Shanghai, China

Osteoarthritis (OA) is a common orthopedic degenerative disease, leading to high disability in activities of daily living. There remains an urgent need to identify the underlying mechanisms and identify new therapeutic targets in OA diagnosis and treatment. Circular RNAs (circRNAs) play a role in the development of multiple diseases. Many studies have reported that circRNAs regulate microRNAs (miRNAs) through an endogenous competitive mechanism. However, it remains unclear if an interplay between circRNAs, miRNAs, and target genes plays a deeper regulatory role in OA. Four datasets were downloaded from the GEO database, and differentially expressed circRNAs (DECs), differentially expressed miRNAs (DEMs), and differentially expressed genes (DEGs) were identified. Functional annotation and pathway enrichment analysis of DEGs and DECs were carried out to determine the main associated mechanism in OA. A protein–protein network (PPI) was constructed to analyze the function of, and to screen out, hub DEGs in OA. Based on the artificial intelligence prediction of protein crystal structures of two hub DEGs, TOP2A and PLK1, digitoxin and oxytetracycline were found to have the strongest affinity, respectively, with molecular docking. Subsequently, overlapping DEMs and miRNAs targeted by DECs obtained target DEMs (DETMs). Intersection of DEGs and genes targeted by DEMs obtained target DEGs (DETGs). Thus, a circRNA–miRNA–mRNA regulatory network was constructed from 16 circRNAs, 32 miRNAs, and 97 mRNAs. Three hub DECs have the largest number of regulated miRNAs and were verified through *in vitro* experiments. In addition, the expression level of 16 DECs was validated by RT-PCR. In conclusion, we constructed a circRNA–miRNA–mRNA regulatory

network in OA and three new hub DECs, hsa_circ_0027914, hsa_circ_0101125, and hsa_circ_0102564, were identified as novel biomarkers for OA.

KEYWORDS

circular RNA, microRNA, osteoarthritis, chondrocytes, regulatory network

Highlights

1. For the first time, a circRNA–miRNA–mRNA regulatory network, constructed from 16 DECs, 32DETMs, and 97 DETGs, was identified in OA chondrocytes.
2. Three hub DECs, hsa_circ_0027914, hsa_circ_0101125, and hsa_circ_0102564, were identified as the hub DECs with the most regulated miRNAs in OA. *In vitro* validation experiments suggested the pro-apoptosis function of these three hub DECs and their potential to be novel biomarkers in OA.
3. Digitoxin and oxytetracycline have the highest affinity for the target genes, *TOP2A* and *PLK1*, and thus were identified as potential drugs for OA therapy.

Introduction

Osteoarthritis (OA) is one of the most common long-term degenerative joint diseases, and the leading cause of disability in elderly people (1). Recent epidemiology studies have reported that the incidence rate of knee OA peaks around the age of 75 years, at 16% (2). The main pathophysiological changes of OA include articular cartilage wear and tear, subchondral bone destruction, and synovium inflammation (1). The pathogenesis of OA is multifactorial, and the molecular biological mechanism remains unclear. To date, few biomarkers of OA have been utilized to develop early diagnosis and treatment.

With deeper understanding of the cellular and molecular biology, the role of post-transcriptional modifications of non-coding RNAs (ncRNAs) in the regulation of messenger RNAs (mRNAs) has received increasing attention (3). Non-coding RNAs (ncRNAs) include microRNAs(miRNAs), circular RNAs (circRNAs), long-non-coding RNAs (lncRNAs), etc. Among these, the functions of miRNAs and circRNAs are the most widely studied owing to their paradoxical effect on mRNA regulation (4). miRNAs are single-stranded RNA molecules (about 18–25 nucleotides in length). At the post-transcriptional level, miRNAs can bind to complementary sites on the 3′-untranslated region (3′-UTR) of target genes to negatively regulate mRNA expression (5). circRNAs, in contrast, are competing endogenous RNAs (ceRNAs), characterized by a closed continuous loop structure lacking a 5′ cap and a poly(A) tail at the 3′ ends (4). The main function of circRNAs is to act as a molecular sponge. CircRNAs can target miRNA and inhibit miRNA transcription, thus enhancing expression of the target gene (6).

Recently, increasing evidence has shown that the interaction between miRNAs and circRNAs plays a vital role in the pathogenesis of many human diseases (7), especially osteoarthritis (OA) (8, 9). CircRNA and miRNAs are strongly related to extracellular matrix (ECM) metabolism and inflammation in OA. For instance, circCDK14 (hsa_circ_0001722) has a protective effect on the ECM and can sponge miR-125a-5p by restoring TGF-β/Smad2 pathways in OA (10). In addition, another circPDE4D protects against OA by binding to miR-103a-3p and targeting the fibroblast growth factor 18 (FGF18) gene (11). Both of these studies found that circRNA competes with miRNA. However, the particular miRNA and circRNA involved in in OA and their potential regulatory interplay remained unidentified.

As shown in Scheme 1, our study aimed to reveal the novel pathogenic mechanism of circRNAs in OA through bioinformatic analysis, and to identify new potential drug targets. Furthermore, the circRNA–miRNA–mRNA network and target gene–protein interaction network are shown, to illustrate the interplay of downstream mRNAs. We also aimed to validate the function of these pathogenic circRNAs through *in vitro* experiments.

Materials and methods

Data derivation

OA-related expression datasets for circRNA (GSE175959), miRNA (GSE79258), and mRNA (GSE114007 and GSE168505) were extracted from the Gene Expression Omnibus (GEO) database (https://www.ncbi.nlm.nih.gov/geo/). The characterization of these datasets is shown in Figure 1A. Owing to the batch nature of the GSE data, we integrated and normalized these data using R's limma package.

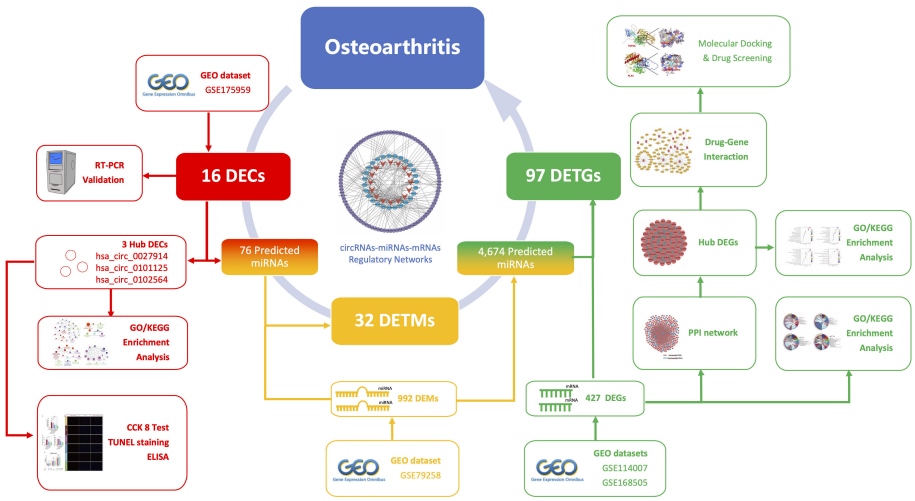

SCHEME 1
The schematic workflow of this study.

Identification of DECs, DEMs, and DEGs

The pretreated datasets were further analyzed using the GEO2R (http://www.ncbi.nlm.nih.gov/geo/geo2r/) for comparison between OA tissue and matched non-arthritic cartilage tissue. The screening thresholds of differentially expressed genes (DEGs), differentially expressed microRNAs (DEMs), and differentially expressed circular RNAs (DECs) were set as p-value < 0.05 and $|\log_2\text{-fold change (FC)}| > 1$. DEGs were divided into two subgroups: upregulated DEGs and downregulated DEGs. Volcano plots were used to visualize DEGs, DEMs, and DECs. Heatmaps were used to better demonstrate the expression profiles of DEGs, and they were created by TBtools software.

Construction of protein–protein interaction (PPI) network and identification of hub genes

A PPI network was constructed using the online STRING database (http://www.string-db.org/) and Cytoscape, as described previously (12). In addition, hub genes were obtained using molecular complex detection (MCODE) v1.5.1.16 (13) (degree of cut-off = 2, max. depth = 100, node score cut-off = 0.2, and k-core = 2).

Functional enrichment analysis of DEGs and DECs

Gene Ontology (GO) and Kyoto Encyclopedia of Genes and Genomes (KEGG) pathway functional enrichment analysis were performed in the Sangerbox database (http://sangerbox.com/Tool) to annotate DEGs and hub DEGs. In addition, functional annotation of hub DECs was carried out based on the analysis of target genes regulated by hub DECs. The enrichment results were visualized by ClueGO V2.5.1 (with a p-value < 0.05 and a gene count > 3).

Drug–gene network analysis

Target drugs of hub genes were further investigated using an online drug–gene interaction database (DGIdb, https://dgidb.genome.wustl.edu/). The drug–gene network was then constructed using Cytoscape.

Homology modeling and molecular docking

With the help of artificial intelligence (AI), protein structural biology has advanced significantly in recent years. AlphaFold v2.0 (https://alphafold.ebi.ac.uk/) was adopted to build the structure of TOP2A and PLK1 using *in silico* modeling as an AI prediction tool. The amino acid sequences of human TOP2A and PLK1 (accession number O15392 and P04818, respectively) were obtained from the UniProt-KB database (http://www.uniprot.org/). The local distance difference test (LDDT) score in the AlphaFold database was used for the evaluation of the stereochemical quality of these predictive models.

After analysis of protein structure, molecular docking helps to mimic the first rank orientation of small-molecule drugs to

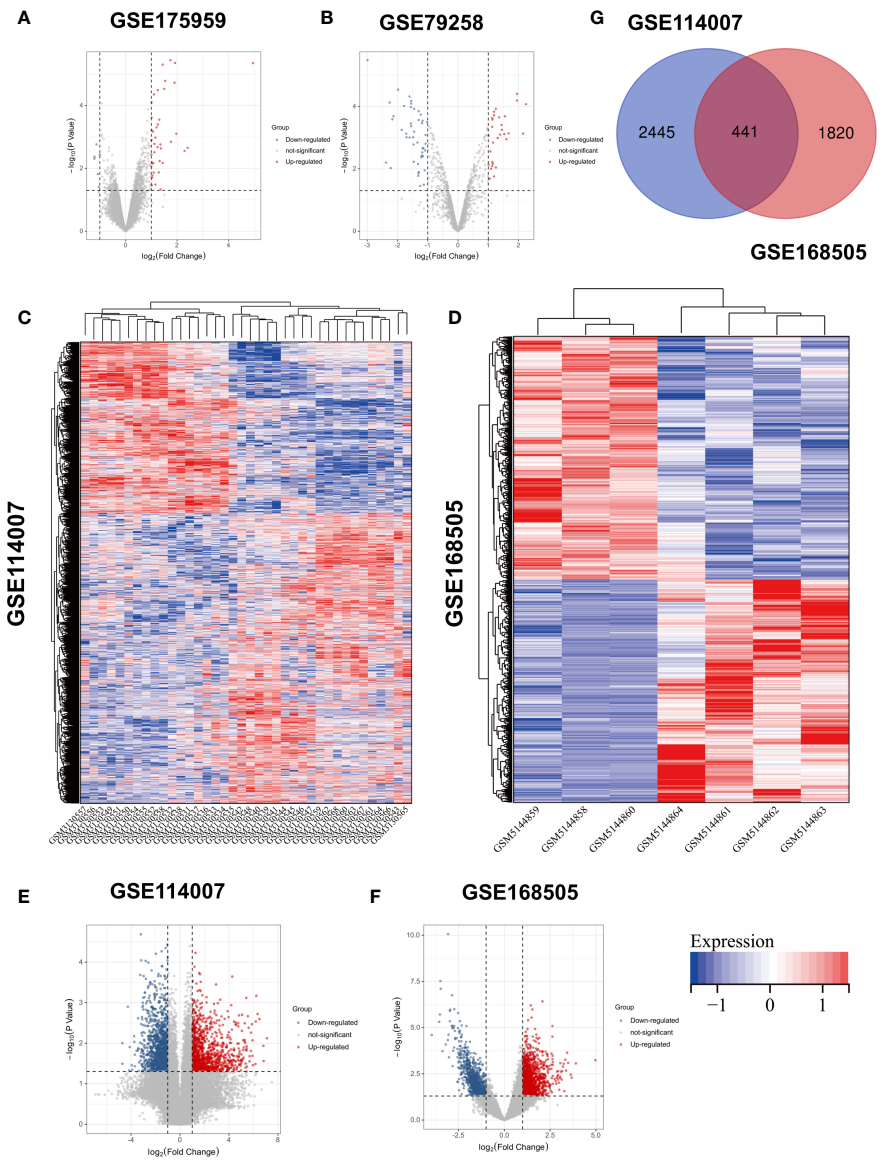

FIGURE 1
Volcano plots of **(A)** GSE175959; **(B)** GSE 79258; Heatmaps of **(C)** GSE114007; **(D)** GSE168505; Volcano plots of **(E)** GSE114007; **(F)** GSE168505. **(G)** Venn diagram of screening DEGs form mRNA expression profile.

macromolecules to better understand drug–gene interaction by computational simulation. Related small molecules were obtained from the PubChem database (https://pubchem.ncbi.nlm.nih.gov). AutoDockTools and PyMol were applied to hydrogenate or delete the crystallographic water and ligands of molecular structure. Molecular docking was performed by AutoDock Vina with default parameters. The geometric structures of selected drugs and candidate genes were then visualized. Docking affinity was also scored. PyMol was applied to analyze the optimal docking conformation.

Prediction of circRNA–miRNA and miRNA–mRNA interactions

CircRNA sponging target miRNAs was predicted by CircBank (http://www.circbank.cn/index.html) (14). The intersection of predicted target miRNAs and DEMs was then considered as differentially expressed target miRNAs (DETMs) for further miRNA–mRNA network construction. Subsequently, miRWalk3.0 (http://zmf.umm.uni-heidelberg.de/apps/zmf/mirwalk3/) was applied to predict target genes of DETMs. Then,

differentially expressed target genes (DETGs) were obtained by taking the intersection of the predicted genes and DEGs. Eventually, circRNA–miRNA–target gene regulatory networks were visualized by Cytoscape. Among the DECs in the ceRNA network, we adopted the DECs with the largest number of regulated miRNAs as the top three ranking hub DECs.

Functional enrichment analysis of hub DECs

To further reveal the function of hub DECs, GO and KEGG pathways analysis of DETGs regulated by hub DECs was performed using ClueGO (https://apps.cytoscape.org/apps/cluego). An adjusted p-value of < 0.05 was considered to indicate significant enrichment.

Tissue samples collection

Five samples of human arthritic cartilage and five samples of human non-arthritic cartilage were collected from patients who had undergone knee arthroplasty surgery in Shanghai Jiao Tong University Affiliated Sixth People's Hospital. All procedures were approved by the Ethics Committee of Shanghai Sixth People's Hospital (No. 2019-134). All aspects of the study were performed in accordance with the Declaration of Helsinki. OA cartilage was harvested from the damaged area of arthritic cartilage layers, while undamaged cartilage harvested from non-arthritic cartilage acted as a control, as described in previous studies (15). All patients signed informed written consent forms. Tissue samples were frozen immediately in liquid nitrogen after isolation and kept frozen until use.

RNA extraction and RT-PCR validation

Total RNA was extracted from cartilage tissue using a total RNA extraction kit (Shabio, Shanghai, China) in accordance with the manufacturer's protocols. For circRNAs, total RNA was then digested with RNase R (Epicenter, Madison, WI, USA) and reverse transcribed into cDNA using NovoScript II reverse transcriptase (Novoprotein, Suzhou, China). RT-PCR was carried out using AceQ Universal SYBR qPCR Master Mix (Vazyme Biotech, Nanjing, China) in an ABI PRISM® 7500 Sequence Detection System (Applied Biosystems Inc., Foster City, CA, USA). Replicate wells were set up for each sample. GAPDH was selected as the internal normalization control. Relative fold expression of circRNA was determined using the $2^{-\Delta\Delta ct}$ method. Primer sequences were synthesized by Sangon Biotech (Shanghai, China). The remaining cDNA and total RNA were dissolved in RNA Follow All solution (New Cell Biotech, Suzhou, China) and placed in a freezer at –80°C.

Cell culture and *in vitro* OA model

Human C28/I2 chondrocytes were obtained from Immocell, China. The cells were obtained and cultured in DMEM/F12 medium containing 10% fetal bovine serum, 1% penicillin, and streptomycin (100 μg/ml). The cells were incubated at 37°C with 5% CO_2. IL-1β, at a concentration of 10 ng/ml, was added to each group of cells to establish the *in vitro* OA model. Untreated cells were used as a control. siRNAs of hsa_circ_0027914, hsa_circ_0101125, and hsa_circ_0102564, made by GenePharma, were added to each well at a concentration of 50 nM and incubated for 24 hours.

TUNEL staining

Th apoptosis level of chondrocytes was detected by using terminal deoxynucleotidyl transferase dUTP nick-end labeling (TUNEL) kits in accordance with the manufacturer's protocol as previously described (16). Specially, the pretreated cell smears were fixed with 4% paraformaldehyde for 30 minutes and incubated with 20 μg/ml proteinase K for 10 minutes. Subsequently, cells were incubated with equilibration buffer solution for 30 minutes and freshly prepared TUNEL staining solution for 1 hour, avoiding exposure to light. Nuclei were stained with 4′,6-diamidino-2-phenylindole (DAPI) for 5 minutes. Randomly selected fields were captured under a fluorescence microscope (Leica, Germany).

CCK-8 assay

The CCK-8 test was applied to detect the proliferation effect on chondrocytes treated with siRNA from the three hub DECs. Chondrocytes were seeded at a density of 5×10^3 cells per well in 96-well plates for 3 consecutive days of testing. CCK-8 solution (10 μl per well) was added to each well and the plates incubated for 3 hours at 37°C following the manufacturer's protocols. Absorbance was examined at 460 nm using a microplate reader (Thermo Fisher Scientific). All three trials were repeated three times to meet statistical requirements.

Enzyme-linked immunosorbent assay

Cells were seeded at a density 1×10^6 cells per well in six-well plates to detect the secretion levels of IL-6 and TNF-α. IL-1β and siRNAs from the three hub DECs were intervened when chondrocytes reached a confluence of 80%. Cell supernatant was harvested from each well and an ELISA kit was used to measure the concentrations of IL-6 and TNF-α following the manufacturer's protocol as in a previous study (11). The absorbance was examined at 450 nm using a microplate reader (Thermo Fisher Scientific). Triplicate experiments were used to obtain the mean value.

Statistical analysis

Statistical analysis was performed using SPSS 16.0 software. Data are shown as means ± SDs. Statistical differences between

two groups were compared using the independent-samples *t*-test. The threshold of statistical difference was set at a *p*-value < 0.05.

Results

Bioinformatics, being a convenient, high-throughput, and predictably accurate tool, is increasingly used by researchers, especially in the study of degenerative diseases such as OA. Gene networks have been widely used to screen pathogenic genes, to identify clinical biomarkers, to elucidate epigenetic regulatory mechanisms, and to identify potential new drug targets for future experimental verification (17). In this study, novel pathogenic circRNAs and their regulation of microRNAs and genes were identified as playing a role in OA pathogenesis. Drugs targeting these genes were screened to identify those with the greatest affinity for these genes.

Identification of DEGs, DEMs, and DECs

Based on the above-mentioned threshold, differentially expressed genes and microRNAs were selected from four GEO datasets, as shown in Table 1. Before screening DEGs in OA, the two independent expression datasets of mRNA processed on different platforms were normalized. The features of four GEO datasets are exhibited as a three-line watch in Table 1. In total, 2,886 DEGs, 2,261 DEGs, 76 DEMs, and 43 DECs were identified in GSE114007, GSE168505, GSE79258, and GSE175959. Volcano plots of GSE17959 (Figure 1A) and GSE79258 (Figure 1B) show the overall upregulated and downregulated DECs, and DEMs in arthritic cartilage and non-arthritic cartilage. Heatmaps (Figures 1C, D) and volcano plots (Figures 1E, F) of GSE114007 and GSE168505 show the distribution of upregulated and downregulated DEGs. The differentially expressed *p*-values of hub genes in GSE114007 and GSE168505 databases are listed in Table 2. A Venn diagram (Figure 1G) of the mRNA datasets overlapping GSE114007 and GSE168505 shows a total of 441 candidate DEGs. A total of 4,265 DEGs with opposite expression trends in these two datasets were excluded. After removing inconsistent expression in both datasets, the remaining 427 DEGs, comprising 367 upregulated DEGS and 60 downregulated DEGs, were considered candidate DEGs.

Construction of a PPI network and identification of hub genes

The interactions between candidate DEGs were determined by constructing a PPI network using the STRING tool. The results were visualized using Cytoscape, as shown in Figure 2. The PPI network was composed of 339 nodes (genes) and 2,854 edges (interactions). Furthermore, hub DEGs were identified by MCODE. As shown in Figure 2, the highest-rated module comprised 56 nodes (genes) and 1,452 edges (interactions). Interestingly, the hub DEGs were all upregulated genes.

Enrichment analysis of DEGs and hub genes

To investigate the biological function and pathways of DEGs, KEGG and GO analyses were carried out on the 427 DEGs. The results of KEGG and GO analyses of hub genes and the related *p*-values are provided in Supplementary Material 2. Figures 3A–C demonstrates the mainly enriched functional annotations from three aspects: the biological process (BP), the cellular components (CCs), and the molecular functions (MFs). From the perspective of the BP, DEGs were mainly enriched during the mitotic cell cycle, cell division, and macrophage activation. From the perspective of CCs, DEGs were mainly involved in the chromosome centromeric region, the kinetochore, and the collagen-containing ECM. From the perspective of MFs, DEGs were mainly focused on protein kinase activity, tubulin binding, oxidoreductase activity, and ECM structural constituents. In addition, the KEGG analysis in Figure 3D shows that DEGs mainly participated in Fc? R-mediated phagocytosis, arachidonic acid metabolism, the mTOR pathway, and p53 pathways. In the case of the hub DEGs shown in Figures 4A–D, the BP items enriched were the mitotic cell cycle and cell cycle process; the CC items enriched were microtubule skeleton modulation and supramolecular complexes; and MF items enriched were cytoskeletal protein binding and protein kinase activity. KEGG results were involved in the p53 signaling pathway and ECM–receptor interaction.

Drug–gene networks

To obtain target drugs for hub DEGs, drug–gene interactions were collected from the DGIdb database; 86 potential drugs for

TABLE 1 Characterization of the four datasets from the GEO database.

Accession no.	Platform	Sample	Non-arthritic cartilage	Osteoarthritic cartilage	circRNA/microRNA/mRNA
GSE175959	GPL21825	Tissues	3	3	circRNA
GSE79258	GPL21599	Tissues	2	2	microRNA
GSE114007	GPL11154/GPL18573	Tissues	18	20	mRNA
GSE168505	GPL16791	Tissues	3	4	mRNA

TABLE 2 Differentially expressed *p*-values of hub genes in the GSE114007 and GSE168505 databases.

Gene	GSE114007 *p*-value	GSE16850 *p*-value	Gene	GSE114007 *p*-value	GSE16850 *p*-value
BIRC5	1.25479E-05	0.01481	DTL	0.004593409	0.020483
ZWINT	1.61251E-05	0.002706	EXO1	0.009738283	0.023251
CCNA2	1.22067E-05	0.014811	NEK2	0.01498041	0.028499
MCM10	0.023361068	0.02301	CEP55	0.000194963	0.030783
ASPM	2.01952E-09	0.027809	CDC25C	0.014188917	0.042123
ANLN	1.32865E-06	0.028623	CDC45	0.006994477	0.017533
CKAP2L	0.000236529	0.037765	ECT2	2.1904E-05	0.044262
PARPBP	0.008837195	0.013339	RRM2	2.84222E-05	0.03409
SKA1	0.001319427	0.048829	KIF23	1.77077E-06	0.022666
DEPDC1	1.29692E-05	0.018933	PLK1	0.000596262	0.043381
AURKB	0.001141327	0.045063	SHCBP1	0.001245922	0.019325
AURKA	1.39417E-05	0.049788	HMMR	0.000200977	0.018348
TTK	3.14754E-05	0.00073	CENPK	0.000197986	0.018214
FAM64A	0.008869907	0.002268	KIF15	0.002073268	0.044941
CDKN3	0.000181842	0.015816	NUSAP1	8.08765E-05	0.012801
BUB1	3.47034E-05	0.025316	NCAPG	8.82967E-05	0.020624
EZH2	4.52304E-06	0.003262	TOP2A	3.61644E-07	0.013508
MELK	4.05136E-05	0.027474	CLSPN	0.000683585	0.037467
KIF14	0.011879799	0.038972	CDK1	4.16892E-05	0.010887
ARHGAP11A	0.004992581	0.004564	KIF20A	4.21525E-05	0.003068
PBK	5.09596E-06	0.021727	BUB1B	0.00010006	0.027953
PTTG1	0.001645643	0.013477	CENPN	1.92797E-06	0.006739
ESCO2	0.047210258	0.020369	NDC80	0.010964047	0.009849
KPNA2	0.000819045	0.035039	UHRF1	0.002325478	0.012213
CDCA8	0.018665118	0.028464	PLK4	0.001191517	0.018608
KIF18A	0.021003146	0.031329	KIF4A	9.43291E-05	0.004651
UBE2C	0.004858359	0.007103	UBE2T	0.010003861	0.004464
NUF2	2.21472E-05	0.035093	CDC20	0.00203521	0.037308

OA were identified. The results were visualized using Cytoscape, as shown in Figure 5. However, the underlying mechanism of drug–gene interaction could not be determined.

Molecular docking

To further investigate the molecular mechanism of drug–gene interaction, molecular docking was performed to identify the drugs with the most potential. The crystal structure of human TOP2A and PLK1 was predicted by AlphaFold v2.0. The LDDT score showed a benign stereochemical property of the predicted structures. The affinity score of AutoDock Vina was applied to evaluate the merits of docking. The scores of the potential drugs for hub DEGs are shown in Figure 6. The results indicate that digitoxin has the strongest binding affinity for TOP2A (0.0–0.0 kcal/mol, |interval score|) and oxytetracycline for PLK1 (0.0–0.0 kcal/mol, |interval score|). The perfect conformation showed that digitoxin interacts with residues of TOP2A (Arg672 and Arg727) through hydrogen bonds. Similar results were observed in the case of oxytetracycline, which interacts with residues of PLK1 (Ser137 and Gly180). Thus, through drug screening, digitoxin and oxytetracycline were found to have potential therapeutic effect in OA.

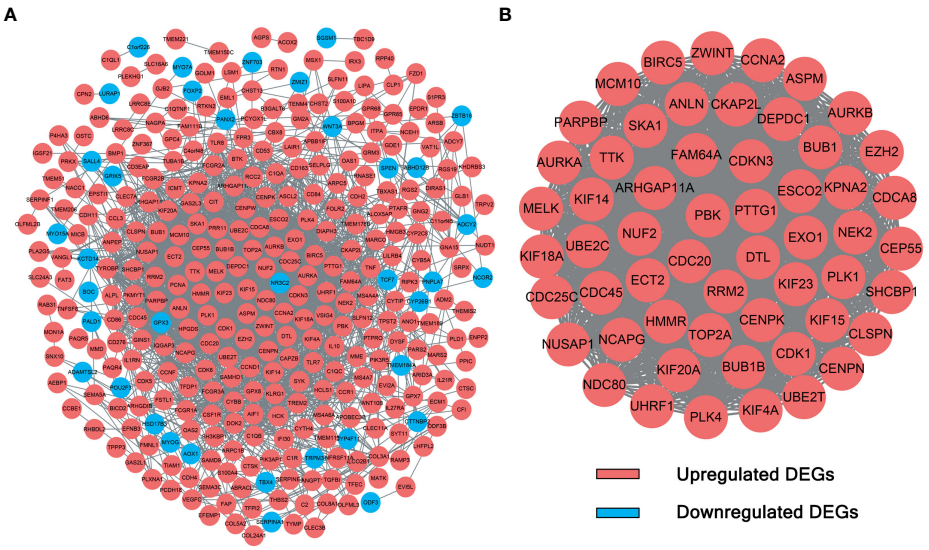

FIGURE 2
PPI network and module analysis. **(A)** The 339 DEGs in the PPI network. **(B)** Hub DEGs identified by module analysis using MCODE.

Construction of the circRNA–miRNA–mRNA regulatory network

CircBank was applied to predict target miRNA of DECs. A total of 76 miRNA genes predicted by circRNAs intersected with 992 DEMs. The 32 overlapping miRNAs were identified as DETMs. miRWalk 3.0 was applied to predict target genes of miRNAs. In our study, a total of 4,674 genes predicted by DETMs intersected with 427 DEGs. The 97 overlapping genes were identified as DETGs for further analysis. We then integrated the circRNA–miRNA network and the miRNA–

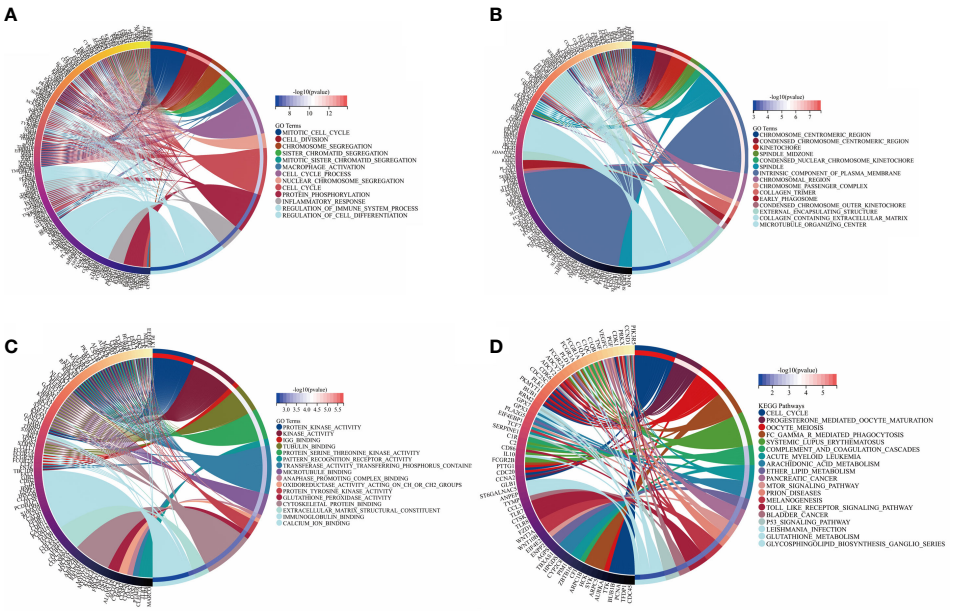

FIGURE 3
GO annotation and KEGG analysis of DEGs. **(A)** BP aspect; **(B)** CC aspect; **(C)** MF aspect; and **(D)** KEGG analysis.

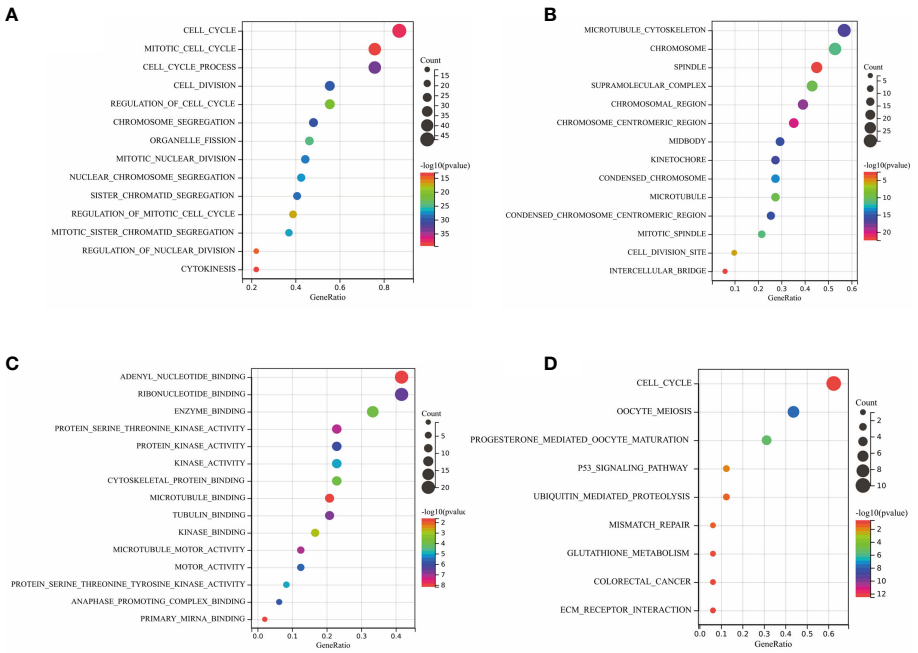

FIGURE 4
GO annotation and KEGG analysis of hub DECs. **(A)** BP aspects; **(B)** CC aspects; **(C)** MF aspects; and **(D)** KEGG analysis.

mRNA network and used Cytoscape to construct an entire regulatory circRNA–miRNA–mRNA network, as shown in Figure 7.

Identification of hub DECs

Based on the established circRNA–miRNA–mRNA regulatory network, three hub DECs were selected based on the top three regulated target miRNAs. These three hub DECs were hsa_circ_0027914, hsa_circ_0101125, and hsa_circ_0102564.

Functional enrichment analysis of hub DECs

Functional annotation of GO analysis and pathway enrichment of KEGG analysis were carried out to further explore the function of hub DECs, as illustrated in Figure 7. Three hub DECs were enriched in regulation of G_2/M transition of the mitotic cell cycle, axon guidance, bone mineralization, and insulin metabolism, in BP terms; cyclin-dependent protein kinase holoenzyme complex, chromosome passenger complex, and lysosomal lumen, in CC terms; and scaffold protein binding, tyrosine protein kinase binding, and phospholipase activator activity, in MF terms. In addition, hub DECs were found to be involved in the Wnt and Hippo signaling pathway, arachidonic acid metabolism, and *Staphylococcus* infection, based on KEGG analysis.

Validation of DECs with RT-PCR

To validate DECs expression in OA, RT-PCR was carried out on OA cartilage and non-arthritic cartilage (n = 5). Most of the results were consistent with our analysis. Eleven DECs were upregulated to a statistically significant degree. In the case of four other DECs, differences were not statistically significant. Furthermore, hsa_circ_0102400 was downregulated in our experiments, as shown in Figure 8. All three hub DECs were, as predicted, markedly upregulated in OA cartilage compared with non-arthritic cartilage.

In vitro verification of functions of hub DECs

In vitro IL-1β-mediated OA chondrocyte models were established to verify the intervention of these three hub DECs through siRNAs. SiRNA interference efficiency has been verified, as shown in Figure S1. TUNEL staining (Figures 9A, B) showed a statistically significant difference in the extent to which apoptosis of chondrocytes was reduced by siRNAs in different hub DECs. ELISA of IL-6 (Figure 9C) and TNF-α (Figure 9D) demonstrated the inhibition of inflammatory cytokine secretion with silencing intervention of these three DECs. The CCK-8 test demonstrated that proliferation of IL-1β-treated chondrocytes was restored by silencing these three hub DECs for 1, 2, and 3 days (Figure 9E). Our preliminary results indicated that silencing of

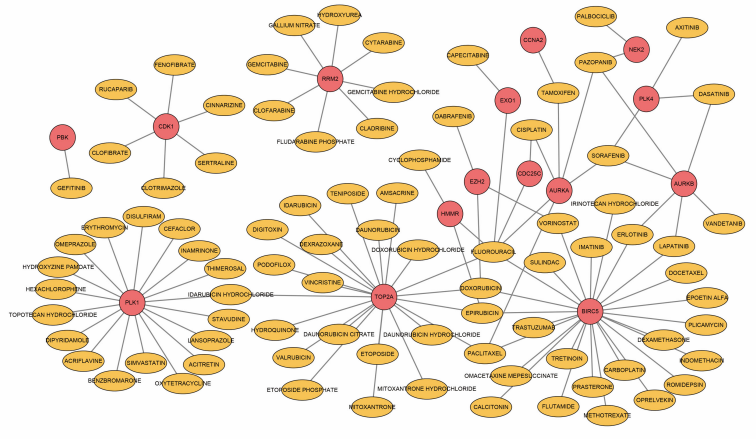

FIGURE 5
Drug–hub DEGs interplay network. Yellow circles, potential target drugs; red circles, upregulated DEGs.

hsa_circ_0027914 in the three hub DECs had the desired effect of reducing IL-1β-mediated apoptosis of OA chondrocytes.

Discussion

Osteoarthritis is the most common degenerative orthopedic disease, and the prevalence of osteoarthritis increases with age in all joints of the body. In contrast to other diseases, OA is not associated with a high mortality rate, but it is a chronic, progressive disease that adversely affects patients' quality of life. However, a lack of understanding of the biological mechanisms underlying the disease etiology and of existing therapeutic strategies for preventing or treating cartilage destruction or for reconstructing the subchondral bone are limited. Symptom-only medications are often rejected by patients for fear of long-term dependence. Therefore, OA drug treatment cannot be limited to symptom relief, and should instead focus on new drug targets based on the latest results of genetic research, which indicates that screening of hub ncRNAs and mRNAs associated with OA is urgently needed. The identification of previously undiscovered ncRNAs would enable the occurrence and development of OA to be recognized at an earlier clinical stage than at present. The prevention of OA or its early diagnosis would improve the prognosis of patients and reduce the need for surgery. Yet, to our knowledge, there have been no reports establishing circRNA–miRNA–mRNA regulatory networks in OA. We have revealed, for the first time, internal interactions among circRNAs, miRNAs, and mRNAs and we revisit OA therapy from a novel angle.

We screened out 427 DEGs by overlapping two mRNA datasets. The results of enrichment analysis of DEGs were closely related to mitotic cell cycle, cell division, and macrophage activation, all of which are closely associated with the pathogenesis of OA, including cartilage and subchondral destruction and synovial inflammation. KEGG results also indicated that DEGs are mainly associated with cell proliferation, apoptosis, and ECM structural constituent. In addition, many ECM structural protein genes, such as *COL24A1* and *COL3A1*, were found in DEGs, which is consistent with widespread destruction of cartilage (18).

To screen out the hub DEGs, 56 hub DEGs were all upregulated as shown in the PPI network. Although most of these hub DEGs were not directly associated with OA, these data are also consistent with the pathological changes in OA. From the perspective of bone and cartilage changes, CDC20 and TOP2A, which are related to cancer cell proliferation and progression, were recently suggested to play a role in rat bone marrow stem cell osteogenesis and chondrogenesis (19). In chondrocytes, upregulation of CDC20 and TOP2A might be an indication of insufficient compensatory cartilage and bone regeneration capacity in response to the destruction of cartilage and subchondral bone. Furthermore, MCM10, a highly conserved pre-replication complex, was recently reported to be a modulator of DNA replication timing (20), suggesting that it plays a potential regulatory role in chondrocyte survival in OA at a deeper genetic level. In addition, another important aspect of OA is the synovial change (21). IL-1RN is one of the cytokines implicated in OA at the inflammation level (22). It has been reported that the IL-1–IL-17 signaling axis induces cartilage destruction and OA development by enhancing the expression of catabolic factors (23). More importantly, IL-1RN polymorphism has an interesting clinical use. The TTG haplotype of IL-1RN is associated with radiographically more severe OA and an increased risk for incident OA (24). In

10.3389/fimmu.2022.1050743

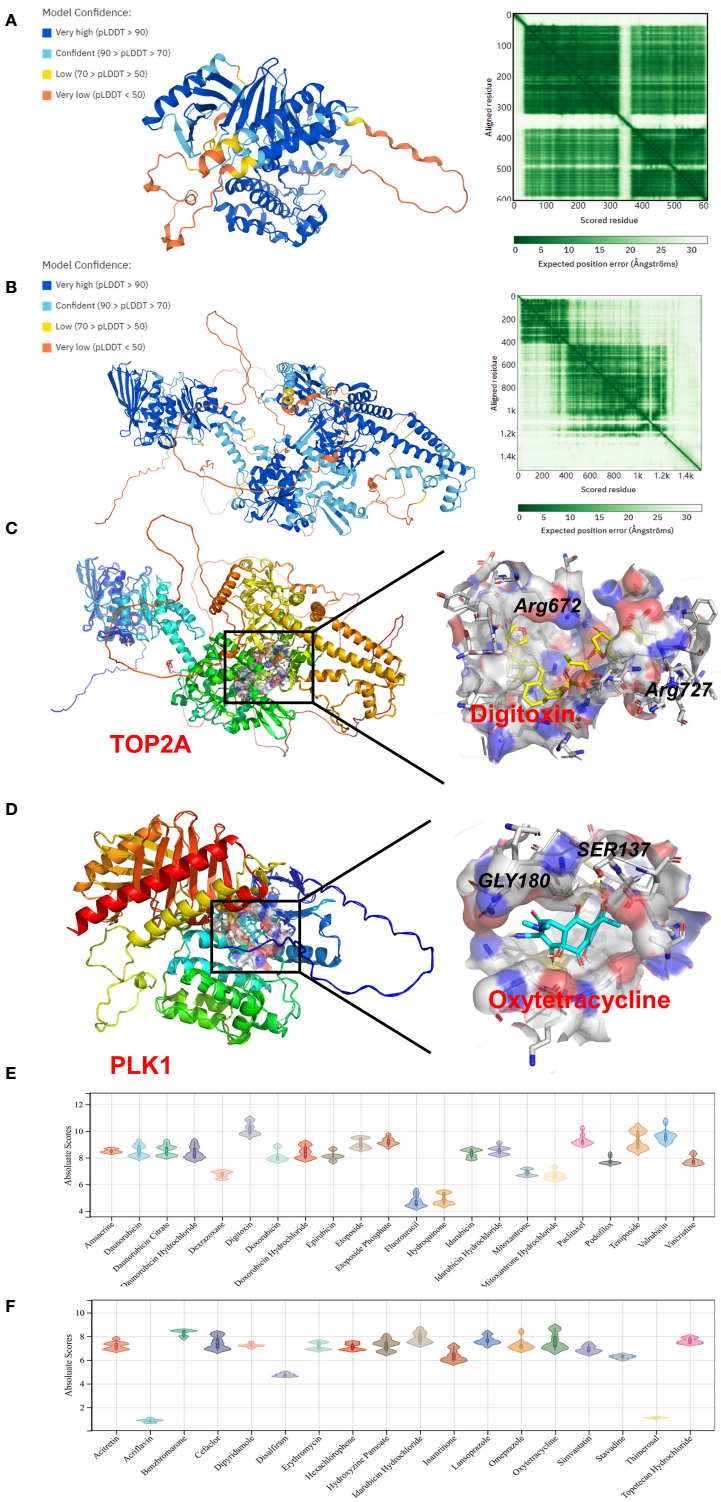

FIGURE 6
Homology modeling and molecular docking results. The crystal structure and evaluation of **(A)** TOP2A and **(B)** PLK1. The best docking positions **(C)** between digitoxin and TOP2A or **(D)** between oxytetracycline and PLK1 are indicated. The absolute value of affinity between predicated small molecules and **(E)** TOP2A or **(F)** PLK1 was exhibited.

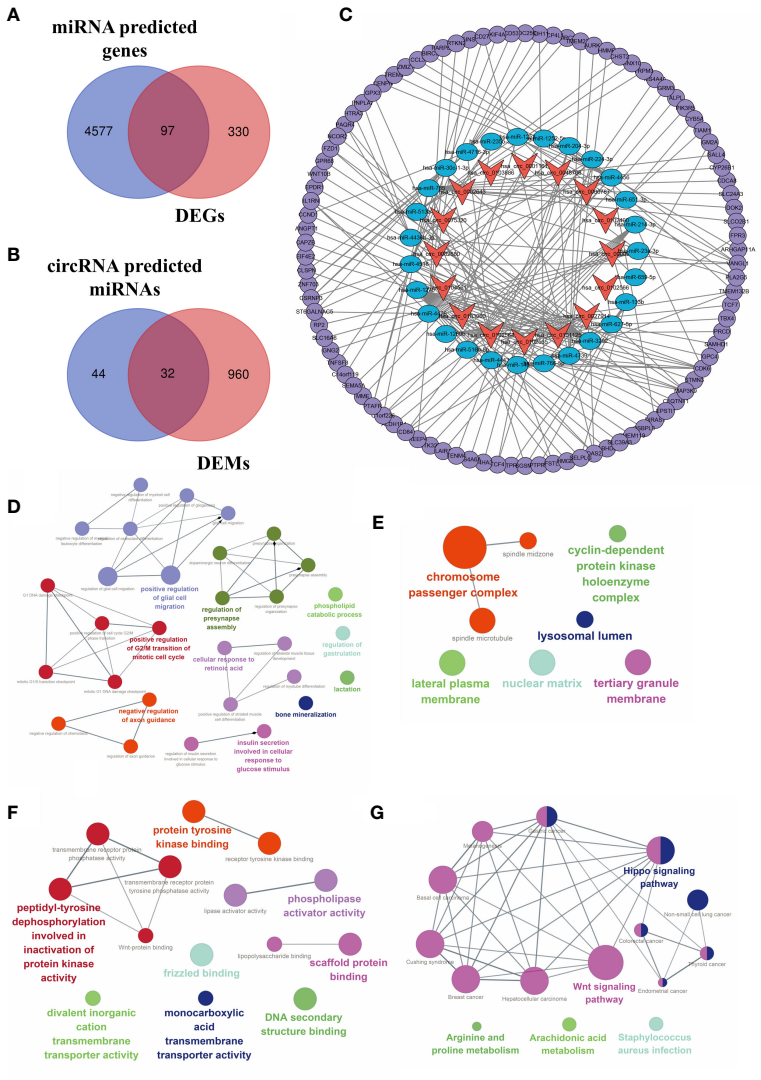

FIGURE 7
Construction of the circRNA–miRNA–mRNA regulatory network. **(A)** Venn diagram of the intersection of DEMs and predicted target genes. **(B)** The intersection of DECs and predicted target miRNAs. **(C)** The circRNA–miRNA–mRNA regulatory network. Orange arrows, DECs; blue ellipses, DETMs; purple circles, DETGs. Function annotation and KEGG analysis of hub DECs. **(D)** BP aspects; **(E)** CC aspects; **(F)** MF aspects; and **(G)** KEGG pathways.

addition, CD53, a molecule vital to lymphocyte trafficking and immunity (25), has been found to play an essential role in OA progression (26). Hence, most of the results of the microarray analysis were in accordance with previous studies and provided supportive evidence for further analysis.

Although many oral pain relief medications, such as non-steroidal anti-inflammatory drugs (NSAIDs), are widely used in the early treatment of OA, they can only treat symptoms owing to the lack of a well-defined target and are always associated with side-effects (for instance, gastrointestinal bleeding in the case of NSAIDs). If oral drugs are ineffective, the injection of prednisone or anesthetic drugs or joint replacement surgery is necessary to relieve patient suffering. Therefore, target drugs for OA urgently need to be developed to avoid progression of degeneration of the joint. Based on our predicted hub DEGs, 86 drugs approved by the Food and Drug Administration of the USA (FDA) were discovered through DGIdb database. Given the top three ranking of target drugs for hub DEGs, TOP2A, PLK1, and BIRC5, computational molecular docking was applied to identify the best candidates. As shown in previous studies, irinotecan has the strongest binding to BIRC5 through hydrogen bond formation (12). In this study, digitoxin and oxytetracycline were found to have the greatest binding affinity for TOP2A and PLK1, respectively. Digitoxin is a cardiac

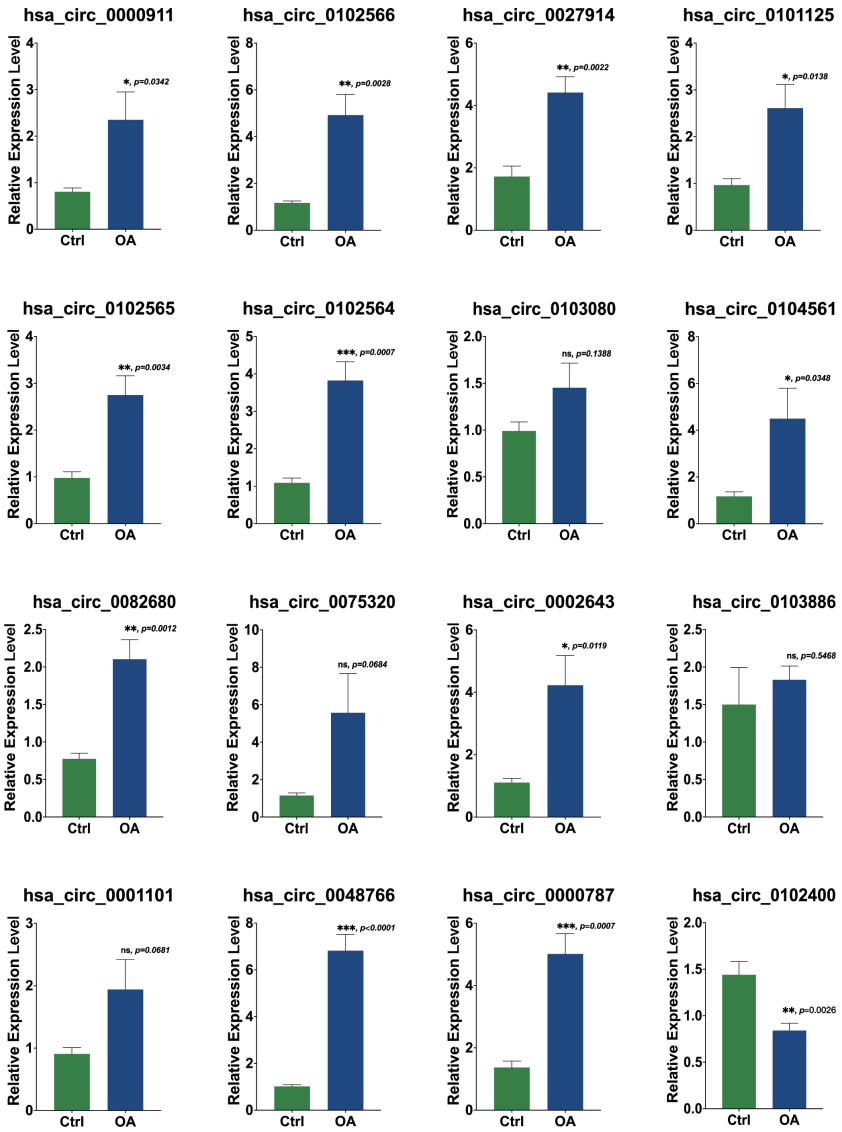

FIGURE 8
Validation of the expression of 16 DECs using RT-PCR. The relative expression levels of hsa_circ_00009, hsa_circ_0102566, hsa_circ_0027914, hsa_circ_0101125, hsa_circ_0102565, hsa_circ_0102564, hsa_circ_0104561, hsa_circ_0082680, hsa_circ_0002643, hsa_circ_0000787, and hsa_circ_0048766 were upregulated in OA cartilage, while the expression levels of hsa_circ_0103080, hsa_circ_0075320, hsa_circ_0001101, and hsa_circ_0103886 were not statistically significantly different. The relative expression level of hsa_circ_0102400 was obviously downregulated. Statistical difference: ***$p < 0.001$; **$p < 0.01$; *$p < 0.05$; ns, $p > 0.05$.

glycoside used in the treatment of congestive heart failure. Cardiac glycosides, such as frugoside, possess interesting anti-inflammatory potential, and can delay OA progression through inhibition of synovial inflammation (27). Oxytetracycline, in contrast, is a tetracycline antibiotic effective against Gram-positive bacteria. Oxytetracycline has already been identified as a chondrogenic compound and a potential OA treatment drug, stimulating cartilage regeneration, as described in a previous study (28). These two drugs are commonly used in clinical practice, and results of the molecular docking experiments might prove to be of medical relevance for the treatment of OA. We expect that our results could provide more insights into OA and potential therapeutic targets.

Over the last few decades, the function of circRNAs has become one of the most discussed issues, and circRNAs have been investigated as novel biomarkers of multiple diseases. Accumulated evidence indicates that circRNAs function as a sponge for the miRNAs involved in post-transcriptional regulation in OA (29). A recent study investigated the circRNA profiles in the osteoarthritic synovium and found

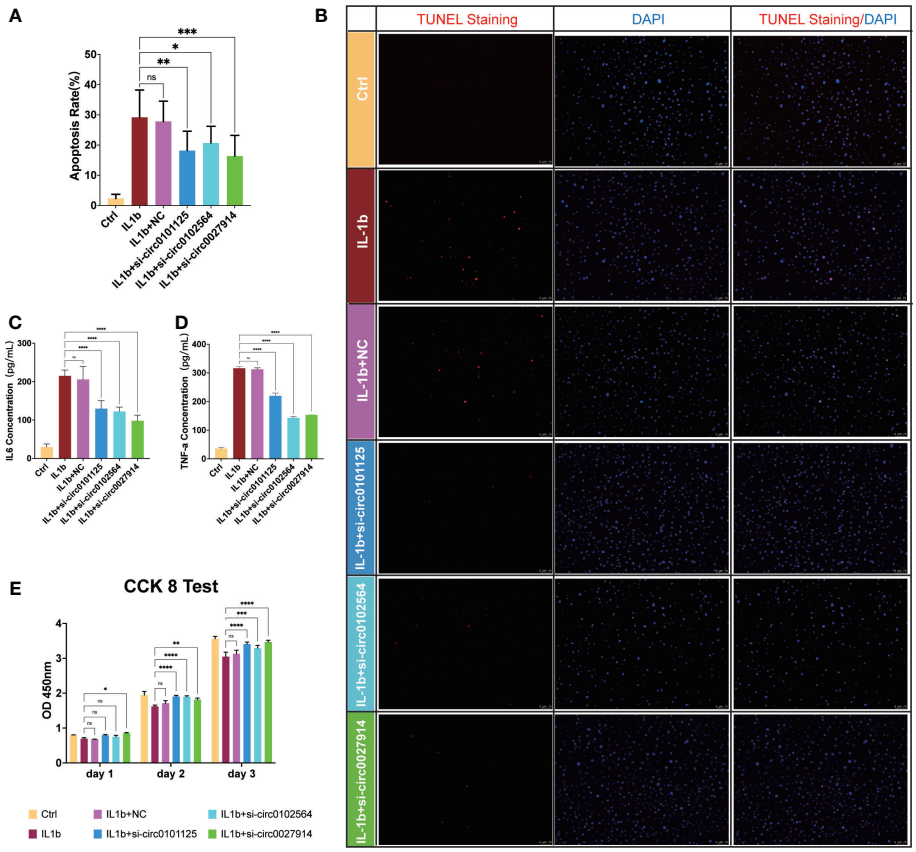

FIGURE 9
Verification of the function of the three hub DECs in an *in vitro* IL-1β-mediated OA chondrocyte model. Representative figures of TUNEL staining **(B)** and quantitative analysis **(A)** demonstrated the alleviation of apoptosis chondrocytes in siRNAs from three hub DECs. ELISA of IL-6 **(C)** and TNF-α **(D)** demonstrated the inhibition of inflammatory cytokine secretion with silencing intervention of these three DECs. **(E)** The CCK-8 test demonstrated that proliferation of IL-1β-treated chondrocytes was restored by silencing these three hub DECs on 1, 2, or 3 days. *****p* < 0.0001; ****p* < 0.001; ***p* < 0.01; **p* < 0.05; ns, *p* > 0.05.

that the hsa_circ_0072697–hsa_miR-6736–5p-LEP/ULK1 axis plays a role in cell senescence regulation (30). In our study, we constructed a network of 16 DECs, regulated miRNAs, and target mRNAs. hsa_circ_0027914, hsa_circ_0101125, and hsa_circ_0102564 were identified as hub DECs based on the number of miRNAs regulated. Functional annotation analysis of hub DECs indicated that DECs are involved in regulation of mitotic cell cycle, axon guidance, bone mineralization, protein kinase binding, etc. The axon guidance suggested the nerve-regulated potential of bone metastasis, which is consistent with previous studies indicating that prostaglandin (PG) E_2-mediated sensory nerve regulation has a role in bone homeostasis (31). Pathway enrichment analysis revealed the involvement of the Wnt and Hippo signaling pathways and arachidonic acid metabolism in OA pathogenesis. Interestingly, a previous study found that the arachidonic acid metabolite prostaglandin D2 (PGD^2) regulates polo-like kinase 1 (PLK1) and mediates chondrocyte apoptosis (32), which is in accordance with our results. Other processes, including bone mineralization and insulin metabolism, have also been closely linked with pathological symptoms in OA, such as the destruction of cartilage and subchondral bone.

Among the 16 DECs, a role has been elucidated only for hsa_circ_0000787, which has been detected in the peripheral blood of patients with type 1 diabetes mellitus (33) and systemic lupus erythematosus (34). However, there have been no studies on its functions or its role in OA. OA pathogenesis of fibrosis circRNA-related studies have been performed on circ_0000423. High levels of expression of circ_0000423 in OA regulate miRNA-27b-3p, and increased levels of the chondrocyte hypertrophy marker MMP-13 have been detected in OA cartilage. Application of AAV-shRNA-circ_0000423 slows the progression of OA by decreasing joint surface fibrosis and osteophyte formation (35). In addition, circHIPK3 (circBase

000284), derived from mesenchymal stem cells, regulates miR-124-3p and MYH9 to prevent chondrocyte apoptosis and hypertrophy in the IL-1β-induced osteoarthritis model (36).

Owing to a lack of experimental studies, we can only speculate on the functions of our novel DECs, based on the functions of the miRNAs or mRNAs they regulate.

hsa_circ_0027914, one of the hub DECs, regulated the greatest number of miRNAs, including hsa-miR-140-3p, hsa-miR-766-5p, hsa-miR-1260b, hsa-miR-516b-5p, hsa-miR-4443, hsa-miR-4739, and hsa-miR-3202. Of these, hsa-miR-140-3p and hsa-miR-766-5p (37) have been reported to participate in the mechanism of OA. MiR-140, the expression of which is especially low in OA cartilage (38), has been recently considered as a promising therapeutic strategy in OA (39). The underlying mechanism might be due to target genes of miR-140, including *ADAMTS5* (40), *MMP13* (41), *CXCR4* (42), *IGFBP5* (43), etc. These target genes are essential regulating genes in cartilage homeostasis, including cartilage degradation and inflammation and cellular fibrosis and hypertrophy in OA (9). Nevertheless, target DEGs in our study mainly focus on cell apoptosis and proliferation. Hence, hsa_circ_0027914 might down-regulate miR-140-3p through a competitive endogenous mechanism and lead to upregulation of DEGs in OA. A recent study has also reported that another circRNA (i.e., hsa_circ_0104595) can sponge miR-140-3p, then target EZH2 (enhancer of zeste homolog 2) to induce apoptosis of chondrocytes in OA (44). Furthermore, when the effect of si-circ-0027914 in reducing apoptosis is taken into consideration, there are reasons to believe that hsa_circ_0027914 plays a vital role in regulating multiple miRNAs and the progression of OA.

Another hub DEC, hsa_circ_0101125, regulated fewer miRNAs, including hsa-miR-3202, hsa-miR-4516, hsa-miR-1275, and hsa-miR-4476. However, the functions of hsa-miR-3202, hsa-miR-4516, and hsa-miR-4476 in OA have not been investigated. According to previous studies in other fields, miR-3202 can promote endothelial cell apoptosis through FAIM (45); miR-4516 inhibits liver cancer cell proliferation and progression through SOX5 (46); miR-4476 could promote glioma progression through APC/β-catenin in the Wnt pathway (47). From the perspective of regulated DEGs, *CCND1* was one of DEGs regulated by miR-3202, according to our analysis. Considering the analogous results of CCND1 regulated by miR-142-5p in chondrocytes, our results suggest that miR-3202/CCND1 may also participate in chondrocyte autophagy and proliferation in OA (48). Hence, in combination with the regulatory role of miR-1275/MMP13 in chondrogenesis (49), it is reasonable to infer that hsa_circ_0101125 might regulate chondrocyte proliferation, migration, and chondrogenesis in OA.

The other hub DEC, hsa_circ_0102564, regulated four miRNAs: hsa-miR-766-5p, hsa-miR-765, hsa-miR-30c-1-3p, and hsa-miR-4716-3p. Owing to the intricated regulated network, miR-766 was also regulated by hsa_circ_0027914, as discussed above. MiR-30c has also recently been considered as a suppressor of bone gamma-carboxyglutamate protein (*BGLAP*) in osteogenesis (50). Target DEGs of miR-30c in our analysis were mostly related to the anti-apoptosis of abnormal tumor cells, including MAP3K9 in lung cancer (46), ST6GALNAC5 in prostate cancer (51), CSRNP3 in clear renal cell carcinoma (52), ZNF703 in breast tumors (53), and CLSPN in brain tumors (54). Thus, upregulation of hsa_circ_0102564 might help reveal the downstream mechanism involved in the abnormal maturation and proliferation of chondrocytes in OA.

In addition to speculating on the biological functions of hub DECs and related DETMs, we found that the role of several other miRNAs in OA pathogenesis is correlated with cell proliferation, migration, and ECM synthesis. For instance, miR-23a-3p, regulated by hsa_circ_0000911, has been found to be an essential regulator of SMAD3/TGF-β in cartilage senescence in OA (55, 56). miR-659-5p, which is regulated by hsa_circ_0000911, despite a lack of osteoarthritis-related studies so far, is an emerging target of the MAPK pathway in breast cancer (57). miR-133b, a cell proliferation regulator, has also been shown to be associated with carcinogenesis (58). The expression of both miR-140-3p and miR-627-5p has been shown to be significantly different in rheumatoid arthritis patients and control subjects, and it is thought that they are mainly involved in the cell proliferation process (59).

To investigate the competing endogenous effect between circRNA and miRNA, a circRNA–miRNA–mRNA regulatory network was established and 16 DECs and 32 DETMs were verified to be coregulators of 97 DETGs. Owing to the complex regulatory mechanism of circRNAs and miRNAs, the complicated network provided a novel insight into the competing endogenous RNA interplay between circRNAs and miRNAs. The three hub DECs could also be potential candidate biomarkers in OA treatment.

RT-PCR was performed to validate expression level of DECs in osteoarthritic cartilages. In comparison with non-arthritic cartilage, expression levels of 11 circRNAs were upregulated and the expression of circRNA was downregulated, as predicted in our analysis. No statistically significant differences in the expression levels of four circRNAs were found. Other *in vitro* studies involving TUNEL staining, the CCK-8 test, and ELISA of IL-6 and TNF-α have demonstrated a decrease in apoptosis following treatment with siRNA from these three circRNAs. CCK-8 showed that IL-1β-treated chondrocyte proliferation was increased by the intervention of hub DECs, especially the group of hsa_circ_0027914. ELISA results have also verified that inflammatory cytokines, including IL-6 and TNF-α, are reduced by the intervention of hub DECs.

Of course, there are inevitably some limitations in our research. Although we performed *in vitro* and *in vivo* experiments, the small sample size of the circRNA and miRNA datasets remains the main limitation of this study. Moreover, the function of downstream target genes and the

predicted drugs were not investigated in this study. Thorough verification of the whole regulatory network should be the subject of future studies. Furthermore, because our biomarker was derived from cartilage, its diagnostic efficiency or related survival analysis could not be completed because of the lack of a worldwide comprehensive database. In addition, functional annotation and pathway enrichment analysis were conducted based on a tumor-related database, and thus our results are not necessarily applicable to OA-related mechanisms and processes. Thus, further studies will shed more light on the functional validation experiments and clinical translational research will be necessary to verify our results. Interaction between circRNA and miRNA is one of the potential biological underlying mechanisms. Whether other ncRNAs, such as lncRNA, also play an important role in OA remains worthy of discussion. We expect to discover more ncRNAs or ncRNAs diagnostic portfolio with high diagnostic efficiency to enhance the accuracy of early screening and improve patients' prognosis.

Conclusion

This is the first study to identify important biomarkers of circRNAs in OA. In addition, we shed light on the regulatory functions and potential molecular mechanisms of the circRNA–miRNA–mRNA network in OA pathogenesis.

Data availability statement

The original contributions presented in the study are included in the article/Supplementary Material. Further enquiries can be directed to the corresponding authors.

Ethics statement

The studies involving human participants were reviewed and approved by the Ethics Committee of Shanghai Sixth People's hospital. The patients/participants provided their written informed consent to participate in this study.

Author contributions

XL, SW, and GW designed this study. XL and HX administered the project and collected data. HX performed the experiments and analyzed these data. XP and SW conducted the bioinformatic analysis. XL wrote this manuscript. YC provided funding and resources. SW and GW modified and discussed this manuscript. All authors contributed to the article and approved the submitted version.

Funding

This study was supported by the National Key Research and Development program of China (grant no. 2020YFC2004900) and Key Projects of Scientific Research and Innovation, Shanghai Municipal Education Commission (grant no. 2019010700002E00043).

Conflict of interest

The authors declare that the research was conducted in the absence of any commercial or financial relationships that could be construed as a potential conflict of interest.

Publisher's note

Supplementary material

The Supplementary Material for this article can be found online at: https://www.frontiersin.org/articles/10.3389/fimmu.2022.1050743/full#supplementary-material

References

1. Hunter DJ, Bierma-Zeinstra S. Osteoarthritis. *Lancet* (2019) 393 (10182):1745–59. doi: 10.1016/S0140-6736(19)30417-9

2. Prieto-Alhambra D, Judge A, Javaid MK, Cooper C, Diez-Perez A, Arden NK. Incidence and risk factors for clinically diagnosed knee, hip and hand osteoarthritis: influences of age, gender and osteoarthritis affecting other joints. *Ann Rheum Dis* (2014) 73(9):1659–64. doi: 10.1136/annrheumdis-2013-203355

3. Djebali S, Davis CA, Merkel A, Dobin A, Lassmann T, Mortazavi A. Landscape of transcription in human cells. *Nature* (2012) 489(7414):101–8. doi: 10.1038/nature11233

4. Patop IL, Wüst S, Kadener S. Past, present, and future of circRNAs. *EMBO J* (2019) 38(16):e100836. doi: 10.15252/embj.2018100836

5. Rupaimoole R, Slack FJ. MicroRNA therapeutics: towards a new era for the management of cancer and other diseases. *Nat Rev Drug Discov* (2017) 16(3):203–22. doi: 10.1038/nrd.2016.246

6. Hansen TB, Jensen TI, Clausen BH, Bramsen JB, Finsen B, Damgaard CK. Natural RNA circles function as efficient microRNA sponges. *Nature* (2013) 495 (7441):384–8. doi: 10.1038/nature11993

7. Kour B, Gupta S, Singh R, Sophiarani Y, Paul P. Interplay between circular RNA, microRNA, and human diseases. *Mol Genet Genomics* (2022) 297(2):277–86. doi: 10.1007/s00438-022-01856-8

8. Ghafouri-Fard S, Poulet C, Malaise M, Abak A, Mahmud Hussen B, Taheriazam A. The emerging role of non-coding RNAs in osteoarthritis. *Front Immunol* (2021) 12:773171. doi: 10.3389/fimmu.2021.773171

9. Kong H, Sun ML, Zhang XA, Wang XQ. Crosstalk among circRNA/lncRNA, miRNA, and mRNA in osteoarthritis. *Front Cell Dev Biol* (2021) 9:774370. doi: 10.3389/fcell.2021.774370

10. Shen P, Yang Y, Liu G, Chen W, Chen J, Wang Q, et al. CircCDK14 protects against osteoarthritis by sponging miR-125a-5p and promoting the expression of Smad2. *Theranostics* (2020) 10(20):9113–31. doi: 10.7150/thno.45993

11. Wu Y, Hong Z, Xu W, Chen J, Wang Q, Chen J, et al. Circular RNA circPDE4D protects against osteoarthritis by binding to miR-103a-3p and regulating FGF18. *Mol Ther* (2021) 29(1):308–23. doi: 10.1016/j.ymthe.2020.09.002

12. Peng X, Mo Y, Liu J, Liu H, Wang S. Identification and validation of miRNA-TF-mRNA regulatory networks in uterine fibroids. *Front Bioengineering Biotechnol* (2022) 10. doi: 10.3389/fbioe.2022.856745

13. Bader GD, Hogue CW. An automated method for finding molecular complexes in large protein interaction networks. *BMC Bioinf* (2003) 4:2. doi: 10.1186/1471-2105-4-2

14. Liu M, Wang Q, Shen J, Yang BB, Ding X. Circbank: a comprehensive database for circRNA with standard nomenclature. *RNA Biol* (2019) 16(7):899–905. doi: 10.1080/15476286.2019.1600395

15. Miao Y, Chen Y, Xue F, Liu K, Zhu B, Gao J, et al. Contribution of ferroptosis and GPX4's dual functions to osteoarthritis progression. *EBioMedicine* (2022) 76:103847. doi: 10.1016/j.ebiom.2022.103847

16. Lin J, Hu W, Gao T, Bao B, Li X, Huang T, et al. Epsilon-poly-l-lysine as an efficient cartilage penetrating and residing drug carrier with high intraarticular injection safety for treating osteoarthritis. *Chem Eng J* (2022) 430(2022):133018. doi: 10.1016/j.cej.2021.133018

17. Hu Y, Lan W, Miller D. Next-generation sequencing for MicroRNA expression profile. *Methods Mol Biol* (2017) 1617:169–77. doi: 10.1007/978-1-4939-7046-9_12

18. Gu HY, Yang M, Guo J, Zhang C, Lin LL, Liu Y, et al. Identification of the biomarkers and pathological process of osteoarthritis: Weighted gene Co-expression network analysis. *Front Physiol* (2019) 10:275. doi: 10.3389/fphys.2019.00275

19. Liu F, Dong J, Zhang P, Zhou D, Zhang Q. Transcriptome sequencing reveals key genes in three early phases of osteogenic, adipogenic, and chondrogenic differentiation of bone marrow mesenchymal stem cells in rats. *Front Mol Biosci* (2021) 8:782054. doi: 10.3389/fmolb.2021.782054

20. Caballero M, Ge T, Rebelo AR, Seo S, Kim S, Brooks K, et al. Comprehensive analysis of DNA replication timing across 184 cell lines suggests a role for MCM10 in replication timing regulation. *Hum Mol Genet* (2022) 31(17):2899–917. doi: 10.1093/hmg/ddac082

21. Scanzello CR, Goldring SR. The role of synovitis in osteoarthritis pathogenesis. *Bone* (2012) 51(2):249–57. doi: 10.1016/j.bone.2012.02.012

22. Budhiparama NC, Lumban-Gaol I, Sudoyo H, Magetsari R, Wibawa T. Interleukin-1 genetic polymorphisms in knee osteoarthritis: What do we know? a meta-analysis and systematic review. *J Orthop Surg (Hong Kong)* (2022) 30 (1):23094990221076652. doi: 10.1177/23094990221076652

23. Na HS, Park JS, Cho KH, Kwon JY, Choi J, Jhun J, et al. Interleukin-1-Interleukin-17 signaling axis induces cartilage destruction and promotes experimental osteoarthritis. *Front Immunol* (2020) 11:730. doi: 10.3389/fimmu.2020.00730

24. Attur M, Zhou H, Samuels J, Krasnokutsky S, Yau M, Scher JU, et al. Interleukin 1 receptor antagonist (IL1RN) gene variants predict radiographic severity of knee osteoarthritis and risk of incident disease. *Ann Rheum Dis* (2020) 79(3):400–7. doi: 10.1136/annrheumdis-2019-216055

25. Yeung L, Gottschalk TA, Hall P, Tsantikos E, Gallagher RH, Kitching AR, et al. Tetraspanin CD53 modulates lymphocyte trafficking but not systemic autoimmunity in Lyn-deficient mice. *Immunol Cell Biol* (2021) 99(10):1053–66. doi: 10.1111/imcb.12501

26. Xu Y, Huang Y, Cai D, Liu J, Cao X. Analysis of differences in the molecular mechanism of rheumatoid arthritis and osteoarthritis based on integration of gene expression profiles. *Immunol Lett* (2015) 168(2):246–53. doi: 10.1016/j.imlet.2015.09.011

27. Wang H, Zhang H, Fan K, Zhang D, Hu A, Zeng X, et al. Frugoside delays osteoarthritis progression *via* inhibiting miR-155-modulated synovial macrophage M1 polarization. *Rheumatol (Oxford)* (2021) 60(10):4899–909. doi: 10.1093/rheumatology/keab018

28. Hojo H, Yano F, Ohba S, Igawa K, Nakajima K, Komiyama Y, et al. Identification of oxytetracycline as a chondrogenic compound using a cell-based screening system. *J Bone Miner Metab* (2010) 28(6):627–33. doi: 10.1007/s00774-010-0179-y

29. Li X, Xie C, Xiao F, Su H, Li Z, Weng J, et al. Circular RNA circ_0000423 regulates cartilage ECM synthesis *via* circ_0000423/miRNA-27b-3p/MMP-13 axis in osteoarthritis. *Aging (Albany NY)* (2022) 14(undefined). doi: 10.18632/aging.204018

30. Liu P, Gao G, Zhou X, Zhang X, Cai Q, Xiang Z, et al. Circular RNA profiles of osteoarthritic synovium. *Mol Omics* (2022) 18(5):439–48. doi: 10.1039/D2MO00066K

31. Chen H, Hu B, Lv X, Zhu S, Zhen G, Wan M, et al. Prostaglandin E2 mediates sensory nerve regulation of bone homeostasis. *Nat Commun* (2019) 10 (1):181. doi: 10.1038/s41467-018-08097-7

32. Zhu F, Wang P, Kontrogianni-Konstantopoulos A, Konstantopoulos K. Prostaglandin (PG)D(2) and 15-deoxy-Delta(12,14)-PGJ(2), but not PGE(2), mediate shear-induced chondrocyte apoptosis *via* protein kinase a-dependent regulation of polo-like kinases. *Cell Death Differ* (2010) 17(8):1325–34. doi: 10.1038/cdd.2010.13

33. Luo S, Deng M, Xie Z, Li X, Huang G, Zhou Z. Circulating circular RNAs profiles associated with type 1 diabetes. *Diabetes Metab Res Rev* (2021) 37(3):e3394. doi: 10.1002/dmrr.3394

34. Luo Q, Zhang L, Fang L, Fu B, Guo Y, Huang Z, et al. Circular RNAs hsa_circ_0000479 in peripheral blood mononuclear cells as novel biomarkers for systemic lupus erythematosus. *Autoimmunity* (2020) 53(3):167–76. doi: 10.1080/08916934.2020.1728529

35. Zhao W, Song Y, Wang QQ, Han S, Li XX, Cui Y, et al. Cryptotanshinone induces necroptosis through Ca2+ release and ROS production in vitro and *in vivo*. *Curr Mol Pharmacol* (2022) 14(8):3400–15. doi: 10.2174/1874467215666220127112201

36. Li S, Liu J, Liu S, Jiao W, Wang X. Mesenchymal stem cell-derived extracellular vesicles prevent the development of osteoarthritis *via* the circHIPK3/miR-124-3p/MYH9 axis. *J Nanobiotechnol* (2021) 19(1):194. doi: 10.1186/s12951-021-00940-2

37. Li J, Yao Z, Xiong H, Cui H, Wang X, Zheng W, et al. Extracellular vesicles from hydroxycamptothecin primed umbilical cord stem cells enhance anti-adhesion potential for treatment of tendon injury. *Stem Cell Res Ther* (2020) 11 (1):500. doi: 10.1186/s13287-020-02016-8

38. Zhang R, Ma J, Yao J. Molecular mechanisms of the cartilage-specific microRNA-140 in osteoarthritis. *Inflamm Res* (2013) 62(10):871–7. doi: 10.1007/s00011-013-0654-8

39. Si HB, Zeng Y, Liu SY, Zhou ZK, Chen YN, Cheng JQ, et al. Intra-articular injection of microRNA-140 (miRNA-140) alleviates osteoarthritis (OA) progression by modulating extracellular matrix (ECM) homeostasis in rats. *Osteoarthritis Cartilage* (2017) 25(10):1698–707. doi: 10.1016/j.joca.2017.06.002

40. Miyaki S, Sato T, Inoue A, Otsuki S, Ito Y, Yokoyama S, et al. MicroRNA-140 plays dual roles in both cartilage development and homeostasis. *Genes Dev* (2010) 24(11):1173–85. doi: 10.1101/gad.1915510

41. Liang ZJ, Zhuang H, Wang GX, Li Z, Zhang HT, Yu TQ, et al. MiRNA-140 is a negative feedback regulator of MMP-13 in IL-1β-stimulated human articular chondrocyte C28/I2 cells. *Inflamm Res* (2012) 61(5):503–9. doi: 10.1007/s00011-012-0438-6

42. Ren T, Wei P, Song Q, Ye Z, Wang Y, Huang L. MiR-140-3p ameliorates the progression of osteoarthritis *via* targeting CXCR4. *Biol Pharm Bull* (2020) 43 (5):810–6. doi: 10.1248/bpb.b19-00959

43. Karlsen TA, de Souza GA, Ødegaard B, Engebretsen L, Brinchmann JE. microRNA-140 inhibits inflammation and stimulates chondrogenesis in a model of interleukin 1β-induced osteoarthritis. *Mol Ther Nucleic Acids* (2016) 5(10):e373. doi: 10.1038/mtna.2016.64

44. Luobu Z, Wang L, Jiang D, Liao T, Luobu C, Qunpei L. CircSCAPER contributes to IL-1β-induced osteoarthritis *in vitro via* miR-140-3p/EZH2 axis. *Bone Joint Res* (2022) 11(2):61–72. doi: 10.1302/2046-3758.112.BJR-2020-0482.R2

45. Huang X, Xie H, Xue G, Ye M, Zhang L. MiR-3202 - promoted H5V cell apoptosis by directly targeting fas apoptotic inhibitory molecule 2 (FAIM2) in high glucose condition. *Med Sci Monit* (2017) 23:975–83. doi: 10.12659/MSM.899443

46. Liang L, Xu WY, Shen A, Cen HY, Chen ZJ, Tan L, et al. Promoter methylation-regulated miR-148a-3p inhibits lung adenocarcinoma (LUAD) progression by targeting MAP3K9. *Acta Pharmacol Sin* (2022) 15(7):1009–23. doi: 10.1038/s41401-022-00893-8

47. Lin J, Ding S, Xie C, Yi R, Wu Z, Luo J, et al. MicroRNA-4476 promotes glioma progression through a miR-4476/APC/β-catenin/c-Jun positive feedback loop. *Cell Death Dis* (2020) 11(4):269. doi: 10.1038/s41419-020-2474-4

48. Man G, Yang H, Shen K, Zhang D, Zhang J, Wu H, et al. Circular RNA RHOT1 regulates miR-142-5p/CCND1 to participate in chondrocyte autophagy and proliferation in osteoarthritis. *J Immunol Res 2022* (2022) p:4370873. doi: 10.1155/2022/4370873

49. Fang P, Zhang LX, Hu Y, Zhang L, Zhou LW. Long non-coding RNA DANCR induces chondrogenesis by regulating the miR-1275/MMP-13 axis in synovial fluid-derived mesenchymal stem cells. *Eur Rev Med Pharmacol Sci* (2019) 23(23):10459–69. doi: 10.26355/eurrev_201912_19685

50. Li Q, Zhou H, Wang C, Zhu Z. Long non-coding RNA Linc01133 promotes osteogenic differentiation of human periodontal ligament stem cells *via*

microRNA-30c / bone gamma-carboxyglutamate protein axis. *Bioengineered* (2022) 13(4):9602–12. doi: 10.1080/21655979.2022.2054912

51. Bai L, Luo L, Gao W, Bu C, Huang J. miR-182 modulates cell proliferation and invasion in prostate cancer *via* targeting ST6GALNAC5. *Braz J Med Biol Res* (2021) 54(8):e9695. doi: 10.1590/1414-431x2020e9695

52. Zhang H, Qiu X, Yang G. The CSRNP gene family serves as a prognostic biomarker in clear cell renal cell carcinoma. *Front Oncol* (2021) 11:620126. doi: 10.3389/fonc.2021.620126

53. Zhang X, Mu X, Huang O, Wang Z, Chen J, Chen D, et al. ZNF703 promotes triple-negative breast cancer cells through cell-cycle signaling and associated with poor prognosis. *BMC Cancer* (2022) 22(1):226. doi: 10.1186/s12885-022-09286-w

54. Hu T, Lei D, Zhou J, Zhang BO. circRNA derived from CLSPN (circCLSPN) is an oncogene in human glioblastoma multiforme by regulating cell growth, migration and invasion *via* ceRNA pathway. *J Biosci* (2021) 46:66. doi: 10.1007/s12038-021-00185-z

55. Röck K, Tigges J, Sass S, Schütze A, Florea AM, Fender AC, et al. miR-23a-3p causes cellular senescence by targeting hyaluronan synthase 2: possible implication for skin aging. *J Invest Dermatol* (2015) 135(2):369–77. doi: 10.1038/jid.2014.422

56. Kang L, Yang C, Song Y, Liu W, Wang K, Li S, et al. MicroRNA-23a-3p promotes the development of osteoarthritis by directly targeting SMAD3 in chondrocytes. *Biochem Biophys Res Commun* (2016) 478(1):467–73. doi: 10.1016/j.bbrc.2016.06.071

57. Wu X, Ding M, Lin J. Three-microRNA expression signature predicts survival in triple-negative breast cancer. *Oncol Lett* (2020) 19(1):301–8. doi: 10.3892/ol.2019.11118

58. Yao B, Zhang Q, Yang Z, An F, Nie H, Wang H, et al. CircEZH2/miR-133b/IGF2BP2 aggravates colorectal cancer progression *via* enhancing the stability of m(6)A-modified CREB1 mRNA. *Mol Cancer* (2022) 21(1):140. doi: 10.1186/s12943-022-01608-7

59. Ormseth MJ, Solus JF, Sheng Q, Ye F, Wu Q, Guo Y, et al. Development and validation of a MicroRNA panel to differentiate between patients with rheumatoid arthritis or systemic lupus erythematosus and controls. *J Rheumatol* (2020) 47(2):188–96. doi: 10.3899/jrheum.181029

frontiers | Frontiers in Immunology

TYPE Original Research
PUBLISHED 10 January 2023
DOI 10.3389/fimmu.2022.1051654

OPEN ACCESS

EDITED BY
Uzma Saqib,
Indian Institute of Technology Indore, India

REVIEWED BY
Qing Xian Luan,
Peking University, China
Pei Shang,
Mayo Clinic, United States

*CORRESPONDENCE
Wei Qiu
qiuweiandmj@163.com
Fuchun Fang
fangfuchun@smu.edu.cn

†These authors have contributed equally to this work and share first authorship

SPECIALTY SECTION
This article was submitted to Inflammation, a section of the journal Frontiers in Immunology

RECEIVED 23 September 2022
ACCEPTED 22 December 2022
PUBLISHED 10 January 2023

CITATION
Yu H, Wu H, Xie Q, Liu Z, Chen Z, Tu Q, Chen J, Fang F and Qiu W (2023) Construction of ceRNA and m6A-related lncRNA networks associated with anti-inflammation of AdipoAI. *Front. Immunol.* 13:1051654. doi: 10.3389/fimmu.2022.1051654

Construction of ceRNA and m6A-related lncRNA networks associated with anti-inflammation of AdipoAI

Hongwen Yu[1†], Hongle Wu[2†], Qiuyan Xie[1†], Zining Liu[1], Zehao Chen[1], Qisheng Tu[3], Jake Chen[3], Fuchun Fang[1*] and Wei Qiu[1*]

[1]Department of Stomatology, Nanfang Hospital, Southern Medical University, Guangzhou, China, [2]Department of Endodontics, Stomatological Hospital, Southern Medical University, Guangzhou, China, [3]Division of Oral Biology, Tufts University School of Dental Medicine, Boston, MA, United States

Background: Adiponectin (APN) is an endogenous adipokine secreted from adipocytes that exerts anti-inflammatory properties. AdipoAI is an orally active adiponectin receptor agonist identified by our group that can emulate APN's anti-inflammatory properties through mechanisms that are not fully understood. LncRNAs, a type of noncoding RNA more than 200 bp in length, have been demonstrated to have abundant biological functions, including in anti-inflammatory responses.

Materials and Result: In the current study, we performed a lncRNA microarray in LPS-induced Raw264.7 cells that were prestimulated with AdipoAI and screened 110 DElncRNAs and 190 DEmRNAs. Enrichment analyses were conducted on total mRNAs and DEmRNAs, including GSVA, ssGSEA, GO/KEGG, GSEA, and PPI analysis. Among all these processes, endocytosis was significantly enriched. A coexpression analysis was built based on DElncRNAs and DEmRNAs. Then, using TargetScan and miRwalk to predict related microRNAs of DElncRNAs and DEmRNAs, respectively, we established competing endogenous RNA (ceRNA) networks including 54 mRNAs from 8 GO items. Furthermore, 33 m6A methylation-related marker genes were obtained from a previous study and used for the construction of an m6A-related lncRNA network by coexpression analysis. We identified FTO as the hub gene of the network and 14 lncRNAs that interacted with it. The expression levels of 10 lncRNAs selected from ceRNA and FTO-related lncRNA networks were validated with qRT–PCR. Finally, macrophage phenotype scores showed that AdipoAI could attenuate the M2b and M2c polarization of macrophages and correlate with the above lncRNAs.

Conclusion: Our work reveals that lncRNAs might be involved in the anti-inflammation process of AdipoAI in LPS-induced macrophages through the

10.3389/fimmu.2022.1051654

ceRNA network and the epigenetic regulation of m6A. Mechanistically, these lncRNAs associated with AdipoAI might be related to endocytosis and polarization in macrophages and provide new candidates for the anti-inflammatory application of APN and its receptor agonist.

KEYWORDS

AdipoAI, m6A related-lncRNA, ceRNA, lipopolysaccharide, anti-inflammation, adiponectin

1 Introduction

Inflammation is an adaptive response triggered by noxious substances and tipped balances, such as infections and injuries (1). Thus, it contributes to two-phase responses, including defending against invading pathogens and provoking pathological processes (2). LPS, a potent inducer of inflammation, contributes to the occurrence of the inflammatory response by activating macrophages and inducing a series of substances, including proinflammatory cytokines and vasoactive mediators (3). Emerging evidence has emphasized that uncontrolled production of proinflammatory cytokines may affect homeostasis and lead to serious consequences, such as septic shock (4). That is, precise tuning of pro- and anti-inflammatory mediators is pivotal for inner homeostasis maintenance.

Adiponectin (APN), an endogenous secretory protein produced by white adipose tissue (5), stimulates downstream signals and is involved in various physical functions, such as improving energy utilization and insulin sensitivity (6). Additionally, APN has been reported to have profound anti-inflammatory effects in numerous diseases, such as type 2 diabetes and periodontitis (7). Specifically, studies indicate that macrophages are the primary target of APN in the anti-inflammation process since it can modulate macrophage functions and inhibit the activation of TLR4 (8–10). However, the requirement of a high dosage of intravenous injection for a constant period as well as the technology scarcity to produce APN proteins on a large scale and with sufficiently high quality act as obstacles for putting APN into clinical practice (11). To address this scarcity, AdipoRon, the first adiponectin receptor agonist, was designed by the University of Tokyo and serves as an orally active small molecule with antidiabetic properties (12). Inspired by it, our previous study also designed a potent adiponectin receptor agonist named AdipoAI, which was proven to inhibit the LPS-induced inflammatory response in macrophages by moderating the interaction between APPL1 and the MyD88 protein (13). As a structural analogue of AdipoRon, AdipoAI showed similar characteristics of orally active acetamide small molecule compound. Interestingly, we found that AdipoAI exerted an approximately eightfold greater than AdipoRon to inhibit the gene expression of inflammatory cytokines in macrophages.

Recently, as sequencing technology has continued to evolve, an upsurge of research on noncoding RNA has appeared in various fields. LncRNAs are collectively classified as noncoding RNAs >200 nucleotides in length (14) and have been shown to play essential roles in multiple physiological activities and pathological processes, including cell differentiation, tissue organ development, and cancer metastasis (15–19). Moreover, numerous reports have shown that lncRNAs involved in such signaling pathways, including NF-kB, MAPK or TLR-related pathways, participate in regulating the inflammatory response of macrophages (20). Attention should be given to competing endogenous RNA (ceRNA) and N6-methyladenosine (m6A) methylation owing to the ceRNA network uncovering the links between mRNAs and ncRNAs (21), while m6A RNA modification serves as a major regulator for RNAs, elucidating the relationship between m6A-related RNA and others (22). Overall, ceRNA and m6A networks are regarded as an important step in discovering the molecular mechanism of lncRNAs in inflammatory homeostasis. Thus, exploring the role of lncRNAs in inflammatory homeostasis could provide novel mechanistic ideas regarding their cointeractions with other molecules.

In the current study, we aimed to further investigate whether lncRNAs contribute to the anti-inflammatory effect of AdipoAI or APN in LPS-induced macrophages. Therefore, we conducted a lncRNA microarray in LPS-induced Raw264.7 cells pretreated with AdipoAI and performed a series of bioinformatics analyses to explore the potential signaling pathways and underlying mechanisms involved in ceRNA- and m6A-related lncRNA networks. Finally, we identified and validated ten ceRNA- and m6A-related lncRNAs, which may provide new therapeutic targets for the anti-inflammatory effects of APN and its receptor agonist.

10.3389/fimmu.2022.1051654

2 Materials and methods

2.1 LncRNA microarray resources and process

Raw264.7 cells were stimulated with AdipoAI for 24 h followed by incubation with 100 ng/ml LPS (E. coli 0111: B4, Sigma-Aldrich, St. Louis, MO, USA) for an additional 6 h. Detailed information of the four groups is shown in the figure legends. Total RNA was extracted from cells, and 5 μg of total RNA from each sample was sent to Arraystar Inc. (Rockville, MD, USA) for microarray analysis. Image processing and data extraction and analysis were also performed by Arraystar Inc. Using their established protocols. Total data from 12 samples were divided into four groups: DMSO, LPS, AdipoAI and LPS +AdipoAI. Then, raw signal intensities were normalized using the quantile method provided by GeneSpring GX v12.1, while low-intensity mRNAs and lncRNAs were filtered. Multiple probes corresponding to the same gene were screened and selected randomly to remove duplications. Then, box plots were constructed by factoextra, and the FactoMineR R package was applied for principal component analysis (PCA) to assess data quality.

2.2 Gene set variation analysis and macrophage phenotype ssGSEA

Gene set variation analysis (GSVA) is a method that estimates the variation in pathway activity over a sample population in an unsupervised manner (23). Enriched pathways of total mRNAs extracted from 12 samples were analyzed by the GSVA R package, while "c2.cp.v7.5.1.symbols.gmt" was used as the molecular signatures' dataset. Subsequently, GSVA scores were displayed by heatmap using the pheatmap R package, and a score matrix was formed. According to the matrix and the threshold of P value<0.05 and |log2 FC (fold change) |≥1.5, the R package limma was used to select differentially expressed pathways among three pairs of samples: DMSO vs. LPS, LPS vs. LPS+AdipoAI, and DMSO vs. AdipoAI. The EnhancedVolcano R package was used for visualization. Furthermore, common pathways among the 3 pairs were identified through a Venn plot created by the EnhancedVolcano R package, and the GSVA scores of each

TABLE 1 Macrophage phenotype-related genes.

Macrophage Type	M1	M2a	M2b	M2c	M2d (TAM)
Related Genes	TNF	IL-10	IL-10	IL-10	IL-10
	IL-1	TGFB1	IL1B	TGFB1	VEGF
	IL-6	CD206	IL-6	CD163	CD206
	IL-12	CD36	TNF	TLR1	CD204
	IL-23	IL1Ra	CD86	TLR8	CD163
	CD80	CD163	CIITA2	ARG1	ARG1
	CD86	ARG1	ARG1	GS	IDO
	CIITA	CARKL	CARKL	STAT3	STAT1
	MHC-II	STAT6	STAT3	STAT6	IRF3
	iNOS	GATA3	IRF4	IRF4	NFKB1
	PFKFB3	SOCS1	NFKB1	NFKB1	
	PKM2	PPARG			
	ACOD1				
	NFKB1				
	STAT1				
	STAT3				
	IRF-4				
	HIF1A				
	AP1				

common pathway were shown by a heatmap generated using the pheatmap R package.

To discover the role of AdipoAI in the regulation of macrophage polarization, a gene set, including a series of macrophage phenotype markers, was obtained from a previous study (24) and is displayed in Table 1. After that, the GSVA R package was applied to the gene set for single-sample gene set enrichment analysis (ssGSEA) and normalization, and the scores were revealed by heatmap using the pheatmap R package.

2.3 Differential expression analysis

Limma is an R software package that provides differential expression analysis for microarray and high-throughput PCR data (25). DEmRNAs and DElncRNAs with a P value<0.05 and |log2 FC (fold change) |≥1.5 as thresholds were selected by the limma package from three pairs of RNA data from total samples: DMSO vs. LPS, LPS vs. LPS+AdipoAI, and DMSO vs. AdipoAI. Furthermore, specific groups of DEmRNAs and DElncRNAs were screened out for investigation of AdipoAI-related potential pathways: upregulated in DMSO vs. LPS while downregulated in both LPS vs. LPS+AdipoAI and DMSO vs. AdipoAI; and downregulated in DMSO vs. LPS while upregulated in both LPS vs. LPS+AdipoAI and DMSO vs. AdipoAI. For visualization, the EnhancedVolcano R package was used to create volcano plots for the three pairs mentioned in the limma analysis. Second, disparities of different subgroups were shown in UpSet plots through the UpSetR R package, and the expression levels of selected DERNAs were revealed by circular heatmap by constructing the circlize R package.

2.4 Bioinformatics for DEmRNAs

Functional enrichment and pathway analysis: Using the ClusterProfiler package and choosing an adjusted P value < 0.05 as the cut-off value and molecular function (MF) as the annotation, we performed GO analysis to DEmRNAs selected as two groups: upregulated in DMSO vs. LPS while downregulated in both LPS+AdipoAI and DMSO vs. AdipoAI; and downregulated in DMSO vs. LPS while upregulated in both LPS+AdipoAI and DMSO vs. AdipoAI. Meanwhile, KEGG analysis was performed on the DEmRNAs, and the cut-off value was set as an adjusted P value < 0.5. Finally, the results are shown in bubble diagrams created by the clusterprofile R package, and a chord diagram was plotted to show mRNAs in each pathway using the circlize R package at the same time.

Gene set enrichment analysis: Gene set enrichment analysis (GSEA) is a type of analytical method for interpreting gene expression data and revealing biological pathways in common among microarray datasets (26). Using c2.cp.reactome.v7.5.1.symbols and c2.cp.kegg.v7.5.1.symbols gene sets as the background and GSEA_4.2.1 software as a tool, GSEA was performed on DEmRNAs that were divided into 3 pairs: DMSO vs. LPS; DMSO vs. AdipoAI; and LPS vs. LPS+AdipoAI.

Construction of the Protein–Protein Interaction (PPI) Network: To explore the interactions of mRNAs and inner biological mechanisms, a PPI network including 190 selected DEmRNAs was constructed by using the string database (https://cn.string-db.org/) as the background and confidence > 0.7 as the cut-off value.

2.5 Coexpression analysis for DEmRNAs-DElncRNAs and construction of the ceRNA network

First, to reveal the interactions between DElncRNAs and DEmRNAs, coexpression analysis was performed by the psych R package. Relevance > 0.97 and p value < 0.001 were set as the thresholds, and the ggcorrplot R package was used for visualization. Second, Cytoscape 3.9.0 was used to build the coexpression network, which was screened by Cytoscape 3.9.0 for hub genes. Since hub genes are critical in regulating networks, we chose the network with the maximum number of hubs for enrichment analyses. Thus, Gluego and GO/KEGG analyses were performed by Cytoscape 3.9.0 and Metascape (https://metascape.org/gp/index.html#/main/step1), respectively. Third, DEmRNAs and DElncRNAs in each enriched pathway were summarized for miRNA-bound DEmRNAs or DElncRNAs. TargetScan 7.2 (https://www.targetscan.org/mmu_72/) was used to predict miRNA-bound DElncRNAs, and MirWalk (http://mirwalk.umm.uni-heidelberg.de/search_genes/) was used to predict miRNA-bound DEmRNAs. Fourth, the identified coexpressed competing triplets were used to build a DEmRNA-miRNA-DElncRNA network, which was visualized by Cytoscape 3.9.0.

2.6 Construction of m6A-related DElncRNA networks based on coexpression analysis

To explore the relationship between m6A methylation and AdipoAI functions, m6A-related DElncRNA networks were established. First, according to previous publications (27–29), a total of 33 m6A mRNA methylation regulators (ALKBH3, ALKBH5, CBLL1, CPSF6, FMR1NB, FTO, HNRNPA2B1, IGF2BP1, IGF2BP3, IGFBP3, LRPPRC, METTL14, METTL16, METTL3, NUDT21, NXF1, PCIF1, PRRC2A, RBM15, RBM15B, RBMX, SRSF10, SRSF3, TRMT112, WTAP, XRN1, YTHDC1, YTHDC2, YTHDF1, YTHDF2, YTHDF3, ZC3H13, and ZCCHC4) were obtained and used for coexpression analysis with 110 DElncRNAs. We set the threshold as p value < 0.01 and

relevance > 0.95, used the psych R package as a tool and created heatmaps by the ggcorrplot package for visualization. DElncRNAs and m6A regulator mRNAs that had interaction relationships were screened out for subsequent coexpression analysis with DEmRNAs based on Spearman analysis. Third, the m6A-related DElncRNA network was built based on DEmRNA-DElncRNA and DEmRNA-m6A regulator mRNA two-tuples by Cytoscape 3.9.0. Radar plots were used to display the expression of the m6A regulator FTO by the ggradar and ggplot2 R packages. Finally, all mRNAs from the network were summarized for GO/KEGG analysis by Metascape.

2.7 Validation

We selected 5 lncRNAs from the m6A-related network based on connectivity and 5 lncRNAs from 8 GO items enriched in ceRNA networks. First, a boxplot was used to reveal the expression levels of selected lncRNAs from four subgroups by the pheatmap and ggplot2 R packages. Then, the vegan package was used for the mantle order test, which is detailed in the following processes.

Total cellular RNA was extracted using a Quick-RNA Miniprep Kit (ZYMO Research, Irvine, CA, USA), and total RNA from mouse tissues was prepared with TRIzol (Life Technologies) according to the manufacturer's instructions followed by reverse transcription and real-time quantitative polymerase chain reaction (qRT-PCR) assays, as we described previously (L. Zhang et al., 2014). One microgram of total RNA was used for reverse transcription using M-MLV Reverse Transcriptase (Thermo Scientific, Waltham, MA, USA) according to the manufacturer's protocol and was detected using PowerUp SYBR Green Master Mix (Thermo Scientific) on a Bio-Rad iQ5 thermal cycler (Bio-Rad Laboratories, Hercules, CA, USA). Differences in expression were evaluated by the comparative cycle threshold method using GAPDH or β-

TABLE 2 Primer sequences chosen for the qRT–PCR experiments.

lncRNA		Sequence (5'->3')
	Forward primer	GGCAGCACAGGAATTTGCAG
AK085671	Reverse primer	TAGACACCAGAGGTTCGCCA
	Forward primer	ATAGACGCAGACCCGATTGT
GM20632	Reverse primer	AAATGAAGCCACCGAGCAC
	Forward primer	AGCTGCTGCTGGCTTCTTAT
AK138558	Reverse primer	TCTGAAACTGCTGTGAGCGA
	Forward primer	GGAGCAGCATGACCTGATGT
PEG13	Reverse primer	TGAGGCACCCAAGTGGAATC
	Forward primer	GCACTTCAGCGTCAAGAAGTC
AK054221	Reverse primer	CCCTCTCCAGTCTAGGTGTT
	Forward primer	GGCCCTGAATGGAGTAACCT
LSS	Reverse primer	ACCCAAGCATGAGCTACAGAA
	Forward primer	TTTCGTGGTAGCTCCTTGGTC
NUPR1	Reverse primer	GTGTGAGGTTAGGACAGGCA
	Forward primer	CCCGAAGCGACATTAACTGC
CTSC	Reverse primer	AGAGCCTCTCAACAGACGAT
	Forward primer	TGGACTGTGGGGAGTGATAGTA
MS4A6B	Reverse primer	ACAATTCTGGCAGGTGTGAATG
	Forward primer	ACCATGTCTGGTTGTGCAGC
PSMB8	Reverse primer	GACATAGGCCACCCACCTT
	Forward primer	AGGTCGGTGTGAACGGATTTG
GADPH	Reverse primer	TGTAGACCATGTAGTTGAGGTCA

actin as a control. The primer sequences chosen for the qRT-PCR experiments are listed in Table 2. Finally, Prism 8.0.2 was used to reveal the selected lncRNA expression levels by bar chart.

2.8 Statistical analysis

The qRT-PCR data were processed with GraphPad Prism software version 8.0.1 (San Diego, CA, USA) and the mean ± standard deviation (mean ± SD) is presented for the quantitative data. Data involving more than two groups were assessed by one-way analysis of variance (ANOVA) and the level of significance was set at P-value < 0.05. The statistical analyses of microarray were performed using R software (Version 4.1.2, httpswww.r-project.org/).

3 Results

3.1 LncRNA microarray

Figure 1 displays a schematic of the workflow of the current study. Total RNA of cells in 12 samples was extracted for microarray analysis and divided into four groups. After normalization, we obtained 16553 lncRNAs and 13342 mRNAs. Box plots and principal component analysis (PCA) results displayed excellent data quality in Supplementary Figure 1.

3.2 GSVA analysis and macrophage phenotype ssGSEA

GSVA was performed on mRNAs from 12 samples, and 928 related pathways were enriched, while a heatmap revealed the scores in Supplementary Figure 2. The limma R package was used to identify differentially expressed pathways in the three groups, and the results are shown in Supplementary Figure 3. After that, intersection pathways among these groups were selected and are shown in Figure 2A. Six pathways were identified as the intersection of the three groups, and their GSVA scores are shown in Figure 2B. Furthermore, to explore the changes in macrophage phenotypes in each group, ssGSEA was conducted and found that AdipoAI could effectively reduce the LPS-induced phenotypic changes of macrophages from the M2b type to the M2c type (Figure 2C).

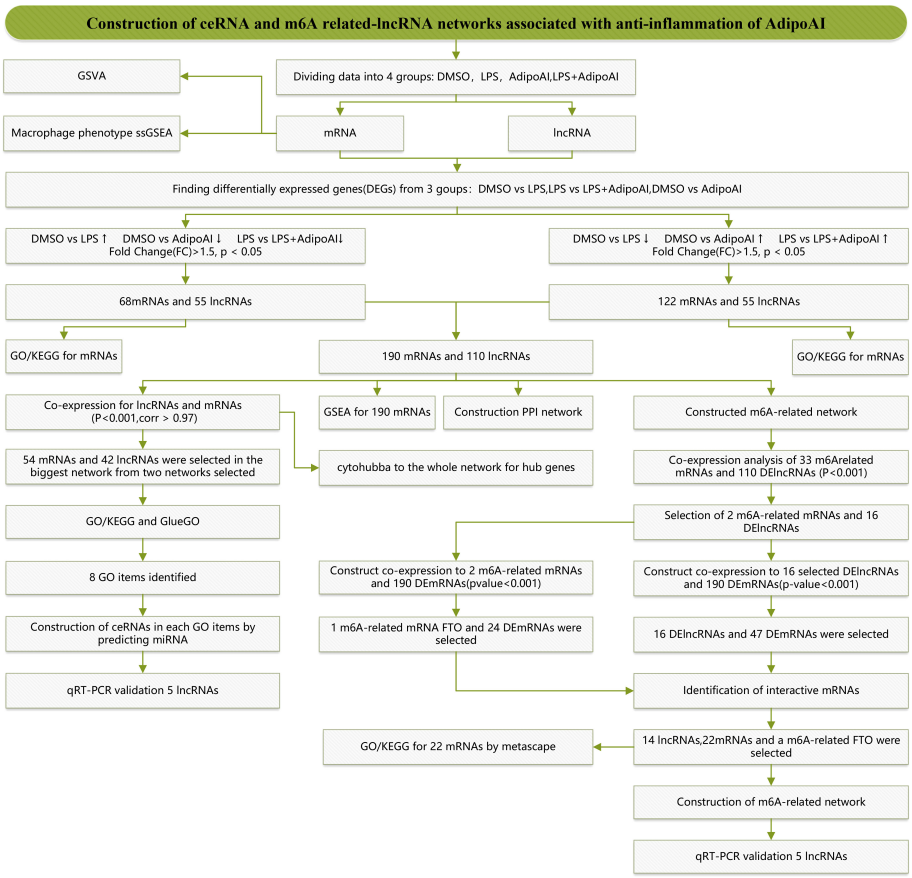

FIGURE 1
Study flow chart.

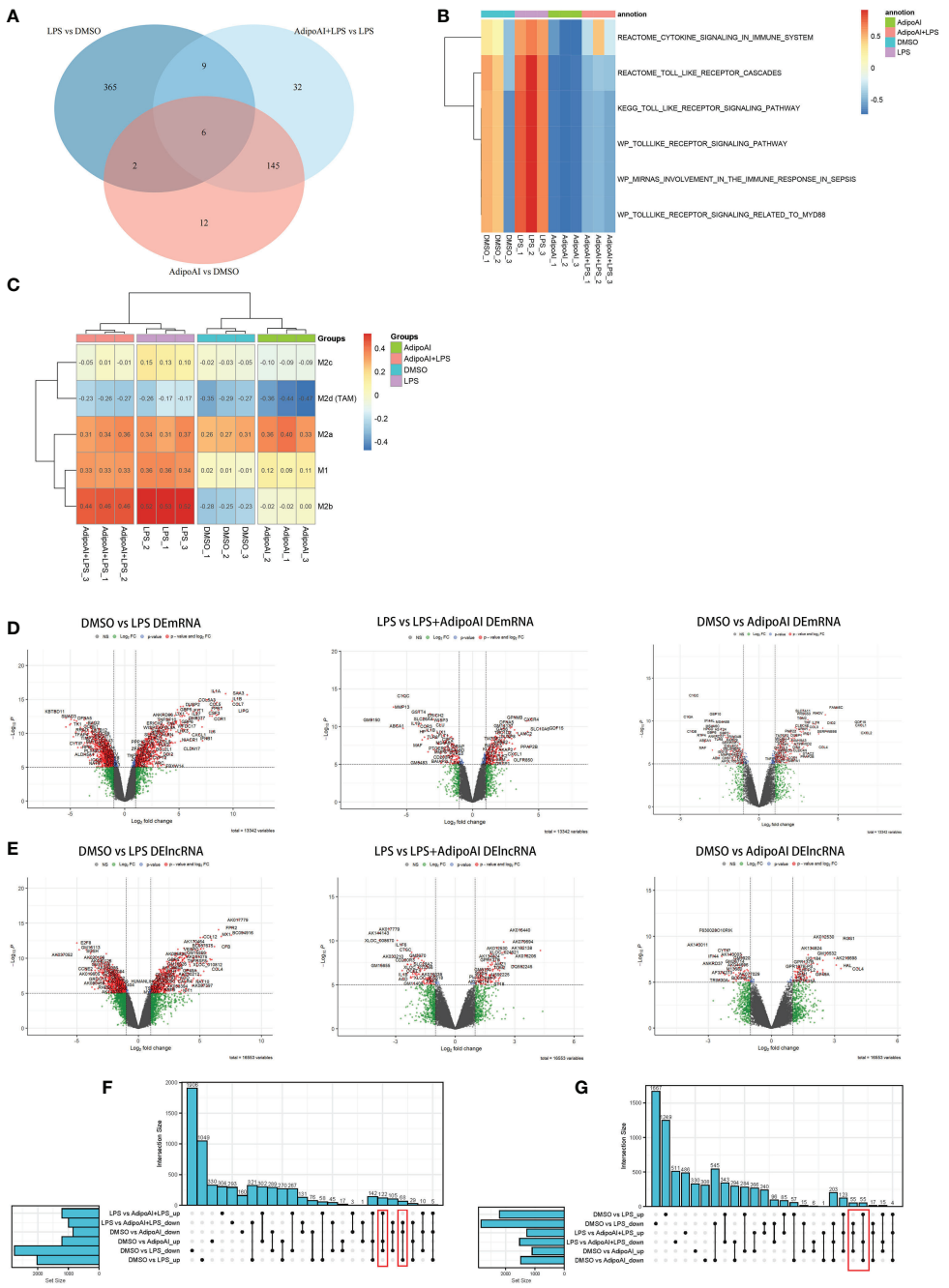

FIGURE 2
GSVA, macrophage phenotype ssGSEA and differential analysis. **(A)** Venn plot of pathways between three groups: DMSO vs. LPS, DMSO vs. AdipoAI and LPS vs. AdipoAI+LPS in GSVA. **(B)** Heatmap of GSVA scores in 12 samples. **(C)** Heatmap of macrophage phenotype ssGSEA scores in 12 samples. **(D)** Volcano plot for the mRNA differential analysis results. **(E)** Volcano plot for the lncRNA differential analysis results. **(F, G)** UpSet plots for the differentially expressed genes of **(F)** DEmRNAs or **(G)** DElncRNAs.

3.3 Identification of 190 DEmRNAs and 110 DElncRNAs

To discover the molecular mechanism of the AdipoAI-related anti-inflammatory effect, the limma package was used to identify DEmRNAs and DElncRNAs related to AdipoAI. A volcano plot (Figures 2D, E) was used to show the results between the 3 subgroups. Upset plots created by UpSetR R package are shown in Figures 2F, G to describe the intersecting lncRNAs and mRNAs between different groups. Fifty-five

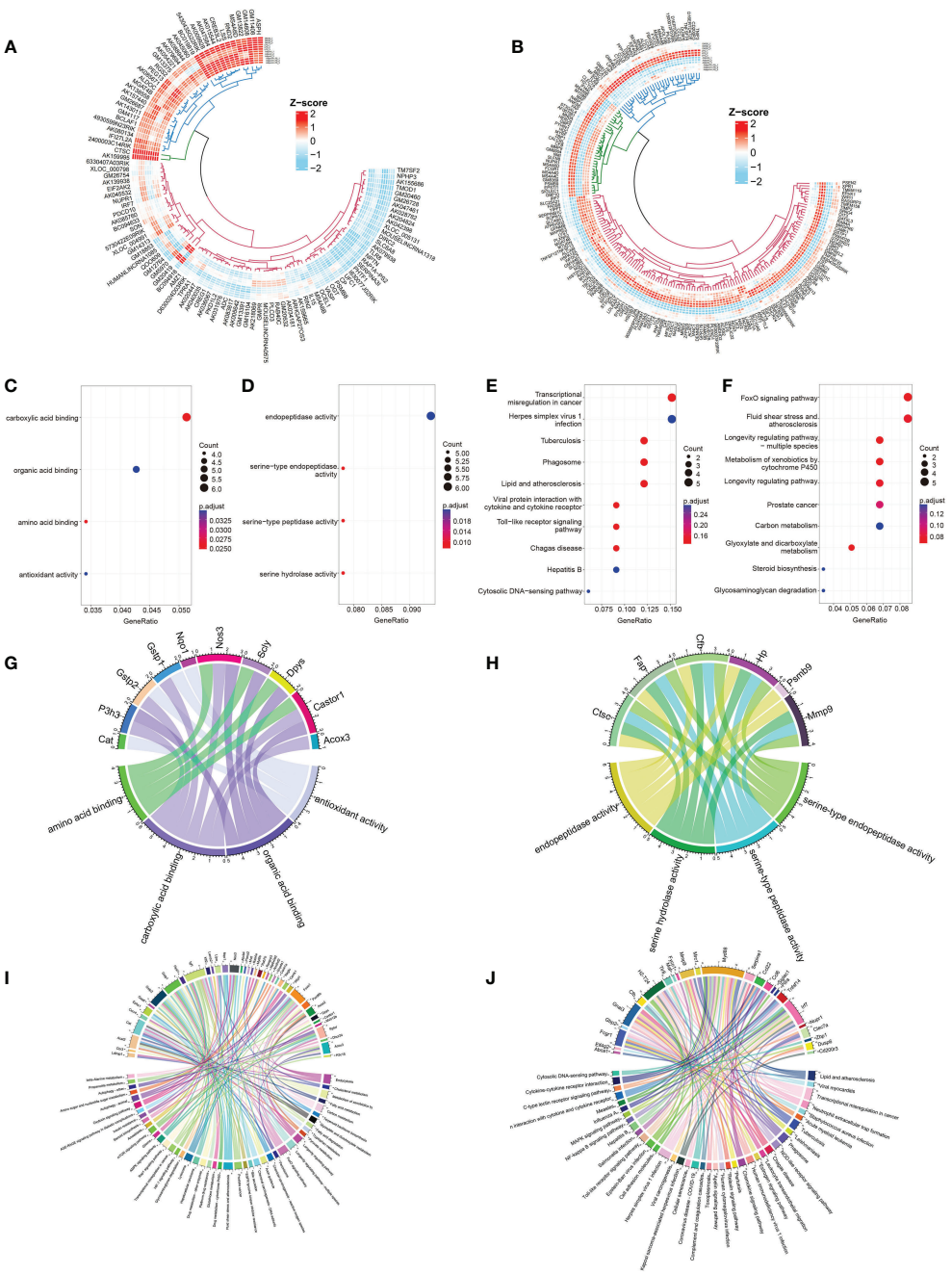

FIGURE 3
Identification and selection of 190 DEmRNAs/110 DElncRNAs and enrichment analysis of the two groups of DEmRNAs. **(A, B)** Circular heatmaps show the common differentially expressed genes among the three groups (LPS vs. DMSO, AdipoAI vs. DMSO and AdipoAI+LPS vs. LPS). **(A)** DElncRNAs. **(B)** DEmRNAs. **(C)** Molecular function enrichment analysis of 122 DEmRNAs (DMSO vs. LPS↓, DMSO vs. AdipoAI↑ and LPS vs. LPS +AdipoAI↑). **(D)** KEGG for 122 DEmRNAs. **(E)** Molecular function enrichment analysis of 68 DEmRNAs (DMSO vs. LPS↑, DMSO vs. AdipoAI↓ and LPS vs. LPS+AdipoAI↓). **(F)**: KEGG for 68 DEmRNAs. **(G–J)** Bubble diagrams showing mRNAs involved in molecular function enrichment analysis and KEGG. **(G)** 122 DEmRNAs in molecular function enrichment analysis. **(H)** 122 DEmRNAs in KEGG. **(I)** 68 DEmRNAs in molecular function enrichment analysis. **(J)** 68 DEmRNAs in KEGG.

DElncRNAs and 68 DEmRNAs were identified as the first group that were upregulated in DMSO vs. LPS but downregulated in both LPS vs. LPS+AdipoAI and DMSO vs. AdipoAI. Simultaneously, 55 DElncRNAs and 122 DEmRNAs were identified as the second group, which was downregulated in DMSO vs. LPS but upregulated in both LPS vs. LPS+AdipoAI and DMSO vs. AdipoAI. Ultimately, 110 DElncRNAs and 190 DEmRNAs were identified and selected for subsequent

processes. In addition, a circular heatmap created by the circlize R package (Figures 3A, B) was used to show the expression levels of 110 DElncRNAs and 190 DEmRNAs in 12 samples.

3.4 Bioinformatics analysis of 190 DEmRNAs

Enrichment analysis of DEmRNAs: Bubble diagrams (Figures 3C–F) revealed the results of GO/KEGG analysis of DEmRNAs in each selected group. A p value < 0.5 was set as the threshold of KEGG, and a p value < 0.05 was set as the threshold for GO analysis. A total of 4 GO terms and top 10 KEGG pathways were enriched in the first group, while 4 GO terms and top 10 KEGG pathways were enriched in the second group. A chord diagram was plotted to show the mRNAs in each pathway (Figures 3G–J).

GSEA for the selection of potential AdipoAI-related pathways: The function of AdipoAI was inferred from the functions of DEmRNAs selected previously; thus, GSEA was performed on 190 DEmRNAs. Against the background of the KEGG database, both LPS vs. LPS+AdipoAI and DMSO vs. AdipoAI enriched a similar pathway when AdipoAI was added: ENDOCYTOSIS. In addition, based on the Reactome database, 2 similar pathways were enriched upon addition of LPS alone in both DMSO vs. LPS and LPS vs. LPS+AdipoAI: REACTOME_SIGNALING_BY_GPCR. Moreover, Figure 4A displays enrichment plots for each enriched pathway screened out by GSEA.

Construction of the PPI network: Figure 4B shows the PPI network built by the STRING online database with 53 nodes and 53 edges. Diagrams were downloaded from the STRING website.

3.5 Construction of the ceRNA network with hub codes

Coexpression results between DElncRNAs and DEmRNAs were visualized by heatmap (Supplementary Figure 4). Figure 5A

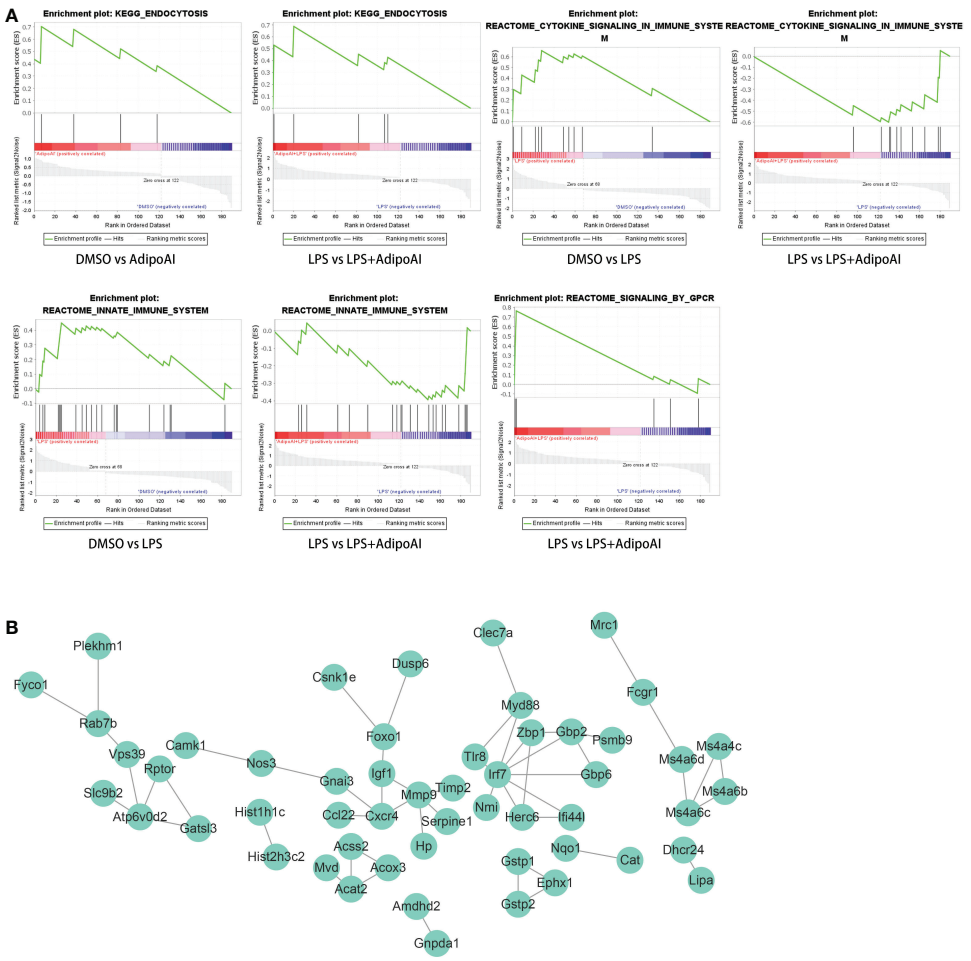

FIGURE 4
GSEA and PPI network for 190 DEmRNAs. **(A)** Gene set enrichment analysis of 190 DEmRNAs. **(B)** PPI network with 53 nodes and 53 edges of 190 DEmRNAs.

shows the coexpression network built by 190 DEmRNAs and 110 DElncRNAs with relevance > 0.97 and P value < 0.001. The cytoHubba results are shown in Figure 5B. We chose the network with the most hub nodes, which contained 58 mRNAs and 42 lncRNAs (Figure 5A with Red Frame). Fifty-eight mRNAs were screened by Gluego analysis and are displayed in Figure 5C. After that, GO/KEGG analysis was performed using Metascape, and 8 GO terms were identified, as shown in Figure 5D. MiRwalk and TargetScan were used to reverse-predict miRNA-bound DEmRNAs and miRNA-bound DElncRNAs, respectively. Therefore, based on the DEmRNA-miRNA-DElncRNA axis in each GO term, ceRNA networks for each term were separately built by Cytoscape and are shown in Figures 6A–H.

3.6 Identification of m6A-related DElncRNAs and construction of an m6A-related DElncRNA network

Thirty-three m6A-related mRNAs were retrieved from a previous study, used to perform a coexpression analysis

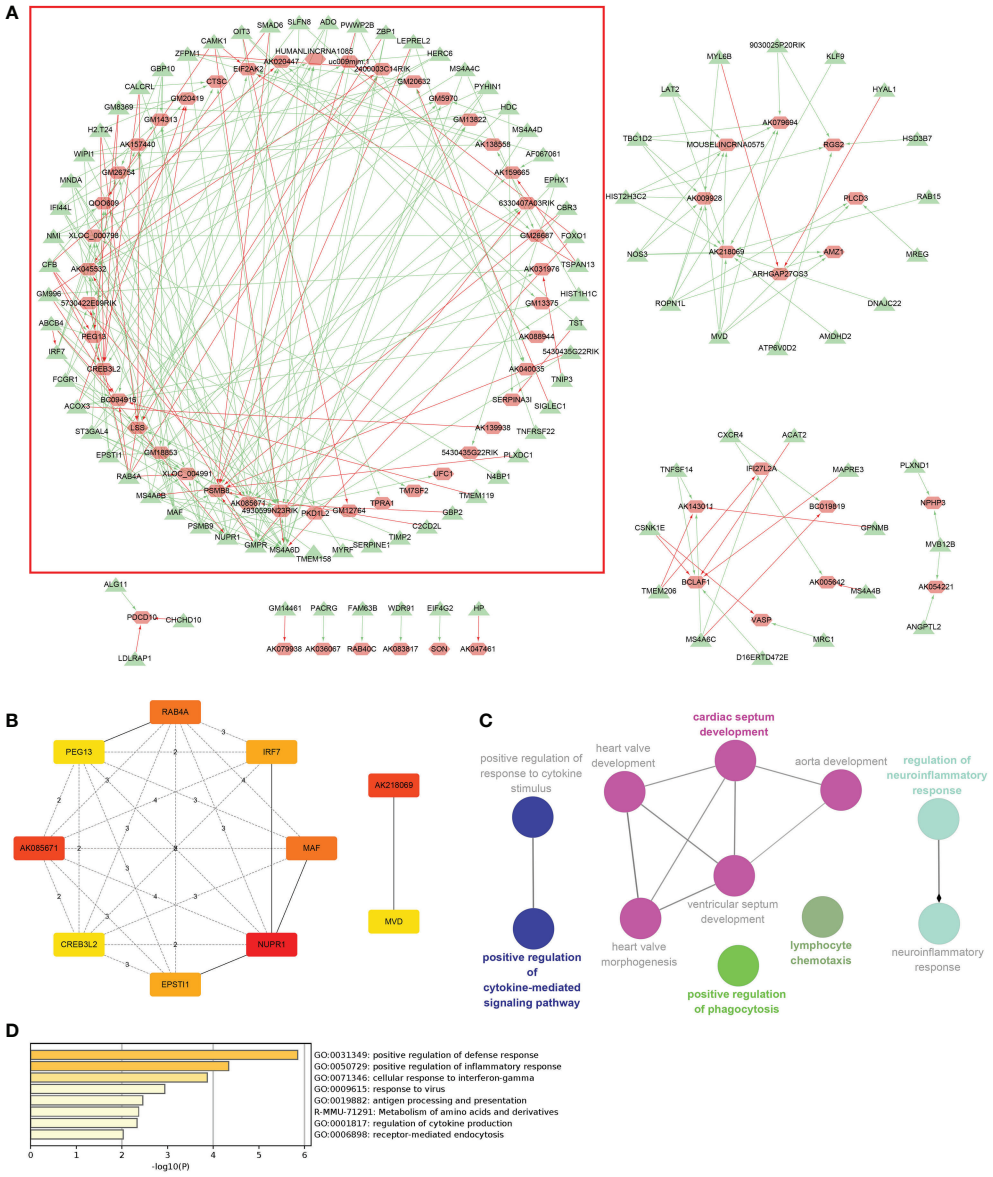

FIGURE 5
Coexpression analysis for DElncRNAs-DEmRNAs. **(A)** The coexpression network of DElncRNAs-DEmRNAs and the largest network with the most hub nodes in the red frame were selected (lncRNA: red; mRNA: green). **(B)** Hub nodes in all networks. **(C)** Gluego for 58 mRNAs in the largest network. **(D)** GO analysis for 58 mRNAs in the largest network.

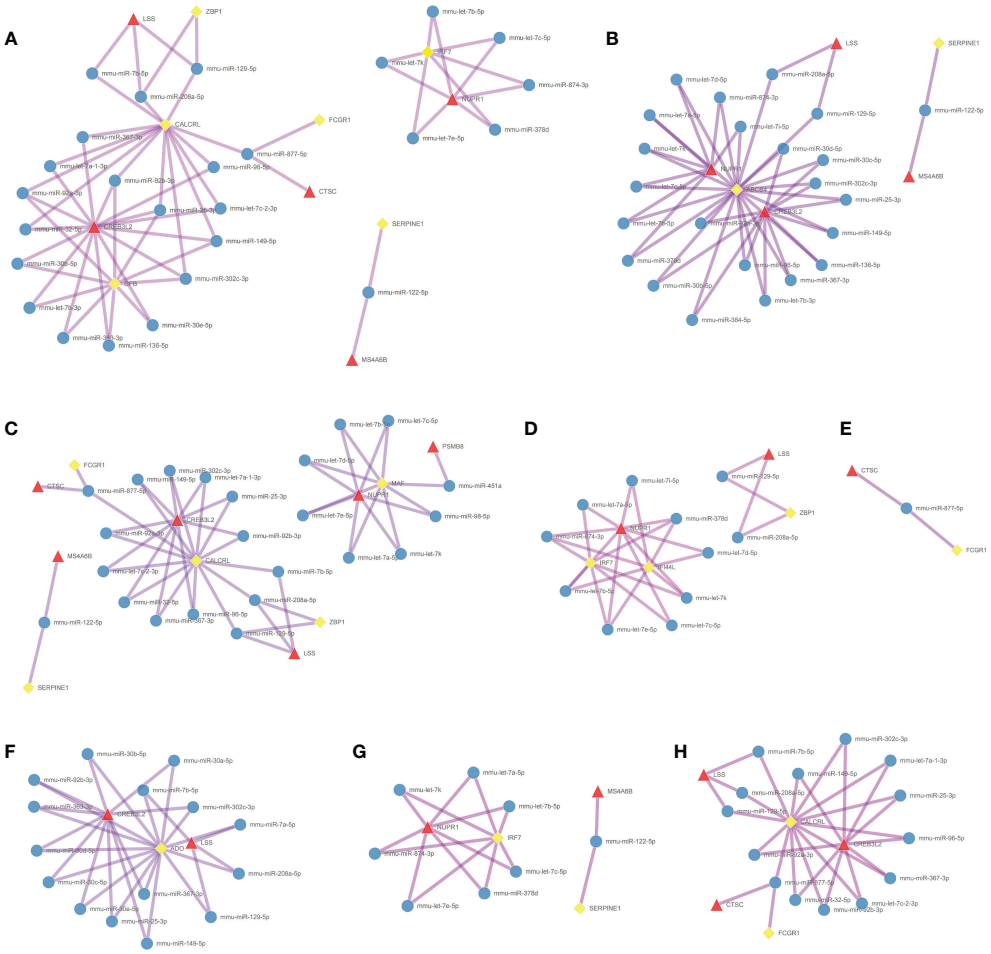

FIGURE 6
Construction of the ceRNA networks. DEmRNA-miRNA-DElncRNA networks of **(A)** positive regulation of defense response, **(B)** cellular response to interferon-gamma, **(C)** positive regulation of inflammatory response, **(D)** response to virus, **(E)** antigen processing and presentation, **(F)** metabolism of amino acids and derivatives, **(G)** regulation of cytokine production, and **(H)** receptor-mediated endocytosis. (Blue Ball: miRNA; Red Triangle: lncRNA; Yellow Square: mRNA).

(Spearman) with 110 previously selected DElncRNAs and visualized by heatmap (Supplementary Figure 5). Then, two m6A-related RNAs and 16 DElncRNAs were screened out, and a heatmap is shown in Supplementary Figure 6. To further confirm the relationship between m6A methylation and AdipoAI-related DERNAs, Spearman analysis of coexpression was performed between 190 DEmRNAs with 2 m6A-related RNAs and 16 DElncRNAs selected previously. Then, the m6A-related mRNA FTO with 24 associated DEmRNAs and 16 DElncRNAs with 47 associated DEmRNAs was screened out (Supplementary Figures 7, 8). Afterwards, we selected the intersection of these results and obtained 14 DElncRNAs, 22 DEmRNAs and the m6A-related mRNA FTO. Based on their inner interactions, the m6A-related DElncRNA network was established and visualized by Cytoscape (Figure 7A). Furthermore, the expression level of the central mRNA FTO was detected, and the radiogram is displayed in Figure 7B. GO analysis was performed on 22 DEmRNAs and resulted in two identified GO terms, as shown in Figure 7C. Finally, a coexpression heatmap was created to verify the results based on 14 DElncRNAs, 22 DEmRNAs and FTO, as shown in Figure 7D.

3.7 qRT–PCR validation of 10 DElncRNAs

To further confirm the functions of the 10 AdipoAI-regulated DElncRNAs selected from the ceRNA and m6A-related DElncRNA networks, a box plot was created to reveal their expression levels among 12 samples, as shown in Figures 8A, B. The results of the mantle order test suggested that most lncRNAs in the ceRNA and m6A networks were related to M2b and M1 macrophage phenotypes (Figures 8C, D). qRT-PCR was used to verify the results shown in Figure 8E. Both

10.3389/fimmu.2022.1051654

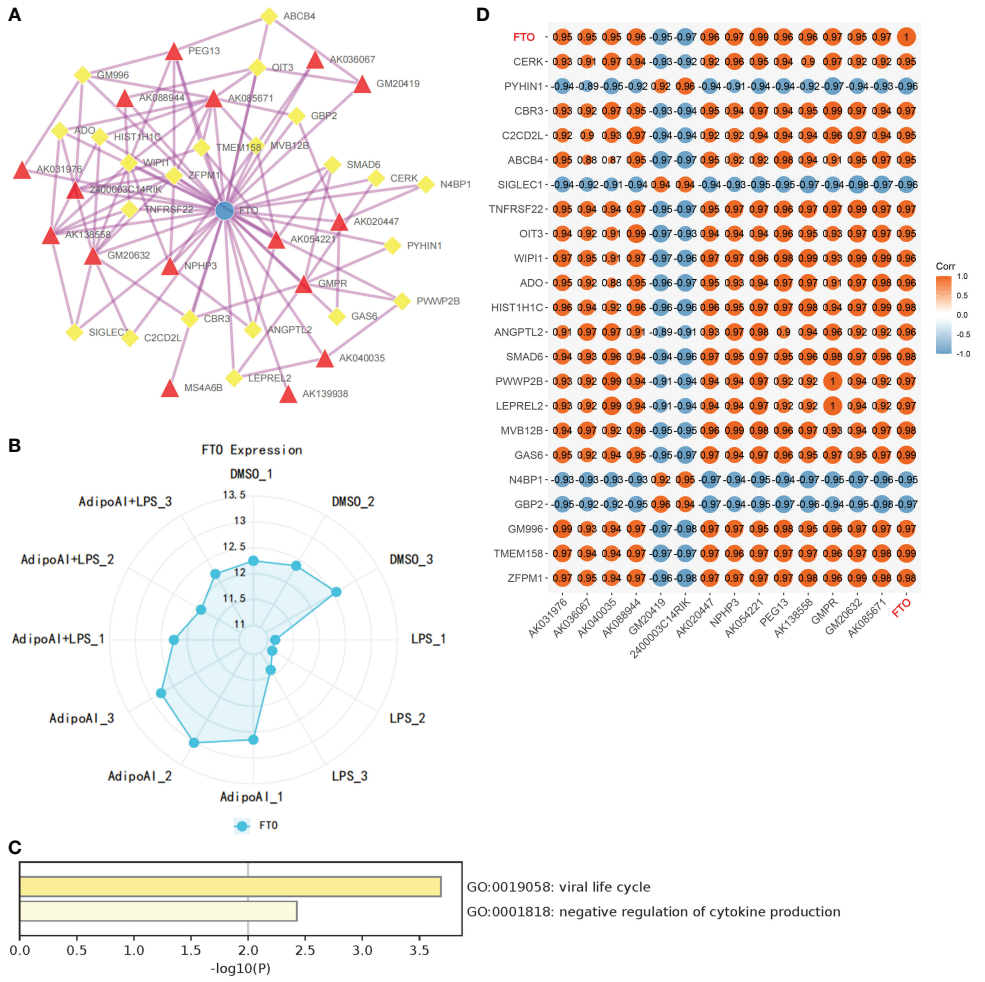

FIGURE 7
Construction of m6A regulator lncRNA–mRNA networks. **(A)** FTO (M6A regulator)-lncRNA–mRNA network. (Blue Ball: m6A regulator; Red Triangle: lncRNA; Yellow Square: mRNA). **(B)** FTO expression levels in 12 samples. **(C)** GO analysis for mRNAs in the network. **(D)** Coexpression validation for FTO, mRNAs and lncRNAs in networks.

data validation and qRT-PCR results showed that these selected DElncRNAs were regulated by AdipoAI.

4 Discussion

Although emerging evidence has shown that APN and its receptor agonists feature anti-inflammatory effects (7, 13), the precise molecular mechanisms remain unclear, especially the functions of lncRNAs. Thus, the current research aimed to provide mechanistic insight into the role played by lncRNAs in the AdipoAI-related anti-inflammatory effect, which attenuated LPS-induced inflammation in macrophages. More importantly, m6A methylation and ceRNA interactions were set as the entry points for further discovering how lncRNAs work in anti-inflammatory effects and macrophage polarization. Transcriptome sequencing and a series of bioinformatic analyses were conducted to elucidate these mechanisms at the high-throughput level.

Initially, enrichment analysis was conducted through GSVA, and the results indicated that AdipoAI inhibited the signal transduction of cytokines in the immune system and the activation of Toll-like receptor signaling pathways, especially signals associated with MYD88. LPS has been proven to affect inflammatory progression and the immune response by inducing cells through TLR4. Notably, TLR4-triggered signal transduction relies on the adaptor proteins myeloid differentiation marker 88 (MyD88) and adaptor-inducing IFNβ (TRIF), which mediate MyD88- and TRIF-dependent signaling pathways while simultaneously containing the Toll-interleukin-1 (IL-1) receptor (TIR) domain (30, 31). According to the enrichment analysis, AdipoR1/APPL1 stably interacted with MyD88. This complex inhibited the activation of the NF-kB, MAPK, and c-Maf pathways and restricted the LPS-induced

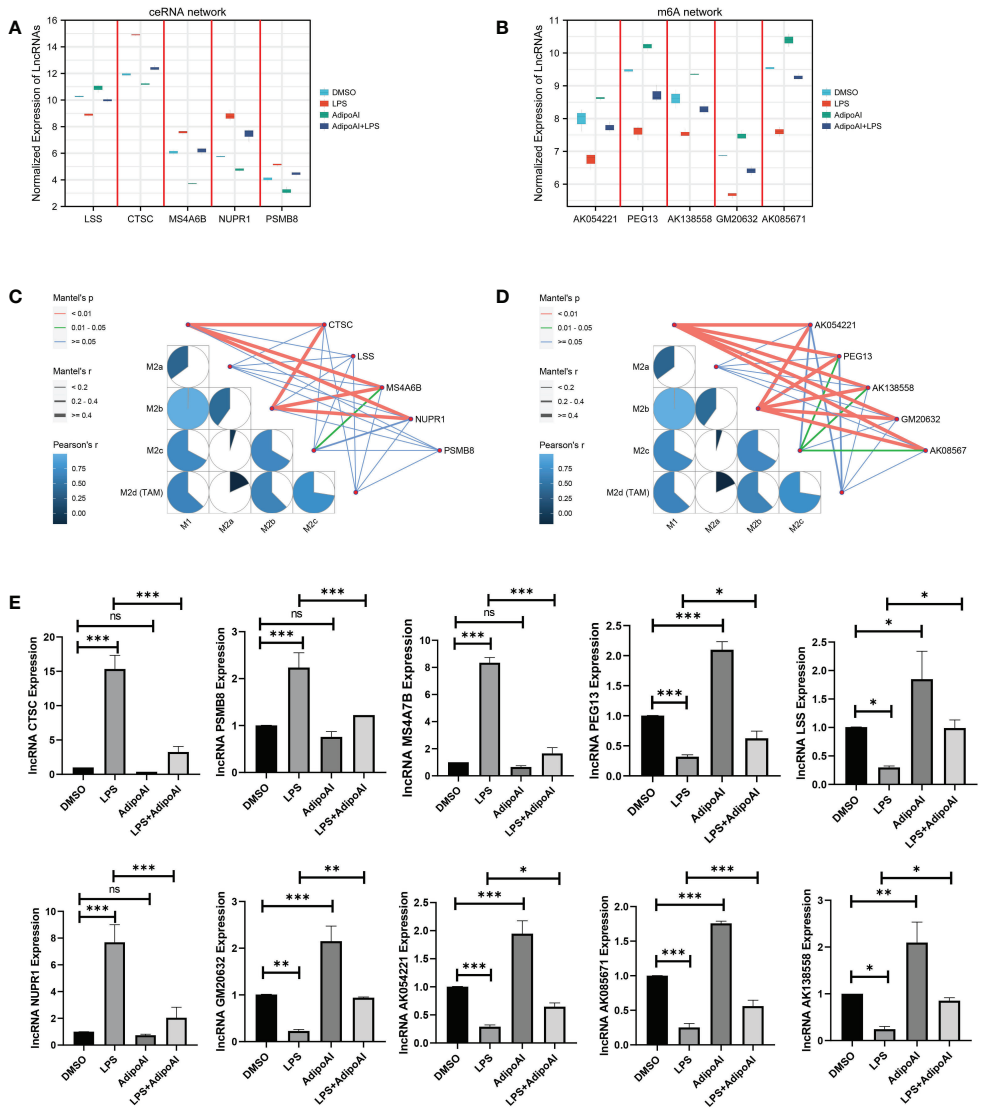

FIGURE 8
Microarray and qRT–PCR validation. **(A)** Box plot for the expression of 5 lncRNAs selected in ceRNA networks. **(B)** Box plot for the expression of 5 lncRNAs selected in the m6A-regulated lncRNA–mRNA networks. **(C, D)** Mantle order test of lncRNAs selected from the ceRNA- and m6A-related DElncRNA networks. **(C)** ceRNA networks, **(D)** m6A-related DElncRNA networks. **(E)** qRT–PCR validation for 10 lncRNAs (n=3). ns: no significant, * P <0.05, ** P <0.01, *** P <0.001.

production of proinflammatory cytokines in macrophages. A previous study was found and was consistent with our results, which strongly supported the reliability of our findings (7).

Differentially expressed lncRNAs and mRNAs were identified among 12 samples, and 110 DElncRNAs and 190 DEmRNAs were screened out and divided into two groups. Since the mechanism of AdipoAI-related anti-inflammatory effects relies on the proteins and RNAs affected by AdipoAI, GO/KEGG analysis was performed for pathway enrichment. Then, GO terms of antioxidant activity, serine and endopeptidase and KEGG pathways, including FoxO signaling and Toll-like receptor signaling, were identified. Notably, antioxidants play essential roles in the regulation of the immune response and inflammation restriction (32), and serine is necessary for LPS-induced expression of IL-1β in macrophages (33). Additionally, the FoxO signaling pathway also regulates innate immune cells (34). Hence, with various enriched pathways closely interacting with the immune response, AdipoAI was proven to be involved in anti-inflammatory mechanisms, particularly in macrophages.

To further clarify the function of AdipoAI on enriched pathways, GSEA was performed on 190 DEmRNAs. Surprisingly, pathways related to cytokines and the innate immune response were inhibited, while the endocytosis

pathway was activated. It has been suggested that the extracellular domain of TLR4 is indispensable for LPS-induced endocytosis (35), and TLR4-related endocytosis is necessary for the signal generation, receptor degradation and signal termination of TRIF-dependent proinflammatory factors (36, 37). Affecting the endocytosis of AdipoR1 may stimulate the phosphorylation of AMPK and ACC, which is mediated by APN and hormones (38, 39). Consequently, endocytosis may contribute to the signaling regulation of APN. In addition, GSEA and other results showed that AdipoAI had a significant correlation with endocytosis; that is, it might serve as the core pathway of AdipoAI-related anti-inflammatory effects.

Recently, a significant moderating role of large-scale biomechanisms has necessitated the investigation of ncRNAs in different fields. lncRNAs and miRNAs are the main constituents of ncRNAs and participate in various biological processes, such as immune responses, by moderating immune-related genes (40, 41). Among them, lncRNAs were identified as transcripts more than 200 nucleotides in length without protein-coding potential (41, 42). In 2011, the ceRNA hypothesis was proposed based on coexpressed competing triplets built by lncRNAs, miRNAs and mRNAs. This suggests a novel theory that lncRNAs and mRNAs compete for binding with one interacting miRNA, thus regulating each other (43) and affecting the miRNA-related negative regulation of gene expression. In previous investigations related to the ceRNA theory and anti-inflammatory effects, lncRNAs have been shown to play an essential role. For example, lncRNAs have been reported to regulate p38 mitogen-activated protein kinase and the nuclear factor-kb signaling pathway through the linc00707/mir-223-5p axis in LPS-induced mrc-5 cells (44). Additionally, lncRNA SNHG16 can upregulate TLR4 through and moderate the miR-15a/16 cluster through the ceRNA network to affect LPS-induced inflammatory pathways (45).

Making use of this theory, we constructed a ceRNA network to further study the mechanistic role played by lncRNAs in AdipoAI-regulated anti-inflammation. Then, a coexpression network was built, and the largest cluster was selected for enrichment analysis, in which 8 terms were identified: positive regulation of defense response, positive regulation of inflammatory response, cellular response to interferon-γ, antigen processing and presentation, regulation of cytokine production, metabolism of amino acids and derivatives and receptor-mediated endocytosis. Among them, a group of items, including regulation of cytokine production, antigen processing and presentation, cellular response to interferon-γ, and receptor-mediated endocytosis, were speculated to be the potential key pathways of AdipoAI-related anti-inflammatory effects since they were reported to be associated with the immune response of macrophages. Given that interferon-γ can activate macrophages and their sensitivities to TLR-induced cellular death (46), these pathways may contribute to the molecular mechanism of AdipoAI-related anti-inflammatory effects. Using TargetScan and mirWalk, we predicted and formed lncRNA–miRNA-mRNA triplets and built ceRNA networks based on triplets in each enriched GO item from the coexpression analysis. Finally, networks were constructed and provided new insight into the mechanistic theory for the role played by lncRNAs in AdipoAI-related anti-inflammatory effects based on the ceRNA theory. Furthermore, 5 lncRNAs from networks were selected as potential therapeutic targets for inflammation since they were discovered to participate in the anti-inflammatory effect caused by APN receptor agonists.

As noted by a recent publication (47), which studied the association between m6A methylation and LPS-induced inflammation in macrophages, the key enzyme for m6A methylation, METTL3, is closely associated with the immune response and inflammatory regulation. Moreover, the expression and biological activity of METTL3 could be enhanced by LPS, while overexpression may significantly reduce the severity of LPS-induced inflammation in macrophages. METTL3 influences these processes through the NF-kB pathway (47). Accordingly, we hypothesized that m6A methylation may contribute to the function of lncRNAs in AdipoAI-related anti-inflammatory effects. Twenty-three mRNAs related to methylation were obtained (27, 28) from recent publications and used for coexpression analyses. A network with the central mRNA FTO was built based on the coexpression relationships among DElncRNAs, DEmRNAs and m6A regulators, revealing the interaction between AdipoAI and m6A methylation. FTO is reported to positively correlate with the expression of APN (48), and the reduction in FTO can inhibit the NLRP3 inflammasome through the FoxO1/NF-kB signaling pathway in macrophages (49). Hence, AdipoAI may regulate the m6A methylation regulator FTO to influence related RNAs, thus affecting immune-related pathways and resulting in an anti-inflammatory effect. Obviously, FTO provides a theoretical basis for the interaction between m6A methylation and anti-inflammatory effects.

Furthermore, as demonstrated by enrichment analysis of mRNAs in m6A networks, these m6A-related mRNAs can suppress the secretion of cytokines. Thus, we speculated that AdipoAI might regulate the secretion of cytokines through the coexpression network. Among the network, lncRNA Peg13 regulates the Wnt/β-catenin pathway through the mir-490-3p/psmd11 axis (50) and attenuates the toxicity of sevoflurane to neural stem cells through the absorption of mir-128-3p while protecting the expression of SOX13 (51). At the same time, Peg13 can also alleviate hypoxic-ischaemic brain injury in neonatal mice *via* the mir-20a-5p/XIAP axis (52). In other studies, knockdown of the m6A-binding protein ythdf2 increased the expression levels of map2k4 and map4k4 mRNA by stabilizing mRNA transcripts. Similarly, the YTHDF2 protein can activate the MAPK and NF-kB signaling pathways and exacerbate the inflammatory reaction in LPS-induced primary Raw264.7 cells to promote the expression of proinflammatory

cytokines (53). Other research (54) proved that LPS treatment promoted Socs1 m6A methylation and sustained SOCS1 induction by promoting FTO degradation. Interestingly, their purpose was to simulate the phenotype of METTL14-deficient macrophages by forcing FTO expression in macrophages, while the results are consistent with ours, strongly proving the reliability of our analyses. As a consequence, we discovered that Socs1 inhibited signal transduction, while AdipoAI suppressed cytokine secretion by affecting related genes; thus, AdipoAI played a role in anti-inflammation by inhibiting the degradation of FTO.

To illuminate how AdipoAI works to influence macrophage phenotypes, ssGSEA was used to reveal scores of different phenotypes in each group of DEmRNAs. The results suggested that AdipoAI could reduce the LPS-induced phenotypic change from the M2b to the M2c type. A previous study (24) showed that the M2b type is associated with tumor progression, immune regulation and the Th2-related response. The M2c type is related to phagocytosis of apoptotic bodies, tissue remodeling and immune suppression (24). In accordance with these publications, AdipoAI may play a key role in macrophage phenotypic changes. The mantle order test suggested that the following genes were related to the M1 and M2b macrophage phenotypes: CTSC, MS4A6B, NUPR1, PEG13, AK054221, AK138558, GM20632, and AK08567. Thus, these genes are critical in both macrophage polarization and AdipoAI-related anti-inflammatory effects.

Notably, all of the sequencing data we extracted were from mice, which may lead to certain limitations. More specific analyses and *in vivo* experiments are necessary for further elucidation of the mechanisms of these newly identified lncRNAs.

In summary, we screened lncRNAs as candidate regulators of the anti-inflammatory mechanism of AdipoAI. Moreover, we identified specific lncRNAs from these processes based on m6A-related DElncRNAs and ceRNA networks, providing a novel reference for the subsequent exploration of the molecular mechanism of AdipoAI-related anti-inflammatory effects.

Data availability statement

The datasets presented in this study can be found in online repositories. The names of the repository/repositories and accession number(s) can be found below: GEO (GSE212065).

Author contributions

HY, FF, and WQ contributed to the conception and design of the research. HY, HW, QX, and WQ contributed to the writing and drafting of the manuscript. ZL and ZC contributed to drawing the figures and tables and analyzing the data. QT, JC, and FF contributed to the critical revision of the manuscript for important intellectual content. All the authors have approved the final version of the manuscript to be published and agree to be accountable for all aspects of the work.

Funding

This research was supported by grants from the National Natural Science Foundation of China [82101024 (WQ)] and the Natural Science Foundation of Guangdong Province [2020A1515110027 (WQ), 2021A1515010854 (FF)].

Acknowledgments

We thank ZhiYi Wang (Department of Radiation Oncology, Nanfang Hospital, Southern Medical University) for his intellectual support.

Conflict of interest

The authors declare that the research was conducted in the absence of any commercial or financial relationships that could be construed as a potential conflict of interest.

Publisher's note

Supplementary material

The Supplementary Material for this article can be found online at: https://www.frontiersin.org/articles/10.3389/fimmu.2022.1051654/full#supplementary-material

SUPPLEMENTARY FIGURE 1
Quality control for lncRNA microarray. **(A)** PCA of lncRNA expression profiles. **(B)** PCA of mRNA expression profiles. **(C)** Boxplot of lncRNAs. **(D)** Boxplot of mRNAs.

SUPPLEMENTARY FIGURE 2
Pheatmap for 928 pathway GSVA scores.

SUPPLEMENTARY FIGURE 3
Volcano plot for differential pathways in the 4 groups. **(A)** Differential pathways: DMSO vs. AdipoAI. **(B)** Differential pathways: DMSO vs. LPS. **(C)** Differential pathways: LPS vs. AdipoAI+LPS.

SUPPLEMENTARY FIGURE 4
Coexpression between DEmRNAs and DElncRNAs.

SUPPLEMENTARY FIGURE 5
Coexpression between 33 m6A-related mRNAs and 110 DElncRNAs.

SUPPLEMENTARY FIGURE 6
Coexpression between 2 m6A-related mRNAs and 16 lncRNAs.

SUPPLEMENTARY FIGURE 7
Coexpression between 2 m6A-related mRNAs and 190 DEmRNAs.

SUPPLEMENTARY FIGURE 8
Coexpression between 16 lncRNAs and 190 DEmRNAs.

References

1. Medzhitov R. Origin and physiological roles of inflammation. *Nature* (2008) 454:428–35. doi: 10.1038/nature07201

2. Barton GM. A calculated response: Control of inflammation by the innate immune system. *J Clin Invest* (2008) 118:413–20. doi: 10.1172/JCI34431

3. Mazgaeen L, Gurung P. Recent advances in lipopolysaccharide recognition systems. *Int J Mol Sci* (2020) 21:379. doi: 10.3390/ijms21020379

4. Raetz CRH, Whitfield C. Lipopolysaccharide endotoxins. *Annu Rev* (2002) 71:635–700. doi: 10.1146/annurev.biochem.71.110601.135414

5. Obata Y, Yamada Y, Takahi Y, Baden MY, Saisho K, Tamba S, et al. Relationship between serum adiponectin levels and age in healthy subjects and patients with type 2 diabetes. *Clin Endocrinol (Oxf)* (2013) 79:204–10. doi: 10.1111/cen.12041

6. Fang H, Judd RL. Adiponectin regulation and function. *Compr Physiol* (2018) p:1031–63. doi: 10.1002/cphy.c170046

7. Gil-Campos M, Cañete RR, Gil A. Adiponectin, the missing link in insulin resistance and obesity. *Clin Nutr* (2004) 23:963–74. doi: 10.1016/j.clnu.2004.04.010

8. Yokota T, Oritani K, Takahashi I, Ishikawa J, Matsuyama A, Ouchi N, et al. Adiponectin, a new member of the family of soluble defense collagens, negatively regulates the growth of myelomonocytic progenitors and the functions of macrophages. *Blood* (2000) 96:1723–32. doi: 10.1182/blood.V96.5.1723

9. Ohashi K, Shibata R, Murohara T, Ouchi N. Role of anti-inflammatory adipokines in obesity-related diseases. *Trends Endocrinol Metab* (2014) 25:348–55. doi: 10.1016/j.tem.2014.03.009

10. Gordon S. Phagocytosis: An immunobiologic process. *Immunity* (2016) 44:463–75. doi: 10.1016/j.immuni.2016.02.026

11. Wu X, Qiu W, Hu Z, Lian J, Liu Y, Zhu X, et al. An adiponectin receptor agonist reduces type 2 diabetic periodontitis. *J Dent Res* (2019) 98:313–21. doi: 10.1177/0022034518818449

12. Okada-Iwabu M, Yamauchi T, Iwabu M, Honma T, Hamagami K, Matsuda K, et al. A small-molecule AdipoR agonist for type 2 diabetes and short life in obesity. *Nature* (2013) 503:493–9. doi: 10.1038/nature12656

13. Qiu W, Wu H, Hu Z, Wu X, Tu M, Fang F, et al. Identification and characterization of a novel adiponectin receptor agonist adipo anti-inflammation agonist and its anti-inflammatory effects. *Vitro vivo. Br J Pharmacol* (2021) 178:280–97. doi: 10.1111/bph.15277

14. Robinson EK, Covarrubias S, Carpenter S. The how and why of lncRNA function: An innate immune perspective. *Biochim Biophys Acta Gene Regul Mech* (2020) 1863:194419. doi: 10.1016/j.bbagrm.2019.194419

15. Batista PJ, Chang HY. Long noncoding RNAs: Cellular address codes in development and disease. *Cell* (2013) 152:1298–307. doi: 10.1016/j.cell.2013.02.012

16. Fatica A, Bozzoni I. Long non-coding RNAs: new players in cell differentiation and development. *Nat Rev Genet* (2014) 15:7–21. doi: 10.1038/nrg3606

17. Liu J, Wang H, Chua N-H. Long noncoding RNA transcriptome of plants. *Plant Biotechnol J* (2015) 13:319–28. doi: 10.1111/pbi.12336

18. Rafiee A, Riazi-Rad F, Havaskary M, Nuri F. Long noncoding RNAs: Regulation, function and cancer. *Biotechnol Genet Eng Rev* (2018) 34:153–80. doi: 10.1080/02648725.2018.1471566

19. Jariwala N, Sarkar D. Emerging role of lncRNA in cancer: A potential avenue in molecular medicine. *Ann Transl Med* (2016) 4:286. doi: 10.21037/atm.2016.06.27

20. Fukata M, Vamadevan AS, Abreu MT. Toll-like receptors (TLRs) and nod-like receptors (NLRs) in inflammatory disorders. *Semin Immunol* (2009) 21:242–53. doi: 10.1016/j.smim.2009.06.005

21. Qi X, Zhang D-H, Wu N, Xiao J-H, Wang X, Ma W. ceRNA in cancer: Possible functions and clinical implications. *J Med Genet* (2015) 52:710–8. doi: 10.1136/jmedgenet-2015-103334

22. Jiang X, Liu B, Nie Z, Duan L, Xiong Q, Jin Z, et al. The role of m6A modification in the biological functions and diseases. *Signal Transd Target Ther* (2021) 6:74. doi: 10.1038/s41392-020-00450-x

23. Hänzelmann S, Castelo R, Guinney J. GSVA: Gene set variation analysis for microarray and RNA-seq data. *BMC Bioinf* (2013) 14:7. doi: 10.1186/1471-2105-14-7

24. Viola A, Munari F, Sánchez-Rodríguez R, Scolaro T, Castegna A. The metabolic signature of macrophage responses. *Front Immunol* (2019) 10:1462. doi: 10.3389/fimmu.2019.01462

25. Ritchie ME, Phipson B, Wu D, Hu Y, Law CW, Shi W, et al. Limma powers differential expression analyses for RNA-sequencing and microarray studies. *Nucleic Acids Res* (2015) 43:e47. doi: 10.1093/nar/gkv007

26. Subramanian A, Tamayo P, Mootha VK, Mukherjee S, Ebert BL, Gillette MA, et al. Gene set enrichment analysis: A knowledge-based approach for interpreting genome-wide expression profiles. *Proc Natl Acad Sci USA* (2005) 102:15545–50. doi: 10.1073/pnas.0506580102

27. Jin Y, Wang Z, He D, Zhu Y, Hu X, Gong L, et al. Analysis of m6A-related signatures in the tumor immune microenvironment and identification of clinical prognostic regulators in adrenocortical carcinoma. *Front Immunol* (2021) 12:637933. doi: 10.3389/fimmu.2021.637933

28. Chen X-Y, Zhang J, Zhu J-S. The role of m6A RNA methylation in human cancer. *Mol Cancer* (2019) 18:103. doi: 10.1186/s12943-019-1033-z

29. Jia H, Hao S, Cao M, Wang L, Bai H, Shui W, et al. m6A-related lncRNAs are potential prognostic biomarkers of cervical cancer and affect immune infiltration. *Dis Markers* (2022) 2022:8700372. doi: 10.1155/2022/8700372

30. Kawai T, Akira S. The role of pattern-recognition receptors in innate immunity: Update on toll-like receptors. *Nat Immunol* (2010) 11:373–84. doi: 10.1038/ni.1863

31. Piao W, Song C, Chen H, Quevedo Diaz MA, Wahl LM, Fitzgerald KA, et al. Endotoxin tolerance dysregulates MyD88- and Toll/IL-1R domain-containing adapter inducing IFN-β-dependent pathways and increases expression of negative regulators of TLR signaling. *J Leukoc Biol* (2009) 86:863–75. doi: 10.1189/jlb.0309189

32. Aderem A, Ulevitch RJ. Toll-like receptors in the induction of the innate immune response. *Nature* (2000) 406:782–7. doi: 10.1038/35021228

33. Spychalowicz A, Wilk G, Śliwa T, Ludew D, Guzik TJ. Novel therapeutic approaches in limiting oxidative stress and inflammation. *Curr Pharm Biotechnol* (2012) 13:2456–66. doi: 10.2174/1389201011208062456

34. Rodriguez AE, Ducker GS, Billingham LK, Martinez CA, Mainolfi N, Suri V, et al. Serine metabolism supports macrophage IL-1β production. *Cell Metab* (2019) 29:1003–11.e4. doi: 10.1016/j.cmet.2019.01.014

35. Manning BD, Toker A. AKT/PKB signaling: Navigating the network. *Cell* (2017) 169:381–405. doi: 10.1016/j.cell.2017.04.001

36. Ciesielska A, Matyjek M, Kwiatkowska K. TLR4 and CD14 trafficking and its influence on LPS-induced pro-inflammatory signaling. *Cell Mol Life Sci* (2021) 78:1233–61. doi: 10.1007/s00018-020-03656-y

37. Kagan JC, Su T, Horng T, Chow A, Akira S, Medzhitov R. TRAM couples endocytosis of toll-like receptor 4 to the induction of interferon-β. *Nat Immunol* (2008) 9:361–8. doi: 10.1038/ni1569

38. Husebye H, Halaas Ø, Stenmark H, Tunheim G, Sandanger Ø, Bogen B, et al. Endocytic pathways regulate toll-like receptor 4 signaling and link innate and adaptive immunity. *EMBO J* (2006) 25:683–92. doi: 10.1038/sj.emboj.7600991

39. Ding Q, Wang Z, Chen Y. Endocytosis of adiponectin receptor 1 through a clathrin- and Rab5-dependent pathway. *Cell Res* (2009) 19:317–27. doi: 10.1038/cr.2008.299

40. Buechler C, Wanninger J, Neumeier M. Adiponectin receptor binding proteins–recent advances in elucidating adiponectin signalling pathways. *FEBS Lett* (2010) 584:4280–6. doi: 10.1016/j.febslet.2010.09.035

41. Atianand MK, Caffrey DR, Fitzgerald KA. Immunobiology of long noncoding RNAs. *Annu Rev Immunol* (2017) 35:177–98. doi: 10.1146/annurev-immunol-041015-055459

42. Mehta A, Baltimore D. MicroRNAs as regulatory elements in immune system logic. *Nat Rev Immunol* (2016) 16:279–94. doi: 10.1038/nri.2016.40

43. Kopp F, Mendell JT. Functional classification and experimental dissection of long noncoding RNAs. *Cell* (2018) 172:393–407. doi: 10.1016/j.cell.2018.01.011

44. Zou X, Gao C, Shang R, Chen H, Wang B. Knockdown of lncRNA LINC00707 alleviates LPS-induced injury in MRC-5 cells by acting as a ceRNA of miR-223-5p. *Biosci Biotechnol Biochem* (2021) 85:315–23. doi: 10.1093/bbb/zbaa069

45. Salmena L, Poliseno L, Tay Y, Kats L, Pandolfi PP. A ceRNA hypothesis: The Rosetta stone of a hidden RNA language? *Cell* (2011) 146:353–8. doi: 10.1016/j.cell.2011.07.014

46. Simpson DS, Pang J, Weir A, Kong IY, Fritsch M, Rashidi M, et al. Interferon-γ primes macrophages for pathogen ligand-induced killing *via* a caspase-8 and mitochondrial cell death pathway. *Immunity* (2022) 55:423–41.e9. doi: 10.1016/j.immuni.2022.01.003

47. Wang J, Yan S, Lu H, Wang S, Xu D. METTL3 attenuates LPS-induced inflammatory response in macrophages *via* NF-κB signaling pathway. *Mediators Inflammation* (2019) 2019:3120391. doi: 10.1155/2019/3120391

48. Terra X, Auguet T, Porras JA, Quintero Y, Aguilar C, Luna AM, et al. Anti-inflammatory profile of FTO gene expression in adipose tissues from morbidly obese women. *Cell Physiol Biochem* (2010) 26:1041–50. doi: 10.1159/000323979

49. Luo J, Wang F, Sun F, Yue T, Zhou Q, Yang C, et al. Targeted inhibition of FTO demethylase protects mice against LPS-induced septic shock by suppressing NLRP3 inflammasome. *Front Immunol* (2021) 12:663295. doi: 10.3389/fimmu.2021.663295

50. Feng H, Gui Q, Zhu W, Wu G, Dong X, Shen M, et al. Long-noncoding RNA Peg13 alleviates epilepsy progression in mice *via* the miR-490-3p/Psmd11 axis to inactivate the wnt/β-catenin pathway. *Am J Transl Res* (2020) 12:7968–81.

51. Jiang Y, Wang Y, Sun Y, Jiang H. Long non-coding RNA Peg13 attenuates the sevoflurane toxicity against neural stem cells by sponging microRNA-128-3p to preserve Sox13 expression. *PloS One* (2020) 15:e0243644. doi: 10.1371/journal.pone.0243644

52. Gao H, Zhang Y, Xue H, Zhang Q, Zhang Y, Shen Y, et al. Long non-coding RNA Peg13 alleviates hypoxic-ischemic brain damage in neonatal mice *via* miR-20a-5p/XIAP axis. *Neurochem Res* (2022) 47:656–66. doi: 10.1007/s11064-021-03474-z

53. Yu R, Li Q, Feng Z, Cai L, Xu Q. m6A reader YTHDF2 regulates LPS-induced inflammatory response. *Int J Mol Sci* (2019) 20:E1323. doi: 10.3390/ijms20061323

54. Du J, Liao W, Liu W, Deb DK, He L, Hsu PJ, et al. N6-adenosine methylation of Socs1 mRNA is required to sustain the negative feedback control of macrophage activation. *Dev Cell* (2020) 55:737–53.e7. doi: 10.1016/j.devcel.2020.10.023

frontiers | Frontiers in Immunology

TYPE Review
PUBLISHED 18 January 2023
DOI 10.3389/fimmu.2022.1083780

OPEN ACCESS

EDITED BY
Chit Laa Poh,
Sunway University, Malaysia

REVIEWED BY
Laurent Dubuquoy,
U1286 Institute for Translational Research in Inflammation (INFINITE), France
Natalia A. Osna,
University of Nebraska Medical Center, United States

*CORRESPONDENCE
Jingmei Liu
464201364@qq.com
Dean Tian
datian@tjh.tjmu.edu.cn

SPECIALTY SECTION
This article was submitted to Inflammation, a section of the journal Frontiers in Immunology

RECEIVED 29 October 2022
ACCEPTED 30 December 2022
PUBLISHED 18 January 2023

CITATION
Gong J, Tu W, Liu J and Tian D (2023) Hepatocytes: A key role in liver inflammation. *Front. Immunol.* 13:1083780. doi: 10.3389/fimmu.2022.1083780

Hepatocytes: A key role in liver inflammation

Jin Gong, Wei Tu, Jingmei Liu* and Dean Tian*

Department of Gastroenterology, Tongji Hospital of Tongji Medical College, Huazhong University of Science and Technology, Wuhan, China

Hepatocytes, the major parenchymal cells in the liver, are responsible for a variety of cellular functions including carbohydrate, lipid and protein metabolism, detoxification and immune cell activation to maintain liver homeotasis. Recent studies show hepatocytes play a pivotal role in liver inflammation. After receiving liver insults and inflammatory signals, hepatocytes may undergo organelle damage, and further respond by releasing mediators and expressing molecules that can act in the microenvironment as well as initiate a robust inflammatory response. In this review, we summarize how the hepatic organelle damage link to liver inflammation and introduce numerous hepatocyte-derived pro-inflammatory factors in response to chronic liver injury.

KEYWORDS

hepatocyte, organelle damage, hepatic inflammation, extracellular vesicles, cytokines

1 Introduction

Chronic liver disease is characterized by hepatocyte injury and inflammation that lead to the development of cirrhosis and liver cancer, accounting for approximately 2 million deaths every year worldwide (1). Multiple etiologies include chronic HBV and HCV infection, nonalcoholic steatohepatitis (NASH), alcoholic liver disease, and autoimmune liver disease cause the global burden of liver disease. Hepatocytes comprise the majority (~85%) of the liver mass, and play a role in various biochemical and metabolic functions (2). Traditional concepts viewed hepatocytes as targets of immune or insults mediated injury, resulting in hepatocyte death which identified as a typical pathological feature in liver disease. However, recent studies have emphasized a role for hepatocyte as active drivers in liver inflammation and fibrosis through intercellular communication (3). Organelle damage, including mitochondria, lysosome, endoplasmic reticulum may determine the severity of hepatocyte injury (4). It is widely accepted that sterile hepatocyte death leads to the release of damage-associated molecular patterns (DAMPs), which are recognized by the innate immune system through pattern recognition receptors, and exaggerate inflammatory response in liver (5). What's more, stressed hepatocytes engage in liver inflammation as well, for they can change their phenotype, make an adaptation to the microenvironment and alter their surrounding cell populations (2). Substantial evidence show that hepatocytes constitutively produce and secrete a variety of mediators that play important roles in immune regulation and fibrosis (6, 7). In this review, we will provide current literature investigating the adaptive and maladaptive alterations of hepatocytes during the initiation of liver injury, and how the

stressed hepatocytes interact with the surrounding cells to trigger a proinflammatory microenvironment in chronic liver disease.

2 Endoplasmic reticulum stress in hepatocytes links to liver inflammation

Endoplasmic reticulum (ER) is the major site of secretory and transmembrane protein folding, calcium homeostasis and lipid synthesis. Upon the accumulation of misfolded proteins in the ER, unfolded protein response (UPR) is activated by three ER-transmembrane sensors, namely PKR like ER kinase (PERK), activating transcription factor 6 (ATF6), and inositol requiring enzyme 1 (IRE1), coordinately through downstream factors including X-box binding protein 1 (XBP1), α-subunit of eukaryotic initiation factor 2 (eIF2α), C/EBP homologous protein (CHOP), activating Transcription Factor 4 (ATF4), to resolve the protein folding defect (8). Sustained or massive ER stress leads to hepatocyte steatosis and apoptosis (9) (Figure 1).

ER stress is observed in many chronic liver diseases. Chronic ER stress plays a causative role in NAFLD progression by promoting lipogenesis, disturbing mitochondrial function and modulating insulin signaling (10). ER stress markers are shown to decline in livers of obese patients following weight loss after bariatric surgery (11). It has confirmed that impaired autophagic flux is associated with increased ER stress in livers from patients with biopsy-proven NASH during the development of NAFLD (12). Various HBV and HCV proteins localize inside the ER lumen and are undergo envelopment. HBV infection can cause ER stress, which enhance HBV viral replication by initiating autophagy (13). Moreover, chronic HCV infection induce ER stress and the minimal expression of UPR target genes, which confers hepatocytes adaptation and resistance to liver injury (14–16). Hepatic PHLDA3 regulates ER stress-induced hepatocyte death through Akt inhibition in HCV hepatitis (17). Besides, it is reported that interferon regulatory factor 3 (IRF3) is activated by ER stress and induce hepatocyte apoptosis in early alcoholic liver disease (18).

Under chronic ER stress, UPR is linked to the activation of several inflammatory response pathways including NFκB, JNK, ROS, IL-6, TNF-α (8, 19). Activated IRE1α induces JNKs activation, and subsequent implicates in cell pro-inflammatory and pro-apoptotic pathways. Knockdown of JNK1 gene protects mice from the

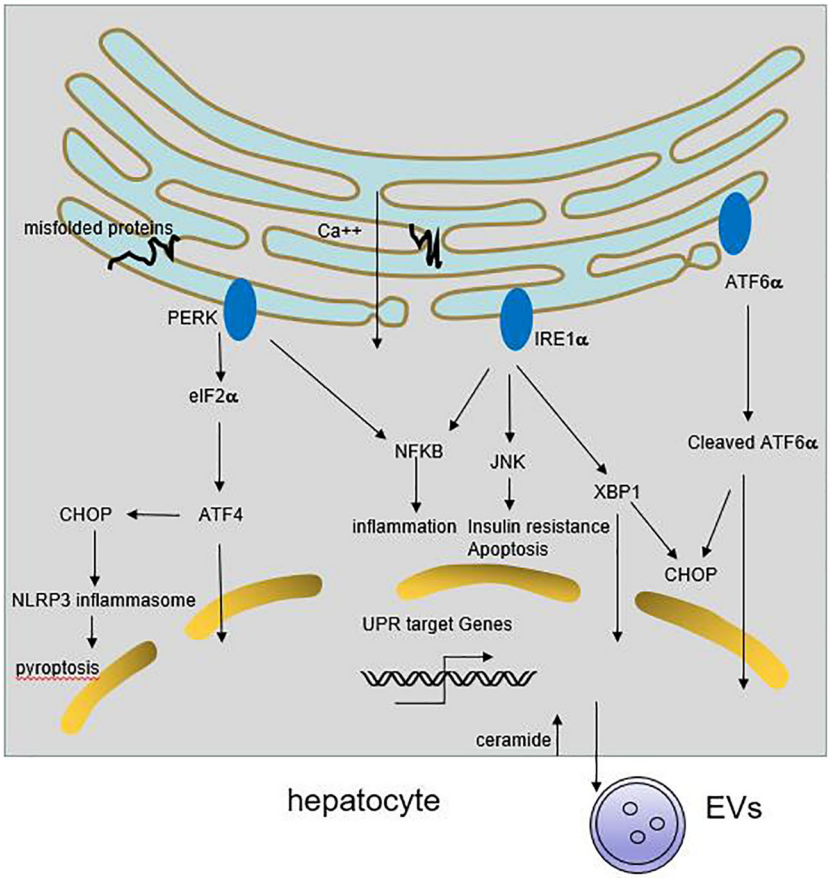

FIGURE 1
Role of ER stress in liver inflammation. Multiple stimuli lead to the activation of UPR response in hepatocyte. The three ER transmembrane sensors, PERK, IRE1 and ATF6, coordinately through downstream signaling cascades to resolve the protein folding defect and promote cell survival. If the adaptive UPR is overwhelmed by sustained or massive ER stress, it leads to hepatocyte steatosis and death. Meanwhile, ER stress may trigger NFκB and JNKs activation, resulting in release of proinflammatory cytokines. On the other hand, ER stress can induce CHOP-dependent NLRP3 inflammasome activation in hepatocytes. Besides, activation of IRE1A in hepatocytes promotes the release of inflammatory extracellular vesicles (EVs), thereby accummulating immune cells infiltration.

development of obesity and insulin resistance (20). Enhanced ER stress can trigger NFκB activation through IRE1α and PERK pathway, followed by the secretion of inflammatory and chemotactic cytokines in hepatocytes (21, 22). Some HCV and HBV protein accumulate at the ER membranes which cause a deregulation of Ca2+ flux, generation of reactive oxygen and nitrogen species, and the resulting ER stress could induce IL-8 transcription (10, 23, 24). ER stress also induces CHOP-dependent NOD-like receptor family, pyrin domain-containing 3 (NLRP3) inflammasome activation in hepatocytes, potentially causing pyroptotic death and hepatic inflammation in patients with HBV-associated liver failure and NAFLD (25, 26). Recent study shows that activation of IRE1A in hepatocytes promotes the release of inflammatory extracellular vesicles (EVs), which recruit macrophages to liver, resulting in liver inflammation and injury in steatohepatitis (27). Therefore, chronic ER stress cause inflammation and the deregulation of lipid metabolism, that further exacerbate liver diseases.

3 Autophagy dysregulation in hepatocytes leads to liver inflammation

Autophagy is a catabolic lysosomal process responsible for clearing damaged proteins, dysfunction organelles and lipid droplets. It is considered as a cellular response to maintain energy balance and in reaction to multiple of cellular stress, such as starvation, hypoxia, and viral infection (28).

Autophagy generally plays a protective role in hepatocytes, since they can protect against steatosis and hepatocyte death. It is reported autophagy can selectively degrades lipid droplets, termed lipophagy, as evidenced by the increase in lipid accumulation upon inhibition of autophagy in hepatocytes (29). Recent studies with specific genetic inhibition of autophagy have established that hepatocytes are more susceptible to various liver injury, such as alcohol, toxic agents, lipotoxic metabolites, and pro-inflammatory factors. Autophagy may promote cell survival by clearing misfolded proteins, lipids and damaged mitochondria (30–33).

Studies show that regulation of autophagy links to the progression of chronic liver diseases. Impaired autophagic flux links to steatosis and progression to NASH in NAFLD patients and mouse models by genetic or phamacological inhibition of autophagy (12). Shen et al. have uncovered pathogenesis of IL-1β-induced liver injury in steatohepatitis by finding that IL-1β becomes cytotoxic and pro-inflammatory to hepatocytes when inhibition of autophagy, leading to cell necrosis and liver inflammation (34). Although autophagy can alleviate hepatocyte apoptosis and steatosis in acute alcohol liver disease (35), decrease autophagic flux in hepatocyte is observed in models of chronic alcohol exposure (36, 37). A significant decrease in UQCRC2 protein expression cause impaired mitophagy, which may aggravate MLKL-mediated hepatocyte necroptosis and inflammation in alcoholic liver disease (38, 39). Furthermore, early autophagy enhance HBV infection and envelopment (40). Inhibition of autophagy by liver-specific knockout of Atg5 in HBV transgenic mice can obviously reduce HBV DNA level (41). Additionally, autophagy plays an important role in HBV-mediated immune response (40). GAL9, a type I IFN-stimulated gene, exerts effect on direct autophagic degradation of HBc in HBV-infected hepatocytes (42). ATG12 is required for HBV replication and impediment of the IFN signaling pathway, as evidence by decreased levels of IFN-α, IFN-β in ATG12-knockdown hepatocytes (43). Autophagy inhibition also abrogates HBx-induced activation of nuclear factor-κB (NF-κB) and production of interleukin-6 (IL-6), IL-8, and CXCL2 (44). Similarly, autophagy is required to promote HCV replication, partly through suppression of innate immunity (45, 46). HCV-induced autophagy can suppress host innate immune response through autophagic degradation of TRAF6, which is an important signaling molecule that mediates the activation of NF-kB and expression of cytokines and interferons (47). Meanwhile, loss of autophagy signaling upregulates HCV-induced cytoplasmic RIG-I signaling and IFN-β–mediated antiviral responses (48). Interference of HCV-induced mitophagy by Drp1 silencing enhances innate immune signaling (49). The correlation between AIH and autophagy in hepatocyte is not clear. It has been observed increased LC3 and p62 expression in hepatocytes of AIH patients, and p62 level is strongly correlated with necroinflammatory grade, which indicates that decreasing autophagic activity may be linked to severity of inflammation in AIH (50).

4 The role of hepatic mitochondrial dysfunction in liver inflammation

Mitochondria are abundant in the liver and required for lipid metabolism and energy production. They can directly or indirectly influence other cellular components such as the lysosomes, the endoplasmic reticulum (ER), and cytosolic pathway, to meet the cellular demands and alleviate mitochondrial dysfunction (51). Generally, mitochondria maintain normal morphology and homeostasis by the way of mitochondrial quality control, including the regulation of mitochondrial fusion, fission, biogenesis, and mitophagy (52). When they fail to adapt to various stress, they can release mitochondrial DNA (mtDNA) in the cytosol or circulation, which could induce cGAS-STING-dependent type I interferon (IFN) response. Furthermore, mtDNA synthesis can activate the NLRP3 inflammasome which initiates inflammation (53). In addition, mitochondrial dysfunction can generate excessive reactive oxygen species (ROS), which stimulate synthesis of cytokines to amplify the inflammatory cascade reaction and cause apoptosis and necrosis of hepatocytes (52) (Figure 2).

Emerging evidence shows that mitochondria dysfunction, especially mitochondria-derived immunogenic components (including its DNA) have profound impacts on the development of various chronic liver diseases. It is reported that NASH patients produce high mitochondrial levels of ROS and ROS-mediated mtDNA damage (54). Moreover, mtDNA is elevated in the serum of NASH patients and in association with histological degree of hepatic fibrosis. The mtDNA released from injured hepatocyte mitochondria could directly activate hepatic stellate cells (HSCs) and promote inflammation through binding to endosomal TLR9 of Kupffer cells (55, 56). Besides, Mitochondrial protein mitofusion 2 (Mfn2) plays an important role in connecting ER membranes to mitochondria and mitochondrial fusion, studies show that hepatic mfn2 deficiency impairs ER-mitochondrial phosphatidylserine transfer and mitochondrial function, leading to ER stress and liver

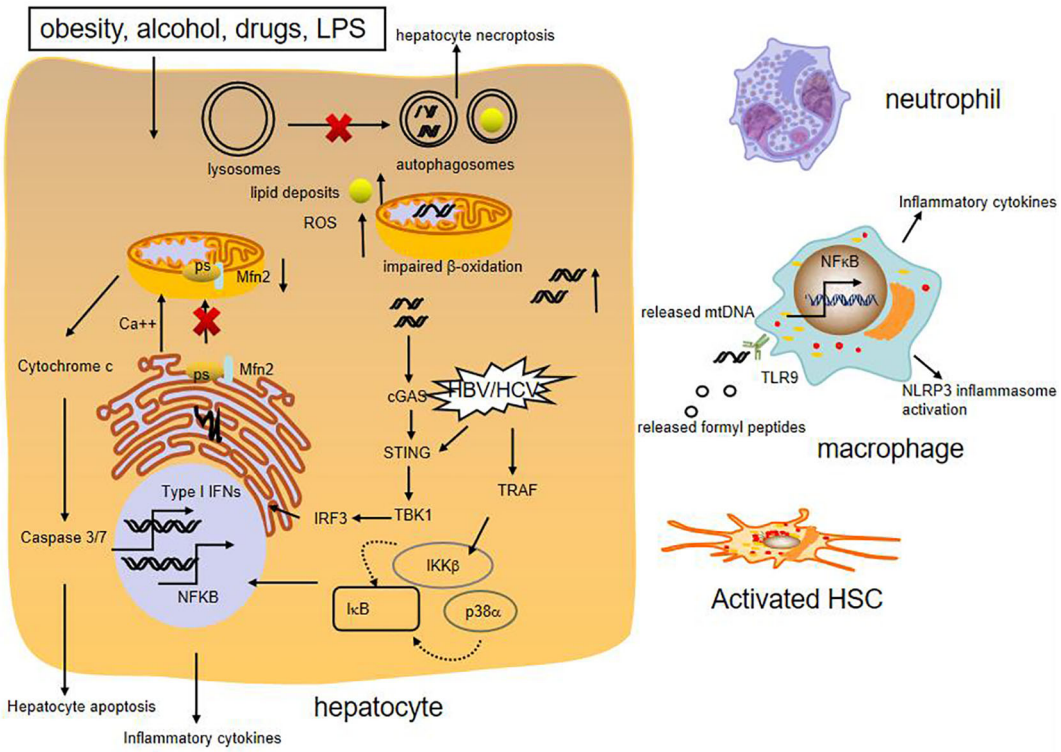

FIGURE 2
Role of mitochondrial damage in liver inflammation. Various liver injury impair mitochondrial respiration and increase ROS formation, cause mtDNA damage. High levels of ROS can increase synthesis of cytokines, which cause apoptosis and necrosis of hepatocytes. The presence of mtDNA in the cytosol or circulation can trigger proinflammatory and type I IFN responses. Moreover, release of mitochondria-derived danger signals, such as mtDNA, formylated proteins, can attract macrophage and neutrohphils, resulting in activation of NFκB and NLRP3 inflammasome. MtDNA also promotes fibrogenic activation of HSCs. Besides, reduced expression of mitochondrial protein Mfn2 leads to deficient ER-mitochondrial phosphatidylserine transfer, which provokes liver inflammation. HBV and HCV can activate innate immune antiviral signaling and inflammatory pathways through induction of type I interferons and expression of inflammatory cytokines by NFκB.

inflammation in NAFLD (57, 58). Mitochondrial dysregulation is also observed in hepatocytes of patients with AIH and experimental mouse model with immune-mediated liver injury. Blockade of dynamin-related protein 1(Drp1)-mediated mitochondrial fission protects mice from concanavalin A (ConA)-induced liver injury (59). In addition, hepatic ATF4 plays a pathological role in alcohol-induced mitochondrial dysfunction and liver injury by repressing TFAM expression, while AMPK protects against alcohol-induced liver injury through up-regulating mitophagy (39, 60). Apart from the above, chronic HBV and HCV infection could induce mitochondrial oxidative stress and mitochondrial antiviral signaling-mediated innate immune signaling as well (61, 62).

5 Mediators involved in intercellular communication

During chronic liver injury, stressed hepatocytes can release mediators that involved in crosstalk between hepatocytes and surrounding cell populations. Besides, hepatocytes serve as liver-resident nonprofessional antigen presenting cells (APCs), resulting in a bias toward immune tolerance.

5.1 Hepatocyte-derived extracellular vesicles in liver inflammation

Extracellular vesicles (EVs) are homogeneous vesicles containing lipid, nuclear acid, proteins, which can be secreted by various cell types to the extracellular space and circulation. EVs include microvesicles, exosomes and apoptotic bodies depending on their source and molecular structure.

A growing body of evidence have identified EVs as a conveyor mediating intercellular communication in liver diseases (63) (List in Table 1). Hepatocyte-derived EVs as pathogenic mediators play a role in NASH (77). Hepatocyte-derived exosomes from early onset obese mice promote insulin sensitivity through miR-3075 (64). The increase in plasma mtDNA contained in EVs of hepatocyte origin could drive NASH development by activation of TLR9 (56). EVs are also shown as mediators of toxic lipid-induced intercellular signaling. Lipotoxic activation of hepatocytes induce release of EVs enriched in ceramide, CXCL10, miR-192-5p, which trigger chemotaxis and inflammatory phenotype switch of macrophages (65–68). Besides, EVs mediate cell-to-cell communication in alcoholic liver disease. In patients with alcoholic hepatitis, the number of circulating EVs is reported higher than those in healthy individuals, and the EVs contain elevated levels of miR122,

TABLE 1 Biosynthesis of secreted extracellular vesicles by hepatocytes.

Molecules	role	liver disease model	references
miR-3075	promote insulin sensitivity, promote proinflammatory activation of macrophages	a HFD diet induced-obesity model	(64)
mtDNA	activate TLR9 on Kupffer cells	Experimental NASH model induced by HFD diet	(56)
ceramides	activate macrophage chemotaxis	hepatocytes treated with palmitate, a HFD diet model with hepatocyte-specific disruption of Ire1a	(27, 65)
TRAIL	activate an inflammatory phenotype in macrophages	hepatocytes treated with palmitate, Experimental NASH model induced by HFD diet	(66)
CXCL10	induce macrophage chemotaxis	hepatocytes treated with palmitate or LPC, a FFC diet-fed Mlk3 deficient mice	(67)
miR-192-5p	activate an inflammatory phenotype in macrophages	Experimental NASH model induced by high-fat high-cholesterol diet	(68)
miR122	activate an inflammatory phenotype in macrophages, potential diagnostic markers	patients with alcoholic hepatitis Experimental AH model induced by alcohol-fed mice	(69, 70)
miR192	potential diagnostic markers	patients with alcoholic hepatitis Experimental AH model induced by alcohol-fed mice	(69)
miR309	potential diagnostic markers	patients with alcoholic hepatitis Experimental AH model induced by alcohol-fed mice	(69)
CD40ligand	activate an inflammatory phenotype in macrophages	Experimental AH model induced by alcohol-fed mice	(71)
HCV RNA	mediate viral transmission to naive hepatocytes, transfer immunomodulatory viral RNA to neighboring immune cells, trigger myeloid- derived suppressor cell expansion, induce apoptosis of hepatitis C virus-specific T cells,	hepatitis C virus-infected hepatocytes chronic HCV infected patients	(72–74)
HBV nucleic acids and proteins	induce active infection in naive human hepatocytes, transmit into NK cells and lead to NK-cell dysfunction, stimulate IFN-γ from NK cells and suppress IL-12p35 mRNA expression, transfer of antiviral molecules from liver nonparenchymal cells to hepatocytes	hepatitis B virus-infected hepatocytes chronic HBV infected patients	(75, 76)

HFD, high fat diet; LPC, lysophosphatidylcholine; FFC, fat, fructose and cholesterol.

miR192 and miR309 (69). Hepatocyte-derived EVs modulate activation of liver marcophages by transferring miRNA-122 and CD40ligand after alcohol exposure (70, 71). In addition, it is reported that exosomes isolated from sera of chronic HBV and HCV infected patients or supernatants of those hepatocytes contain viral RNA, which can mediate viral transmission to naive hepatocytes (72, 75). These hepatic derived-exosomes involve in host innate immune response and virus-mediated immunosuppression. HCV-associated exosomes can transfer immunomodulatory viral RNA from infected cells to neighboring immune cells and trigger myeloid-derived suppressor cell expansion (73). EVs from hepatitis C virus-infected cells stimulate monocytes to produce galectin-9, which induces apoptosis of hepatitis C virus-specific T cells and increases inhibitory regulatory T cells (74). Similarly, HBV components are observed to be transmitted into NK cells by exosomes, resulting in NK-cell dysfunction (75). Exosomes also can regulate innate immune response against HBV through inducing NKG2D ligand expression in macrophages, which stimulates IFN-γ from NK cells, and suppressing IL-12p35 mRNA expression to counteract he host innate immune response (76). In a word, EVs exert a crucial role on the crosstalk between hepatocytes and nonparenchymal liver cells.

5.2 Hepatic cytokines involved in liver inflammation

Hepatocytes can produce diverse cytokines to regulate liver injury, repair, and inflammation in liver injury. Here, we make a summary of cytokines that involved in the pathogenesis of chronic liver diseases below.

IL-6 can be synthesized by hepatocytes in response to specific stimuli to induce acute phase response, it implicates in the liver regeneration following partial hepatectomy and exerts antiviral effects on limiting the replication of HBV in hepatocytes (78, 79). Moreover, substantial studies show that IL-6 trans-signaling promotes inflammation in chronic liver diseases (80). Excessive lipid accumulation in hepatocytes stimulates IL11 protein secretion, autocrine IL11 activity drives lipotoxicity and underlies the transition from NAFLD to NASH (81). Interleukin 33 (IL-33) functions as an “alarmin” released from hepatocytes in response to tissue damages. It exerts protective effects on hepatocytes through the activation of autophagy and suppression of cell death, meanwhile, it

regulates host innate immunity by recruitment and activation of ST2-positive target immune cells in the liver (82). Furthermore, it is responsible for repressing viral transcription, protein production and genome replication in HBV-infected hepatocytes (83). IL-32 is markedly induced in hepatocytes in various liver diseases. It plays an important role in inflammatory response by promoting proinflammatory cytokines such as IL-1β and tumor necrosis factor alpha (TNF-α) (84, 85). IL32 also has a critical role in the pathogenesis of NAFLD, partly due to its association with hepatocyte insulin resistance and cholesterol homeostasis (86, 87). Besides, it can suppress HBV transcription and replication (88). Hepatocyte also can produce several chemokines to attract immune cells in response to liver injury. For example, hepatocyte can express chemokine MCP-1, which recruits macrophages to promote liver steatosis and inflammation in alcoholic and non-alcoholic fatty liver disease. Moreover, hepatic MCP-1 expression is found to regulate fatty acid oxidation resulting in steatosis during chronic alcohol exposure (89, 90). Apart from the above, hepatocytes can secrete high amounts of CXCL1, leading to hepatic neutrophil infiltration through TLR2 and TLR9-dependent pathway in alcohol-mediated liver injury (91). Hepatocyte is the main source for necrotic cell-induced CXCL1 production, which dependent of NF-κB activation by Kupffer cells, resulting in neutrophils mobilization and finally clearing dead cells (92). Another study shows that hepatocyte-specific gp130 signaling is sufficient to induce CXCL1 expression, independent of NF-κB activation, triggering a robust systemic innate immune response (93). Steatotic hepatocytes also can stimulate IL-8 production, an active neutrophil chemoattractant, potentially contributing to hepatic inflammation (94).

5.3 Role of hepatocytes in antigen-presentation

In clinical hepatitis, viral or autoimmune especially, hepatocytes can directly modulate immune cells *via* cell-cell interactions. Hepatocytes could function as nonprofessional APCs because they express MHC class II during inflammation. MHC-II overexpressing hepatocytes are capable of activating CD4+ T-cells *in vitro*, but they only induce T helper cell (Th) 2 differentiation, which impair antiviral CD8 T-cell responses and viral clearance (95, 96). Hepatocytes appear to play a role in the liver tolerogenic effect. They can activate CD8+ T cells in a manner that leads to apoptosis of these cells since lack of either costimulatory signals or CD4+ T cell help (97). What's more, the hepatocytes may endocytose and kill CD8+ T cells that recognize them, a process known as suicidal emperipolesis (98). In viral infection, virus-positive hepatocytes can be eliminated by activated circulating CD8+ T-cells through directly recognizing antigen on hepatocytes, leading to CD8+T-cell exhaustion (99). Among the underlying mechanism, Notch signaling may performed an important regulatory role in the interaction between hepatocytes and T cells activation. It is reported hepatocytes fine -tune liver inflammation by upregulation of Jagged1 and activation of Notch signaling in Th1 cells, resulting in induction of IL10-producing CD4+ T cells (100). Besides, Notch signaling contributes to liver inflammation by regulation of interleukin-22-producing cells in hepatitis B virus infection (101). In addition, hepatocytes may induce tolerance *via* Notch-mediated conversion of CD4(+) T cells into Foxp3(+) Tregs upon TCR stimulation (102). Apart from these, intercellular adhesion molecule 1 (ICAM-1) is involved in CD4+ T cell engulfment by hepatocytes and huh-7 cells by facilitating T cell early adhesion and internalization (103).

6 Conclusion

A growing number of evidences have demonstrated stressed hepatocytes exert a pivotal role on the development of inflammation and fibrosis *via* cell-cell interactions during liver injury. In this review, we summarize the role of hepatic organelle disorders in the pathogenesis of chronic liver diseases, especially, their links to liver inflammation. Furthermore, we introduce a wide variety of pro-inflammatory signals carried by hepatocyte derived-EVs that can deliver the message to neighbor target cells and in the circulation to modulate immune response. Besides, we conclude several cytokines and chemokines of hepatocyte origin which engage in chronic liver diseases. Finally, we address briefly antigen-presentation properties of hepatocytes in immune regulation. Understanding of the molecular mechanisms involved in the regulation of hepatic organelle damage, as well as role of hepatocyte in immune regulation may provide us novel insights of dysregulated inflammation during liver injury and identify new therapeutic targets for various liver diseases.

Author contributions

JG and JL contributed to select the topic of the manuscript. WT collected relevant literature. JG wrote the manuscript. JL and DT reviewed and edited the final version of manuscript. All authors contributed to the article and approved the submitted version.

Funding

This study was supported by grants from the National Natural Science Foundation of China (No. 81900504).

Conflict of interest

The authors declare that the research was conducted in the absence of any commercial or financial relationships that could be construed as a potential conflict of interest.

Publisher's note

References

1. Asrani SK, Devarbhavi H, Eaton J, Kamath PS. Burden of liver diseases in the world. *J Hepatol* (2019) 70(1):20. doi: 10.1016/j.jhep.2018.09.014

2. Tu T, Calabro SR, Lee A, Maczurek AE, Budzinska MA, Warner FJ, et al. Hepatocytes in liver injury: Victim, bystander, or accomplice in progressive fibrosis? *J Gastroenterol Hepatol* (2015) 30(12):1696–704. doi: 10.1111/jgh.13065

3. Wree A, Holtmann TM, Inzaugarat ME, Feldstein AE. Novel drivers of the inflammatory response in liver injury and fibrosis. *Semin Liver Dis* (2019) 39(3):275–82. doi: 10.1055/s-0039-1685515

4. Rinella ME. Nonalcoholic fatty liver disease: A systematic review. *Jama* (2015) 313 (22):2263–73. doi: 10.1001/jama.2015.5370

5. Luedde T, Kaplowitz N, Schwabe RF. Cell death and cell death responses in liver disease: Mechanisms and clinical relevance. *Gastroenterology* (2014) 147(4):765–83.e4. doi: 10.1053/j.gastro.2014.07.018

6. Zhou Z, Xu MJ, Gao B. Hepatocytes: A key cell type for innate immunity. *Cell Mol Immunol* (2016) 13(3):301–15. doi: 10.1038/cmi.2015.97

7. Seki E, Schwabe RF. Hepatic inflammation and fibrosis: Functional links and key pathways. *Hepatology* (2015) 61(3):1066–79. doi: 10.1002/hep.27332

8. Malhi H, Kaufman RJ. Endoplasmic reticulum stress in liver disease. *J Hepatol* (2011) 54(4):795–809. doi: 10.1016/j.jhep.2010.11.005

9. Mollica MP, Lionetti L, Putti R, Cavaliere G, Gaita M, Barletta A. From chronic overfeeding to hepatic injury: Role of endoplasmic reticulum stress and inflammation. *Nutr Metab Cardiovasc Dis* (2011) 21(3):222–30. doi: 10.1016/j.numecd.2010.10.012

10. Liu C, Zhou B, Meng M, Zhao W, Wang D, Yuan Y, et al. FOXA3 induction under endoplasmic reticulum stress contributes to non-alcoholic fatty liver disease. *J Hepatol* (2021) 75(1):150–62. doi: 10.1016/j.jhep.2021.01.042

11. Gregor MF, Yang L, Fabbrini E, Mohammed BS, Eagon JC, Hotamisligil GS, et al. Endoplasmic reticulum stress is reduced in tissues of obese subjects after weight loss. *Diabetes* (2009) 58(3):693–700. doi: 10.2337/db08-1220

12. Gonzalez-Rodriguez A, Mayoral R, Agra N, Valdecantos MP, Pardo V, Miquilena-Colina ME, et al. Impaired autophagic flux is associated with increased endoplasmic reticulum stress during the development of NAFLD. *Cell Death Dis* (2014) 5:e1179. doi: 10.1038/cddis.2014.162

13. Wang X, Wei Z, Cheng B, Li J, He Y, Lan T, et al. Endoplasmic reticulum stress promotes HBV production by enhancing use of the autophagosome/multivesicular body axis. *Hepatology* (2022) 75(2):438–54. doi: 10.1002/hep.32178

14. Joyce MA, Walters KA, Lamb SE, Yeh MM, Zhu LF, Kneteman N, et al. HCV induces oxidative and ER stress, and sensitizes infected cells to apoptosis in SCID/Alb-uPA mice. *PloS Pathog* (2009) 5(2):e1000291. doi: 10.1371/journal.ppat.1000291

15. Merquiol E, Uzi D, Mueller T, Goldenberg D, Nahmias Y, Xavier RJ, et al. HCV causes chronic endoplasmic reticulum stress leading to adaptation and interference with the unfolded protein response. *PloS One* (2011) 6(9):e24660. doi: 10.1371/journal.pone.0024660

16. Asselah T, Bieche I, Mansouri A, Laurendeau I, Cazals-Hatem D, Feldmann G, et al. *In vivo* hepatic endoplasmic reticulum stress in patients with chronic hepatitis c. *J Pathol* (2010) 221(3):264–74. doi: 10.1002/path.2703

17. Han CY, Lim SW, Koo JH, Kim W, Kim SG. PHLDA3 overexpression in hepatocytes by endoplasmic reticulum stress *via* IRE1-Xbp1s pathway expedites liver injury. *Gut* (2016) 65(8):1377–88. doi: 10.1136/gutjnl-2014-308506

18. Petrasek J, Iracheta-Vellve A, Csak T, Satishchandran A, Kodys K, Kurt-Jones EA, et al. STING-IRF3 pathway links endoplasmic reticulum stress with hepatocyte apoptosis in early alcoholic liver disease. *Proc Natl Acad Sci USA* (2013) 110(41):16544–9. doi: 10.1073/pnas.1308331110

19. Li X, Wang Y, Wang H, Huang C, Huang Y, Li J. Endoplasmic reticulum stress is the crossroads of autophagy, inflammation, and apoptosis signaling pathways and participates in liver fibrosis. *Inflammation Res* (2015) 64(1):1–7. doi: 10.1007/s00011-014-0772-y

20. Hirosumi J, Tuncman G, Chang L, Gorgun CZ, Uysal KT, Maeda K, et al. A central role for JNK in obesity and insulin resistance. *Nature* (2002) 420(6913):333–6. doi: 10.1038/nature01137

21. Luedde T, Schwabe RF. NF-kappaB in the liver–linking injury, fibrosis and hepatocellular carcinoma. *Nat Rev Gastroenterol Hepatol* (2011) 8(2):108–18. doi: 10.1038/nrgastro.2010.213

22. Lebeaupin C, Vallee D, Hazari Y, Hetz C, Chevet E, Bailly-Maitre B. Endoplasmic reticulum stress signalling and the pathogenesis of non-alcoholic fatty liver disease. *J Hepatol* (2018) 69(4):927–47. doi: 10.1016/j.jhep.2018.06.008

23. Scrima R, Piccoli C, Moradpour D, Capitanio N. Targeting endoplasmic reticulum and/or mitochondrial Ca(2+) fluxes as therapeutic strategy for HCV infection. *Front Chem* (2018) 6:73. doi: 10.3389/fchem.2018.00073

24. Tsuge M, Hiraga N, Zhang Y, Yamashita M, Sato O, Oka N, et al. Endoplasmic reticulum-mediated induction of interleukin-8 occurs by hepatitis b virus infection and contributes to suppression of interferon responsiveness in human hepatocytes. *Virology* (2018) 525:48–61. doi: 10.1016/j.virol.2018.08.020

25. Han CY, Rho HS, Kim A, Kim TH, Jang K, Jun DW, et al. FXR inhibits endoplasmic reticulum stress-induced NLRP3 inflammasome in hepatocytes and ameliorates liver injury. *Cell Rep* (2018) 24(11):2985–99. doi: 10.1016/j.celrep.2018.07.068

26. Lebeaupin C, Proics E, de Bieville CH, Rousseau D, Bonnafous S, Patouraux S, et al. ER stress induces NLRP3 inflammasome activation and hepatocyte death. *Cell Death Dis* (2015) 6:e1879. doi: 10.1038/cddis.2015.248

27. Dasgupta D, Nakao Y, Mauer AS, Thompson JM, Sehrawat TS, Liao CY, et al. IRE1A stimulates hepatocyte-derived extracellular vesicles that promote inflammation in mice with steatohepatitis. *Gastroenterology* (2020) 159(4):1487–503.e17. doi: 10.1053/j.gastro.2020.06.031

28. Gual P, Gilgenkrantz H, Lotersztajn S. Autophagy in chronic liver diseases: The two faces of janus. *Am J Physiol Cell Physiol* (2017) 312(3):C263–C73. doi: 10.1152/ajpcell.00295.2016

29. Singh R, Kaushik S, Wang Y, Xiang Y, Novak I, Komatsu M, et al. Autophagy regulates lipid metabolism. *Nature* (2009) 458(7242):1131–5. doi: 10.1038/nature07976

30. Shen Y, Malik SA, Amir M, Kumar P, Cingolani F, Wen J, et al. Decreased hepatocyte autophagy leads to synergistic IL-1beta and TNF mouse liver injury and inflammation. *Hepatology* (2020) 72(2):595–608. doi: 10.1002/hep.31209

31. Czaja MJ, Ding WX, Donohue TMJr., Friedman SL, Kim JS, Komatsu M, et al. Functions of autophagy in normal and diseased liver. *Autophagy* (2013) 9(8):1131–58. doi: 10.4161/auto.25063

32. Zhou B, Kreuzer J, Kumsta C, Wu L, Kamer KJ, Cedillo L, et al. Mitochondrial permeability uncouples elevated autophagy and lifespan extension. *Cell* (2019) 177 (2):299–314.e16. doi: 10.1016/j.cell.2019.02.013

33. Amir M, Zhao E, Fontana L, Rosenberg H, Tanaka K, Gao G, et al. Inhibition of hepatocyte autophagy increases tumor necrosis factor-dependent liver injury by promoting caspase-8 activation. *Cell Death Differ* (2013) 20(7):878–87. doi: 10.1038/cdd.2013.21

34. Francis H, Wu N, Alpini G, Meng F. Hepatocyte autophagy: Maintaining a toxic-free environment. *Hepatology* (2020) 72(2):371–4. doi: 10.1002/hep.31219

35. Ding WX, Li M, Chen X, Ni HM, Lin CW, Gao W, et al. Autophagy reduces acute ethanol-induced hepatotoxicity and steatosis in mice. *Gastroenterology* (2010) 139 (5):1740–52. doi: 10.1053/j.gastro.2010.07.041

36. Lin CW, Zhang H, Li M, Xiong X, Chen X, Chen X, et al. Pharmacological promotion of autophagy alleviates steatosis and injury in alcoholic and non-alcoholic fatty liver conditions in mice. *J Hepatol* (2013) 58(5):993–9. doi: 10.1016/j.jhep.2013.01.011

37. Chao X, Wang S, Zhao K, Li Y, Williams JA, Li T, et al. Impaired TFEB-mediated lysosome biogenesis and autophagy promote chronic ethanol-induced liver injury and steatosis in mice. *Gastroenterology* (2018) 155(3):865–79.e12. doi: 10.1053/j.gastro.2018.05.027

38. Zhou Y, Wu R, Wang X, Jiang Y, Xu W, Shao Y, et al. Activation of UQCRC2-dependent mitophagy by tetramethylpyrazine inhibits MLKL-mediated hepatocyte necroptosis in alcoholic liver disease. *Free Radic Biol Med* (2022) 179:301–16. doi: 10.1016/j.freeradbiomed.2021.11.008

39. Lu X, Xuan W, Li J, Yao H, Huang C, Li J. AMPK protects against alcohol-induced liver injury through UQCRC2 to up-regulate mitophagy. *Autophagy* (2021) 17(11):3622–43. doi: 10.1080/15548627.2021.1886829

40. Lin Y, Zhao Z, Huang A, Lu M. Interplay between cellular autophagy and hepatitis b virus replication: A systematic review. *Cells* (2020) 9(9). doi: 10.3390/cells9092101

41. Tian Y, Sir D, Kuo CF, Ann DK, Ou JH. Autophagy required for hepatitis b virus replication in transgenic mice. *J Virol* (2011) 85(24):13453–6. doi: 10.1128/JVI.06064-11

42. Miyakawa K, Nishi M, Ogawa M, Matsunaga S, Sugiyama M, Nishitsuji H, et al. Galectin-9 restricts hepatitis b virus replication *via* p62/SQSTM1-mediated selective autophagy of viral core proteins. *Nat Commun* (2022) 13(1):531. doi: 10.1038/s41467-022-28171-5

43. Kunanopparat A, Hirankarn N, Kittigul C, Tangkijvanich P, Kimkong I. Autophagy machinery impaired interferon signalling pathways to benefit hepatitis b virus replication. *Asian Pac J Allergy Immunol* (2016) 34(1):77–85. doi: 10.12932/AP0636.34.1.2016

44. Luo MX, Wong SH, Chan MT, Yu L, Yu SS, Wu F, et al. Autophagy mediates HBx-induced nuclear factor-kappaB activation and release of IL-6, IL-8, and CXCL2 in hepatocytes. *J Cell Physiol* (2015) 230(10):2382–9. doi: 10.1002/jcp.24967

45. Chu JYK, Ou JJ. Autophagy in HCV replication and protein trafficking. *Int J Mol Sci* (2021) 22(3). doi: 10.3390/ijms22031089

46. Chan ST, Ou JJ. Hepatitis c virus-induced autophagy and host innate immune response. *Viruses* (2017) 9(8). doi: 10.3390/v9080224

47. Chan ST, Lee J, Narula M, Ou JJ. Suppression of host innate immune response by hepatitis c virus *via* induction of autophagic degradation of TRAF6. *J Virol* (2016) 90 (23):10928–35. doi: 10.1128/JVI.01365-16

48. Ke PY, Chen SS. Activation of the unfolded protein response and autophagy after hepatitis c virus infection suppresses innate antiviral immunity *in vitro*. *J Clin Invest* (2011) 121(1):37–56. doi: 10.1172/JCI41474

49. Kim SJ, Syed GH, Khan M, Chiu WW, Sohail MA, Gish RG, et al. Hepatitis c virus triggers mitochondrial fission and attenuates apoptosis to promote viral persistence. *Proc Natl Acad Sci USA* (2014) 111(17):6413–8. doi: 10.1073/pnas.1321114111

50. Szekerczes T, Gogl A, Illyes I, Mandl J, Borka K, Kiss A, et al. Autophagy, mitophagy and MicroRNA expression in chronic hepatitis c and autoimmune hepatitis. *Pathol Oncol Res* (2020) 26(4):2143–51. doi: 10.1007/s12253-020-00799-y

51. Mottis A, Herzig S, Auwerx J. Mitocellular communication: Shaping health and disease. *Science* (2019) 366(6467):827–32. doi: 10.1126/science.aax3768

52. Mansouri A, Gattolliat CH, Asselah T. Mitochondrial dysfunction and signaling in chronic liver diseases. *Gastroenterology* (2018) 155(3):629–47. doi: 10.1053/j.gastro.2018.06.083

53. Youle RJ. Mitochondria-striking a balance between host and endosymbiont. *Science* (2019) 365(6454). doi: 10.1126/science.aaw9855

54. Koliaki C, Szendroedi J, Kaul K, Jelenik T, Nowotny P, Jankowiak F, et al. Adaptation of hepatic mitochondrial function in humans with non-alcoholic fatty liver is lost in steatohepatitis. *Cell Metab* (2015) 21(5):739–46. doi: 10.1016/j.cmet.2015.04.004

55. An P, Wei LL, Zhao S, Sverdlov DY, Vaid KA, Miyamoto M, et al. Hepatocyte mitochondria-derived danger signals directly activate hepatic stellate cells and drive progression of liver fibrosis. *Nat Commun* (2020) 11(1):2362. doi: 10.1038/s41467-020-16092-0

56. Garcia-Martinez I, Santoro N, Chen Y, Hoque R, Ouyang X, Caprio S, et al. Hepatocyte mitochondrial DNA drives nonalcoholic steatohepatitis by activation of TLR9. *J Clin Invest* (2016) 126(3):859–64. doi: 10.1172/JCI83885

57. Hou J, Zhang J, Cui P, Zhou Y, Liu C, Wu X, et al. TREM2 sustains macrophage-hepatocyte metabolic coordination in nonalcoholic fatty liver disease and sepsis. *J Clin Invest* (2021) 131(4). doi: 10.1172/JCI135197

58. Hernandez-Alvarez MI, Sebastian D, Vives S, Ivanova S, Bartoccioni P, Kakimoto P, et al. Deficient endoplasmic reticulum-mitochondrial phosphatidylserine transfer causes liver disease. *Cell* (2019) 177(4):881–95.e17. doi: 10.1016/j.cell.2019.04.010

59. He GW, Gunther C, Kremer AE, Thonn V, Amann K, Poremba C, et al. PGAM5-mediated programmed necrosis of hepatocytes drives acute liver injury. *Gut* (2017) 66 (4):716–23. doi: 10.1136/gutjnl-2015-311247

60. Hao L, Zhong W, Dong H, Guo W, Sun X, Zhang W, et al. ATF4 activation promotes hepatic mitochondrial dysfunction by repressing NRF1-TFAM signalling in alcoholic steatohepatitis. *Gut* (2021) 70(10):1933–45. doi: 10.1136/gutjnl-2020-321548

61. Li XD, Sun L, Seth RB, Pineda G, Chen ZJ. Hepatitis c virus protease NS3/4A cleaves mitochondrial antiviral signaling protein off the mitochondria to evade innate immunity. *Proc Natl Acad Sci USA* (2005) 102(49):17717–22. doi: 10.1073/pnas.0508531102

62. Waris G, Huh KW, Siddiqui A. Mitochondrially associated hepatitis b virus X protein constitutively activates transcription factors STAT-3 and NF-kappa b *via* oxidative stress. *Mol Cell Biol* (2001) 21(22):7721–30. doi: 10.1128/MCB.21.22.7721-7730.2001

63. Kostallari E, Valainathan S, Biquard L, Shah VH, Rautou PE. Role of extracellular vesicles in liver diseases and their therapeutic potential. *Adv Drug Delivery Rev* (2021) 175:113816. doi: 10.1016/j.addr.2021.05.026

64. Ji Y, Luo Z, Gao H, Dos Reis FCG, Bandyopadhyay G, Jin Z, et al. Hepatocyte-derived exosomes from early onset obese mice promote insulin sensitivity through miR-3075. *Nat Metab* (2021) 3(9):1163–74. doi: 10.1038/s42255-021-00444-1

65. Kakazu E, Mauer AS, Yin M, Malhi H. Hepatocytes release ceramide-enriched pro-inflammatory extracellular vesicles in an IRE1alpha-dependent manner. *J Lipid Res* (2016) 57(2):233–45. doi: 10.1194/jlr.M063412

66. Hirsova P, Ibrahim SH, Krishnan A, Verma VK, Bronk SF, Werneburg NW, et al. Lipid-induced signaling causes release of inflammatory extracellular vesicles from hepatocytes. *Gastroenterology* (2016) 150(4):956–67. doi: 10.1053/j.gastro.2015.12.037

67. Ibrahim SH, Hirsova P, Tomita K, Bronk SF, Werneburg NW, Harrison SA, et al. Mixed lineage kinase 3 mediates release of c-X-C motif ligand 10-bearing chemotactic extracellular vesicles from lipotoxic hepatocytes. *Hepatology* (2016) 63(3):731–44. doi: 10.1002/hep.28252

68. Liu XL, Pan Q, Cao HX, Xin FZ, Zhao ZH, Yang RX, et al. Lipotoxic hepatocyte-derived exosomal MicroRNA 192-5p activates macrophages through Rictor/Akt/Forkhead box transcription factor O1 signaling in nonalcoholic fatty liver disease. *Hepatology* (2020) 72(2):454–69. doi: 10.1002/hep.31050

69. Momen-Heravi F, Saha B, Kodys K, Catalano D, Satishchandran A, Szabo G. Increased number of circulating exosomes and their microRNA cargos are potential novel biomarkers in alcoholic hepatitis. *J Transl Med* (2015) 13:261. doi: 10.1186/s12967-015-0623-9

70. Momen-Heravi F, Bala S, Kodys K, Szabo G. Exosomes derived from alcohol-treated hepatocytes horizontally transfer liver specific miRNA-122 and sensitize monocytes to LPS. *Sci Rep* (2015) 5:9991. doi: 10.1038/srep09991

71. Verma VK, Li H, Wang R, Hirsova P, Mushref M, Liu Y, et al. Alcohol stimulates macrophage activation through caspase-dependent hepatocyte derived release of CD40L containing extracellular vesicles. *J Hepatol* (2016) 64(3):651–60. doi: 10.1016/j.jhep.2015.11.020

72. Bukong TN, Momen-Heravi F, Kodys K, Bala S, Szabo G. Exosomes from hepatitis c infected patients transmit HCV infection and contain replication competent viral RNA in complex with Ago2-miR122-HSP90. *PloS Pathog* (2014) 10(10):e1004424. doi: 10.1371/journal.ppat.1004424

73. Wang L, Cao D, Wang L, Zhao J, Nguyen LN, Dang X, et al. HCV-associated exosomes promote myeloid-derived suppressor cell expansion *via* inhibiting miR-124 to regulate T follicular cell differentiation and function. *Cell Discov* (2018) 4:51. doi: 10.1038/s41421-018-0052-z

74. Harwood NM, Golden-Mason L, Cheng L, Rosen HR, Mengshol JA. HCV-infected cells and differentiation increase monocyte immunoregulatory galectin-9 production. *J Leukoc Biol* (2016) 99(3):495–503. doi: 10.1189/jlb.5A1214-582R

75. Yang Y, Han Q, Hou Z, Zhang C, Tian Z, Zhang J. Exosomes mediate hepatitis b virus (HBV) transmission and NK-cell dysfunction. *Cell Mol Immunol* (2017) 14(5):465–75. doi: 10.1038/cmi.2016.24

76. Kouwaki T, Fukushima Y, Daito T, Sanada T, Yamamoto N, Mifsud EJ, et al. Extracellular vesicles including exosomes regulate innate immune responses to hepatitis b virus infection. *Front Immunol* (2016) 7:335. doi: 10.3389/fimmu.2016.00335

77. Ibrahim SH, Hirsova P, Gores GJ. Non-alcoholic steatohepatitis pathogenesis: sublethal hepatocyte injury as a driver of liver inflammation. *Gut* (2018) 67(5):963–72. doi: 10.1136/gutjnl-2017-315691

78. Fazel Modares N, Polz R, Haghighi F, Lamertz L, Behnke K, Zhuang Y, et al. IL-6 trans-signaling controls liver regeneration after partial hepatectomy. *Hepatology* (2019) 70(6):2075–91. doi: 10.1002/hep.30774

79. Palumbo GA, Scisciani C, Pediconi N, Lupacchini L, Alfalate D, Guerrieri F, et al. IL6 inhibits HBV transcription by targeting the epigenetic control of the nuclear cccDNA minichromosome. *PloS One* (2015) 10(11):e0142599. doi: 10.1371/journal.pone.0142599

80. Giraldez MD, Carneros D, Garbers C, Rose-John S, Bustos M. New insights into IL-6 family cytokines in metabolism, hepatology and gastroenterology. *Nat Rev Gastroenterol Hepatol* (2021) 18(11):787–803. doi: 10.1038/s41575-021-00473-x

81. Dong J, Viswanathan S, Adami E, Singh BK, Chothani SP, Ng B, et al. Hepatocyte-specific IL11 cis-signaling drives lipotoxicity and underlies the transition from NAFLD to NASH. *Nat Commun* (2021) 12(1):66. doi: 10.1038/s41467-020-20303-z

82. Arshad MI, Piquet-Pellorce C, Samson M. IL-33 and HMGB1 alarmins: sensors of cellular death and their involvement in liver pathology. *Liver Int* (2012) 32(8):1200–10. doi: 10.1111/j.1478-3231.2012.02802.x

83. Gao Z, Shen Z, Wu J, Song Y, Liu N, Deng Q, et al. Interleukin-33 mediates both immune-related and non-immune-related inhibitory effects against hepatitis b virus. *Antiviral Res* (2022) 206:105404. doi: 10.1016/j.antiviral.2022

84. Pan X, Cao H, Lu J, Shu X, Xiong X, Hong X, et al. Interleukin-32 expression induced by hepatitis b virus protein X is mediated through activation of NF-kappaB. *Mol Immunol* (2011) 48(12-13):1573–7. doi: 10.1016/j.molimm.2011.03.012

85. Moschen AR, Fritz T, Clouston AD, Rebhan I, Bauhofer O, Barrie HD, et al. Interleukin-32: A new proinflammatory cytokine involved in hepatitis c virus-related liver inflammation and fibrosis. *Hepatology* (2011) 53(6):1819–29. doi: 10.1002/hep.24285

86. Dali-Youcef N, Vix M, Costantino F, El-Saghire H, Lhermitte B, Callari C, et al. Interleukin-32 contributes to human nonalcoholic fatty liver disease and insulin resistance. *Hepatol Commun* (2019) 3(9):1205–20. doi: 10.1002/hep4.1396

87. Damen M, Dos Santos JC, Hermsen R, Adam van der Vliet J, Netea MG, Riksen NP, et al. Interleukin-32 upregulates the expression of ABCA1 and ABCG1 resulting in reduced intracellular lipid concentrations in primary human hepatocytes. *Atherosclerosis* (2018) 271:193–202. doi: 10.1016/j.atherosclerosis.2018.02.027

88. Kim DH, Park ES, Lee AR, Park S, Park YK, Ahn SH, et al. Intracellular interleukin-32gamma mediates antiviral activity of cytokines against hepatitis b virus. *Nat Commun* (2018) 9(1):3284. doi: 10.1038/s41467-018-05782-5

89. Obstfeld AE, Sugaru E, Thearle M, Francisco AM, Gayet C, Ginsberg HN, et al. C-c chemokine receptor 2 (CCR2) regulates the hepatic recruitment of myeloid cells that promote obesity-induced hepatic steatosis. *Diabetes* (2010) 59(4):916–25. doi: 10.2337/db09-1403

90. Mandrekar P, Ambade A, Lim A, Szabo G, Catalano D. An essential role for monocyte chemoattractant protein-1 in alcoholic liver injury: Regulation of proinflammatory cytokines and hepatic steatosis in mice. *Hepatology* (2011) 54 (6):2185–97. doi: 10.1002/hep.24599

91. Roh YS, Zhang B, Loomba R, Seki E. TLR2 and TLR9 contribute to alcohol-mediated liver injury through induction of CXCL1 and neutrophil infiltration. *Am J Physiol Gastrointest Liver Physiol* (2015) 309(1):G30–41. doi: 10.1152/ajpgi.00031.2015

92. Su L, Li N, Tang H, Lou Z, Chong X, Zhang C, et al. Kupffer cell-derived TNF-alpha promotes hepatocytes to produce CXCL1 and mobilize neutrophils in response to necrotic cells. *Cell Death Dis* (2018) 9(3):323. doi: 10.1038/s41419-018-0377-4

93. Schumacher N, Yan K, Gandrass M, Muller M, Krisp C, Hasler R, et al. Cell-autonomous hepatocyte-specific GP130 signaling is sufficient to trigger a robust innate immune response in mice. *J Hepatol* (2021) 74(2):407–18. doi: 10.1016/j.jhep.2020.09.021

94. Joshi-Barve S, Barve SS, Amancherla K, Gobejishvili L, Hill D, Cave M, et al. Palmitic acid induces production of proinflammatory cytokine interleukin-8 from hepatocytes. *Hepatology* (2007) 46(3):823–30. doi: 10.1002/hep.21752

95. Herkel J, Jagemann B, Wiegard C, Lazaro JF, Lueth S, Kanzler S, et al. MHC class II-expressing hepatocytes function as antigen-presenting cells and activate specific CD4 T lymphocytes. *Hepatology* (2003) 37(5):1079–85. doi: 10.1053/jhep.2003.50191

96. Wiegard C, Wolint P, Frenzel C, Cheruti U, Schmitt E, Oxenius A, et al. Defective T helper response of hepatocyte-stimulated CD4 T cells impairs antiviral CD8 response and viral clearance. *Gastroenterology* (2007) 133(6):2010–8. doi: 10.1053/j.gastro.2007.09.007

97. Bertolino P, Trescol-Biemont MC, Rabourdin-Combe C. Hepatocytes induce functional activation of naive CD8+ T lymphocytes but fail to promote survival. *Eur J Immunol* (1998) 28(1):221–36. doi: 10.1002/(SICI)1521-4141(199801)28:01<221::AID-IMMU221>3.0.CO;2-F

98. Crispe IN. Hepatocytes as immunological agents. *J Immunol* (2016) 196(1):17–21. doi: 10.4049/jimmunol.1501668

99. Mehrfeld C, Zenner S, Kornek M, Lukacs-Kornek V. The contribution of non-professional antigen-presenting cells to immunity and tolerance in the liver. *Front Immunol* (2018) 9:635. doi: 10.3389/fimmu.2018.00635

100. Burghardt S, Erhardt A, Claass B, Huber S, Adler G, Jacobs T, et al. Hepatocytes contribute to immune regulation in the liver by activation of the notch signaling pathway in T cells. *J Immunol* (2013) 191(11):5574–82. doi: 10.4049/jimmunol.1300826

101. Wei X, Wang JP, Hao CQ, Yang XF, Wang LX, Huang CX, et al. Notch signaling contributes to liver inflammation by regulation of interleukin-22-Producing cells in hepatitis b virus infection. *Front Cell Infect Microbiol* (2016) 6:132. doi: 10.3389/fcimb.2016.00132

102. Burghardt S, Claass B, Erhardt A, Karimi K, Tiegs G. Hepatocytes induce Foxp3 (+) regulatory T cells by notch signaling. *J Leukoc Biol* (2014) 96(4):571–7. doi: 10.1189/jlb.2AB0613-342RR

103. Davies SP, Reynolds GM, Wilkinson AL, Li X, Rose R, Leekha M, et al. Hepatocytes delete regulatory T cells by enclysis, a CD4(+) T cell engulfment process. *Cell Rep* (2019) 29(6):1610–20.e1614. doi: 10.1016/j.celrep.2019.09.068

frontiers | Frontiers in Immunology

TYPE Review
PUBLISHED 18 January 2023
DOI 10.3389/fimmu.2022.1095577

OPEN ACCESS

EDITED BY
Mirza S. Baig,
Indian Institute of Technology Indore, India

REVIEWED BY
Bettina Grötsch,
University Hospital Erlangen, Germany
Hua Ren,
East China Normal University, China

*CORRESPONDENCE
Yunhua Zhou
hzhuster@outlook.com
Xiangjie Liu
liuxiangjie1968@126.com

SPECIALTY SECTION
This article was submitted to Inflammation, a section of the journal Frontiers in Immunology

RECEIVED 11 November 2022
ACCEPTED 30 December 2022
PUBLISHED 18 January 2023

CITATION
Gao Z, Gao Z, Zhang H, Hou S, Zhou Y and Liu X (2023) Targeting STING: From antiviral immunity to treat osteoporosis. *Front. Immunol.* 13:1095577. doi: 10.3389/fimmu.2022.1095577

Targeting STING: From antiviral immunity to treat osteoporosis

Zhonghua Gao[1], Zhongguo Gao[2], Hao Zhang[1], Shoubo Hou[3], Yunhua Zhou[4]* and Xiangjie Liu[1]*

[1]Department of Geriatrics, Liyuan Hospital, Tongji Medical College, Huazhong University of Science and Technology, Wuhan, Hubei, China, [2]Department of Medical Laboratory Technology, School of Biomedical Engineering, Hubei University of Medicine, Shiyan, Hubei, China, [3]Department of General Practice, General Hospital of Central Theater Command, Wuhan, Hubei, China, [4]Department of Wound Repair Surgery, Liyuan Hospital, Tongji Medical College, Huazhong University of Science and Technology, Wuhan, Hubei, China

The cGAS-STING signaling pathway can trigger innate immune responses by detecting dsDNA from outside or within the host. In addition, the cGAS-STING signaling pathway has emerged as a critical mediator of the inflammatory response and a new target for inflammatory diseases. STING activation leads to dimerization and translocation to the endoplasmic reticulum Golgi intermediate compartment or Golgi apparatus catalyzed by TBK1, triggers the production of IRF3 and NF-κB and translocates to the nucleus to induce a subsequent interferon response and pro-inflammatory factor production. Osteoporosis is a degenerative bone metabolic disease accompanied by chronic sterile inflammation. Activating the STING/IFN-β signaling pathway can reduce bone resorption by inhibiting osteoclast differentiation. Conversely, activation of STING/NF-κB leads to the formation of osteoporosis by increasing bone resorption and decreasing bone formation. In addition, activation of STING inhibits the generation of type H vessels with the capacity to osteogenesis, thereby inhibiting bone formation. Here, we outline the mechanism of action of STING and its downstream in osteoporosis and discuss the role of targeting STING in the treatment of osteoporosis, thus providing new ideas for the treatment of osteoporosis.

KEYWORDS

osteoporosis, STING, IFN-β, NF-κB, type H vessels

1 Introduction

The stimulator of interferon genes (STING, also known as MITA, MPYS, ERIS, and TMEM173) is a pattern recognition receptor (PRR) that recognizes nucleic acids of pathogenic microorganisms or cell membrane components, among others (1). It acts as the first line of defense of cells against pathogenic invasion. Initially found in the endoplasmic reticulum (ER) membrane of the innate immune cells and later also found to be expressed in T cells and other cells, it recognizes released DNA and triggers innate immune activation with essential functions in infection, inflammation, and cancer (2). STING, a necessary protein of natural immunity, plays a crucial role in antiviral immunity by activating nuclear factor-

kappa B (NF-κB) and interferon regulatory factor 3 (IRF3) and producing type I interferon (IFN-I) independently of Toll-like receptors (TLRs, another type of PRR) (2).

The cGAS-STING in the innate immune response is vital in defending against pathogenic microbial invasion (3). In addition to its antiviral immune function, STING can cause inflammatory and autoimmune diseases (4). Activation of STING causes the transcription of inflammatory genes and increases pro-inflammatory cytokines. The increase of overpowering pro-inflammatory factors then causes inflammatory and autoimmune diseases (5). Therefore, STING is also the inflammatory protein that triggers chronic inflammation (6). The cGAS-STING pathway mediates the cellular inflammatory response and thus plays a crucial role in the pathogenesis of inflammatory diseases such as ischemic myocardial infarction (MI), nonalcoholic steatohepatitis (NASH), traumatic brain injury (TBI), and silicosis (7). A chronic low-grade inflammatory state accompanies aging. The cGAS-STING pathway can also induce the senescence-associated secretory phenotype (SASP) through the accumulation of cytoplasmic DNA during aging, which leads to the development of aging-related diseases (8).

Hundreds of millions worldwide are affected by bone-related diseases such as osteoporosis, degenerative disc disease, and rheumatoid arthritis. Osteoporosis is an age-related degenerative disease of bone, mainly due to changes in the bone microenvironment and structural degeneration, resulting in reduced bone density (9). It seriously endangers patients' quality of life and lives due to the extreme risk of fractures and others and causes a substantial financial burden on society. Osteoporosis is also a sterile inflammatory disease characterized by the activation of NF-κB at the molecular level, which promotes osteoclast-mediated bone resorption and inhibits osteoblast-induced bone formation (10). Notably, STING can act as an upstream of NF-κB, stimulating its activation and transcription, thus mediating pro-inflammatory effects and playing a role in the pathogenesis of osteoporosis (Figure 1). IFN-β is also a downstream target of STING. However, unlike NF-κB, although IFN-β is induced by STING activation in osteoclasts, it can inhibit osteoclast activation through negative feedback (11). In addition, STING can act on vascular endothelial cells (ECs) to regulate the formation of type H vessels, which can control bone formation. STING activation can impair their formation and thus affect bone formation (12) (Table 1). Therefore, the role of STING in osteoporosis deserves further investigation to determine how to target STING for osteoporosis treatment.

2 cGAS-STING pathway

The cGAS-STING pathway is a significant component of the host's innate immune response to viral infection. The cGAS senses pathogenic DNA to activate STING to modulate the type 1 interferon response to trigger a natural immune response. Herpes simplex virus 1 (HSV-1) is a double-stranded DNA virus sensed by the cGAS to activate STING and induce innate antiviral immunity (22). Similarly, other DNA viruses, such as HIV and CMV, can trigger cGAS-STING

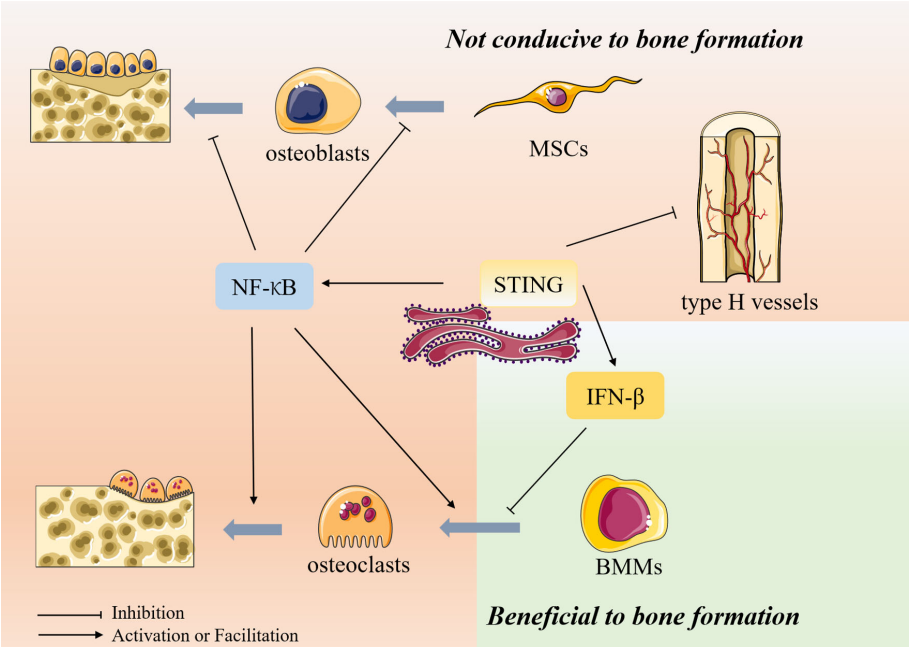

FIGURE 1
The role of STING in bone metabolism Bone metabolism is mainly composed of osteoblast-mediated bone formation and osteoclast-mediated bone resorption. In addition, type H vessels also can induce bone formation and thus participate in bone remodeling. Osteoblasts are differentiated from mesenchymal stem cells (MSCs), whereas osteoclasts are differentiated from bone marrow macrophages. STING can act as an upstream of NF-κB, stimulating its activation and transcription and thus exerting biological effects. NF-κB inhibits the differentiation of MSCs toward osteogenesis and inhibits osteoblast activity, thus inhibiting bone formation. In osteoclasts, NF-κB can promote osteoclast production and activity, thereby promoting bone resorption. IFN-β is also a downstream target of STING. However, unlike NF-κB, although IFN-β is induced in osteoclasts after activation by STING, it can inhibit osteoclast activation through its negative feedback, thereby inhibiting bone resorption. In addition, STING can inhibit the formation of type H vessels, inhibiting bone formation.

TABLE 1 Summary of research on targeting STING and it signaling pathways in bone metabolism.

Disease	Interventions	Mechanism &Target	Model	Effects
OA	Deficient in STING (13)	Inhibiting STING / IFN-I signaling	DNase II$^{-/-}$/ IFNAR$^{-/-}$ double-knockout arthritis mice	Inhibiting abnormal bone formation
	Itaconate (14)	Inhibiting STING/NF-κB axis, Promoting M2 polarization in macrophages	OA mouse	Inhibiting chondrocyte senescence and ECM degeneration, Attenuating osteoarthritis
IVDD	Lipopolysaccharide (LPS) (15)	Activating cGAS/STING pathway	vertebral inflammation-induced caudal IVDD (VI-IVDD) rat	Building a novel model of VI-IVDD
	STING knock-down (16)	Inhibiting cGAS/STING pathway	puncture-induced IVDD rat	Alleviating IVDD development
	Epigallocatechin-3-Gallate (17)	Inhibiting cGAS/STING/ NLRP3 pathway	H_2O_2 -Treated NP cells	Protecting NP cells from apoptosis
Bone Loss (including OP)	STING agonists (18) (DMXAA, ADU-S100)	Activating STING/IFN-I signaling	Lewis lung carcinoma or breast cancer -induced bone loss mice	Reducing bone loss
	CDNs (19)	Activating STING/IFN-β signaling	RANKL-induced BMMs, calvarial implantation mouse	Inhibiting osteoclast differentiation and bone resorption
	Tmem173(STING) overexpression (20)	Overexpressing STING	RANKL-induced BMMs	Inhibiting osteoclast differentiation
	RTA-408 (21)	Inhibiting STING /NF-κB signaling	OVX-induced bone loss	Attenuating osteoclastogenesis
Bone Fracture, Bone Defect	2′,3′-cGAMP (12)	Activating STING	Bone fracture and defect mice	Inhibiting type H vessel formation, Delaying bone healing
	STING inhibitors (12) (C-176 and H-151)	Inhibiting STING		Enhancing type H vessel formation, Accelerating bone healing

(23, 24). STING also plays a vital role in the immune response induced by RNA viruses (25). RNA viruses, like dengue virus and SARS-CoV-2, have no DNA and cannot induce cGAS autonomously. However, these RNA viruses can activate the cGAS-STING pathway by triggering intracellular mitochondrial stress damage to release mitochondrial DNA (mtDNA), thereby generating antiviral immunity (26). In addition, cGAS can sense bacterial DNA and the host's DNA, such as senescent apoptotic cells, extracellular vesicles, and chromatin fragments (27). Thus, the cGAS-STING pathway is critical in many disease processes, including autoimmune diseases, inflammatory diseases, degenerative diseases, and cancer (5, 28).

STING is a PRR on the ER that does not bind directly to DNA. Pathogenic microbes and damaged host cells can release free double-stranded DNA (dsDNA) (29). Then dsDNA is recognized by the cytoplasmic DNA sensor, the cyclic GMP-AMP synthase (cGAS) (30). The ds DNA binding to cGAS triggers the conversion of ATP and GTP to cGAMP (2′,3′-cyclic GMP–AMP) (31). The cGAMP is canonical cyclic dinucleotides (CDNs) that bind and activate STING (32). CDNs are essential second messengers produced by cyclic dinucleotide synthase, which is widely distributed and can trigger from various cellular signaling cascades, as well as being an activating ligand for STING (33, 34). The binding of cGAMP to STING triggers STING conformational transition, dimerization, and translocation to the endoplasmic reticulum-Golgi intermediate compartment (ERGIC) and Golgi apparatus (Golgi) (35). Then STING dimers recruit TBK1, which phosphorylates STING and induces IRF3 (36). STING also leads to NF-κB activation. IRF3 and NF-κB are translocated to the nucleus to induce the production of IFN-I and other cytokines involved in the host immune response (37)(Figure 2).

Classical STING activation induces the critical transcription factor IRF3 *via* the cGAS-STING pathway, which promotes IFN-I secretion and activates NF-κB to trigger pro-inflammatory cytokines. In recent years, atypical patterns of STING activation have also been identified. Keratinocytes generate an innate immune response within hours of etoposide-induced DNA damage, which involves the DNA sensing adapter STING but is not dependent on cGAS (38). And this non-canonical STING signaling predominantly activates NF-κB rather than IRF3, which induces IFN-I production. This also provides another way of thinking for future STING research.

Although it has been reported that cytoplasmic DNA-mediated STING-dependent inflammatory response requires activation of NF-κB *via* TBK1 (39), at the same time, activation of TBK1 can also cause IFN-β production. However, investigators have found that selective activation of NF-κB can occur in the cGAS-STING pathway, while a parallel path blocks activation of the IRF3/IFN system (40). In late 2019, SARS-CoV-2 emerged as a highly infectious coronavirus that causes a human respiratory disease called COVID-19. SARS-CoV-2 infection can cause respiratory symptoms ranging from mild to severe, resulting in lasting lung damage or death (41). One of the hallmarks of severe COVID-19 is low levels of IFN-I and high levels of expression of inflammatory cytokines or chemokines such as IL-6 and tumor necrosis factor (TNF) (42–44). This unbalanced immune response fails to limit viral transmission and leads to severe systemic symptoms. Specific activation of NF-κB and blockade of IRF3 nuclear translocation occurs in SARS-CoV-2 infected cells, and STING-targeted drugs can attenuate this NF-κB response (44). This NF-κB response is induced by mtDNA released from cellular oxidative stress injury (44, 45). MtDNA mediates the activation of

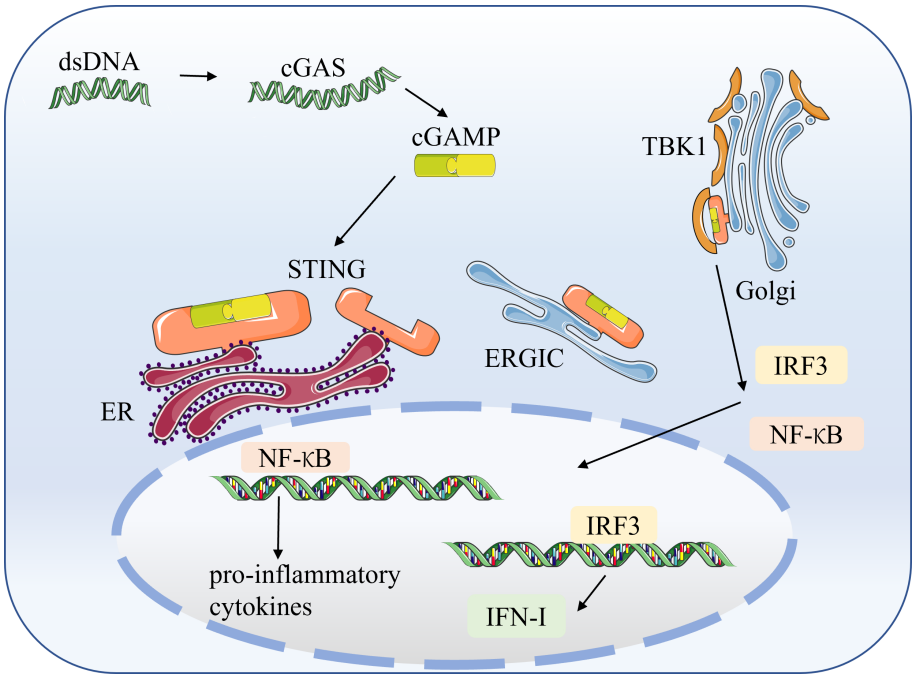

FIGURE 2
The cGAS-STING signaling pathway STING is a pattern recognition receptor (PRR) on the endoplasmic reticulum (ER) that does not bind directly to DNA. Pathogenic microorganisms and damaged host cells can release double-stranded DNA (dsDNA). The cytoplasmic DNA sensor, cyclic GMP–AMP synthase (cGAS), recognizes dsDNA and catalyzes the synthesis of cGAMP from ATP and GTP. The cGAMP binds to STING, triggering STING conformational transitions, dimerization, and translocation to the endoplasmic reticulum-Golgi intermediate compartment (ERGIC) and the Golgi apparatus (Golgi). The dimerized STING recruits TBK1, which induces the production of IRF3 and NF-κB. Subsequently, IRF3 and NF-κB translocate to the nucleus to induce the production of IFN-I and pro-inflammatory factors.

cGAS-STING. Furthermore, cancer studies found that the classical NF-κB pathway in the cGAS-STING pathway enhances anti-tumor effects by promoting IFN-I expression. In contrast, the non-classical NF-κB pathway impedes anti-tumor effects by decreasing IFN-I expression (40). Activation of STING triggers NF-κB activation that can be generated independently of IFN-I.

3 STING/IFN-β and osteoporosis

Bone, the body's central axis system, provides physical support and protection, is involved in calcium metabolism and endocrine regulation, and promotes the hematopoietic system in the bone marrow (10). In response to normal wear and mechanical forces as well as the aging process, bone in the adult skeleton undergoes continuous remodeling in which damaged or failing microscopic parts of the bone are removed by osteoclasts and subsequently replaced by new bone laid down by osteoblasts (46). Bone remodeling is a continuous dynamic process that includes bone formation and bone resorption activities, generally in balance, thus maintaining bone homeostasis (47). Bone homeostasis depends on the functional balance between bone-forming cells (osteoblasts) and bone-resorbing cells (osteoclasts) (48). Disruption of bone homeostasis is the frequent pathophysiological mechanism of bone metabolic diseases (49). Excessive osteoclast activity can lead to bone diseases such as osteoporosis, Paget's disease, and rheumatoid arthritis.

Osteoclast differentiation is initiated by bone marrow macrophages (BMMs) through stimulation of receptor activators of nuclear factor-κB ligand (RANKL) and macrophage colony-stimulating factor (M-CSF) (50). Osteoblasts release RANKL and osteoprotegerin (OPG) to regulate bone homeostasis. RANK, the receptor of RANKL, is expressed in osteoclasts. Furthermore, RANK-RANKL interaction activates downstream signaling pathways such as NF-κB, MAPK, and AKT, thereby inducing the expression of osteoclast-associated genes, including c-Fos and NFATc1 (51). Additional studies have shown that osteoclastogenesis generates reactive oxygen species (ROS), and these ROS can induce the activation of downstream signaling pathways, such as NF-κB and MAPK, which also play a role in osteoclast differentiation and bone resorption (52). Conversely, OPG binds to RANK to reduce RANK-RANKL signaling, thereby balancing bone resorption (53). C-Fos is essential for osteoclast differentiation, and lack of c-Fos can lead to osteosclerosis. It interacts with NFATc1, then activates multiple target genes for osteoclast function, triggering a transcriptional regulatory cascade (54). RANKL interactions have been shown to induce IFN-β production through the induction of c-Fos genes (11)(Figure 3).

3.1 Relationship between IFN-β and osteoporosis

IFN-β belongs to type I interferons. The human body produces three known types of interferons: type I, type II, and type III (55).

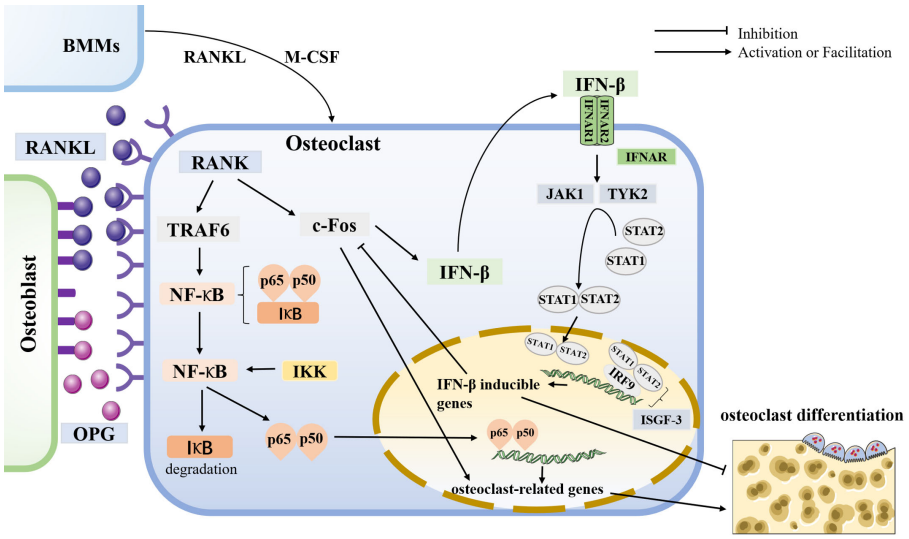

FIGURE 3
osteoclastogenesis and the role of IFN-β in it Osteoclasts are differentiated from BMMs by stimulating receptor activators for nuclear factor-κB ligand (RANKL) and macrophage colony-stimulating factor (M-CSF). Osteoblasts release RANKL and osteoprotegerin (OPG) to regulate bone homeostasis. RANK is a receptor for RANKL, expressed in osteoclasts. In osteoclasts, RANK-RANKL interaction activates downstream signaling pathways that induce the expression of osteoclast-associated genes such as c-Fos and TRAF6. In comparison, OPG binds to RANK to reduce RANK-RANKL signaling to balance bone resorption. C-Fos is essential for osteoclast differentiation. The RANK-RANKL interaction has been shown to induce IFN-β production by the c-Fos. IFN receptor (IFNAR) is a class of heterodimers on the cell membrane consisting of two subunits, IFNAR1 and IFNAR2. IFN-β binds to its receptor to activate the downstream protein kinases JAK1 and TYK2, then activating the transcription factors STAT1 and STAT2, forming a dimer that can enter the nucleus and bind to IRF9 to constitute ISGF-3, which exerts its IFN-β mediated transcriptional effects to inhibit osteoclast production. Thus, IFN-β forms negative feedback, inhibiting osteoclast differentiation. In addition, TRAF6 is essential for osteoclastogenesis and induces the production of NF-κB. In the resting state, NF-κB in the cytoplasm binds to the inhibitor protein IκB while leaving NF-κB inactive. IκB kinase (IKK) phosphorylates NF-κB to degrade IκB, and the released p65 and p50 subunits enter the nucleus for transcription of osteoclast-related genes, thus inducing bone resorption.

Type I interferons are mainly IFN-α and IFN-β, secreted by innate immune cells. Type II interferons, IFN-γ, is mainly produced by activated T cells. Type III interferons include IFN-λ, whose known distribution and function are minimal. Type I interferons are mainly produced by surface or internal receptors of innate immune cells (TLRs, NLRs, RLRs, and cGAS) binding to specific antigens from outside or inside the host (56). IFN receptors (IFNAR) are a class of heterodimers located on the cell membrane and consist of two subunits, IFNAR1 and IFNAR2, and widely distributed, including monocytes, macrophages, B cells, T cells, epithelial cells, endothelial cells, and tumor cells (57). Ligand receptor binding activates downstream protein kinases JAK1 and TYK2, and kinase activation activates cytoplasmic transcription factors STAT1 and STAT2, forming a dimer that enters the nucleus to assist IRF9 in transcribing some downstream effector genes (56). Type I interferons can play a biological role in antiviral and immunomodulatory, inhibiting specific cell growth and proliferation and killing tumor cells (58, 59). Therefore, interferon therapy has been used to treat common viral diseases such as hepatitis (60) and various cancers (61).

When osteoclasts are induced to produce IFN-β, the binding of IFN-β to its bioreceptor activates ISGF-3 (formed by the aggregation of STAT1, STAT2, and IRF9) *via* the classical JAK/STAT pathway, initiating a signal transduction cascade (62). Then, c-Fos will be inhibited, leading to the inhibition of osteoclast production and activity (11). Thereby, IFN-β forms negative feedback of its own (Figure 3). Thus, IFN-β also plays a vital role in regulating bone homeostasis. In addition, osteoclasts express iNOS and release NO, and the NO produced by this pathway also acts as a negative feedback signal to limit RANKL-stimulated osteoclastogenesis (63). In iNOS-deficient bone marrow cells, RANKL-induced NO production was inhibited, leading to an increase in the number of terminally differentiated osteoblasts (64). Direct administration of IFN-β in RAW264.7 cells stimulated iNOS expression in the absence of RANKL, thereby upregulating NO expression. NO, like IFN-β, inhibited osteoclast differentiation. These results suggest that IFN-β may be a key mediator of iNOS-derived NO induction by RANKL in developing osteoclasts and that iNOS can mediate the inhibitory effect of IFN-β on osteoclasts (65).

Another interaction of IFN-β involved in the regulation of bone homeostasis is 4-1BBL with 4-1BB. 4-1BB, also known as CD137, is similar to RANK and is a member of the same TNF receptor family, encoded by the TNFRSF9 gene. Upon its activation, antigen-presenting cells, such as dendritic cells, B cells, and macrophages, express 4-1BBL (66). Osteoclast precursors can express 4-1BB and 4-BBL after exposure to RANKL (67). In BMMs co-stimulated by M-CSF and RANKL, 4-1BBL mRNAs are upregulated (68). In the animal model, 4-1BB knockout mice also showed increased bone mass compared to the wild group. The number of osteoclasts was significantly reduced in the presence of immobilized recombinant 4-1BB (4-1BB-Fc). 4-1BB can induce the binding activity of IRF3, and IRF3 is activated by 4-1BB stimulation, which induces IFN-β (11, 69, 70). It is not difficult to speculate that the decrease in osteoclast activity caused by 4-1BB should be due to the inhibition of c-Fos expression by IFN-β.

3.2 Targeting STING/IFN-β in osteoporosis

As a critical signal transduction molecule involved in the innate immune response, STING, triggered by cytoplasmic DNA from pathogens and hosts, can induce type I interferon and pro-inflammatory cytokine secretion, defend against viral and intracellular bacterial infections, and regulate the spontaneous anti-tumor immune response *in vivo*. Targeted STING is a new tool for immunotherapy. In addition to immune or oncological diseases, the role of STING in bone metabolic diseases has been the focus of attention in recent years. DNase II is a nuclease that degrades dsDNA. Lack of DNase II causes DNA accumulation in cells and produces several cytokines, including type I IFN (71). Mice lacking DNase II and IFNAR were able to develop distal aggressive inflammatory arthritis (72). However, this arthritis was eliminated in the absence of STING (71, 73). Surprisingly, the arthritis model (DNase $II^{-/-}$/ $IFNAR^{-/-}$ double-knockout mice) showed aberrant accumulation of bone in both long bones and the spleen at sites of local DNA accumulation (13). STING deficiency inhibited bone accumulation (13), revealing a potential role of the STING pathway in bone, although the exact mechanism is unclear.

Patients with advanced cancer often suffer from severe pain due to bone metastases and bone destruction with osteolytic lesions (74). Agonists of the immunomodulator STING have significantly protected against pain (75), bone destruction (13, 19), and local tumor burden (76). One of its effects is alleviating cancerous bone pain by regulating osteoclast function in the tumor microenvironment to prevent local bone destruction, which depends on host-intrinsic STING/IFN-β signaling. Bone metastases in patients with cancer produce osteolytic bone destruction due to tumor-induced osteoclast formation and activation (77). Bone loss was significantly reduced in Lewis lung carcinoma (LLC) or breast cancer mice treated with DMXAA and ADU-S100, two different STING agonists, similar to zoledronic acid (ZA) (18). In contrast, the reversal effect of DMXAA on bone loss was eliminated in the STING knockout group of mice. Thus, the inhibitory effect of STING agonists on bone resorption is dependent on STING. Systemic administration of STING agonists also promotes a robust IFN-I response in the systemic and bone cancer tumor microenvironment. DMXAA treatment does not prevent bone destruction in IFNAR1-deficient mice. IFNAR is required for IFN signaling (57). Thus, the protective effects of STING agonists against cancerous bone destruction require IFN-I signaling (18).

STING, also known as Tmem173, has been shown to inhibit osteoclast differentiation and activity by regulating IFN-β production. It inhibits the expression of osteoclast-specific genes and related enzymes and downregulates the activation of osteoclast-specific transcription factors (20). CDNs are symbiotic bacterial-derived second messengers in the intestine that regulates bacterial survival, colonization, and biofilm formation and have immunomodulatory activity by inducing type I interferon expression by macrophages through the STING signaling pathway (34, 78). CDNs dose-dependently inhibit M-CSF and RANKL-induced differentiation of bone marrow macrophages to osteoclasts and induce phosphorylation of TBK1 and IRF3, representative features of STING activation (19). In contrast, inhibition of osteoclast differentiation was reversed in STING knockdown BMMs. These suggest that the STING signaling pathway plays a crucial role in CDNs-mediated inhibition of osteoclast differentiation. In addition, CDNs increased the expression of IFN-β, a member of the IFN-I family, which has also been identified as a typical negative regulator of RANKL-induced osteoclast differentiation (79, 80). RANKL induces IFN-β expression *via* c-Fos (81). In turn, IFN-β binds to IFNAR on the membrane, which activates ISGF-3 and prevents RANKL-induced c-Fos expression from inhibiting osteoclast differentiation (11). The inhibitory effect of CDNs on osteoclast differentiation was absent in the presence of antibodies blocking IFNAR, and no inhibitory effect was observed in knockout IFNAR macrophages (19). These also confirm that CDNs induce phosphorylation of STAT1, which mediates IFNAR signaling. Experiments performed with a mouse cranial implant model showed that CDNs inhibit RANKL-induced bone resorption (19). These results suggest STING induces IFN-β to inhibit osteoclast differentiation and bone resorption.

It is well known that IFN-I response is a weapon against viruses. IFN-I is induced during STING-mediated immune responses. IFN-I can also be stimulated by the osteoclast-specific gene c-Fos and ultimately inhibits osteoclast production and activation through IFNAR transmission (11, 82). STING regulates the inhibitory effect of IFN-I on osteoclasts, and the knockdown of STING reverses this effect (79). Knockdown of STING can offset this effect (19). Therefore, targeting STING/IFN-β to increase IFN-β expression and thereby inhibit osteoclast bone resorption is expected to be a new approach to treating osteoporosis. In addition, interferon therapy has been used in the clinic. And IFN-β has a relatively good clinical tolerability and safety profile. However, it faces several tests when using IFN-β to treat bone metabolic diseases, including osteoporosis. First, as with other protein drugs, treatment with interferon results in the production of neutralizing antibodies in the patient (83). Second, effective delivery of the drug to the bone microenvironment is another challenge in using IFN-β for treating bone metabolic diseases (84). Targeting STING to increase the level of interferon in the body may solve these problems faced by treatment with interferon alone. In addition, the inhibitory effect of IFN-β on osteoclasts is mainly due to its negative feedback mechanism. However, the action of IFN-β is also inhibited by another kind of negative feedback. Suppressors of cytokine signaling (SOCS)-1 and SOCS-3 in response to RANKL can act as inhibitory factors that significantly inhibit IFN-β signaling (85). Thus IFN-β-mediated inhibition of osteoclastogenesis has a potential counteracting pathway. It may be the same challenge for targeting STING/IFN-β with interferon therapy alone.

4 STING/NF-κB and osteoporosis

Past studies have indicated that the cGAS-STING pathway is a key component of the innate immune response as a host defense against multiple pathogens. At the same time, sustained STING activity may lead to fatal inflammatory diseases (39). The continuous secretion of pro-inflammatory cytokines enhances tissue destruction and impairs the organism's homeostasis, thus affecting functional integrity. NF-κB is a downstream target of STING signaling and can be activated by it. NF-κB is a ubiquitous transcription factor activated by various stimuli, including infection, inflammation, and oxidative stress (86). The aging process is

accompanied by a chronic and persistent inflammatory state (87). NF-κB is also a hub of the aging process, promoting transcription and expression of various genes associated with inflammation and can regulate inflammatory signaling during aging induced by oxidative stress (88). NF-κB is associated with many age-related diseases and inflammatory diseases (89), including Alzheimer's disease (90), diabetes mellitus (91), cancer (92), and autoimmune and inflammatory diseases (93). Activation of NF-κB signaling was found in senescent ARPE-19, and NF-κB was confirmed to be a downstream target of STING in oxidative stress-induced senescent retinal pigment epithelium (RPE) (94). In microgliomas, polyglutamine binding protein 1 (PQBP1) activates cGAS-STING by interacting with sensing extrinsic tau 3R/4R proteins (95). Activation of the PQBP1-cGAS-STING pathway leads to nuclear translocation of NF-κB and expression of inflammatory genes, resulting in brain inflammation and cognitive dysfunction in mice. Psoriasis, a chronic inflammatory skin disease, is associated with innate and adaptive immune responses. STING antagonist H-151 ameliorates psoriasis by inhibiting STING/NF-κB-mediated inflammation (96).

Inflammation is also closely associated with bone metabolism diseases, including osteoporosis (97), osteoarthritis(OA) (98), intervertebral disc degeneration(IVDD) (99), bone lysis (100), and spondyloarthritis (101). STING upregulation was found to be associated with the development of IVDD. And vertebral inflammation mediated by activation of the cGAS/STING molecular pathway is a novel form of animal model used to induce disc degeneration (15). Excessive accumulation of ROS can lead to DNA damage, which activates the cGAS/STING pathway (102). ROS-induced DNA damage is thought to be one of the leading causes of nucleus pulposus (NP) cell degeneration during IVDD progression (103). Moreover, the knockdown of STING expression can attenuate ROS-induced disc degeneration (16). Similarly, pharmacological inhibition of STING also protects NP cells from inflammation-induced apoptosis (17). Moreover, the process of OA is also accompanied by increased expression of STING and NF-κB, and exogenous supplementation with itaconate can inhibit the STING/NF-κB signaling pathway to alleviate the progression of OA (14). Osteoporosis, an age-related disease of bone metabolism, is also an inflammatory disease. Elevated levels of NF-κB can also be found in osteoporosis models. Aging-associated bone loss is characterized by decreased bone formation and increased bone resorption, and it is often referred to as senile osteoporosis (104). Aging is a biological process characterized by changes in the redox state of the organism and inflammatory responses induced by oxidative stress (105). Oxidative stress can release mtDNA (106), which can act as an upstream of the cGAS-STING signaling pathway and activate STING (107). The activation and transduction of STING are crucial in the development and progression of aging-related diseases (108, 109). Therefore the application of targeting STING/NF-κB in osteoporosis is worth exploring.

4.1 NF-κB

NF-κB is one of the best-characterized transcription factors that regulate inflammation and innate and adaptive immune responses (110). Activation of NF-κB signaling leads to the production of various inflammatory cytokines, chemokines, adhesion molecules, transcription factors, and antimicrobial effector molecules that initiate and mimic inflammatory responses and coordinate the immediate host response to pathogens and tissue damage. The NF-κB transcription factor family includes five members p50 (NF-κB1), p52 (NF-κB2), RelA (p65), RelB, and c-Rel (111). All NF-κB subunits have a structurally conserved N-terminal sequence spanning 300 amino acid residues called the Rel homology structural domain (RHD) (112). The RHD is responsible for DNA binding, dimerization, and nuclear translocation of NF-κB subunits, which can divide into three structural components - the N-terminal structural domain (NTD), the dimerization structural domain (DD), and the nuclear localization sequence (NLS) polypeptide - all of which mediate the various activities of the RHD and subsequent NF-κB signaling (110, 113, 114). Subunits RelA, RelB, and c-Rel are produced as mature proteins. In contrast, the p50 and p52 subunits are produced by the precursor proteins (113).

In the resting state, NF-κB subunits bind to IκB proteins, inhibiting their activity and maintaining NF-κB subunits in an inactive state (115). In turn, IκB kinase (IKK) can degrade these inhibitory proteins (116). Once activated by upstream signaling cascades, phosphorylated IKK degrades the IκB protein and releases the subunits of the NF-κB. Then these subunits go into the nucleus as dimers and participate in the transcription of various target genes (10). For example, the functional subunits p65 and p50 enter the nucleus and bind to target genes, producing large amounts of inflammatory mediators, and the gene products further activate NF-κB, causing an expanded cascade of uncontrolled inflammatory responses. More and more NF-κB target genes have been identified (117), including various cytokines such as interleukin (IL) and TNF, interferons, and antiapoptotic proteins, such as BIRC2, BIRC3, and BCL2L1.

4.2 Relationship between NF-κB and osteoporosis

Bone homeostasis is necessary for the maintenance of normal bone function. Bone homeostasis is maintained by bone remodeling mediated by osteoblasts and osteoclasts, which are responsible for bone formation and resorption (48). Osteoblasts and osteoclasts are the essential cells that regulate bone homeostasis. NF-κB is the master transcription factor that regulates the inflammatory response and bone remodeling process (118, 119). Chronic inflammation induces excess pro-inflammatory cytokines, disrupting homeostasis (120). These result in abnormal bone remodeling, including osteosclerotic and osteolytic lesions (121).

Pro-inflammatory cytokines driven by NF-κB are powerful signals to regulate bone homeostasis (122). Elevated expression of TNF, IL-1, IL-6, and IL-7 has been found in various chronic inflammatory bone diseases, including osteoarthritis (123), osteoporosis (124), and periodontal disease (125). These pro-inflammatory cytokines are all produced by macrophages, lymphocytes, osteoblasts, and bone marrow stromal cells under the regulation of NF-κB and stimulate NF-κB signaling in target cells, which further serves to amplify inflammation (126). Osteoclasts are specialized cells of the monocyte-macrophage lineage responsible for

bone resorption. In contrast, osteoblasts are differentiated from mesenchymal stem cells to osteogenesis and are responsible for establishing new bone. NF-κB has an essential role in osteoblasts and osteoclasts, thus affecting bone regulation.

4.2.1 Role of NF-κB in bone resorption

NF-κB signaling is directly involved in the differentiation and activation of osteoclasts responsible for bone resorption (127). The binding of RANKL to RANK triggers a complex and unique signaling cascade that controls lineage commitment and activation of osteoclasts (128). Activating NF-κB signaling in osteoclasts is essential for their differentiation and activation (54). TNF receptor–associated factor (TRAF) proteins are cytoplasmic adaptor proteins that bind to various receptors of the TNF receptor (TNFR) superfamily. An essential role of TRAFs in RANK-RANKL signaling is inducing NF-κB (51). Among TRAFs, TRAF6 is the most critical adaptor of RANK-RANKL-induced osteoclastogenesis (129). Genetic experiments have shown that TRAF6 is required for osteoclast formation and activation (130). Like mice lacking NF-κB p50 and p52 subunits (131), TRAF6-deficient mice develop severe osteoporosis (132).

Usually, NF-κB in the cytoplasm is bound to the inhibitory protein IκB while keeping NF-κB in a resting state. While various stimuli lead to the activation of IKK, which leads to the degradation of IκB bound to the NF-κB subunits, the released NF-κB enters the nucleus as a homodimer or a heterodimer and activates transcription, thus exerting biological effects. For example, released p65 and p50 subunits enter the nucleus for transcription of osteoclast-related genes, thus inducing bone resorption (21). IKK is a complex of three subunits, IKKα (also known as IKK1), IKKβ (also known as IKK2), and IKKγ(also known as NEMO). IKKβ is required for osteolysis *in vitro* and *in vivo*, and the knockdown of IKKβ can lead to bone loss in mice (133). While IKKα is required for RANK ligand-induced osteoclast formation *in vitro*, it is not required *in vivo* (134). Thus, targeting IKK can regulate the NF-κB activity of osteoclasts and prevent bone loss, providing a new idea for the treatment of osteoporosis (135). In conclusion, NF-κB is an essential mediator of osteoclastogenesis (136), which leads to excessive bone resorption and osteoporosis. Pharmacotherapy can inhibit RANKL-mediated osteoclastic formation by targeting the NF-κB pathway to attenuate inflammatory factors and ROS production and can reduce bone loss *in vivo* in ovariectomized (OVX) model (137).

4.2.2 Role of NF-κB in bone formation

Osteoblasts derived from mesenchymal stem cells (MSCs) are responsible for bone formation. NF-κB activity is suppressed in mature osteoblasts, so NF-κB activation in osteoblasts inhibits bone formation (136). NF-κB activation occurs in bone trabeculae of naturally aging mice (138). Increased NF-κB activity was found in MSCs isolated from aged mice compared to young mice, and inhibition of the NF-κB pathway partially rescued the reduction in osteogenesis in aged MSCs (139). And increased RANKL and reduced OPG expression was observed in aged MSCs, which resulted in increased RANKL/OPG ratio and osteoclast activation. Chronic NF-κB activation has also been shown to impair the differentiation of MSCs along the osteogenic pathway and osteoblast-mediated bone formation (140).

In the absence of NF-κB activation, prolonged c-Jun N-terminal kinase (JNK) activation, which regulates FOSL1 (also known as Fra1) expression, contributes to bone formation (126, 141). Mice specifically lacking IKK-β in osteoblasts exhibit increased bone mass, mainly because reduced NF-κB activity by IKK-β deficiency increases JNK activity and Fra1 expression, ultimately leading to increased bone formation to maintain bone mass in OVX mice (142). Fra1 is an important transcription factor involved in bone matrix formation (143). Chronic inflammation can inhibit bone formation. For example, the pro-inflammatory factor TNF-α inhibits osteoblast differentiation (144), but the IKK inhibitor BAY11-7082 rescues the TNF-α-induced inhibition of osteoblast differentiation by inhibiting NF-κB (145). Thus, inhibition of osteoblast NF-κB can promote bone formation. A decrease in NF-κB activity in osteoblasts leads to an increase in bone formation (146). The NF-κB inhibitor, S1627, upregulates the mRNA of osteoblast-specific genes (such as type I collagen and alkaline phosphatase) to increase osteoblast differentiation and bone formation *in vitro* (147). Moreover, it can increase bone formation to repair bone defects in a mouse cranial defect model and alleviate osteoporosis in the OVX mouse model. Therefore, targeting NF-κB could provide a novel and effective therapeutic strategy for osteoporosis and other inflammatory bone diseases.

4.3 Targeting STING/NF-κB in osteoporosis

Excessive accumulation of ROS leading to redox imbalance and overactive osteoclasts is associated with the progression of osteoporosis. The process of osteoclastogenesis is accompanied by the production of ROS, which plays a role in osteoclast differentiation and bone resorption (52). In addition, ROS-induced mtDNA release induces inflammation through the activation of cGAS/STING (148). ROS can induce NF-κB through the RANKL/RANK cascade reaction, which is further involved in osteoclastogenesis (149). In addition to promoting type I interferon production in the innate immune response (150), STING can also act as an NF-κB upstream of NF-κB, stimulating its production.

In the past, it was generally considered that NF-κB activation *via* STING is exclusively dependent on TBK1. However, studies have now demonstrated that TBK1 is dispensable for NF-κB, although TBK1 and its kinase activity are essential for STING-dependent IRF3 activation and INF-I. In fact, TBK1 and IKK redundantly drive NF-κB activation when the IFN-I reaction is triggered by TBK1 and its homolog, IKK (151). Inhibition by TBK1/IKK kinase indicates that IRF3 activation highly depends on TBK1 kinase activity. In contrast, NF-κB sensitivity to TBK1/IKK kinase inhibition is significantly reduced, and TBK1 was dispensable for NF-κB activation downstream of STING *in vitro* and *in vivo* (151). So, NF-κB production can be activated by STING through a non-classical pathway, a process that is independent of IFN-β (44). In addition, non-classical STING signaling activates NF-κB pathways mainly through K63-mediated ubiquitination and has no effect on IFN-I (38).

CDNs can inhibit osteoclast differentiation by inducing IFN-β through STING signaling (19), suggesting that activation of STING can inhibit osteoclast differentiation through IFN-β. A sustained activation state of STING can cause a series of inflammatory responses in the organism. NF-κB, acting as a pro-inflammatory gene, is involved in osteoclastogenesis as another downstream of

STING. In contrast to NF-κB, nuclear factor erythroid2-related factor 2 (Nrf2), a critical antioxidant molecule, has been shown to inhibit osteoclast formation and bone resorption by reducing ROS (152). In addition, Nrf2 negatively regulates STING signaling (153).

RTA-408 was found to act as an activator of Nrf2 that inhibits STING expression and subsequent NF-κB activation but does not affect IFN-β expression (21). RTA-408 inhibits RANKL-induced K63 ubiquitination of STING by suppressing the interaction between STING and the E3 ubiquitin ligase TRAF6. As a downstream of STING, NF-κB was also inhibited by RTA-408, mainly by suppressing IκBα protein degradation, preventing p65 from translocating to the nucleus and thus rendering NF-κB inactive. Overexpression of STING rescued the inhibitory effect of RTA-408 on NF-κB signaling and osteoclastogenesis. *In vivo* experiments showed that RTA-408 attenuated osteoclastogenesis-induced bone loss in C57BL/6 mice by inhibiting STING-mediated NF-κB (21). Thus, inhibition of STING-dependent NF-κB signaling could inhibit osteoclastogenesis and reduce bone loss. Targeting STING/NF-κB may be a promising pathway for the future treatment of osteoporosis.

5 STING/type H vessels and osteoporosis

In recent years, it has been found that in addition to osteogenic and osteoclastic effects, angiogenesis also plays a vital role in bone homeostasis in the mammalian skeletal system. Type H vessels that can induce bone formation have been discovered recently and are named for their high expression of EMCN and CD31 (154). Angiogenesis, the development of new blood vessels from pre-existing vessels, is closely associated with osteogenesis during skeletal development and bone remodeling. Blood vessels provide bone tissue with essential nutrients, oxygen, growth factors, and hormones and play a crucial role in the regulation of bone formation (155).

5.1 Relationship between type H vessels and osteoporosis

Osteogenesis is linked to angiogenesis (156). The close spatial and temporal link between osteogenesis and angiogenesis has been termed "angiogenesis-osteogenesis coupling" (157). Type H vessels are located near the epiphyseal growth plate, the epiphyseal periosteum, and the endosteum. Type H vessels are densely surrounded by osteoprogenitors expressing Osterix, a potent promoter of bone formation (158). These osteoprogenitor cells can differentiate into osteoblasts and osteocytes. Under aging conditions, osteoblasts are significantly reduced in the long bones of mice (159), which is associated with a decrease in Type H vessels and reduced bone mass (160). The abundance of Type H vessels is an essential indicator of bone loss in elderly subjects and patients with osteoporosis (161).

PDGF-BB is a chemotactic and mitogenic factor of the PDGF family, produced by hematopoietic stem cells (162). It is essential for promoting the migration, proliferation, and differentiation of various mesenchymal cell types, such as endothelial progenitor cells and mesenchymal stem cells, to promote angiogenesis and osteogenesis (163, 164). PDGF-BB enhanced type H vessels and bone formation during bone plastination and remodeling. The concentration of PDGF-BB was decreased in the OVX mouse model (165). Pharmacological stimulation was able to secrete PDGF-BB to stimulate H-type angiogenesis, thereby promoting osteogenesis to prevent bone loss in OVX mice (166). Glucocorticoids reduce vascularity and blood flow to the bone, causing osteonecrosis and bone loss (167, 168). Glucocorticoid-induced osteoporosis (GIO) is also common osteoporosis. In GIO mouse models, glucocorticoids inhibit PDGF-BB secretion by pre-osteoblasts, inhibiting Type H vessels and reducing osteogenic capacity (169). And L-235, a cathepsin K inhibitor, prevents bone loss by inhibiting osteoclast-inducing bone resorption while maintaining PDGF-BB secreted by preosteoclasts preserving Type H vessels (169).

HIF-1α is a transcription factor that mediates the cellular response to an altered oxygen environment and controls angiogenesis (170).HIF-1α plays a crucial role in bone formation, regeneration plays a key role in bone formation and regeneration, and its expression and activity are regulated by hypoxia Oxygen is required for the high metabolic demand of osteoblasts. Therefore, osteoblasts and nearby ECs may increase HIF-1α expression during relative hypoxia during osteogenesis (155). And ECs express HIF-1α at high levels in young mice, which decreases with age and is associated with a decrease in ECs and age-dependent bone loss. Activation of hypoxic signaling in ECs increased the number of Type H vessels and enhanced angiogenesis and osteogenesis (171). EC-specific deletion of HIF-1α resulted in a significant decrease in osteoblast producers and was associated with reduced trabecular formation. Thus, HIF-1α signaling is vital in regulating type H vascular abundance and couples angiogenesis to osteogenesis (172). Tetramethylpyrazine activates the AMPK/mTOR/HIF-1α signaling pathway to induce type H vessel angiogenesis and improve bone homeostasis in aging mice (173). This provides an additional therapeutic target for the treatment of age-related osteoporosis.

5.2 Targeting STING/type H vessels in osteoporosis

Type H vessels also play an indelible role in bone remodeling. Osteoblasts, osteoclasts, and periosteal cells interact with vascular endothelial cells. The STING signaling pathway may act directly on these cells, thereby affecting the angiogenic process. Several studies have shown an association between STING and angiogenesis. STING is expressed in endothelial cells, and cGAMP leads to the activation of cGAS-STING in endothelial cells (174, 175). STING-associated vascular disease (SAVI), with onset in infancy, is an autoinflammatory disease caused by mutations in STING function, which can cause vascular and pulmonary syndromes and cause systemic inflammatory responses (176, 177).

Previous studies have shown that STING can affect angiogenesis in multiple ways. In the zebrafish xenograft model, exogenous administration of cGAMP can activate STING-dependent STAT3, leading to the inhibition of tumor vascular proliferation and migration (178). Palmitic acid (PA) induces mtDNA into the cytoplasm by inducing mitochondrial damage, activating the cGAS-STING-IRF3 signaling (179). Activation of the cGAS-STING-IRF3 pathway dysregulates the Hippo-YAP pathway and inhibits angiogenesis. In

addition, STING-IRF3 can trigger endothelial inflammation in response to PA-induced mitochondrial damage (180). In retinal microangiopathy, mtDNA drives inflammation of microvascular endothelial cells *via* the cGAS-STING signaling pathway (181). Inflammation in the physiological state is a protective mechanism for tissue damage and the basis for tissue repair and regeneration. Nevertheless, an excessive inflammatory response can impair the integrity of the tissue and its function. The persistent inflammatory state of the vascular endothelium leads to impaired angiogenesis and poor bone healing, which affects bone reconstruction (182).

Activation of the STING signaling pathway impairs angiogenesis, including type H vessels. In addition, the prolonged inflammatory response stimulated by the STING pathway delays the bone healing process. Activation of STING inhibits angiogenesis both *in vitro* and *in vivo* and slows the bone healing process *in vivo* (12). Conversely, inhibition of STING accelerated bone healing by enhancing type H vessel formation during coupled osteogenesis (12). Therefore, targeting STING to enhance type H vessel formation and thus promote osteogenesis provides a new idea for the treatment of osteoporosis.

6 Conclusions

Osteoporosis is a bone metabolic disease and an aseptic inflammatory disease. In recent years, bone immunology has become a hot research topic in bone metabolic diseases by studying the functional interactions between the skeletal and immune systems, including various cytokines and transcription factors that affect both systems, to explore new immunological therapeutic avenues for bone metabolic diseases. STING is the core of natural immunity and a new target for immunotherapy. The core of IFN-β treatment for osteoporosis is also inseparable from bone immunology. With the discovery that IFN-β can play a unique role in regulating bone homeostasis, targeting the STING/IFN-β signaling pathway is also emerging as a potential therapeutic tool for osteoporosis. However, the STING pathway has a dual role in bone metabolism. In addition to its immune function, STING can also act as an inflammatory protein to induce NF-κB, thereby mediating the development and progression of various inflammatory diseases, including osteoporosis. But in studies on osteoclastic inhibition by STING/IFN-β, the effect of another STING downstream signaling molecule, NF-κB, had rarely been considered, which is a drawback of related studies. If NF-κB is not disturbed in the activation of STING/IFN-β pathway to inhibit osteoclastic resorption, it will be a more rigorous and appropriate choice. The classical STING/NF-κB pathway, the cGAS-STING pathway, is dependent on the activation of TBK1, which not only activates NF-κB but also mediates the production of IFN-β by activating IRF3. In contrast, the non-classical STING/NF-κB pathway blocks the production of IRF3/IFN-β in parallel. Inhibition of NF-κB activation and, thus, osteoclast differentiation by targeting STING without affecting the level of IFN-β has been shown to alleviate bone loss in the OVX mice. Therefore, targeting the STING/NF-κB pathway is also expected to be a new therapy for osteoporosis. In addition, activation of STING leads to a prolonged inflammatory response that delays revascularization and inhibits the production of type H vessels, which are closely related to osteogenesis and can induce bone formation. Targeting STING/type H vessels also promotes bone reconstruction and osteogenesis by promoting tape H vessel formation. To enhance bone formation and inhibit bone resorption, a STING inhibitor would be a reasonable choice if it were designed to specifically target NF-κB rather than IFN-β.

Overall, STING has a unique role in osteoporosis. The drugs commonly used in clinical to treat osteoporosis are mainly bisphosphonates, which inhibit bone resorption, and calcitonin and estrogen drugs, which can also promote osteoblastogenesis, but they all have many side effects. Therefore, how to safely and effectively treat osteoporosis remains a challenge to tackle. Targeted STING has been applied in antiviral immunotherapy and does represent a rather promising therapeutic option in the new field of treatment of osteoporosis. Targeted STING not only has the ability to directly inhibit osteoclast-mediated bone resorption and promote osteoblast-mediated bone formation but also can promote type H vascular angiogenesis to indirectly enhance the osteogenic effect. However, the network of regulatory pathways involved in STING is also very complex, and the decrease in IFN-β production-mediated bone resorption due to STING activation is in contradiction with the increase in bone resorption and decrease in bone formation mediated by NF-κB activation and type H vascular inhibition. Targeting STING as a therapeutic option for osteoporosis requires balancing these conflicting biological effects. Therefore, there is still much room for exploration of the STING pathway in bone metabolism.

Author contributions

ZG (1st author) conceived and drafted the manuscript. HZ, SH, YZ, and XL discussed the concepts of the manuscript. ZG (1st author) and ZG (2nd author) drew the figures. YZ and XL reviewed and revised the manuscript. All authors contributed to the article and approved the submitted version.

Funding

This study was supported by the National Key R&D Program of China (2018YFC2002000).

Conflict of interest

The authors declare that the research was conducted in the absence of any commercial or financial relationships that could be construed as a potential conflict of interest.

Publisher's note

References

1. Cheng Z, Dai T, He X, Zhang Z, Xie F, Wang S, et al. The interactions between cGAS-STING pathway and pathogens. *Signal Transduct Target Ther* (2020) 5:91. doi: 10.1038/s41392-020-0198-7

2. Ishikawa H, Barber GN. STING is an endoplasmic reticulum adaptor that facilitates innate immune signalling. *Nature* (2008) 455:674–8. doi: 10.1038/nature07317

3. Xia P, Wang S, Gao P, Gao G, Fan Z. DNA Sensor cGAS-mediated immune recognition. *Protein Cell* (2016) 7:777–91. doi: 10.1007/s13238-016-0320-3

4. Zhou R, Xie X, Li X, Qin Z, Wei C, Liu J, et al. The triggers of the cGAS-STING pathway and the connection with inflammatory and autoimmune diseases. *Infect Genet Evol* (2020) 77:104094. doi: 10.1016/j.meegid.2019.104094

5. Skopelja-Gardner S, An J, Elkon KB. Role of the cGAS-STING pathway in systemic and organ-specific diseases. *Nat Rev Nephrol* (2022) 18:558–72. doi: 10.1038/s41581-022-00589-6

6. Li T, Chen ZJ. The cGAS-cGAMP-STING pathway connects DNA damage to inflammation, senescence, and cancer. *J Exp Med* (2018) 215:1287–99. doi: 10.1084/jem.20180139

7. Wan D, Jiang W, Hao J. Research advances in how the cGAS-STING pathway controls the cellular inflammatory response. *Front Immunol* (2020) 11:615. doi: 10.3389/fimmu.2020.00615

8. Paul BD, Snyder SH, Bohr VA. Signaling by cGAS-STING in neurodegeneration, neuroinflammation, and aging. *Trends Neurosci* (2021) 44:83–96. doi: 10.1016/j.tins.2020.10.008

9. Gao Z, Chen Z, Xiong Z, Liu X. Ferroptosis - a new target of osteoporosis. *Exp Gerontol* (2022) 165:111836. doi: 10.1016/j.exger.2022.111836

10. Lin T-H, Pajarinen J, Lu L, Nabeshima A, Cordova LA, Yao Z, et al. NF-κB as a therapeutic target in inflammatory-associated bone diseases. *Adv Protein Chem Struct Biol* (2017) 107:117–54. doi: 10.1016/bs.apcsb.2016.11.002

11. Abraham AK, Ramanathan M, Weinstock-Guttman B, Mager DE. Mechanisms of interferon-β effects on bone homeostasis. *Biochem Pharmacol* (2009) 77:1757–62. doi: 10.1016/j.bcp.2009.01.007

12. Chen X, He W, Sun M, Yan Y, Pang Y, Chai G. STING inhibition accelerates the bone healing process while enhancing type h vessel formation. *FASEB J* (2021) 35:e21964. doi: 10.1096/fj.202100069RR

13. Baum R, Sharma S, Organ JM, Jakobs C, Hornung V, Burr DB, et al. STING contributes to abnormal bone formation induced by deficiency of DNase II in mice. *Arthritis Rheumatol* (2017) 69:460–71. doi: 10.1002/art.39863

14. Ni L, Lin Z, Hu S, Shi Y, Jiang Z, Zhao J, et al. Itaconate attenuates osteoarthritis by inhibiting STING/NF-κB axis in chondrocytes and promoting M2 polarization in macrophages. *Biochem Pharmacol* (2022) 198:114935. doi: 10.1016/j.bcp.2022.114935

15. Su Q, Cai Q, Li Y, Ge H, Zhang Y, Zhang Y, et al. A novel rat model of vertebral inflammation-induced intervertebral disc degeneration mediated by activating cGAS/STING molecular pathway. *J Cell Mol Med* (2021) 25:9567–85. doi: 10.1111/jcmm.16898

16. Guo Q, Zhu D, Wang Y, Miao Z, Chen Z, Lin Z, et al. Targeting STING attenuates ROS induced intervertebral disc degeneration. *Osteoarthritis Cartilage* (2021) 29:1213–24. doi: 10.1016/j.joca.2021.04.017

17. Tian Y, Bao Z, Ji Y, Mei X, Yang H. Epigallocatechin-3-Gallate protects H2O2-induced nucleus pulposus cell apoptosis and inflammation by inhibiting cGAS/Sting/NLRP3 activation. *Drug Des Devel Ther* (2020) 14:2113–22. doi: 10.2147/DDDT.S251623

18. Wang K, Donnelly CR, Jiang C, Liao Y, Luo X, Tao X, et al. STING suppresses bone cancer pain *via* immune and neuronal modulation. *Nat Commun* (2021) 12:4558. doi: 10.1038/s41467-021-24867-2

19. Kwon Y, Park O-J, Kim J, Cho J-H, Yun C-H, Han SH. Cyclic dinucleotides inhibit osteoclast differentiation through STING-mediated interferon-β signaling. *J Bone Miner Res* (2019) 34:1366–75. doi: 10.1002/jbmr.3701

20. Ch C, Is P JP, Ky Y HJ, J K, Ys J. Transmembrane protein 173 inhibits RANKL-induced osteoclast differentiation. *FEBS Lett* (2015) 589:836–841. doi: 10.1016/j.febslet.2015.02.018

21. Sun X, Xie Z, Hu B, Zhang B, Ma Y, Pan X, et al. The Nrf2 activator RTA-408 attenuates osteoclastogenesis by inhibiting STING dependent NF-κb signaling. *Redox Biol* (2020) 28:101309. doi: 10.1016/j.redox.2019.101309

22. Huang J, You H, Su C, Li Y, Chen S, Zheng C. Herpes simplex virus 1 tegument protein VP22 abrogates cGAS/STING-mediated antiviral innate immunity. *J Virol* (2018) 92:e00841–18. doi: 10.1128/JVI.00841-18

23. Lahaye X, Gentili M, Silvin A, Conrad C, Picard L, Jouve M, et al. NONO detects the nuclear HIV capsid to promote cGAS-mediated innate immune activation. *Cell* (2018) 175:488–501.e22. doi: 10.1016/j.cell.2018.08.062

24. Wilski NA, Stotesbury C, Del Casale C, Montoya B, Wong E, Sigal LJ, et al. STING sensing of murine cytomegalovirus alters the tumor microenvironment to promote antitumor immunity. *J Immunol* (2020) 204:2961–72. doi: 10.4049/jimmunol.1901136

25. Fan YM, Zhang YL, Luo H, Mohamud Y. Crosstalk between RNA viruses and DNA sensors: Role of the cGAS-STING signalling pathway. *Rev Med Virol* (2022) 32:e2343. doi: 10.1002/rmv.2343

26. Sun B, Sundström KB, Chew JJ, Bist P, Gan ES, Tan HC, et al. Dengue virus activates cGAS through the release of mitochondrial DNA. *Sci Rep* (2017) 7:3594. doi: 10.1038/s41598-017-03932-1

27. Hopfner K-P, Hornung V. Molecular mechanisms and cellular functions of cGAS-STING signalling. *Nat Rev Mol Cell Biol* (2020) 21:501–21. doi: 10.1038/s41580-020-0244-x

28. Kwon J, Bakhoum SF. The cytosolic DNA-sensing cGAS-STING pathway in cancer. *Cancer Discovery* (2020) 10:26–39. doi: 10.1158/2159-8290.CD-19-0761

29. Kato K, Omura H, Ishitani R, Nureki O. Cyclic GMP-AMP as an endogenous second messenger in innate immune signaling by cytosolic DNA. *Annu Rev Biochem* (2017) 86:541–66. doi: 10.1146/annurev-biochem-061516-044813

30. Chen Q, Sun L, Chen ZJ. Regulation and function of the cGAS-STING pathway of cytosolic DNA sensing. *Nat Immunol* (2016) 17:1142–9. doi: 10.1038/ni.3558

31. Liu H, Moura-Alves P, Pei G, Mollenkopf H-J, Hurwitz R, Wu X, et al. cGAS facilitates sensing of extracellular cyclic dinucleotides to activate innate immunity. *EMBO Rep* (2019) 20:e46293. doi: 10.15252/embr.201846293

32. Zhang X, Shi H, Wu J, Zhang X, Sun L, Chen C, et al. Cyclic GMP-AMP containing mixed phosphodiester linkages is an endogenous high-affinity ligand for STING. *Mol Cell* (2013) 51:226–35. doi: 10.1016/j.molcel.2013.05.022

33. Annibal A, Ripa R, Ballhysa E, Latza C, Hochhard N, Antebi A. Mass spectrometric characterization of cyclic dinucleotides (CDNs). *vivo. Anal Bioanal Chem* (2021) 413:6457–68. doi: 10.1007/s00216-021-03628-6

34. Jenal U, Reinders A, Lori C. Cyclic di-GMP: Second messenger extraordinaire. *Nat Rev Microbiol* (2017) 15:271–84. doi: 10.1038/nrmicro.2016.190

35. Taguchi T, Mukai K, Takaya E, Shindo R. STING operation at the ER/Golgi interface. *Front Immunol* (2021) 12:646304. doi: 10.3389/fimmu.2021.646304

36. Zhou R, Zhang Q, Xu P. TBK1, a central kinase in innate immune sensing of nucleic acids and beyond. *Acta Biochim Biophys Sin (Shanghai)* (2020) 52:757–67. doi: 10.1093/abbs/gmaa051

37. Liu Y, Lu X, Qin N, Qiao Y, Xing S, Liu W, et al. STING, a promising target for small molecular immune modulator: A review. *Eur J Med Chem* (2021) 211:113113. doi: 10.1016/j.ejmech.2020.113113

38. Dunphy G, Flannery SM, Almine JF, Connolly DJ, Paulus C, Jønsson KL, et al. Non-canonical activation of the DNA sensing adaptor STING by ATM and IFI16 mediates NF-κB signaling after nuclear DNA damage. *Mol Cell* (2018) 71:745–760.e5. doi: 10.1016/j.molcel.2018.07.034

39. Abe T, Barber GN. Cytosolic-DNA-mediated, STING-dependent proinflammatory gene induction necessitates canonical NF-κB activation through TBK1. *J Virol* (2014) 88:5328–41. doi: 10.1128/JVI.00037-14

40. Hou Y, Liang H, Rao E, Zheng W, Huang X, Deng L, et al. Non-canonical NF-κB antagonizes STING sensor-mediated DNA sensing in radiotherapy. *Immunity* (2018) 49:490–503.e4. doi: 10.1016/j.immuni.2018.07.008

41. Wiersinga WJ, Rhodes A, Cheng AC, Peacock SJ, Prescott HC. Pathophysiology, transmission, diagnosis, and treatment of coronavirus disease 2019 (COVID-19): A review. *JAMA* (2020) 324:782–93. doi: 10.1001/jama.2020.12839

42. Mehta P, McAuley DF, Brown M, Sanchez E, Tattersall RS, Manson JJ. HLH across speciality collaboration, UK. COVID-19: consider cytokine storm syndromes and immunosuppression. *Lancet* (2020) 395:1033–4. doi: 10.1016/S0140-6736(20)30628-0

43. Wen W, Su W, Tang H, Le W, Zhang X, Zheng Y, et al. Immune cell profiling of COVID-19 patients in the recovery stage by single-cell sequencing. *Cell Discovery* (2020) 6:31. doi: 10.1038/s41421-020-0168-9

44. Neufeldt CJ, Cerikan B, Cortese M, Frankish J, Lee J-Y, Plociennikowska A, et al. SARS-CoV-2 infection induces a pro-inflammatory cytokine response through cGAS-STING and NF-κB. *Commun Biol* (2022) 5:45. doi: 10.1038/s42003-021-02983-5

45. Berthelot J-M, Lioté F. COVID-19 as a STING disorder with delayed over-secretion of interferon-beta. *EBioMedicine* (2020) 56:102801. doi: 10.1016/j.ebiom.2020.102801

46. Boyce BF, Li J, Xing L, Yao Z. Bone remodeling and the role of TRAF3 in osteoclastic bone resorption. *Front Immunol* (2018) 9:2263. doi: 10.3389/fimmu.2018.02263

47. Siddiqui JA, Partridge NC. Physiological bone remodeling: Systemic regulation and growth factor involvement. *Physiol (Bethesda)* (2016) 31:233–45. doi: 10.1152/physiol.00061.2014

48. Kim J-M, Lin C, Stavre Z, Greenblatt MB, Shim J-H. Osteoblast-osteoclast communication and bone homeostasis. *Cells* (2020) 9:E2073. doi: 10.3390/cells9092073

49. Feng X, McDonald JM. Disorders of bone remodeling. *Annu Rev Pathol* (2011) 6:121–45. doi: 10.1146/annurev-pathol-011110-130203

50. Boyle WJ, Simonet WS, Lacey DL. Osteoclast differentiation and activation. *Nature* (2003) 423:337–42. doi: 10.1038/nature01658

51. Wada T, Nakashima T, Hiroshi N, Penninger JM. RANKL-RANK signaling in osteoclastogenesis and bone disease. *Trends Mol Med* (2006) 12:17–25. doi: 10.1016/

j.molmed.2005.11.007

52. Agidigbi TS, Kim C. Reactive oxygen species in osteoclast differentiation and possible pharmaceutical targets of ROS-mediated osteoclast diseases. *Int J Mol Sci* (2019) 20:E3576. doi: 10.3390/ijms20143576

53. Boyce BF, Xing L. The RANKL/RANK/OPG pathway. *Curr Osteoporos Rep* (2007) 5:98–104. doi: 10.1007/s11914-007-0024-y

54. Yao Z, Getting SJ, Locke IC. Regulation of TNF-induced osteoclast differentiation. *Cells* (2021) 11:132. doi: 10.3390/cells11010132

55. Walter MR. The role of structure in the biology of interferon signaling. *Front Immunol* (2020) 11:606489. doi: 10.3389/fimmu.2020.606489

56. Peignier A, Parker D. Impact of type I interferons on susceptibility to bacterial pathogens. *Trends Microbiol* (2021) 29:823–35. doi: 10.1016/j.tim.2021.01.007

57. Zanin N, Viaris de Lesegno C, Lamaze C, Blouin CM. Interferon receptor trafficking and signaling: Journey to the cross roads. *Front Immunol* (2020) 11:615603. doi: 10.3389/fimmu.2020.615603

58. McNab F, Mayer-Barber K, Sher A, Wack A, O'Garra A. Type I interferons in infectious disease. *Nat Rev Immunol* (2015) 15:87–103. doi: 10.1038/nri3787

59. Dunn GP, Koebel CM, Schreiber RD. Interferons, immunity and cancer immunoediting. *Nat Rev Immunol* (2006) 6:836–48. doi: 10.1038/nri1961

60. Tang LSY, Covert E, Wilson E, Kottilil S. Chronic hepatitis b infection: A review. *JAMA* (2018) 319:1802–13. doi: 10.1001/jama.2018.3795

61. Stiff A, Carson W. Investigations of interferon-lambda for the treatment of cancer. *J Innate Immun* (2015) 7:243–50. doi: 10.1159/000370113

62. Michalska A, Blaszczyk K, Wesoly J, Bluyssen HAR. A positive feedback amplifier circuit that regulates interferon (IFN)-stimulated gene expression and controls type I and type II IFN responses. *Front Immunol* (2018) 9:1135. doi: 10.3389/fimmu.2018.01135

63. Sunyer T, Rothe L, Kirsch D, Jiang X, Anderson F, Osdoby P, et al. Ca2+ or phorbol ester but not inflammatory stimuli elevate inducible nitric oxide synthase messenger ribonucleic acid and nitric oxide (NO) release in avian osteoclasts: autocrine NO mediates Ca2+-inhibited bone resorption. *Endocrinology* (1997) 138:2148–62. doi: 10.1210/endo.138.5.5144

64. Brandi ML, Hukkanen M, Umeda T, Moradi-Bidhendi N, Bianchi S, Gross SS, et al. Bidirectional regulation of osteoclast function by nitric oxide synthase isoforms. *Proc Natl Acad Sci U.S.A.* (1995) 92:2954–8. doi: 10.1073/pnas.92.7.2954

65. Zheng H, Yu X, Collin-Osdoby P, Osdoby P. RANKL stimulates inducible nitric-oxide synthase expression and nitric oxide production in developing osteoclasts. an autocrine negative feedback mechanism triggered by RANKL-induced interferon-beta *via* NF-kappaB that restrains osteoclastogenesis and bone resorption. *J Biol Chem* (2006) 281:15809–20. doi: 10.1074/jbc.M513225200

66. Kwon B, Moon CH, Kang S, Seo SK, Kwon BS. 4-1BB: still in the midst of darkness. *Mol Cells* (2000) 10:119–26. doi: 10.1007/s10059-000-0119-0

67. J Y, Oj P, Yj L, Hm J, Km W YC. The 4-1BB ligand and 4-1BB expressed on osteoclast precursors enhance RANKL-induced osteoclastogenesis *via* bi-directional signaling. *Eur J Immunol* (2008) 38:1598–1690. doi: 10.1002/eji.200737650

68. Shin H-H, Lee E-A, Kim S-J, Kwon BS, Choi H-S. A signal through 4-1BB ligand inhibits receptor for activation of nuclear factor-kappaB ligand (RANKL)-induced osteoclastogenesis by increasing interferon (IFN)-beta production. *FEBS Lett* (2006) 580:1601–6. doi: 10.1016/j.febslet.2006.01.091

69. Sarkar SN, Peters KL, Elco CP, Sakamoto S, Pal S, Sen GC. Novel roles of TLR3 tyrosine phosphorylation and PI3 kinase in double-stranded RNA signaling. *Nat Struct Mol Biol* (2004) 11:1060–7. doi: 10.1038/nsmb847

70. Aksoy E, Vanden Berghe W, Detienne S, Amraoui Z, Fitzgerald KA, Haegeman G, et al. Inhibition of phosphoinositide 3-kinase enhances TRIF-dependent NF-kappa b activation and IFN-beta synthesis downstream of toll-like receptor 3 and 4. *Eur J Immunol* (2005) 35:2200–9. doi: 10.1002/eji.200425801

71. Ahn J, Gutman D, Saijo S, Barber GN. STING manifests self DNA-dependent inflammatory disease. *Proc Natl Acad Sci U.S.A.* (2012) 109:19386–91. doi: 10.1073/pnas.1215006109

72. Kawane K, Ohtani M, Miwa K, Kizawa T, Kanbara Y, Yoshioka Y, et al. Chronic polyarthritis caused by mammalian DNA that escapes from degradation in macrophages. *Nature* (2006) 443:998–1002. doi: 10.1038/nature05245

73. Baum R, Sharma S, Carpenter S, Li Q-Z, Busto P, Fitzgerald KA, et al. Cutting edge: AIM2 and endosomal TLRs differentially regulate arthritis and autoantibody production in DNase II-deficient mice. *J Immunol* (2015) 194:873–7. doi: 10.4049/jimmunol.1402573

74. Weilbaecher KN, Guise TA, McCauley LK. Cancer to bone: a fatal attraction. *Nat Rev Cancer* (2011) 11:411–25. doi: 10.1038/nrc3055

75. Donnelly CR, Jiang C, Andriessen AS, Wang K, Wang Z, Ding H, et al. STING controls nociception *via* type I interferon signalling in sensory neurons. *Nature* (2021) 591:275–80. doi: 10.1038/s41586-020-03151-1

76. Corrales L, Glickman LH, McWhirter SM, Kanne DB, Sivick KE, Katibah GE, et al. Direct activation of STING in the tumor microenvironment leads to potent and systemic tumor regression and immunity. *Cell Rep* (2015) 11:1018–30. doi: 10.1016/j.celrep.2015.04.031

77. Brodowicz T, O'Byrne K, Manegold C. Bone matters in lung cancer. *Ann Oncol* (2012) 23:2215–22. doi: 10.1093/annonc/mds009

78. Margolis SR, Wilson SC, Vance RE. Evolutionary origins of cGAS-STING signaling. *Trends Immunol* (2017) 38:733–43. doi: 10.1016/j.it.2017.03.004

79. Jin L, Hill KK, Filak H, Mogan J, Knowles H, Zhang B, et al. MPYS is required for IFN response factor 3 activation and type I IFN production in the response of cultured phagocytes to bacterial second messengers cyclic-di-AMP and cyclic-di-GMP. *J Immunol* (2011) 187:2595–601. doi: 10.4049/jimmunol.1100088

80. Xiong Q, Zhang L, Ge W, Tang P. The roles of interferons in osteoclasts and osteoclastogenesis. *Joint Bone Spine* (2016) 83:276–81. doi: 10.1016/j.jbspin.2015.07.010

81. Feng X. RANKing intracellular signaling in osteoclasts. *IUBMB Life* (2005) 57:389–95. doi: 10.1080/15216540500137669

82. Yim HY, Park C, Lee YD, Arimoto K-I, Jeon R, Baek SH, et al. Elevated response to type I IFN enhances RANKL-mediated osteoclastogenesis in Usp18-knockout mice. *J Immunol* (2016) 196:3887–95. doi: 10.4049/jimmunol.1501496

83. Basu A, Yang K, Wang M, Liu S, Chintala R, Palm T, et al. Structure-function engineering of interferon-beta-1b for improving stability, solubility, potency, immunogenicity, and pharmacokinetic properties by site-selective mono-PEGylation. *Bioconjug Chem* (2006) 17:618–30. doi: 10.1021/bc050322y

84. Weinstock-Guttman B, Hong J, Santos R, Tamaño-Blanco M, Badgett D, Patrick K, et al. Interferon-beta modulates bone-associated cytokines and osteoclast precursor activity in multiple sclerosis patients. *Mult Scler* (2006) 12:541–50. doi: 10.1177/1352458506070605

85. Hayashi T, Kaneda T, Toyama Y, Kumegawa M, Hakeda Y. Regulation of receptor activator of NF-kappa b ligand-induced osteoclastogenesis by endogenous interferon-beta (INF-beta) and suppressors of cytokine signaling (SOCS). the possible counteracting role of SOCSs- in IFN-beta-inhibited osteoclast formation. *J Biol Chem* (2002) 277:27880–6. doi: 10.1074/jbc.M203836200

86. Oeckinghaus A, Hayden MS, Ghosh S. Crosstalk in NF-κB signaling pathways. *Nat Immunol* (2011) 12:695–708. doi: 10.1038/ni.2065

87. He S, Sharpless NE. Senescence in health and disease. *Cell* (2017) 169:1000–11. doi: 10.1016/j.cell.2017.05.015

88. Chung HY, Lee EK, Choi YJ, Kim JM, Kim DH, Zou Y, et al. Molecular inflammation as an underlying mechanism of the aging process and age-related diseases. *J Dent Res* (2011) 90:830–40. doi: 10.1177/0022034510387794

89. Salminen A, Huuskonen J, Ojala J, Kauppinen A, Kaarniranta K, Suuronen T. Activation of innate immunity system during aging: NF-kB signaling is the molecular culprit of inflamm-aging. *Ageing Res Rev* (2008) 7:83–105. doi: 10.1016/j.arr.2007.09.002

90. Seo E-J, Fischer N, Efferth T. Phytochemicals as inhibitors of NF-κB for treatment of alzheimer's disease. *Pharmacol Res* (2018) 129:262–73. doi: 10.1016/j.phrs.2017.11.030

91. Olefsky JM, Glass CK. Macrophages, inflammation, and insulin resistance. *Annu Rev Physiol* (2010) 72:219–46. doi: 10.1146/annurev-physiol-021909-135846

92. Zinatizadeh MR, Schock B, Chalbatani GM, Zarandi PK, Jalali SA, Miri SR, et al. (NF-kB) signaling in cancer development and immune diseases. *Genes Dis* (2021) 8:287–97. doi: 10.1016/j.gendis.2020.06.005

93. Barnabei L, Laplantine E, Mbongo W, Rieux-Laucat F, Weil R. NF-κB: At the borders of autoimmunity and inflammation. *Front Immunol* (2021) 12:716469. doi: 10.3389/fimmu.2021.716469

94. Chen Q, Tang L, Zhang Y, Wan C, Yu X, Dong Y, et al. STING up-regulates VEGF expression in oxidative stress-induced senescence of retinal pigment epithelium *via* NF-κB/HIF-1α pathway. *Life Sci* (2022) 293:120089. doi: 10.1016/j.lfs.2021.120089

95. Jin M, Shiwaku H, Tanaka H, Obita T, Ohuchi S, Yoshioka Y, et al. Tau activates microglia *via* the PQBP1-cGAS-STING pathway to promote brain inflammation. *Nat Commun* (2021) 12:6565. doi: 10.1038/s41467-021-26851-2

96. Pan Y, You Y, Sun L, Sui Q, Liu L, Yuan H, et al. The STING antagonist h-151 ameliorates psoriasis *via* suppression of STING/NF-κB-mediated inflammation. *Br J Pharmacol* (2021) 178:4907–22. doi: 10.1111/bph.15673

97. Mundy GR. Osteoporosis and inflammation. *Nutr Rev* (2007) 65:S147–151. doi: 10.1111/j.1753-4887.2007.tb00353.x

98. Goldring MB, Otero M. Inflammation in osteoarthritis. *Curr Opin Rheumatol* (2011) 23:471–8. doi: 10.1097/BOR.0b013e328349c2b1

99. Lyu F-J, Cui H, Pan H, Mc Cheung K, Cao X, Iatridis JC, et al. Painful intervertebral disc degeneration and inflammation: from laboratory evidence to clinical interventions. *Bone Res* (2021) 9:7. doi: 10.1038/s41413-020-00125-x

100. Haynes DR. Bone lysis and inflammation. *Inflammation Res* (2004) 53:596–600. doi: 10.1007/s00011-004-1303-z

101. Briot K, Roux C. Inflammation, bone loss and fracture risk in spondyloarthritis. *RMD Open* (2015) 1:e000052. doi: 10.1136/rmdopen-2015-000052

102. Smith JA. STING, the endoplasmic reticulum, and mitochondria: Is three a crowd or a conversation? *Front Immunol* (2020) 11:611347. doi: 10.3389/fimmu.2020.611347

103. Saberi M, Zhang X, Mobasheri A. Targeting mitochondrial dysfunction with small molecules in intervertebral disc aging and degeneration. *Geroscience* (2021) 43:517–37. doi: 10.1007/s11357-021-00341-1

104. Qadir A, Liang S, Wu Z, Chen Z, Hu L, Qian A. Senile osteoporosis: The involvement of differentiation and senescence of bone marrow stromal cells. *Int J Mol Sci*

(2020) 21:E349. doi: 10.3390/ijms21010349

105. Rea IM, Gibson DS, McGilligan V, McNerlan SE, Alexander HD, Ross OA. Age and age-related diseases: Role of inflammation triggers and cytokines. *Front Immunol* (2018) 9:586. doi: 10.3389/fimmu.2018.00586

106. Sharma P, Sampath H. Mitochondrial DNA integrity: Role in health and disease. *Cells* (2019) 8:100. doi: 10.3390/cells8020100

107. Liu Z, Wang M, Wang X, Bu Q, Wang Q, Su W, et al. XBP1 deficiency promotes hepatocyte pyroptosis by impairing mitophagy to activate mtDNA-cGAS-STING signaling in macrophages during acute liver injury. *Redox Biol* (2022) 52:102305. doi: 10.1016/j.redox.2022.102305

108. Zhong W, Rao Z, Rao J, Han G, Wang P, Jiang T, et al. Aging aggravated liver ischemia and reperfusion injury by promoting STING-mediated NLRP3 activation in macrophages. *Aging Cell* (2020) 19:e13186. doi: 10.1111/acel.13186

109. Zhang D, Liu Y, Zhu Y, Zhang Q, Guan H, Liu S, et al. A non-canonical cGAS-STING-PERK pathway facilitates the translational program critical for senescence and organ fibrosis. *Nat Cell Biol* (2022) 24:766–82. doi: 10.1038/s41556-022-00894-z

110. Huxford T, Hoffmann A, Ghosh G. Understanding the logic of IκB:NF-κB regulation in structural terms. *Curr Top Microbiol Immunol* (2011) 349:1–24. doi: 10.1007/82_2010_99

111. Hayden MS, Ghosh S. Shared principles in NF-kappaB signaling. *Cell* (2008) 132:344–62. doi: 10.1016/j.cell.2008.01.020

112. Ghosh S, May MJ, Kopp EB. NF-kappa b and rel proteins: Evolutionarily conserved mediators of immune responses. *Annu Rev Immunol* (1998) 16:225–60. doi: 10.1146/annurev.immunol.16.1.225

113. Courtois G, Gilmore TD. Mutations in the NF-kappaB signaling pathway: implications for human disease. *Oncogene* (2006) 25:6831–43. doi: 10.1038/sj.onc.1209939

114. Leibowitz SM, Yan J. NF-κB pathways in the pathogenesis of multiple sclerosis and the therapeutic implications. *Front Mol Neurosci* (2016) 9:84. doi: 10.3389/fnmol.2016.00084

115. Napetschnig J, Wu H. Molecular basis of NF-κB signaling. *Annu Rev Biophys* (2013) 42:443–68. doi: 10.1146/annurev-biophys-083012-130338

116. Mercurio F, Zhu H, Murray BW, Shevchenko A, Bennett BL, Li J, et al. IKK-1 and IKK-2: cytokine-activated IkappaB kinases essential for NF-kappaB activation. *Science* (1997) 278:860–6. doi: 10.1126/science.278.5339.860

117. Ghosh S, Karin M. Missing pieces in the NF-kappaB puzzle. *Cell* (2002) 109 Suppl:S81–96. doi: 10.1016/s0092-8674(02)00703-1

118. Hadjidakis DJ, Androulakis II. Bone remodeling. *Ann New York Acad Sci* (2006) 1092:385–96. doi: 10.1196/annals.1365.035

119. Lawrence T. The nuclear factor NF-kappaB pathway in inflammation. *Cold Spring Harb Perspect Biol* (2009) 1:a001651. doi: 10.1101/cshperspect.a001651

120. Adamopoulos IE. Inflammation in bone physiology and pathology. *Curr Opin Rheumatol* (2018) 30:59–64. doi: 10.1097/BOR.0000000000000449

121. Theoleyre S, Wittrant Y, Tat SK, Fortun Y, Redini F, Heymann D. The molecular triad OPG/RANK/RANKL: involvement in the orchestration of pathophysiological bone remodeling. *Cytokine Growth Factor Rev* (2004) 15:457–75. doi: 10.1016/j.cytogfr.2004.06.004

122. Cheng T, Zhang X. NFkappaB gene silencing inhibits wear particles-induced inflammatory osteolysis. *Med Hypotheses* (2008) 71:727–9. doi: 10.1016/j.mehy.2008.07.003

123. Wang T, He C. Pro-inflammatory cytokines: The link between obesity and osteoarthritis. *Cytokine Growth Factor Rev* (2018) 44:38–50. doi: 10.1016/j.cytogfr.2018.10.002

124. Fujita T, Matsui T, Nakao Y, Shiozawa S, Imai Y. Cytokines and osteoporosis. *Ann N Y Acad Sci* (1990) 587:371–5. doi: 10.1111/j.1749-6632.1990.tb00178.x

125. Hegde R, Awan KH. Effects of periodontal disease on systemic health. *Dis Mon* (2019) 65:185–92. doi: 10.1016/j.disamonth.2018.09.011

126. Krum SA, Chang J, Miranda-Carboni G, Wang C-Y. Novel functions for NFκB: inhibition of bone formation. *Nat Rev Rheumatol* (2010) 6:607–11. doi: 10.1038/nrrheum.2010.133

127. Asagiri M, Takayanagi H. The molecular understanding of osteoclast differentiation. *Bone* (2007) 40:251–64. doi: 10.1016/j.bone.2006.09.023

128. Boyce BF, Xing L. Functions of RANKL/RANK/OPG in bone modeling and remodeling. *Arch Biochem Biophys* (2008) 473:139–46. doi: 10.1016/j.abb.2008.03.018

129. Yamamoto M, Gohda J, Akiyama T, Inoue J-I. TNF receptor-associated factor 6 (TRAF6) plays crucial roles in multiple biological systems through polyubiquitination-mediated NF-κB activation. *Proc Jpn Acad Ser B Phys Biol Sci* (2021) 97:145–60. doi: 10.2183/pjab.97.009

130. Darnay BG, Ni J, Moore PA, Aggarwal BB. Activation of NF-kappaB by RANK requires tumor necrosis factor receptor-associated factor (TRAF) 6 and NF-kappaB-inducing kinase. *Identification novel TRAF6 interaction motif. J Biol Chem* (1999) 274:7724–31. doi: 10.1074/jbc.274.12.7724

131. Iotsova V, Caamaño J, Loy J, Yang Y, Lewin A, Bravo R. Osteopetrosis in mice lacking NF-kappaB1 and NF-kappaB2. *Nat Med* (1997) 3:1285–9. doi: 10.1038/nm1197-1285

132. Lomaga MA, Yeh WC, Sarosi I, Duncan GS, Furlonger C, Ho A, et al. TRAF6 deficiency results in osteopetrosis and defective interleukin-1, CD40, and LPS signaling. *Genes Dev* (1999) 13:1015–24. doi: 10.1101/gad.13.8.1015

133. Ruocco MG, Karin M. IKK{beta} as a target for treatment of inflammation induced bone loss. *Ann Rheum Dis* (2005) 64 Suppl 4:iv81–85. doi: 10.1136/ard.2005.042721

134. Ruocco MG, Maeda S, Park JM, Lawrence T, Hsu L-C, Cao Y, et al. I{kappa}B kinase (IKK){beta}, but not IKK{alpha}, is a critical mediator of osteoclast survival and is required for inflammation-induced bone loss. *J Exp Med* (2005) 201:1677–87. doi: 10.1084/jem.20042081

135. Ruocco MG, Karin M. Control of osteoclast activity and bone loss by IKK subunits: new targets for therapy. *Adv Exp Med Biol* (2007) 602:125–34. doi: 10.1007/978-0-387-72009-8_16

136. Boyce BF, Yao Z, Xing L. Functions of nuclear factor kappaB in bone. *Ann N Y Acad Sci* (2010) 1192:367–75. doi: 10.1111/j.1749-6632.2009.05315.x

137. Lee S-Y, Lee K-S, Yi SH, Kook S-H, Lee J-C. Acteoside suppresses RANKL-mediated osteoclastogenesis by inhibiting c-fos induction and NF-κB pathway and attenuating ROS production. *PloS One* (2013) 8:e80873. doi: 10.1371/journal.pone.0080873

138. Yu B., Chang J., Liu Y., Li J., Kevork K., Al-Hezaimi K. Wnt4 signaling prevents skeletal aging and inflammation by inhibiting nuclear factor-κB. *Nat Med* (2014) 20:1009–1017. doi: 10.1038/nm.3586

139. Lin T-H, Gibon E, Loi F, Pajarinen J, Córdova LA, Nabeshima A, et al. Decreased osteogenesis in mesenchymal stem cells derived from the aged mouse is associated with enhanced NF-κB activity. *J Orthop Res* (2017) 35:281–8. doi: 10.1002/jor.23270

140. Lin T, Tamaki Y, Pajarinen J, Waters HA, Woo DK, Yao Z, et al. Chronic inflammation in biomaterial-induced periprosthetic osteolysis: NF-κB as a therapeutic target. *Acta Biomater* (2014) 10:1–10. doi: 10.1016/j.actbio.2013.09.034

141. Liu J, Lin A. Role of JNK activation in apoptosis: a double-edged sword. *Cell Res* (2005) 15:36–42. doi: 10.1038/sj.cr.7290262

142. Jimi E, Takakura N, Hiura F, Nakamura I, Hirata-Tsuchiya S. The role of NF-κB in physiological bone development and inflammatory bone diseases: Is NF-κB inhibition "Killing two birds with one stone"? *Cells* (2019) 8:1636. doi: 10.3390/cells8121636

143. Eferl R, Hoebertz A, Schilling AF, Rath M, Karreth F, Kenner L, et al. The fos-related antigen fra-1 is an activator of bone matrix formation. *EMBO J* (2004) 23:2789–99. doi: 10.1038/sj.emboj.7600282

144. Gilbert L, He X, Farmer P, Boden S, Kozlowski M, Rubin J, et al. Inhibition of osteoblast differentiation by tumor necrosis factor-alpha. *Endocrinology* (2000) 141:3956–64. doi: 10.1210/endo.141.11.7739

145. Yamazaki M., Fukushima H., Shin M., Katagiri T., Takahashi D., Takahashi T., et al Tumor necrosis factor alpha represses bone morphogenetic protein (BMP) signaling by interfering with the DNA binding of smads through the activation of NF-kappaB. *J Biol Chem* (2009) 284:35987–35995. doi: 10.1074/jbc.M109.070540

146. Chang J, Wang Z, Tang E, Fan Z, McCauley L, Franceschi R, et al. Inhibition of osteoblastic bone formation by nuclear factor-kappaB. *Nat Med* (2009) 15:682–9. doi: 10.1038/nm.1954

147. Alles N, Soysa NS, Hayashi J, Khan M, Shimoda A, Shimokawa H, et al. Suppression of NF-kappaB increases bone formation and ameliorates osteopenia in ovariectomized mice. *Endocrinology* (2010) 151:4626–34. doi: 10.1210/en.2010-0399

148. Quan Y, Xin Y, Tian G, Zhou J, Liu X. Mitochondrial ROS-modulated mtDNA: A potential target for cardiac aging. *Oxid Med Cell Longev* (2020) 2020:9423593. doi: 10.1155/2020/9423593

149. Gloire G, Legrand-Poels S, Piette J. NF-kappaB activation by reactive oxygen species: fifteen years later. *Biochem Pharmacol* (2006) 72:1493–505. doi: 10.1016/j.bcp.2006.04.011

150. Burdette DL, Monroe KM, Sotelo-Troha K, Iwig JS, Eckert B, Hyodo M, et al. STING is a direct innate immune sensor of cyclic di-GMP. *Nature* (2011) 478:515–8. doi: 10.1038/nature10429

151. Balka KR, Louis C, Saunders TL, Smith AM, Calleja DJ, D'Silva DB, et al. TBK1 and IKKε act redundantly to mediate STING-induced NF-κB responses in myeloid cells. *Cell Rep* (2020) 31:107492. doi: 10.1016/j.celrep.2020.03.056

152. Sun Y-X, Xu A-H, Yang Y, Li J. Role of Nrf2 in bone metabolism. *J BioMed Sci* (2015) 22:101. doi: 10.1186/s12929-015-0212-5

153. Olagnier D, Brandtoft AM, Gunderstofte C, Villadsen NL, Krapp C, Thielke AL, et al. Nrf2 negatively regulates STING indicating a link between antiviral sensing and metabolic reprogramming. *Nat Commun* (2018) 9:3506. doi: 10.1038/s41467-018-05861-7

154. Zhang J, Pan J, Jing W. Motivating role of type h vessels in bone regeneration. *Cell Prolif* (2020) 53:e12874. doi: 10.1111/cpr.12874

155. Peng Y, Wu S, Li Y, Crane JL. Type h blood vessels in bone modeling and remodeling. *Theranostics* (2020) 10:426–36. doi: 10.7150/thno.34126

156. Yang Y-Q, Tan Y-Y, Wong R, Wenden A, Zhang L-K, Rabie ABM. The role of vascular endothelial growth factor in ossification. *Int J Oral Sci* (2012) 4:64–8. doi: 10.1038/ijos.2012.33

157. Grosso A, Burger MG, Lunger A, Schaefer DJ, Banfi A, Di Maggio N. It takes two to tango: Coupling of angiogenesis and osteogenesis for bone regeneration. *Front Bioeng*

Biotechnol (2017) 5:68. doi: 10.3389/fbioe.2017.00068

158. Zhou X, Kunkel G, Zhang Z, Deng JM, Behringer RR, et al. The novel zinc finger-containing transcription factor osterix is required for osteoblast differentiation and bone formation. *Cell* (2002) 108:17–29. doi: 10.1016/s0092-8674(01)00622-5

159. Farr JN, Khosla S. Cellular senescence in bone. *Bone* (2019) 121:121–33. doi: 10.1016/j.bone.2019.01.015

160. Zhu Y, Ruan Z, Lin Z, Long H, Zhao R, Sun B, et al. The association between CD31hiEmcnhi endothelial cells and bone mineral density in Chinese women. *J Bone Miner Metab* (2019) 37:987–95. doi: 10.1007/s00774-019-01000-4

161. Wang L, Zhou F, Zhang P, Wang H, Qu Z, Jia P, et al. Human type h vessels are a sensitive biomarker of bone mass. *Cell Death Dis* (2017) 8:e2760. doi: 10.1038/cddis.2017.36

162. Wang H, Yin Y, Li W, Zhao X, Yu Y, Zhu J, et al. Over-expression of PDGFR-β promotes PDGF-induced proliferation, migration, and angiogenesis of EPCs through PI3K/Akt signaling pathway. *PloS One* (2012) 7:e30503. doi: 10.1371/journal.pone.0030503

163. Ball SG, Shuttleworth CA, Kielty CM. Mesenchymal stem cells and neovascularization: role of platelet-derived growth factor receptors. *J Cell Mol Med* (2007) 11:1012–30. doi: 10.1111/j.1582-4934.2007.00120.x

164. Andrae J, Gallini R, Betsholtz C. Role of platelet-derived growth factors in physiology and medicine. *Genes Dev* (2008) 22:1276–312. doi: 10.1101/gad.1653708

165. Xie H, Cui Z, Wang L, Xia Z, Hu Y, Xian L, et al. PDGF-BB secreted by preosteoclasts induces angiogenesis during coupling with osteogenesis. *Nat Med* (2014) 20:1270–8. doi: 10.1038/nm.3668

166. Huang J, Yin H, Rao S-S, Xie P-L, Cao X, Rao T, et al. Harmine enhances type h vessel formation and prevents bone loss in ovariectomized mice. *Theranostics* (2018) 8:2435–46. doi: 10.7150/thno.22144

167. Jiang Y, Liu C, Chen W, Wang H, Wang C, Lin N. Tetramethylpyrazine enhances vascularization and prevents osteonecrosis in steroid-treated rats. *BioMed Res Int* (2015) 2015:315850. doi: 10.1155/2015/315850

168. Pufe T, Scholz-Ahrens KE, Franke ATM, Petersen W, Mentlein R, Varoga D, et al. The role of vascular endothelial growth factor in glucocorticoid-induced bone loss: evaluation in a minipig model. *Bone* (2003) 33:869–76. doi: 10.1016/j.bone.2003.08.002

169. Yang P, Lv S, Wang Y, Peng Y, Ye Z, Xia Z, et al. Preservation of type h vessels and osteoblasts by enhanced preosteoclast platelet-derived growth factor type BB attenuates glucocorticoid-induced osteoporosis in growing mice. *Bone* (2018) 114:1–13. doi: 10.1016/j.bone.2018.05.025

170. Pugh CW, Ratcliffe PJ. Regulation of angiogenesis by hypoxia: Role of the HIF system. *Nat Med* (2003) 9:677–84. doi: 10.1038/nm0603-677

171. Kusumbe AP, Ramasamy SK, Adams RH. Coupling of angiogenesis and osteogenesis by a specific vessel subtype in bone. *Nature* (2014) 507:323–8. doi: 10.1038/nature13145

172. Riddle RC, Khatri R, Schipani E, Clemens TL. Role of hypoxia-inducible factor-1alpha in angiogenic-osteogenic coupling. *J Mol Med (Berl)* (2009) 87:583–90. doi: 10.1007/s00109-009-0477-9

173. Gao B, Lin X, Jing H, Fan J, Ji C, Jie Q, et al. Local delivery of tetramethylpyrazine eliminates the senescent phenotype of bone marrow mesenchymal stromal cells and creates an anti-inflammatory and angiogenic environment in aging mice. *Aging Cell* (2018) 17:e12741. doi: 10.1111/acel.12741

174. Demaria O, De Gassart A, Coso S, Gestermann N, Di Domizio J, Flatz L, et al. STING activation of tumor endothelial cells initiates spontaneous and therapeutic antitumor immunity. *Proc Natl Acad Sci U.S.A.* (2015) 112:15408–13. doi: 10.1073/pnas.1512832112

175. Baris AM, Fraile-Bethencourt E, Anand S. Nucleic acid sensing in the tumor vasculature. *Cancers (Basel)* (2021) 13:4452. doi: 10.3390/cancers13174452

176. Liu Y, Jesus AA, Marrero B, Yang D, Ramsey SE, Sanchez GAM, et al. Activated STING in a vascular and pulmonary syndrome. *N Engl J Med* (2014) 371:507–18. doi: 10.1056/NEJMoa1312625

177. Crow YJ, Casanova J-L. STING-associated vasculopathy with onset in infancy–a new interferonopathy. *N Engl J Med* (2014) 371:568–71. doi: 10.1056/NEJMe1407246

178. Jiang X, Liu G, Hu Z, Chen G, Chen J, Lv Z. cGAMP inhibits tumor growth in colorectal cancer metastasis through the STING/STAT3 axis in a zebrafish xenograft model. *Fish Shellfish Immunol* (2019) 95:220–6. doi: 10.1016/j.fsi.2019.09.075

179. Yuan L, Mao Y, Luo W, Wu W, Xu H, Wang XL, et al. Palmitic acid dysregulates the hippo-YAP pathway and inhibits angiogenesis by inducing mitochondrial damage and activating the cytosolic DNA sensor cGAS-STING-IRF3 signaling mechanism. *J Biol Chem* (2017) 292:15002–15. doi: 10.1074/jbc.M117.804005

180. Mao Y, Luo W, Zhang L, Wu W, Yuan L, Xu H, et al. STING-IRF3 triggers endothelial inflammation in response to free fatty acid-induced mitochondrial damage in diet-induced obesity. *Arterioscler Thromb Vasc Biol* (2017) 37:920–9. doi: 10.1161/ATVBAHA.117.309017

181. Guo Y, Gu R, Gan D, Hu F, Li G, Xu G. Mitochondrial DNA drives noncanonical inflammation activation *via* cGAS-STING signaling pathway in retinal microvascular endothelial cells. *Cell Commun Signal* (2020) 18:172. doi: 10.1186/s12964-020-00637-3

182. Huang J, Han Q, Cai M, Zhu J, Li L, Yu L, et al. Effect of angiogenesis in bone tissue engineering. *Ann BioMed Eng* (2022) 50:898–913. doi: 10.1007/s10439-022-02970-9

frontiers | Frontiers in Immunology

TYPE Review
PUBLISHED 24 January 2023
DOI 10.3389/fimmu.2022.1053136

OPEN ACCESS

EDITED BY
Mirza S. Baig,
Indian Institute of Technology
Indore, India

REVIEWED BY
Milica Milovan Borovcanin,
University of Kragujevac, Serbia
Ivana Kawikova,
Quinnipiac University, United States

*CORRESPONDENCE
Fang Deng
deng_fang@jlu.edu.cn

SPECIALTY SECTION
This article was submitted to Inflammation, a section of the journal Frontiers in Immunology

RECEIVED 25 September 2022
ACCEPTED 05 December 2022
PUBLISHED 24 January 2023

CITATION
Gong S and Deng F (2023) Renin-angiotensin system: The underlying mechanisms and promising therapeutical target for depression and anxiety.
Front. Immunol. 13:1053136.
doi: 10.3389/fimmu.2022.1053136

Renin-angiotensin system: The underlying mechanisms and promising therapeutical target for depression and anxiety

Sizhu Gong and Fang Deng*

Department of Neurology, First Affiliated Hospital of Jilin University, Changchun, China

Emotional disorders, including depression and anxiety, contribute considerably to morbidity across the world. Depression is a serious condition and is projected to be the top contributor to the global burden of disease by 2030. The role of the renin-angiotensin system (RAS) in hypertension and emotional disorders is well established. Evidence points to an association between elevated RAS activity and depression and anxiety, partly through the induction of neuroinflammation, stress, and oxidative stress. Therefore, blocking the RAS provides a theoretical basis for future treatment of anxiety and depression. The evidence for the positive effects of RAS blockers on depression and anxiety is reviewed, aiming to provide a promising target for novel anxiolytic and antidepressant medications and/or for improving the efficacy of currently available medications used for the treatment of anxiety and depression, which independent of blood pressure management.

KEYWORDS

deprssion, anxiety, renin-angiotensin system, angiotensin II, neuroinflammation

1 Introduction

Emotional disorders, including depression and anxiety, contribute considerably to morbidity across the world (1). Anxiety disorders are the most common class of disorders listed in the Diagnostic and Statistical Manual of Mental Disorders, Fifth Edition (DSM-V), which are complex interactions between biological, psychological, temperamental, and environmental factors (2). As a group, anxiety disorders represent a heterogeneous group of illnesses that are characterized by excessive fear and anxiety, hypervigilance, and related behavioral disturbances (3). Furthermore, anxiety is one of the most common comorbid disorders with major depressive disorder (MDD) (4, 5). A large psychiatric cohort study has reported that depression preceded anxiety in 18% of such comorbid

cases, while in 57% of the cases anxiety preceded depression (5). Comorbid anxiety and many core depression symptoms may be caused by hyperactivity of the hypothalamic-pituitary-adrenal (HPA) axis combined with amygdala dysfunction (4). The amygdala is a key element of anxiety circuitry and produces behavioral responses associated with fear and anxiety by integrating information from sensory inputs in the cortex and thalamus (6). Similarly, some neuroimaging studies have reported enhanced amygdala glucose metabolism and activation in patients with depression (7), and that depression-associated anxiety is accompanied by an increase in amygdala volume (8). First-degree relatives of individuals with anxiety have an increased risk of developing anxiety disorders or depression (9). Importantly, however, only 40–70% of patients with depression respond to pharmacological treatment and therapies often have a delayed onset (10), and anxiety associated with depression often leads to reduced responses and decreased compliance with pharmacotherapy (6). Consequently, emotional disorders are a serious public health issue, and identifying novel targets for their treatment is worthy of further attention.

The role of the renin-angiotensin system (RAS) in hypertension and emotional disorders is well established. Evidence points to an association between elevated RAS activity and depression and anxiety, partly through the induction of neuroinflammation, stress, and oxidative stress (11). Importantly, blocking RAS can have anti-inflammatory and anti-oxidative stress effects, providing a theoretical basis for future treatment of anxiety and depression. Captopril and enalapril (angiotensin-converting enzyme inhibitors; ACEIs) may rapidly improve depressive moods in hypertensive patients (12). This has sparked significant interest in RAS targets. The evidence for the positive effects of RAS blockers on depression and anxiety is reviewed here to evaluate a promising target for novel anxiolytic and antidepressant medications. Furthermore, this knowledge may aid the improvement of the efficacy of currently available medications used for the treatment of anxiety and depression, which are independent of blood pressure management.

2 Overview of RAS

RAS-blockers or RAS inhibitors are classes of medications that block the renin-angiotensin axis, primarily inhibiting angiotensin (Ang) II activity. Examples include ACEIs and selective Ang II type 1 receptor blockers (ARBs) (13). The most common ACEIs include captopril, enalapril, lisinopril, perindopril, ramipril, and imidapril. The most common ARBs include losartan, irbesartan, candesartan, telmisartan, and valsartan. As effective first-line antihypertensive medications, ACEIs and ARBs have been shown to minimize the risk of cardiovascular and renal events as well as mortality (14). These classes of drugs target Ang II, however, differences in their mechanisms of action impact their effects on other pathways and receptors, which may have therapeutic implications. For example, ACEIs inhibit RAS activation by preventing the conversion of Ang I to Ang II, resulting in reduced activation of both Ang II type 1 (AT1/AT1) receptors and Ang II type 2 (AT2/AT2) receptors (15). Moreover, ACEIs prevent the degradation of Ang-(1–7) by angiotensin-converting enzyme (ACE), thereby the level increased due to a build-up caused by the lack of degradation of Ang-(1–7) (15). Additionally, ACEIs block the degradation of bradykinin, leading to activation of the β-2 receptor and promotion of nitric oxide (NO) release with vasodilatory and tissue-protective effects (13). One study showed that ACEIs rapidly ameliorate depressive behaviors *via* the bradykinin-dependent activation of the target of the rapamycin complex (10). Unlike ACEIs, ARBs block RAS by antagonizing the binding of Ang II to the AT1 receptor and activating the AT2 receptors, thus producing insufficient Ang II to elevate Ang-(1–7) level (16). High levels of Ang-(1–7) reduce anxiety and depression behaviors, providing positive benefits (see below). RAS blockers shift the balance to increase circulating levels of Ang-(1–7), this may contribute to shunt the ACE/Ang II/AT1 pathway toward the ACE2/Ang-(1–7)/MasR pathway providing beneficial effects on mood disorders (17).

Although RAS is widely acknowledged as a cardiovascular circulation hormonal system, it is found in a variety of organs, including the brain. The RAS is composed of two pathways that are mutually antagonistic that maintain the balance through angiotensin-converting enzyme 2 (ACE2): the classical pathway angiotensin-converting enzyme/angiotensin II/angiotensin II type 1 receptor (ACE/Ang II/AT_1R) and the non-classical pathway angiotensin-converting enzyme 2/angiotensin- (1–7)/Mas receptor (ACE2/Ang-(1–7)/MasR).

2.1 Classical pathway: ACE/Ang II/AT_1R

The classical pathway contains renin, angiotensin (Ang) II, angiotensin-converting enzyme (ACE), angiotensin II type 1 receptor (AT_1R/AT1R), and angiotensin II type 2 receptor (AT_2R/AT2R). Renin is an aspartyl protease typically produced in the juxtaglomerular cells of the kidney, and it cleaves angiotensinogen (ATN, an inactive peptide formed and secreted by the liver) to produce angiotensin I (Ang I). Ang I has few physiological effects and produces Ang II as a substrate for ACE. Ang II exerts several physiological effects: constriction of blood vessels, stimulation of aldosterone secretion, and release of catecholamines. Ang II acts by binding to the AT_1R and AT_2R. When Ang II activates the AT_1 receptor, it causes neurotoxicity, such as vasoconstriction, pro-inflammatory, apoptotic, and anti-diuresis. Furthermore, increased circulating levels of Ang II disrupt blood-brain barrier (BBB) integrity, allowing circulating Ang II to

access the brain parenchyma and trigger the AT_1R directly, producing oxidative stress and brain inflammation (18). AT_2R is activated by Ang II and may counterbalance AT_1R neurotoxic effects and determine a neuroprotective role in RAS activation, such as vasodilation, diuresis, anti-fibrosis, antihypertensive, and cognitive improvement. AT_2R activation is important in blunting the negative effects of AT_1R, such as neuroinflammation and oxidative stress (19). However, evidence shows that AT_1 receptors predominate in adult tissues and AT_2 receptors predominated in the developing brain (20).

2.2 Non-classical pathway: ACE2/Ang-(1–7)/MasR

The non-classical axis is neuroprotective and composes angiotensin-converting enzyme 2/angiotensin-(1–7)/Mas receptor axis (ACE2/Ang-(1–7)/MasR). The non-classical axis exerts neuroprotective effects, such as promoting the release of NO and promoting anti-inflammatory, anti-fibrotic, and vasodilatation effects. In the brain, all components of the ACE2/Ang-(1–7)/MasR axis are expressed. ACE2 correlates with AT_1R and Ang II levels and ACE2 overexpression results in the downregulation of AT_1R and increases the expression of AT_2R and MasR. As a homologous enzyme of ACE, ACE2 is found in the hippocampus and cerebral cortex that cleaves Ang II to produce Ang-(1–7), which activates the Mas receptor and produces an inverse regulation of the ACE/Ang II/AT1 pathway (21, 22). Ang-(1–7) generated in the rat hippocampus has been reported (23). As for the Mas receptor, it was a G protein-coupled receptor specific for Ang-(1–7), which is expressed in brains and other different organs, including the hippocampus, amygdala, and cortex (21).

3 The relationship between RAS and depression/anxiety

In addition to the systemic RAS, all the components of the RAS independently exist in the brain involving the pathophysiology of depression and anxiety. Hyperactivation of the ACE/Ang II/AT1R classical pathway accelerate the disease process *via* activated AT1R, while AT2R plays a protective role (24). We will discuss the evidence and mechanisms of RAS involvement in depression and anxiety in this part (Figure 1A) (Table 1).

3.1 ACE/Ang II/AT1R and depression/anxiety

Angiotensinogen is the glycoprotein precursor of angiotensin II. Voigt et al. were the first time to describe transgenic rats with low brain angiotensinogen behavioral phenotype as characterized by increased anxiety-related behaviors (41). Subsequently, studies showed low angiotensinogen concentration in the brain leads to anxiety-like behaviors accompanied by a depression-like state (25).

Ang II was previously discovered as a pro-hypertensive factor present in areas of the brain associated with cardiovascular and has recently been found to be associated with motor activity, anxiety, learning, and memory (20). Additionally, increased Ang II level is significantly associated with depression, anxiety, hyperactivity of the HPA axis, and stress (28, 42). For instance, treatment with Ang II for 14 consecutive days had significant anxious-like behaviors and bidirectional synaptic plasticity impairment, and increase expression of $GABA_AR\alpha1$ (γ-aminobutyric acid A receptor) (27). Administered Ang II for 3 weeks induced cognitive impairment and anxiety-like behaviors as shown by spending less time in the four center squares in the open field tests (OFT) (26). Telmisartan and imipramine reversed chronic Ang II infusion-induced behavioral changes, including changes in TST and forced swimming test (FST) (28). Losartan microinjects into the hippocampus CA1 region showed an anxiolytic-like effect in bilateral olfactory bulbectomy rats (OBX, rat model of depression), indicating the involvement of Ang II in the pathogenesis of anxiety by activating AT_1R (42). Whereas microinjections Ang II (0.1,0.5,1.0μg) into the CA1 hippocampal area, at a dose of 0.1μg shows some anxiolytic effects manifested as an increasing number of entries into the open arms in the elevated plus maze (EPM) (29). The results are inconsistent with previous studies, but there may be anxiolytic and anxiety effects of Ang II in a dose-related U-shaped manner.

Furthermore, hyperactivation of AT_1a receptors is associated with promoting anxiety-like behaviors in the brain (31). Deletion of AT_1a receptors ($AT_1a-/-$) from the paraventricular nucleus (PVN) attenuated anxiety-like behaviors in rodents as manifested by increased time spent in the open arms of the EPM (31). Further, ($AT_1a-/-$)mice reduced flight behavior in the elevated T-maze test (a model of anxiety and panic) and diminished fear responses despite threat levels (30).

Chronically infused intracerebroventricular (i.c.v.) AT_2 receptors agonist evokes anxiolytic-like effects (32). Treatment with selective AT_2 receptor antagonist PD123319 decreased the open arms exploration in EPM and changed the pattern of swimming during the FST (33). AT_2 receptor-deficient mice increased anxiety-like behaviors, which can be reversed by captopril, and show no depression-like behaviors compared to wild-type mice, providing a theoretical basis for ACEIs for the treatment of emotional disorders (35). Recently, it was reported that the modulatory role of the AT_2 receptor in the development of depressive-like behavior (43). Administration of AT_2R antagonist PD123319 into the prefrontal cortex reversed the antidepressant effect of losartan (34), indicating AT_2R has positive effects on depression and anxiety.

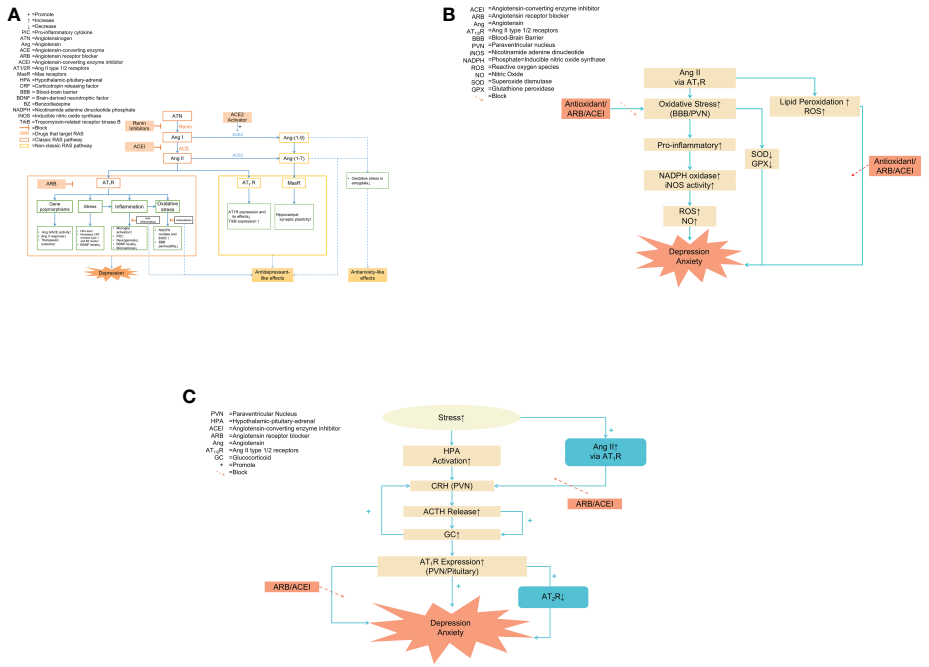

FIGURE 1
(A) The overview of RAS and the role of the RAS in the pathophysiology of anxiety and depression. Notes: The blue dashed line pointed to the positive effects, such as antidepressant-like and anxiolytic effects. Two key regulatory pathways: the classical axis ACE/Ang II/AT1 receptor pathway and the non-classical pathway ACE2/Ang-(1–7)/Mas receptor pathway. Under physiological conditions, the two pathways regulated each other and maintained a dynamic balance. Ang II aggravated oxidative stress and inflammation response by activating AT1R to upregulate the ACE/Ang II/AT1R pathway, promoting the development of emotional disorders. Ang II activated non-classical pathways by activating AT2R and MasR, producing antidepressant-like and anxiolytic effects. Thus, the beneficial effects of RAS blockers may be due to inhibiting oxidative stress and inflammation by directly targeting Ang II and its AT1 receptor. Other potential targets of anxiolytic drugs include renin, ACE2, AT2 receptors, and Mas receptors. **(B)** RAS and oxidative stress in depression and anxiety Notes: The pro-inflammatory effects of Ang II were largely mediated by increased oxidative stress. During inflammation, Ang II activated AT_1R to promote the oxidative stress process by increasing NADPH oxidase and iNOS activity in the BBB and PVN, resulting in an accumulation of ROS and NO and ultimately aggravating emotional disorders. Antioxidant enzyme activity was decreased during oxidative stress, which was prevented by RAS blockers and antioxidants. Furthermore, Ang II directly increased ROS generation and triggered lipid peroxidation, inhibited by RAS inhibitors and antioxidants. **(C)** HPA and RAS. Notes: The type of stress caused HPA axis activation and increased the downstream hormones such as CRH, ACTH, and GC, eventually promoting anxiety and depression. Stress increased Ang II levels, which in turn raised the expression of CRH mRNA, induced the release of ACTH and GC, and enhanced the stimulatory effects of CRH through AT1R located in the pituitary and PVN. The absence of AT2 receptor transcription enhanced the AT1 receptor expression in brain areas and was involved in regulating the HPA axis, which was associated with anxiety and depression. Pretreatment with RAS blockers attenuated neuroendocrine responses, preventing the development of stress-induced anxiety/depression-like behaviors. **(C)** RAS and oxidative stress in depression and anxiety. Notes: The pro-inflammatory effects of Ang II were largely mediated by increased oxidative stress. During inflammation, Ang II activated AT_1R to promote the oxidative stress process by increasing NADPH oxidase and iNOS activity in the BBB and PVN, resulting in an accumulation of ROS and NO and ultimately aggravating emotional disorders. Antioxidant enzyme activity was decreased during oxidative stress, which was prevented by RAS blockers and antioxidants. Furthermore, Ang II directly increased ROS generation and triggered lipid peroxidation, inhibited by RAS inhibitors and antioxidants.

3.2 ACE2/Ang-(1–7)/MasR and antidepressant/anxiolytic effect

Walther was the first to discover that the ACE2/Ang-(1–7)/MasR pathway is associated with the development of anxiety, demonstrating that upregulating ACE2 significantly improved anxiety-like behaviors (40). ACE2 is essential for maintaining the balance between ACE2/Ang-(1–7)/Mas receptor and the ACE/Ang II/AT_1R pathway. The main function of ACE2 is to inhibit ACE activity by decreasing Ang II bioavailability and increasing Ang-(1–7) levels. Thus, the overexpression of ACE2 not only is related to the upregulation of AT_2R and Mas receptors but also to the downregulation of AT_1R and ACE (44). Elevated ACE2 activity decreases anxiety-like behaviors and inhibits stress-induced activation of the HPA axis in male mice (45). However, in female mice, increasing ACE2 expression only produces anxiolysis without reversing HPA axis activity (45). Consistent with the effect, central administration of diminazen aceturate to mice, an ACE2 activator reduces anxiety-like behaviors in EPM (36).

Ang-(1–7) is associated with reduced depressive and anxious behaviors as a selective non-competitive antagonist of Ang II at type 1 Ang II receptors (46). Overexpression of circulation Ang-(1–7) produced anxiolytic-like effects have been found in transgenic rats

TABLE 1 The relationship between RAS components and depression/anxiety.

RASComponent	Compounds	Species	Mode of Administration	Measure Method	Main Findings	Reference
ATN		Low ATN TGR			Anxiety/depression-like behaviors↑	(25)
Ang II		UMS rats	21 days	OFT	Anxiety-like behaviors↑ Cognition↑	(26)
		Adult C57 mice	14 days		Anxiety-like behaviors↑ Synaptic plasticity↓	(27)
		Adult male C57BL/6	21 days	TST FST	Depressive–like behaviors↑ HPA axis↑	(28)
		Male SD rats	Microinjected into hippocampal CA1 0.1μg	EPM	Anxiolytic-like	(29)
AT_1R		(AT1A−/−) mice		ETM	Anxiolytic Fear responses↓	(30)
		(AT1A−/−) mice in PVN		EPM OFT	Anxiolytic	(31)
AT_2R	Agonist Novokinin	Male Wistar rats with T1DM	ICV	EPM TMRA	Anxiolytic Cognition↑ Spatial memory↑	(32)
	Antagonist PD123319	Male Wistar rats	Microinjected into MeA (100 nL/side)	EPM FST	Anxiety-like behaviors↑	(33)
	Antagonist PD123319	Male Wistar rats and female C57BL/6 mice		FST	Anxiety-like behaviors↑	(34)
		AT2R-deficient mice		EPM OFT	Anxiety-like behaviors↑	(35)
ACE2		Male mice overexpressing ACE2		EPM	Anxiolytic	(36)
	Activator diminazen aceturate	C57BL/6 mice		EPM	Anxiolytic	(36)
Ang-(1–7)		Adult male TGR (ASrAOGEN)	1μmol/μL	EPM FST	Anxiolytic Anti-depressant	(25)
		Adult male Wistar rats		EPM	Anxiolytic	(37)
		TGR rats (mRen2)27	1μL	EPM FST NSF	Anxiolytic Antidepressant	(38)
		Adult male SD rats	0.5μg in 0.5μL	OFT EPM	Anxiolytic	(39)
Mas		Mas-deficient rats		EPM	Anxiety-like behaviors↑	(40)
	Antagonist A-779	Male Wistar rats	Microinjected into MeA (100 nL/side)	EPM FST	Anxiety-like behaviors↑	(33)
	A-779	C57BL/6 mice		EPM	Anxiety-like behaviors↑	(36)

ATN, angiotensinogen; UMS, unpredictable mild stress; OFT, open field test; FST, forced swim test; TST, tail suspension test; EPM, elevated-plus-maze; ICV, intracerebroventricular; AT_2R, AT2 receptors; AT_1R, AT1 receptors; AT1aR, AT1a receptors; PVN, paraventricular nucleus; ↓, means decreased; ↑, means increased; TGR(ASrAOGEN), transgenic rats with low brain angiotensinogen; TGR, transgenic rat; (AT1A−/−), AT1A receptor knockout mice; ETM, elevated T-maze; TMRA, T-maze rewarded alternation test; T1DM, type 1 diabetes mellitus; MeA, medial amygdaloid nucleus; IP/i.p., intraperitoneally; LDB, light-dark box; NIH, novelty-induced hypophagia; NSF, novelty suppressed feeding; VCT, vogel conflict test; MasR, Mas receptors; ACEI, angiotensin-converting enzyme inhibitors; ARB, angiotensin II receptor blockers.

(37), which were manifested by increasing the percentage of time spent and frequency of entries in the open arms and decreasing stretching in closed arms of the EPM (38, 47). In addition, overexpression of Ang-(1–7) reverses the increase in heart rate associated with emotional stress and demonstrates less anxious behaviors in transgenic rats (48). Low angiotensinogen levels in the brain lead to anxiety-like behaviors and depression-like behaviors, while intracerebroventricular administration of Ang-(1–7), selective serotonin reuptake inhibitor fluoxetine, enalapril (ACEI) attenuated behavioral changes in transgenic hypertensive rats, as shown by spending a lower percentage of time in the open arms of EPM and decreasing immobility time in FST (25, 38).

Centrally injecting the MasR antagonist reverses the ACE2 and Ang-(1–7)-induced anxiolytic effects, indicating the anxiolytic effects of ACE2/Ang-(1–7)/MasR pathway due to activate Mas receptors (36, 47). Pre-treatment with A779 (a selective Mas receptor antagonist) enhances the anxiety-like effects (38), showing decreases open arms exploration in the EPM and changes the pattern of swimming during the forced swim test (33). MasR-deficient mice influence hippocampal synaptic plasticity and exhibit increased anxiety behaviors in EPM (40). Taken together, the upregulation of the ACE/Ang II/AT1R pathway accelerates the process of the emotional disorder and the non-classical axis ACE2/Ang-(1–7)/MasR has neuroprotective effects on emotional disorders.

3.3 RAS blockers-induced mood-elevating effects

ACEIs and ARBs have been shown to have protective and potential therapeutic benefits in mood disorders (49)(Table 2). Saavedra et al. proposed that Ang II expression is associated with mood disorders and that reducing brain Ang II levels might decrease anxiety and depression in animal models (57). For example, treatment with captopril had significant antidepressant activity as shown by the forced swim-induced behavioral despair (immobility) test in mice. In addition, it reversed escape deficits in the learned helplessness model (55, 58). Studies in rodents injected with losartan systemically and locally to the anterior prefrontal cortex and medial amygdaloid nucleus have shown antidepressant effects as evidenced by decreased immobility time in the FST (33, 34).

Chronic administration of the ACEI perindopril has anxiolytic effects on rats (56). Chronic cerebral hypoperfusion induces ACE/Ang II/AT1R overexpression in the hippocampus and causes anxiety. Candesartan and perindopril attenuate anxiety-like behavior and improve memory impairment by downregulating the ACE/Ang II/AT1R pathway and upregulating the ACE2/Ang-(1–7)/MasR pathway in the hippocampus (52). Ang II-induced rats spent significantly less time in the open arms of the elevated plus maze (EPM), this effect was abolished by the administration of valsartan and losartan (53, 59). Losartan effectively attenuated hyperactivity and anxiogenic behaviors in mice as seen in the EPM, social-interaction tests, and open field tests (OFT) (51) (50). Moreover, telmisartan treatment prevented diet-induced anxiety-like behaviors in behavioral tests (54).

4 Potential mechanisms of RAS blockers-induced antidepressant/anxiolytic effects

4.1 RAS-related gene and development of depression

The main RAS-related gene polymorphisms are found in the angiotensinogen gene, ACE, and the angiotensin 1 receptor gene, which have alleles associated with high levels of Ang II, high ACE activity, and elevated Ang II response, respectively. The ACE insertion/deletion (I/D) polymorphism determines functional variations of the ACE gene that significantly influence ACE plasma concentrations, which account for 30–40% of the variation in plasma ACE levels (60). Baghai et al. investigated the genetic association between 35 single-nucleotide polymorphisms (SNPs) and an I/D polymorphism in the ACE gene. They reported that carrying the T-allele is correlated with higher ACE serum activity, in which the highest ACE activities are found in patients homozygous for the T-allele, and the lowest is noted in patients homozygous for the A-allele (61). This research indicates that enhanced ACE activity is associated with depressive symptoms and increased susceptibility to affective disorders (61). In addition, a study based on the Iranian population showed that high serum ACE activity is associated with the pathogenesis of depression (62). The GG genotype of the A2350G polymorphism is associated with MDD and exhibits significantly higher serum ACE activity than AA or AG. Furthermore, certain variants of the ACE gene, such as the D allele, are more frequently noted in patients with affective disorders and associated with a higher risk of affective disorders (63). The D allele may be associated with the severity of depression in DD genotypes carriers of ACE I/D polymorphism (64).

In fact, in individuals with depression, the ACE I/D polymorphism is significantly associated with HPA axis hyperactivity. Patients with depression carrying the D/D variant of the ACE gene show considerably greater activation of the HPA axis (65). Cortisol secretion is increased in patients carrying homozygous T-alleles, showing higher HPA axis activity (61). In addition, the I/D polymorphism of the ACE gene is associated with both late-life depression and cortisol secretion (66).

Polymorphisms of the RAS-related gene variants have also been associated with a higher risk of depression (67). Saab et al.

TABLE 2 Anxiolytic/anti-depressant effect of RAS blockers.

RAS Component	Compounds	Species	Mode of Administration	Measure Method	Main Findings	Reference
ARB	Losartan	Male RHR (Wistar strain albino rats)	5, 10 mg/kg q.d. orally	OFT EPM SIT	Anxiolytic	(50)
		Male SHR	15 mg/kg/d for 2 months oral gavage	NORT OFT	Cognition↑ Neuroplasticity↑	(51)
		Male Wistar rats	10 mg/kg, i.p.	OFT	Anxiolytic Cognition↑	(43)
		Male Wistar rats	Microinjected into MeA (100 nL/side)	FST	Anti-depressant	(33)
		Male Wistar rats; female C57BL6/j mice	10, 30, 45 mg/kg, i.p.	FST	Anti-depressant Cognition↑	(34)
	Candesartan	Male SHR	1 mg/kg/d for 4 weeks intragastric administration	OFT NORT MWM	Anxiolytic Cognition↑	(52)
	Valsartan	Male Wistar rats	10 mg/kg orally	OFT EPM CAR Chimney test	Anxiolytic Cognition↑	(53)
	Telmisartan	C57 mice with high-fat diet	8 mg/kg q.d. Oral gavage	OFT OPRT Barnes maze	Anxiolytic CBF↑	(54)
		Adult male C57BL/6		TST FST	Anti-depressant	(28)
AECI	Captopril	AT2R-deficient mice	0.1, 1.0 mg/kg, i.p.	EPM OFT	Anxiolytic	(35)
		Male Wistar A.F. rats	4, 8, 16, 32 mg/kg/day, i.p.	Learned Helplessness Paradigm	Anti-depressant	(55)
	Enalapril	Male RHR (Wistar strain albino rats)	4 mg/kg q.d. orally	OFT EPM SIT	Anxiolytic	(50)
	Perindopril	Male SD rats	0.1, 1.0 mg/kg/d	Water maze EPM	Anxiolytic Cognition↑ Spatial memory↑	(56)
		Male SHR	1 mg/kg/d for 4 weeks intragastric administration	OFT NORT MWM	Anxiolytic Cognition↑	(52)

FST, forced swim test; OFT, open field test; OBX, bilateral olfactory bulbectomy rats (a rat model of depression); SHR, spontaneously hypertensive rats; NORT, Novel-Object Recognition Test; MWM, Morris Water Maze Test; SD rats, Sprague–Dawley rats; i.c.v., Intracerebroventricular; CAR, Conditioned Avoidance Responses; PFC, prefrontal cortex; RHR, renal hypertensive rats; SIT, social interaction test; CBF, cerebral blood flow; OPRT, object place recognition test, TST, tail suspension test; FST, forced swimming test; MeA, medial amygdaloid nucleus i.p., intraperitoneally; HBP, hypertensive patients.

collected buccal cells from 132 patients with major depression and their first-degree relatives (case controls) in Lebanon (67). Their study showed that the angiotensin receptor type 1 (A1166C) CC genotype is more common in patients with depression, indicating that the CC genotype is significantly associated with depression (p=0.036) (67). A population-based cohort study found the ACE gene (rs1799752) is associated with the incidence of major depression in older individuals in followed up for over 12 years (68). Moreover, variation in the angiotensin II type 1 receptor has been linked with depression

diagnosis and frontotemporal brain volumes (69). Two haplotype-tagging SNPs, rs10935724 (p=0.0487) and rs12721331(p=0.0082) showed statistically significant changes in frequency between diagnostic cohorts (69).

4.2 RAS-related gene and depression therapeutic outcome

Clinically, the ACE I/D polymorphism seems to influence the therapeutic outcome in patients with depression, including the onset of action of antidepressant pharmacotherapies and the responses to selective serotonin reuptake inhibitors (SSRIs) (70), which plays an important role in the individualized treatment of depression. To investigate the impact of ACE2 gene variants on the antidepressant efficacy of SSRIs, a randomized, controlled trial was completed, involving 200 patients with newly diagnosed depression who underwent fluoxetine or sertraline for 6 weeks, along with ACE2 allele genotyping (71). The result showed that the patients with GA and AA genotypes respond significantly better to sertraline and confirm the role of G8790A in response to some SSRIs (71). Elevated levels of substance P are associated with mood symptoms, such as depression (72) and treatment with substance P receptor antagonists has antidepressant properties (73). DD allele carriers possessing higher ACE activity can promote the degradation of substance P, which may be related to having a positive impact on antidepressant treatment efficacy (63, 72). Another study conducted a survey among 313 patients with depression receiving various antidepressant treatments and found patients with the D/D and I/D genotypes have shorter hospitalization durations and better treatment outcomes than those with the I/I genotype (74). Surprisingly, when the 313 patients were classified by sex, the ACE I/D polymorphism only influences the therapeutic outcome in women with major depression, not men. This may be due to the sex-dependent influence of the ACE I/D polymorphism on therapeutic outcomes in antidepressant therapies through the influence of gonadal hormones (74). Based on this study, the D allele has a beneficial effect on the onset of therapy for depression and can be used as a predictor of faster onset of different antidepressant treatments, but the I-allele seemed to have a delayed effect on therapy (74). Another study enrolled 273 patients with MDD who received various antidepressant treatments and assessed the severity of depression with the Hamilton Depression Scale-17 (HAMD) before and after 4 weeks of therapy (75). That study revealed that patients carrying the D allele respond better to antidepressant treatment than those carrying other genotypes (75). More than 70% of AT1 CC homozygotes have a 50% reduction in the HAMD-17 scale within 4 weeks of antidepressant treatment, implying that patients with a haplotype combining the CC and DD/ID genotypes respond better to treatment than those with a single allele (75). Although the therapeutic outcome in various genotypes is related to pharmaceutical variety, the findings demonstrate that the ACE gene may generate varied antidepressant effects.

4.3 RAS blockers inhibit neuroinflammation

Inflammation is triggered by cellular damage caused by infection or injury. The term “neuroinflammation” refers to an immune-related process that occurs within the brain and spinal cord as a result of harm induced by infection, psychological or physical stress, or indirectly as a result of infection emerging in the periphery (76). Subsequently, innate immune cells in the brain (microglia, astrocytes, and oligodendroglia) are activated in response to inflammatory stimuli including the production of cytokines, chemokines, and secondary inflammatory mediators such as prostaglandins (77).

The brain lacks T- and B-cells that are involved in cellular and humoral immunity but contain innate immune cells, including macrophages and dendritic cells (78). Macrophages in the brain referred to as microglia, are the primary immune cells and contain surface membrane receptors recognizing neurotransmitters and hormones (79). Microglia respond to local and systemic inflammatory stimuli by producing pro-inflammatory cytokines (PIC), including interleukin-1α and β (IL-1α and IL-1β), tumor necrosis factor α (TNF-α), and interleukin-6 (IL-6) (79). In addition, microglia produce the anti-inflammatory cytokines IL-10 and transforming growth factor (TGF)-β. Activated microglia also trigger a chain reaction between chemokines, prostaglandins, and NO. In addition to the direct promotion of brain inflammation, chemokines such as CCR2 promote the recruitment of peripheral immune cells into the brain, thereby increasing the effects of inflammation (80).

Appropriate central inflammatory responses are essential to protect the brain from infection and restore homeostasis; however, prolonged inflammation is harmful. Long-term neuroinflammation leads to the activation of peripheral macrophages and central microglia and nerve dysfunction (76). Moreover, excessive responses may lead to decreased levels of brain-derived neurotrophic factors chronic inflammation, and neuronal damage. Sustained activation of the immune response increases inflammation and nitro-oxidative stress, ultimately leading to changes in monoamine levels that increase the risk of many neurological and psychiatric disorders (81). Such a procedure most likely occurs in chronic psychiatric disorders such as depression (82).

In recent years it has become apparent that inflammation is associated with psychiatric disorders. For example, depression is characterized by a chronic low-grade inflammatory state, increased levels of peripheral inflammatory cytokines, and microglial activation (83–85). Clinically, high levels of

inflammatory markers are associated with the development of depression (83). In the general population, an elevated C-reactive protein (CRP) level is linked to a higher risk of developing depression (86). Elevated levels of inflammatory cytokines have been observed in both peripheral and cerebrospinal fluid in patients with depression (87). Particularly, elevated levels of circulating pro-inflammatory mediators have been found in patients with treatment-refractory depression (TRD), including TNF-α, IL-6, IL-1β, CRP, and macrophage inflammatory protein-1 (88).

Consequently, it has been hypothesized that medications that suppress levels of pro-inflammatory cytokines might also contribute to treating depression (87, 89). Some antidepressants with known anti-inflammatory effects have been shown to reduce the level of IL-6 and IL-1β in patients with MDD (88, 90). The use of anti-cytokine and anti-tumor necrosis factor drugs (e.g. infliximab, etanercept, and adalimumab) has been associated with significant improvements in depressive symptoms (91). LPS promotes the activation of microglia and induces depressive-like symptoms, while treatment with anti-inflammatory medication alleviates depressive symptoms (92, 93).

In addition to the regulation of blood pressure, the RAS is also an important regulator of the inflammatory states in the nervous system (94). Excessively elevated Ang II levels enhance plasma cytokine levels such as IL-6, interferon-γ (IFN-γ), TNF-α, and IL-1β (95). IL-6 levels increase the most after Ang II infusion, and plasma IFN-γ levels also increases significantly (96). Cytokine expression is controlled at the transcriptional level by pro-inflammatory transcription factors, such as nuclear factor kappa B (NF-κB) and activator protein-1 (AP-1) (97). Ang II induces the differentiation of immune cells and promotes the production of cytokines through NF-κB and/or AP-1, initiating an inflammatory cascade that leads to microglial activation (98). These findings suggest that the RAS has an intimate and complex regulatory role in the immune system.

ARBs have been proven to effectively inhibit inflammation by reducing gene expression of brain pro-inflammatory cytokines (99)(Table 3). Ang II facilitates the production of IL-1β and NO. This effect is reversed by losartan, which inhibits NF-κB and AP-1 (110). Administration of candesartan reduces brain AT1R synthesis and inhibits LPS-induced acute brain inflammation throughout the inflammatory cascade, including decreased production and release to the circulation of centrally acting pro-inflammatory cytokines; reduction of brain pro-inflammatory cytokines, cytokine, and prostanoid receptors; and reduced microglial activation (105, 106). Pretreatment with candesartan (1 mg/kg/d, for 3 d before the LPS treatment) lessens LPS-induced ACTH and corticosterone release and reduces gene expression of cyclooxygenase-2 (COX-2), IL-6, and TNF-α (105). Moreover, candesartan prevents the synthesis and release of the pro-inflammatory hormone aldosterone (108). In the pituitary, candesartan decreases the expression of the genes for IL-6, iNOS, and COX-2 (109). It also lessens the release of inflammatory markers such as TNF-, IL-1, and IL-6 in the circulation (109). AT1 receptor blockades are demonstrated to provide superior neuroprotective properties to ACE inhibition (107). In the rat model of neuroinflammation, candesartan (1 nM) inhibits LPS-induced neuroinflammation more effectively even at lower dosages and increases AT2R and anti-inflammatory IL-10 expression than perindopril (1 μM) (107). Systemic administration of telmisartan directly ameliorates the IL-1β-induced neuronal inflammatory response and inhibits oxidative stress (102). Administration of telmisartan attenuates chronic intermittent hypoxia (CIH)-induced neuronal apoptosis and decreases levels of CD45 (leukocyte common antigen), CRP, and IL-6 in the hippocampus and circulation through inhibiting inflammatory response (103). Intranasal administration of telmisartan (1 mg/kg; two months) significantly reduces glial activation in the brain and ameliorates the synthesis of NO, iNOS, TNF-α, as well as IL1-β (104).

Consequently, it is hypothesized that medications with anti-inflammatory effects might also have antidepressant potential. Losartan and ramipril can reverse depression-like behaviors in restraint-stressed mice and insulin resistance through anti-inflammatory mechanisms (112). Administration of irbesartan reduces the level of inflammatory mediators and reverses Ang II-induced depressive-like behaviors as manifested by decreased immobility times in the modified forced swim test (MFST) and the TST (100). Pretreatment with losartan significantly improves FST performance and prevents LPS-induced anhedonia and anxiety-like behaviors in addition to preventing LPS-induced higher levels of the pro-inflammatory cytokine (TNF, IL-1, and IL-6) (99, 116). A model of diabetes-associated depression rats exhibited depression-like behavior, which can be therapeutically reversed by losartan (20 mg/kg) *via* altering diabetes-induced neuroinflammatory responses (111). Telmisartan effectively reduces the concentration of pro-inflammatory mediators, including NO, IL-6, and IL-1β, in depressed rats with diabetes (101). Moreover, in a rat model of post-traumatic stress disorder (PTSD), treatment with captopril decreases pro-inflammatory cytokines levels and inhibits microglial activation in the hypothalamus (114). More importantly, the anxiolytic/antidepressant effects of RAS blockers may be mediated by their anti-inflammatory effects, providing new treatment directions.

4.4 RAS blockers inhibit oxidative stress

Oxidative stress occurs when there is an imbalance between the production of reactive oxygen species (ROS) and endogenous antioxidant enzymes. Antioxidant enzymes, such as catalase (CAT), superoxide dismutase (SOD), and glutathione peroxidase (GPX), maintain low levels of ROS *in vivo*. Excessive ROS generation and exhaustion of anti-oxidative defense-

TABLE 3 RAS blockers inhibit inflammation.

RAS Component	Compounds	Species	Mode of Administration	Measure Method	Main Findings	Reference
AT1R		AT1aR knockout mice		EPM	Anxiolytic Neuroinflammation↓	(31)
ACE2		Male SD rats	Bilateral microinjected ACE2 into PVN		Anxiolytic PIC↓	(44)
ARB	Irbesartan	Swiss albino mice of UCMS	40mg/kg i.p./p.o.	MFST TST OFT	Antidepressant 5-HT levels↑	(100)
	Telmisartan	Wistar rats with DM	0.05mg/kg, p.o. for 21days	FST OFT EPM	Antidepressant NO↓, IL-6↓, IL-1β↓	(101)
		SK-N-SH human neuroblasts Primary rat cortical neurons	10 ng/ml		Neuronal inflammatory response to IL-1β↓ COX-2 PGE2↓ JNK/c-Jun pathway↓	(102)
		Male SD rats	10 mg/kg for 8 weeks		CD45, IL-6, CRP↓	(103)
		5XFAD mice Primary neonatal rat glial cells	1 mg/kg/day intranasal for 2 months		TNF-α, IL1-β↓ iNOS↓ Aβ burden and CD11b↓	(104)
	Candesartan	WH rats and SHR	1 mg/kg per day for 14 days	EPM	Anxiolytic PIC↓ Microglia activation↓	(105)
		Male SD rats	1 mg/kg oral gavage for 2 weeks	EPM FST NSFT	Anxiolytic Antidepressant IL-1β, IL-6, Cox2↓, iNOS↓, IL-10↑	(106)
		Male SD rats	0.1 mg/kg Orally for 5 days		Astroglia, microglial, STAT3 activation↓ NFκB↓ TNF-α↓ PP2A activation↓ IL-10↑	(107)
		Male Wistar Hanover rats	1 mg/kg/d, s.c. for 3 days		PIC↓ COX-2, IL-6↓ LIF, IκB-α↓	(108) (109)
	Losartan	Microglial cells	10^{-5}m		IL-1↓ NF-κB ↓ AP-1 activation↓	(110)
		Wistar rats	ICV 50 μg		NF-κB↑ AP-1↑	(98)
		Wistar rats of DM	20 mg/kg for 2 weeks	FST OFT	Antidepressant Neuroinflammation↓	(111)
		Male LACA mice of CRS	20 mg/kg for 30 days	FST	Antidepressant Insulin levels↑ Locomotor activity↑	(112)
ACEI	Lisinopril	Wistar rats	ICV 50 μg		NF-κB↑ AP-1↑	(98)
	Enalapril Ramipril	Wistar rats of DM	(40mg/bwkg/d) (10μg/bwkg/d) for 2 weeks	FST OFT	Antidepressant IL-1a mRNA↓	(113)

(Continued)

TABLE 3 Continued

RAS Component	Compounds	Species	Mode of Administration	Measure Method	Main Findings	Reference
					IL-6 mRNA↓ TNF-α mRNA↓	
	Ramipril	Male LACA mice subjected to CRS	10, 20mg/kg for 30days	FST	Antidepressant Locomotor activity↑	(112)
		Male SD rats	1 μM Orally for 5 days		Astroglia, microglia, STAT3 activation↓ NFκB↓ TNF-α↓ AT2R expression↑	(107)
	Captopril	Male SD rats	0.5 mg/ml for 2 weeks		TNF-α↓ PIC↓	(114)
		MRL/lpr lupus-prone mouse model	5 mg/kg every other day i.p. for 2 weeks	Rotarod Test FST EPM	Antidepressant 5-HT levels↑ IFNα levels↓ Microglial activation↓	(115)

IL-1β, interleukin-1β; IL-6, interleukin-6; NO, nitric oxide; SD, Sprague-Dawley; DM, diabetes mellitus; MR, mineralocorticoid-receptor; TNF-α, tumor necrosis factor-α; IL-1a, interleukin-1a; i.c.v., intracerebroventricular; AP-1, activator protein-1; PIC, pro-inflammatory cytokine; i.p., intraperitoneal; p.o., oral route; CRS, Chronic restraint stress; IFNα, interferon-α; MFST, Modified forced swim test; TST, tail suspension test; OFT, open-field test; UCMS, unpredictable mild stress, WH rats, Wistar Hannover rats; MWM, Morris water maze; PA, passive avoidance; MBT, Marble burying task; NSFT, Novelty-Suppressed Feeding Test; Cox-2, cyclooxygenase-2, NOS, Nitric oxide synthase, LIF, leukemia inhibitory factor; iNOS, inducible nitric oxidase synthase; MIF migration inhibitory factor; NFκB Nuclear factor-kappa B; pSTAT3, Phosphorylated signal transducer and activator of transcription 3; PP2A, Protein phosphatase-2A; PGE2, prostaglandin E2; JNK, c-Jun N-terminal kinase; NOS, Nitric oxide synthase; CIH, chronic intermittent hypoxia; CD45, leukocyte common antigen; CRP, C-reactive protein; 5XFAD, five familial Alzheimer's disease transgenic mouse; CD11b expression, a marker for microglia; SPT, sucrose preference test; BDNF-TrkB-CREP, brain-derived neurotrophic factor-tropomyosin receptor kinase B-cyclic adenosine monophosphate response element-binding protein.

produced pro-inflammatory mediators results in damage to vital macromolecules and induces cellular apoptosis (117). Another major consequence of ROS-derived damage is lipid peroxidation. The brain is particularly susceptible to damage from reactive oxygen species because of its elevated oxygen consumption and lower levels of endogenous antioxidant enzymes (118).

Many studies have highlighted associations between oxidative stress and the development of affective disorders, and that antioxidants can improve symptoms of emotional disorders (119). Increased levels of oxidative stress markers, pro-inflammatory cytokines, and lipid peroxidation are observed in patients with anxiety and depression (120). Depression patients have significantly higher levels of F8-isoprostanes and lower GPX activity, two markers of oxidative stress, compared to healthy controls (121). Moreover, antioxidant treatment improves diabetes-induced depressive-like behaviors, increases levels of antioxidant enzymes CAT and SOD in brain tissue, and reduces oxidative stress in the hippocampus (118). Additionally, the administration of antioxidants shows an anxiolytic effect (122, 123). F2-isoprostanes and oxidized glutathione are positively associated with total Hamilton Anxiety ratings and the severity of anxiety in MDD (124). Moderate treadmill exercises prevent anxiety-like behaviors and the production of oxidative stress markers in the hippocampus, amygdala, and locus coeruleus (125). Importantly, antioxidants have the same effects as treadmill exercises, performing an anxiolytic effect (125), indicating that oxidative stress metabolites play an important role in mood disorders.

RAS overactivation is involved in oxidative stress *via* increasing Ang II levels and oxidative stress in the central nervous system is associated with depression (126) (Figure 1B). Ang II induces the production of superoxide anion and impairs cerebral microvascular endothelial function *in vivo* (127). Ang II stimulates inflammatory responses in the microvascular endothelium of the brain through AT1R, allowing more interaction between immune cells and the endodermis, and in turn, leading to disrupted BBB permeability partly *via* oxidative stress cascades (128). Ang II increases leukocyte adhesion 2.6-fold and BBB permeability 3.8-fold in male mice *via* oxidative stress-mediated cerebral microvascular inflammation (128). Furthermore, Ang II directly increases the production of ROS and subsequently induces lipid peroxidation and modification (129).

After systemic inflammation in the brain, nicotinamide adenine dinucleotide phosphate (NADPH) oxidase and inducible nitric oxide synthase (iNOS) activities rise, resulting in an accumulation of ROS and NO (126). During inflammation, Ang II promotes the oxidative stress process by increasing NADPH oxidase and iNOS activity in the BBB and PVN (126), and ARBs attenuate iNOS activity (126)(Table 4). Moreover, pretreatment with losartan at 3 mg/kg attenuates NO metabolite accumulation in hippocampal and cortical tissues (116). Treatment with telmisartan attenuates CIH-induced neuronal apoptosis in the hippocampus by

suppressing NOS activity and inhibiting excessive NO generation (103). In addition, RAS blockers have a positive effect on depression as a comorbidity. Administration of RAS blockers prevents indices of systemic oxidative/nitrosative stress increased in rats with diabetes mellitus by inhibiting oxidative stress (131). Treatment with perindopril reduces severe acute respiratory syndrome-related coronavirus 2 spike protein-induced inflammatory and oxidative stress responses in cells and significantly blunted apoptosis and ROS (130).

The limbic system, comprised primarily of the amygdala and hippocampus, includes widely distributed AT1 receptors and is sensitive to oxidative stress 184). Oxidative stress upregulates angiotensin-1 receptor levels and elevates NF-κB-mediated pro-inflammatory factors levels (IL-6, TNF-α) in these brain areas, leading to anxiety-like behaviors (132, 133). Candesartan significantly inhibits nuclear translocation of NF-κB expression, while also decreasing ROS levels and increasing IL-10 levels in the cortex and hippocampus (133). Captopril and

TABLE 4 RAS blockers inhibit oxidative stress.

RAS Component	Compounds	Species	Mode of Administration	Measure Method	Main Findings	Reference
Ang- (1–7)		Adult male Wistar rats			GPX↑ MDA↓	(37)
AT_2R	Blocker PD-123177	Male Wistar rats	0.1 mg/kg/b.w. i.c.v. for 7 days	PA Y-maze	Antidepressants Memory↑ SOD↑ GPX↑ MDA↓	(37)
ARB	Losartan	Male Wistar rats	0.1 mg/kg i.c.v.		SOD↑ GPX↑ MDA↓	(59)
		Male Wistar rats	0.1 mg/kg/b.w. i.c.v. for 7 days	PA Y-maze	Memory↑ SOD↑, GPX↑ MDA↓	(37)
		Male LACA mice of CRS	20 mg/kg for 30 days	FST	Antidepressant MDA↓ Nitrite↓	(112)
	Telmisartan	Primary rat cortical neurons	10 ng/ml		NOX-4 mRNA expression↓ NADPH, ROS↓	(102)
		Male SD rats	10 mg/kg for 8 weeks		iNOS, NO↓ MDA↓	(67)
	Candesartan	Male Wistar Hanover rats	1 mg/kg/d, s.c. for 3 days		nNOS/eNOS activity↓ iNOS↓	(109)
		Male SD rats	0.1 mg/kg Orally for 5 days		ROS↓ Nitrite↓	(107)
	Irbesartan	Swiss albino mice of UCMS	40 mg/kg i.p./p.o.	MFST TST OFT	Antidepressant CAT↑ MDA↓	(100)
ACEI	Ramipril	Male LACA mice of CRS	10,20mg/kg for 30 days	FST	Antidepressant MDA↓ Nitrite↓	(112)
	Captopril	Male Wistar rats	0.1 mg/kg/b.w. i.c.v. for 7 days	PA Y-maze	Memory↑ SOD, GPX↑ MDA↓	(37)
	Perindopril	Male SD rats	1 μM Orally for 5 days		ROS↓	(107)
		THP-1 cells	100 μM		TNF-α, IL-17↓ Apoptosis↓ ROS↓	(130)

GPX, glutathione peroxidase; MDA, malondialdehyde; SOD, superoxide dismutase; MBT, Marble burying task; NOX-4, NADPH oxidase-4; NOS, Nitric oxide synthase; NO, nitric oxide; CIH, chronic intermittent hypoxia; iNOS, inducible nitric oxide synthase; CAT, catalase; HCD, high cholesterol diet; TABRS, thiobarbituric acid reactive substances, CUMS, chronic unpredictable mild stress; BDNF–TrkB-CREP, brain-derived neurotrophic factor-tropomyosin receptor kinase B–cAMP response element-binding protein; NSF, novel-suppressed feeding test, OFT, open-field test; TST, tail suspension test; FST, forced swimming test; SPT, sucrose preference test.

losartan reverse the disruption of BBB permeability and prevent Ang II-induced enhancement of oxidative stress in the hippocampus (59, 134). Moreover, captopril and losartan decrease lipid peroxidation levels, reduce anxiety-like behaviors, and increase antioxidant enzymes including SOD and GPX (59, 134). Furthermore, antioxidant treatment improves Ang II-induced disruption of BBB permeability and prevented anxiety-like behaviors in rats (135). LPS injection raises the concentration of malondialdehyde (MDA), a marker of lipid peroxidation, in hippocampus tissue (99). Losartan prominently increases the activity of antioxidant enzymes and reduces lipid peroxidation, such as MDA (99, 136). Pretreatment with losartan (3 mg/kg) significantly decreases MDA levels and reverses the negative effects of LPS on the activity of CAT and SOD in the hippocampal and cortical tissues (116). Consistent with losartan, telmisartan suppresses CIH-induced lipid peroxidation and overexpression of inflammatory mediators in the hippocampus (103). Irbesartan, alone or in combination with fluoxetine, significantly decreases the levels of thiobarbituric acid reactive substances, CAT, and MDA, and reverses the reduction in GSH levels in unpredictable chronic mild stress (UCMS) mice (100). Taken together, RAS blockers improve emotional disorders through anti-oxidative stress effects.

4.5 RAS blockers inhibit stress responses

4.5.1 RAS, corticotropin-releasing factor, and stress

In response to stress stimulation, the subgenual prefrontal cortex is suppressed and the amygdala is activated, which activates the HPA axis (137). As the major stress mediator and crucial regulatory center of the neuroendocrine system, HPA releases corticotropin-releasing factor (CRF) to regulate stress responses (138). When the HPA axis is activated, CRF is released from the paraventricular nucleus(PVN) into the portal circulation, stimulating the pituitary to produce and release adrenocorticotropic hormone (ACTH). ACTH further stimulates the glucocorticoid (GC) hormone cortisol synthesis and release by the adrenal cortex (139). Interestingly, increased CRF in the cerebrospinal fluid and hyperactivation of the HPA axis have been reported in both anxiety and depression (140, 141).

Corticotrophin-releasing factor or hormone (CRH) is a 41 amino acid neuropeptide that mediated the neuroendocrine, immunological, autonomic, and behavioral responses to stress (142). In various animal models of anxiety disorders, centrally injected CRF induces anxiety-like responses such as sleep disturbances, loss of appetite, and anhedonia (143). CRF antagonists show anxiolytic effects in a variety of animal models (143). In addition, a large literature indicates that stress responses upregulate the transcription and expression of Ang II-related receptors and enhance the expression of central Ang II (144–146). Ang II, as a stress hormone, increases the expression of CRF mRNA through AT1R, which contributes to increasing the expression of CRF receptors and promoting CRF release during stress (147, 148). Ang II stimulates ACTH and GC secretion through pituitary AT1R and/or activates Ang II afferent terminals innervating present in PVN neurons enhancing the stimulatory effect of CRF (149, 150)(Figure 1C).

The various stressors enhance Ang II levels and affect the expression of receptors. Pavel reported that ARBs prevent the response of the HPA axis to isolate stress and reduce the expression of CRH receptors and benzodiazepine receptors, demonstrating that ARBs exert powerful anti-anxiety properties by downregulating CRH receptor type and benzodiazepine receptors in stress models (151, 152). Saavedra et al. pretreated rats for 13 days with candesartan (0.5 mg/kg/day) followed by 24 h of isolation in metabolic cages, and they found that candesartan blocks the stress-induced augments of CRF in the cortical and prevents benzodiazepine receptors from binding in the paraventricular nucleus and cortex (153). Injecting Ang II-induced depressive-like behaviors *via* microglia activation and activates the HPA axis (28), pretreatment with candesartan (1.0mg/kg/days for 14 days) attenuates the response of the HPA axis to stress and reduces cold restraint stress (placed in plastic restraining devices and maintained at 4°C for 2 h)-induced ulceration of the gastric mucosa eventrally (154). Candesartan increases gastric blood flow by 40-50% and prevents gastric ulcer formation by 70-80% after cold-restraint stress (154). Administration of losartan effectively attenuates the stress-induced fear memory impairment and prevents the development of depression-like behaviors caused by chronic mild unpredictable stress (CMS) (116, 155). Low doses of candesartan completely reverse chronic restraint stress (2 h/21 days in tight plastic tubes)-induced memory deficits (156). Isolation stress increases AT1 receptor binding in the PVN and anterior pituitary. The administration of candesartan is sufficient to block the isolation stress (24h isolation in individual metabolic cages)-induced increased binding of AT_1R to PVN and to reduce the HPA response to stress (157)(Table 4).

Systemic administration of angiotensin II receptor antagonist inhibits stress-induced anxiety (158). Ovariectomized rats treated with losartan decreased plasma corticosterone levels ($p<0.05$) and AT1R mRNA expression in the CA3 region of the hippocampus (159). Administration of losartan improves anxiety responses in stressed rats *via* blockade of the AT1 receptor within the amygdala under both non-stress and acutely stressed rats (160). In sub-chronic swim stress models, pretreatment with losartan (10 mg/kg) decreases anxiety-like and stress behaviors as manifested by enhancing the tendency to spend more time in the center area in the OFT (43). Chronic stress lead to neuropsychiatric disorders, such as anxiety and depression, the neuroprotective effect of losartan alleviates chronic fatiguing stress-induced anxiety-like

behaviors (161). Moreover, pretreatment of losartan reveres the chronic restraint stress-induced increased anxiety-like behaviors and decreased motor activity (162).

Empirical studies in animals show RAS blockers exert antidepressive effects. Treatment with losartan significantly abolishes the increased Ang II level and prevents the development of stress-induced depression-like behaviors in UCMS rats (163). Chronic administration of irbesartan significantly increases swimming and climbing times, decreases immobility times in the MFST, and decreases immobility time in the tail suspension test in UCMS rats (100). Administration with telmisartan for five weeks notably prevents the depression-like behaviors in OFT and sucrose preference test (SPT) in animals under chronic stress (164).

4.5.2 RAS, 5-HT, and stress

Serotonin (5-HT) is an important neuromodulatory transmitter and decreased 5-HT production may result in mood disturbance, aggression, and other neuropsychological impairment (165). There is an interaction between Ang II and 5-HT, particularly in the hippocampus, and brain Ang II regulates stress-related effects by modulating 5-HT release and synthesis (166, 167). The major serotonin metabolite 5-hydroxyindoleaceticacid (5-HIAA) is significantly elevated in the striatum after Ang II administration, indicating that Ang II increases the 5-HT levels (167). Furthermore, the AT1 receptor antagonist losartan reduces basal levels of 5HIAA (167). However, irbesartan (an ARB) increases time spent in the center of the OFT and elevates the 5-HT levels in UCMS rats (100), suggesting the biphasic response of Ang II on 5-HT synthesis (166). It is speculated that the biphasic response was related to the concentration of Ang II. Ang II stimulated tryptophan (TRP) hydroxylase at high concentrations to increase the synthesis of 5-HT. At low concentrations, an inhibitory effect is found, Ang II inhibits tryptophan hydroxylase resulting in decreasing 5-HT levels (166). Above all, it represents a subtle regulation of serotonin and the RAS system.

Perindopril (1.0 mg/kg/day) and candesartan (10 mg/kg/day) were administered *via* drinking water for 1 week, and serotonin levels increase in the prefrontal cortex and hippocampus, suggesting that decreased Ang II levels are associated with increased serotonin (168). Systemic administration of captopril increased serotonin levels and decrease depressive-like behaviors (115). In addition, captopril significantly increases the concentration of 5-HT and 5-HIAA in the parabrachial lateral nucleus (169). Administration with telmisartan for five weeks notably prevents the depression-like behaviors in OFT and SPT, and enhances expression of 5-HT transporter in the hippocampus of mice through activation of peroxisome proliferator-activated receptor δ, indicating RAS blockers improve stress-induced depressive symptoms in animals under chronic stress (164). Although these findings support that Ang II regulates stress by altering 5-HT levels in the brain, the association between Ang II and 5-HT in the formation of stress-related behaviors needs further investigation.

4.5.3 RAS, sympathetic/parasympathetic, and stress

Stress generally triggers the autonomic nervous system, which is one of the major neural pathways (170). Depression is characterized by autonomic imbalance, with elevated sympathetic tone and weak parasympathetic tone, or both (171). A study of more than 600 subjects reports that depression and anxiety are shown to be more significantly and positively linked with the activation of the sympathetic nervous system (SNS), and depression is negatively correlated with parasympathetic nervous system (PNS) activation (172). SNS is stimulated in response to stress and increases the concentration of serum catecholamines to maintain body homeostasis (173). Indeed, patients with depression have been reported to have elevated catecholamines in plasma and cerebrospinal fluid (CSF) (174).

Norepinephrine (NE), one of the catecholamine hormones, is a major monoamine neurotransmitter that widely affects multiple brain regions (175). Noradrenergic hyperactivity has been shown to be an important component of the stress response and dysregulation of noradrenergic signaling has been implicated in the pathogenesis of anxiety and depression disorders. In fact, RAS has a complex bidirectional interaction with the autonomic nervous system activity under both physiological and pathophysiological conditions *via* receptors localized to peripheral and central sites of action (176). In the brain, Ang II increases sympathetic discharge and decreases vagal discharge. As a neuromodulator, Ang II stimulates ganglionic transmission and catecholamine release from adrenal medullary chromaffin cells and potentiated NE release from sympathetic nerve terminals in the periphery (177). In addition, there is some evidence that Ang II inhibits norepinephrine reuptake to promote neurotransmission (177). Administration of angiotensin-converting enzyme inhibitors can attenuate sympathetic neurotransmission and facilitate parasympathetic (175). In addition, Ang-(1–7) inhibits sympathetic tone and facilitates parasympathetic tone effects in experimental animal models, which will become an attractive treatment for autonomic nerve dysfunction (178).

In rat hypothalamic tissue, losartan partially reduces norepinephrine secretion (179). Also, noradrenaline levels are also shown to be significantly reduced in the striatum after chronic candesartan, although the mechanism is unclear (168). Ang II elevates catecholamines in the periphery and central, and pretreatment with Ang II receptor antagonism losartan significantly attenuates neuroendocrine responses, indicating Ang II activates sympathetic-adrenomedullary system activity through AT1R during stress (180). Although these findings

support that Ang II regulated stress-related behaviors by altering NE levels, the association between Ang II and NE and sympathetic and parasympathetic in the formation of stress-related behaviors needs further investigation.

In clinical studies, elevated catecholamine activity impaired prefrontal cortex (PFC) function under stress and is associated with PTSD and other anxiety disorders (181). Chronic stress exposure leads to dendritic atrophy in PFC and enhances the noradrenergic NE system in the PFC (181). Cerebrospinal fluid norepinephrine concentrations are significantly higher in patients with chronic PTSD than in healthy subjects (182). Moreover, CSF norepinephrine concentrations are shown to be more significantly and positively link with the severity of PTSD symptoms, rather than plasma norepinephrine concentrations (182). Gold observed significant elevations in twenty-four-hour indices of norepinephrine secretion in both cerebrospinal fluid and plasma in severely depressed patients, compared with the control group (183). Clinical studies find that alpha-1 receptor blockers or alpha-2A receptor agonists can reduce the high concentration of NE release during stress, suggesting targeting the autonomic nervous system can be utilized as a pharmaceutical therapy for stress-related symptoms (181, 184). Taken together, the above finding indicates that RAS is involved in stress and that inhibiting RAS reduced the effects of stress.

4.6 RAS blockers elevate brain-derived neurotrophic factor levels

Brain-derived neurotrophic factor (BDNF) is a neurotrophic factor bound to its receptor tropomyosin-related receptor kinase B (TrkB). BDNF is associated with the neurobiology of depression and antidepressant effects (185). BDNF plays an important role in neuronal growth, maturation, and survival and it mainly has the following functions (186): (1) increase synaptic plasticity and affect learning and memory. (2) promote neurogenesis, especially in the hippocampus. Further, the expression of BDNF is regulated *via* cyclic adenosine monophosphate response element-binding protein (CREB), and the phosphorylated cyclic adenosine monophosphate response element-binding protein (pCREB) level in the hippocampus was one of the pathogenesis of depression (187). TrkB signaling is essential for antidepressants, activating TrkB and increasing levels of BDNF (188). Hippocampal biopsies showed that individuals with major depression reveal lower levels of BDNF and its receptor TrkB, and long-term use of antidepressants promotes increased BDNF levels (111). Chauhan et al. revealed that in depressed patients with low BDNF levels, after four weeks of antidepressant treatment, the serum BDNF levels and depressive symptoms significantly improve (189).

BDNF exhibits a negative regulatory effect on brain inflammation along with inflammation and oxidative stress (83, 189). RAS performs an integral effect in mediating BDNF, which is essential in the neurobiology of depression and antidepressant effects (34). Decreased BDNF levels in the hippocampal are associated with depressive-like behaviors in UCMS rats and losartan minimizes depressive-like behaviors *via* modulating the BDNF pathway (113, 190)(Table 5). Losartan treatment significantly elevates TrkB and p-CREB protein levels and reduces NF-κB protein, IL-6, and TNF-α mRNA levels, and facilitates the BDNF-TrkB-CREB, indicating that the TrkB signal promoted neuronal survival (111). Losartan exerts neuroprotective effects by alleviating neuroinflammatory responses and elevating BDNF levels in astrocyte (111). Oral administration of candesartan ameliorates chronic neuroinflammation-induced behavioral changes and apoptosis by inhibiting Ang II-induced NF-κB inflammatory signaling and enhancing the phosphorylated CREB and BDNF expression level in the cortex and hippocampus regions (133). In the case of AT1R blockade, AT2R activation increases the expression of AT2R mRNA (192). The antidepressant-like effect of losartan may increase the binding of Ang II to AT2R by inhibiting AT1R, finally, increase the surface levels of TrkB and coupling of TRK/FYN in the hippocampus and ventral medial prefrontal cortex (vmPFC) prelimbic aspects (34).

Reduced BDNF levels promote oxidative stress processes that lead to anxiety (120, 132). For example, social stress lowers BDNF and glutathione reductase levels, leading to oxidative stress-induced anxiety/depression-like behaviors in rats (193). Impaired hippocampal neurogenesis and reduced BDNF levels were observed in UCMS mice. Orally administration of valsartan (10–40 mg/kg/day, 4 weeks) promotes the hippocampus neurogenesis and the BDNF expression, exerting an antidepressant-like effect, which may be one of the mechanisms for its antidepressant (191). Importantly, the antidepressant-like property is dose-dependent, with the maximum effect obtained when valsartan is administered at a dose of 40 mg/kg/day (191).

5 Clinical data

To date, no randomized controlled trial has examined the impact of ACEIs or ARBs on depression. However, case reports and observational studies have demonstrated a bidirectional relationship between antihypertensive medications and depression, indicating mood-improving effects of RAS blockers, whereas other antihypertensive agents did not (Table 6). For example, losartan positively affects individuals with high-trait anxiety and prevents the development of anxiety disorders (205). In hypertensive individuals without a psychiatric history, discontinuation of valsartan (160 mg/day) is accompanied by anxiety symptoms such as palpitations, insomnia, and increased

TABLE 5 RAS blockers reduce stress responses and elevate BDNF levels.

RAS Component	Compounds	Species	Mode of Administration	Measure Method	Main Findings	Reference
AT1R		AT1aR knockout mice in PVN		EPM	CRH gene transcription↓	(31)
AT2R	Agonist Novokinin	Male Wistar rats of T1DM	i.c.v.	EPM TMRA	Corticosterone↓	(32)
ARB	Telmisartan	Male Wistar rats of DM	0.5mg/kg, p.o. for 21days	FST OFT EPM	Antidepressant Serum cortisol↓	(101)
	Candesartan	Rats of CRS		EPM	Anxiolytic Sympathetic↓	(151)
		Male Wistar rats of isolation stress	0.5 mg/kg/day for 13 days		Anxiolytic CRF1R and BZ binding↓	(153)
		Male Wistar rats of isolation stress	4 mg/day per os for 3 months		Corticosterone↓ Aldosterone↓ Catecholamines↓ HPA response to stress↓	(157)
		Male Wistar rats of isolation stress	1 mg/kg/d, s.c. for 3 d		ACTH↓	(109)
	Losartan	Male SD rats of CMS	20 mg/kg/day for 7 weeks	SPT FST Y-maze test	Antidepressant Cognition↑	(163)
		Female long evans rats of Ovx	10mg/kg/day	SPT OFT EPM NORT	Anxiolytic Cognition↑ Corticosterone↓	(159)
		Male rats	2,4ug injected into amygdala	EPM	Anxiolytic	(160)
		Male LACA mice of CFS	10 and 20 mg/kg, ip for 21 days		Anxiolytic TNF-α, CRP↓	(161)
		Male Wistar rats of CFS	10 mg/kg for 10 days	OFT	Anxiolytic Stress↓	(162)
		Male LACA mice of CFS	20 mg/kg	FST	Antidepressant Corticosterone↓	(112)
		Wistar rats of DM	20 mg/kg for 2weeks	FST OFT	Antidepressant BDNF↑	(111)
	Valsartan	Male C57BL/6J mice of CUMS	40 mg/kg/d, p.o. for 4 weeks	NSF FST OFT TST SPT	Antidepressant Anxiolytic BDNF↑	(191)
ACEI	Ramipril	Male LACA mice of CFS	10,20mg/kg for 30 days	FST	Antidepressant Corticosterone↓	(112)
		Wistar rats of DM	10μg/bwkg/d for 2 weeks	FST OFT	Antidepressant BDNF↑	(113)
	Enalapril	Wistar rats of DM	40mg/bwkg/d for 2 weeks	FST OFT	Antidepressant BDNF↑	(113)

HPA, hypothalamic-pituitary-adrenal; CMS, chronic mild unpredictable stress; CFS, Chronic fatigue stress; CSR, chronically stressed rats; CRS, chronic resistance stress; BZR, Benzodiazepine receptors; CRH/CRF, Corticotropin-Releasing Hormone/factor; CRF1R, Corticotropin-Releasing Factor Receptor; UCMS, unpredictable chronic mild stress.

TABLE 6 Clinical data of RAS blockers.

Compounds	Study Design	Clinical Population	Main Findings	Reference
SSRI **SSRI+RAS**	PSM cohort study	SSRI users 30,311 SSRI+RAS 30,311 A total of 49,327 1997 to 2012	Risk for psychiatric hospital contacts↓	(194)
ACEI **ARB**	Nationwide population-based study in Danish	1,576,253 individuals 2005 to 2015	Rate of incident depression↓	(195)
ACEI **ARB**	Meta-analysis of Randomized clinical trials		Mental health domain of quality of life↑	(196)
ACEI **ARB**		378 patients with HBP	Rates of antidepressant usage↓	(197)
ACEI **CCB** **β-blockers**	Nationwide Population-Based Study in Danish	5.4 million individuals 2005 and 2015	Rates of depression↓	(198)
ACEI **ARB**	Prospective study	144,066 patients	Risk of mood disorders admissions↓ Risk for mood disorder↓ β-blockers and CCB higher risk	(199)
Candesartan	4 mg/d orally for 3 months	17 patients with T2DM	Interpersonal sensitivity↓ Depression ratings↓ Sensitivity of the adrenals to ACTH↓ Expression of AT1R↓	(148)
Enalapril **Captopril**	15.5 ± 1.54 mg/day for 1.66 ± 0.51 years	15 HBP patients	Anti-depressant Cognition↑	(200)
Captopril	12.5,50 mg	50-year-old woman with MDD	Anti-depressant	(201)
Captopril	12.5, 25 mg	41-year-old man with MDD	Anti-depressant	(202)
Captopril	50 mg t.i.d./4 weeks	Patiens with HBP	Anti-depressant	(203) (204)
Losartan	50 mg orally	30 anxious individuals	Anxiolytic	(205)

PSM, propensity scores matched; 95%-CI, 95%-confidence intervals; HRR, hazard rate ratio; HBP, hypertension; CCB, calcium antagonists; ACEI, angiotensin-converting enzyme inhibitors; ARB, angiotensin II receptor blockers; T2DM, type 2 diabetes.

respiratory rate (206). These anxiety symptoms were significantly relieved with recontinuation of valsartan (80 mg/day) (206). A recent neuroimaging study showed that losartan prevents sustained amygdala activation in individuals with high-trait anxiety and leads to increased activation in other brain areas associated with threat processing, such as the insula and putamen (205). A recent study reports a significant association between the presence of an ACE inhibitor/ARB medication and decreased post-traumatic stress disorder symptoms compared with other blood pressure medications, including β-blockers, calcium channel blockers, and diuretics (207).

Moreover, captopril and enalapril partly reverse the significant negative emotional effects of hypertension (12). Several cases have reported that captopril has mood-improving properties and antidepressant effects (202–204). Patients treated with captopril had significantly reduced total Hamilton Depression Scale (HAMD) scores and corrected neuroendocrine dysfunction during one-year follow-up (201). Moreover, captopril (12.5 mg b.i.d.2 weeks) decreases HAMD-21 scores and improves depressive symptomatology in patients with recurrent unipolar major depression (208). Captopril and enalapril improve depressive and anxiety symptoms in patients with hypertension (200). Hertzman reported that ten patients who suffered from hypertension and mood disorders (major depressive disorder or bipolar disorder) had improved mood with a combination of antidepressants and lisinopril, and no serious negative effects were reported by any of these patients while using lisinopril (209). A clinical trial reported that ACE inhibitors reduced the likelihood of depression risk and significantly improved general well-being, work performance, and cognitive function in 625 white men with mild hypertension administered captopril for 6 months (210). Two prospective multicenter randomized trials have shown that captopril has a significant tendency to reduce depressive symptoms compared with other antihypertensive drugs (211). Subsequently, another ACE inhibitor (enalapril) showed a significant improvement in health-related quality of life (HRQoL) compared to selective beta-blockers, although the overall tolerability of the two drugs was similar (212). In a clinical trial that enrolled 387 subjects aged 75+ years with hypertension in Italy, the results showed that the use of ACE

inhibitors was associated with significantly better HRQoL among older adults (213). A case-control study enrolled 972 patients with both diabetes and depression, and the results suggest that those given ACEIs show a lower odds ratio for depression (OR 1.3, 95% confidence interval (95%CI):0.8–2.2) compared to beta-blockers (OR 2.6, 95% CI:1.1–7.0) and calcium channel blockers (OR 2.2, 95% CI:1.2–4.2) (214). Patients with type 2 diabetes and depressive symptoms received chronic candesartan administration for at least three months, which significantly improved interpersonal sensitivity and depression ratings and reset the HPA axis by reducing the sensitivity of the adrenals to ACTH and expression of AT1R (148).

In clinical and cohort studies, targeted RAS compounds have neuropsychiatric advantages through their anti-inflammatory properties, especially in depression (215). A Danish nationwide population-based study enrolled 1 576 253 subjects exposed to one of the six drugs(low-dose aspirin, statins, allopurinol, ACEIs, ARBs, and non-aspirin non-steroidal anti-inflammatory drugs) during the exposure period from 2005 to 2015. The incidence of depression decreased in patients taking ACEIs and ARBs, suggesting that these agents may act on inflammation and the stress response system (195). A recent meta-analysis identified 11 randomized controlled trials on the effects of antihypertensives on mental health and reported that ACEI and AT_1R blockers have better effects on quality of life, anxiety, and mental well-being than placebo and other antihypertensives (196). Nasr analyzed data from 378 patients whom both suffered from hypertension and depression and found that patients being treated with an ACEI or ARB showed significantly lower rates of antidepressant usage, while beta-blocker and calcium channel blocker usage led to the highest rate of antidepressant usage (197). Consistent with these studies, Boal et al. analyzed cohort data and found that the use of RAS blockers in patients was associated with a low prevalence of depressive symptoms. The risk of affective disorders is reduced with the usage of ACEIs or Ang II receptor blockers, whereas the risk is increased with the administration of beta-blockers or calcium channel blockers (199). A nationwide population-based study showed that 3747190 subjects were exposed to antihypertensive drugs between 2005 to 2015. The findings of this study suggest that patients who continue to use classes of angiotensin agents, calcium antagonists, and β-blockers have significantly decreased rates of depression, whereas those using diuretic medication do not (198). A retrospective cohort study to investigate the distinct effects of antihypertensives on depression enrolled 181,709 patients and found that other antihypertensives may have a negative effect on the risk of depression compared with ARBs (216). Furthermore, 58.6 million patients aged 18–90 years were enrolled to study the influence of antihypertensive drugs on the onset and recurrence of psychiatric disorders (217). This study showed that ARB users exhibited the lowest incidence of psychotic, affective, and anxiety disorders for the first and recurrent diagnoses compared with CCB and β-blockers (217). However, there are limited randomized clinical trials on ACEI- and ARB-targeting medications and depression, which raises the possibility that future clinical research should conduct trials to examine these apparent advantages.

Despite the success demonstrated, a significant limitation is that not all research has revealed that ACEIs and ARBs have positive benefits on mood disorders, and these opposing results provide a new perspective for future clinical therapy. A small double-blind pilot study of eight patients was conducted to assess whether captopril has euphoric effects in the treatment of hypertension and found that the administration of captopril failed to elevate depressive mood (218). This result may be due to the small sample size of this study. A case report shows the dose of captopril is increased from 25 mg t.i.d. to 37.5 mg q.i.d. and the patient becomes intensely dysphoric within 2 days (203). When the captopril dose was raised to 37.5 mg q.i.d, anxiety and dysphoria reappeared. Furthermore, the dose was increased to 50 mg q.i.d., and the patient exhibited incoherent speech and suicidal ideation. It should be noted that although several studies have found that captopril has a positive effect on depression, its anxiolytic effect may be dose-dependent. In future studies, more attention should be paid to the frequency and different dosages of RAS blockers and the negative effects of different doses on mood.

In contrast, some epidemiological studies highlight concerns regarding possible links between the use of RAS blockers and increased risk of suicide, although the underlying mechanisms remain unknown (49). Mamdani et al. carried out a population-based nested case-control study, which included 964 patients and 3856 controls. The study found that ARB exposure is associated with a higher risk of suicide compared with ACEI (adjusted odds ratio, 1.63; 95% CI, 1.33–2.00). The preferred use of ACEI instead of ARB should be explored whenever possible, especially in individuals with severe mental disorders (219). Nonetheless, when a subsequent analysis was performed in 2020, a nationwide population-based propensity score matching study demonstrated that ARB use was not associated with an increased risk of suicide compared to non-ARB use (220). In summary, evidence from epidemiological studies suggests that the relationship between RAS medication use and suicide is inconsistent. Even if a direct cause-and-effect link exists, it is difficult to prove whether higher or lower RAS contributes to increased suicide risk.

Furthermore, most studies investigating the role of RAS in mood disorders have focused on pharmacological compounds that target ACE or AT1 receptors. Recently, several novel pharmacological compounds have been discovered, including ACE2 activators, Mas receptor agonists, AT2 receptor agonists, and renin blockers (221, 222), and further work to understand their roles is required.

6 Conclusion

A growing body of experimental and clinical data highlights the important role of the RAS in the pathophysiology of mood disorders. In this review, we presented an overview of the RAS, which consisted of two mutually antagonistic pathways that maintain balance through ACE2. The ACE/Ang II/AT1R classical pathway aggravates depression and anxiety by activating AT1R, while the non-classical pathway exerts anxiety/antidepressant effects by activating MasR. Moreover, RAS, mainly Ang II, is involved in the pathological process of depression by promoting inflammation, oxidative stress, and stress responses and reducing BDNF levels. Similarly, agents that inhibit RAS reduce inflammation, oxidative stress, and stress responses and facilitate neurogenesis. This may be the underlying mechanism of RAS blocker treatment for anxiety and depression. The full potential of RAS blockers as antidepressants and anti-anxiety drugs has not yet been elucidated. Hence, in future work, large-scale, randomized, controlled clinical trials are necessary to evaluate the therapeutic efficiency of RAS compounds in emotional disorders. RAS blockers need to be tested as potential therapies for emotional disorders, such as comorbid cardiovascular/cerebrovascular disease and depression. Furthermore, the role of RAS blockers in males and females in emotional disorders and pharmaceutical dosage in men and women should be carefully established.

Thus, RAS blockers may be a promising strategy for the treatment of mood disorders in the future. However, to realize the full therapeutic potential of RAS in mood disorders, further research is required.

Author contributions

SG performed information collection and drafted the manuscript. FD supervised the review and approved the final version of the manuscript. All authors contributed to the article and approved the submitted version.

Funding

This work was supported by a grant from the National Natural Science Foundation of China [grant number 82071293].

Conflict of interest

The authors declare that the research was conducted in the absence of any commercial or financial relationships that could be construed as a potential conflict of interest.

Publisher's note

All claims expressed in this article are solely those of the authors and do not necessarily represent those of their affiliated organizations, or those of the publisher, the editors and the reviewers. Any product that may be evaluated in this article, or claim that may be made by its manufacturer, is not guaranteed or endorsed by the publisher.

References

1. Machado MO, Veronese N, Sanches M, Stubbs B, Koyanagi A, Thompson T, et al. The association of depression and all-cause and cause-specific mortality: an umbrella review of systematic reviews and meta-analyses. *BMC Med* (2018) 16 (1):112. doi: 10.1186/s12916-018-1101-z

2. Clark DA, Beck AT. Cognitive theory and therapy of anxiety and depression: Convergence with neurobiological findings. *Trends Cogn Sci* (2010) 14(9):418–24. doi: 10.1016/j.tics.2010.06.007

3. Regier DA, Kuhl EA, Kupfer DJ. The DSM-5: Classification and criteria changes. *World Psychiatry* (2013) 12(2):92–8. doi: 10.1002/wps.20050

4. Young EA, Abelson JL, Cameron OG. Effect of comorbid anxiety disorders on the hypothalamic-pituitary-adrenal axis response to a social stressor in major depression. *Biol Psychiatry* (2004) 56(2):113–20. doi: 10.1016/j.biopsych.2004.03.017

5. Lamers F, van Oppen P, Comijs HC, Smit JH, Spinhoven P, van Balkom AJLM, et al. Comorbidity patterns of anxiety and depressive disorders in a large cohort study: the Netherlands study of depression and anxiety (NESDA). *J Clin Psychiatry* (2011) 72(3):341–8. doi: 10.4088/JCP.10m06176blu

6. Babaev O, Piletti Chatain C, Krueger-Burg D. Inhibition in the amygdala anxiety circuitry. *Exp Mol Med* (2018) 50(4):1–16. doi: 10.1038/s12276-018-0063-8

7. Drevets WC, Price JL, Bardgett ME, Reich T, Todd RD, Raichle ME. Glucose metabolism in the amygdala in depression: relationship to diagnostic subtype and plasma cortisol levels. *Pharmacol Biochem Behav* (2002) 71(3):431–47. doi: 10.1016/S0091-3057(01)00687-6

8. Frodl T, Meisenzahl E, Zetzsche T, Bottlender R, Born C, Groll C, et al. Enlargement of the amygdala in patients with a first episode of major depression. *Biol Psychiatry* (2002) 51(9):708–14. doi: 10.1016/S0006-3223(01)01359-2

9. Smoller JW. The genetics of stress-related disorders: PTSD, depression, and anxiety disorders. *Neuropsychopharmacology* (2016) 41(1):297–319. doi: 10.1038/npp.2015.266

10. Luo H, Wu PF, Cao Y, Jin M, Shen TT, Wang J, et al. Angiotensin-converting enzyme inhibitor rapidly ameliorates depressive-type behaviors *via* bradykinin-dependent activation of mammalian target of rapamycin complex 1. *Biol Psychiatry* (2020) 88(5):415–25. doi: 10.1016/j.biopsych.2020.02.005

11. Welcome MO, Mastorakis NE. Stress-induced blood brain barrier disruption: Molecular mechanisms and signaling pathways. *Pharmacol Res* (2020) 157:104769. doi: 10.1016/j.phrs.2020.104769

12. Karwowska-Polecka W, Halicka D, Jakubów P, Braszko JJ. [The effect of enalapril and captopril on emotional processes in hypertensive patients]. *Psychiatr Pol* (2002) 36(4):591–601.

13. Robles NR, Cerezo I, Hernandez-Gallego R. Renin-angiotensin system blocking drugs. *J Cardiovasc Pharmacol Ther* (2014) 19(1):14–33. doi: 10.1177/1074248413501018

14. Turnbull F. Blood pressure lowering treatment trialists' collaboration. effects of different blood-pressure-lowering regimens on major cardiovascular events: results of prospectively-designed overviews of randomised trials. *Lancet* (2003) 362 (9395):1527–35. doi: 10.1016/s0140-6736(03)14739-3

15. Miller AJ, Arnold AC. The renin-angiotensin system in cardiovascular autonomic control: recent developments and clinical implications. *Clin Auton Res* (2019) 29(2):231–43. doi: 10.1007/s10286-018-0572-5

16. Kucharewicz I, Pawlak R, Matys T, Pawlak D, Buczko W. Antithrombotic effect of captopril and losartan is mediated by angiotensin-(1-7). *Hypertension* (2002) 40(5):774–9. doi: 10.1161/01.HYP.0000035396.27909.40

17. Yousif MHM, Dhaunsi GS, Makki BM, Qabazard BA, Akhtar S, Benter IF. Characterization of angiotensin-(1-7) effects on the cardiovascular system in an experimental model of type-1 diabetes. *Pharmacol Res* (2012) 66(3):269–75. doi: 10.1016/j.phrs.2012.05.001

18. Biancardi VC, Stern JE. Compromised blood-brain barrier permeability: novel mechanism by which circulating angiotensin II signals to sympathoexcitatory centres during hypertension: AngII-mediated BBB breakdown. *J Physiol* (2016) 594 (6):1591–600. doi: 10.1113/JP271584

19. Sabuhi R, Ali Q, Asghar M, Al-Zamily NRH, Hussain T. Role of the angiotensin II AT2 receptor in inflammation and oxidative stress: opposing effects in lean and obese zucker rats. *Am J Physiol Renal Physiol* (2011) 300(3): F700–706. doi: 10.1152/ajprenal.00616.2010

20. Saavedra JM, Ando H, Armando I, Baiardi G, Bregonzio C, Juorio A, et al. Anti-stress and anti-anxiety effects of centrally acting angiotensin II AT1 receptor antagonists. *Regul Pept* (2005) 128(3):227–38. doi: 10.1016/j.regpep.2004.12.015

21. Gironacci MM, Vicario A, Cerezo G, Silva MG. The depressor axis of the renin-angiotensin system and brain disorders: a translational approach. *Clin Sci (Lond)* (2018) 132(10):1021–38. doi: 10.1042/CS20180189

22. Fraga-Silva RA, Pinheiro SVB, Gonçalves ACC, Alenina N, Bader M, Souza Santos RA. The antithrombotic effect of angiotensin-(1-7) involves mas-mediated NO release from platelets. *Mol Med* (2008) 14(1):28–35. doi: 10.2119/2007-00073.Fraga-Silva

23. Pereira MGAG, Souza LL, Becari C, Duarte DA, Camacho FRB, Oliveira JAC, et al. Angiotensin II-independent angiotensin-(1-7) formation in rat hippocampus: involvement of thimet oligopeptidase. *Hypertension* (2013) 62 (5):879–85. doi: 10.1161/HYPERTENSIONAHA.113.01613

24. Armando I, Terrón JA, Falcón-Neri A, Takeshi I, Häuser W, Inagami T, et al. Increased angiotensin II AT_1 receptor expression in paraventricular nucleus and hypothalamic-Pituitary-Adrenal axis stimulation in AT_2 receptor gene disrupted mice. *Neuroendocrinology* (2002) 76(3):137–47. doi: 10.1159/000064525

25. Kangussu LM, Almeida-Santos AF, Bader M, Alenina N, Fontes MAP, Santos RAS, et al. Angiotensin-(1-7) attenuates the anxiety and depression-like behaviors in transgenic rats with low brain angiotensinogen. *Behav Brain Res* (2013) 257:25–30. doi: 10.1016/j.bbr.2013.09.003

26. Duchemin S, Belanger E, Wu R, Ferland G, Girouard H. Chronic perfusion of angiotensin II causes cognitive dysfunctions and anxiety in mice. *Physiol Behav* (2013) 109:63–8. doi: 10.1016/j.physbeh.2012.10.005

27. Gao N, Wang H, Xu X, Yang Z, Zhang T. Angiotensin II induces cognitive decline and anxiety-like behavior *via* disturbing pattern of theta-gamma oscillations. *Brain Res Bull* (2021), 174:84–91. doi: 10.1016/j.brainresbull.2021.06.002

28. Park HS, You MJ, Yang B, Jang KB, Yoo J, Choi HJ, et al. Chronically infused angiotensin II induces depressive-like behavior *via* microglia activation. *Sci Rep* (2020) 10(1):22082. doi: 10.1038/s41598-020-79096-2

29. Belcheva I, Georgiev V, Chobanova M, Hadjiivanova C. Behavioral effects of angiotensin II microinjected into CA1 hippocampal area. *Neuropeptides* (1997) 31 (1):60–4. doi: 10.1016/S0143-4179(97)90021-4

30. Choy KHC, Chavez CA, Yu J, Mayorov DN. The effect of angiotensin AT1A inactivation on innate and learned fear responses in mice and its relationship to blood pressure. *Psychoneuroendocrinology* (2019), 107:208–16. doi: 10.1016/j.psyneuen.2019.05.004

31. Wang L, Hiller H, Smith JA, de Kloet AD, Krause EG. Angiotensin type 1a receptors in the paraventricular nucleus of the hypothalamus control cardiovascular reactivity and anxiety-like behavior in male mice. *Physiol Genomics* (2016) 48(9):667–76. doi: 10.1152/physiolgenomics.00029.2016

32. Pechlivanova D, Petrov K, Grozdanov P, Nenchovska Z, Tchekalarova J, Stoynev A. Intracerebroventricular infusion of angiotensin AT2 receptor agonist novokinin aggravates some diabetes-mellitus-induced alterations in wistar rats. *Can J Physiol Pharmacol* (2018) 96(5):471–8. doi: 10.1139/cjpp-2017-0428

33. Moreno-Santos B, Marchi-Coelho C, Costa-Ferreira W, Crestani CC. Angiotensinergic receptors in the medial amygdaloid nucleus differently modulate behavioral responses in the elevated plus-maze and forced swimming test in rats. *Behav Brain Res* (2021) 397:112947. doi: 10.1016/j.bbr.2020.112947

34. Diniz CRAF, Casarotto PC, Fred SM, Biojone C, Castrén E, Joca SRL. Antidepressant-like effect of losartan involves TRKB transactivation from angiotensin receptor type 2 (AGTR2) and recruitment of FYN. *Neuropharmacology* (2018) 135:163–71. doi: 10.1016/j.neuropharm.2018.03.011

35. Okuyama S, Sakagawa T, Chaki S, Imagawa Y, Ichiki T, Inagami T. Anxiety-like behavior in mice lacking the angiotensin II type-2 receptor. *Brain Res* (1999) 821(1):150–9. doi: 10.1016/S0006-8993(99)01098-7

36. Wang L, de Kloet AD, Pati D, Hiller H, Smith JA, Pioquinto DJ, et al. Increasing brain angiotensin converting enzyme 2 activity decreases anxiety-like behavior in male mice by activating central mas receptors. *Neuropharmacology* (2016) 105:114–23. doi: 10.1016/j.neuropharm.2015.12.026

37. Bild W, Ciobica A. Angiotensin-(1–7) central administration induces anxiolytic-like effects in elevated plus maze and decreased oxidative stress in the amygdala. *J Affect Disord* (2013) 145(2):165–71. doi: 10.1016/j.jad.2012.07.024

38. Almeida-Santos AF, Kangussu LM, Moreira FA, Santos RAS, Aguiar DC, Campagnole-Santos MJ. Anxiolytic- and antidepressant-like effects of angiotensin-(1–7) in hypertensive transgenic (mRen2)27 rats. *Clin Sci* (2016) 130(14):1247–55. doi: 10.1042/CS20160116

39. Zhu D, Sun M, Liu Q, Yue Y, Lu J, Lin X, et al. Angiotensin (1–7) through modulation of the NMDAR–nNOS–NO pathway and serotonergic metabolism exerts an anxiolytic-like effect in rats. *Behav Brain Res* (2020) 390:112671. doi: 10.1016/j.bbr.2020.112671

40. Walther T, Balschun D, Voigt JP, Fink H, Zuschratter W, Birchmeier C, et al. Sustained long term potentiation and anxiety in mice lacking theMas protooncogene. *J Biol Chem* (1998) 273(19):11867–73. doi: 10.1074/jbc.273.19.11867

41. Voigt JP, Hörtnagl H, Rex A, van Hove L, Bader M, Fink H. Brain angiotensin and anxiety-related behavior: The transgenic rat TGR(ASrAOGEN) 680. *Brain Res* (2005) 1046(1–2):145–56. doi: 10.1016/j.brainres.2005.03.048

42. Tashev R, Ivanova M. Involvement of hippocampal angiotensin 1 receptors in anxiety-like behaviour of olfactory bulbectomized rats. *Pharmacol Rep* (2018) 70 (5):847–52. doi: 10.1016/j.pharep.2018.03.001

43. Ranjbar H, Aghaei I, Moosazadeh M, Shabani M. Angiotensin II type 1 receptor blocker losartan attenuates locomotor, anxiety-like behavior and passive avoidance learning deficits in a sub-chronic stress model. *Iranian J Basic Med Sci [Internet]* (2018) 21(8):856–62. doi: 10.22038/ijbms.2018.27113.6632

44. Sriramula S, Cardinale JP, Lazartigues E, Francis J. ACE2 overexpression in the paraventricular nucleus attenuates angiotensin II-induced hypertension. *Cardiovasc Res* (2011) 92(3):401–8. doi: 10.1093/cvr/cvr242

45. de Kloet AD, Cahill KM, Scott KA, Krause EG. Overexpression of angiotensin converting enzyme 2 reduces anxiety-like behavior in female mice. *Physiol Behav* (2020) 224:113002. doi: 10.1016/j.physbeh.2020.113002

46. Mahon JM, Carr RD, Nicol AK, Henderson IW. Angiotensin(1-7) is an antagonist at the type 1 angiotensin II receptor. *J Hypertens* (1994) 12(12):1377–81.

47. Kangussu LM, Almeida-Santos AF, Moreira FA, Fontes MAP, Santos RAS, Aguiar DC, et al. Reduced anxiety-like behavior in transgenic rats with chronically overproduction of angiotensin-(1–7): Role of the mas receptor. *Behav Brain Res* (2017) 331:193–8. doi: 10.1016/j.bbr.2017.05.026.

48. Moura Santos D, Ribeiro Marins F, Limborço-Filho M, de Oliveira ML, Hamamoto D, Xavier CH, et al. Chronic overexpression of angiotensin-(1-7) in rats reduces cardiac reactivity to acute stress and dampens anxious behavior. *Stress* (2017) 20(2):189–96. doi: 10.1080/10253890.2017.1296949

49. Sanches M, Teixeira AL. The renin-angiotensin system, mood, and suicide: Are there associations? *World J Psychiatry* (2021) 11(9):581–8.

50. Srinivasan J, Suresh B, Ramanathan M. Differential anxiolytic effect of enalapril and losartan in normotensive and renal hypertensive rats. *Physiol Behav* (2003) 78(4–5):585–91. doi: 10.5498/wjp.v11.i9.581.

51. Coatl-Cuaya H, Tendilla-Beltrán H, de Jesús-Vásquez LM, Garcés-Ramírez L, Gómez-Villalobos M de J, Flores G. Losartan enhances cognitive and structural neuroplasticity impairments in spontaneously hypertensive rats. *J Chem Neuroanat* (2022) 120:102061. doi: 10.1016/j.jchemneu.2021.102061

52. Feng P, Wu Z, Liu H, Shen Y, Yao X, Li X, et al. Electroacupuncture improved chronic cerebral hypoperfusion-induced anxiety-like behavior and memory impairments in spontaneously hypertensive rats by downregulating the ACE/Ang II/AT1R axis and upregulating the ACE2/Ang-(1-7)/MasR axis. *Neural Plast* (2020) 2020:9076042. doi: 10.1155/2020/9076042

53. Braszko JJ. Valsartan abolishes most of the memory-improving effects of intracerebroventricular angiotensin II in rats. *Clin Exp Hypertens* (2005) 27 (8):635–49. doi: 10.1080/10641960500298723

54. Huber G, Ogrodnik M, Wenzel J, Stölting I, Huber L, Will O, et al. Telmisartan prevents high-fat diet-induced neurovascular impairments and reduces anxiety-like behavior. *J Cereb Blood Flow Metab* (2021) 41(9):2356–69. doi: 10.1177/0271678X211003497

55. Martin P, Massol J, Puech AJ. Captopril as an antidepressant? effects on the learned helplessness paradigm in rats. *Biol Psychiatry* (1990) 27(9):968–74. doi: 10.1016/0006-3223(90)90034-Y

56. Jenkins TA, Chai SY. Effect of chronic angiotensin converting enzyme inhibition on spatial memory and anxiety-like behaviours in rats. *Neurobiol Learn Memory* (2007) 87(2):218–24. doi: 10.1016/j.nlm.2006.08.010

57. Saavedra JM, Sánchez-Lemus E, Benicky J. Blockade of brain angiotensin ii At1 receptors ameliorates stress, anxiety, brain inflammation and ischemia: Therapeutic implications. *Psychoneuroendocrinology* (2011) 36(1):1–18. doi: 10.1016/j.psyneuen.2010.10.001

58. Giardina WJ, Ebert DM. Positive effects of captopril in the behavioral despair swim test. *Biol Psychiatry* (1989) 25(6):697–702. doi: 10.1016/0006-3223(89)90240-0

59. Ciobica A, Hritcu L, Bild W, Padurariu M, Bild V. P.4.b.011 effects of angiotensin II and its specific receptor antagonists on anxiety status and some oxidative stress markers in rat. *Eur Neuropsychopharmacol* (2011) 21:S538–9. doi: 10.1016/S0924-977X(11)70876-8

60. Jeunemaitre X. [Genetic polymorphisms in the renin-angiotensin system]. *Therapie* (1998) 53(3):271–7.

61. Baghai TC, Binder EB, Schule C, Salyakina D, Eser D, Lucae S, et al. Polymorphisms in the angiotensin-converting enzyme gene are associated with unipolar depression, ACE activity and hypercortisolism. *Mol Psychiatry* (2006) 11(11):1003–15. doi: 10.1038/sj.mp.4001884

62. Firouzabadi N, Shafiei M, Bahramali E, Ebrahimi SA, Bakhshandeh H, Tajik N. Association of angiotensin-converting enzyme (ACE) gene polymorphism with elevated serum ACE activity and major depression in an Iranian population. *Psychiatry Res* (2012) 200(2–3):336–42. doi: 10.1016/j.psychres.2012.05.002

63. Arinami T, Li L, Mitsushio H, Itokawa M, Hamaguchi H, Toru M. An insertion/deletion polymorphism in the angiotensin converting enzyme gene is associated with both brain substance p contents and affective disorders. *Biol Psychiatry* (1996) 40(11):1122–7. doi: 10.1016/S0006-3223(95)00597-8

64. Ghorbani E, Mohammadi M, Malakouti SK, Mohammadi-Kangarani H, Abdollahi E, Torab M, et al. Association of ACE gene Insertion/Deletion polymorphism with suicidal attempt in an Iranian population. *Biochem Genet* (2021) 59(1):31–41. doi: 10.1007/s10528-020-09986-7

65. Baghai TC, Schule C, Zwanzger P, Minov C, Zill P, Ella R, et al. Hypothalamic-pituitary-adrenocortical axis dysregulation in patients with major depression is influenced by the insertion/deletion polymorphism in the angiotensin I-converting enzyme gene. *Neurosci Lett* (2002) 328(3):299–303. doi: 10.1016/S0304-3940(02)00527-X

66. Ancelin ML, Carrière I, Scali J, Ritchie K, Chaudieu I, Ryan J. Angiotensin-converting enzyme gene variants are associated with both cortisol secretion and late-life depression. *Transl Psychiatry* (2013) 3:e322. doi: 10.1038/tp.2013.95

67. Saab YB, Gard PR, Yeoman MS, Mfarrej B, El-Moalem H, Ingram MJ. Renin–angiotensin-system gene polymorphisms and depression. *Prog Neuropsychopharmacol Biol Psychiatry* (2007) 31(5):1113–8. doi: 10.1016/j.pnpbp.2007.04.002

68. Zettergren A, Kern S, Gustafson D, Gudmundsson P, Sigström R, Östling S, et al. The ACE gene is associated with late-life major depression and age at dementia onset in a population-based cohort. *Am J Geriatr Psychiatry* (2017) 25(2):170–7. doi: 10.1016/j.jagp.2016.06.009

69. Taylor WD, Benjamin S, McQuoid DR, Payne ME, Krishnan RR, MacFall JR, et al. AGTR1 gene variation: Association with depression and frontotemporal morphology. *Psychiatry Res: Neuroimaging* (2012) 202(2):104–9. doi: 10.1016/j.pscychresns.2012.03.007

70. Baghai TC, Schüle C, Zwanzger P, Minov C, Schwarz MJ, de Jonge S, et al. Possible influence of the insertion/deletion polymorphism in the angiotensin I-converting enzyme gene on theraputic outcome in affective disorders. *Mol Psychiatry* (2001) 6(3):258–9. doi: 10.1038/sj.mp.4000857

71. Firouzabadi N, Farshadfar P, Haghnegahdar M, Alavi-Shoushtari A, Ghanbarinejad V. Impact of ACE2 genetic variant on antidepressant efficacy of SSRIs. *Acta Neuropsychiatr* (2022) 34(1):30–6. doi: 10.1017/neu.2021.32

72. Skidgel RA, Erdös EG. The broad substrate specificity of human angiotensin I converting enzyme. In: *Clinical and experimental hypertension. part a: Theory and practice* (1987), vol. 9:(2–3):243–59. Available at: https://www.tandfonline.com/doi/abs/10.3109/10641968709164184.

73. Kramer MS, Cutler N, Feighner J, Shrivastava R, Carman J, Sramek JJ, et al. Distinct mechanism for antidepressant activity by blockade of central substance p receptors. *Science* (1998) 281(5383):1640–5. doi: 10.1126/science.281.5383.1640

74. Baghai TC, Schule C, Zill P, Deiml T, Eser D, Zwanzger P, et al. The angiotensin I converting enzyme insertion/deletion polymorphism influences therapeutic outcome in major depressed women, but not in men. *Neurosci Lett* (2004) 363(1):38–42. doi: 10.1016/j.neulet.2004.03.052

75. Bondy B, Baghai TC, Zill P, Schule C, Eser D, Deiml T, et al. Genetic variants in the angiotensin I-converting-enzyme (ACE) and angiotensin II receptor (AT1) gene and clinical outcome in depression. *Prog Neuropsychopharmacol Biol Psychiatry* (2005) 29(6):1094–9. doi: 10.1016/j.pnpbp.2005.03.015

76. Leonard BE. Inflammation and depression: a causal or coincidental link to the pathophysiology? *Acta Neuropsychiatr* (2018) 30(1):1–16. doi: 10.1017/neu.2016.69

77. Licinio J, Wong ML. Pathways and mechanisms for cytokine signaling of the central nervous system. *J Clin Invest* (1997) 100(12):2941–7.

78. Dantzer R, O'Connor JC, Freund GG, Johnson RW, Kelley KW. From inflammation to sickness and depression: when the immune system subjugates the brain. *Nat Rev Neurosci* (2008) 9(1):46–56.

79. Ah M, Cl R. The role of inflammation in depression: from evolutionary imperative to modern treatment target. *Nat Rev Immunol* (2016) 16(1):22–34.

80. Prinz M, Priller J. Tickets to the brain: role of CCR2 and CX3CR1 in myeloid cell entry in the CNS. *J Neuroimmunol* (2010) 224(1–2):80–4.

81. Moylan S, Berk M, Dean OM, Samuni Y, Williams LJ, O'Neil A, et al. Oxidative & nitrosative stress in depression: why so much stress? *Neurosci Biobehav Rev* (2014) 45:46–62.

82. Leonard BE. Inflammation, depression and dementia: are they connected? *Neurochem Res* (2007) 32(10):1749–56.

83. Porter GA, O'Connor JC. Brain-derived neurotrophic factor and inflammation in depression: Pathogenic partners in crime? *World J Psychiatry* (2022) 12(1):77–97.

84. Osimo EF, Baxter LJ, Lewis G, Jones PB, Khandaker GM. Prevalence of low-grade inflammation in depression: a systematic review and meta-analysis of CRP levels. *Psychol Med* (2019) 49(12):1958–70.

85. Leonard B, Maes M. Mechanistic explanations how cell-mediated immune activation, inflammation and oxidative and nitrosative stress pathways and their sequels and concomitants play a role in the pathophysiology of unipolar depression. *Neurosci Biobehav Rev* (2012) 36(2):764–85.

86. Wium-Andersen MK, Orsted DD, Nordestgaard BG. Elevated c-reactive protein, depression, somatic diseases, and all-cause mortality: a mendelian randomization study. *Biol Psychiatry* (2014) 76(3):249–57.

87. Miller AH, Maletic V, Raison CL. Inflammation and its discontents: The role of cytokines in the pathophysiology of major depression. *Biol Psychiatry* (2009) 65(9):732–41. doi: 10.1016/j.biopsych.2008.11.029

88. Yang C, Wardenaar KJ, Bosker FJ, Li J, Schoevers RA. Inflammatory markers and treatment outcome in treatment resistant depression: A systematic review. *J Affect Disord* (2019) 257:640–9. doi: 10.1016/j.jad.2019.07.045

89. Strawbridge R, Hodsoll J, Powell TR, Hotopf M, Hatch SL, Breen G, et al. Inflammatory profiles of severe treatment-resistant depression. *J Affect Disord* (2019) 246:42–51. doi: 10.1016/j.jad.2018.12.037

90. Hannestad J, DellaGioia N, Bloch M. The effect of antidepressant medication treatment on serum levels of inflammatory cytokines: A meta-analysis. *Neuropsychopharmacol* (2011) 36(12):2452–9. doi: 10.1038/npp.2011.132

91. Kappelmann N, Lewis G, Dantzer R, Jones PB, Khandaker GM. Antidepressant activity of anti-cytokine treatment: a systematic review and meta-analysis of clinical trials of chronic inflammatory conditions. *Mol Psychiatry* (2018) 23(2):335–43. doi: 10.1038/mp.2016.167

92. O'Connor JC, Lawson MA, André C, Moreau M, Lestage J, Castanon N, et al. Lipopolysaccharide-induced depressive-like behavior is mediated by indoleamine 2,3-dioxygenase activation in mice. *Mol Psychiatry* (2009) 14(5):511–22. doi: 10.1038/sj.mp.4002148

93. Kreisel T, Frank MG, Licht T, Reshef R, Ben-Menachem-Zidon O, Baratta MV, et al. Dynamic microglial alterations underlie stress-induced depressive-like behavior and suppressed neurogenesis. *Mol Psychiatry* (2014) 19(6):699–709. doi: 10.1038/mp.2013.155

94. Tao SH, Ren XQ, Zhang LJ, Liu MY. Association between common cardiovascular drugs and depression. *Chin Med J (Engl)* (2021) 134(22):2656–65. doi: 10.1097/CM9.0000000000001875

95. Zhang L, Du J, Hu Z, Han G, Delafontaine P, Garcia G, et al. IL-6 and serum amyloid a synergy mediates angiotensin II-induced muscle wasting. *J Am Soc Nephrol* (2009) 20(3):604–12. doi: 10.1681/ASN.2008060628

96. Recinos A, LeJeune WS, Sun H, Lee CY, Tieu BC, Lu M, et al. Angiotensin II induces IL-6 expression and the jak-STAT3 pathway in aortic adventitia of LDL receptor-deficient mice. *Atherosclerosis* (2007) 194(1):125–33. doi: 10.1016/j.atherosclerosis.2006.10.013

97. Kranzhöfer R, Browatzki M, Schmidt J, Kübler W. Angiotensin II activates the proinflammatory transcription factor nuclear factor-kappaB in human monocytes. *Biochem Biophys Res Commun* (1999) 257(3):826–8. doi: 10.1006/bbrc.1999.0543

98. Watanabe K, Taniguchi M, Miyoshi M, Shimizu H, Imoto T, Sato K, et al. Effects of central injection of angiotensin-converting-enzyme inhibitor and angiotensin type 1 receptor antagonist on the brain NF-kappaB and AP-1 activities of rats given LPS. *Peptides* (2006) 27(6):1538–46. doi: 10.1016/j.peptides.2005.11.005

99. Salmani H, Hosseini M, Baghcheghi Y, Moradi-Marjaneh R, Mokhtari-Zaer A. Losartan modulates brain inflammation and improves mood disorders and memory impairment induced by innate immune activation: The role of PPAR-γ activation. *Cytokine* (2020) 125:154860. doi: 10.1016/j.cyto.2019.154860

100. Ayyub M, Najmi A, Akhtar M. Protective effect of irbesartan an angiotensin (AT1) receptor antagonist in unpredictable chronic mild stress induced depression in mice. *Drug Res (Stuttg)* (2016) 67(01):59–64. doi: 10.1055/s-0042-118172

101. Aswar U, Chepurwar S, Shintre S, Aswar M. Telmisartan attenuates diabetes induced depression in rats. *Pharmacol Rep* (2017) 69(2):358–64. doi: 10.1016/j.pharep.2016.12.004

102. Pang T, Wang J, Benicky J, Sánchez-Lemus E, Saavedra JM. Telmisartan directly ameliorates the neuronal inflammatory response to IL-1β partly through the JNK/c-jun and NADPH oxidase pathways. *J Neuroinflamm* (2012) 9(1):588. doi: 10.1186/1742-2094-9-102

103. Yuan X, Guo X, Deng Y, Zhu D, Shang J, Liu H. Chronic intermittent hypoxia-induced neuronal apoptosis in the hippocampus is attenuated by telmisartan through suppression of iNOS/NO and inhibition of lipid peroxidation and inflammatory responses. *Brain Res* (2015) 1596:48–57. doi: 10.1016/j.brainres.2014.11.035

104. Torika N, Asraf K, Danon A, Apte RN, Fleisher-Berkovich S. Telmisartan modulates glial activation: *In vitro* and *In vivo* studies. *PloS One* (2016) 11(5): e0155823. doi: 10.1371/journal.pone.0155823

105. Benicky J, Sánchez-Lemus E, Honda M, Pang T, Orecna M, Wang J, et al. Angiotensin II AT1 receptor blockade ameliorates brain inflammation. *Neuropsychopharmacol* (2011) 36(4):857–70. doi: 10.1038/npp.2010.225

106. Gong X, Hu H, Qiao Y, Xu P, Yang M, Dang R, et al. The involvement of renin-angiotensin system in lipopolysaccharide-induced behavioral changes, neuroinflammation, and disturbed insulin signaling. *Front Pharmacol* (2019) 10:318. doi: 10.3389/fphar.2019.00318

107. Bhat SA, Goel R, Shukla R, Hanif K. Angiotensin receptor blockade modulates NFκB and STAT3 signaling and inhibits glial activation and neuroinflammation better than angiotensin-converting enzyme inhibition. *Mol Neurobiol* (2016) 53(10):6950–67. doi: 10.1007/s12035-015-9584-5

108. Sanchez-Lemus E, Murakami Y, Larrayoz-Roldan IM, Moughamian AJ, Pavel J, Nishioku T, et al. Angiotensin II AT1 receptor blockade decreases lipopolysaccharide-induced inflammation in the rat adrenal gland. *Endocrinology* (2008) 149(10):5177–88. doi: 10.1210/en.2008-0242

109. Sánchez-Lemus E, Benicky J, Pavel J, Saavedra JM. *In vivo* angiotensin II AT1 receptor blockade selectively inhibits LPS-induced innate immune response and ACTH release in rat pituitary gland. *Brain Behav Immun* (2009) 23(7):945–57. doi: 10.1016/j.bbi.2009.04.012

110. Miyoshi M, Miyano K, Moriyama N, Taniguchi M, Watanabe T. Angiotensin type 1 receptor antagonist inhibits lipopolysaccharide-induced stimulation of rat microglial cells by suppressing nuclear factor κB and activator protein-1 activation: Lipopolysaccharide-induced stimulation of rat microglial cells. *Eur J Neurosci* (2008) 27(2):343–51. doi: 10.1111/j.1460-9568.2007.06014.x

111. Lenart L, Balogh DB, Lenart N, Barczi A, Hosszu A, Farkas T, et al. Novel therapeutic potential of angiotensin receptor 1 blockade in a rat model of diabetes-associated depression parallels altered BDNF signalling. *Diabetologia* (2019) 62 (8):1501–13. doi: 10.1007/s00125-019-4888-z

112. Singh B, Mourya A, Sah SP, Kumar A. Protective effect of losartan and ramipril against stress induced insulin resistance and related complications: Anti-inflammatory mechanisms. *Eur J Pharmacol* (2017) 801:54–61. doi: 10.1016/j.ejphar.2017.02.050

113. Balogh DB, Molnar A, Hosszu A, Lakat T, Hodrea J, Szabo AJ, et al. Antidepressant effect in diabetes-associated depression: A novel potential of RAAS inhibition. *Psychoneuroendocrinology* (2020) 118:104705. doi: 10.1016/j.psyneuen.2020.104705

114. Xue B, Yu Y, Wei SG, Beltz TG, Guo F, Felder RB, et al. Stress-induced sensitization of angiotensin II hypertension is reversed by blockade of angiotensin-converting enzyme or tumor necrosis factor-α. *Am J Hypertens* (2019) 32(9):909–17. doi: 10.1093/ajh/hpz075

115. Nocito C, Lubinsky C, Hand M, Khan S, Patel T, Seliga A, et al. Centrally acting angiotensin-converting enzyme inhibitor suppresses type I interferon responses and decreases inflammation in the periphery and the CNS in lupus-prone mice. *Front Immunol* (2020) 11:573677. doi: 10.3389/fimmu.2020.573677

116. Salmani H, Hosseini M, Beheshti F, Baghcheghi Y, Sadeghnia HR, Soukhtanloo M, et al. Angiotensin receptor blocker, losartan ameliorates neuroinflammation and behavioral consequences of lipopolysaccharide injection. *Life Sci* (2018) 203:161–70. doi: 10.1016/j.lfs.2018.04.033

117. Bhatt S, Nagappa AN, Patil CR. Role of oxidative stress in depression. *Drug Discov Today* (2020) 25(7):1270–6. doi: 10.1016/j.drudis.2020.05.001

118. Réus GZ, Dos Santos MAB, Abelaira HM, Titus SE, Carlessi AS, Matias BI, et al. Antioxidant treatment ameliorates experimental diabetes-induced depressive-like behaviour and reduces oxidative stress in brain and pancreas. *Diabetes Metab Res Rev* (2016) 32(3):278–88. doi: 10.1002/dmrr.2732

119. Salim S. Oxidative stress and psychological disorders. *Curr Neuropharmacol* (2014) 12(2):140–7. doi: 10.2174/1570159X11666131120230309

120. Vaváková M, Ďuračková Z, Trebatická J. Markers of oxidative stress and neuroprogression in depression disorder. *Oxid Med Cell Longevity* (2015) 2015:1–12. doi: 10.1155/2015/898393

121. Diniz BS, Mendes-Silva AP, Silva LB, Bertola L, Vieira MC, Ferreira JD, et al. Oxidative stress markers imbalance in late-life depression. *J Psychiatr Res* (2018) 102:29–33. doi: 10.1016/j.jpsychires.2018.02.023

122. Lee SY, Lee SJ, Han C, Patkar AA, Masand PS, Pae CU. Oxidative/nitrosative stress and antidepressants: Targets for novel antidepressants. *Prog Neuropsychopharmacol Biol Psychiatry* (2013) 46:224–35. doi: 10.1016/j.pnpbp.2012.09.008

123. Hovatta I, Juhila J, Donner J. Oxidative stress in anxiety and comorbid disorders. *Neurosci Res* (2010) 68(4):261–75. doi: 10.1016/j.neures.2010.08.007

124. Steenkamp LR, Hough CM, Reus VI, Jain FA, Epel ES, James SJ, et al. Severity of anxiety- but not depression- is associated with oxidative stress in major depressive disorder. *J Affect Disord* (2017) 219:193–200. doi: 10.1016/j.jad.2017.04.042

125. Salim S, Sarraj N, Taneja M, Saha K, Tejada-Simon MV, Chugh G. Moderate treadmill exercise prevents oxidative stress-induced anxiety-like behavior in rats. *Behav Brain Res* (2010) 208(2):545–52. doi: 10.1016/j.bbr.2009.12.039

126. Rodriguez-Perez AI, Borrajo A, Rodriguez-Pallares J, Guerra MJ, Labandeira-Garcia JL. Interaction between NADPH-oxidase and rho-kinase in angiotensin II-induced microglial activation: NADPH-oxidase and rho-kinase interaction. *Glia* (2015) 63(3):466–82. doi: 10.1002/glia.22765

127. Pedreanez A, Arcaya JL, Carrizo E, Mosquera J. Forced swimming test increases superoxide anion positive cells and angiotensin II positive cells in the cerebrum and cerebellum of the rat. *Brain Res Bull* (2006) 71(1–3):18–22. doi: 10.1016/j.brainresbull.2006.07.018

128. Zhang M, Mao Y, Ramirez SH, Tuma RF, Chabrashvili T. Angiotensin II induced cerebral microvascular inflammation and increased blood–brain barrier permeability *via* oxidative stress. *Neuroscience* (2010) 171(3):852–8. doi: 10.1016/j.neuroscience.2010.09.029

129. Lee SH, Fujioka S, Takahashi R, Oe T. Angiotensin II-induced oxidative stress in human endothelial cells: Modification of cellular molecules through lipid peroxidation. *Chem Res Toxicol* (2019) 32(7):1412–22. doi: 10.1021/acs.chemrestox.9b00110

130. Barhoumi T, Alghanem B, Shaibah H, Mansour FA, Alamri HS, Akiel MA, et al. SARS-CoV-2 coronavirus spike protein-induced apoptosis, inflammatory, and oxidative stress responses in THP-1-Like-Macrophages: Potential role of angiotensin-converting enzyme inhibitor (Perindopril). *Front Immunol* (2021) 12:728896. doi: 10.3389/fimmu.2021.728896

131. Onozato ML, Tojo A, Goto A, Fujita T, Wilcox CS. Oxidative stress and nitric oxide synthase in rat diabetic nephropathy: effects of ACEI and ARB. *Kidney Int* (2002) 61(1):186–94. doi: 10.1046/j.1523-1755.2002.00123.x

132. Salim S, Asghar M, Taneja M, Hovatta I, Chugh G, Vollert C, et al. Potential contribution of oxidative stress and inflammation to anxiety and hypertension. *Brain Res* (2011), 1404:63–71. doi: 10.1016/j.brainres.2011.06.024

133. Goel R, Bhat SA, Hanif K, Nath C, Shukla R. Angiotensin II receptor blockers attenuate lipopolysaccharide-induced memory impairment by modulation of NF-κB-Mediated BDNF/CREB expression and apoptosis in spontaneously hypertensive rats. *Mol Neurobiol* (2018) 55(2):1725–39. doi: 10.1007/s12035-017-0450-5

134. Bild W, Hritcu L, Stefanescu C, Ciobica A. Inhibition of central angiotensin II enhances memory function and reduces oxidative stress status in rat hippocampus. *Biol Psychiatry* (2013) 43:79–88. doi: 10.1016/j.pnpbp.2012.12.009

135. Patki G, Salvi A, Liu H, Atrooz F, Alkadhi I, Kelly M, et al. Tempol treatment reduces anxiety-like behaviors induced by multiple anxiogenic drugs in rats. *PloS One* (2015) 10(3):e0117498. doi: 10.1371/journal.pone.0117498

136. AlSaad AMS, Alasmari F, Abuohashish HM, Mohany M, Ahmed MM, Al-Rejaie SS. Renin angiotensin system blockage by losartan neutralize hypercholesterolemia-induced inflammatory and oxidative injuries. *Redox Rep* (2020) 25(1):51–8. doi: 10.1080/13510002.2020.1763714

137. Gold PW. The organization of the stress system and its dysregulation in depressive illness. *Mol Psychiatry* (2015) 20(1):32–47. doi: 10.1038/mp.2014.163

138. Cohen S, Janicki-Deverts D, Doyle WJ, Miller GE, Frank E, Rabin BS, et al. Chronic stress, glucocorticoid receptor resistance, inflammation, and disease risk. *Proc Natl Acad Sci U S A* (2012) 109(16):5995–9. doi: 10.1073/pnas.1118355109

139. Juruena MF, Bocharova M, Agustini B, Young AH. Atypical depression and non-atypical depression: Is HPA axis function a biomarker? a systematic review. *J Affect Disord* (2018) 233:45–67. doi: 10.1016/j.jad.2017.09.052

140. Boyer P. Do anxiety and depression have a common pathophysiological mechanism? *Acta Psychiatr Scand Suppl* (2000) 406):24–9. doi: 10.1111/j.0065-1591.2000.acp29[dash]04.x

141. Kalin NH. Novel insights into pathological anxiety and anxiety-related disorders. *Am J Psychiatry* (2020) 177(3):187–9. doi: 10.1176/appi.ajp.2020.20010057

142. Chalmers DT, Lovenberg TW, De Souza EB. Localization of novel corticotropin-releasing factor receptor (CRF2) mRNA expression to specific subcortical nuclei in rat brain: comparison with CRF1 receptor mRNA expression. *J Neurosci* (1995) 15(10):6340–50. doi: 10.1523/JNEUROSCI.15-10-06340.1995

143. Holsboer F. The rationale for corticotropin-releasing hormone receptor (CRH-r) antagonists to treat depression and anxiety. *J Psychiatr Res* (1999) 33 (3):181–214. doi: 10.1016/S0022-3956(98)90056-5

144. Yang G, Xi ZX, Wan Y, Wang H, Bi G. Changes in circulating and tissue angiotensin II during acute and chronic stress. *Biol Signals* (1993) 2(3):166–72. doi: 10.1159/000109488

145. Peng J, Kimura B, Phillips MI. The predominant role of brain angiotensinogen and angiotensin in environmentally induced hypertension. *Regul Peptides* (2002) 110(1):25–32. doi: 10.1016/S0167-0115(02)00156-8

146. Castren E, Saavedra JM. Repeated stress increases the density of angiotensin II binding sites in rat paraventricular nucleus and subfornical organ. *Endocrinology* (1988) 122(1):370–2. doi: 10.1210/endo-122-1-370

147. Jezova D, Ochedalski T, Kiss A, Aguilera G. Brain angiotensin II modulates sympathoadrenal and hypothalamic pituitary adrenocortical activation during stress: Neuropeptide y. *J Neuroendocrinol* (2008) 10(1):67–72. doi: 10.1046/j.1365-2826.1998.00182.x

148. Pavlatou MG, Mastorakos G, Lekakis I, Liatis S, Vamvakou G, Zoumakis E, et al. Chronic administration of an angiotensin II receptor antagonist resets the hypothalamic–pituitary–adrenal (HPA) axis and improves the affect of patients with diabetes mellitus type 2: Preliminary results: Research report. *Stress* (2008) 11 (1):62–72. doi: 10.1080/10253890701476621

149. Veltmar A, Culman J, Qadri F, Rascher W, Unger T. Involvement of adrenergic and angiotensinergic receptors in the paraventricular nucleus in the angiotensin II-induced vasopressin release. *J Pharmacol Exp Ther* (1992) 263(3):1253–60.

150. Rivier C, Vale W. Effect of angiotensin II on ACTH release *in vivo*: role of corticotropin-releasing factor. *Regul Pept* (1983) 7(3):253–8. doi: 10.1016/0167-0115(83)90018-6

151. Pavel J, Benicky J, Murakami Y, Sanchez-Lemus E, Saavedra JM. Peripherally administered angiotensin II AT $_1$ receptor antagonists are anti-stress compounds in vivo. *Ann New York Acad Sci* (2008) 1148(1):360–6. doi: 10.1196/annals.1410.006

152. Saavedra JM, Benicky J. Brain and peripheral angiotensin II play a major role in stress. *Stress* (2007) 10(2):185–93. doi: 10.1080/10253890701350735

153. Saavedra JM, Armando I, Bregonzio C, Juorio A, Macova M, Pavel J, et al. A centrally acting, anxiolytic angiotensin II AT1 receptor antagonist prevents the isolation stress-induced decrease in cortical CRF1 receptor and benzodiazepine binding. *Neuropsychopharmacol* (2006) 31(6):1123–34. doi: 10.1038/sj.npp.1300921

154. Bregonzio C, Armando I, Ando H, Jezova M, Baiardi G, Saavedra JM. Anti-inflammatory effects of angiotensin II AT1 receptor antagonism prevent stress-induced gastric injury. *Am J Physiol Gastrointest Liver Physiol* (2003) 285(2):G414–423. doi: 10.1152/ajpgi.00058.2003

155. Costa R, Tamascia ML, Sanches A, Moreira RP, Cunha TS, Nogueira MD, et al. Tactile stimulation of adult rats modulates hormonal responses, depression-like behaviors, and memory impairment induced by chronic mild stress. In: *Role of angiotensin II. Behav Brain Res* (2020) 379:112250. doi: 10.1016/j.bbr.2019.112250. Available at: https://reader.elsevier.com/reader/sd/pii/S0166432819304784?token=89053D7496A3BE06CDD995A8EE12059DFC1F1D89BA4C836C07522F9DFA6CDC552C257BF51C70A785D342B9A91BC7DD7E&originRegion=us-east-1&originCreation=20220420031144.

156. Braszko JJ, Wincewicz D, Jakubów P. Candesartan prevents impairment of recall caused by repeated stress in rats. *Psychopharmacol (Berl)* (2013) 225(2):421–8. doi: 10.1007/s00213-012-2829-3

157. Armando I, Carranza A, Nishimura Y, Hoe KL, Barontini M, Terrón JA, et al. Peripheral administration of an angiotensin II AT1 receptor antagonist decreases the hypothalamic-Pituitary-Adrenal response to isolation stress. *Endocrinology* (2001) 142(9):3880–9. doi: 10.1210/endo.142.9.8366

158. Barnes NM, Costall B, Kelly ME, Murphy DA, Naylor RJ. Anxiolytic-like action of DuP753, a non-peptide angiotensin II receptor antagonist. *Neuroreport* (1990) 1(1):20–1. doi: 10.1097/00001756-199009000-00006

159. Campos GV, de Souza AMA, Ji H, West CA, Wu X, Lee DL, et al. The angiotensin type 1 receptor antagonist losartan prevents ovariectomy-induced cognitive dysfunction and anxiety-like behavior in long Evans rats. *Cell Mol Neurobiol* (2020) 40 (3):407–20. doi: 10.1007/s10571-019-00744-x

160. Llano López LH, Caif F, García S, Fraile M, Landa AI, Baiardi G, et al. Anxiolytic-like effect of losartan injected into amygdala of the acutely stressed rats. *Pharmacol Rep* (2012) 64(1):54–63. doi: 10.1016/S1734-1140(12)70730-2

161. Kumar A, Singh B, Mishra J, Sah SP, Pottabathini R. Neuroprotective mechanism of losartan and its interaction with nimesulide against chronic fatigue stress. *Inflammopharmacology* (2015) 23(6):291–305. doi: 10.1007/s10787-015-0238-z

162. Pechlivanova DM, Stoynev AG, Tchekalarova JD. The effects of chronic losartan pretreatment on restraint stress-induced changes in motor activity, nociception and pentylenetetrazol generalized seizures in rats. *Folia Med* (2011) 53(2):69–73. doi: 10.2478/v10153-010-0040-z

163. Costa R, Tamascia ML, Sanches A, Moreira RP, Cunha TS, Nogueira MD, et al. Tactile stimulation of adult rats modulates hormonal responses, depression-like behaviors, and memory impairment induced by chronic mild stress: Role of angiotensin II. *Behav Brain Res* (2020) 379:112250. doi: 10.1016/j.bbr.2019.112250

164. Li Y, Cheng KC, Liu KF, Peng WH, Cheng JT, Niu HS. Telmisartan activates PPARδ to improve symptoms of unpredictable chronic mild stress-induced depression in mice. *Sci Rep* (2017) 7(1):14021. doi: 10.1038/s41598-017-14265-4

165. McALLISTER-WILLIAMS RH, Ferrier IN, Young AH. Mood and neuropsychological function in depression: the role of corticosteroids and serotonin. *Psychol Med* (1998) 28(3):573–84. doi: 10.1017/S0033291798006680

166. Nahmod VE, Finkielman S, Benarroch EE, Pirola CJ. Angiotensin regulates release and synthesis of serotonin in brain. *Science* (1978) 202(4372):1091–3. doi: 10.1126/science.152460

167. Bali A, Jaggi AS. Angiotensin as stress mediator: role of its receptor and interrelationships among other stress mediators and receptors. *Pharmacol Res* (2013) 76:49–57. doi: 10.1016/j.phrs.2013.07.004

168. Jenkins TA. Effect of angiotensin-related antihypertensives on brain neurotransmitter levels in rats. *Neurosci Lett* (2008) 444(2):186–9. doi: 10.1016/j.neulet.2008.08.021

169. Tanaka J, Miyakubo H, Kawakami A, Hayashi Y, Nomura M. Involvement of NMDA receptor mechanisms in the modulation of serotonin release in the lateral parabrachial nucleus in the rat. *Brain Res Bull* (2006) 71(1–3):311–5. doi: 10.1016/j.brainresbull.2006.09.017

170. Stone LB, McCormack CC, Bylsma LM. Cross system autonomic balance and regulation: Associations with depression and anxiety symptoms. *Psychophysiology* (2020) 57(10):e13636. doi: 10.1111/psyp.13636

171. Streeter CC, Gerbarg PL, Saper RB, Ciraulo DA, Brown RP. Effects of yoga on the autonomic nervous system, gamma-aminobutyric-acid, and allostasis in epilepsy, depression, and post-traumatic stress disorder. *Med Hypotheses* (2012) 78 (5):571–9. doi: 10.1016/j.mehy.2012.01.021

172. Lin KD, Chang LH, Wu YR, Hsu WH, Kuo CH, Tsai JR, et al. Association of depression and parasympathetic activation with glycemic control in type 2 diabetes mellitus. *J Diabetes Complications* (2022) 36(8):108264. doi: 10.1016/j.jdiacomp.2022.108264

173. Selye H. A syndrome produced by diverse nocuous agents. 1936. *J Neuropsychiatry Clin Neurosci* (1998) 10(2):230–1. doi: 10.1176/jnp.10.2.230a

174. Grippo AJ, Johnson AK. Stress, depression and cardiovascular dysregulation: a review of neurobiological mechanisms and the integration of research from preclinical disease models. *Stress* (2009) 12(1):1–21. doi: 10.1080/10253890802046281

175. Vatta MS, Bianciotti LG, Locatelli AS, Papouchado ML, Fernández BE. Monophasic and biphasic effects of angiotensin II and III on norepinephrine uptake and release in rat adrenal medulla. *Can J Physiol Pharmacol* (1992) 70 (6):821–5. doi: 10.1139/y92-110

176. Piano MR, Prasun M. Neurohormone activation. *Crit Care Nurs Clin North Am* (2003) 15(4):413–21. doi: 10.1016/S0899-5885(02)00096-5

177. Fabiani ME, Sourial M, Thomas WG, Johnston CI, Johnston CI, Frauman AG. Angiotensin II enhances noradrenaline release from sympathetic nerves of the rat prostate *via* a novel angiotensin receptor: implications for the pathophysiology of benign prostatic hyperplasia. *J Endocrinol* (2001) 171(1):97–108. doi: 10.1677/joe.0.1710097

178. Machado-Silva A, Passos-Silva D, Santos RA, Sinisterra RD. Therapeutic uses for angiotensin-(1-7). *Expert Opin Ther Pat* (2016) 26(6):669–78. doi: 10.1080/13543776.2016.1179283

179. Rodriguez-Campos M, Kadarian C, Rodano V, Bianciotti L, Fernandez B, Vatta M. AT-1 receptor and phospholipase c are involved in angiotensin III modulation of hypothalamic noradrenergic transmission. *Cell Mol Neurobiol* (2000) 20(6):747–62. doi: 10.1023/A:1007059010571

180. Kregel KC, Stauss H, Unger T. Modulation of autonomic nervous system adjustments to heat stress by central ANG II receptor antagonism. *Am J Physiol* (1994) 266(6 Pt 2):R1985–1991. doi: 10.1152/ajpregu.1994.266.6.R1985

181. Arnsten AFT, Raskind MA, Taylor FB, Connor DF. The effects of stress exposure on prefrontal cortex: Translating basic research into successful treatments for post-traumatic stress disorder. *Neurobiol Stress* (2015) 1:89–99. doi: 10.1016/j.ynstr.2014.10.002

182. Geracioti TD, Baker DG, Ekhator NN, West SA, Hill KK, Bruce AB, et al. CSF norepinephrine concentrations in posttraumatic stress disorder. *Am J Psychiatry* (2001) 158(8):1227–30. doi: 10.1176/appi.ajp.158.8.1227

183. Gold PW, Wong ML, Goldstein DS, Gold HK, Ronsaville DS, Esler M, et al. Cardiac implications of increased arterial entry and reversible 24-h central and peripheral norepinephrine levels in melancholia. *Proc Natl Acad Sci U S A* (2005) 102(23):8303–8. doi: 10.1073/pnas.0503069102

184. Strawn JR, Geracioti TD. Noradrenergic dysfunction and the psychopharmacology of posttraumatic stress disorder. *Depress Anxiety* (2008) 25 (3):260–71. doi: 10.1002/da.20292

185. Numakawa T, Suzuki S, Kumamaru E, Adachi N, Richards M, Kunugi H. BDNF function and intracellular signaling in neurons. *Histol Histopathol* (2010) 25 (2):237–58. doi: 10.14670/HH-25.237

186. Alonso M, Vianna MRM, Depino AM, Mello e Souza T, Pereira P, Szapiro G, et al. BDNF-triggered events in the rat hippocampus are required for both short- and long-term memory formation. *Hippocampus* (2002) 12(4):551–60. doi: 10.1002/hipo.10035

187. Chen DY, Bambah-Mukku D, Pollonini G, Alberini CM. Glucocorticoid receptors recruit the CaMKIIα-BDNF-CREB pathways to mediate memory consolidation. *Nat Neurosci* (2012) 15(12):1707–14. doi: 10.1038/nn.3266

188. Saarelainen T, Hendolin P, Lucas G, Koponen E, Sairanen M, MacDonald E, et al. Activation of the TrkB neurotrophin receptor is induced by antidepressant drugs and is required for antidepressant-induced behavioral effects. *J Neurosci* (2003) 23(1):349–57. doi: 10.1523/JNEUROSCI.23-01-00349.2003

189. Chauhan VS, Khan SA, Kulhari K. Correlation of brain-derived neurotrophic factor with severity of depression and treatment response. *Med J Armed Forces India* (2020). doi: 10.1016/j.mjafi.2020.09.014

190. Tayyab M, Shahi MH, Farheen S, Mariyath PMM, Khanam N, Hossain MM. Exploring the potential role of sonic hedgehog cell signalling pathway in antidepressant effects of nicotine in chronic unpredictable mild stress rat model. *Heliyon* (2019) 5(5):e01600. doi: 10.1016/j.heliyon.2019.e01600

191. Ping G, Qian W, Song G, Zhaochun S. Valsartan reverses depressive/anxiety-like behavior and induces hippocampal neurogenesis and expression of BDNF protein in unpredictable chronic mild stress mice. *Pharmacol Biochem Behav* (2014) 124:5–12. doi: 10.1016/j.pbb.2014.05.006

192. Shibata K, Makino I, Shibaguchi H, Niwa M, Katsuragi T, Furukawa T. Up-regulation of angiotensin type 2 receptor mRNA by angiotensin II in rat cortical cells. *Biochem Biophys Res Commun* (1997) 239(2):633–7. doi: 10.1006/bbrc.1997.7521

193. Patki G, Solanki N, Atrooz F, Allam F, Salim S. Depression, anxiety-like behavior and memory impairment are associated with increased oxidative stress and inflammation in a rat model of social stress. *Brain Res* (2013) 1539:73–86. doi: 10.1016/j.brainres.2013.09.033

194. Köhler-Forsberg O, Petersen L, Berk M, Gasse C, Østergaard SD. The effect of combined treatment with SSRIs and renin-angiotensin system (RAS) drugs: A propensity score matched cohort study. *Eur Neuropsychopharmacol* (2020) 32:120–30. doi: 10.1016/j.euroneuro.2020.01.004

195. Kessing LV, Rytgaard HC, Gerds TA, Berk M, Ekstrøm CT, Andersen PK. New drug candidates for depression - a nationwide population-based study. *Acta Psychiatr Scand* (2019) 139(1):68–77. doi: 10.1111/acps.12957

196. Brownstein DJ, Salagre E, Köhler C, Stubbs B, Vian J, Pereira C, et al. Blockade of the angiotensin system improves mental health domain of quality of life: A meta-analysis of randomized clinical trials. *Aust N Z J Psychiatry* (2018) 52 (1):24–38. doi: 10.1177/0004867417721654

197. Nasr SJ, Crayton JW, Agarwal B, Wendt B, Kora R. Lower frequency of antidepressant use in patients on renin-Angiotensin-Aldosterone system modifying medications. *Cell Mol Neurobiol* (2011) 31(4):615–8. doi: 10.1007/s10571-011-9656-7

198. Kessing LV, Rytgaard HC, Ekstrøm CT, Torp-Pedersen C, Berk M, Gerds TA. Antihypertensive drugs and risk of depression: A nationwide population-based study. *Hypertension* (2020) 76(4):1263–79. doi: 10.1161/HYPERTENSIONAHA.120.15605

199. Boal AH, Smith DJ, McCallum L, Muir S, Touyz RM, Dominiczak AF, et al. Monotherapy with major antihypertensive drug classes and risk of hospital admissions for mood disorders. *Hypertension* (2016) 68(5):1132–8. doi: 10.1161/HYPERTENSIONAHA.116.08188

200. Braszko JJ, Karwowska-Polecka W, Halicka D, Gard PR. Captopril and enalapril improve cognition and depressed mood in hypertensive patients. *J Basic Clin Physiol Pharmacol* (2003) 14(4):323–43. doi: 10.1515/JBCPP.2003.14.4.323

201. Germain L, Chouinard G. Captopril treatment of major depression with serial measurements of blood cortisol concentrations. *Biol Psychiatry* (1989) 25 (4):489–93. doi: 10.1016/0006-3223(89)90203-5

202. Germain L, Chouinard G. Treatment of recurrent unipolar major depression with captopril. *Biol Psychiatry* (1988) 23(6):637–41. doi: 10.1016/0006-3223(88)90010-8

203. Zubenko GS, Nixon RA. Mood-elevating effect of captopril in depressed patients. *Am J Psychiatry* (1984) 141(1):110–1. doi: 10.1176/ajp.141.1.110

204. Deicken RF. Captopril treatment of depression. *Biol Psychiatry* (1986) 21 (14):1425–8. doi: 10.1016/0006-3223(86)90334-3

205. Reinecke A, Browning M, Klein Breteler J, Kappelmann N, Ressler KJ, Harmer CJ, et al. Angiotensin regulation of amygdala response to threat in high-Trait-Anxiety individuals. *Biol Psychiatry Cognit Neurosci Neuroimaging* (2018) 3 (10):826–35. doi: 10.1016/j.bpsc.2018.05.007

206. Shad MU. Is there an association between anxiety symptoms and valsartan treatment? *J Affect Disord* (2020) 261:111–2. doi: 10.1016/j.jad.2019.10.004

207. Khoury NM, Marvar PJ, Gillespie CF, Wingo A, Schwartz A, Bradley B, et al. The renin-angiotensin pathway in posttraumatic stress disorder: angiotensin-converting enzyme inhibitors and angiotensin receptor blockers are associated with fewer traumatic stress symptoms. *J Clin Psychiatry* (2012) 73(6):849–55. doi: 10.4088/JCP.11m07316

208. Cohen BM, Zubenko GS. Captopril in the treatment of recurrent major depression. *J Clin Psychopharmacol* (1988) 8(2):143–4. doi: 10.1097/00004714-198804000-00018

209. Hertzman M, Adler LW, Arling B, Kern M. Lisinopril may augment antidepressant response. *J Clin Psychopharmacol* (2005) 25(6):618–20. doi: 10.1097/01.jcp.0000186736.99523.1d

210. Breckenridge A. Angiotensin converting enzyme inhibitors and quality of life. *Am J Hypertens* (1991) 4(1 Pt 2):79S–82S. doi: 10.1093/ajh/4.1.79S

211. Hill JF, Bulpitt CJ, Fletcher AE. Angiotensin converting enzyme inhibitors and quality of life: the European trial. *J Hypertens Suppl* (1985) 3(2):S91–94.

212. Edmonds D, Vetter H, Vetter W. Angiotensin converting enzyme inhibitors in the clinic: quality of life. *J Hypertens Suppl* (1987) 5(3):S31–35. doi: 10.1097/00004872-198708003-00007

213. Laudisio A, Giovannini S, Finamore P, Gemma A, Bernabei R, Incalzi RA, et al. Use of ACE-inhibitors and quality of life in an older population. *J Nutr Health Aging* (2018) 22(10):1162–6. doi: 10.1007/s12603-018-1135-0

214. Rathmann W, Haastert B, Roseman JM, Giani G. Cardiovascular drug prescriptions and risk of depression in diabetic patients. *J Clin Epidemiol* (1999) 52 (11):1103–9. doi: 10.1016/S0895-4356(99)00082-7

215. Vian J, Pereira C, Chavarria V, Köhler C, Stubbs B, Quevedo J, et al. The renin-angiotensin system: a possible new target for depression. *BMC Med* (2017) 15(1):144. doi: 10.1186/s12916-017-0916-3

216. Cao YY, Xiang X, Song J, Tian YH, Wang MY, Wang XW, et al. Distinct effects of antihypertensives on depression in the real-world setting: A retrospective cohort study. *J Affect Disord* (2019) 259:386–91. doi: 10.1016/j.jad.2019.08.075

217. Colbourne L, Luciano S, Harrison PJ. Onset and recurrence of psychiatric disorders associated with anti-hypertensive drug classes. *Transl Psychiatry* (2021) 11(1):319. doi: 10.1038/s41398-021-01444-1

218. Callender JS, Hodsman GP, Hutcheson MJ, Lever AF, Robertson JI. Mood changes during captopril therapy for hypertension. a double-blind pilot study. *Hypertension* (1983) 5(5 Pt 2):III90–93. doi: 10.1161/01.hyp.5.5_pt_2.iii90

219. Mamdani M, Gomes T, Greaves S, Manji S, Juurlink DN, Tadrous M, et al. Association between angiotensin-converting enzyme inhibitors, angiotensin receptor blockers, and suicide. *JAMA Netw Open* (2019) 2(10):e1913304. doi: 10.1001/jamanetworkopen.2019.13304

220. Lin SY, Lin CL, Lin CC, Hsu WH, Lin CD, Wang IK, et al. Association between angiotensin receptor blockers and suicide: nationwide population-based propensity score matching study. *J Affect Disord* (2020) 276:815–21. doi: 10.1016/j.jad.2020.07.106

221. Vasile S, Hallberg A, Sallander J, Hallberg M, Åqvist J, Gutiérrez-de-Terán H. Evolution of angiotensin peptides and peptidomimetics as angiotensin II receptor type 2 (AT2) receptor agonists. *Biomolecules* (2020) 10(4):649. doi: 10.3390/biom10040649

222. Tamargo M, Tamargo J. Future drug discovery in renin-angiotensin-aldosterone system intervention. *Expert Opin Drug Discov* (2017) 12(8):827–48. doi: 10.1080/17460441.2017.1335301

frontiers | Frontiers in Immunology

TYPE Original Research
PUBLISHED 27 January 2023
DOI 10.3389/fimmu.2023.1089809

OPEN ACCESS

EDITED BY
Uzma Saqib,
Indian Institute of Technology Indore, India

REVIEWED BY
Koji Yasutomo,
Tokushima University, Japan
Jing-hua Wang,
Daejeon University, Republic of Korea

*CORRESPONDENCE
Xiao-peng Ma
pengpengma@163.com
Huan-gan Wu
wuhuangan@126.com

†These authors have contributed equally to this work

SPECIALTY SECTION
This article was submitted to Inflammation, a section of the journal Frontiers in Immunology

RECEIVED 04 November 2022
ACCEPTED 16 January 2023
PUBLISHED 27 January 2023

CITATION
Wang X-j, Zhang D, Yang Y-t, Li X-y, Li H-n, Zhang X-p, Long J-y, Lu Y-q, Liu L, Yang G, Liu J, Hong J, Wu H-g and Ma X-p (2023) Suppression of microRNA-222-3p ameliorates ulcerative colitis and colitis-associated colorectal cancer to protect against oxidative stress *via* targeting BRG1 to activate Nrf2/HO-1 signaling pathway. *Front. Immunol.* 14:1089809. doi: 10.3389/fimmu.2023.1089809

Suppression of microRNA-222-3p ameliorates ulcerative colitis and colitis-associated colorectal cancer to protect against oxidative stress *via* targeting BRG1 to activate Nrf2/HO-1 signaling pathway

Xue-jun Wang[1,2†], Dan Zhang[3†], Yan-ting Yang[1†], Xiao-ying Li[1], Hong-na Li[1], Xiao-peng Zhang[1], Jun-yi Long[1], Yun-qiong Lu[1], Li Liu[1], Guang Yang[3], Jie Liu[3], Jue Hong[3], Huan-gan Wu[1,3*] and Xiao-peng Ma[1,3*]

[1]Yueyang Hospital of Integrated Traditional Chinese and Western Medicine, Shanghai University of Traditional Chinese Medicine, Shanghai, China, [2]Eye Institute and Department of Ophthalmology, Eye & ENT Hospital, Fudan University, Shanghai, China, [3]Shanghai Research Institute of Acupuncture and Meridian, Shanghai University of Traditional Chinese Medicine, Shanghai, China

Oxidative stress is an important pathogenic factor in ulcerative colitis (UC) and colitis-associated colorectal cancer (CAC), further impairing the entire colon. Intestinal epithelial cells (IECs) are crucial components of innate immunity and play an important role in maintaining intestinal barrier function. Recent studies have indicated that microRNA-222-3p (miR-222-3p) is increased in colon of UC and colorectal cancer (CRC) patients, and miR-222-3p is a crucial regulator of oxidative stress. However, whether miR-222-3p influences IEC oxidative stress in UC and CAC remains unknown. This study investigated the effect of miR-222-3p on the regulation of IEC oxidative stress in UC and CAC. An *in vitro* inflammation model was established in NCM460 colonic cells, mouse UC and CAC models were established *in vivo*, and IECs were isolated. The biological role and mechanism of miR-222-3p-mediated oxidative stress in UC and CAC were determined. We demonstrated that miR-222-3p expression was notably increased in dextran sulfate sodium (DSS)-induced NCM460 cells and IECs from UC and CAC mice. *In vitro*, these results showed that the downregulation of miR-222-3p reduced oxidative stress, caspase-3 activity, IL-1β and TNF-α in DSS-induced NCM460 cells. We further identified BRG1 as the target gene of miR-222-3p, and downregulating miR-222-3p alleviated DSS-induced oxidative injury *via* promoting BRG1-mediated activation Nrf2/HO-1 signaling in NCM460 cells. The *in vivo* results demonstrated that inhibiting miR-222-3p in IECs significantly relieved oxidative stress and inflammation in the damaged colons of UC and CAC mice, as evidenced by decreases in ROS, MDA, IL-1β and TNF-α levels and increases in GSH-Px levels. Our study further demonstrated that inhibiting miR-

222-3p in IECs attenuated oxidative damage by targeting BRG1 to activate the Nrf2/HO-1 signaling. In summary, inhibiting miR-222-3p in IECs attenuates oxidative stress by targeting BRG1 to activate the Nrf2/HO-1 signaling, thereby reducing colonic inflammation and tumorigenesis.

KEYWORDS

ulcerative colitis (UC), colitis-associated colorectal cancer (CAC), oxidative stress, miR-222-3p, BRG1/Nrf2/HO-1 pathway

Introduction

Ulcerative colitis (UC), a type of inflammatory bowel disease (IBD), is a chronic inflammatory disease of the colonic mucosa. The peak age of UC onset is between 30 and 40 years, which is increasing in incidence and prevalence (1, 2). UC patients have significantly increased risks of developing colorectal cancer (CRC) in the long term, and chronic inflammation is a driver of tumor progression (3, 4). Studies have shown that the deficiency of intestinal epithelial cells (IECs) homeostasis maintenance can lead to chronic inflammation and inflammatory cancer transformation (5–8).

Oxidative stress has long been recognized as one of the main pathogenic factors of UC and colitis-associated colorectal cancer (CAC) (9). Under normal conditions, reactive oxygen species (ROS) in intestinal tissue have bactericidal effects and participate in intestinal defense. However, excessive ROS production exceeds the buffering capacity of the host's antioxidant defense, and the resulting oxidative stress can lead to lipid peroxidation, inflammatory responses, and intestinal mucosal barrier damage (9, 10). ROS generated by chronic inflammatory infiltration are thought to contribute to the generation of dysplastic lesions. Excessive ROS production can lead to DNA damage, which can become oncogenic (11, 12).

MicroRNAs (miRNAs, miRs) are noncoding single-stranded small RNAs approximately 17-25 nucleotides in length that are critical regulators of gene expression (13). MiRNAs can bind to the 3' untranslated region (3'-UTR) of mRNAs, resulting in translational inhibition or the degradation of target mRNAs (14). MiRNAs have been shown to play critical roles in managing molecular and cellular processes in cancer and inflammation (15, 16). Among miRNAs, microRNA-222-3p (miR-222-3p) is a major regulator of oxidative stress and inhibiting the expression of miR-222-3p can significantly reduce the development of oxidative stress (17, 18). Recently, there is evidence suggesting an increased in the miR-222-3p expression in the colonic mucosal tissues of UC patients and in the colorectal tissues of CRC patients (19, 20). However, whether miR-222-3p plays a role in regulating oxidative stress in the colon in UC and CAC has not been investigated.

Brahma-related gene 1 (BRG1; SMARCA4) is an ATPase subunit of the SWI/SNF chromatin remodeling complex, which changes the structure of chromatin by hydrolyzing the energy released by ATP (21, 22). Studies have shown that BRG1 is crucial to maintain the homeostasis of IECs to prevent colitis and tumorigenesis, and the expression of BRG1 in the IECs of UC patients is significantly reduced (12). BRG1 deletion led to excess ROS levels in mice, resulting in defective colonic barrier integrity, and the oxidative stress generated by ROS showed that the mice were highly susceptible to colitis and CAC (12, 23). Studies have shown that BRG1 is a potential target gene of miR-222-3p, and miR-222-3p directly binds to the 3'-UTR of BRG1, thereby inhibiting the transcription and translation of BRG1 (24). By inhibiting miR-222-3p, BRG1 expression can be significantly increased (24), and BRG1 further activates the antioxidant Nrf2/HO-1 signaling to resist oxidative stress (25, 26).

Nuclear factor erythroid 2-related factor 2 (Nrf2) is an critical transcription factor associated with the cellular antioxidant response and a central regulator that maintains intracellular redox homeostasis (27). Under physiological conditions, Nrf2 exists in the cytoplasm and combines with Kelch-like ECH-associated protein 1 (Keap1) to form a complex, and Nrf2 is degraded by proteases, maintaining an inhibited state (28–30). However, after exposure to oxidative stress, Nrf2 is released from the Keap1/Nrf2 complex and translocates into the nucleus to form a dimer with the small Maf protein, associates with the antioxidant response element (ARE) and further exerts antioxidant and anti-inflammatory effects by activating the downstream antioxidant protein heme oxygenase-1 (HO-1) (31).

Therefore, we hypothesized that miR-222-3p could promote ulcerative colitis and tumorigenesis by regulating oxidative stress in IECs and that the BRG1/Nrf2/HO-1 pathway was involved in this process (Figure 1). Our study aims to explore the effect of miR-222-3p on the regulation of IECs oxidative stress in UC and CAC through the BRG1/Nrf2/HO-1 pathway.

Materials and methods

Cell culture

Human NCM460 colonic cells (INCELL, San Antonio, TX) were purchased from Ningbo Mingzhou Biotechnology Co., Ltd. (Ningbo, China) and cultured in Minimul Essential Medium (MEM, Gibco, Rockville, MD) supplemented with 10% (v/v) FBS and 1% penicillin/streptomycin (Gibco, Rockville, MD). The cells were cultured in a humidified atmosphere of 95% air and 5% CO_2 at 37°C.

Establishment of a dextran sulfate sodium-induced inflammation model in NCM460 cells

According to previous methods, NCM460 cells were placed under specific conditions (5% CO_2/95% air) at 37°C for 24 h. Afterward, NCM460 cells were exposed to 20 mg/mL dextransulfate sodium (DSS) for 12 h (32, 33).

Cell transfection

The miR-222-3p mimics, miR-222-3p inhibitor, and negative control miRNA (miR-NC) were purchased from Shanghai GenePharma (Shanghai, China) and transfected into cells using Lipofectamine 2000 (Thermo Fisher Scientific, USA) according to the manufacturer's protocols. BRG1 shRNA and negative control shRNA (NC-shRNA) were purchased from Shanghai Genechem Co., Ltd. (Shanghai, China) and transfected into cells according to the manufacturer's instructions.

Cell counting kit-8 assay

NCM460 cell viability was assessed using a Cell Counting Kit-8 (CCK-8) assay from KeyGen BioTech (Nanjing, China) according to the manufacturer's instructions. Briefly, the cells were added into 96-well plates at a density of 1×10^4 cells/well and cultured for 24 h. After being transfected and treated, the cells were mixed with 10 μL/well CCK-8 reagent at 37°C for 1.5 h. NCM460 cell viability was determined by determining the absorbance at 450 nm using a microplate reader (BioTek, USA).

Luciferase reporter assay

To validate BRG1 as the target gene of miR-222-3p, a dual-luciferase reporter assay was performed. Briefly, the mutated sequences of the binding sites were designed, and the corresponding vectors were constructed by Shanghai Genechem Co., Ltd. (Shanghai, China). The reporter vector was cotransfected with miR-222-3p mimics into NCM460 cells using Lipofectamine 2000 (Thermo Fisher Scientific, USA). After 48 h, according to the manufacturer's instructions, the activity of luciferase was detected using a dual-luciferase reporter assay (Beyotime, Shanghai, China).

RNA isolation and quantitative real-time PCR

The expression levels of miR-222-3p, BRG1, Nrf2 and HO-1 mRNA were measured by qRT–PCR. In brief, total RNA was

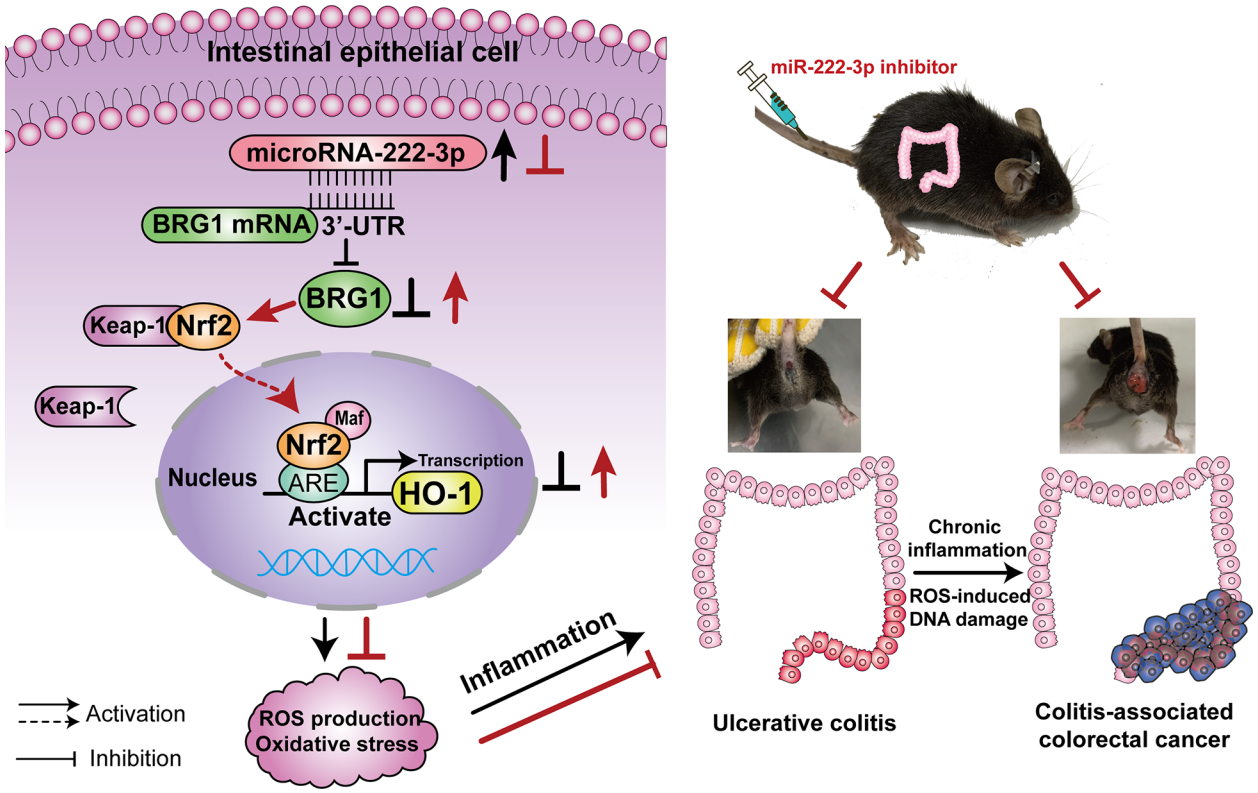

FIGURE 1
Illustration of the mechanisms of miR-222-3p in UC and CAC. MiR-222-3p directly controls oxidative stress *via* the BRG1/Nrf2/HO-1 pathway in IECs. MiR-222-3p overexpression leads to the inhibition of the BRG1/Nrf2/HO-1 pathway, which results in excessive ROS production and oxidative stress thereby compromising mucosal barrier integrity and promoting UC. Chronic inflammation combined with ROS-induced DNA damage promotes the malignant progression of CAC. UC, Ulcerative colitis; CAC, Colitis-associated colorectal cancer.

extracted from NCM460 cells and mouse IECs with TRIzol reagent (Invitrogen, Carlsbad, CA, USA). For miRNA analysis, cDNA synthesis was carried out using an EZ-press microRNA Reverse Transcription Kit (EZBioscience, USA). For mRNA analysis, total RNA was reverse transcribed using the PrimeScript RT Reagent Kit with gDNA Eraser (Takara, Japan). qRT–PCR was performed with a Roche Light Cycler 480 II using TB Green™ Premix Ex Taq™ (Tli RNaseH Plus) (Takara, Japan). The relative amounts of transcripts were calculated using the $2^{-\Delta\Delta Ct}$ formula. To normalize the data, U6 served as the internal reference for miRNAs, and GAPDH as the internal reference for mRNAs. The specific primer sequences were shown in Supplementary Table 2.

Western blot analysis

The protein expression levels of BRG1, Nu-Nrf2, HO-1, Keap-1 and caspase-3 were measured by Western blotting. Generally, total proteins were extracted from NCM460 cells and mouse IECs using RIPA buffer containing protease inhibitors (Roche, Basel, Switzerland), and nuclear proteins were extracted from cells with a nuclear protein extraction kit (Beyotime, Shanghai, China). Then, the protein concentrations were detected with a BCA protein assay kit (Beyotime, Shanghai, China). 10% SDS-PAGE was used to separate equal amount of proteins (40 μg) and transferred onto a PVDF membrane (Millipore, Boston, MA, USA) by electroblotting. The membrane was then blocked with 5% BSA and incubated with the appropriate primary antibodies, including anti-BRG1 (1:1000, Abcam, Cambridge, U.K), anti-Nrf2 (1:1000, CST, Danvers, MA, USA), anti-HO-1 (1:1000, CST, Danvers, MA, USA), anti-Keap-1 (1:1000, Abcam, Cambridge, U.K.), anti-β-actin (1:1000, Beyotime, Shanghai, China), and anti-Lamin B2 (1:1000, CST, Danvers, MA, USA) at 4°C overnight. Afterward, the membrane was incubated with secondary antibodies (1:5000; Beyotime, Shanghai, China) conjugated with peroxidase for 1 h at room temperature. The proteins were detected by an enhanced chemiluminescence (ECL) kit (Beyotime, Shanghai, China). Protein expression was analyzed using Image J software.

Dichlorofluorescein diacetate assay

ROS generation was detected using a 6-carboxy-2′,7′-dichlorodihydrofluorescein diacetate (DCFH-DA) ROS assay kit (Beyotime, Shanghai, China). For NCM460 cells were treated with DCFH-DA (10 μmol/L) and incubated for 20 min at 37°C. Afterward, NCM60 cells were observed under a fluorescence microscope, and the IOD intensity of ROS was analyzed by Image-Pro Plus. For IECs, cells were treated with DCFH-DA (10 μmol/L) and incubated for 20 min at 37°C. The fluorescence intensity in IECs was detected using a fluorescence microplate reader (488 nm excitation wavelength and 525 nm emission wavelength).

Glutathione peroxidase assay and malondialdehyde assay

According to the manufacturer's protocol, glutathione peroxidase (GSH-Px) activities of NCM460 cells and mouse IECs were determined using a total glutathione peroxidase assay kit (Beyotime, Shanghai, China), and malondialdehyde (MDA) levels of NCM460 cells and mouse IECs were measured using a lipid peroxidation MDA assay kit (Beyotime, Shanghai, China).

Caspase-3 activity assay

Apoptosis of NCM460 cells and mouse IECs were measured using a Caspase 3 Activity Assay Kit (Beyotime, Shanghai, China). Briefly, cells were lysed with cell lysis buffer, and the supernatant was collected by centrifugation. Then, 50 μL supernatant was added to 40 μL assay buffer and 10 μL caspase-3 substrate and incubated in 96-well plates (Ac-DEVD-pNA) at 37° C for 6 h. The absorbance values at 405 nm were analyzed by a microplate reader (BioTek, USA).

Enzyme-linked immunosorbent assay

The levels of IL-1β and TNF-α in the cell-free supernatants of NCM460 cells and mouse IECs were examined by enzyme-linked immunosorbent assay (ELISA) using IL-1β (Shanghai Simuwu Biotechnology Co., Ltd, Shanghai, China) and TNF-α enzyme-linked immunosorbent assay kits (Shanghai Simuwu Biotechnology Co., Ltd, Shanghai, China), respectively. Cell-free supernatants were collected, and IL-1β and TNF-α levels were measured according to the manufacturer's instructions. The absorbance at 450 nm was measured by a microplate reader (BioTek, USA).

Mice ethics

Male C57BL/6 mice (6-8 weeks old) were purchased from Shanghai SLAC Laboratory Animal Co., Ltd. (Shanghai, China; License no: SYXK (Shanghai) 2018-0040) and used for DSS-induced UC models and azoxymethane (AOM)/DSS-induced CAC mouse models. All animal experiment protocols were implemented in accordance with the International Guiding Principles for Biomedical Research Involving Animals recommended by the World Health Organization and were approved by the Ethics Committee of Yueyang Clinical Medicine School, Shanghai University of Traditional Chinese Medicine (No. YYLAC-2020-094-1, YYLAC-2020-085-1).

AAV9-GFP construction and tail vein injection

The miR-222-3p inhibitor (AAV-222-3p inhibitor) and a negative control (AAV-NC) recombinant adeno-associated virus-green fluorescence protein vector 9 (AAV9-GFP) was obtained from Shanghai Genechem Co., Ltd. (Shanghai, China). In brief, 1×10^{11} particles of AAV in 200 μL PBS were injected into the tail veins of mice. After 2 months, the colon and rectum were removed, and the fluorescence intensity of AAV9-GFP was measured with a fluorescence microscope (Supplementary Figures 1, 2).

Induction of UC and CAC

According to a previous study (12), AAVs were first injected into mice's tail veins. Two months later, the mice were first subjected to BRG1 deletion with tamoxifen (100 mg/kg body weight) (Sigma –Aldrich, USA) for 3 consecutive days, and then the UC and CAC models were induced. To induce UC, the mice were fed 3% DSS (MW, 36–50 kDa; MP Biomedicals) for 3 days, followed by regular drinking water. In the CAC experiments, mice were intraperitoneally injected with AOM (10 mg/kg body weight) (Sigma–Aldrich, USA). After 7 days, 3% DSS was offered *via* drinking water for 4 days, followed by 16 days of normal drinking water. This DSS treatment cycle was repeated three times. The following day, the mice were sacrificed, and the large intestines were dissected to record the size and number of tumors. Intestinal tissues were then fixed in 4% paraformaldehyde for H&E staining.

Assessment of colonic inflammation

The disease activity index (DAI) and colon macroscopic damage indices (CMDIs) were measured to evaluate the symptoms of UC in the mice. The DAI was measured according to a previous standard scoring system (34). Mouse body weight, colon length, stool consistency, and rectal bleeding were observed. Briefly, the DAI scores were defined as follows: weight loss (0 = no loss, 1 = 5–10%, 2 = 10–15%, 3 = 15–20%, 4=>20%); rectal bleeding (0= no blood, 1 = occult blood 1+, 2 = occult blood 2+, 3 = occult blood 3+, 4 = occult blood 4+); and the appearance of diarrhea (0 = none, 2 = mild diarrhea, 4 = gross diarrhea). The mice were sacrificed, the abdominal cavity was opened, and the length and weight of the colon were recorded. Subsequently, the colon tissues were washed in ice-cold PBS to clear fecal residue. CMDIs were assessed (35). The scores are shown in Supplementary Table 1.

Isolation and culture of IECs

IECs were isolated from mice according to a previous study (12). The colons were cut into 6-8 mm pieces, rinsed three times with ice cold PBS containing 2% fetal calf serum, and incubated with digestion buffer (5% penicillin/streptomycin with 1% collagenase type I and 1% Dispase II) for 45 min at 37 °C. Then, the cells were passed through a 100 μm cell strainers (Corning, USA). After being centrifuged, the cells were plated in petri dishes overnight and cultured in epithelial cell culture medium with 1% penicillin/streptomycin and 10% Fetal bovine serum (FBS). The next day, the cells were digested with 0.25% trypsin (containing EDTA) for 2 min to remove other cells. Subsequently, the supernatant was removed, and 0.25% trypsin (containing EDTA) was added for 4 min for digestion. Finally, IECs in suspension were collected and placed in a petri dish for 24 h. The purity of the IECs was determined by immunofluorescence (IF) analysis (Supplementary Figure 3).

The isolated IECs were incubated for 24 h, after which cells were fixed with 4% paraformaldehyde, permeabilized in 0.25% Triton X-100 and incubated with 5% BSA. After being incubated with diluted antibodies against CK19 (1:100, Proteintech, USA) at 4°C overnight, the cells were exposed to secondary antibodies conjugated with the fluorophore FITC (1:500, Proteintech, USA) for 2 h in the dark at room temperature and treated with DAPI (1:1000, Beijing Solarbio Science & Technology Co., Ltd, Beijing, China) for 5 min. The cells were observed with a fluorescence microscope and photographed (Olympus Corporation, Japan).

Hematoxylin and eosin staining

Histopathological specimens of colon tissues were fixed with 4% paraformaldehyde. The samples were embedded in paraffin and sliced into 4 μm sections. The prepared paraffin sections were stained with H&E (36), sealed and observed using a microscope (Olympus Corporation, Japan).

Immunohistochemistry

Immunohistochemistry was performed to analyze the expression of BRG1 in the colon tissues according to standard protocols. The sections were heated at 60°C and deparaffinized. Then, the sections were placed in citric acid for antigen retrieval, and blocked with 5% BSA for 20 min, followed by stained with an anti-BRG1 antibody (1:200, Abcam, Cambridge, U. K) overnight at 4°C. The next day, the sections were observed with a microscope (Olympus Corporation, Japan).

Statistical analysis

SPSS 25.0 statistical software (IBM, Armonk, NY, USA) was used for statistical analyses. All data (except for the CMDIs score) in the different experimental groups are presented as the mean ± SD and were analyzed using one-way ANOVA test. The least significant difference (LSD) method was used when pairwise tests indicated that the variances of the different groups were equal, and the Games-Howell method was used when the variances were unequal. CMDIs data are expressed as the median (*P25, P75*) and were analyzed using a nonparametric test (Kruskal–Wallis). $P < 0.05$ was considered statistically significant.

Results

miR-222-3p downregulation protects NCM460 cells from DSS-induced injury

DSS has been reported to induce injury in cell and animal models of UC (33). To establish a UC model at the cellular level, a DSS-induced NCM460 cell injury model was constructed in our study. We first used the CCK-8 assay to evaluate the damage to DSS-induced NCM460 cells. As shown in Figure 2A, various concentrations of DSS decreased cell viability. In particular, 20 mg/mL DSS reduced the viability of NCM460 to less than 50%. To understand the biological function of miR-222-3p in regulating NCM460 cell injury under inflammatory conditions, we conducted miR-222-3p gain-of-function

and loss-of-function experiments. We found that miR-222-3p expression was significantly higher in cells treated with DSS (Figure 2B), and the transfection of miR-222-3p mimics further significantly promoted the expression of miR-222-3p transfection of a miR-222-3p inhibitor markedly downregulated the expression of miR-222-3p in cells compared with transfection of a negative control (Figure 2B). The results suggest that miR-222-3p is a DSS-responsive miRNA in NCM460 cells.

We then examined the effect of miR-222-3p on cell viability by CCK-8 assay. We found that DSS significantly reduced cell viability, while miR-222-3p overexpression further decreased the viability of DSS-induced NCM460 cells (Figure 2C). However, miR-222-3p downregulation significantly increased DSS-induced NCM460 cell viability (Figure 2C). Caspase-3 activity showed that miR-222-3p overexpression significantly promoted DSS-induced apoptosis, whereas miR-222-3p downregulation decreased DSS-induced apoptosis (Figure 2D). These results suggest that inhibiting miR-222-3p protects NCM460 cells from DSS-induced cell viability impairment and apoptosis.

To further explore the biological function of miR-222-3p in DSS-induced NCM460 cell injury, we measured the effect of miR-222-3p on DSS-induced oxidative stress and inflammation. We found that miR-222-3p overexpression promoted ROS and MDA generation in DSS-induced NCM460 cells (Figures 2E, F, H), while inhibiting miR-222-3p significantly reduced the production of ROS and MDA in DSS-induced cells (Figures 2E, F, H). In addition, miR-222-3p overexpression decreased the level of glutathione peroxidase (GSH-Px) in DSS-induced NCM460 cells, while miR-222-3p knockdown enhanced it (Figure 2G).

We examined inflammatory factors in DSS-treated NCM460 cell supernatants and found that IL-1β and TNF-α were increased, and miR-222-3p overexpression further upregulated IL-1β and TNF-α

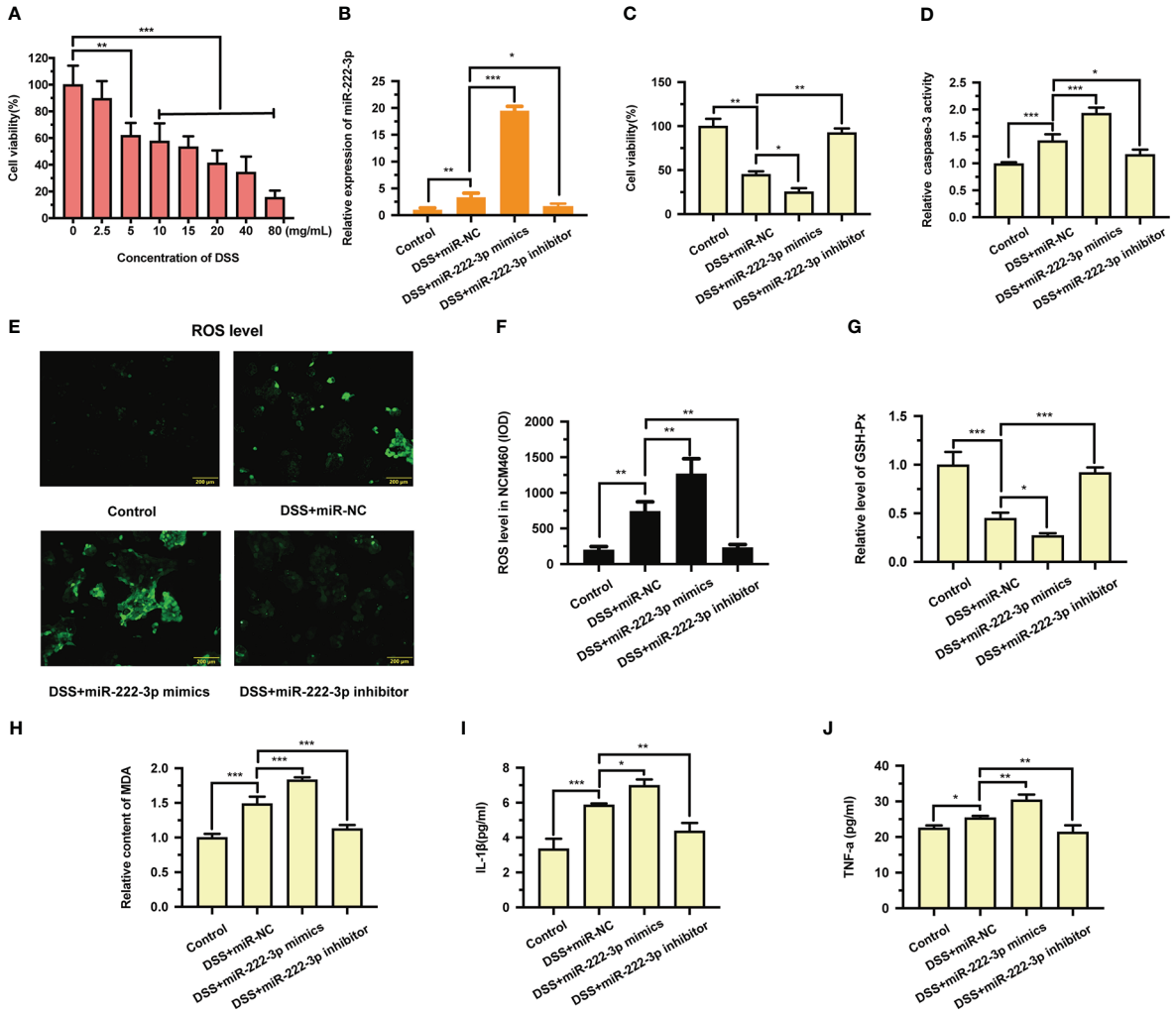

FIGURE 2
Effects of miR-222-3p on DSS-induced cell injury in the NCM460 cells. **(A)** Effect of DSS on NCM460 cell viability was detected by CCK-8 assay. **(B)** The effect of miR-222-3p mimics or inhibitor transfection on miR-222-3p expression was assessed by qRT-PCR from NCM460 cells. **(C)** Effect of miR-222-3p on NCM460 cell viability was measured using the CCK-8 assay. **(D)** Effect of miR-222-3p on NCM460 cell apoptosis was measured by caspase-3 activity assay. **(E, F)** Living cell microscopy. Effect of miR-222-3p on NCM460 cell ROS level was measured by DCFH-DA ROS assay kit. **(G, H)** Effect of miR-222-3p on the level of GSH-Px **(G)** and the content of MDA **(H)** were measured by corresponding kits from NCM460 cells. **(I, J)** Effect of miR-222-3p on the inflammatory factors, including IL-1β and TNF-α in the NCM460 cell supernatant were determined by ELISA. Data are presented as the mean ± SD (n = 3). $^{*}P < 0.05$, $^{**}P < 0.01$, $^{***}P < 0.001$. Control: control group; DSS+miR-NC: DSS+negative control miRNA group; DSS+miR-222-3p mimics: miR-222-3p mimics group; DSS +miR-222-3p inhibitor: miR-222-3p inhibitor group. Scale bar: 200 μm.

levels in DSS-induced NCM460 cell supernatants (Figures 2I, J). When DSS-induced NCM460 cells were treated with the miR-222-3p inhibitor, IL-1β and TNF-α were significantly decreased (Figures 2I, J). These results show that miR-222-3p downregulation reduced oxidative stress and inflammation in DSS-induced NCM460 cells.

BRG1 is a potential target gene of miR-222-3p

To explore the underlying mechanism of miR-222-3p regulating NCM460 cell injury under inflammatory condition, we searched for potential downstream target genes of miR-222-3p by bioinformatic analysis. Studies have shown that BRG1 is a key regulator of oxidative stress and apoptosis (12, 23) and is predicted to be a target gene of miR-222-3p (24).

The 3′-UTR of BRG1 has a conserved binding site for miR-222-3p (Figure 3A). To investigate whether miR-222-3p directly targets to the BRG1 3′-UTR, a dual luciferase assay was performed (Figure 3B). The results showed that miR-222-3p overexpression significantly inhibited the luciferase activity of the luciferase reporter vector containing the wild-type BRG1 3′-UTR (Figure 3B). However, miR-222-3p overexpression did not have any effect on the luciferase activity of the reporter vector containing the mutant BRG1 3′-UTR (Figure 3B). Therefore, we found that miR-222-3p directly bound to BRG1.

In addition, we also detected the regulatory effect of miR-222-3p on BRG1. The results showed that BRG1 expression was inhibited by miR-222-3p overexpression, while promoted by miR-222-3p inhibition (Figures 3C, D, E). Overall, these results demonstrate that miR-222-3p can directly bind to BRG1 and negatively regulate its expression.

Inhibiting miR-222-3p promotes the activation of Nrf2/HO-1 signaling

Studies have shown that BRG1 alleviates oxidative stress by activating Nrf2/HO-1 signaling (25, 26). Considering the regulation of BRG1 by miR-222-3p, we supposed that miR-222-3p could regulate the Nrf2/HO-1 signaling pathway. Our results demonstrated that miR-222-3p overexpression impaired nuclear Nrf2 protein expression and intracellular Nrf2 mRNA expression (Figures 3F-H), while miR-222-3p inhibition markedly promoted nuclear Nrf2 protein expression and intracellular Nrf2 mRNA expression (Figures 3F-H).

Moreover, miR-222-3p overexpression downregulated the mRNA (Figure 3I) and protein (Figures 3J, K) expression of HO-1 in DSS-induced NCM460 cells, whereas miR-222-3p inhibition upregulated the mRNA (Figures 3I) and protein (Figures 3J, K) expression of HO-1. These results suggest that miR-222-3p downregulation promotes the activation of Nrf2/HO-1 signaling.

Downregulation of BRG1 reverses the protective effect of miR-222-3p inhibition on DSS-induced NCM460 cell injury

To further confirm whether miR-222-3p inhibition relieves DSS-induced NCM460 cell injury by upregulating BRG1 expression, we examined the effect of BRG1 downregulation on the protection induced by miR-222-3p inhibition. We found that the transfection of BRG1 shRNA significantly abrogated the promotion of BRG1 expression induced by miR-222-3p inhibition (Figures 4A-C). Moreover, the promotion of Nrf2/HO-1 signaling by miR-222-3p inhibition was also significantly abolished by BRG1 knockdown (Figures 4D-I). As expected, the protective effect of miR-222-3p inhibition against DSS-induced NCM460 cell necrosis, apoptosis, oxidative stress and inflammation was also reversed by BRG1 knockdown (Figures 4J-Q). Overall, these results demonstrated that miR-222-3p downregulation attenuates DSS-induced NCM460 cell injury by upregulating BRG1 expression.

The miR-222-3p inhibitor relieves DSS-induced colonic injury

Considering the impact of miR-222-3p on UC, we hypothesized that the miR-222-3p inhibitor would have therapeutic potential and tested the effect of the miR-222-3p inhibitor *in vivo* using a DSS-induced UC mouse model. Recombinant adeno-associated virus (AAV) vector-mediated gene transfer to IECs provides a mature method of intestinal transduction (37). Based on previous studies, we selected AAV serotype 9 with high intestinal transduction efficiency (38), and transfected mice with AAV-miR-222-3p inhibitor (AAV-222-3p inhibitor) or AAV-negative control vectors (AAV-NC) through tail vein injection. To determine intestinal efficiency *in vivo*, frozen colon tissue sections were analyzed by fluorescence to measure the scatteration and expression of the AAV-222-3p inhibitor and AAV-NC in the mice. We showed that the AAV-222-3p inhibitor and AAV-NC were dramatically present in colonic epithelial cells (Supplementary Figure 1).

After successful AAV transfection, we extracted mouse IECs. To identify cells extracted from the colon as IECs, we stained the cells with immunofluorescence. The results showed that after the cells were fluorescently stained with the IEC-specific marker CK19, they showed the unique spindle shape of IECs (Supplementary Figure 2). Therefore, the extracted cells were mouse IECs. To confirm the expression of miR-222-3p, we performed qRT–PCR. Compared with that in the normal control group, the miR-222-3p expression in the UC group was significantly increased. However, the miR-222-3p expression was significantly suppressed by transfection of miR-222-3p inhibitor (Figure 5A). These results further demonstrated that the miR-222-3p inhibitor was transfected into IECs.

Mice in the UC and AAV-NC groups exhibited significant appetite and weight loss, diarrhea, mucus bloody stool and colon injury, and these mice had higher DAI scores and CMDIs than normal control mice (Figures 5B, C). The miR-222-3p inhibitor ameliorated DSS-induced colitis manifestations, DAI scores and CMDIs (Figures 5B, C). The shortening of the colon can show the severity of colon injury. Compared with that in the normal control group, there was a decrease in colon length in the UC group (Figures 5D, E). In contrast, the colons of mice in the AAV-222-3p inhibitor group were considerably longer (Figures 5D, E).

Colonic pathophysiologic structure was observed by HE staining (Figures 5F-I). Intestinal epithelial necrosis, goblet cell disorder and loss, continuous ulcers, and a large number of inflammatory cells

infiltration in the mucosa and submucosa were observed in the UC and AAV-NC groups (Figures 5G, H). Pretreatment with the miR-222-3p inhibitor significantly attenuated colonic damage. Damage to intestinal epithelial tissue, goblet cells and glands was repaired, and arrows indicate ulcer healing sites (Figure 5I). Thus, our results show that miR-222-3p is involved in colon inflammation and that a miR-222-3p inhibitor that can reach IECs can attenuate colonic immune inflammation in UC mice.

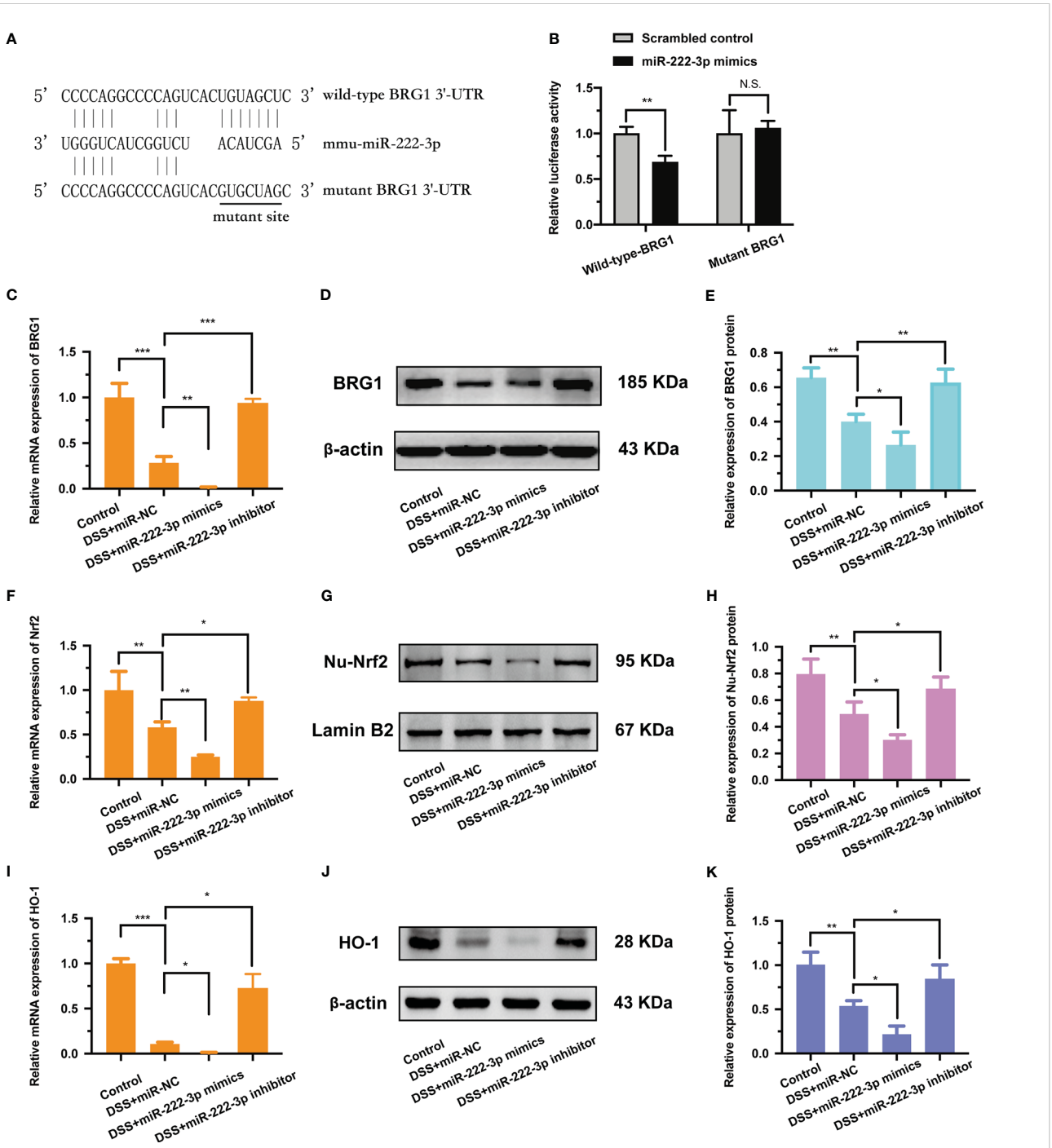

FIGURE 3
BRG1 is the potential target gene of miR-222-3p and inhibition of miR-222-3p promotes the activation of Nrf2/HO-1 signaling. **(A)** The alignment of miR-222-3p with the seed regions in BRG1 3′-UTR. **(B)** Designed wild-type or mutant sequences of BRG1 binding to miR-222-3p, and relative luciferase activity was detected by dual-luciferase reporter assay. **(C)** Relative BRG1 mRNA expression was determined by qRT-PCR from NCM460 cells. **(D, E)** Relative BRG1 protein expression was determined by Western blot from NCM460 cells. **(F)** Relative Nrf2 mRNA expression was determined by qRT-PCR from NCM460 cells. **(G, H)** Relative Nu-Nrf2 protein expression was determined by Western blot from NCM460 cells. **(I)** Relative HO-1 mRNA expression was determined by qRT-PCR from NCM460 cells. **(J, K)** Relative HO-1 protein expression was determined by Western blot from NCM460 cells. Data are presented as the mean ± SD (n = 3). $^{*}P < 0.05$, $^{**}P < 0.01$, $^{***}P < 0.001$. Control: control group; DSS+miR-NC: DSS+negative control miRNA group; DSS+miR-222-3p mimics: miR-222-3p mimics group; DSS+miR-222-3p inhibitor: miR-222-3p inhibitor group. Scale bar: 200 μm.

The miR-222-3p inhibitor activates Nrf2/HO-1 signaling pathway in UC mouse IECs by targeting BRG1

As stated previously, the miR-222-3p inhibitor significantly decreased the level of miR-222-3p compared with that in the UC group. To explore the relationship between BRG1 and miR-222-3p in IECs of UC mice, we analyzed the BRG1 expression in the colon tissues of UC mice by immunohistochemistry (Figure 5J-M). The results revealed that there was lower BRG1 staining detected in IECs in the UC group than in the normal control group, while miR-222-3p inhibitor increased positive BRG1 staining in IECs (Figures 5J-M). In addition, we further detected the mRNA and protein expression of BRG1 in IECs by qRT–PCR and Western blotting (Figures 6A-C). The results also showed that the expression of BRG1 was decreased in the UC group compared with the normal control group. However, the miR-222-3p inhibitor improved BRG1 expression compared with that in the UC group. The changes in miR-222-3p and BRG1 expression in

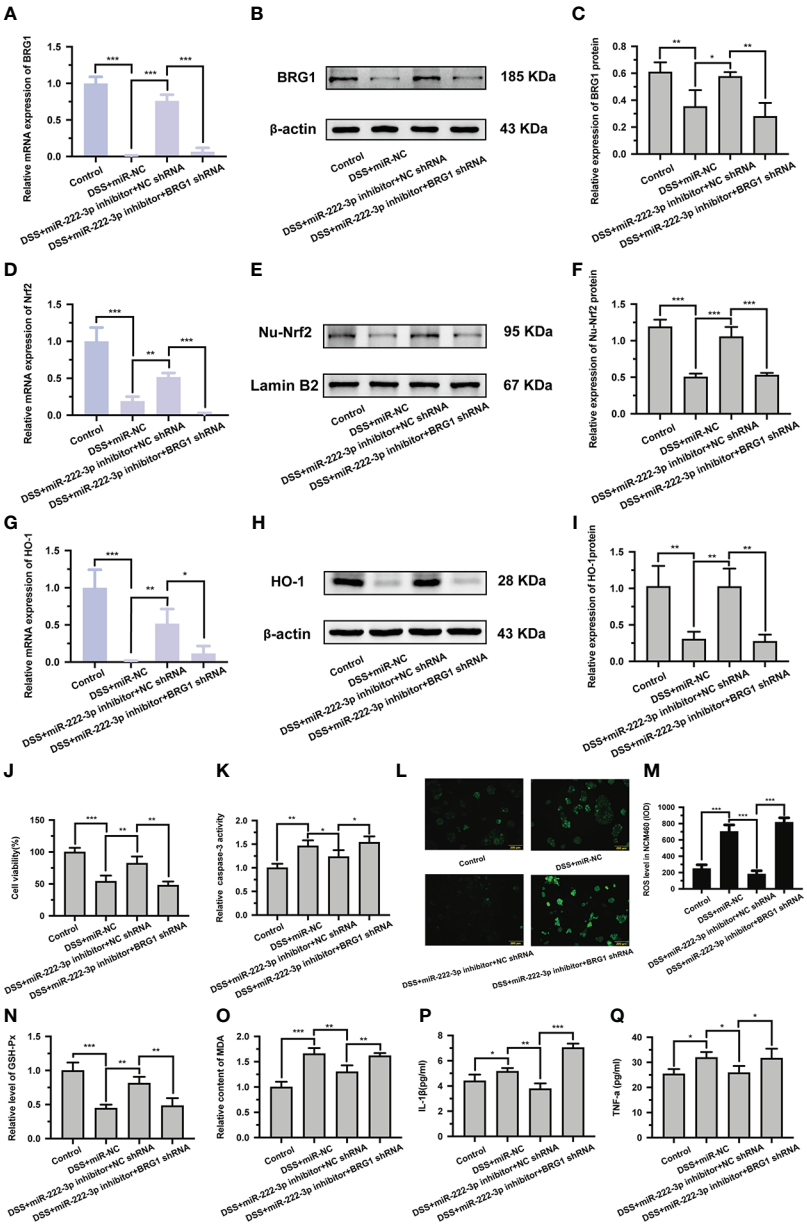

FIGURE 4
Knockdown of BRG1 reverses the protective effect of miR-222-3p inhibition in DSS-induced NCM460 cell injury. **(A)** Relative BRG1 mRNA expression was determined by qRT-PCR from NCM460 cells. **(B, C)** Relative BRG1 protein expression was determined by Western blot from NCM460 cells. **(D)** Relative Nrf2 mRNA expression was determined by qRT-PCR from NCM460 cells. **(E, F)** Relative Nu-Nrf2 protein expression was determined by Western blot from NCM460 cells. **(G)** Relative HO-1 mRNA expression was determined by qRT-PCR from NCM460 cells. **(H, I)** Relative HO-1 protein expression was determined by Western blot from NCM460 cells. **(J)** NCM460 cell viability was assessed using the CCK-8 assay. **(K)** NCM460 cell apoptosis was measured by caspase-3 activity assay. **(L, M)** Living cell microscopy. NCM460 cell ROS level was measured by DCFH-DA ROS assay kit. **(N, O)** the level of GSH-Px **(N)** and the content of MDA **(O)** were measured by corresponding kits from NCM460 cells. **(P, Q)** The inflammatory factors of IL-1β and TNF-α in the cell supernatant were determined by ELISA from NCM460 cells. Data are presented as the mean ± SD (n = 3). *$P < 0.05$, **$P < 0.01$, ***$P < 0.001$. Control: control group; DSS+miR-NC: DSS+negative control miRNA group; DSS+miR-222-3p inhibitor+NC shRNA: miR-222-3p inhibitor+ negative control shRNA group; DSS+miR-222-3p inhibitor+BRG1 shRNA: miR-222-3p inhibitor+BRG1 shRNA group. Scale bar: 200 μm.

the DSS+miR-NC group and DSS+miR-222-3p inhibitor group were consistent with the *in vitro* results. The animal results were consistent with the cell experiments. Altogether, these results indicate that the expression levels of miR-222-3p and BRG1 are negatively correlated in the IECs of DSS-induced UC mice.

Research in recent years has revealed that BRG1 protects cells from oxidative damage by activating Nrf2/HO-1 signaling (39). Therefore, we further examined the relationship between BRG1 and Nrf2/HO-1 signaling in IECs. qRT–PCR and Western blotting were used to measure the protein and mRNA levels of Nrf2, HO-1 and Keap-1 (Figures 6D-K). As expected, the results showed that the miR-222-3p inhibitor increased the level of Nrf2 nuclear translocation and HO-1 in the IECs of DSS-induced UC mice (Figures 6D-I). Moreover, Western blot analysis showed that Keap-1 expression in the IECs of DSS-induced UC mice was apparently decreased by the miR-222-3p inhibitor (Figures 6J, K). These results showed that the miR-222-3p inhibitor activated Nrf2/HO-1 signaling in DSS-induced UC mouse IECs by targeting BRG1.

The miR-222-3p inhibitor relieves oxidative stress and inflammation in IECs of UC mice

We further explored the effect of the miR-222-3p inhibitor on oxidative stress and inflammation in UC mice. As shown in Figure 6L and Supplementary Figure 3, DSS treatment induced marked apoptosis in IECs, while the miR-222-3p inhibitor significantly attenuated these changes. In addition, ROS and MDA levels in IECs were distinctly increased after DSS treatment (Figures 6M, O), while the miR-222-3p inhibitor markedly decreased ROS and MDA levels in the IECs of DSS-induced mice (Figures 6M, O). DSS treatment similarly decreased the GSH-Px level in IECs, while the miR-222-3p inhibitor reversed this change (Figure 6N). These results showed that the miR-222-3p inhibitor relieved apoptosis and oxidative stress in IECs from DSS-induced UC mice.

Then, the production of inflammatory cytokines was determined to evaluate the anti-inflammatory effects of the miR-222-3p inhibitor. As shown in Figures 6P and Q, DSS increased the levels of IL-1β and TNF-α in the supernatant of IECs, while the miR-222-3p inhibitor

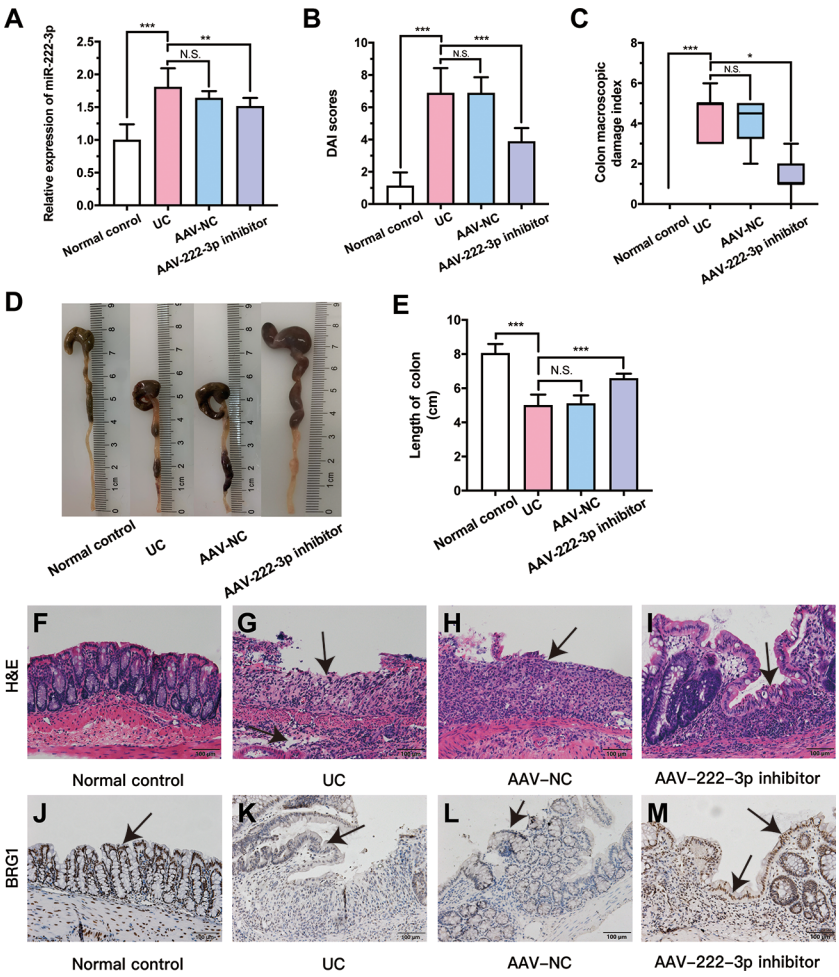

FIGURE 5
MiR-222-3p inhibitor relieves DSS-induced damage of colon. **(A)** qRT-PCR analysis of miR-222-3p in the IECs from DSS-induced mice. **(B)** DAI scores. **(C)** CMDIs. **(D)** Colon images. **(E)** Colon length. (F~I) morphological observation with hematoxylin and eosin (H&E)-stained colon sections as indicated, and arrows indicate ulcer healing sites. (J~M) Immunohistochemical analyses of BRG1 expression in colon tissues, and arrows indicate IECs locations. Data are presented as the median (*P25, P75*) (n = 8) in **(C)** and mean ± SD in **(A, B, E)** (n = 8). $^{*}P < 0.05$, $^{**}P < 0.01$, $^{***}P < 0.001$. Normal control: Normal control group; UC: UC group; AAV-NC: UC+ AAV-negative control group; AAV-222-3p inhibitor: UC+ miR-222-3p inhibitor group. N.S., no significance. Scale bar: 100 μm

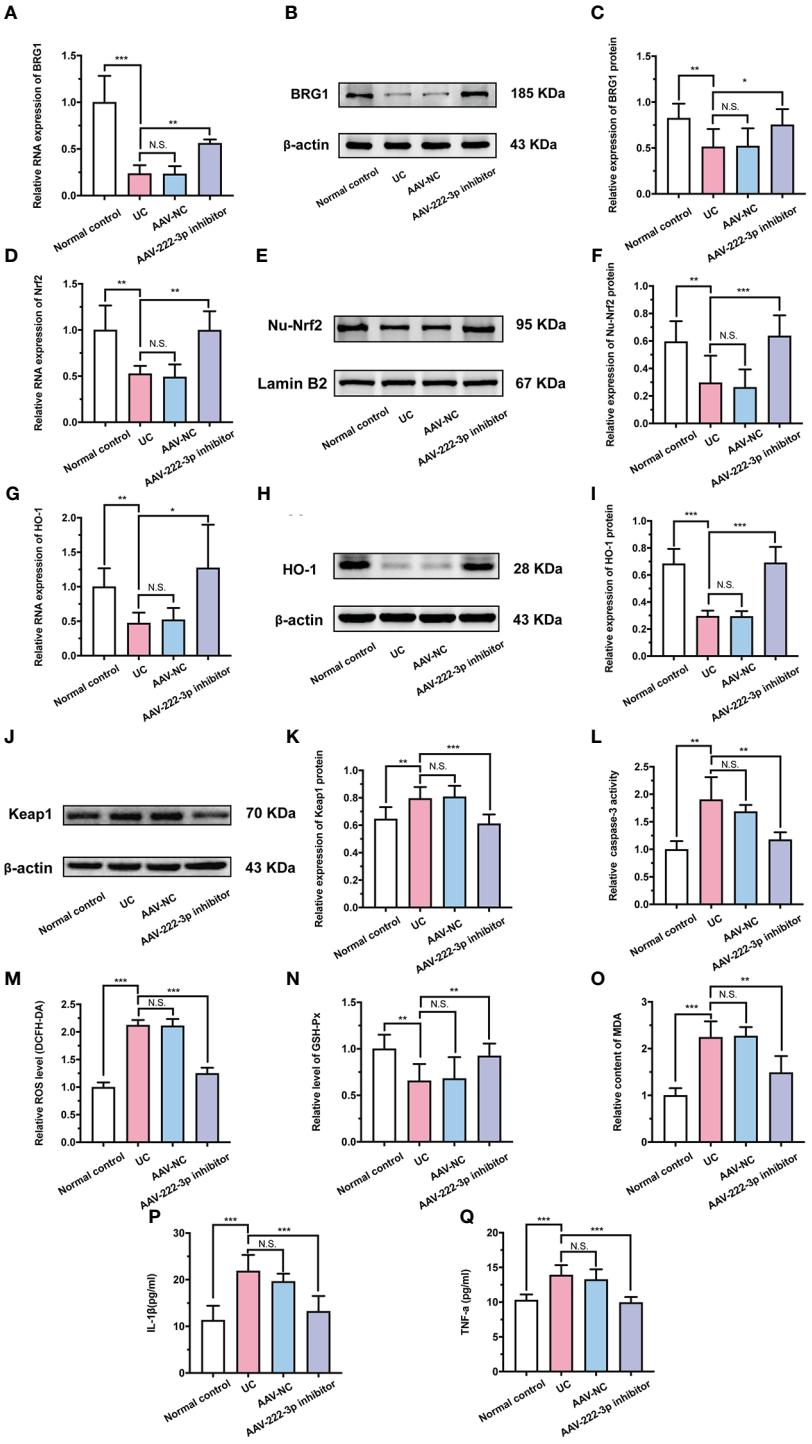

FIGURE 6
MiR-222-3p inhibitor attenuates oxidative damage by targeting BRG1 to activate Nrf2/HO-1 signaling pathway in IECs of UC mice. **(A)** Relative BRG1 mRNA expression was determined by qRT-PCR in the IECs from DSS-induced mice. **(B, C)** Relative BRG1 protein expression was determined by Western blot in the IECs from DSS-induced mice. **(D)** Relative Nrf2 mRNA expression was determined by qRT-PCR in the IECs from DSS-induced mice. **(E, F)** Relative Nu-Nrf2 protein expression was determined by Western blot in the IECs from DSS-induced mice. **(G)** Relative HO-1 mRNA expression was determined by qRT-PCR in the IECs from DSS-induced mice. **(H, I)** Relative HO-1 protein expression was determined by Western blot in the IECs from DSS-induced mice. **(J, K)** Relative Keap-1 protein expression was determined by Western blot in the IECs from DSS-induced mice. **(L)** IECs apoptosis was measured by caspase-3 activity assay from DSS-induced mice. **(M)** IECs ROS level was measured by DCFH-DA ROS assay kit from DSS-induced mice. **(N, O)** the level of GSH-Px **(N)** and the content of MDA **(O)** were measured by corresponding kits in the IECs from DSS-induced mice. **(P, Q)** IL-1β and TNF-α in the IECs supernatant were determined by ELISA from DSS-induced mice. Data are presented as the mean ± SD (n = 8). *$P < 0.05$, **$P < 0.01$, ***$P < 0.001$. Normal control: Normal control group; UC: UC group; AAV-NC: UC+ AAV-negative control group; AAV-222-3p inhibitor: UC+ miR-222-3p inhibitor group. N.S., no significance.

significantly inhibited these increases (Figures 6P, Q). These results demonstrated the efficacy of the miR-222-3p inhibitor in alleviating oxidative stress and inflammation in UC mice. In conclusion, the miR-222-3p inhibitor attenuates DSS-induced oxidative stress in IECs by targeting BRG1 to activate the Nrf2/HO-1 signaling pathway and thereby relieve inflammation.

miR-222-3p inhibition in IECs protects mice from CAC

To further determine whether miR-222-3p in IECs regulates the development of intestinal tumorigenesis, we used AOM/DSS to induce CAC in miR-222-3p inhibitor-treated mice. After successful AAV transfection (Supplementary Figure 4), we extracted mouse IECs. To confirm the expression of miR-222-3p, we performed qRT–PCR (Figure 7A). Consistent with the results in UC mice, the expression of miR-222-3p was also significantly elevated in the CAC group compared with the normal control group (Figure 7A). However, the miR-222-3p inhibitor decreased miR-222-3p expression (Figure 7A). These results further demonstrated that the miR-222-3p inhibitor was transfected into IECs.

Mice with CAC developed more and larger tumors than normal controls (Figures 7B-E). However, the numbers and volumes of macroscopically visible tumors were significantly decreased in miR-222-3p inhibitor mice compared with CAC mice (Figures 7B-E). Histologic analysis revealed that tumor cells could break through the basement membrane and grow invasively outward, and the nuclei become enlarged and hyperchromatic, reaching the level of adenocarcinoma in the CAC and AAV-NC groups (Figures 7G, H). In sharp contrast, the miR-222-3p inhibitor largely curtailed tumor development, the lesions that developed were mainly graded as mild-to-moderate dysplasia, and slightly enlarged and hyperchromatic nuclei were observed (Figure 7I). These results showed that the

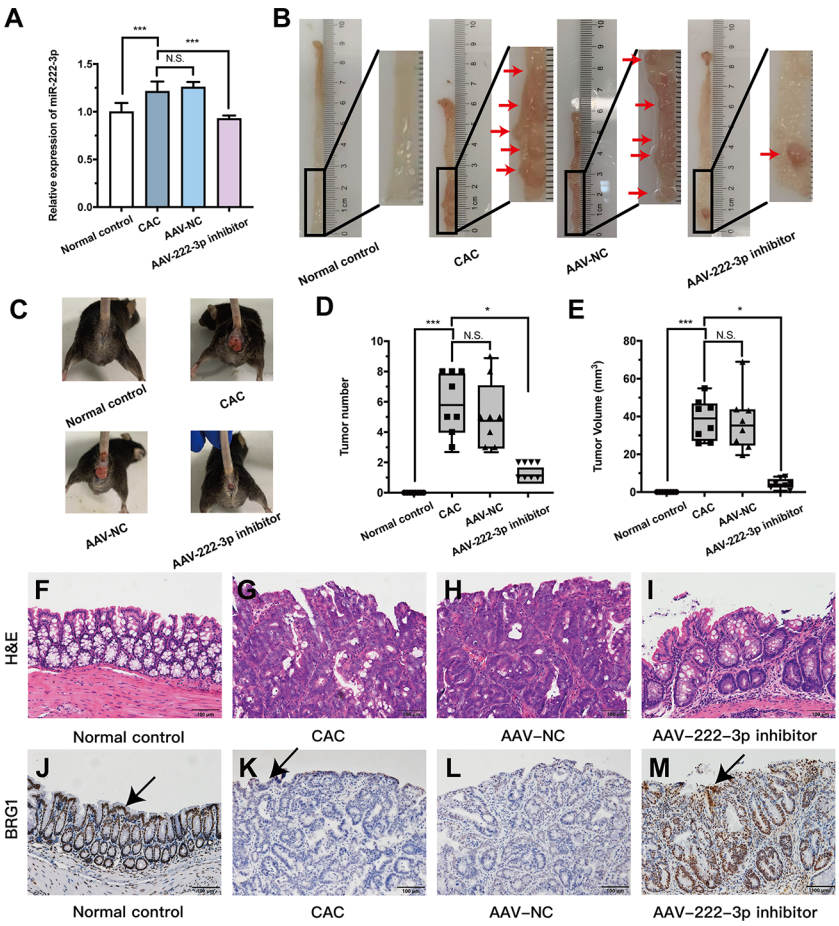

FIGURE 7
MiR-222-3p inhibitor plays CAC-suppressive roles *in vivo*. **(A)** qRT-PCR analysis of miR-222-3p in the IECs from AOM/DSS-induced mice. **(B)** Macroscopic images of tumors in the intestines of AOM/DSS-induced mice. **(C)** Images of AOM/DSS-induced mice. **(D, E)** Intestinal tumor numbers and tumor volumes were recorded. **(F–I)** morphological observation with H&E-stained colon sections as indicated. **(J–M)** Immunohistochemical analyses of BRG1 expression in colon tissues, and arrows indicate IECs locations. Data are presented as the median (*P25, P75*) (n = 8) in **(D, E)** and mean ± SD in **(A)** (n = 8). $^{*}P < 0.05$, $^{***}P < 0.001$. Normal control: Normal control group; CAC: CAC group; AAV-NC: CAC+ AAV-negative control group; AAV-222-3p inhibitor: CAC+ miR-222-3p inhibitor group. Scale bar: 100 μm. N.S., no significance.

miR-222-3p inhibitor rendered the mice resistant to AOM/DSS-induced CAC.

The miR-222-3p inhibitor protects IECs from oxidative stress by activating the BRG1/Nrf2/HO-1 pathway in CAC mice

Based on the UC results, we further explored the connection between BRG1 and miR-222-3p in AOM/DSS-induced colonic IECs. Immunohistochemistry showed that the BRG1 staining detected in IECs was also lower in AOM/DSS-induced mice than that in normal control group (Figures 7J-M). However, miR-222-3p inhibitor increased the positive BRG1 staining in IECs (Figures 7J-M). We further detected the mRNA and protein expression of BRG1. As shown in Figures 8A-C, compared to that in the normal control group, BRG1 expression was reduced in the IECs of AOM/DSS-induced mice, while miR-222-3p increased BRG1 expression. This result is consistent with the cell experiments and UC results. In conclusion, miR-222-3p can negatively regulate the expression level of BRG1 in DSS-induced or AOM/DSS-induced mouse IECs.

In addition, the results showed that the level of HO-1 and Nrf2 nuclear translocation in IECs were upregulated by miR-222-3p inhibitor treatment of AOM/DSS-induced CAC mice (Figures 8D-I). Moreover, the miR-222-3p inhibitor decreased the expression of Keap-1 (Figures 8J, K). These results showed that the miR-222-3p inhibitor activated Nrf2/HO-1 signaling in AOM/DSS-induced CAC mouse IECs by targeting BRG1.

We further explored the effect of the miR-222-3p inhibitor on oxidative stress and inflammation in AOM/DSS-induced colonic IECs. ROS and MDA levels in IECs were increased after AOM/DSS treatment (Figures 8L, N), while the miR-222-3p inhibitor markedly reversed these changes (Figures 8L, N). AOM/DSS treatment decreased GSH-Px levels in IECs, while the miR-222-3p inhibitor increased GSH-Px levels (Figure 8M). As shown in Figures 8O and P, DSS treatment increased the relative levels of IL-1β and TNF-α in the supernatants of IECs, while the miR-222-3p inhibitor significantly inhibited these changes (Figures 8O, P).

Collectively, these data indicated that the miR-222-3p inhibitor protected IECs from oxidative stress by activating the BRG1/Nrf2/HO-1 pathway in AOM/DSS-induced CAC mice, thereby inhibiting the inflammatory-cancer transition.

Discussion

Although much attention has been given to the important role of adaptive immunity in intestinal mucosal inflammation, IECs are one of the most crucial components of innate immunity and play an important role in maintaining intestinal barrier function (40–42). A compromised epithelial barrier and concomitant hyperimmune response to the gut microbiota are implicated in the pathogenesis of IBD and CAC (12, 43, 44). Studies have reported that miRNAs are key regulators of IEC barriers, regulating the growth and apoptosis of IECs and tight junctions between IECs (13, 45–47). There is evidence to indicate that miR-222-3p expression is upregulated in the colonic mucosal tissues of UC patients and in the colorectal tissues of CRC patients (19, 20). MiR-222-3p inhibits VDR and activates STAT3 signaling pathway in RAW264.7 cells by targeting SOCS1, which in turn exacerbates inflammatory responses (19). Oxidative stress has long been recognized as one of the main pathogenic factors of UC and CAC (9, 48). MiR-222-3p is an important regulator of oxidative stress (18). Under oxidative stress conditions, the expression of miR-222-3p is significantly increased, and inhibiting miR-222-3p can significantly reduce oxidative stress and improve cellular oxidative damage and apoptosis (18, 49, 50). However, whether miR-222-3p is involved in the occurrence and development of UC and CAC by regulating oxidative stress in IECs is still unknown.

In our study, we demonstrated that IEC expression of miR-222-3p was significantly increased in mice with UC and CAC. We generated DSS-induced or AOM/DSS-induced mice to establish experimental models of UC and CAC and found that miR-222-3p induced intestinal oxidative stress and inflammation, possibly by inhibiting the BRG1/Nrf2/HO-1 pathway in IECs, damaged the integrity of the intestinal barrier and induced colon tumorigenesis (Figure 1). Furthermore, we found that the downregulation of miR-222-3p relieved oxidative stress in IECs *via* targeting BRG1 to promote the Nrf2/HO-1 signaling pathway, thereby improving colitis and tumorigenesis (Figure 1).

First, *in vitro* experiments confirmed that inhibiting miR-222-3p could protect NCM460 colonic cells from DSS-induced oxidative injury (Figure 2). Cell viability and caspase-3 experiments showed that treatment with miR-222-3p inhibitor significantly alleviated DSS-induced cell death and apoptosis in NCM460 colonic cells (Figures 2C, D). We found that miR-222-3p downregulation reduced oxidative stress and inflammation in DSS-induced NCM460 cells by examining the levels of oxidative stress markers (including ROS, GSH-Px and MDA) and inflammatory factors (including IL-1β and TNF-α) in cells (Figures 2E-J). However, the TNF-α results indicated that the difference among samples is small even if there is statistical difference. It may be that the dispersion between samples is small. Therefore, we further verified whether miR-222-3p can regulate TNF-α content in UC and CAC mice *in vivo*. The results showed that the results *in vivo* were consistent with those *in vitro* (Figure 6Q) (Figure 8P).

In this study, we identified BRG1 as a target gene of miR-222-3p by dual-luciferase assays, and the 3′-UTR of BRG1 has a conserved binding site for miR-222-3p (Figures 3A, B). We further showed that miR-222-3p downregulation increased BRG1 expression and promoted the activation of antioxidant Nrf2/HO-1 signaling (Figures 3C-K). Previous studies have shown that BRG1 is an important gene that regulates cellular oxidative stress and apoptosis (51, 52), and BRG1 overexpression reverses the lncRNA-TUG1-induced decrease in cell viability and oxidative stress (53). In addition, BRG1 can activate Nrf2/HO-1 signaling, reduce ROS production and MDA levels, and increase the antioxidant enzyme Superoxide Dismutase (SOD), thereby inhibiting oxidative stress and apoptosis (39, 54), while after BRG1 knockout, the expression of Nrf2 and HO-1 significantly decreased, and ROS increased, which in turn aggravated oxidative damage (25, 39, 54, 55). Our results confirmed that miR-222-3p downregulation alleviated DSS-induced apoptosis, oxidative stress and inflammation by promoting BRG1-mediated activation of Nrf2/HO-1 signaling in NCM460 cells *in vitro* (Figure 4).

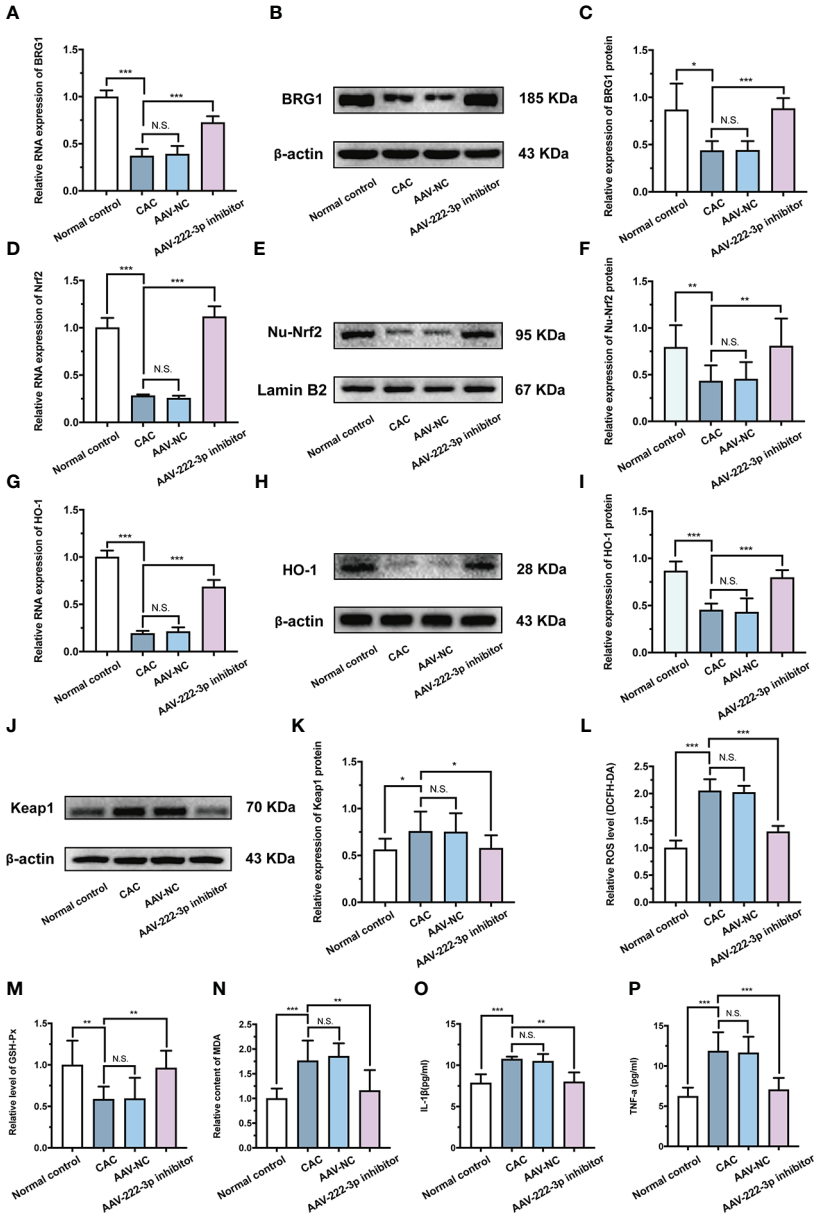

FIGURE 8
miR-222-3p inhibitor protects IECs from oxidative stress by activating the BRG1/Nrf2/HO-1 pathway in CAC mice. **(A)** Relative BRG1 mRNA expression was determined by qRT-PCR in the IECs from AOM/DSS-induced mice. **(B, C)** Relative BRG1 protein expression was determined by Western blot in the IECs from AOM/DSS-induced mice. **(D)** Relative Nrf2 mRNA expression was determined by qRT-PCR in the IECs from AOM/DSS-induced mice. **(E, F)** Relative Nu-Nrf2 protein expression was determined by Western blot in the IECs from AOM/DSS-induced mice. **(G)** Relative HO-1 mRNA expression was determined by qRT-PCR in the IECs from AOM/DSS-induced mice. **(H, I)** Relative HO-1 protein expression was determined by Western blot in the IECs from AOM/DSS-induced mice. **(J, K)** Relative Keap-1 protein expression was determined by Western blot in the IECs from AOM/DSS-induced mice. **(L)** IECs ROS level was measured by DCFH-DA ROS assay kit from AOM/DSS-induced mice. **(M, N)** the level of GSH-Px **(M)** and the content of MDA **(N)** were measured by corresponding kits in the IECs from AOM/DSS-induced mice. **(O, P)** IL-1β and TNF-α in the IECs supernatant were determined by ELISA from AOM/DSS-induced mice. Data are presented as the mean ± SD (n = 8). $^{*}P < 0.05$, $^{**}P < 0.01$, $^{***}P < 0.001$. Normal control: Normal control group; CAC: CAC group; AAV-NC: CAC+ AAV-negative control group; AAV-222-3p inhibitor: CAC+ miR-222-3p inhibitor group. N.S., no significance.

Based on these results, we further evaluated the *in vivo* protective effects of the AAV-miR-222-3p inhibitor using DSS-induced UC mice. After successful AAV-miR-222-3p inhibitor transfection, we extracted mouse IECs. We found that the level of miR-222-3p was dramatically higher in the IECs of DSS-induced UC mice (Figure 5A). However, inhibiting miR-222-3p alleviated colon shortening and decreased CMDI and DAI scores in DSS-induced UC mice (Figures 5B-E). HE staining showed that colonic damage was significantly improved after UC mice were transfected with the AAV-miR-222-3p inhibitor (Figures 5F-I). The reductions in ROS and MDA levels increased GSH-Px levels in IECs further confirmed the enhanced antioxidant effects of the miR-222-3p inhibitor (Figures 6M–O), and the miR-222-3p inhibitor markedly reduced the levels of inflammatory markers, including IL-1β and TNF-α, in the supernatants of IECs from DSS-induced UC mice (Figures 6P, Q).

Previous studies indicated that BRG1 deletion caused spontaneous colitis in mice, which was accompanied by increased GM-CSF production in intestinal ILC3s. In contrast, the

overexpression of BRG1 promoted T-bet-mediated suppression of GM-CSF in ILC3s, thereby ameliorating colitis in Rag1-/-Smarca4ΔILC3 mice (23). Another study showed that BRG1 expression was significantly reduced in the IECs of UC patients, and BRG1 deletion led to excess ROS in mouse IECs, resulting in oxidative stress and apoptosis, which made these animals highly susceptible to DSS-induced colitis (12). Our findings indicated that inhibiting miR-222-3p could activate BRG1 expression in the IECs of UC mice (Figures 5J-M) (Figures 6A-C).

The Nrf2/HO-1 signaling pathway is an important endogenous antioxidative stress pathway that plays an important role in colitis. By mediating the degradation of Keap1 in the cytoplasm, Nrf2/HO-1 signaling is activated, further significantly increasing the activities of the antioxidant enzymes SOD and GSH-Px, reducing the activities of myeloperoxidase (MPO) and MDA and caspase-3, and inhibiting the levels of the proinflammatory cytokines IL-6, TNF-α and IL-1β in colitis (56, 57). Our findings clearly revealed that the presence of the miR-222-3p inhibitor in IECs attenuated oxidative damage by targeting BRG1 to activate the Nrf2/HO-1 signaling pathway, reduced the protein expression of Keap1, and thereby relieved colonic immune inflammation in DSS-induced UC mice (Figure 6) (Supplementary Figure 3).

Previous studies have shown that miRNAs play crucial roles in the progression of IBD to CRC (58). Local miRNA expression profile in colon may be involved in the genesis and development of CRC (59). Therefore, after clarifying the pathogenic role of miR-222-3p in the development of UC, we further explored the role of miR-222-3p in CAC mice. Consistent with the increased expression of miR-222-3p in IECs with DSS-induced UC, IECs treated with the miR-222-3p inhibitor were resistant to the development of CAC mice (Figure 7), indicating that inhibiting miR-222-3p may regulate CAC development.

Our study identified BRG1 as a target gene of miR-222-3p that regulates IEC function. Inhibiting miR-222-3p can target BRG1 to activate Nrf2/HO-1 signaling in the IECs of CAC mice and reduce Keap1 protein expression (Figures 7J-M) (Figures 8A-K). BRG1 deletion leads to compensatory regeneration, as well as DNA damage induced by ROS in an inflammatory environment, which promotes the malignant progression of AOM/DSS-induced CRC (12), and Nrf2-knockout mice also exhibit increased sensitivity to CAC (60). This finding was further confirmed by the reduction in CAC in BRG1-overexpressing or Nrf2-overexpressing mice (12, 61). Therefore, previous studies and the present study have confirmed that BRG1 and Nrf2 play important roles in the prevention of inflammation-related colorectal cancer.

Further results showed that inhibiting miR-222-3p reduced the levels of ROS and MDA in IECs, increased the level of GSH-Px, and reduced the levels of the inflammatory factors IL-1β and TNF-α in the supernatants of IECs (Figures 8L-P). Previous studies also showed that in the context of oxidative damage in CAC mice, the activities of the antioxidant enzymes GSH-Px and SOD in colon tissue were significantly reduced, and ROS and MDA levels were significantly increased (9, 62). However, increasing the expression of Nrf2 and HO-1 can increase the activity of the antioxidant enzyme SOD, reduce the levels of MDA, inhibit the levels of the inflammatory markers NF-κB, TNF-α, IL-1β and MPO in CAC mice, and have a certain preventive effect on the occurrence of CAC (63, 64). Thus, our data suggest that the presence of a miR-222-3p inhibitor in IECs may protect the gut of CAC mice from oxidative damage and inflammation by targeting BRG1 to activate Nrf2/HO-1 signaling.

In summary, we found that miR-222-3p expression was significantly increased in DSS-induced NCM460 cells and IECs from UC and CAC mice. We identified BRG1 as a target gene of miR-222-3p and that miR-222-3p not only induces intestinal oxidative stress and inflammation, possibly by inhibiting the BRG1/Nrf2/HO-1 pathway in IECs and impairing epithelial integrity but also promotes colon tumorigenesis. However, inhibiting miR-222-3p in IECs attenuates oxidative stress by targeting BRG1 to activate the Nrf2/HO-1 signaling pathway, and thereby alleviating colonic inflammation and tumorigenesis. Because miR-222-3p inhibitors support intestinal inflammation and neoplastic suppression, they could potentially serve as agents for the treatment of patients with UC and CAC and may provide insights into other human diseases related to miR-222-3p.

This study has some limitations. We did not construct miR-222-3p-overexpressing mice. In future studies, we plan to construct miR-222-3p-overexpressing mice to verify whether miR-222-3p overexpression can spontaneously induce colitis and tumorigenesis through oxidative stress. In addition, miR-222-3p inhibitors are not yet in the preclinical development stage. By using miR-222-3p inhibitor, it will be interesting to see if blocking miR-222-3p can prevent/treat colitis and colon tumorigenesis. If successful, a miR-222-3p inhibitor will provide a potential agent for the treatment of patients with IBD or CAC.

Data availability statement

The original contributions presented in the study are included in the article/Supplementary Material. Further inquiries can be directed to the corresponding authors.

Ethics statement

The animal study was reviewed and approved by Ethics Committee of Yueyang Clinical Medicine School, Shanghai University of Traditional Chinese Medicine (No. YYLAC-2020-094-1, YYLAC-2020-085-1).

Author contributions

X-JW: Study design, data collection, data interpretation, manuscript preparation. DZ: Study design, manuscript preparation. Y-TY: Study design, manuscript preparation. X-YL: Data collection. H-NL: Data collection. X-PZ: Data collection. J-YL: Data collection. Y-QL: Statistical analysis. LL: Statistical analysis. GY: Data interpretation. JL: Literature search. JH: Literature search. H-GW: Study design, literature search. X-PM: Study design, data interpretation, funds collection. All authors have read and approved the manuscript. All authors contributed to the article and approved the submitted version.

Funding

This work was supported by National Natural Science Foundation of China (No. 82104985, No.81674073); Natural Science Foundation of Shanghai (No. 20ZR1453000, No. 19ZR1451600); Outstanding Leader Plan of Shanghai (No.060).

Conflict of interest

The authors declare that the research was conducted in the absence of any commercial or financial relationships that could be construed as a potential conflict of interest.

Publisher's note

Supplementary material

The Supplementary Material for this article can be found online at: https://www.frontiersin.org/articles/10.3389/fimmu.2023.1089809/full#supplementary-material

References

1. Ungaro R, Mehandru S, Allen PB, Peyrin-Biroulet L, Colombel J-F. Ulcerative colitis. *Lancet* (2017) 389:1756–770. doi: 10.1016/s0140-6736(16)32126-2

2. Segal JP, LeBlanc JF, Hart AL. Ulcerative colitis: An update. *Clin Med (Lond)* (2021) 21:135–139. doi: 10.7861/clinmed.2021-0080

3. Shah SC, Itzkowitz SH. Colorectal cancer in inflammatory bowel disease: Mechanisms and management. *Gastroenterology* (2022) 162:715–730.e713. doi: 10.1053/j.gastro.2021.10.035

4. Nadeem MS, Kumar V, Al-Abbasi FA, Kamal MA, Anwar F. Risk of colorectal cancer in inflammatory bowel diseases. *Semin Cancer Biol* (2020) 64:51–60. doi: 10.1016/j.semcancer.2019.05.001

5. Ravindran R, Loebbermann J, Nakaya HI, Khan N, Ma H, Gama L, et al. The amino acid sensor GCN2 controls gut inflammation by inhibiting inflammasome activation. *Nature* (2016) 531:523–27. doi: 10.1038/nature17186

6. Rescigno M. The intestinal epithelial barrier in the control of homeostasis and immunity. *Trends Immunol* (2011) 32:256–64. doi: 10.1016/j.it.2011.04.003

7. Takahashi N, Vereecke L, Bertrand MJ, Duprez L, Berger SB, Divert T, et al. RIPK1 ensures intestinal homeostasis by protecting the epithelium against apoptosis. *Nature* (2014) 513:95–9. doi: 10.1038/nature13706

8. Garo LP, Ajay AK, Fujiwara M, Gabriely G, Raheja R, Kuhn C, et al. MicroRNA-146a limits tumorigenic inflammation in colorectal cancer. *Nat Commun* (2021) 12:2419. doi: 10.1038/s41467-021-22641-y

9. Wang Z, Li S, Cao Y, Tian X, Zeng R, Liao DF, et al. Oxidative stress and carbonyl lesions in ulcerative colitis and associated colorectal cancer. *Oxid Med Cell Longev* (2016) 2016:9875298. doi: 10.1155/2016/9875298

10. Lambert GP. Stress-induced gastrointestinal barrier dysfunction and its inflammatory effects. *J Anim Sci* (2009) 87:E101–108. doi: 10.2527/jas.2008-1339

11. Rogler G. Chronic ulcerative colitis and colorectal cancer. *Cancer Lett* (2014) 345:235–41. doi: 10.1016/j.canlet.2013.07.032

12. Liu M, Sun T, Li N, Peng J, Fu D, Li W, et al. BRG1 attenuates colonic inflammation and tumorigenesis through autophagy-dependent oxidative stress sequestration. *Nat Commun* (2019) 10:4614. doi: 10.1038/s41467-019-12573-z

13. Zhou J, Liu J, Gao Y, Shen L, Li S, Chen S. miRNA-based potential biomarkers and new molecular insights in ulcerative colitis. *Front Pharmacol* (2021) 12:707776. doi: 10.3389/fphar.2021.707776

14. Stavast CJ, Erkeland SJ. The non-canonical aspects of MicroRNAs: Many roads to gene regulation. *Cells* (2019) 8:1465. doi: 10.3390/cells8111465

15. O'Connell RM, Rao DS, Baltimore D. microRNA regulation of inflammatory responses. *Annu Rev Immunol* (2012) 30:295–312. doi: 10.1146/annurev-immunol-020711-075013

16. Nicoloso MS, Spizzo R, Shimizu M, Rossi S, Calin GA. MicroRNAs–the micro steering wheel of tumour metastases. *Nat Rev Cancer* (2009) 9:293–302. doi: 10.1038/nrc2619

17. Liu XX, Wang MJ, Kan QN, Li C, Xiao Z, Jiang YH, et al. Kukoamine a improves mycoplasma pneumoniae pneumonia by regulating miR-222-3p/Superoxide dismutase 2. *BioMed Res Int* (2022) 2022:2064013. doi: 10.1155/2022/2064013

18. Wu C, Liu Z, Ma L, Pei C, Qin L, Gao N, et al. MiRNAs regulate oxidative stress related genes *via* binding to the 3' UTR and TATA-box regions: A new hypothesis for cataract pathogenesis. *BMC Ophthalmol* (2017) 17:142. doi: 10.1186/s12886-017-0537-9

19. Xia F, Bo W, Ding J, Yu Y, Wang J. MiR-222-3p aggravates the inflammatory response by targeting SOCS1 to activate STAT3 signaling in ulcerative colitis. *Turk J Gastroenterol* (2022) 33:934–44. doi: 10.5152/tjg.2022.21769

20. Liu S, Sun X, Wang M, Hou Y, Zhan Y, Jiang Y, et al. A microRNA 221- and 222-mediated feedback loop maintains constitutive activation of NFκB and STAT3 in colorectal cancer cells. *Gastroenterology* (2014) 147:847–859.e811. doi: 10.1053/j.gastro.2014.06.006

21. Ho L, Crabtree GR. Chromatin remodelling during development. *Nature* (2010) 463:474–84. doi: 10.1038/nature08911

22. Trotter KW, Archer TK. The BRG1 transcriptional coregulator. *Nucl Recept Signal* (2008) 6:e004. doi: 10.1621/nrs.06004

23. Qi X, Qiu J, Chang J, Ji Y, Yang Q, Cui G, et al. Brg1 restrains the pro-inflammatory properties of ILC3s and modulates intestinal immunity. *Mucosal Immunol* (2021) 14:38–52. doi: 10.1038/s41385-020-0317-3

24. Seeley JJ, Baker RG, Mohamed G, Bruns T, Hayden MS, Deshmukh SD, et al. Induction of innate immune memory *via* microRNA targeting of chromatin remodelling factors. *Nature* (2018) 559:114–9. doi: 10.1038/s41586-018-0253-5

25. Ge M, Chen H, Zhu Q, Cai J, Chen C, Yuan D, et al. Propofol post-conditioning alleviates hepatic ischaemia reperfusion injury *via* BRG1-mediated Nrf2/HO-1 transcriptional activation in human and mice. *J Cell Mol Med* (2017) 21:3693–704. doi: 10.1111/jcmm.13279

26. Wang S, Zeng X, Yang Y, Li S, Wang Y, Ye Q, et al. Hypothermic oxygenated perfusion ameliorates ischemia-reperfusion injury of fatty liver in mice *via* Brg1/Nrf2/HO-1 axis. *Artif Organs* (2022) 46:229–38. doi: 10.1111/aor.14076

27. Suzuki T, Motohashi H, Yamamoto M. Toward clinical application of the Keap1-Nrf2 pathway. *Trends Pharmacol Sci* (2013) 34:340–6. doi: 10.1016/j.tips.2013.04.005

28. Ooi BK, Goh BH, Yap WH. Oxidative stress in cardiovascular diseases: Involvement of Nrf2 antioxidant redox signaling in macrophage foam cells formation. *Int J Mol Sci* (2017) 18:2336. doi: 10.3390/ijms18112336

29. Dinkova-Kostova AT, Holtzclaw WD, Kensler TW. The role of Keap1 in cellular protective responses. *Chem Res Toxicol* (2005) 18:1779–91. doi: 10.1021/tx050217c

30. Furukawa M, Xiong Y. BTB protein Keap1 targets antioxidant transcription factor Nrf2 for ubiquitination by the cullin 3-Roc1 ligase. *Mol Cell Biol* (2005) 25:162–71. doi: 10.1128/mcb.25.1.162-171.2005

31. Loboda A, Damulewicz M, Pyza E, Jozkowicz A, Dulak J. Role of Nrf2/HO-1 system in development, oxidative stress response and diseases: An evolutionarily conserved mechanism. *Cell Mol Life Sci* (2016) 73:3221–47. doi: 10.1007/s00018-016-2223-0

32. Bhattacharyya S, Dudeja PK, Tobacman JK. ROS. Hsp27, and IKKbeta mediate dextran sodium sulfate (DSS) activation of IkappaBa, NFkappaB, and IL-8. *Inflammation Bowel Dis* (2009) 15:673–83. doi: 10.1002/ibd.20821

33. Xu LL, Liu T, Wang L, Li L, Wu YF, Li CC, et al. 3-(1H-Benzo[d]imidazol-6-yl)-5-(4-fluorophenyl)-1,2,4-oxadiazole (DDO7232), a novel potent Nrf2/ARE inducer, ameliorates DSS-induced murine colitis and protects NCM460 cells against oxidative stress *via* ERK1/2 phosphorylation. *Oxid Med Cell Longev* (2018) 2018:3271617. doi: 10.1155/2018/3271617

34. Mei Y, Wang Z, Zhang Y, Wan T, Xue J, He W, et al. FA-97, a new synthetic caffeic acid phenethyl ester derivative, ameliorates DSS-induced colitis against oxidative stress by activating Nrf2/HO-1 pathway. *Front Immunol* (2019) 10:2969. doi: 10.3389/fimmu.2019.02969

35. Wallace JL, Keenan CM, Gale D, Shoupe TS. Exacerbation of experimental colitis by nonsteroidal anti-inflammatory drugs is not related to elevated leukotriene B4 synthesis. *Gastroenterology* (1992) 102:18–27. doi: 10.1016/0016-5085(92)91779-4

36. Wang XJ, Li XY, Guo XC, Liu L, Jin YY, Lu YQ, et al. LncRNA-miRNA-mRNA network analysis reveals the potential biomarkers in crohn's disease rats treated with

herb-partitioned moxibustion. *J Inflammation Res* (2022) 15:1699–716. doi: 10.2147/jir.S351672

37. Hasbrouck NC, High KA. AAV-mediated gene transfer for the treatment of hemophilia b: Problems and prospects. *Gene Ther* (2008) 15:870–5. doi: 10.1038/gt.2008.71

38. Polyak S, Mach A, Porvasnik S, Dixon L, Conlon T, Erger KE, et al. Identification of adeno-associated viral vectors suitable for intestinal gene delivery and modulation of experimental colitis. *Am J Physiol Gastrointest Liver Physiol* (2012) 302:G296–308. doi: 10.1152/ajpgi.00562.2010

39. Sun W, Yu J, Kang Q. Upregulation of heme oxygenase-1 by Brahma-related gene 1 through Nrf2 signaling confers protective effect against high glucose-induced oxidative damage of retinal ganglion cells. *Eur J Pharmacol* (2020) 875:173038. doi: 10.1016/j.ejphar.2020.173038

40. Nalle SC, Turner JR. Intestinal barrier loss as a critical pathogenic link between inflammatory bowel disease and graft-versus-host disease. *Mucosal Immunol* (2015) 8:720–30. doi: 10.1038/mi.2015.40

41. Hooper LV. Epithelial cell contributions to intestinal immunity. *Adv Immunol* (2015) 126:129–72. doi: 10.1016/bs.ai.2014.11.003

42. Su L, Nalle SC, Shen L, Turner ES, Singh G, Breskin LA, et al. TNFR2 activates MLCK-dependent tight junction dysregulation to cause apoptosis-mediated barrier loss and experimental colitis. *Gastroenterology* (2013) 145:407–15. doi: 10.1053/j.gastro.2013.04.011

43. Luissint AC, Parkos CA, Nusrat A. Inflammation and the intestinal barrier: Leukocyte-epithelial cell interactions, cell junction remodeling, and mucosal repair. *Gastroenterology* (2016) 151:616–32. doi: 10.1053/j.gastro.2016.07.008

44. Ordás I, Eckmann L, Talamini M, Baumgart DC, Sandborn WJ. Ulcerative colitis. *Lancet* (2012) 380:1606–19. doi: 10.1016/s0140-6736(12)60150-0

45. He C, Yu T, Shi Y, Ma C, Yang W, Fang L, et al. MicroRNA 301A promotes intestinal inflammation and colitis-associated cancer development by inhibiting BTG1. *Gastroenterology* (2017) 152:1434–1448.e1415. doi: 10.1053/j.gastro.2017.01.049

46. Bian Z, Li L, Cui J, Zhang H, Liu Y, Zhang CY, et al. Role of miR-150-targeting c-myb in colonic epithelial disruption during dextran sulphate sodium-induced murine experimental colitis and human ulcerative colitis. *J Pathol* (2011) 225:544–53. doi: 10.1002/path.2907

47. Wang H, Chao K, Ng SC, Bai AH, Yu Q, Yu J, et al. Pro-inflammatory miR-223 mediates the cross-talk between the IL23 pathway and the intestinal barrier in inflammatory bowel disease. *Genome Biol* (2016) 17:58. doi: 10.1186/s13059-016-0901-8

48. Qin Z, Yuan X, Liu J, Shi Z, Cao L, Yang L, et al. Albuca bracteata polysaccharides attenuate AOM/DSS induced colon tumorigenesis *via* regulating oxidative stress, inflammation and gut microbiota in mice. *Front Pharmacol* (2022) 13:833077. doi: 10.3389/fphar.2022.833077

49. Markopoulos GS, Roupakia E, Tokamani M, Vartholomatos G, Tzavaras T, Hatziapostolou M, et al. Senescence-associated microRNAs target cell cycle regulatory genes in normal human lung fibroblasts. *Exp Gerontol* (2017) 96:110–22. doi: 10.1016/j.exger.2017.06.017

50. Xu X, Gao R, Li S, Li N, Jiang K, Sun X, et al. Circular RNA circZNF292 regulates H (2) O(2) -induced injury in human lens epithelial HLE-B3 cells depending on the regulation of the miR-222-3p/E2F3 axis. *Cell Biol Int* (2021) 45:1757–67. doi: 10.1002/cbin.11615

51. Ge M, Yao W, Yuan D, Zhou S, Chen X, Zhang Y, et al. Brg1-mediated Nrf2/HO-1 pathway activation alleviates hepatic ischemia-reperfusion injury. *Cell Death Dis* (2017) 8:e2841. doi: 10.1038/cddis.2017.236

52. Gao S, Yang Z, Shi R, Xu D, Li H, Xia Z, et al. Diabetes blocks the cardioprotective effects of sevoflurane postconditioning by impairing Nrf2/Brg1/HO-1 signaling. *Eur J Pharmacol* (2016) 779:111–21. doi: 10.1016/j.ejphar.2016.03.018

53. Ming N, Na HST, He JL, Meng QT, Xia ZY. Propofol alleviates oxidative stress *via* upregulating lncRNA-TUG1/Brg1 pathway in hypoxia/reoxygenation hepatic cells. *J Biochem* (2019) 166:415–21. doi: 10.1093/jb/mvz054

54. Li F, Liang J, Tong H, Zhu S, Tang D. Inhibition of microRNA-199a-5p ameliorates oxygen-glucose deprivation/reoxygenation-induced apoptosis and oxidative stress in HT22 neurons by targeting Brg1 to activate Nrf2/HO-1 signalling. *Clin Exp Pharmacol Physiol* (2020) 47:1020–29. doi: 10.1111/1440-1681.13265

55. Liu X, Yuan X, Liang G, Zhang S, Zhang G, Qin Y, et al. BRG1 protects the heart from acute myocardial infarction by reducing oxidative damage through the activation of the NRF2/HO1 signaling pathway. *Free Radic Biol Med* (2020) 160:820–36. doi: 10.1016/j.freeradbiomed.2020.09.012

56. Wang R, Luo Y, Lu Y, Wang D, Wang T, Pu W, et al. Maggot extracts alleviate inflammation and oxidative stress in acute experimental colitis *via* the activation of Nrf2. *Oxid Med Cell Longev* (2019) 2019:4703253. doi: 10.1155/2019/4703253

57. Khodir AE, Said E, Atif H, ElKashef HA, Salem HA. Targeting Nrf2/HO-1 signaling by crocin: Role in attenuation of AA-induced ulcerative colitis in rats. *Biomed Pharmacother* (2019) 110:389–99. doi: 10.1016/j.biopha.2018.11.133

58. Josse C, Bours V. MicroRNAs and inflammation in colorectal cancer. *Adv Exp Med Biol* (2016) 937:53–69. doi: 10.1007/978-3-319-42059-2_3

59. Ranjha R, Aggarwal S, Bopanna S, Ahuja V, Paul J. Site-specific MicroRNA expression may lead to different subtypes in ulcerative colitis. *PloS One* (2015) 10:e0142869. doi: 10.1371/journal.pone.0142869

60. Khor TO, Huang MT, Prawan A, Liu Y, Hao X, Yu S, et al. Increased susceptibility of Nrf2 knockout mice to colitis-associated colorectal cancer. *Cancer Prev Res (Phila)* (2008) 1:187–91. doi: 10.1158/1940-6207.Capr-08-0028

61. Pandurangan AK, Saadatdoust Z, Esa NM, Hamzah H, Ismail A. Dietary cocoa protects against colitis-associated cancer by activating the Nrf2/Keap1 pathway. *Biofactors* (2015) 41:1–14. doi: 10.1002/biof.1195

62. Wang J, Ding K, Wang Y, Yan T, Xu Y, Deng Z, et al. Wumei pill ameliorates AOM/DSS-induced colitis-associated colon cancer through inhibition of inflammation and oxidative stress by regulating s-adenosylhomocysteine hydrolase- (AHCY-) mediated hedgehog signaling in mice. *Oxid Med Cell Longev* (2022) 2022:4061713. doi: 10.1155/2022/4061713

63. Trivedi PP, Jena GB, Tikoo KB, Kumar V. Melatonin modulated autophagy and Nrf2 signaling pathways in mice with colitis-associated colon carcinogenesis. *Mol Carcinog* (2016) 55:255–67. doi: 10.1002/mc.22274

64. Wang X, Saud SM, Zhang X, Li W, Hua B. Protective effect of shaoyao decoction against colorectal cancer *via* the Keap1-Nrf2-ARE signaling pathway. *J Ethnopharmacol* (2019) 241:111981. doi: 10.1016/j.jep.2019.111981

frontiers | Frontiers in Immunology

TYPE Original Research
PUBLISHED 24 March 2023
DOI 10.3389/fimmu.2023.1142240

OPEN ACCESS

EDITED BY
Chit Laa Poh,
Sunway University, Malaysia

REVIEWED BY
Martin P. Alphonse,
Johns Hopkins Medicine, United States
John Cijiang He,
Icahn School of Medicine at Mount Sinai, United States

*CORRESPONDENCE
Zhihua Zheng
zhzhihua@mail.sysu.edu.cn
Hui-yao Lan
hylan@cuhk.edu.hk
Jinhong Li
lijinhong0414@hotmail.com

†These authors have contributed equally to this work

SPECIALTY SECTION
This article was submitted to Inflammation, a section of the journal Frontiers in Immunology

RECEIVED 11 January 2023
ACCEPTED 13 March 2023
PUBLISHED 24 March 2023

CITATION
Zhu E, Liu Y, Zhong M, Liu Y, Jiang X, Shu X, Li N, Guan H, Xia Y, Li J, Lan H-y and Zheng Z (2023) Targeting NK-1R attenuates renal fibrosis *via* modulating inflammatory responses and cell fate in chronic kidney disease. *Front. Immunol.* 14:1142240. doi: 10.3389/fimmu.2023.1142240

Targeting NK-1R attenuates renal fibrosis *via* modulating inflammatory responses and cell fate in chronic kidney disease

Enyi Zhu[1†], Yang Liu[1†], Ming Zhong[1†], Yu Liu[1], Xi Jiang[2], Xiaorong Shu[3], Na Li[1], Hui Guan[1], Yin Xia[4], Jinhong Li[1*], Hui-yao Lan[5,6*] and Zhihua Zheng[1*]

[1]Department of Nephrology, Center of Kidney and Urology, the Seventh Affiliated Hospital, Sun Yat-sen University, Shenzhen, China, [2]Department of Clinical Laboratory, the Seventh Affiliated Hospital, Sun Yat-sen University, Shenzhen, China, [3]Department of Cardiology, Sun Yat-sen Memorial Hospital of Sun Yat-sen University, Guangzhou, China, [4]Faculty of Medicine, School of Biomedical Sciences, The Chinese University of Hong Kong, Hong Kong, Hong Kong SAR, China, [5]Departments of Medicine & Therapeutics, Li Ka Shing Institute of Health Sciences, Lui Che Woo Institute of Innovative Medicine, The Chinese University of Hong Kong, Hong Kong, Hong Kong SAR, China, [6]Guangdong-Hong Kong Joint Laboratory for Immune and Genetic Kidney Disease, Guangdong Provincial People's Hospital and Guangdong Academy of Medical Sciences, Guangzhou, China

Background: Renal fibrosis is the final common pathway of chronic kidney disease (CKD), which is clinically irreversible and without effective therapy. Renal tubules are vulnerable to various insults, and tubular injury is involving in the initiation and evolution of renal inflammation and fibrosis. Neurokinin-1 receptor (NK-1R) functions by interacting with proinflammatory neuropeptide substance P (SP), exerting crucial roles in various neurological and non-neurological diseases. However, its roles in renal inflammation and fibrosis are still unknown.

Methods: We collected renal biopsy specimens and serum samples of individuals with or without CKD. Additionally, knockout mice lacking NK-1R expression, SP addition and NK-1R pharmacological antagonist treatment in the unilateral ureteral obstruction (UUO) model, and NK-1R-overexpressed HK-2 cells were employed.

Results: Renal SP/NK-1R and serum SP were increased in patients with CKD and mice experiencing UUO and correlated with renal fibrosis and function. SP addition enhanced UUO-induced progressive inflammatory responses and renal fibrosis, whereas genetically or pharmacologically targeting NK-1R attenuated these effects. Mechanistically, TFAP4 promoted NK-1R transcription by binding to its promoter, which was abolished by mutation of the binding site between TFAP4 and NK-1R promoter. Furthermore, SP acted through the NK-1R to activate the JNK/p38 pathways to modulate cell fate of tubular epithelial cells including growth arrest, apoptosis, and expression of profibrogenic genes.

Conclusion: Our data reveals that SP/NK-1R signaling promotes renal inflammatory responses and fibrosis, suggesting NK-1R could be a potential therapeutic target for the patients with CKD.

KEYWORDS

targeted therapy, neuropeptide, substance P, NK-1R, renal inflammation, macrophages, renal fibrosis, chronic kidney disease

Introduction

Renal fibrosis, regarded as the key pathological process leading to the chronic kidney disease (CKD), is becoming a grievous public-health concern (1, 2). Renal tubules are the dominant element of the kidney, and increasing research is focused on the causative effect of renal tubular epithelial cells (renal TECs) on the initiation and evolution of renal fibrosis (3). Upon renal injuries, TECs undergo various abnormal changes, including cell cycle arrest, apoptosis, and cellular senescence as well as partial epithelial-to-mesenchymal transition (EMT), which consequently facilitates renal fibrosis by generating proinflammatory and profibrogenic responses *via* autocrine and paracrine effects (4, 5). Accumulating evidence shows that kidney fibrogenesis involves the collaboration of multiple signaling pathways, such as transforming growth factor-β (TGF-β)/SMAD, mitogen-activated protein kinases (MAPK), nuclear factor-κB (NF-κB), and Wnt/β-catenin (6–9). Nevertheless, the fundamental mechanisms that drives renal TECs to trigger renal tubulointerstitial fibrosis remain to be determined.

Neurokinin-1 receptor (NK-1R) is encoded by the *TACR1* gene and serves as the high-affinity G protein-coupled receptor for substance P (SP), which is encoded in exon 3 of the *TAC1* gene and represents a proinflammatory neuropeptide of tachykinin family. NK-1R is widely detected in multiple cell types, including nerve cells (e.g., microglia, neurons, and astrocytes), immune cells (e.g., dendritic cells, lymphocytes, and macrophages), endothelial cells, smooth muscle cells, together with epithelial cells (10, 11). SP is also extensively distributed throughout not only in neuronal but also in non-neuronal tissues as well as in the body fluids including blood (12). SP/NK-1R axis exerts critical effects on multifarious cell activities, such as apoptosis, chemotaxis, and inflammation, and thus participates in regulating various physiological/pathological processes, including pain, emesis, neurological diseases (e.g., pruritus, epilepsy, Alzheimer's disease), cardiovascular diseases (e.g., heart failure, cardiomyopathy, and myocardial infarction), inflammatory diseases (e.g., rheumatoid arthritis, osteoarthritis, and psoriasis), and cancer (13).

NK-1R antagonists are presently being studied as analgesic, anti-emetic, and anti-inflammatory drugs, which have been approved for preventing chemotherapy-induced nausea and emesis by the U.S. Food and Drug Administration (14). Previous studies have revealed that SP/NK-1R may play a critical role in fibrotic disorders, such as myocardial fibrosis and liver fibrosis (15). During aortocaval fistula-mediated volume overload, the SP/NK-1R axis promotes adverse myocardial remodeling by activating cardiac mast cells, resulting in elevated levels of tumor necrosis factor-α (TNF-α) together with matrix metalloproteinase (MMP) activity, and later ECM remodeling (16). In cytokine-mediated liver injury, inactivation of SP/NK-1R significantly reduces inflammatory cell infiltration and liver cell apoptosis (17). Moreover, upon cholestatic liver injury, serum SP level and SP/NK-1R expression in the liver are up-regulated, leading to SP/NK-1R pathway hyperactivation, which promotes liver fibrosis by mediating cell aging in hepatic stellate cells and cholangiocytes as well as enhancing the biliary secretion of TGF-β1 (18). However, the impact of the SP/NK-1R pathway on TEC dysfunction and consequent renal fibrosis is still unclear.

The present work revealed highly increased SP/NK-1R levels within the kidneys and serum SP levels in patients with CKD and in mice experiencing unilateral ureteral obstruction (UUO), which were strongly associated with the severity of renal fibrosis and renal functional impairment. UUO-induced renal inflammation and fibrosis were ameliorated by genetic deletion of NK-1R but aggravated by SP administration. In addition, pharmacological inhibition of NK-1R also attenuated renal inflammation and fibrosis. Mechanistically, our study showed that NK-1R was a direct target of the transcription factor activating enhancer-binding protein 4 (TFAP4). TFAP4 directly bound to the NK-1R promoter to promote its transcription. Furthermore, we also elucidated that SP/NK-1R signaling promoted JNK and p38 phosphorylation in renal tubular cells, whereby it modulated cell fate of TECs, including G2/M arrest, apoptosis, and profibrogenic/proinflammatory responses to consequently accelerate renal inflammation and fibrosis. Therefore, this study demonstrates that activation of the SP/NK-1R axis in tubular cells contributes to renal inflammation and fibrosis. Targeting this pathway may be a promising strategy for renal fibrosis and CKD treatment.

Materials and methods

Reagents

Substance P (SP, GC15649; GLPBIO, CA, USA), SR140333 (GC11256; GLPBIO), SP600125 (GC15344; GLPBIO) and SB239063 (GC10054; GLPBIO) were used. PBS was used as

vehicle control for SP, and DMSO as a control for SR140333, SP600125, and SB239063.

Human samples and clinical information

Human renal biopsies from patients living with CKD (stage 3–5, n = 21), together with 6 surgically removed adjacent non-tumor kidney tissues of individuals with renal cancer as relatively normal control and human serum samples from 28 CKD patients (stage 3–5) and 20 healthy persons were collected from the Seventh Affiliated Hospital, Sun Yat-sen University, Shenzhen, China. Clinical information and laboratory examination data of indicated individuals were collected. The clinical characteristics of patients with CKD are shown in Supplementary Table S1. The baseline features between patients with CKD and control individuals are shown in Supplementary Table S2. Human samples protocols gained approval from the Institutional Research Ethics Committee at the Seventh Affiliated Hospital, Sun Yat-sen University (Approval No. KY AF/SC-07/01.0) and informed consent was obtained from all individuals.

Animals

We obtained 8–12-week-old wild-type C57BL/6J male mice from GemPharmatech Co. Ltd, Nanjing, China. NK-1R knockout ($NK\text{-}1R^{-/-}$) C57BL/6J mice were also generated by GemPharmatech using the CRISPR-Cas9 system. The left ureter was ligated to construct the UUO mouse model according to a previous description (19). Mice were euthanized 7 or 14 days after UUO surgery. Animal experimental protocols gained approval from the Institutional Research Ethics Committee at the Sun Yat-sen University (Approval No. SYSU-IACUC-2022-000226) and were carried out following the relevant guidelines and the Guide for the Care and Use of Laboratory Animals (NIH publications Nos. 80-23, revised 1996).

Histology and immunohistochemistry assay

After harvesting kidney tissues, Masson's trichrome and periodic acid-Schiff (PAS) staining were performed to assess tubular/tubulointerstitial injury and fibrosis, respectively. Immunohistochemistry analyses were carried out using antibodies against NK-1R (NB300-119, diluted 1:400; Novus Biologicals, Littleton, CO, USA), SP (DF7522, 1:200; Affinity Biosciences, Jiangsu, China), Collagen1 (14695-1-AP, 1:400; Proteintech, Wuhan, China); F4/80 (70076, 1:400; Cell Signaling Technology, Beverly, MA, USA), α-SMA (19245, 1:200; Cell Signaling Technology); MCP-1(A7277, 1:2500; ABclonal Technology, Wuhan, China), TNF-α (A11534, 1:400; ABclonal Technology), TFAP4 (12017-1-AP, 1:100; Proteintech). The fibrotic-, NK-1R-, SP-, Collagen I-, F4/80-, α-SMA-, MCP-1-, TNF-α- and TFAP4-positive areas were measured in 10 randomly chosen high-power fields per kidney section using ImageJ software, version 1.53e (National Institutes of Health, Bethesda, USA).

ELISA assay

Serum samples from both human and mice were collected for SP detection. SP level was determined with ELISA kits (Cusabio, Wuhan, China) in line with specific protocols.

TUNEL assay

The ApopTag Plus Peroxidase *In Situ* Apoptosis Detection Kit (Chemicon, Temecula, CA, USA) was adopted for TUNEL assay in detecting apoptotic cell rate in line with specific protocols. Later, fluorescence microscopy was performed to determine the apoptotic cell number in 10 randomly chosen high-power fields per kidney section.

RNA isolation and real-time quantitative PCR

This work utilized Trizol reagent (ThermoFisher Scientific, Darmstadt, Germany) to extract total RNA and reverse-transcribe it using the Quantitec Reverse Transcription Kit (Ruizhen Bio, Guangzhou, China) in line with the specific protocols. The mRNA expression levels were quantified by RT-qPCR using a SYBR Green PCR kit (Ruizhen Bio). All reactions were conducted in duplicate. The $2^{-\Delta\Delta Ct}$ approach was implemented to determine gene levels, with β-actin as a reference. Primers for β-actin, NK-1R, SP, Collagen1, a-SMA, MCP-1, TNF-α, CTGF, MMP9, and TFAP4 are described in Supplementary Table S3.

Western blotting assay

RIPA buffer (Beyotime, Shanghai, China) supplemented with protease and phosphorylase inhibitors was added to lyse both kidney tissues and HK-2 cells. Later, proteins were separated through SDS-PAGE, followed by transfer on PVDF membranes. Thereafter, 5% BSA was added to block membranes under room temperature (RT) for a 1-h period, followed by primary antibody incubation, including NK-1R (ab183713, 1:1000; Abcam, Cambridge, MA, USA), SP (DF7522, 1:1000; Affinity Biosciences); α-SMA (19245, 1:5000), phosphorylated-p38 (4511, 1:1000), p38 (8690, 1:1000), phosphorylated-ERK (4370, 1:1000), ERK (4695, 1:1000), Cell Signaling Technology; phosphorylated-JNK (ab124956, 1:1000; Abcam), JNK (ab179461, 1:1000; Abcam); TFAP4 (12017-1-AP, 1:500; Proteintech), Collagen1 (14695-1-AP, 1:1000; Proteintech), and GAPDH (60004-1-Ig, 1:20000; Proteintech) under 4°C overnight. Afterward, HRP-labeled secondary antibodies (15015, 15014, diluted 1:10000; Proteintech) were added to further incubate membranes for 1 hour at RT. Protein detection was performed

through WB Chemiluminescence Detection, with GAPDH being the endogenous reference.

Cell culture and transfection

We cultivated HK-2 cells within DMEM/f12 containing 10% fetal bovine serum (FBS), 1% penicillin/streptomycin (P/S) under 5% CO2 and 37°C conditions. By adopting ClonExpress® One Step Cloning Kit (Vazyme Biotech, Nanjing, China), overexpression plasmids pCDH-NK-1R and pCDH-TFAP4 were produced by inserting full-length NK-1R or TFAP4 in pCDH-CMV-MCS-EF1-Puro's EcoR I/BamH I sites. For producing lentiviruses, the overexpression plasmid, psPAX2 was co-transfected with pMD2.G plasmid into HEK293T cells using Lipofectamine 2000 (Invitrogen, Carlsbad, CA, USA). Then, this work collected the lentiviral supernatant and preserved it under −80°C prior to analysis. Later, lentiviral supernatant that contained polybrene (8 μg/mL) was added to infect HK-2 cells, and then screened by puromycin (2 μg/mL) for obtaining HK-2 cells stably overexpressing NK-1R or TFAP4.

Cell counting assay

We cultivated NK-1R-overexpressed HK-2 cells (5×10^4) into the 12-well plate and then subjected to treatment with 20 μM SP with or without 10 μM SR140333 for 48 hours prior to calculating cell number with Countstar (ALIT Life Sciences, Shanghai, China).

Colony formation assay

We maintained NK-1R-overexpressed HK-2 cells (5×10^2) into the six-well plate for 1 day, and then subjected to treatment with 20 μM SP with or without 10 μM SR140333 for another 8 days. Methanol was added to fix colonies, followed by 0.1% crystal violet staining as well as counting.

Flow cytometry

Apoptotic cell proportion and cell cycle distribution were evaluated by FCM. NK-1R-overexpressed HK-2 cells were incubated with the indicated treatment (20 μM SP, 10 μM SR140333, 5 μM SP600125, 2.5 μM SB239063) for 48 hours, and then evaluated by staining with Annexin V/DAPI staining using Annexin V-APC/DAPI Apoptosis Kit (Elabscience Biotechnology, Wuhan, China) or with propidium iodide (PI) by adopting Cell Cycle Analysis Kit (4A Biotech, Beijing, China). Thereafter, fluorescence-activated cell sorting (FACS) was carried out (CytoFLEX, Beckman Coulter, Miami, FL, USA).

Luciferase report assay

Luciferase activities were determined by dual-luciferase reporter assay (Promega). *Renilla* luciferase that expresses pRL-TK (Promega) served as the endogenous reference for amending heterogeneities of transfection efficiency. To explore how TFAP4 affected the activity of the NK-1R promoter, 25 ng pRL-TK and 50 ng *firefly* luciferase reporter plasmid [p-(−1.5/+0.1k), p-mutA or p-mutB] and 150 ng pCDH-CMV-MCS-EF1-Puro or pCDH-TFAP4 were co-transfected into cells for 48 hours.

ChIP assay

To confirm the interaction between proteins and target gene promoters, a ChIP assay was conducted as previously described (20) with some modifications. A 1% formaldehyde solution was added to cross-link HK-2 cells in a 10-cm dish for a 10-min period at RT and then collected by DTT solution. Subsequently, the cells were resuspended within SDS lysis buffer, followed by sonication 4°C for shearing DNA to 200–750 bp. After mixing with dilution buffer, the chromatin complexes were immunoprecipitated with 4 μg of anti-TFAP4 antibody (Proteintech) or isotype-matched rabbit control IgG (A7016; Beyotime) at 4°C overnight, followed by collection with 20 μL of Protein A/G MagBeads (Bimake) at 4°C for 2 hours. The bead-bound immunocomplexes were washed by pre-chilled IP lysis buffer, followed by elution with elution buffer and reverse crosslink of the DNA-protein. After purification of the immunoprecipitated DNA, semi-quantitative PCR and RT-qPCR were conducted by specific primers listed in Supplementary Table S3.

Data extraction and processing

The gene expression profile (GSE66494) of human CKD kidneys was obtained in Gene Expression Omnibus (GEO, http://www.ncbi.nlm.nih.gov/geo/). Moreover, the R software limma package (version 4.1.1) was applied in identifying differentially expressed genes (DEGs) of CKD compared with non-CKD kidney tissues upon the thresholds of |log2 (Fold Change, FC)| >= 1 together with false discovery rate (FDR) < 0.05. Up-regulated DEGs were later enriched by a Kyoto Encyclopedia of Genes and Genomes (KEGG) analysis based on the Database for Annotation, Visualization, and Integrated Discovery (DAVID, https://david.ncifcrf.gov/). NK-1R co-expressed genes in GSE66494 were selected with cut-off of $p < 0.05$ and r >= 0.3 using Spearman's correlation coefficient analysis. NK-1R potential transcriptional factors were predicted by ConTra v3 (http://bioit2.irc.ugent.be/contra/v3/) with a threshold of $p < 0.05$. Then, up-regulated DEGs, NK-1R co-expressed genes, and predicted NK-1R transcriptional factors were intersected.

RNA-seq analysis

We added 20 μM SP or PBS to NK-1R-overexpressed HK-2 cells for a 48-h incubation period, followed by harvesting for RNA isolation using Trizol reagent. RNA preparation, library construction, and sequencing on the platform DNBSEQ (sequencing length, PE150) were conducted by the Beijing Genomics Institute (BGI, Shenzhen, China). Clean reads were obtained by eliminating raw sequencing reads, which were then mapped to the reference genome of Homo sapiens (GCF_000001405.39_GRCh38.p13) using HISAT (21). The expression levels of genes were quantified by RSEM (22) and DEGs between groups were selected according to DESeq2 (23) under the |log2 (FC)| >= 1 and FDR < 0.05. KEGG enrichment analysis of DEGs was based on the DAVID database.

Statistics analysis

GraphPad Prism version 9.0.2 (GraphPad Software Inc., San Diego, CA, USA) was utilized for statistical analysis. Results were represented by mean ± SEM from three or more individual assays. Differences between the two groups were compared by unpaired Student's t-test. Multiple comparisons among groups were made using one-way ANOVA test followed by Bonferroni adjustment (assuming equal SDs) or Brown-Forsythe and Welch ANOVA tests followed by Dunnett T3 adjustment (assuming unequal SDs). For correlation analysis, a linear regression analysis was performed with Spearman's correlation coefficients. $p < 0.05$ stood for statistical significance.

Results

Renal SP/NK-1R and serum SP levels are elevated in patients with CKD and correlated with severe renal fibrosis and declined kidney function

To assess the expression and cellular localization of SP and NK-1R, kidney biopsies were collected from 21 patients with CKD (stage 3-5) and 6 adjacent relatively normal kidney tissues from surgically removed renal cell carcinoma (RCC) tissues were obtained as controls.

Immunohistochemistry demonstrated that both SP and NK-1R were predominantly localized to renal TECs, and their expression notably increased in CKD kidneys compared with control kidneys (Figure 1A). In addition, Masson's trichrome staining showed that CKD kidney tissues with higher SP and NK-1R expression exhibited more severe tubulointerstitial fibrosis (Figure 1B). Spearman's correlation analysis revealed that fibrotic extents in CKD kidneys were positively correlated with renal NK-1R ($r = 0.507$, $p = 0.019$) or SP ($r = 0.468$, $p = 0.033$) expression levels (Figure 1C). Based on the median NK-1R expression level in CKD kidneys, the samples were classified into low- and high-NK-1R groups. Relationships between renal NK-1R expression and the clinical characteristics of patients with CKD were shown in Supplementary Table S4. Compared to CKD patients with low NK-1R expression, CKD patients with high NK-1R expression had lower hemoglobin (Hb, $p = 0.023$) levels, decreased estimated glomerular filtration rates (eGFR, $p=0.035$), and increased serum cystatin c (Cys C, $p = 0.043$) levels (Figure 1D). Meanwhile, enzyme-linked immunosorbent assay (ELISA) revealed that serum SP levels were up-regulated in patients with CKD (Figure 1E) and were correlated to clinical features (Supplementary Table S5). Compared with CKD patients with low serum SP levels, those with high serum SP levels displayed worse renal function as indicated by elevated levels of serum creatinine (Scr, $p = 0.003$), blood urea nitrogen (BUN, $p = 0.012$), Cys C ($p = 0.0011$) and decreased eGFR ($p = 0.008$) (Figure 1F). Thus, our results suggest that renal SP and NK-1R expression are augmented and strongly correlated with renal fibrotic extent and renal functional impairment in patients with CKD.

Renal SP and NK-1R expression are upregulated in the mouse UUO kidneys

UUO is a widely used as an animal model of renal fibrosis, which exhibits renal inflammation and fibrosis similar to CKD (24). As revealed by RT-qPCR assay, SP and NK-1R mRNA levels were significantly elevated in kidneys 7 and 14 days after UUO surgery (Figure 2A), and the serum levels of SP protein increased time-dependently during the UUO injury (Figure 2B). In addition, both Western blotting and immunohistochemistry detected that compared to sham-operated kidneys, the UUO kidneys showed a marked increase in the expression of SP and NK-1R in a time-dependent manner (Figures 2C, D). Consistent with the observations in human CKD, SP and NK-1R were mainly expressed in TECs of UUO kidneys (Figure 2D). These findings indicate that tubular SP and NK-1R may be involved in regulation of renal fibrosis.

Genetic deletion of NK-1R protects UUO mice from the development of renal inflammation and fibrosis

To identify the role of the SP/NK-1R axis in renal fibrosis, NK-1R knockout ($NK\text{-}1R^{-/-}$) mice were generated (Supplementary Figure 1A) and subjected to UUO for 14 days. Compared with $NK\text{-}1R^{+/+}$ mice, $NK\text{-}1R^{-/-}$ counterparts showed alleviated renal inflammation as showed by decreases in mRNA and protein levels of proinflammatory factors monocyte chemoattractant protein-1 (MCP-1) and TNF-α (Figure 3A and Supplementary Figure 1B). Consistently, immune cell infiltration and F4/80 positive macrophage numbers were reduced in $NK\text{-}1R^{-/-}$ kidneys compared with $NK\text{-}1R^{+/+}$ kidneys as shown by PAS and F4/80 staining respectively (Figure 3C).

As inflammation is closely associated with renal fibrosis (25), we therefore examined renal fibrosis in $NK\text{-}1R^{-/-}$ mice. The mRNA and

10.3389/fimmu.2023.1142240

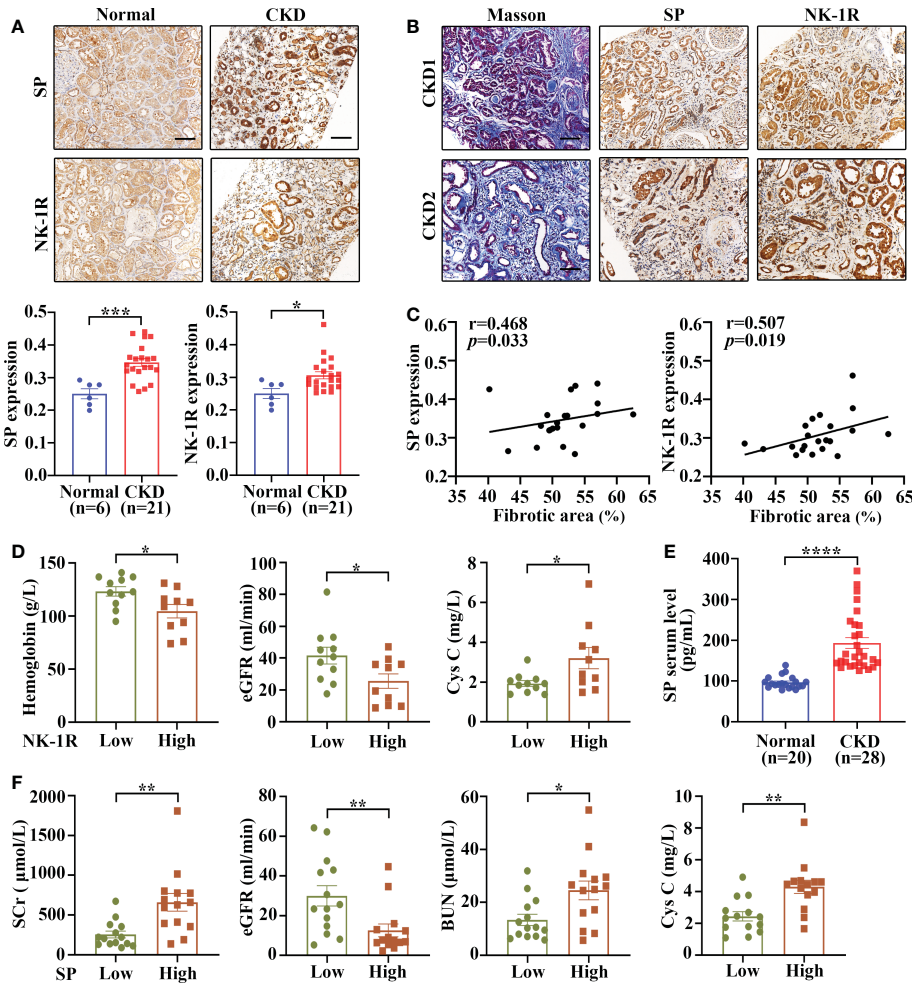

FIGURE 1
Renal SP/NK-1R and serum SP were up-regulated in patients with CKD and related to renal fibrosis and function. **(A)** The expression levels of NK-1R and SP were significantly increased in the fibrotic kidneys of patients with CKD, as assessed by immunohistochemistry staining. Representative sections (upper panels) and quantitative data (lower panels) are shown. **(B, C)** Spearman's correlation coefficient analysis showed that the expression levels of renal NK-1R and SP were positively correlated with renal fibrotic extents in 21 CKD individuals. Representative sections of immunohistochemistry staining and Masson's trichrome are exhibited in **(B)**. **(D)** Correlation between clinical characteristics and high/low renal expression of NK-1R in 21 CKD patients. The median NK-1R level was selected as the cut-off value for separating high from low NK-1R expression groups. **(E)** ELISA analysis displayed increased serum SP levels in CKD patients. **(F)** Correlation between clinical characteristics and high/low serum SP levels in 28 CKD patients. Samples were classified into high and low SP level groups using the cutoff of median SP level. Scale bar, 100 μm. Data are shown as mean ± SEM. *$p < 0.05$; **$p < 0.01$; ***$p < 0.001$; ****$p < 0.0001$.

protein levels of α-smooth muscle actin (α-SMA) and collagen I were lower in NK-1R$^{-/-}$ kidneys than in NK-1R$^{+/+}$ kidneys following UUO (Figures 3A, B and Supplementary Figure 1B). Masson's trichrome showed decreased collagen matrix deposition in NK-1R$^{-/-}$ UUO kidneys (Figure 3C). These results suggest that deletion of NK-1R attenuates UUO-induced fibrosis.

PAS showed that deletion of NK-1R effectively lessened UUO-induced tubule injury (Figure 3C). Renal cell apoptosis has been implicated in the progression of renal fibrosis. Interestingly, TUNEL positive cell numbers were increased by UUO in NK-1R$^{+/+}$ mice, which were decreased in NK-1R$^{-/-}$ mice (Figure 3C). These results suggest that deletion of NK-1R attenuates UUO-induced renal inflammation, apoptosis, and fibrosis.

Administration of SP promotes renal inflammation and fibrosis induced by UUO

It is well accepted that SP signals primarily through NK-1R. To further explore the role of the SP/NK-1R axis in kidney disease, SP, an agonist of NK-1R, was administered to mice after UUO surgery. As shown by RT-qPCR, Western blotting and immunohistochemistry, administration of SP obviously augmented the mRNA and protein levels of proinflammatory/profibrogenic factors in kidneys 14 days after UUO (Figures 4A, B and Supplementary Figure 2). Moreover, SP also significantly increased the influx of inflammatory cells, F4/80-positive macrophages, TUNEL-positive apoptotic cells and renal fibrosis (Figure 4C). These results confirm that activation of the SP/

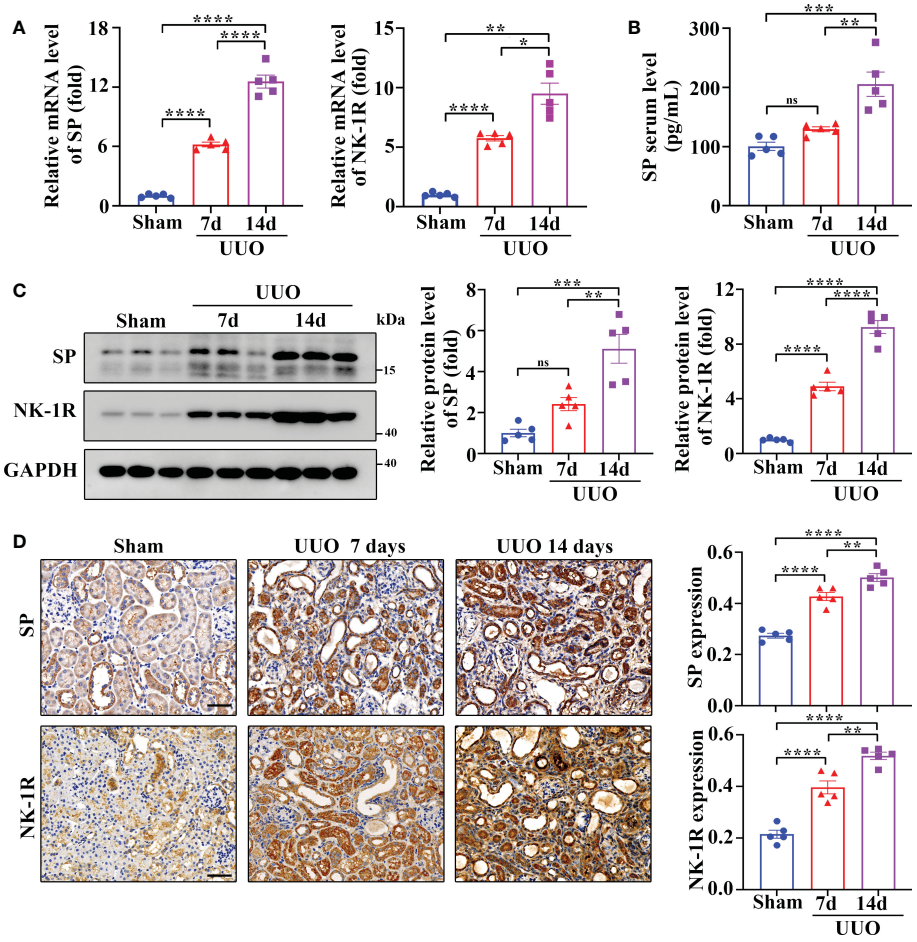

FIGURE 2
Renal SP/NK-1R and serum SP were overexpressed in a mouse unilateral ureteral obstruction (UUO) model. **(A)** RT-qPCR exhibited increased levels of SP and NK-1R mRNA in cortical lysates of kidneys on days 7 and 14 after UUO. **(B)** ELISA analysis displayed elevated serum SP levels on days 7 and 14 after UUO. **(C, D)** Western blot analysis and immunochemistry staining showed that the protein levels of renal SP and NK-1R in cortical tissues were up-regulated on days 7 and 14 after UUO. Representative images (left panels) and quantitative data (right panels) are shown. Scale bar, 50 μm. Data are shown as mean ± SEM from groups of five mice. *$p < 0.05$; **$p < 0.01$; ***$p < 0.001$; ****$p < 0.0001$; ns, not significant.

NK-1R axis amplifies renal inflammation, apoptosis, and fibrosis induced by UUO.

Treatment with a pharmacological NK-1R inhibitor attenuates renal inflammation and fibrosis induced by UUO

To examine if targeting NK-1R has a therapeutic effect on renal fibrosis, we treated UUO mice with an NK-1R-specific pharmacologic inhibitor, SR140333 (NK-1Ri). Administration of NK-1Ri significantly down-regulated expression of profibrogenic and proinflammatory factors in kidneys 14 days after UUO surgery (Figures 5A, B and Supplementary Figure 3). In addition, both histological and TUNEL analyses also detected the amelioration of tubule injury, renal inflammation, and fibrosis, as well as the reduction of apoptotic cell number, in mice treated with NK-1Ri (Figure 5C). These results unravel the promising therapeutic effects of pharmacological inhibition of NK-1R on progressive renal fibrosis.

TFAP4 is up-regulated in fibrotic kidneys and transcriptionally activates NK-1R expression

To determine the regulatory mechanism of UUO-induced NK-1R expression, we analyzed the expression array data (GSE66494) of kidney biopsies from patients with CKD (Figures 6A, B). In order to identify the potential transcriptional factors that enhance NK-1R expression, we first selected 3457 up-regulated genes (log2 FC >= 1 and FDR < 0.05). Next, we calculated the Spearman's correlation between NK-1R and other genes expression in GSE66494 and generated 2805 NK-1R coexpressed genes ($r >= 0.3$, $p < 0.05$). Last, 14 potential transcription factors were predicted by ConTra v3

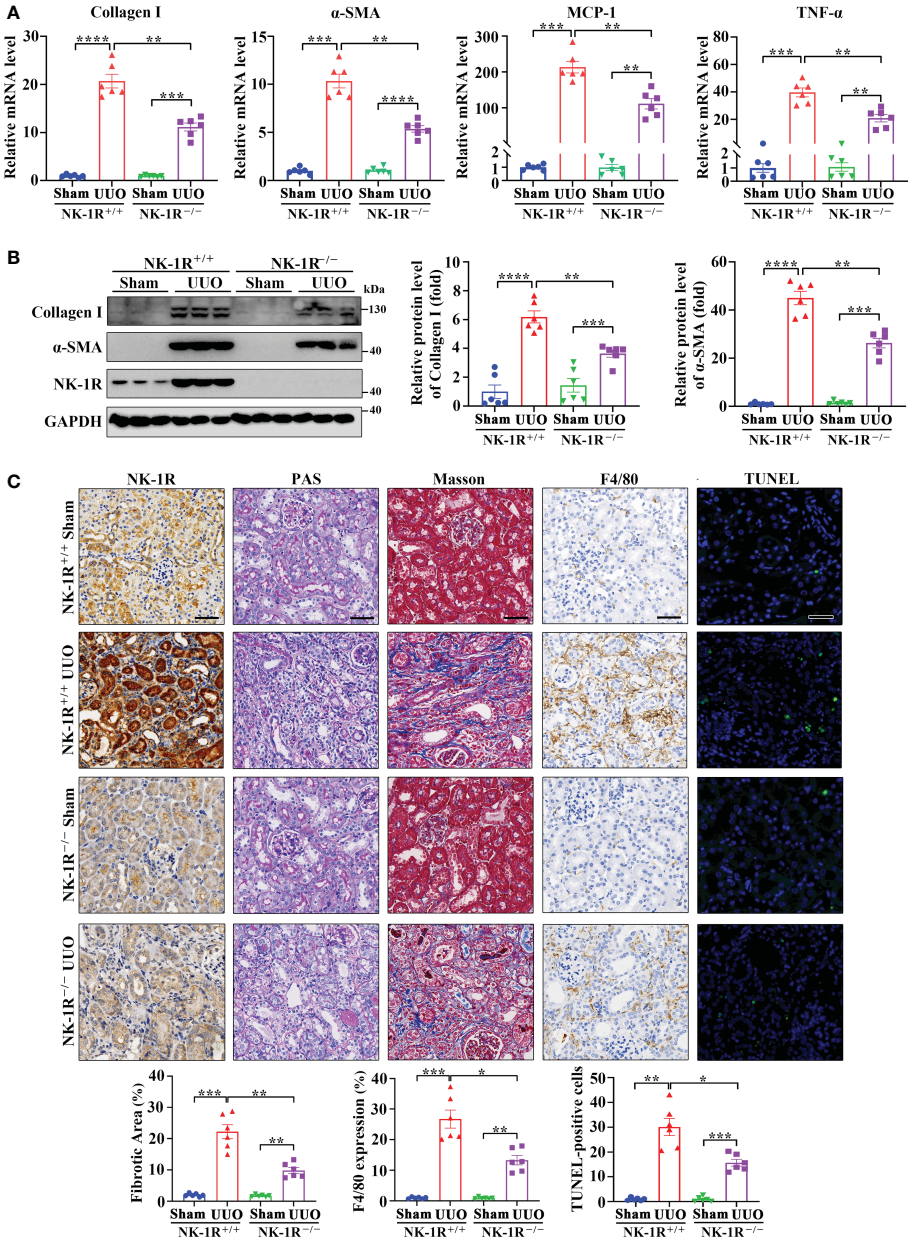

FIGURE 3
Genetic deletion of NK-1R alleviated UUO-induced renal fibrosis, inflammation, and apoptosis. **(A, B)** RT-qPCR **(A)** and Western blotting **(B)** displayed the reduced mRNA **(A)** and protein **(B)** levels of Collagen I, α-SMA, MCP-1, and TNF-α in renal cortical tissues of NK-1R knockout (NK-1R$^{-/-}$) UUO mice, compared with NK-1R wildtype (NK-1R$^{+/+}$) UUO mice. **(C)** Immunochemistry staining of NK-1R and F4/80, PAS, Masson's trichrome, and TUNEL analysis showed that the deletion of NK-1R attenuated UUO-induced renal fibrosis, infiltration of F4/80-positive inflammatory cells, and apoptosis. For **(A–C)**, mouse kidneys were excised on day 14 after UUO. Analysis of TUNEL-positive cells was counted by fluorescence microscopy in ten randomly selected high-power fields per kidney section. Scale bar, 50 μm. Data are shown as mean ± SEM from groups of six mice. *$p < 0.05$; **$p < 0.01$; ***$p < 0.001$; ****$p < 0.0001$.

to bind to the NK-1R promoter. TFAP4 was the only one that was found in all three sets of genes and thus was selected for further investigation (Figures 6C–E). Interestingly, TFAP4 mRNA levels increased in CKD along with elevated SP and NK-1R mRNA levels (Figure 6D).

TFAP4 protein expression was also increased in mouse UUO kidney (Figure 6F) and in patients with CKD (Figure 6G). TFAP4 expression in the CKD kidney was positively correlated to fibrotic extent (r = 0.46, $p = 0.04$) as well as NK-1R expression (r = 0.52, $p = 0.02$) (Supplementary Figures 4A, B). We then explored whether TFAP4 regulates NK-1R expression in HK-2 cells. As shown in Figures 6H, I, TFAP4 overexpression stimulated NK-1R expression at both mRNA and protein levels. As predicted by JASPAR (26), the 1500-bp sequence upstream of TSS of the NK-1R gene contains two potential TFAP4 binding sites (site A and B) (Figure 6J). This sequence displayed visible promoter activity, which was enhanced

10.3389/fimmu.2023.1142240

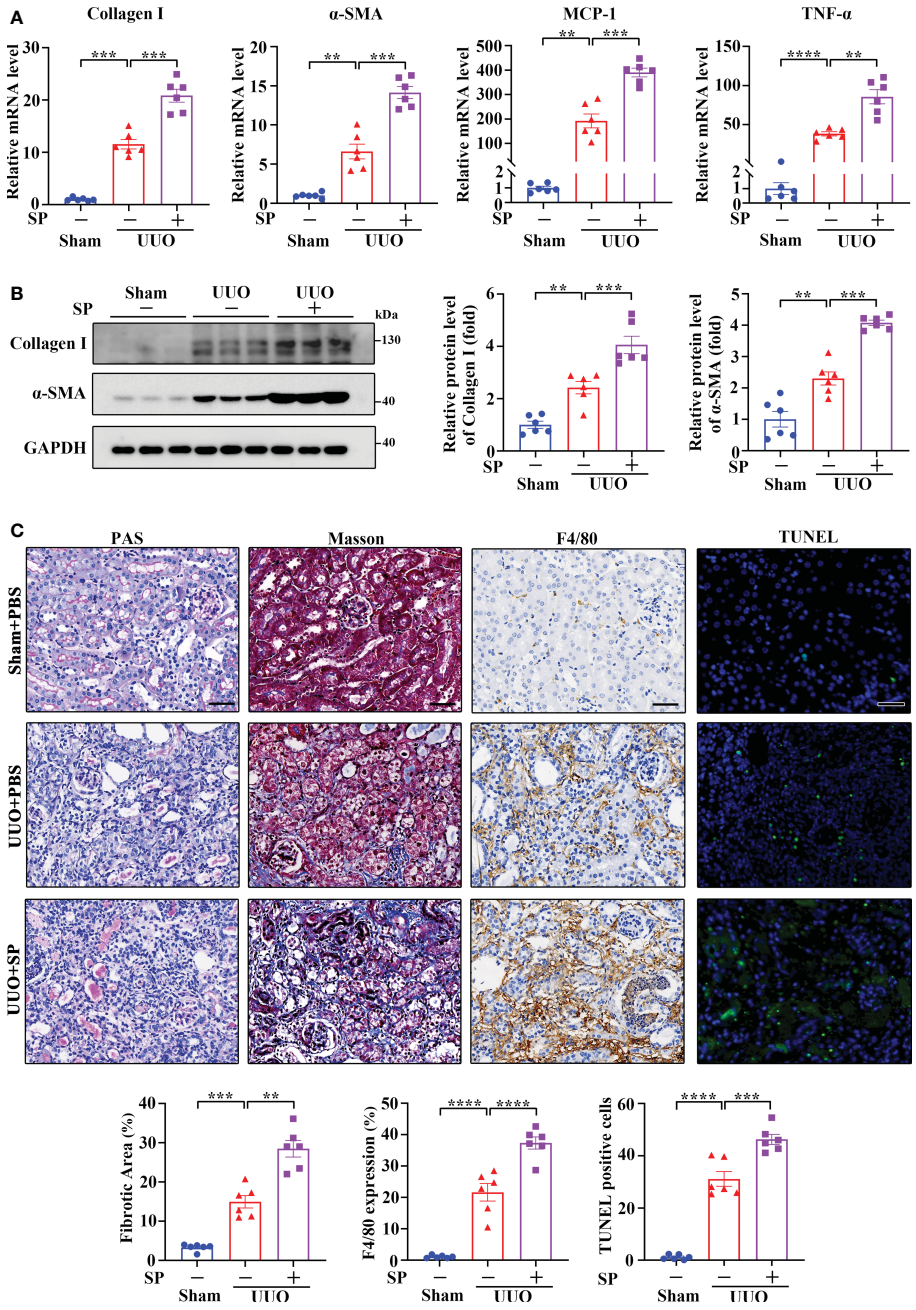

FIGURE 4
Administration of SP exacerbated UUO-induced renal fibrosis, inflammation, and apoptosis. **(A–C)** RT-qPCR **(A)**, Western blotting **(B)**, PAS, Masson's trichrome, F4/80 immunochemistry staining, and TUNEL analysis **(C)**. Results showed that SP administration in established UUO mice enhanced the expression of Collagen I, α-SMA, MCP-1, and TNF-α at mRNA and/or protein levels, which was accompanied by aggravated renal fibrosis, infiltration of F4/80-positive inflammatory cells, and apoptosis. For **(A–C)**, sham and UUO mice were subjected to vehicle (PBS) or SP (40 nM/kg body weight) by tail vein injection three times a week for 14 days. The quantitative analysis of TUNEL-positive cells was achieved by fluorescence microscopy in 10 randomly chosen high-power fields per kidney section. Scale bar, 50 μm. Data are shown as mean ± SEM from groups of six mice. $^{**}p < 0.01$; $^{***}p < 0.001$; $^{****}p < 0.0001$.

by TFAP4 overexpression and suppressed by mutation in the site B but not the site A (Figure 6K). Consistently, ChIP assays demonstrated the binding of TFAP4 to the NK-1R promoter (Figure 6L). Thus, these findings suggest that TFAP4 regulates NK-1R transcription by binding to the NK-1R promoter directly.

NK-1R promotes renal inflammation and fibrosis *via* the JNK and p38 pathway

We then examined the machanisms through which the SP/NK-1R axis regulates renal inflammation and fibrosis in HK-2 cells

10.3389/fimmu.2023.1142240

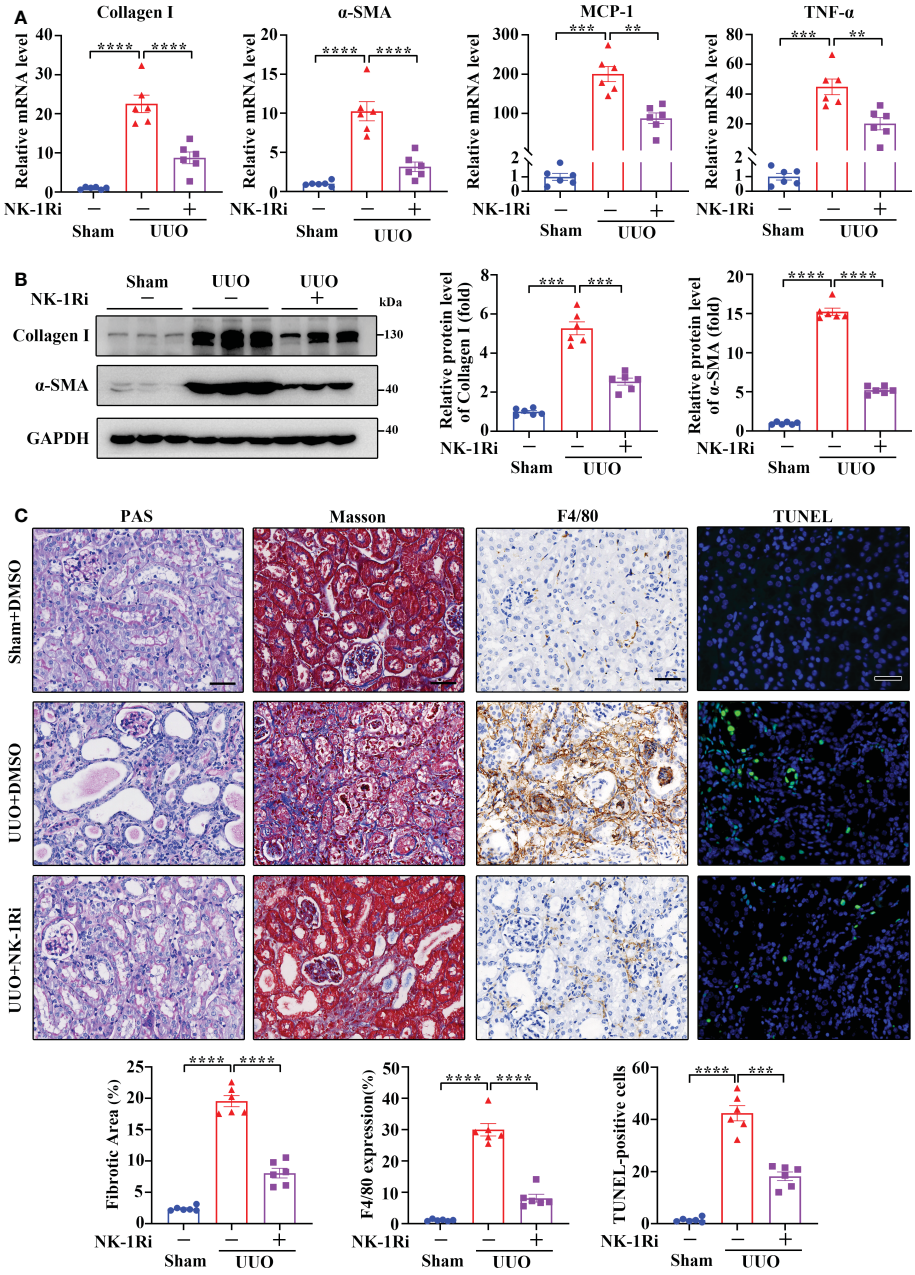

FIGURE 5
Inhibition of NK-1R with a pharmacological antagonist attenuated UUO-induced renal fibrosis, inflammation, and apoptosis. **(A, B)** RT-qPCR **(A)** and Western blotting **(B)** showed that the inhibition of NK-1R antagonized the UUO-induced increase in Collagen I, α-SMA, MCP-1, and TNF-α at the mRNA and/or protein levels in renal cortical tissues on day 14 after UUO. For B, representative images (left panels) and quantitative data (right panels) are shown. **(C)** PAS, Masson's trichrome, F4/80 immunochemistry staining, and TUNEL analysis displayed that the inhibition of NK-1R impeded renal fibrosis, infiltration of F4/80-positive inflammatory cells, and apoptosis mediated by UUO surgery. Representative images (upper panels) and quantitative data (lower panels) are shown. For **(A–C)**, sham and UUO mice were administered intraperitoneally with vehicle (DMSO) or a specific NK-1R inhibitor (NK-1Ri) SR140333 (1 mg/kg body weight) every day for 14 days. + or –, with (+) or without (–) the indicated treatment. TUNEL-positive cells were counted by fluorescence microscopy in ten randomly selected high-power fields per kidney section. Scale bar, 50 μm. Data are shown as mean ± SEM from groups of six mice. $^{**}p < 0.01$; $^{***}p < 0.001$; $^{****}p < 0.0001$.

stably overexpressing NK-1R (Supplementary Figure 5A). We found that addition of SP significantly suppressed the growth and colony formation of NK-1R-overexpressing HK-2 cells, whereas, these suppressive effects were reversed by the NK-1R-specific pharmacological inhibitor (Figure 7A and Supplementary Figure 5B). In addition, SP administration induced apoptosis and G2/M arrest in NK-1R-overexpressing HK-2 cells, which was also blocked by inhibition of NK-1R (Figure 7B). Interestingly, in SP-treated HK-2 cells that stably overexpressed NK-1R, the expression levels of profibrogenic factors, including connective tissue growth factor (CTGF) and MMP9, were obviously elevated, but these were markedly antagonized by NK-1R inhibition (Supplementary

10.3389/fimmu.2023.1142240

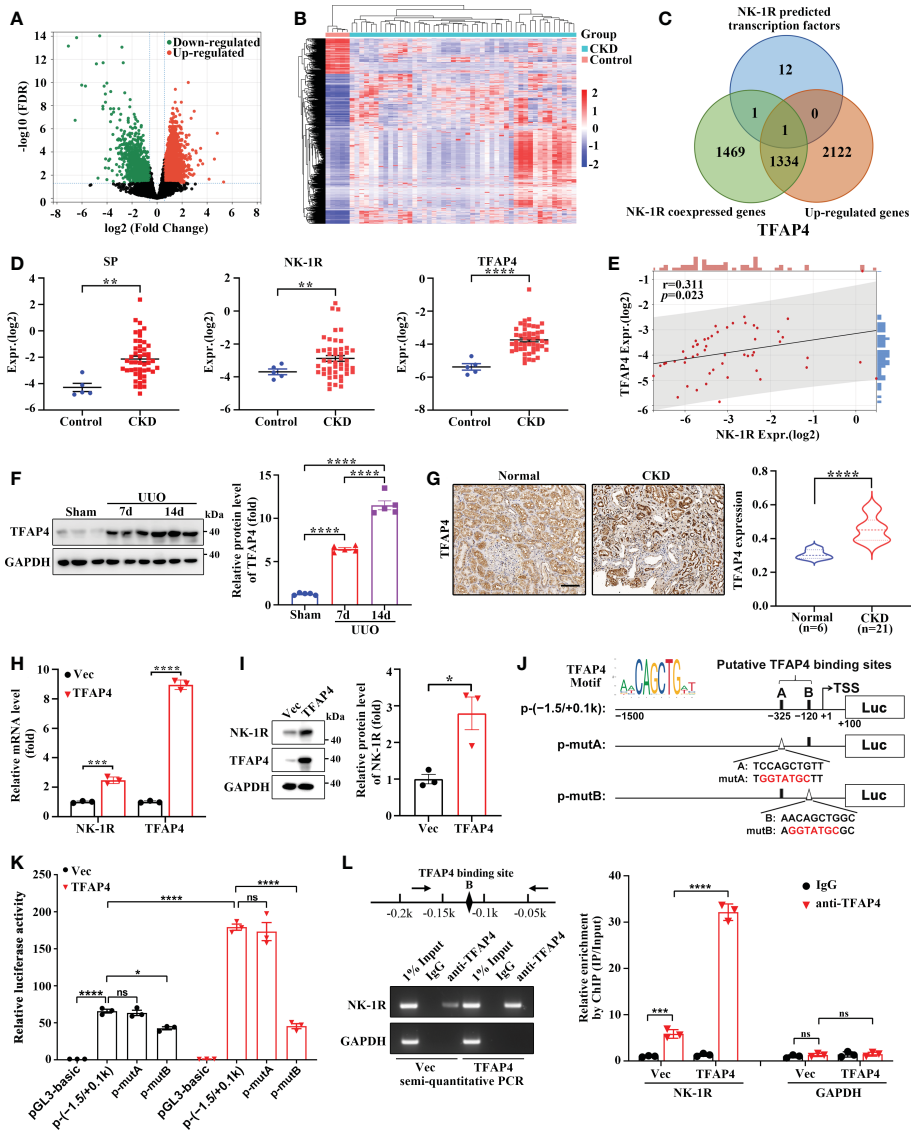

FIGURE 6
TFAP4 is dysregulated in fibrotic kidneys and transcriptionally activates NK-1R expression. **(A, B)** The volcano plot **(A)** and heatmap **(B)** of DEGs between CKD and non-CKD patients from GSE66494 with the threshold of FDR < 0.05 and |log2 (Fold Change)| > = 1. **(C)** Venn diagram of ConTra v3-predicted NK-1R transcription factors overlapping NK-1R co-expressed genes and up-regulated genes in GSE66494. **(D)** The mRNA levels of renal NK-1R, SP, and TFAP4 increased in CKD patients based on GSE66494. **(E)** Correlation between the expression of NK-1R and TFAP4 in GSE66494. **(F, G)** Western blotting **(F)** and immunochemistry staining **(G)** showed the up-regulated expression of renal TFAP4 protein in UUO mice and CKD patients, respectively. **(H, I)** Real-time quantitative PCR **(H)** and Western blotting **(I)** showed that the stable overexpression of TFAP4 increased NK-1R mRNA and protein levels in HK-2 cells. **(J, K)** Overexpression of TFAP4 enhanced the activity of the NK-1R promoter, whereas the mutation of the potential TFAP4 binding site B but not A reduced its activity. Schematic diagram for firefly luciferase reporter plasmids containing -1.5 to +0.1 k region of NK-1R is shown. Potential TFAP4 binding sites (BS) in the NK-1R promoter are depicted as a close rectangle A/B, and mutant TFAP4 BS are depicted as an open triangle A/B. **(L)** ChIP assay showed that TFAP4 directly interacted with the NK-1R promoter *in vivo*. The antibody-precipitated DNA was amplified by semi-quantitative PCR for 30 cycles (left) and real-time quantitative PCR (right). The promoter of GAPDH was used as a negative control. Data are presented as mean ± SEM. *$p < 0.05$; **$p < 0.01$; ***$p < 0.001$; ****$p < 0.0001$; ns, not significant.

Figure 5C). Collectively, SP/NK-1R axis activation promoted apoptosis, G2/M arrest and profibrogenic factor expression in TECs.

To explore the regulatory mechanisms of SP/NK-1R axis in HK-2 cell activities, we treated the stable NK-1R-overexpressing HK-2 cells with and without SP. RNA-seq identified that 399 DEGs were detected in SP-treated cells compared with PBS-treated (control) cells with 307 being up-regulated and 92 down-regulated (|log2 FC| >= 1 and FDR < 0.05) (Figures 7C, D). KEGG analysis revealed the major enrichment of DEGs in the MAPK pathway, cytokine–cytokine receptor interaction, and PI3K-Akt pathway (Figure 7E). It has been well documented that MAPK signaling contributes to inflammation, apoptosis, and fibrosis. We then investigated whether the MAPK pathway was altered by SP/NK-1R activation in HK-2 cells. Phosphorylation of p38 and JNK, but not ERK, was highly up-regulated time-dependently by SP treatment in NK-1R-overexpressing HK-2 cells (Figure 7F). Furthermore, pharmacologically inhibiting NK-1R drastically

10.3389/fimmu.2023.1142240

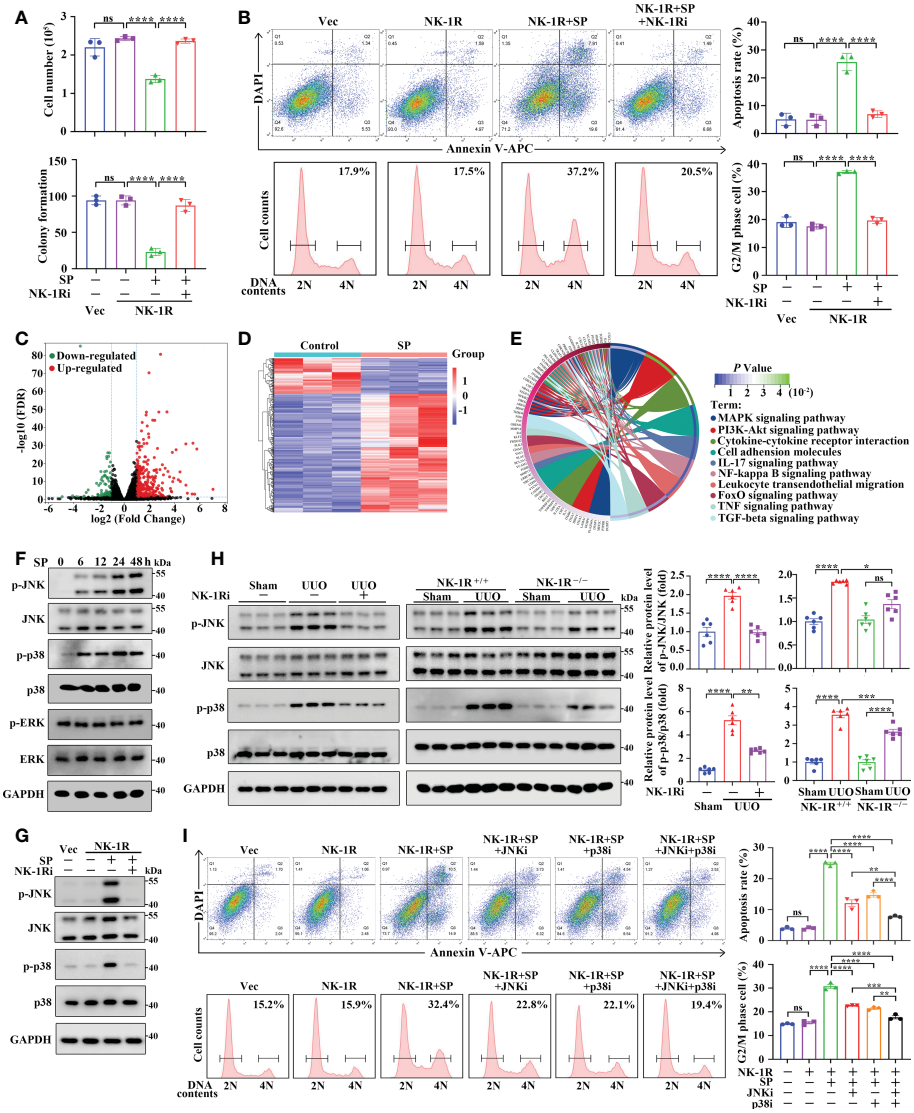

FIGURE 7
SP mediates renal inflammation and fibrosis through an NK-1R-dependent JNK/p38 mechanism *in vivo* and *in vitro*. **(A, B)** The NK-1R inhibitor abrogated the suppressive effect of SP on cell growth and colony formation **(A)** and abolished SP-induced apoptosis and G2/M arrest **(B)** in NK-1R-overexpressed HK-2 cells. For B, representative images (left panels) and quantitative data (right panels) are shown. **(C, D)** The volcano plot **(C)** and heatmap **(D)** of differentially expressed genes (DEGs) between NK-1R-overexpressed HK-2 cells treated with SP or its control using the criteria of FDR < 0.05 and |log2 (Fold Change)| > = 1. **(E)** The circos plot for the KEGG enrichment of indicated DEGs. **(F, G)** Western blotting showed a time-dependent increase in phosphorylated JNK and p38 but not ERK levels in NK-1R-overexpressed HK-2 cells upon SP incubation and that treatment with the NK-1R inhibitor blocked SP-induced increases in the expression of phosphorylated p38 and JNK. **(H)** Inhibition of NK-1R using both an NK-1R inhibitor and genetic knock-out strategies impaired the UUO-mediated elevation of phosphorylated JNK and p38 levels in mouse kidneys. **(I)** p38- or JNK-specific inhibitors or their combination significantly attenuated SP-stimulated G2/M arrest and apoptosis. For H and I, representative images (left panels) and quantitative data (right panels) are shown. Data are presented as mean ± SEM. *$p < 0.05$; **$p < 0.01$; ***$p < 0.001$; ****$p < 0.0001$; ns, not significant.

repressed SP-induced JNK and p38 phosphorylation (Figure 7G). Consistent with the *in vitro* results, the increased p38 and JNK phosphorylation in UUO kidneys was attenuated by pharmacological inhibition or genetic deletion of NK-1R (Figure 7H).

To confirm the role of JNK and p38 in SP/NK-1R-mediated renal fibrosis, two inhibitors, namely, SP600125 (the JNK inhibitor) and SB203580 (the p38 inhibitor) were used to further assess whether MAPKs mediate the effects of the SP/NK-1R signaling on G2/M arrest, apoptosis and expression of profibrogenic genes. Results showed that treatment with SP600125 or SB203580 partially antagonized the stimulatory effects of SP on apoptosis and G2M arrest as well as profibrogenic gene levels in NK-1R-overexpressing HK-2 cells. Of note, the combined use of p38 and JNK inhibitors further inhibited SP-induced G2M arrest, apoptosis, and profibrogenic gene production (Figure 7I and Supplementary Figure 5D). Collectively, these results suggest that the SP/NK-1R axis may promote apoptosis and G2/M arrest as well as profibrogenic gene levels by activating the JNK and p38/MAPK pathways in TECs.

Discussion

As a prevalent pathological hallmark of end-stage kidney disorders irrespective of the initial cause, renal fibrosis is featured with excessive ECM accumulation upon renal injury, leading to the destruction of normal renal structure and eventual kidney failure (27). Hence, renal fibrosis is well associated with renal dysfunction and is a poor prognostic indicator (28). Increasing evidence has revealed that TECs play an indispensable role in both initial and progressive stages of kidney fibrosis by undergoing various functional changes (such as programmed cell death, senescence, and cell cycle arrest) after injury, resulting from deregulation of pivotal factors/signaling pathways (26). Therefore, further investigation of the molecular mechanism underlying renal TECs abnormity is vital for understanding the pathogenesis of renal fibrosis. The SP/NK-1R pathway is related to the pathogenesis of diverse diseases, such as neurological, cardiovascular, and gastrointestinal diseases (13), as well as myocardial and liver fibrosis (18, 29). Nevertheless, the impact of the SP/NK-1R pathway on renal TEC dysfunction and consequent renal fibrosis remains unexplored. In the present study, as outlined in Figure 8, we identified that SP/NK-1R axis activation, arising from elevated SP and NK-1R levels upon injury, could augment renal cell apoptosis, G2/M arrest, proinflammatory/profibrogenic factors production, resulting in progressive renal fibrosis. Mechanistically, we found that NK-1R was a direct target of TFAP4 and TFAP4 promoted NK-1R transcription by binding to the NK-1R promoter. Furthermore, we also uncovered that SP acted *via* the NK-1R to activate the JNK and p38 pathways to induce G2/M arrest, apoptosis, and expression of proinflammatory/profibrogenic genes. More importantly, we also provided the first evidence for targeting the SP/NK-1R axis as a novel therapy for the patients with CKD.

Previous studies have well elucidated the extensive involvement of the SP/NK-1R axis in physiological or pathological processes related to central and peripheral nervous systems (e.g., pain, emesis, and neurodegenerative diseases). However, increasing evidence has also shown the expression of SP and NK-1R in non-neuronal tissues and cells (e.g., the liver, lung, and immune, epithelial, and endothelial cells) (30, 31). Indeed, NK-1R is found to promote inflammation, apoptosis, and fibrogenesis by associating with its ligand SP (15). It is reported that SP can bind to NK-1R to activate cardiac mast cells to increase TNF-α and MMPs expression and promote myocardial remodeling upon aortocaval fistula-induced volume overload (16). It can also provoke HSC/cholangiocyte senescence and liver cell apoptosis by stimulating TGF-β1 secretion after liver injury, leading to liver fibrosis (16, 18). Nevertheless, whether SP/NK-1R regulates renal fibrosis remains unknown.

In this study, we identified that expression of SP and NK-1R was significantly increased in the fibrotic kidney in patients with CKD and in mice after UUO and was positively correlated with the fibrotic extent in the renal interstitium. Serum SP levels were also increased in CKD individuals and UUO mice. More importantly, CKD patients with high NK-1R expression or SP levels exhibited lower eGFR, indicating that the activation of SP/NK-1R may contribute to the progression of CKD. Further investigations revealed that both genetic deletion and pharmacological inhibition of NK-1R remarkably impeded UUO-induced proinflammatory/profibrogenic responses as indicated by decreased macrophage infiltration, TNF-α/MCP-1/α-SMA/Collagen I levels, and renal cell apoptosis, whereas SP administration significantly enhanced these inflammatory and fibrogenic responses. Altogether, we find that the SP/NK-1R pathway mediates renal fibrosis progression.

Although SP and NK-1R levels are generally up-regulated in response to different injuries in diverse cell types, the regulatory mechanism of SP/NK-1R expression remains unclear. It has been reported that TFAP4, a member of the basic helix–loop–helix leucine-zipper (bHLH-LZ) family (32), is associated with c-Myc-

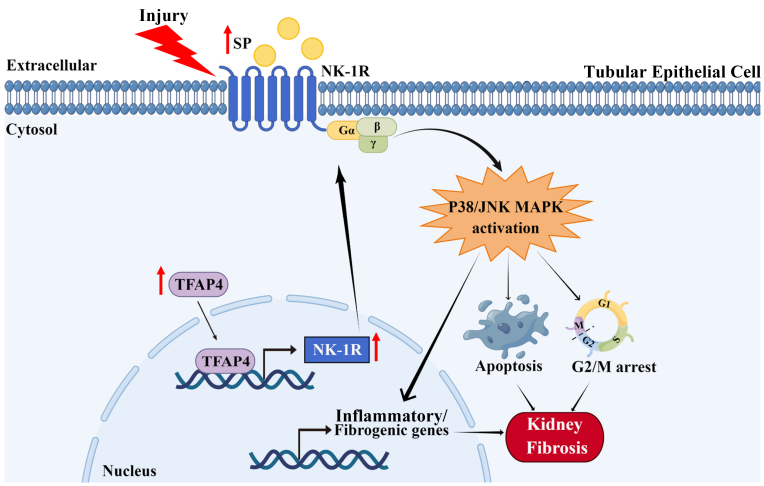

FIGURE 8
Schematic diagram generated by Figdraw for the proposed mechanism by which the SP/NK-1R axis contributes to the pathogenesis of renal fibrosis *via* modulating inflammatory responses and cell fate of tubular epithelial cells through JNK/p38 signaling pathway in CKD.

mediated renal fibrosisby by inducing integrin αv-mediated TGF-β signaling (33). However, no direct evidence has yet revealed the regulatory role of TFAP4 in renal fibrosis. Hyperactivation of TFAP4 has been observed in various human malignancies (e.g., intestinal, lymphoid and liver cancer) (34–36). In the present study, we identified that increased renal TFAP4 levels were closely correlated to the fibrotic index and NK-1R levels in patients with CKD. Moreover, KEGG enrichment analysis suggested that TFAP4 might be associated with multiple signaling pathways (Supplementary Figure 4C), such as neuroactive ligand-receptor interaction, MAPK, and Wnt signaling pathways. More importantly, we uncovered that NK-1R expression was regulated by TFAP4 as TFAP4 could bind to the promoter region of NK-1R to regulate its transcription. In the present study, therefore, TFAP4 may be a regulatory mechanism responsible for NK-1R overexpression in renal fibrosis.

Renal fibrosis involves different types of resident cells, including renal TECs and myofibroblasts. It is reported that apoptosis and cell cycle arrest of renal TECs initiate adaptive repair in response to kidney injury (37). Previous studies have demonstrated that maladaptive cell death results in the loss of resident renal TECs and that apoptotic tubule communicates with adjacent profibrogenic cell types (e.g., fibroblasts, myofibroblasts), eventually promoting fibrosis (37). Of these processes, the G2/M phase arrest of renal TECs after kidney injury contributes to persistent transcription of profibrogenic factors such as CTGF and Collagen I (38, 39). Given that SP and NK-1R were mainly expressed in renal TECs, we used HK-2 cells that stably overexpressed NK-1R to further investigate the relationship between SP/NK-1R and tubular injury as well as fibrogenesis *in vitro*. We found that SP treatment suppressed the growth and induced G2/M arrest, apoptosis, and profibrogenic factor production in NK-1R-overexpressing HK-2 cells. Correspondingly, the above effects of SP were almost abolished by a specific NK-1R antagonist, indicating that SP functioned through NK-1R activation. We thus propose that the SP/NK-1R axis may contribute to renal fibrosis at least partly by provoking phenotypic changes in tubular epithelium cells.

To explore the mechanism underlying SP/NK-1R-mediated tubular injury and fibrogenesis, RNA-seq and KEGG pathway enrichment analyses were performed. We found that the SP/NK-1R axis was associated with several signaling pathways closely related to renal fibrosis, such as MAPK and PI3K-Akt. The MAPK kinase superfamily includes four typical subgroups, including JNK, p38, ERK1/2, and ERK5, and it is worth noting that the first three members are dominant responders to extracellular and intracellular stresses (40). Extensive studies have suggested that MAPKs participate in multiple events such as cell differentiation, cell death, and inflammation, and play a critical role in various diseases (41). We found that SP treatment induced the phosphorylation of p38 and JNK but not ERK1/2 *in vitro*, which was completely blocked by the NK-1R antagonist. In addition, the stimulatory effect of UUO injury on phosphorylated p38/JNK levels was attenuated by the pharmacological inhibition and genetic deletion of NK-1R *in vivo*. Furthermore, treatment with JNK or p38 inhibitors partially abolished apoptosis, G2/M arrest, and fibrogenesis mediated by SP in NK-1R-overexpressing HK-2 cells, and the combined use of JNK and p38 inhibitors enhanced these suppressive effects. Collectively, these data indicated that SP/NK-1R may induce injury and profibrogenic responses in HK-2 cells by activating JNK/p38 MAPKs.

In conclusion, we identify the SP/NK-1R axis as a novel pathway whose activation leads to renal inflammation and fibrosis. Our study uncovers a regulatory mechanism of NK-1R expression whereby TFAP4 increases NK-1R transcription by directly binding to its promoter. Moreover, SP/NK-1R axis activation, may stimulate p38/JNK signaling to promote cell apoptosis and G2/M arrest as well as proinflammatory/profibrogenic responses, resulting in renal fibrosis. Thus, targeting SP/NK-1R axis with NK-1R pharmacological antagonists may represent a promising treatment for renal inflammation and fibrosis in chronic and end-stage kidney disease.

Data availability statement

The datasets presented in this study can be found in online repositories. The names of the repository/repositories and accession number(s) can be found below: GSE216743 (GEO) GSE66494 (GEO).

Ethics statement

Human samples protocols gained approval from the Institutional Research Ethics Committee at the Seventh Affiliated Hospital, Sun Yat-sen University. The patients/participants provided their written informed consent to participate in this study. Animal experimental protocols gained approval from the Institutional Research Ethics Committee at the Sun Yat-sen University.

Author contributions

EZ, YaL, and MZ were responsible for most of the experiments. XJ, recruited the patient samples and collected clinical data. YuL, NL and HG were responsible for statistical analysis and data interpretation. XS was responsible for the generation of schematic diagram. YX were responsible for modifying the manuscript. JL, H-YL and ZZ designed the study and prepared the manuscript. All authors contributed to the article and approved the submitted version.

Funding

This study was supported by grants from the Health and Medical Research Fund of National Nature Science Founding of China (NSFC 81900673), Shenzhen Technology Project (JCYJ20190809120801655, JCYJ20180307150634856) and Sanming Project of Medicine in Shenzhen (SZSM201911013), and the Guangdong-Hong Kong-Macao-Joint Labs Program from Guangdong Science and Technology (2019B121205005).

Conflict of interest

The authors declare that the research was conducted in the absence of any commercial or financial relationships that could be construed as a potential conflict of interest.

Publisher's note

All claims expressed in this article are solely those of the authors and do not necessarily represent those of their affiliated organizations, or those of the publisher, the editors and the reviewers. Any product that may be evaluated in this article, or claim that may be made by its manufacturer, is not guaranteed or endorsed by the publisher.

Supplementary material

The Supplementary Material for this article can be found online at: https://www.frontiersin.org/articles/10.3389/fimmu.2023.1142240/full#supplementary-material

References

1. Eddy AA. Overview of the cellular and molecular basis of kidney fibrosis. *Kidney Int Suppl* (2014) 4(1):2–8. doi: 10.1038/kisup.2014.2

2. Bikbov B, Purcell CA, Levey A. S, Smith M, Abdoli A, Abebe M, et al. Global, regional, and national burden of chronic kidney disease, 1990-2017: A systematic analysis for the global burden of disease study 2017. *Lancet (London England)* (2020) 395(10225):709–33. doi: 10.1016/S0140-6736(20)30045-3

3. Liu B, Tang T, Lv L, Lan H. Renal tubule injury: A driving force toward chronic kidney disease. *Kidney Int* (2018) 93:568–79. doi: 10.1016/j.kint.2017.09.033

4. Zhou D, Liu Y. Renal fibrosis in 2015: Understanding the mechanisms of kidney fibrosis. *Nat Rev Nephrol* (2016) 12:68–70. doi: 10.1038/nrneph.2015.215

5. Gewin L. Renal fibrosis: Primacy of the proximal tubule. *Matrix Biol* (2018) 68:248–62. doi: 10.1016/j.matbio.2018.02.006

6. Sánchez-López E, Rayego S, Rodrigues-Díez R, Rodriguez JS, Rodrigues-Díez R, Rodríguez-Vita J, et al. CTGF promotes inflammatory cell infiltration of the renal interstitium by activating NF-kappaB. *J Am Soc Nephrol JASN* (2009) 20(7):1513–26. doi: 10.1681/ASN.2008090999

7. Meng X, Nikolic-Paterson D, Lan H. TGF-β: the master regulator of fibrosis. *Nat Rev Nephrol* (2016) 12:325–38. doi: 10.1038/nrneph.2016.48

8. Bozic M, et al. Protective role of renal proximal tubular alpha-synuclein in the pathogenesis of kidney fibrosis. *Nat Commun* (2020) 11:1943. doi: 10.1038/s41467-020-15732-9

9. Schunk S, Floege J, Fliser D, Speer T. WNT-β-catenin signalling - a versatile player in kidney injury and repair. *Nat Rev Nephrol* (2021) 17:172–84. doi: 10.1038/s41581-020-00343-w

10. Calvillo L, Gironacci M, Crotti L, Meroni P, Parati G. Neuroimmune crosstalk in the pathophysiology of hypertension. *Nat Rev Cardiol* (2019) 16:476–90. doi: 10.1038/s41569-019-0178-1

11. Muñoz M, Coveñas R. The neurokinin-1 receptor antagonist aprepitant, a new drug for the treatment of hematological malignancies: Focus on acute myeloid leukemia. *J Clin Med* (2020) 9(6):1659. doi: 10.3390/jcm9061659

12. Suvas S. Role of substance p neuropeptide in inflammation, wound healing, and tissue homeostasis. *J Immunol (Baltimore Md. 1950)* (2017) 199:1543–52. doi: 10.4049/jimmunol.1601751

13. Thom C, Ehrenmann J, Vacca S, Waltenspühl Y, Schöppe J, Medalia O, et al. Structures of neurokinin 1 receptor in complex with G and G proteins reveal substance p binding mode and unique activation features. *Sci Adv* (2021) 7(50):eabk2872. doi: 10.1126/sciadv.abk2872

14. Zhang Y, Yang Y, Zhang Z, Fang W, Kang S, Luo Y, et al. Neurokinin-1 receptor antagonist-based triple regimens in preventing chemotherapy-induced nausea and vomiting: A network meta-analysis. *J Natl Cancer Institute* (2017) 109(2). doi: 10.1093/jnci/djw217

15. Peng L, Agogo G, Guo J, Yan M. Substance p and fibrotic diseases. *Neuropeptides* (2019) 76:101941. doi: 10.1016/j.npep.2019.101941

16. Melendez G. C, Li J, Law BA, Janicki JS, Supowit SC, Levick S. P. Substance p induces adverse myocardial remodelling *via* a mechanism involving cardiac mast cells. *Cardiovasc Res* (2011) 92(3):420–9. doi: 10.1093/cvr/cvr244

17. Bang R, Biburger M, Neuhuber W, Tiegs G. Neurokinin-1 receptor antagonists protect mice from CD95- and tumor necrosis factor-alpha-mediated apoptotic liver damage. *J Pharmacol Exp Ther* (2004) 308:1174–80. doi: 10.1124/jpet.103.059329

18. Wan Y, Meng F, Wu N, Zhou T, Venter J, Francis H, et al. Substance p increases liver fibrosis by differential changes in senescence of cholangiocytes and hepatic stellate cells. *Hepatol (Baltimore Md.)* (2017) 66(2):528–41. doi: 10.1002/hep.29138

19. Li Y, Yuan Y, Huang ZX, Chen H, Lan R, Wang Z, et al. GSDME-mediated pyroptosis promotes inflammation and fibrosis in obstructive nephropathy. *Cell Death differentiation* (2021) 28(8):2333–50. doi: 10.1038/s41418-021-00755-6

20. Zhang LZ, Yang JE, Luo YW, Liu FT, Yuan YF, Zhuang SM. A p53/lnc-Ip53 negative feedback loop regulates tumor growth and chemoresistance. *Advanced Sci (Weinheim Baden-Wurttemberg Germany)* (2020) 7(21):2001364. doi: 10.1002/advs.202001364

21. Kim D, Langmead B, Salzberg S. HISAT: A fast spliced aligner with low memory requirements. *Nat Methods* (2015) 12:357–60. doi: 10.1038/nmeth.3317

22. Li B, Dewey C. RSEM: Accurate transcript quantification from RNA-seq data with or without a reference genome. *BMC Bioinf* (2011) 12:323. doi: 10.1186/1471-2105-12-323

23. Love M, Huber W, Anders S. Moderated estimation of fold change and dispersion for RNA-seq data with DESeq2. *Genome Biol* (2014) 15:550. doi: 10.1186/s13059-014-0550-8

24. Forbes M, Thornhill B, Chevalier R. Proximal tubular injury and rapid formation of atubular glomeruli in mice with unilateral ureteral obstruction: a new look at an old model. *Am J Physiol Renal Physiol* (2011) 301:F110–117. doi: 10.1152/ajprenal.00022.2011

25. Li X, Pan J, Li H, Li G, Liu X, Liu B, et al. DsbA-l mediated renal tubulointerstitial fibrosis in UUO mice. *Nat Commun* (2020) 11:4467. doi: 10.1038/s41467-020-18304-z

26. Liu Y. Cellular and molecular mechanisms of renal fibrosis. *Nat Rev Nephrol* (2011) 7:684–96. doi: 10.1038/nrneph.2011.149

27. Ruiz-Ortega M, Rayego-Mateos S, Lamas S, Ortiz A, Rodrigues-Diez R. Targeting the progression of chronic kidney disease. *Nat Rev Nephrol* (2020) 16:269–88. doi: 10.1038/s41581-019-0248-y

28. Berchtold L, Crowe LA, Combescure C, Kassaï M, Aslam I, Legouis D, et al. Diffusion-magnetic resonance imaging predicts decline of kidney function in chronic kidney disease and in patients with a kidney allograft. *Kidney Int* (2022) 101(4):804–13. doi: 10.1016/j.kint.2021.12.014

29. Levick S, Murray D, Janicki J, Brower G. Sympathetic nervous system modulation of inflammation and remodeling in the hypertensive heart. *Hypertension (Dallas Tex. 1979)* (2010) 55:270–6. doi: 10.1161/HYPERTENSIONAHA.109.142042

30. Muñoz M, Coveñas R. Involvement of substance p and the NK-1 receptor in human pathology. *Amino Acids* (2014) 46:1727–50. doi: 10.1007/s00726-014-1736-9

31. Steinhoff M, von Mentzer B, Geppetti P, Pothoulakis C, Bunnett N. Tachykinins and their receptors: contributions to physiological control and the mechanisms of disease. *Physiol Rev* (2014) 94:265–301. doi: 10.1152/physrev.00031.2013

32. Jackstadt R, Röh S, Neumann J, Jung P, Hoffmann R, Horst D, et al. AP4 is a mediator of epithelial-mesenchymal transition and metastasis in colorectal cancer. *J Exp Med* (2013) 210(7):1331–50. doi: 10.1084/jem.20120812

33. Shen Y, Miao N, Wang B, Xu J, Gan X, Xu D, et al. C-myc promotes renal fibrosis by inducing integrin αv-mediated transforming growth factor-β signaling. *Kidney Int* (2017) 92(4):888–99. doi: 10.1016/j.kint.2017.03.006

34. Jaeckel S, Kaller M, Jackstadt R, Götz U, Müller S, Boos S, et al. Ap4 is rate limiting for intestinal tumor formation by controlling the homeostasis of intestinal stem cells. *Nat Commun* (2018) 9:3573. doi: 10.1038/s41467-018-06001-x

35. Song J, Xie C, Jiang L, Wu G, Zhu J, Zhang S, et al. Transcription factor AP-4 promotes tumorigenic capability and activates the wnt/β-catenin pathway in hepatocellular carcinoma. *Theranostics* (2018) 8(13):3571–83. doi: 10.7150/thno.25194

36. Tonc E, Takeuchi Y, Chou C, Xia Y, Holmgren M, Fujii C, et al. Unexpected suppression of tumorigenesis by c-MYC *via* TFAP4-dependent restriction of stemness in b lymphocytes. *Blood* (2021) 138(24):2526–38. doi: 10.1182/blood.2021011711

37. Li L, Fu H, Liu Y. The fibrogenic niche in kidney fibrosis: components and mechanisms. *Nat Rev Nephrol* (2022) 18(9):545–57. doi: 10.1038/s41581-022-00590-z

38. Yang L, Besschetnova T, Brooks C, Shah J, Bonventre J. Epithelial cell cycle arrest in G2/M mediates kidney fibrosis after injury. *Nat Med* (2010) 16:535–43. doi: 10.1038/nm.2144

39. Li H, Peng X, Wang Y, Cao S, Xiong L, Fan J, et al. Atg5-mediated autophagy deficiency in proximal tubules promotes cell cycle G2/M arrest and renal fibrosis. *Autophagy* (2016) 12:1472–86. doi: 10.1080/15548627.2016.1190071

40. Mathien S, Tesnière C, Meloche S. Regulation of mitogen-activated protein kinase signaling pathways by the ubiquitin-proteasome system and its pharmacological potential. *Pharmacol Rev* (2021) 73:263–96. doi: 10.1124/pharmrev.120.000170

41. Ronkina N, Gaestel M. MAPK-activated protein kinases: Servant or partner? *Annu Rev Biochem* (2022) 91:505–40. doi: 10.1146/annurev-biochem-081720-114505

frontiers | Frontiers in Immunology

TYPE Review
PUBLISHED 29 March 2023
DOI 10.3389/fimmu.2023.1140791

OPEN ACCESS

EDITED BY
Chit Laa Poh,
Sunway University, Malaysia

REVIEWED BY
Wei Qiu,
Southern Medical University, China
Rongjun Wan,
Xiangya Hospital, Central South University, China
Xiaoxi Lv,
Chinese Academy of Medical Sciences and Peking Union Medical College, China

*CORRESPONDENCE
Ying Wei
weiying_acup@126.com
Jingcheng Dong
jcdong2004@126.com

†These authors have contributed equally to this work

SPECIALTY SECTION
This article was submitted to Inflammation, a section of the journal Frontiers in Immunology

RECEIVED 09 January 2023
ACCEPTED 17 March 2023
PUBLISHED 29 March 2023

CITATION
Lv X, Tang W, Qin J, Wang W, Dong J and Wei Y (2023) The crosslinks between ferroptosis and autophagy in asthma. *Front. Immunol.* 14:1140791. doi: 10.3389/fimmu.2023.1140791

The crosslinks between ferroptosis and autophagy in asthma

Xiaodi Lv[1,2†], Weifeng Tang[1,2†], Jingjing Qin[1,2], Wenqian Wang[1,2], Jingcheng Dong[1,2*] and Ying Wei[1,2*]

[1]Department of Integrative Medicine, Huashan Hospital, Fudan University, Shanghai, China, [2]Institutes of Integrative Medicine, Fudan University, Shanghai, China

Autophagy is an evolutionarily conserved cellular process capable of degrading various biological molecules and organelles *via* the lysosomal pathway. Ferroptosis is a type of oxidative stress-dependent regulated cell death associated with the iron accumulation and lipid peroxidation. The crosslinks between ferroptosis and autophagy have been focused on since the dependence of ferroptosis on autophagy was discovered. Although the research and theories on the relationship between autophagy and ferroptosis remain scattered and fragmented, the crosslinks between these two forms of regulated cell death are closely related to the treatment of various diseases. Thereof, asthma as a chronic inflammatory disease has a tight connection with the occurrence of ferroptosis and autophagy since the crosslinked signal pathways may be the crucial regulators or exactly regulated by cells and secretion in the immune system. In addition, non-immune cells associated with asthma are also closely related to autophagy and ferroptosis. Further studies of cross-linking asthma inflammation with crosslinked signaling pathways may provide us with several key molecules that regulate asthma through specific regulators. The crosslinks between autophagy and ferroptosis provide us with a new perspective to interpret and understand the manifestations of asthma, potential drug discovery targets, and new therapeutic options to effectively intervene in the imbalance caused by abnormal inflammation in asthma. Herein, we introduce the main molecular mechanisms of ferroptosis, autophagy, and asthma, describe the role of crosslinks between ferroptosis and autophagy in asthma based on their common regulatory cells or molecules, and discuss potential drug discovery targets and therapeutic applications in the context of immunomodulatory and symptom alleviation.

KEYWORDS

asthma, autophagy, crosslinks, ferroptosis, targets

1 Introduction

The scientific observation of regulated cell death (RCD) historically originated in 1842 when dying cells in toads were discovered by Karl Vogt. And when the term "apoptosis" was coined in 1972 by Andrew Wyllie, Alastair Currie1, and John Kerr, the surge in RCD research started. Since then, various types of forms of RCD have been explored in the context of the role in multiple pathological and physiological processes of different diseases, the macroscopic morphological alterations, the molecular mechanisms and signaling pathways associated with activation or regulation, and the program in response to varieties of stresses, especially oxidative stress. With multiple novel forms of RCD identified, the core and specific molecular mechanisms have been discovered to insulate the particular form of RCD from others. The research on the regulation of these forms of RCD provided us with novel targets for treating a wide range of diseases. However, it has been increasingly apparent that these molecular programs are deeply interwoven. Studies probing cell death crosstalk have demonstrated multiple molecular interactions between signal transduction pathways and shown that numerous cell death programs are involved in the pathogenesis and pathophysiological process of various diseases. For example, the pyroptotic molecules can activate apoptotic substrates and vice versa, while inhibition of one type of cell death pathway by the pathogen or other signaling defects can result in another pathway of RCD compensating (1–4).

The crosslinks between ferroptosis and macroautophagy/autophagy have been focused on since the form of autophagy-dependent ferroptosis was discovered. The initiation of autophagy is mediated by the unc-51-like kinase (ULK) complex, which can be inhibited by mTOR complex 1 (mTORC1) or activated by 5′-AMP-activated protein kinase (AMPK) (the kinase can be activated by stress signals). Then, PI3P-binding molecules can be recruited after the activation of vacuolar protein sorting 34 (VPS34) to form a phagosome (an isolated pre-autophagosomal structure) (5–8). The autophagosome (AP) formation depends on LC3 lipidation that LC3 is cleaved into the soluble form LC3I acting as a precursor to LC3II, a docking point covalently attaching to the phagosome membrane for cargo receptors (Figure 1A) (9–11). These receptors play a central role in the selective recruitment of specific cargoes with ubiquitin labeling during autophagy (Figure 1A). Then, an AP can be formed when the phagosome extends and eventually closes (Figure 1A). When transported to the perinuclear region and fused with proximal lysosomes, cargoes can be degraded and nutrients can be recycled through lysosomal hydrolases, along with the formation of autolysosomes (ALs) (12–15). Ferroptosis is initiated with lipid peroxidation which is uncontrolled and lethal resulting in subsequent rupture of the plasma membrane through iron catalysis, containing enzymatic (lipoxygenases) and non-enzymatic (Fenton's reaction) mechanisms. Iron accumulation and lipid peroxidation are two critical mediators in ferroptosis. Autophagy can modulate ferroptosis based on particular lysosomal degradation of specific organelles or proteins leading to iron accumulation and lipid peroxidation. Similarly, ferroptosis can regulate the formation of ALs to affect the process of autophagy. For example, ferroptosis induction has been proven to have a tight connection with the turnover of lipidated LC3 and the fusion of the AP with lysosomes (16, 17).

Furthermore, the signal transduction pathways or principal signal molecules of two forms of RCD may be common or cross-linked. The research on these crosslinked pathways and molecules can provide more effective pharmacological targets for improving the prognosis of multiple patients. In addition, both ferroptosis and autophagy have been proven to have a tight connection with innate and adaptive immunity. On the one hand, the activation of immune cells can be regulated by these two forms of RCD. On the other hand, the immune and inflammatory signaling can be controlled by the pathways or proteins of ferroptosis and autophagy.

Asthma is a heterogeneous and complex disorder characterized by asthmatic inflammation in the airways. In addition to the chronic inflammation, airway remodeling, and bronchial hyper-reactivity comprise the specific pathogenesis of asthma along with the interaction of non-immune cells such as epithelial cells and airway smooth muscle (ASM) cells, and immune cells including the cells from the innate and adaptive immune systems. Immune factors and various genetic factors interplay in an array of disorders after being stimulated by different environmental factors. Asthma attacks occur over periods of many years, which creates additional therapeutic challenges. Long term structural airway alteration involves multiple cell types and leads to non-reversible obstruction of airflow causing chronic symptoms and, in rare cases, death. New targets for asthmatic therapy have been always discovered based on various areas of lung research to circumvent some of the current limitations of conventional asthma therapy that include tachyphylaxis to beta adrenergic agonists, corticosteroid insensitivity, off-target effects of corticosteroids, and improvement of effective treatments to reverse obstructive airway remodeling.

Autophagy and ferroptosis as two crucial forms of RCD have been proved to enrich the strategies of asthmatic therapy. For example, a randomized clinical trial demonstrated that Carbamazepine, an anticonvulsant drug and autophagy inducer had high efficacy in therapy of moderate or severe bronchial asthma (18). Carbamazepine has been shown to induce antimicrobial autophagy through mTOR-independent pathway, suggesting that autophagy induction by repurposed drug could provide an easily implementable potential therapy for some asthma phenotypes (19). Similarly, ferroptosis was reported to have a tight connection with type 2 high asthma. The elevated expression of ALOX15 (arachidonate 15- lipoxygenase), a key enzyme of lipid peroxidation, in the bronchial epithelium or eosinophils of BALF in both childhood and adult asthmatics is associated with allergen sensitization and airway inflammation (20, 21). Furthermore, Phosphatidylethanolamine binding protein 1 (PEBP1), the crosslinked regulatory molecule of ferroptosis and autophagy, has been discovered to affect the function and survival of asthmatic epithelial cells. PEBP1 which is also called rheostat between ferroptosis and autophagy in HAECs can interact with ALOX15 to induce ferroptosis in asthmatic HAECs by generating 15-

hydroperoxyeicosaetetranoic acid (15-HpETE-PE). In addition, when the process of PEBP1 binding with LC3-I is inhibited, autophagic pro-survival pathways would be activated in asthmatic HAECs and subsequently, cell destruction would be limited (22).

However, the role of ferroptosis and autophagy in asthma is mostly preclinical evidence, a series of evaluation criteria should be developed before clinical application. As such a large player in general function of cells associated with asthma, autophagy and ferroptosis do provide multiple therapeutic targets. Determining the roles they play in different cell types is key to understanding how to specifically target them. Moreover, in order to reach the best clinical outcome, it is also crucial to consider the stage of development of the disease. Indeed, depending if asthmatic patients are in the initiation or exacerbation phases of the pathogenesis, the specific cell type to be targeted should be considered.

It can be further concluded that the therapeutic schedules to attenuate the symptoms and improve the prognosis for asthma patients can be established based on regulating the innate and adaptive immunity *via* modulating the progress of autophagy and ferroptosis, or discovering some crosslinked targets of ferroptosis and autophagy in various cells which are crucial in asthmatic pathogenesis. All in all, the crosslinks between ferroptosis and autophagy may provide us with more effective targets in various specific cell types to treat asthma.

$CD11b^+$ cDCs can maturate and migrate depending on the transcription factor IRF4 with the effect of danger signals and 'instructive' cytokines produced by HAECs. The typical function of DCs as antigen-presenting cells is to internalize antigens and present antigen-derived peptides to T cells. When activated by the innate immune system, $CD4^+$T cells can differentiate into multiple functional subsets of helper T cells such as Th2 cells, Th17 cells, Th1 cells, and Treg cells. Both Th2 cells and ILC2 cells contribute to eosinophilic inflammation by upregulating the expression of GATA-3 which can promote the production of Th2 cytokines, and increase the production of IL-5 to modulate the development of eosinophils, IL-13 leading to goblet cell metaplasia and bronchial hyperreactivity, IL-4 affecting the mature and activation of Th9 cells which can promote the IgE synthesis by B cells. Both Th1 and Th17 cells can result in neutrophilic inflammation by respectively secreting IFN-γ or TNFαand IL-17A or IL-17F Treg cells, a subset of $CD4^+$ T cells, also originate from Th0 cells. The fate of follicular helper T cells (TFH) can be adopted by Th cells producing IL-21 so that IgE can be induced by B lymphocytes.

2 The role of autophagy in ferroptosis

Ferroptosis is promoted by iron accumulation and lipid peroxidation. The progress of both initiation and advancement of ferroptosis involves autophagy. The process of autophagy can be divided into non-selective autophagy and selective autophagy. Non-selective autophagy has long been thought to be the main form of bulk degradation pathway, which randomly engulfs a portion of the cytoplasm into autophagosomes and then delivers them to lysosome for degradation. Selective autophagy, however, specifically recognizes and degrades the particular cargo, either a protein complex, an organelle, or lipid droplets (23). Nonselective autophagy is primarily a starvation response, whereas cells use selective autophagy for a variety of purposes, such as remodeling to adapt to changing environmental/nutritional conditions and to eliminate damaged organelles.

2.1 The role of selective autophagy in ferroptosis

The selective autophagy processes which influence ferroptosis included two main parts in the context of regulating the level of iron and modulating lipid peroxidation.

2.1.1 The role of selective autophagy in regulating the level of iron

The level of iron can be regulated by ferritinophagy mediated by nuclear receptor coactivator 4 (NCOA4) (Figure 1B) (16, 17). The role of ferritinophagy in iron accumulation promotes the development of ferroptosis. Hence, the suppression of ferritinophagy can increase iron storage and limit ferroptosis by modulating the genetic expression of LC3, autophagy-related gene (ATG)3, ATG5, ATG7, ATG13 or ELAV-like RNA-binding protein 1 (ELAVL1/HuR) (24, 25). Furthermore, the strategy of suppressing ferroptosis from the perspective of upregulating iron storage can be achieved by poly (RC)- binding proteins (PCBPs) and ferritin mitochondrial (FTMT). PCBPs acting as iron chaperones can deliver $Fe2^+$ to ferritin, thereby limiting ferroptosis (26). Similarly, when the principal iron storage protein in mitochondria, FTMT, is upregulated, ferroptosis induced by erastin can be inhibited (27).

2.1.2 The role of selective autophagy in modulating lipid peroxidation

The selective autophagy plays a crucial role in modulating lipid peroxidation. Thereof, lipophagy and clockophagy have a tight relationship with free lipid accumulation. Mitophagy and chaperon-mediated autophagy (CMA) are respectively responsible for impaired oxidative phosphorylation and lipid ROS accumulation.

Lipophagy can decompose lipid droplets (LDs) which are necessary for cells to resist oxidative stress. Lipid peroxidation has been proved to be induced by polyunsaturated fatty acids (PUFAs) which can be transported into their center along with the formation of LDs (Figure 1C) (28).

Hence, when lipophagy is initiated and enhanced, lipid peroxidation can be triggered due to the increased PUFAs and result in subsequent ferroptosis. Furthermore, ferroptosis promoted by lipophagy can be suppressed after the knockdown of Rab7a member RAS oncogene family (RAB7A) *in vitro* (29).

Compared to the direct relation between lipophagy and free lipid accumulation, the mechanism of clockophagy regulating ferroptosis presents complex. Aryl hydrocarbon receptor nuclear translocator-like (ARNTL/BMAL1) as the center circadian clock protein can be degraded by clockophagy and result in negative modulation of the transcription factor hypoxia-inducible factor 1

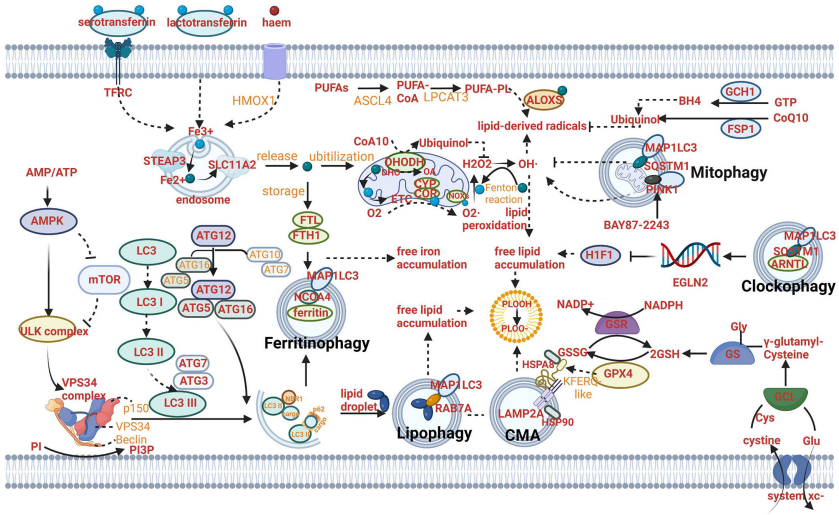

FIGURE 1
Mechanism of autophagy-dependent ferroptosis. **(A)** The mechanism of autophagy: AMPK can activate ULK complex to induce VPS34 complex and suppress the activity of mTOR and ULK complex. The autophagosome (AP) formation depends on LC3 lipidation that LC3 is cleaved into the soluble form LC3I acting as a precursor to LC3II. These receptors play a central role in the selective recruitment of specific cargoes with ubiquitin labeling during autophagy. **(B)** The mechanism of ferritinophagy: Fe^{2+} can be exported as ferritin through exosomes. NCOA4-mediated ferritinophagy (namely, the autophagic degradation of ferritin) promotes ferroptosis by increasing intracellular iron (Fe^{2+}) levels. **(C)** The mechanism of lipophagy: Lipophagy (namely, the autophagic degradation of lipid droplets) increases the levels of free fatty acids available for subsequent lipid peroxidation during ferroptosis. **(D)** The mechanism of CMA: Chaperone-mediated autophagy is involved in GPX4 degradation for ferroptosis. **(E)** The mechanism of mitophagy: Mitophagy (the autophagic degradation of mitochondria) has a dual role in ferroptosis. **(F)** The mechanism of clockophagy: Sequestosome 1-mediated degradation of ARNTL by autophagy (a process termed clockophagy) regulates HIF1α, facilitating ferroptosis. **(G)** The mechanism of ferroptosis: The cystine/glutamate transporter (also known as system xc^-) imports cystine into cells with a 1:1 counter-transport of glutamate. Once in cells, cystine (Cys_2) can be oxidized to cysteine (Cys), which is used to synthesize glutathione (GSH) in a reaction catalysed by glutamate–cysteine ligase (GCL) and glutathione synthetase (GSS). By using GSH as a reducing cofactor, glutathione peroxidase GPX4 is capable of reducing lipid hydroperoxides to lipid alcohols. The GSH–GPX4 antioxidation system has an important role in protecting cells from ferroptosis. The AIFM2–CoQ10, ESCRT-III membrane repair and GCH1–BH_4 systems can also inhibit ferroptosis. Several proteins (including serotransferrin, transferrin receptor (TFRC), solute carrier family 40 member 1 (SLC40A1), ferritin components (FTH1 and FTL), nuclear receptor co-activator 4 (NCOA4) and prominin 2) control ferroptosis through the regulation of iron metabolism. Acetyl-CoA carboxylase (ACAC)-mediated fatty acid synthesis or lipophagy-mediated fatty acid release induces the accumulation of intracellular free fatty acids, which fuels ferroptosis. Long-chain fatty acid–CoA ligase 4 (ACSL4) and lysophospholipid acyltransferase 5 (LPCAT3) promote the incorporation of polyunsaturated fatty acids (PUFAs) into phospholipids to form polyunsaturated fatty acid-containing phospholipids (PUFA–PLs), which are vulnerable to free radical-initiated oxidation mediated by lipoxygenases (ALOXs).

(HIF1) through transcriptionally upregulating the expression of Egl-9 family HIF2, which is responsible for upregulating expression of specific genes involved in regulating the transport and combination of fatty acids and lipids (for example, FABP3 and FABP7). When HIF1 is deficient, downregulation of these proteins produced by the aforementioned specific genes can stimulate ferroptosis by preventing the combination of lipids and fatty acids and their transportation from the plasma membrane to mitochondria, and promoting their peroxidation (30). Sequestosome 1 (SQSTM1/P62) as the autophagy receptor for clockophagy mediates ARNTL degradation and promotes ferroptosis (Figure 1F) (30).

The effect of CMA on lipid peroxidation centers on the function of degradation of the antioxidant defense systems. In addition, CMA can provide a pathway to degrade various proteins from the cytoplasm in lysosomes directly (31). All pathways begin with a combination of heat shock protein family A (Hsp70) member 8 (HSPA8/HSC70) and proteins with a KFERQ-like motif (Figure 1D). Then the lysosomes can degrade these specific proteins with the particular motif through the recognition of the lysosome-associated membrane protein type 2A (LAMP2A). A key enzyme of the antioxidant defense systems called glutathione peroxidase 4 (GPX4) in ferroptosis is a protein containing KEFRQ-like motif. It has been proven to be degraded by HSP90-mediated CMA during erastin-induced ferroptosis. 2-amino-5-chloro-N,3-dimethylbenzamide (CDDO) can block the combination between HSP90 and LAMP2A. Therefore, when erastin-induced ferroptosis occurs, CDDO can suppress the progress by preventing the degradation of GPX4 mediated by CMA (32). GPX4 plays a principal role in maintaining the intracellular antioxidant environment according to reducing phospholipid hydroperoxide production (AA/AdA-PE-OOH) (which is the immediate cause of lipid peroxidation and ferroptosis) to the corresponding phospholipid alcohol (PLOH). The activity or expression of GPX4 is affected by GSH and selenium (33, 34). When GPX is synthesized, selenium can replace the sulfur of cysteine (amino acid of an emerging polypeptide chain) and involve in the generation of selenocysteine (Sec) due to the stop codon UGA "recoded" by a selenocysteine insertion sequence (SECIS). The anti-ferroptotic activity of GPX4 can be enhanced through a selenocysteine residue at 46 (U46) (33). In the catalytic cycle of GPX4, GSH can reduce the selenic acid (-SeOH) to the

intermediate selenide disulfide (-Se-SG). Finally, the second GSH can activate GPX4, and glutathione disulfide (GS-SG) can be released (Figure 1G). The synthetic reaction of GSH originates from system xc^-, the cystine/glutamate transporter (Figure 1G). The transporter can import cystine into cells and meanwhile transport the same quantities of glutamate out of cells. System xc^- is composed of SLC3A2 and SLC7A11 (Figure 1G). Like CMA degrading GPX4, the whole antioxidant system can be the target for the modulation of ferroptosis. For example, the activity of SCL7A11 can be inhibited by AMPK-mediated BECN1 phosphorylation, hence promoting ferroptosis and meanwhile inducing the progress of autophagy (24, 35). BECN1 mRNA can be stabilized by m6A modification. Furthermore, the role of YTHDF1 has been identified as a key m6A reader protein for BECN1 mRNA stability and therefore proved to activate autophagy *via* recognizing the m6A binding site within BECN1 coding regions and regulate ferroptosis (36). Besides, a CD44 variant (CD44v) can promote GSH synthesis by the interaction with system xc^- and stabilize system xc^- expression (37). The synthesis reaction of GSH can be catalyzed by glutamate-cysteine ligase (GCL) and glutathione synthetase (GSS) when the cystine oxidized to cysteine (Cys) or by cystathionine beta-synthase through a trans-sulfuration pathway which can be negatively regulated by *CARS1* (the important member from the aminoacyl-tRNA synthetase family) (38, 39).

Mitophagy can regulate lipid peroxidation through modulating the function of mitochondria. Most cellular ROS derives from mitochondria. ROS includes a series of byproducts of aerobic metabolism such as hydroxyl radicals (•OH), superoxide anion (O2•–), singlet oxygen (1O2) and hydrogen peroxide (H2O2). On one hand, mitophagy can selectively degrade mitochondria to clear dysfunctional organelles and decrease levels of ROS, therefore, preventing ferroptosis from the perspective of lipid peroxidation prevention. Until now, the identified cargo receptors that take part in mitophagy included CALCOCO2, OPTN, SQSTM1,TAX1BP1 and others (40). Mitochondrial ROS is important for both autophagy and ferroptosis induction, although the molecular switches which can determine the bifurcation between these two different types of RCD remain elusive (41–43). On the other hand, mitophagy can promote ferroptotic death by a mitochondrial complex I inhibitor (BAY87-2243) or heme oxygenase 1 (HMOX1). Inhibition of complex I of the mitochondrial respiratory chain can depolarize the mitochondrial membrane potential, mitophagy stimulation, ROS increase and cellular ferroptotic death (44). HMOX1 can mediate redox regulation of ferroptosis with enhanced endoplasmic reticulum (ER) stress and mitophagy (Figure 1E) (45).

The role of autophagy in modulating the absorption, utilization and export of iron is still under exploration. For example, the autophagic degradation of transferrin receptor (TFRC) (which can combine with transferrin and release iron [Fe^{2+}] from transferrin into the cytoplasm through solute carrier family 11 member 2 [SLC11A2]) has been proven to be impaired due to WDR45 mutation and promote ferroptosis (Figure 1G) (46).

2.2 The role of non-selective autophagy in ferroptosis

2.2.1 The role of non-selective autophagy in regulating the level of iron

Iron export as the connection between non-selective autophagy and ferroptosis provided various molecular targets. Fe^{2+} can be exported as ferritin through exosomes, or by SLC40A1 in the cell membrane. Furthermore, the overexpression of SLC40A1 has been proven to activate the autophagy flux *via* AMPK/mTOR/ULK1 and AMPK/ULK1 signaling pathways to meet the energy requirements of cell and decrease the ratio of AMP : ATP (47). The regulatory network of iron export affecting the progress of ferroptosis and the AMP : ATP ratio affecting the progress of autophagy has been crosslinked and the key molecule SLC40A1 may become a critical target for regulating both ferroptosis and autophagy (Figure 2A).

2.2.2 The role of non-selective autophagy in modulating lipid peroxidation

The role of autophagy in modulating lipid peroxidation needs to be further explored from the perspective of regulating the biosynthesis of PUFAs (the substrate of the reaction catalyzed by acyl-CoA synthetase long-chain family member4 [ACSL4] and lysophospholipid acyltransferase-3 [LPCAT3]). AMPK regulation of ferroptosis has been proven to play a critical role in PUFAs biosynthesis and phosphorylation of acyl-CoA carboxylase with the analysis of functional and lipidomic (43). Both the progress of iron export and lipid biosynthesis have a tight connection with AMPK which is also the principal enzyme to stimulate the ULK complex. Doxorubicin (Dox) cardiotoxicity- induced ferroptosis can be alleviated by epigallocatechin-3-gallate due to the upregulation and activation of AMP-activated protein kinase α2 (48). The underlying mechanism can link the increased energy supply to the modulation of ferroptosis. PUFA-PLs catalyzed by ASCL4 and LPCAT3 can be further oxidized by multiple oxygenases, for example, CYP/CYP450, PTGS/COX (prostaglandin-endoperoxide synthase), and ALOXs to produce the hydroperoxides AA-PE-OOH or AdA-PE-OOH which result in the immediate cause of lipid peroxidation (Figure 1G). ALOXs are nonheme iron dioxygenases and have 6 subtypes in humans, namely ALOX12 (arachidonate 12- lipoxygenase, 12S type), ALOX12B (arachidonate 12- lipoxygenase, 12 R type), ALOX15, ALOX15B (arachidonate 15-lipoxygenase type B), ALOX5 (arachidonate 5-lipoxygenase)and ALOXE3 (arachidonate lipoxygenase 3) (49).

Lipid peroxidation can also be mediated in a non-enzymatic manner through the Fenton reaction in which $Fe2^+$ reacts with H2O2 to generate $Fe3^+$, HO·, and OH-. The membrane lipids can be oxidized by these free radical ions (Figure 1G). Both the generator of ROS through the Fenton reaction and several heme or nonheme iron-containing enzymes have a close relationship with iron accumulation. Therefore, the role of autophagy in modulating the absorption, utilization and export of iron may be recognized from the perspective of affecting the process of lipid peroxidation.

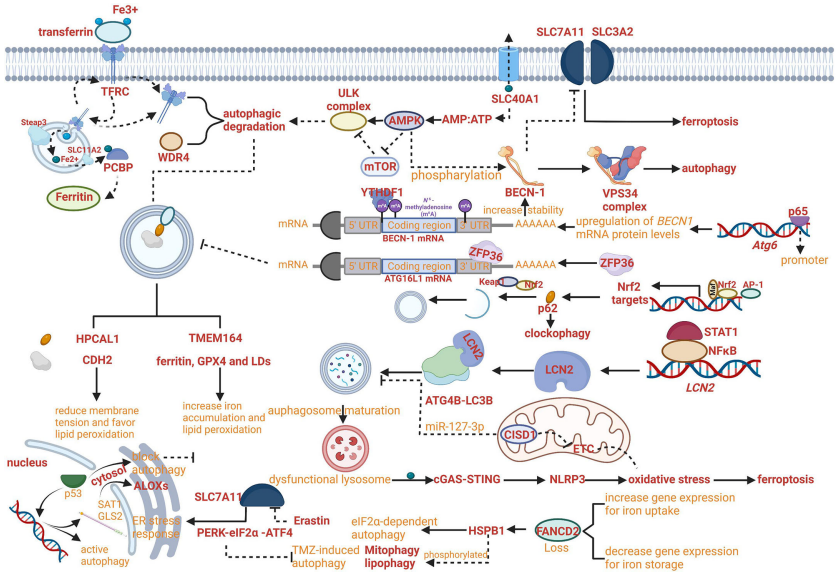

FIGURE 2
Crosslinks between ferroptosis and autophagy. **(A)** The regulatory network of iron export affecting the progress of ferroptosis and the AMP : ATP ratio affecting the progress of autophagy has been crosslinked. **(B)** NF-κB family member p65/RelA can increase autophagy coupled with upregulating levels of *BECN1* mRNA and protein. **(C)** RNA-binding protein ZFP36/TTP can inhibit autophagy activation by destabilizing autophagy related 16 like 1 (ATG16L1) mRNA. **(D)** The Keap1-Nrf2 system has been proven to involve in the phosphorylation of p62 on the cargo. **(E)** Increased lipocalin 2 (LCN2) can reduce autophagy flux by regulating ATG4B activity and LC3-II lipidation and activate inflammasome-ferroptosis processes. **(F)** HSPB1 disrupts STAT3/PKR complex, facilitates PKR-dependent eIF2α phosphorylation and activates eIF2α-dependent autophagy. **(G)** Erastin-induced ferroptosis can promote the activation of the endoplasmic reticulum (ER) stress response that is regulated by PERK-eIF2α (eukaryotic initiation factor 2α)-ATF4 (activating transcription factor 4) pathway which can inhibit TMZ-induced autophagy. **(H)** HPCAL1 as an autophagy receptor for the selective degradation of cadherin 2 (CDH2) can increase susceptibility to ferroptosis.

2.3 The novel and comprehensive role of autophagy in ferroptosis

The growing evidence proved that the role of autophagy in ferroptosis regulation was not limited exclusively to aforementioned mechanism. For example, the novel regulation mechanism can be based on reducing membrane tension facilitated by hippocalcin like 1 (HPCAL1). The autophagy receptor for the selective degradation of cadherin 2 (CDH2) can reduce membrane tension and favor lipid peroxidation (Fenton reaction) to increase susceptibility to ferroptosis (Figure 2H) (50). In addition, increased lipocalin 2 (LCN2) can reduce autophagy flux by regulating ATG4B activity and LC3-II lipidation and activate inflammasome-ferroptosis processes (Figure 2E) (51).

With the development of research, the increasing roles of autophagy have been reported to be comprehensive with multiple crosslinked mechanisms for regulating ferroptosis. For example, TMEM164- mediated autophagy can increase iron accumulation and lipid peroxidation by degrading ferritin, GPX4 and LDs (52). Insufficient cellular autophagy can turn off antioxidant defense mediated by nuclear factor NF-E2-related factor (Nrf2) while initiating Nrf2-induced iron accumulation and lipid peroxidation, resulting in the advancement of ferroptosis. The Keap1-Nrf2 system has been proven to involve in the phosphorylation of p62 on the cargo, which can regulate clockophagy to affect the process of ferroptosis (Figure 2D) (53). However, the relevant signaling pathways need to be further explored (54).

Meanwhile, the regulatory network of autophagy-dependent ferroptosis was enriched. For example, RNA-binding protein ZFP36/TTP can inhibit autophagy activation by destabilizing autophagy related 16 like 1 (ATG16L1) mRNA *via* binding to the AU-rich elements (AREs) within the 3′-untranslated region. The downregulation of ZFP36 can activate ferritinophagy and induce ferroptosis by regulating the signaling pathway of autophagy (Figure 2C) (55).

3 The role of ferroptosis in autophagy

Autophagy is a dynamic process relying on the maturation and formation of specific membrane structures including phagophores, APs, and ALs, which can be generated from the plasma membrane, Golgi complex, recycling endosomes and the ER mitochondria-ER-associated membrane (56, 57). Mechanistically, ATG proteins play an indispensable role in the regulation of autophagy concerning initiation, progression and maintenance. Genetic screens in yeast have identified over 40 ATG genes regulating the expression of ATG proteins which can interact with other factors by multiple posttranslational modifications (58). The phagophore and AP formation can be governed by the joint influence of both ATG proteins and other factors. It has been proved that synaptosome-associated protein29 (SNAP29), the homotypic fusion and vacuole protein sorting (HOPS) complex, vesicle-associated membrane protein 8(VAMP8), regulatory lipids, certain cytoskeleton motor

proteins, syntaxin 17 (STX17) are involved in the formation of AL (59).

Although the direct evidence supporting the critical role of ferroptosis in autophagy is limited, the hypothesis that ferroptosis can regulate autophagy has been confirmed gradually based on the molecular connection between ferroptosis and autophagy. Indeed, erastin-induced ferroptosis can promote the activation of the endoplasmic reticulum (ER) stress response that is regulated by PERK-eIF2α (eukaryotic initiation factor 2α)-ATF4 (activating transcription factor 4) pathway which can inhibit TMZ-induced autophagy (Figure 2G) (60, 61). Besides, it has been reported that the process of protective autophagy can be induced by iron deprivation with antitumor drugs, which can also be reversed by ferric ammonium citrate (FAC) through iron supplementation (62).

The regulation of autophagy may have a tight connection with ferroptosis in the context of inducing different immune and inflammatory reactions, increasing lipid peroxidation or ROS products (which may impair the function of lysosome to suppress autophagy or induce the damage of mitochondria to initiate the subsequent onset of autophagy), and affecting the common signal transduction pathways.

For example, the lipid peroxidation product 4HNE as a pro-inflammatory mediator can activate the nuclear factor-κB (NF-κB) pathway which is a crucial regulator in the context of monocyte-to-macrophage differentiation through autophagy (63, 64). In the promoter of the human *BECN1*autophagic gene (*Atg6*), a conserved NF-κB binding site has been found. Therefore, the NF-κB family member p65/RelA can increase autophagy coupled with upregulating levels of *BECN1* mRNA and protein in different cellular systems (Figure 2B) (65). Meanwhile, the NF-κB pathway can be activated by a pattern-recognition receptor, advanced glycosylation end-product-specific receptor(AGER/RAGE), in peripheral macrophages by HMGB1 (a typical DAMP participating in multiple types of cell death released by ferroptotic cells) (66, 67). DAMPs such as HMGB1 result in chemotherapy resistance coupled with the upregulation of autophagy (68).

The common signal molecules or pathways also play a critical role in the crosslinks between ferroptosis and autophagy. For example, in the cytosol, p53 can block autophagy in a transcription-independent manner, whereas in the nucleus, p53 can activate autophagy in a transcription-dependent way (69). Meanwhile, nuclear p53 can accelerate the expression of glutaminase 2 (GLS2) and spermidine/spermine N1-acetyltransferase 1 (SAT1) which can induce lipid peroxidation through ALOXs (70). Furthermore, the activity and expression of SLC7A11 can be negatively regulated by p53 resulting in ferroptosis, whereas p53 has been proved to antagonize ferroptosis by the formation of the dipeptidyl-peptidase-4 (DPP4)-p53 complex (71, 72). When the ability of DPP4 to form NADPH oxidase 1 (NOX1) complexes with NOX1 in the nucleus is blocked, ROS production can be reduced and ferroptosis can be inhibited (73). p53-mediated ferroptosis can be upregulated by acetylation of p53 (74). However, the induction of p53 deacetylation, due to either the activation of the deacetylase Sirtuin 1 (Sirt1) or the mutation of the acetylated lysine site in p52 can promote autophagy (75).

Another critical crosslinked signaling pathway was STAT3/Nrf2/GPX4. On one hand, impairing STAT3/Nrf2/GPX4 signaling pathway can reactivate ferroptosis, which can be used to attenuate drug resistance (76). On the other hand, cytoplasmic STAT3 can suppress autophagy through binding to protein kinase B (PKB) (the inhibition of PKB/Akt can be induced by the activation of mTORC1 and result in the inhibition of autophagy), in turn, promote mitochondrial localization of STAT3 and its phosphorylation induced by IL-6 (77, 78).

Some crucial crosslinked molecules have been explored to find the connection between ferroptosis and autophagy. The mitochondrial protein, CDGSH iron sulfur domain 1 (CISD1, also called mitoNEET) can mediate the crosstalk between oxidative stress and mitochondrial iron uptake in the outer membrane of mitochondria. The expression of CISD1 has a tight connection with both autophagy and ferroptosis. The overexpression of CISD1 can effectively inhibit autophagic cell death, which can be modulated by a specific regulator miR-127-3p (79–81). In addition to regulating autophagy, overexpression of CISD1 can also limit ferroptosis by a guard against lipid peroxidation induced by ROS from mitochondria (82).

Besides, heat shock protein family B (small) member 1 (HSPB1, also called HSP27 in humans or HSP25 in mice) was confirmed to be central in regulation of autophagy and ferroptosis, which is a molecular chaperone with a function in counteracting protein misfolding and aggregation. The mutations in *Hspb1/HSP25*, both targeting its catalytic alpha-crystallin domain and the C-terminus, can downregulate autophagy levels (83). In detail, HSPB1 disrupts STAT3/PKR complex, facilitates PKR-dependent eIF2α phosphorylation and activates eIF2α-dependent autophagy (Figure 2F) (84).The phosphorylated HSPB1 involves in mitophagy and lipophagy (85, 86). It has also been found that phosphorylated HSPB1 induced by erastin can block cytoskeleton-mediated iron uptake and subsequent lipid peroxidation under ferroptosis (Figure 2F) (87). Previous studies have confirmed that the expression of HSBP1 can be upregulated with the loss of FANCD2 which is the central protein of the Fanconi anemia (FA) pathway (88). In addition, loss of FANCD2 is also closely related to increased gene expression for iron uptake (such as transferrin and transferrin receptor) and decreased gene expression for iron storage (such as FTH) and iron export (such as hepcidin antimicrobial peptide) in ferroptosis (89). Meanwhile, FANCD2-deficient cells have been proven to behave hypersensitive to oxidative stress and impaired autophagy leading to DNA crosses links (90).

Another principal crosslinked target called NEDD4 (neural precursor cell expressed developmentally down-regulated protein 4) is a member of the HECT E3 ubiquitin ligases, which is closely related to the mTOR signaling pathway and promotes autophagy (91). Meanwhile, NEDD4 can also regulate oxidative damage and iron metabolism by the degradation of voltage-dependent anion channels (VDAC) (which can mediate the transport of ions and metabolites in eukaryotic cells across the outer membrane of mitochondria) and lactotransferrin (LTF) (that can specifically bind and transport iron) (92, 93).

4 The crosslinks between ferroptosis and autophagy in asthma

Both autophagy and ferroptosis are involved in various diseases, and crosslinks between autophagy and ferroptosis in various diseases have been emerging. Autophagy and ferroptosis can be initiated as a defense against varieties of intra- and extra-cellular stress stimuli, which can be achieved in large part through a synergistic immune response. The immune response can lead to alterations of multiple signal molecules which may induce a new round of ferroptosis or autophagy of various cells. The crosslinked intra- and extra- signal molecules or pathways affect the function of leukocytic or non-leukocytic cells and influence the progress of various diseases. The deepened cognition of the role of crosslinks between ferroptosis and autophagy in diseases may provide new targets for therapy, novel signal pathways associated with the pathogenesis of the disease, innovative paradigms to recognize and regulate the immune and inflammatory reactions and in general therapeutic benefits for patients.

Although the links between asthma and ferroptosis or autophagy have been confirmed, the role of crosslinks between these two forms of RCD remains unclear. In the latter section, we demonstrate recent advances in the evolving comprehension of the interface between autophagy, ferroptosis and asthma from the perspective of functional cells involved in the pathogenesis of asthma. We discuss how the crosslinked signal pathways in immune or non-immune cells affect the pathogenesis of asthma, how these two forms of RCD reciprocally induce the occurrence of each other through immune and inflammatory signals, how emerging concepts about the crosslinks between ferroptosis and autphagy reshape our understanding of immunity and asthma.

IL-13 can increase LC3II expression and then induce autophagy. Meanwhile, IL-13 can induce ferroptosis. IL-33 can activate autophagy through the inhibition of mTORC1. Autophagy can decrease the level of p62 and increase secretion of IL-18.

4.1 The crosslinks and HAECs

HAECs can promote the regeneration of tissues and protect the body from stimuli, allergens and pathogens by releasing inflammatory response mediators and cytokines such as thymic stromal lymphopoietin (TSLP) and chemokine (C-X-C motif) ligand (CXCL)-8, CXCL1, IL-25, IL-33 and activating innate and adaptive immune systems. The various allergens and proteases can induce the expression of the epithelial cytokines and then promote Th2 immunity by activating conventional dendritic cells (cDCs) and by activating innate lymphoid type-2 (ILC2) cells and basophils that could efficiently polarize IL-4 and/or IL-13 for promoting Th2 immunity and decreasing tolerance to inhaled allergens (94–98). In ongoing asthma, HAECS continue to fuel inflammation in the airway by activating incoming monocytes to adopt an immunogenic phenotype and by generating cytokines and chemokines to activate neutrophils, eosinophils, and other cells of the innate immune system (Figure 3) (99). Epithelial cells also substantially contribute to airway remodeling by releasing repair cytokines along with the repeated cycles of injury and repair (100).

The upregulation of IL-13 can not only increase autophagic flux (that can be prevented by *Atg5* knockdown) and expression of LC3-II in order to induce autophagy and then stimulate goblet cell formation and MUC5AC secretion from HAECs (Figure 4), but also promote the occurrence of ferroptosis by upregulating the expression of ALOXs such as ALOX5 and ALOX15 (Figure 4) (101, 102). When blocking autophagy in HAECs, the generation of ROS can be inhibited through the activation of the NADPH oxidase DUOX1 (103). The suppression of ROS production can also negatively regulate the process of ferroptosis. NOD-like receptor

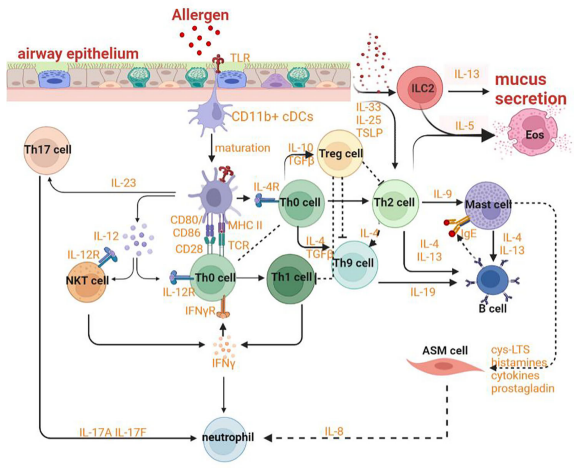

FIGURE 3
Mechanism of asthma.

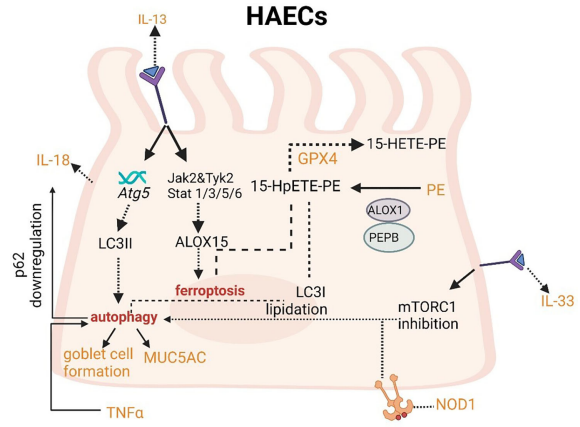

FIGURE 4
Crosslinks between ferroptosis and autophagy in HAECs.

(NLRs) signaling pathway mediated activation of HAECs interacting with eosinophils, which may trigger allergic asthma (104). Nucleotide-binding oligomerization domain-containing protein 1 (NOD1) and NOD2 that can initiate NF-κB-dependent and mitogen-activated protein kinase (MAPK)-dependent gene transcription are crucial for innate immune responses (105). NOD1 agonists have been proven to induce autophagy in HAECs and the activation of NOD1 can increase the levels of GPX4 and other iron and ferroptosis regulatory proteins in macrophages (106, 107). Cellular ferroptotic death has been proven to be more likely to trigger inflammatory signal molecules than apoptotic death by the less effective macrophages (108). TNFα as a critical pro-inflammatory cytokine produced by macrophages in the airway lumen and bronchial mucosa can promote the initiation of the HAECs autophagy (109). Autophagy in HAECs can decrease the level of p62 the autophagy receptor for clockophagy and downregulate the level of ferroptosis, which has a tight connection with increased secretion of IL-18 (Figure 4) (110). Inflammatory response mediators and cytokines released by HAECs can activate the innate and adaptive immune systems such as chemokine (C-X-C motif) ligand (CXCL)-8, CXCL1, thymic stromal lymphopoietin (TSLP), IL-33, and IL-25. Thereof, IL-33 can activate autophagy through the inhibition of mTORC1 and be inhibited by *LC3B* knockdown (Figure 4) (111).

In mature DC, ATG5 and MAP1LC3B involve in the regulation of TLR stimulation. ATG7 involves the regulation of the STING signal pathway which can promote autophagy through the lipidation of MAP1LC3. The signal pathway of TLR4 can induce NF-κB–dependent proinflammatory cytokines. When TLR4 binds to NOX4 or its isoenzymes, ferroptosis would be induced. HMGB1 can promote autophagy by releasing the basic autophagic gene Beclin 1. CMA contributed to the antigen-presenting process through overexpression of LAMP2A.

In T cells, Beclin1 has been shown to negatively modulate the generation of Th2 cytokines IL-5 and IL-13 and upregulate the production of IL-17 and IFN-γ by co-culturing $CD4^+$ T cells. After being activated by TCR/CD28 co-stimulation, Treg cells can induce the expression of GPX4. $CD8^+$ T cells can induce ferroptosis of surrounding macrophages and other activated immune cells to accelerate inflammation through IFN-γ which can down-regulate the expression of SLC7A11 and SLC3A2.

4.2 The crosslinks and antigen-presenting cells in the innate immune system

The interaction between epithelial cells and DCs plays an indispensable role in sensitization to allergens and the advancement of asthma. Both HAECs and lung cDCs can express pattern-recognition receptors and can be directly activated by allergens (112). $CD11b^+$ cDCs can maturate and migrate depending on the transcription factor IRF4 with the effect of danger signals and 'instructive' cytokines produced by HAECs (Figure 3) (113). After stimulation by ILC2 cells secreting IL-13, these cells then would induce Th2 and Th17 responses in draining mediastinal lymph nodes (114). With the help of basophils, DCs can sustain Th2 responses in the lymph nodes. When the lung is exposed to allergens repeatedly, $CD11c^{hi}$ DCs will actively participate in the TH2 effector phase of asthma (115). After being stimulated by allergens, effector Th2 cells could be recruited by CCL22 and CCL17 produced by macrophages and/or $CD11c^{hi}$ monocytic DCs with poor migration capability (115). Poorly migratory $CD11c^{hi}$ monocytic DCs have some similar features as macrophages, for example, the ability to express FcεRI and CD64 (115).

The crosslinks between ferroptosis and autophagy can affect DCs in the context of functional maturation, migration, antigen presentation, and MHC-II presentation of extracellular (phagocytosed) antigens. DCs endure two opposite functional and phenotypic states of maturation. The maturation from a tolerogenic state to the activated one occurs with the help of pathogen-associated molecular patterns (PAMPs), the most characterized type of TLRs. ATG5 and MAP1LC3B regulate TLR stimulation to promote the maturation of DCs (Figure 5) (116). Both two autophagy proteins also involve in TLR4-mediated responses in DCs. The signal pathway of TLR4 can promote the innate immune responses by inducing NF-κB–dependent proinflammatory cytokines after activated by adaptor MYD88 or by accelerating the generation of type I IFN after activated by the adaptor TCR adaptor molecule 1 (TICAM1/TRIF). Furthermore, when TLR4 binds to NOX4 or its isoenzymes, TICAM1 would be activated and ferroptosis would be induced (117). On one hand, autophagy can regulate TLR signaling transduction by acting upstream. On the other hand, autophagy can be modulated by the activation of TLR. For example, the initiation of TLR4 has recently been proven to inhibit autophagy due to the activation of mTORC1 (118). However, the combinatorial initiation of NOD2 and TLR4 has been proven to promote autophagy, indicating that the impact of NOD2 on the regulation of autophagy is predominant over TLR4 initiation (Figure 5) (119). The maturation endows DCs with the migratory capability to activate naïve T cells and promote effector T cell responses in secondary lymphoid tissues. Migration of DCs can also be regulated through autophagy affecting the modulation of their cytoskeleton (120). ATG7 and ATG16L can regulate the

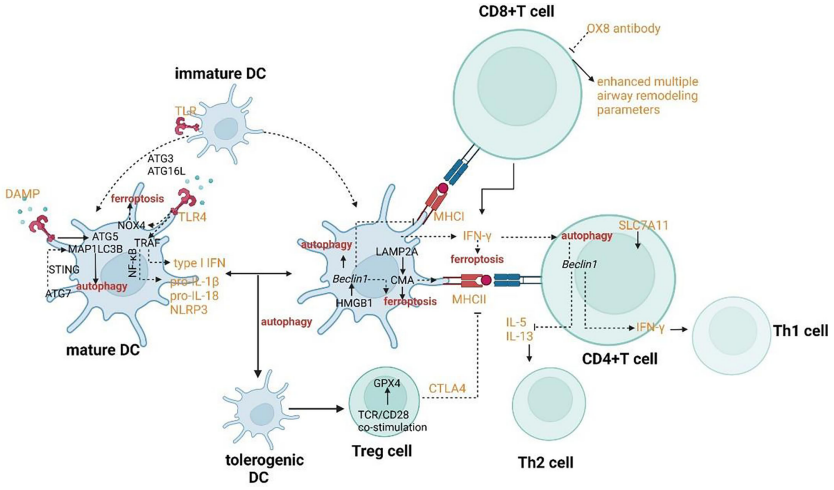

FIGURE 5
Crosslinks between ferroptosis and autophagy in dendritic cells and T cells.

recruitment and migration of CDs to promote their communication with lymphocytes and to coordinate the adaptive immune responses. ATG7 also involves IFN-α secretion by DCs. It has been confirmed that the induction of IFN-αwas facilitated by the cGAS-STING signal pathway (121–123). Hence, it can be concluded that ATG7 involves the regulation of the STING signal pathway which can promote autophagy through the lipidation of MAP1LC3 (Figure 5). Furthermore, the release of 8-OHG from ferroptotic cells can co-activate the STING1-dependent inflammatory pathway (124).

The typical function of DCs as antigen-presenting cells is to internalize antigens and present antigen-derived peptides to T cells. The exogenous and endogenous can be presented by DCs to $CD4^+$ T and $CD8^+$ T cells by MHC class II and class I, respectively. MHC-I can present the extracellular proteins by a process called cross-presentation. CMA has been proved to contribute to the antigen-presenting process by mediating the translocation of substrates across the lysosomal/late endosomal membrane during CMA through overexpression of LAMP2A (Figure 5) (125). Therefore, the process of antigen presentation involved with CMA may also result in the ferroptosis of DCs. When DCs exposed to the ferroptotic cells, the antigen processing and presentation by DCs may reduce (126). In process of MHC class II-restricted antigen presentation, the cytosol galectin 8 can directly recruit the macroautophagic machinery for lysosome degradation of the damaged endosome and the ubiquitinated endosome cargo can recruit the LC3 anchor proteins such as p62 for targeting to APs (127–129). The signal pathway of autophagy-dependent ferroptosis is also involved in extracellular antigen processing for MHC-I presentation. Some specific types of allergen can be surrounded by IFN-γ collaboration with autophagy proteins such as ATG3, ATG5, ATG7 and ATG16L1 so that the vacuolar membrane can be broken and the allergen can be exposed to the cytosol and degraded successively, possibly by autophagy (130). The exposure results in p62 association with the allergen, which can promote $CD8^+$T-cell responses (131). The lower secretion of IFN-γin DCs may result from haploinsufficiency of an essential protein, Beclin-1 and result in the downregulation of MHC-I presentation and the suppression of system xc^- which can induce ferroptosis (132, 133). In addition to IFN-γ, HGMB1 also plays a crucial role in the coordination of ferroptosis and autophagy in the innate immune system. When mature DCs secrete this leaderless cytokine, T-cell and B-cell responses can be activated (134). Meanwhile, the prototypical DAMP involves the stimulation of inflammatory response in peripheral macrophages by activating AGER/RAGE (67). HMGB1 can also promote autophagy by releasing the basic autophagic gene Beclin 1 from the BCL-2 complex (Figure 5) (86).

The polarization of macrophages has been shown to contribute to the pathogenesis of asthma. Typically, macrophages can be polarized into the M1 phenotype with increased cellular immunity and pro-inflammatory cytokines production by IFN-γ or LPS and M2 phenotype with increased anti-inflammatory responses to promote tissue repair and humoral immunity (135, 136). Nowadays, the bimodal subdivision has been abandoned in favor of a model of a spectrum of polarization changes in macrophages that better illustrates the great variety in macrophage responses to stimuli (137). The alteration of cellular processes such as efferocytosis, phagocytosis, and (anti-) inflammatory cytokine generation results in the pathology of asthma. The crosslinks between ferroptosis and autophagy provide us with novel targets and new therapeutic strategies by regulating the function and polarization of macrophages. p53 acetylation and ROS production due to iron overload can lead to M1 polarization with the upregulating expression of M1 markers including IL-1β, IL-6, and TNF-α and decreasing levels of M2 markers such as TGM2 (Figure 6) (138, 139). M1 polarization can also be stimulated by the suppression of the mTOR pathway which is the master controller of autophagy (140). NF-κB can be activated after M1 polarization, in fact, the activation of NF-κB is able to drive macrophages to either M1 or M2 polarization (141, 142). NF-κB p65 cytosolic ubiquitination induced by TLR2 signal can result in its degradation by p62-mediated autophagy. The

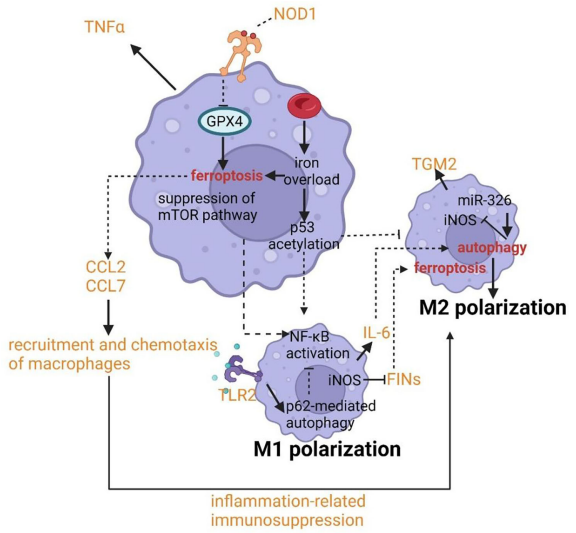

FIGURE 6
Crosslinks between ferroptosis and autophagy in macrophages.

repression of autophagy can rescue the activity of NF-κB and drive macrophages to M2 phenotype (143, 144). Similarly, IL-6 and CCL2 can trigger M2 phenotype by inducing autophagy in macrophages (Figure 6) (145). The chemotaxis and recruitment of macrophages can be assisted by CCL2 and CCL7 regulated by ferroptosis inducing expression of inflammation-related genes (146–148). In addition, along with the occurrence of ferroptotic cellular death, inflammation-related immunosuppression can be formed through macrophage polarization (149). Inducible nitric oxide synthase (iNOS) as the critical marker of macrophage M1/M2 polarization has been uncovered to have a potential relationship with ferroptosis and autophagy. The overexpression of miR-326 can promote autophagy along with the downregulation of iNOS expression (149). And the higher activity and enrichment of iNOS in M1 phagocytes compared to M2 phagocytes confers higher resistance to ferroptosis induced by reagents (150). An important feature of asthma is the altered colonization of microbes resulting from the defective phagocytosis of monocytes and macrophages. Hence both limiting immune activity and defective phagocytosis will promote the development of asthma due to cellular ferroptotic death or defects of LC3-associated phagocytosis (LAP). Unluckily, ferroptosis of macrophages has been proven to be triggered by iron overload when scavenging aged erythrocytes (151). LAP can promote antigen presentation to T cells by MHC-II and help to clear pathogens *via* engulfment and phagosome acidification (152–154). Therefore, the deepened cognition of signal pathways and molecules associated with LAP such as the TLR9 pathway, TRAF3 and IRF7 may provide novel targets for asthmatic therapy.

IL-6 can trigger M2 phenotype by inducing autophagy in macrophages. The chemotaxis and recruitment of macrophages can be assisted by CCL2 and CCL7 regulated by ferroptosis inducing expression of inflammation-related genes. p53 acetylation can lead to M1 polarization with the upregulating expression of M1 markers including IL-1β, IL-6, and TNF-α and decreasing levels of M2 markers such as TGM2.

4.3 The crosslinks and the adaptive immune system

With the deepened research on asthma, the paradigm of cognition on asthma has gradually transformed from a single disease into a syndrome (101, 155). The endotypes which are defined as distinct pathophysiology due to different asthma phenotypes can differ in terms of genetic susceptibility, age of onset, clinical presentation, environmental risk factors, prognosis and response to standard and new therapies (156, 157). The underlying immunological basis of multiple asthma endotypes has a close relationship with the adaptive immune system, especially with T cells. When activated by the innate immune system, $CD4^+$T cells can differentiate into multiple functional subsets of helper T cells such as Th2 cells, Th17 cells, Th1 cells, and Treg cells. Both Th2 cells and ILC2 cells contribute to eosinophilic inflammation by upregulating the expression of GATA-3 which can promote the production of Th2 cytokines, upregulate the expression of chemokine receptors such as CCR4, CCR8 and CRTH2, and increase the production of IL-5 to modulate the development of eosinophils, IL-13 leading to goblet cell metaplasia and bronchial hyperreactivity, IL-4 affecting the mature and activation of Th9 cells which can promote the IgE synthesis by B cells. Both Th1 and Th17 cells can result in neutrophilic inflammation by respectively secreting IFN-γ or TNFαand IL-17A or IL-17F Treg cells, a subset of $CD4^+$ T cells, also originate from Th0 cells and can express transcription factor forkhead box P3 (Foxp3) and IL-2 receptor (CD25) to suppress allergic responses (Figure 3). The fate of follicular helper T cells (TFH) can be adopted by Th cells producing IL-21 so that IgE can be induced by B lymphocytes. DCs can sustain Th2 responses with the help of basophils in lymph nodes. The crosslinks regulation of ferroptosis and autophagy in adaptive immunity including in antigen presentation, mutation and activation of effector cells, and immune signaling regulation may provide us with new modulatory strategies and novel targets to effectively alleviate asthmatic inflammation and symptoms.

The role of ferroptosis and autophagy in antigen presentation of $CD4^+$ T cells can be recognized from MHC class II presentation perspectives, DC-mediated T cell activation, and some key signaling molecule production. MHC class II antigens can derive from both extracellular and intracellular sources. Thereof, autophagy plays an essential role in delivering materials into lysosomes to promote the generation of intracellular sources for MHC class II antigens. In addition, autophagy involves the antigens' capture after their evasion from phagosomes and delivers them into lysosomes to promote $CD4^+$ T cells (158). The formation of AP-like structures has been reported to emanate from MHC class II compartments (MIICs) in DCs, which contain the markers of AP Atg16L1 and LC3 as well as the principal molecular machinery involved in antigen-processing (159). The phagocytosis of macrophages can be

regulated by the iron accumulation, generation of lipid peroxidation and the release of ROS, which means that ferroptosis can modulate the MHC class II antigens production through alteration of the derivation of MHC class II antigens. The production of MHC class II can be downregulated by cytotoxic T lymphocyte antigen 4 (CTLA-4) and other inhibitory molecules secreted by Treg cells. Meanwhile, Treg cells can induce $CD4^+$ T cells to produce anti-inflammatory cytokines such as TGF-β and IL-10 (160). The upregulated amount of $CD4^+CD25^+$Treg cells has been reported in asthmatic patients with corticosteroid therapy (161). Therefore, if the crosslinks between autophagy and ferroptosis can effectively regulate the activity and amount of the inflammatory T cells and anti-inflammatory T cells, the prognosis of asthma may be improved drastically. Much research has been conducted to find the distinguished receptors which may be the potential targets for asthmatic therapy if the effect is poles apart after activated by common signal molecules regulating ferroptosis or/and autophagy on or in different subsets of T cells. In human naive $CD4^+$ T cells, SLC7A11 has been proven to be deficient. However, when $CD4^+$ T cells are activated, the ferroptosis-related protein can be drastically upregulated (162, 163). Autophagy is carried out constitutively to low levels in $CD4^+$ T cells and can be induced following T-cell receptor activation (164). Multiple genetic model systems have been applied to explore the role of the specific expression product in regulating the function and amount of T cells. The levels of autophagy can be upregulated in T cells with a deletion in $Atg5^{-/-}$, $Atg7^{-/-}$, $Atg3^{-/-}$ and $Vps34^{-/-}$ in the lymph nodes (164–168). In autophagy-deficient T cells, ferroptosis may also be easily induced due to the increase in mitochondrial load with enhanced levels of ROS. The reducing extracellular microenvironment is necessary for $CD4^+$ T cells to activate and proliferate from the perspective of the maintenance of intracellular GSH levels. The mechanisms inspire us to modulate the heterogeneity of $CD4^+$T cells or even T cells by the various distribution of sensitivity on the signal molecules of autophagy and ferroptosis in order to generally recover the balance of inflammatory and anti-inflammatory responses.

The activation of T cells has always been the focus for researchers to explore in order to explain the pathogenesis of asthma and find novel targets for treatment. The regulation of Th2 subsets has a tight connection with the function of eosinophils, while the effect on Th1 and Th17 subsets may influence the pathogenesis of neutrophilic inflammation. The activation of Treg cells can also be modulated for anti-inflammation reactions. $CD4^+$ T cells can be activated by DCs through autophagy as judged by their capability to secrete IFN-γ (119). Beclin1 has been shown to negatively modulate the generation of Th2 cytokines IL-5 and IL-13 and upregulate the production of IL-17 and IFN-γ by co-culturing $CD4^+$ T cells (Figure 5) (169). IFN-γ as a critical modulator of autophagy and activation of $CD4^+$ T cells also has the crosstalk with ferroptosis. $CD8^+$ T cells can induce ferroptosis of surrounding macrophages and other activated immune cells to accelerate inflammation through IFN-γ which can down-regulate the expression of SLC7A11 and SLC3A2 (Figure 5) (170). Although our recognition of the potential roles of $CD8^+$ T cells in asthma is still limited, the positive role of $CD8^+$ T cells has been demonstrated. It has been found that rats formerly sensitized and treated with OX8 antibody (which can lead to the consumption of $CD8\alpha^+$ T cells) have enhanced multiple airway remodeling parameters such as mucus production and airway smooth muscle volume, airway inflammation and epithelial cell proliferation (171–173). After being activated by TCR/CD28 co-stimulation, Treg cells can induce the expression of GPX4 (Figure 5) (174, 175). Deletion of GPX4 in Treg cells can result in ferroptosis and the production of IL-1β which can mediate lung neutrophilia and IL-33 expression (174, 175). The activation of Treg cells also has a tight connection with autophagy. Tolerogenic DCs can induce enhanced proliferation of $CD25^+$ $Foxp3^+$ Treg cells. Furthermore, the tolerance to drive the DC phenotype to tolerogenic functions is induced by autophagy (176). TCRγδ$^+$ T cells have been shown to be activated resulting from the improved DC numbers and costimulatory molecule expression in Atg16L1-deficient mice (177). γδ T cells are an important subset of innate-like T cells in asthma. Another subset of this group is called natural killer T (NKT) cells. Regardless of the occurrence of Th2 cells, NKT cells can involve in allergic responses in asthma. Meanwhile, they can accelerate airway hyperresponsiveness (AHR) in the defect of adaptive immune responses, particularly in situations with viral infections or neutrophils (178). γδ T cells have a tight connection with HAECs as an immune surveillance guarder, responding to tissue damage and endogenous stress signals. Hence, a major paradox should focus on the fact that the modulation of T cells with the crosslinks between autophagy and ferroptosis may alleviate the allergic responses for asthmatic patients, while the protection against HAECs may be destroyed further because of the impaired effect of γδ T cells. The research on the signaling pathway which can regulate T cells with inflammation causing the effect but protect the function and integrality of T cells with body protective effect needs to be further explored.

B cells in asthma mainly function as antigen-presenting cells, which are crosslinked by high affinity IgE receptor FcεRI to enhance the activity of basophils and mast cells (Figure 3). Antigen-specific IgE in serum can promote the pathogenesis of asthma by inducing the immediate response of basophils and mast cells. B cells are activated by IL-13 and IL-14 from Th2 cells and basophils, IL-19 from Th19 cells, IL-4 and IL-13 from mast cells. Therefore, the regulation of B cells with respect to their activation or amount can be intervened from the perspective of T cells modulation which both ferroptosis and autophagy have already been shown to involve. Besides, B cells can also promote airway inflammation and induce AHR in the absence of T cells (179). Hence, the role of crosslinks between ferroptosis and autophagy in the direct regulation of B cells is also necessary for asthmatic therapy.

The specific deletion of *Atg5* in B cells has been proved to acquire a deficient transition for these autophagy insufficient B-cell progenitors between pro- and pre-B-cell phases in the bone marrow, indicating the critical role of autophagy in B-cell development (180). In addition to the process of advancement in the center, B cells can also be severely influenced by both ferroptosis and autophagy in the periphery. B cells include two main subgroups. One of them called B1-lymphocytes (B1a and Bib lymphocytes) arising from fetal liver precursors always gather in

peritoneal and pleural cavities as well as mucosal tissues. Another group called B2-lymphocytes (follicular B lymphocytes and marginal zone B (MZB) lymphocytes) derived from precursors in the bone marrow are enriched in secondary lymphoid organs. B1 lymphocytes and MZB always involve in the rapid humoral response to achieve the natural defense, while follicular B lymphocytes play an essential role in response to exogenous antigens. Compared with follicular B cells, MZB cells and B1 cells have a tighter connection with ferroptosis. The enhanced ferroptosis sensitivity and fatty acid uptake resulted from the higher expression of CD36 (the protein in charge of fatty acid transport) lead to the regulators targeting GPX4 easily inducing the activation of maintenance, progression and antibody response of B1 cells and MZB cells (Figure 7) (181). The role of autophagy has been confirmed to be a particular requirement in B1a cells homeostasis (182). Follicular B cells differentiate into plasma cells and memory B cells with high affinity and long life characterized by selection and mutation, through the germinal center (GC) reaction induced by TFH cells. On one hand, plasma cells require autophagy for sustainable immunoglobulin production (182). On the other hand, TFH cells have been reported to present vulnerable to ferroptosis and the selenium-GPX4-ferroptosis axis plays a principal role in the regulation of homeostasis of TFH cells (183).

Effector B cells can be divided into BE1 and BE2 lymphocytes from the perspective of cytokine secretion. Thereof, BE1 lymphocytes can generate IFN-γ to promote the transition between Th0 cells and Th1 cells, while BE2 lymphocytes can produce IL-4 to induce Th0 cells differentiation to Th2. Hence, the regulation of B cells by ferroptosis and autophagy may coordinate the immune system in asthma according to modulating the differentiation of T cells. IL-4 as a cytokine of crucial effector Th2 in allergic asthma can also induce autophagy in B cells dependent on JAK signaling *via* an mTOR-independent, PtdIns3K-dependent pathway, which can aggravate asthma through multiple mechanisms (Figure 7) (184).

Erastin, a ferroptosis activator, has been proven to induce lipid peroxidation to down-regulate members of the bone morphogenetic protein (BMP) family and promote the differentiation of peripheral blood mononuclear cells to B cells (185). This provides us with a direction: can the number of B cells also be regulated, and how can we use this mechanism to control and alter the sensitivity of B cells to autophagy or ferroptosis (maybe facilitating differentiation of B cells to B1 cells for enhancing ferroptosis sensitivity or inducing effector B lymphocytes into BE1 cells to decrease autophagy inducing asthma exacerbation).

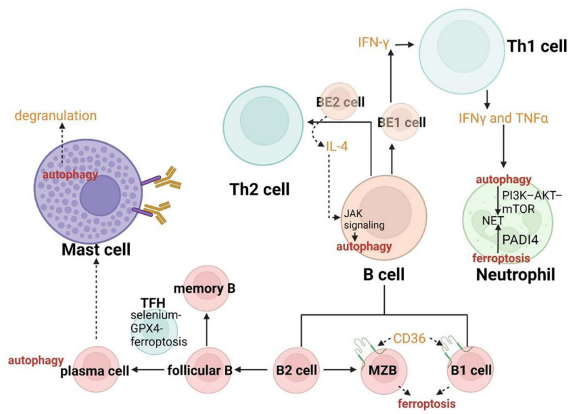

FIGURE 7
Crosslinks between ferroptosis and autophagy in B cells, mast cells and neutrophils.

In B cells, IL-4 can induce autophagy dependent on JAK signaling. The enhanced ferroptosis sensitivity resulted from the higher expression of CD36 lead to the regulators targeting GPX4 easily inducing antibody response of B1 cells and MZB cells.

In neutrophils, NETs formation has a tight connection with peptidyl arginine deiminase 4 (PADI4) and NOX. The PI3K–AKT–mTOR axis is a bridge connecting NET induction and autophagy.

Autophagy plays a critical role in the degranulation of mast cells.

4.4 The crosslinks and other cells

In asthma, varieties of cells directly result in abnormal symptoms and syndromes by inducing pathophysiologic and histopathologic modification. For example, both eosinophils and mast cells can enhance the permeability of blood vessels. Mast cells contribute to airway remodeling and bronchoconstriction. Eosinophils, neutrophils, basophils and mast cells play an essential role in asthmatic inflammation (Figure 3). It is necessary for relieving discomfort and improving prognosis in asthma patients to explore the role of crosslinks between ferroptosis and autophagy plays in these cells.

4.4.1 Eosinophils

Eosinophils play a key role in the eosinophilic inflammatory response. Eosinophils can be recruited to the lung from bone marrow by DCs secreting C-C Motif Chemokine Ligand (CCL)-17 and CCL22. Subsequently, Th2 cells and DCs can be further recruited in asthmatic inflammatory reactions.

The count of eosinophils in BALF positively related with the expression of LC3-II in lung homogenates, indicating that autophagy has a close relationship with the eosinophilic inflammation as well as the severity of asthma. Eosinophilic inflammation has also been shown to alleviate after intranasal treatment with Atg5 shRNA in the context of significantly improved AHR, decreased amount of eosinophils and IL-5 levels in BALF (autophagy can be induced in isolated blood eosinophils in response to IL-5 treatment), and improved histological inflammatory features (186). Meanwhile, eosinophilic inflammation can also be suppressed through ferroptosis-induced agents (FINs) promoting eosinophil death. Furthermore, FIN-induced cellular death can be remarkably attenuated by N-acetylcysteine and GSH (187).

4.4.2 Neutrophils

Neutrophils, as the primary "first line" interaction between primary effector cells and the immune response, gather at the injured position of HEACs from the bone marrow and release

chemokines including CXCL-1 and CXCL-8. Neutrophils can also degrade elastin and type-3 collagen (principal components of extracellular matrix) through secreting elastin and proteinase 3, when activated by Th17 cells or Th1 cells. *Meanwhile*, they can fight against pathogens through phagocytosis, degranulation, and neutrophil extracellular traps (NETs). NETs formation has been proven to be upregulated in asthma and has a tight connection with peptidyl arginine deiminase 4 (PADI4) and NOX (Figure 7) (188, 189). Both ferroptosis and autophagy can affect the formation of NETs. Stage 3 of NET vacuolization can be influenced by autophagy due to the involvement in the externalization of cytosolic and membrane-bound proteins (190, 191). The PI3K–AKT–mTOR axis is a bridge connecting NET induction and autophagy and has a prominent effect on both (Figure 7). Oxidized lipids can promote PADI4-related NETs formation (192). Hence, both autophagy and ferroptosis may control the process of NETs formation to modulate the resistance of neutrophils to pathogens. This idea may efficiently confront the problem of asthmatic therapy, about increasing susceptibility to pathogens due to decreasing anti-inflammatory and antiviral mediators. Autophagy has also been proved to influence the degranulation of neutrophils and ROS production according to NOX and modulate neutrophil-mediated inflammation (193). Ferroptosis may involve the recruitment of neutrophils (194). Therefore, regulation of neutrophilic autophagy and ferroptotic tissue damage may be the approach to alleviate the destruction caused by neutrophilic inflammation (for example cysteinyl leukotrienes [Cys-LTS] and inflammasomes generated by neutrophils can aggravate airway narrowing and promote bronchoconstriction) in asthma.

4.4.3 Mast cells

Mast cells are granulocytic and hematopoietic leukocytes that degranulate to mediate inflammatory responses. In asthma, the activation of mast cells is stimulated by immune or non-immune cells (such as nerve cells) and various cell surface receptors including TLRs, FcεRI receptors, hormone receptors and cytokine receptors. Autophagy plays a critical role in the degranulation of mast cells (Figure 7) (195). If these two forms of RCD can be proved to connect with the regulation of activation of mast cells, it will be reasonable to conclude that the function of mast cells in asthma can be further modulated by ferroptosis and autophagy. The target mutation of GPX4 or GPX4 conditional deletion facilitates instant neuronal death with varieties of ferroptotic characteristics (196). In this way, neuropeptide from nerve cells may be regulated to modulate the activity of mast cells.

When the mechanism of how ferroptosis and autophagy influence the stimulation or dysfunction of the basophils is better known, airway remodeling and asthmatic airway inflammation can be better controlled.

The increased expression of autophagy markers is linked to the increased accumulation of ASM mass. ferroptosis participate in the pathogenesis of airway mass in airway remodeling.

4.4.4 ASM cells

ASM is involved not only in airflow obstruction but also in airway inflammation in asthma. The role of crosslinks between autophagy and ferroptosis in abnormal function (increased contractility/decreased relaxation) of ASM cells or the regulation of the size and number may provide new targets for asthmatic therapy and create the new idea for studying the modulatory network of ASM pathogenesis in asthma. The concomitant expression and association of autophagy with airway modeling have been found. ASM mass is increased in asthma and correlates with poor lung function and increased airway responsiveness to multiple contractile agonists, pollens, allergens and so forth. The increased expression of autophagy markers linked to the increased accumulation of ASM mass confirmed that autophagy plays an indispensable role in airway remodeling (Figure 8) (197). In addition, autophagy has been shown to be a necessary mechanism for changing the phenotype of HAECs to mesenchymal cells (198, 199). In addition to autophagy, ferroptosis may also participate in the pathogenesis of airway mass in airway remodeling with the differentially regulated expression of SCL9A14 and SCL7A11 (Figure 8) (200, 201). Furthermore, key enzymes of PUFAs biosynthesis, the major enzymes correlated with lipid peroxidation and principal proteins related to iron accumulation have been reported to co-express differentially in asthmatic ASM cells (200, 201). Studies of these associated changes may guide us to identify new asthma biomarkers and targets and novel cross-linked regulatory networks to better treat exacerbations of asthma resulting from ASM-inducing airway remodeling, bronchoconstriction and inflammation.

5 Conclusion

Both ferroptosis and autophagy are involved in various diseases. The role of these two forms of RCD in treatment has expanded drastically with novel mechanistic details about the regulation and molecular crosstalk between pathways, and the crosslinked effects with immunity and inflammation, which are all previously viewed as independent emerging as topics of particular interest. In this review, we summarize the mechanism of ferroptosis and autophagy and demonstrate the mutual regulation and influence of both of them. Reliance on the common signal pathways and molecules provides multiple potential therapeutic targets. However, the complicated mechanisms of ferroptosis and autophagy make some conclusions contradictory. For example, in macrophages, the suppression of mTOR pathway can activate NF-κB signal

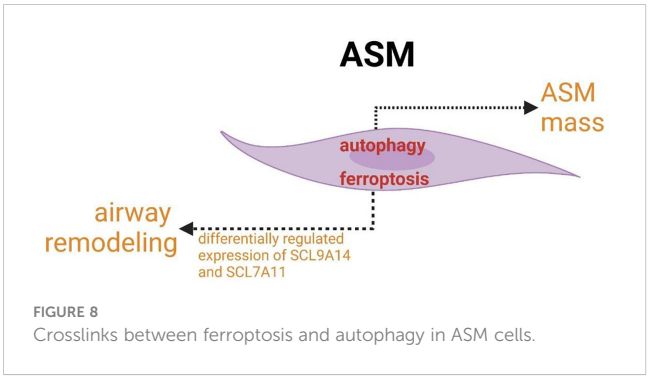

FIGURE 8
Crosslinks between ferroptosis and autophagy in ASM cells.

pathway, which can enhance the progress of autophagy. But the autophagy induced by TLR2 suppressed NF-κB activation. In DCs, IFN-γ may promote inflammation through ferroptosis, however, suppress the generation of inflammatory cytokines through autophagy. These contradictory mechanisms need to be further explored.

In general, for asthma patients, the deepened cognition of common characteristics of ferroptosis and autophagy can be beneficial based on the modulation of target cells or molecules in the direction of equilibrium. This makes it necessary to clarify the exactly crosslinked molecular events and accurate crosslinked effects with the immunity and inflammation, as well as the clarified upstream and downstream mechanisms when autophagy and ferroptosis trigger cell death or we use the crosslinks between ferroptosis and autophagy to implement a therapeutic schedule. Moreover, to improve the prevention, diagnosis, treatment and prognosis of asthma, researchers should explore more about the crosslinks between ferroptosis and autophagy in asthma-related cells and utilize this accumulated knowledge by refining the relationship between immune homeostasis, regulatory mechanisms, inflammation alleviation and symptom relief. If more specific markers of crosslinked pathways can be discovered and relevant key molecular modulators or novel regulatory approaches based on definite mediators performed by immune cells and signals can be confirmed to be effective in asthmatic therapy, the crosslinks between ferroptosis and autophagy and the role in asthma can be further understood, and the regulation of the crosslinked pathways from perspective of cells and molecules will bring the great therapeutic potential for asthma patients.

Author contributions

XL and WT wrote the original draft manuscript. JQ, WW, JD and YW reviewed and edited the manuscript. JD and YW supervised the manuscript. All authors contributed to the article and approved the submitted version.

Funding

This work was supported by grants from the National Natural Science Foundation of China (Grant No. 82174495).

Conflict of interest

The authors declare that the research was conducted in the absence of any commercial or financial relationships that could be construed as a potential conflict of interest.

Publisher's note

References

1. Zheng M, Williams EP, Malireddi RS, Karki R, Banoth B, Burton A, et al. Impaired NLRP3 inflammasome activation/pyroptosis leads to robust inflammatory cell death *via* caspase-8/RIPK3 during coronavirus infection. *J Biol Chem* (2020) 295 (41):14040–52. doi: 10.1074/jbc.RA120.015036

2. Sarhan J, Liu BC, Muendlein HI, Li P, Nilson R, Tang AY, et al. Caspase-8 induces cleavage of gasdermin d to elicit pyroptosis during yersinia infection. *Proc Natl Acad Sci* (2018) 115(46):E10888–E97. doi: 10.1073/pnas.1809548115

3. Malireddi R, Gurung P, Kesavardhana S, Samir P, Burton A, Mummareddy H, et al. Innate immune priming in the absence of TAK1 drives RIPK1 kinase activity–independent pyroptosis, apoptosis, necroptosis, and inflammatory disease. *J Exp Med* (2020) 217(3). doi: 10.1084/jem.20191644

4. Kesavardhana S, Malireddi RS, Burton AR, Porter SN, Vogel P, Pruett-Miller SM, et al. The Zα2 domain of ZBP1 is a molecular switch regulating influenza-induced PANoptosis and perinatal lethality during development. *J Biol Chem* (2020) 295 (24):8325–30. doi: 10.1074/jbc.RA120.013752

5. Backer JM. The intricate regulation and complex functions of the class III phosphoinositide 3-kinase Vps34. *Biochem J* (2016) 473(15):2251–71. doi: 10.1042/BCJ20160170

6. Ohashi Y, Tremel S, Williams RL. VPS34 complexes from a structural perspective. *J Lipid Res* (2019) 60(2):229–41. doi: 10.1194/jlr.R089490

7. Lahiri V, Hawkins WD, Klionsky DJ. Watch what you (self-) eat: autophagic mechanisms that modulate metabolism. *Cell Metab* (2019) 29(4):803–26. doi: 10.1016/j.cmet.2019.03.003

8. Ktistakis NT, Tooze SA. Digesting the expanding mechanisms of autophagy. *Trends Cell Biol* (2016) 26(8):624–35. doi: 10.1016/j.tcb.2016.03.006

9. Gatica D, Lahiri V, Klionsky DJ. Cargo recognition and degradation by selective autophagy. *Nat Cell Biol* (2018) 20(3):233–42. doi: 10.1038/s41556-018-0037-z

10. Tanida I, Ueno T, Kominami E. LC3 conjugation system in mammalian autophagy. *Int J Biochem Cell Biol* (2004) 36(12):2503–18. doi: 10.1016/j.biocel.2004.05.009

11. Lamark T, Kirkin V, Dikic I, Johansen T. NBR1 and p62 as cargo receptors for selective autophagy of ubiquitinated targets. *Cell Cycle (Georgetown Tex)* (2009) 8 (13):1986–90. doi: 10.4161/cc.8.13.8892

12. Shibutani ST, Yoshimori T. A current perspective of autophagosome biogenesis. *Cell Res* (2014) 24(1):58–68. doi: 10.1038/cr.2013.159

13. Orsi A, Razi M, Dooley H, Robinson D, Weston A, Collinson L, et al. Dynamic and transient interactions of Atg9 with autophagosomes, but not membrane integration, are required for autophagy. *Mol Biol Cell* (2012) 23(10):1860–73. doi: 10.1091/mbc.e11-09-0746

14. Wang Y, Li L, Hou C, Lai Y, Long J, Liu J, et al. SNARE-mediated membrane fusion in autophagy. *Semin Cell Dev Biol* (2016) 60:97–104. doi: 10.1016/j.semcdb.2016.07.009

15. Zhao YG, Codogno P, Zhang H. Machinery, regulation and pathophysiological implications of autophagosome maturation. *Nat Rev Mol Cell Biol* (2021) 22(11):733–50. doi: 10.1038/s41580-021-00392-4

16. Gao M, Monian P, Pan Q, Zhang W, Xiang J, Jiang X. Ferroptosis is an autophagic cell death process. *Cell Res* (2016) 26(9):1021–32. doi: 10.1038/cr.2016.95

17. Hou W, Xie Y, Song X, Sun X, Lotze MT, Zeh HJIII, et al. Autophagy promotes ferroptosis by degradation of ferritin. *Autophagy* (2016) 12(8):1425–8. doi: 10.1080/15548627.2016.1187366

18. Lomia M, Tchelidze T, Pruidze M. Bronchial asthma as neurogenic paroxysmal inflammatory disease: a randomized trial with carbamazepine. *Respir Med* (2006) 100 (11):1988–96. doi: 10.1016/j.rmed.2006.02.018

19. Schiebler M, Brown K, Hegyi K, Newton SM, Renna M, Hepburn L, et al. Functional drug screening reveals anticonvulsants as enhancers of mTOR-independent autophagic killing of mycobacterium tuberculosis through inositol depletion. *EMBO Mol Med* (2015) 7(2):127–39. doi: 10.15252/emmm.201404137

20. Ono E, Mita H, Taniguchi M, Higashi N, Hasegawa M, Miyazaki E, et al. Concentration of 14, 15-leukotriene C4 (eoxin C4) in bronchoalveolar lavage fluid. *Clin Exp Allergy* (2009) 39(9):1348–52. doi: 10.1111/j.1365-2222.2009.03261.x

21. Hajek AR, Lindley AR, Favoreto S, Carter R, Schleimer RP, Kuperman DA. 12/15-lipoxygenase deficiency protects mice from allergic airways inflammation and increases secretory IgA levels. *J Allergy Clin Immunol* (2008) 122(3):633–9. e3. doi: 10.1016/j.jaci.2008.06.021

22. Zhao J, Dar HH, Deng Y, St. Croix CM, Li Z, Minami Y, et al. PEBP1 acts as a rheostat between prosurvival autophagy and ferroptotic death in asthmatic epithelial cells. *Proc Natl Acad Sci* (2020) 117(25):14376–85. doi: 10.1073/pnas.1921618117

23. Hubbard VM, Valdor R, Macian F, Cuervo AM. Selective autophagy in the maintenance of cellular homeostasis in aging organisms. *Biogerontology* (2012) 13:21–35. doi: 10.1007/s10522-011-9331-x

24. Zhang Z, Yao Z, Wang L, Ding H, Shao J, Chen A, et al. Activation of ferritinophagy is required for the RNA-binding protein ELAVL1/HuR to regulate ferroptosis in hepatic stellate cells. *Autophagy* (2018) 14(12):2083–103. doi: 10.1080/15548627.2018.1503146

25. Park E, Chung SW. ROS-mediated autophagy increases intracellular iron levels and ferroptosis by ferritin and transferrin receptor regulation. *Cell Death Disease* (2019) 10(11):1–10. doi: 10.1038/s41419-019-2064-5

26. Protchenko O, Baratz E, Jadhav S, Li F, Shakoury-Elizeh M, Gavrilova O, et al. Iron chaperone poly rC binding protein 1 protects mouse liver from lipid peroxidation and steatosis. *Hepatology* (2021) 73(3):1176–93. doi: 10.1002/hep.31328

27. Wang Y-Q, Chang S-Y, Wu Q, Gou Y-J, Jia L, Cui Y-M, et al. The protective role of mitochondrial ferritin on erastin-induced ferroptosis. *Front Aging Neurosci* (2016) 8:308. doi: 10.3389/fnagi.2016.00308

28. Bailey AP, Koster G, Guillermier C, Hirst EM, MacRae JI, Lechene CP, et al. Antioxidant role for lipid droplets in a stem cell niche of drosophila. *Cell* (2015) 163 (2):340–53. doi: 10.1016/j.cell.2015.09.020

29. Bai Y, Meng L, Han L, Jia Y, Zhao Y, Gao H, et al. Lipid storage and lipophagy regulates ferroptosis. *Biochem Biophys Res Commun* (2019) 508(4):997–1003. doi: 10.1016/j.bbrc.2018.12.039

30. Yang M, Chen P, Liu J, Zhu S, Kroemer G, Klionsky DJ, et al. Clockophagy is a novel selective autophagy process favoring ferroptosis. *Sci Adv* (2019) 5(7):eaaw2238. doi: 10.1126/sciadv.aaw2238

31. Dice JF. Chaperone-mediated autophagy. *Autophagy* (2007) 3(4):295–9. doi: 10.4161/auto.4144

32. Wu Z, Geng Y, Lu X, Shi Y, Wu G, Zhang M, et al. Chaperone-mediated autophagy is involved in the execution of ferroptosis. *Proc Natl Acad Sci* (2019) 116 (8):2996–3005. doi: 10.1073/pnas.1819728116

33. Ingold I, Berndt C, Schmitt S, Doll S, Poschmann G, Buday K, et al. Selenium utilization by GPX4 is required to prevent hydroperoxide-induced ferroptosis. *Cell* (2018) 172(3):409–22. e21. doi: 10.1016/j.cell.2017.11.048

34. Ursini F, Maiorino M. Lipid peroxidation and ferroptosis: the role of GSH and GPx4. *Free Radical Biol Med* (2020) 152:175–85. doi: 10.1016/j.freeradbiomed.2020.02.027

35. Song X, Zhu S, Chen P, Hou W, Wen Q, Liu J, et al. AMPK-mediated BECN1 phosphorylation promotes ferroptosis by directly blocking system xc–activity. *Curr Biol* (2018) 28(15):2388–99. e5. doi: 10.1016/j.cub.2018.05.094

36. Shen M, Li Y, Wang Y, Shao J, Zhang F, Yin G, et al. N6-methyladenosine modification regulates ferroptosis through autophagy signaling pathway in hepatic stellate cells. *Redox Biol* (2021) 47:102151. doi: 10.1016/j.redox.2021.102151

37. Ishimoto T, Nagano O, Yae T, Tamada M, Motohara T, Oshima H, et al. CD44 variant regulates redox status in cancer cells by stabilizing the xCT subunit of system xc– and thereby promotes tumor growth. *Cancer Cell* (2011) 19(3):387–400. doi: 10.1016/j.ccr.2011.01.038

38. Hayano M, Yang W, Corn C, Pagano N, Stockwell B. Loss of cysteinyl-tRNA synthetase (CARS) induces the transsulfuration pathway and inhibits ferroptosis induced by cystine deprivation. *Cell Death Differentiation* (2016) 23(2):270–8. doi: 10.1038/cdd.2015.93

39. Wang L, Cai H, Hu Y, Liu F, Huang S, Zhou Y, et al. A pharmacological probe identifies cystathionine β-synthase as a new negative regulator for ferroptosis. *Cell Death disease* (2018) 9(10):1–17. doi: 10.1038/s41419-018-1063-2

40. Liu J, Kuang F, Kroemer G, Klionsky DJ, Kang R, Tang D. Autophagy-dependent ferroptosis: machinery and regulation. *Cell Chem Biol* (2020) 27(4):420–35. doi: 10.1016/j.chembiol.2020.02.005

41. Gao M, Yi J, Zhu J, Minikes AM, Monian P, Thompson CB, et al. Role of mitochondria in ferroptosis. *Mol Cell* (2019) 73(2):354–63. e3. doi: 10.1016/j.molcel.2018.10.042

42. Li C, Zhang Y, Liu J, Kang R, Klionsky DJ, Tang D. Mitochondrial DNA stress triggers autophagy-dependent ferroptotic death. *Autophagy* (2021) 17(4):948–60. doi: 10.1080/15548627.2020.1739447

43. Lee H, Zandkarimi F, Zhang Y, Meena JK, Kim J, Zhuang L, et al. Energy-stress-mediated AMPK activation inhibits ferroptosis. *Nat Cell Biol* (2020) 22(2):225–34. doi: 10.1038/s41556-020-0461-8

44. Basit F, Van Oppen LM, Schöckel L, Bossenbroek HM, Van Emst-de Vries SE, Hermeling JC, et al. Mitochondrial complex I inhibition triggers a mitophagy-dependent ROS increase leading to necroptosis and ferroptosis in melanoma cells. *Cell Death Disease* (2017) 8(3):e2716–e. doi: 10.1038/cddis.2017.133

45. Chang L-C, Chiang S-K, Chen S-E, Yu Y-L, Chou R-H, Chang W-C. Heme oxygenase-1 mediates BAY 11–7085 induced ferroptosis. *Cancer letters* (2018) 416:124–37. doi: 10.1016/j.canlet.2017.12.025

46. Xiong Q, Li X, Li W, Chen G, Xiao H, Li P, et al. WDR45 mutation impairs the autophagic degradation of transferrin receptor and promotes ferroptosis. *Front Mol biosciences* (2021) 8:645831. doi: 10.3389/fmolb.2021.645831

47. Peng Y, Yang J, Li Z, Chen S, Tang X, Zhou J. Overexpression of SLC40A1 inhibits the malignancy of hepatocellular carcinoma MHCC-97H cells by stimulation of autophagy. *Biomed Signal Process Control* (2022) 75:103554. doi: 10.1016/j.bspc.2022.103554

48. He H, Wang L, Qiao Y, Yang B, Yin D, He M. Epigallocatechin-3-gallate pretreatment alleviates doxorubicin-induced ferroptosis and cardiotoxicity by upregulating AMPKα2 and activating adaptive autophagy. *Redox Biol* (2021) 48:102185. doi: 10.1016/j.redox.2021.102185

49. Haeggstrom JZ, Funk CD. Lipoxygenase and leukotriene pathways: biochemistry, biology, and roles in disease. *Chem Rev* (2011) 111(10):5866–98. doi: 10.1021/cr200246d

50. Chen X, Song X, Li J, Zhang R, Yu C, Zhou Z, et al. Identification of HPCAL1 as a specific autophagy receptor involved in ferroptosis. *Autophagy* (2022) 19(1):1–21. doi: 10.1080/15548627.2022.2059170

51. Gupta U, Ghosh S, Wallace CT, Shang P, Xin Y, Nair AP, et al. Increased LCN2 (lipocalin 2) in the RPE decreases autophagy and activates inflammasome-ferroptosis processes in a mouse model of dry AMD. *Autophagy* (2022) 19(1):1–20. doi: 10.1080/15548627.2022.2062887

52. Liu J, Liu Y, Wang Y, Li C, Xie Y, Klionsky DJ, et al. TMEM164 is a new determinant of autophagy-dependent ferroptosis. *Autophagy* (2022) 19(3):1–12. doi: 10.1080/15548627.2022.2111635

53. Ichimura Y, Waguri S, Sou Y-s, Kageyama S, Hasegawa J, Ishimura R, et al. Phosphorylation of p62 activates the Keap1-Nrf2 pathway during selective autophagy. *Mol Cell* (2013) 51(5):618–31. doi: 10.1016/j.molcel.2013.08.003

54. Peng Q, Liu H, Luo Z, Zhao H, Wang X, Guan X. Effect of autophagy on ferroptosis in foam cells *via* Nrf2. *Mol Cell Biochem* (2022) 477(5):1597–606. doi: 10.1007/s11010-021-04347-3

55. Zhang Z, Guo M, Li Y, Shen M, Kong D, Shao J, et al. RNA-Binding protein ZFP36/TTP protects against ferroptosis by regulating autophagy signaling pathway in hepatic stellate cells. *Autophagy* (2020) 16(8):1482–505. doi: 10.1080/15548627.2019.1687985

56. Dikic I, Elazar Z. Mechanism and medical implications of mammalian autophagy. *Nat Rev Mol Cell Biol* (2018) 19(6):349–64. doi: 10.1038/s41580-018-0003-4

57. Tooze SA, Yoshimori T. The origin of the autophagosomal membrane. *Nat Cell Biol* (2010) 12(9):831–5. doi: 10.1038/ncb0910-831

58. Xie Y, Kang R, Sun X, Zhong M, Huang J, Klionsky DJ, et al. Posttranslational modification of autophagy-related proteins in macroautophagy. *Autophagy* (2015) 11 (1):28–45. doi: 10.4161/15548627.2014.984267

59. Nakamura S, Yoshimori T. New insights into autophagosome–lysosome fusion. *J Cell science* (2017) 130(7):1209–16. doi: 10.1242/jcs.196352

60. Chen D, Rauh M, Buchfelder M, Eyupoglu IY, Savaskan N. The oxido-metabolic driver ATF4 enhances temozolamide chemo-resistance in human gliomas. *Oncotarget* (2017) 8(31):51164. doi: 10.18632/oncotarget.17737

61. Rahmani M, Davis EM, Crabtree TR, Habibi JR, Nguyen TK, Dent P, et al. The kinase inhibitor sorafenib induces cell death through a process involving induction of endoplasmic reticulum stress. *Mol Cell Biol* (2007) 27(15):5499–513. doi: 10.1128/MCB.01080-06

62. Yang C, Ma X, Wang Z, Zeng X, Hu Z, Ye Z, et al. Curcumin induces apoptosis and protective autophagy in castration-resistant prostate cancer cells through iron chelation. *Drug design Dev Ther* (2017) 11:431. doi: 10.2147/DDDT.S126964

63. Bhattacharya A, Ghosh P, Singh A, Ghosh A, Bhowmick A, Sinha DK, et al. Delineating the complex mechanistic interplay between NF-κβ driven mTOR depedent autophagy and monocyte to macrophage differentiation: A functional perspective. *Cell signalling* (2021) 88:110150. doi: 10.1016/j.cellsig.2021.110150

64. Jang EJ, Kim DH, Lee B, Lee EK, Chung KW, Moon KM, et al. Activation of proinflammatory signaling by 4-hydroxynonenal-Src adducts in aged kidneys. *Oncotarget* (2016) 7(32):50864. doi: 10.18632/oncotarget.10854

65. Copetti T, Bertoli C, Dalla E, Demarchi F, Schneider C. p65/RelA modulates BECN1 transcription and autophagy. *Mol Cell Biol* (2009) 29(10):2594–608. doi: 10.1128/MCB.01396-08

66. Kang R, Chen R, Zhang Q, Hou W, Wu S, Cao L, et al. HMGB1 in health and disease. *Mol aspects Med* (2014) 40:1–116. doi: 10.1016/j.mam.2014.05.001

67. Wen Q, Liu J, Kang R, Zhou B, Tang D. The release and activity of HMGB1 in ferroptosis. *Biochem Biophys Res Commun* (2019) 510(2):278–83. doi: 10.1016/j.bbrc.2019.01.090

68. Liu L, Yang M, Kang R, Wang Z, Zhao Y, Yu Y, et al. DAMP-mediated autophagy contributes to drug resistance. *Autophagy* (2011) 7(1):112–4. doi: 10.4161/auto.7.1.14005

69. Tasdemir E, Maiuri MC, Morselli E, Criollo A, D'Amelio M, Djavaheri-Mergny M, et al. A dual role of p53 in the control of autophagy. *Autophagy* (2008) 4(6):810–4. doi: 10.4161/auto.6486

70. Ou Y, Wang S-J, Li D, Chu B, Gu W. Activation of SAT1 engages polyamine metabolism with p53-mediated ferroptotic responses. *Proc Natl Acad Sci* (2016) 113 (44):E6806–E12. doi: 10.1073/pnas.1607152113

71. Jiang L, Kon N, Li T, Wang S-J, Su T, Hibshoosh H, et al. Ferroptosis as a p53-mediated activity during tumour suppression. *Nature* (2015) 520(7545):57–62. doi: 10.1038/nature14344

72. Zhang W, Gai C, Ding D, Wang F, Li W. Targeted p53 on small-molecules-induced ferroptosis in cancers. *Front Oncol* (2018) 8:507. doi: 10.3389/fonc.2018.00507

73. Xie Y, Zhu S, Song X, Sun X, Fan Y, Liu J, et al. The tumor suppressor p53 limits ferroptosis by blocking DPP4 activity. *Cell Rep* (2017) 20(7):1692–704. doi: 10.1016/j.celrep.2017.07.055

74. Wang S-J, Li D, Ou Y, Jiang L, Chen Y, Zhao Y, et al. Acetylation is crucial for p53-mediated ferroptosis and tumor suppression. *Cell Rep* (2016) 17(2):366–73. doi: 10.1016/j.celrep.2016.09.022

75. Sun M, Li J, Mao L, Wu J, Deng Z, He M, et al. p53 deacetylation alleviates sepsis-induced acute kidney injury by promoting autophagy. *Front Immunol* (2021) 12. doi: 10.3389/fimmu.2021.685523

76. Liu Q, Wang K. The induction of ferroptosis by impairing STAT3/Nrf2/GPx4 signaling enhances the sensitivity of osteosarcoma cells to cisplatin. *Cell Biol Int* (2019) 43(11):1245–56. doi: 10.1002/cbin.11121

77. Castets P, Rion N, Théodore M, Falcetta D, Lin S, Reischl M, et al. mTORC1 and PKB/Akt control the muscle response to denervation by regulating autophagy and HDAC4. *Nat Commun* (2019) 10(1):1–16. doi: 10.1038/s41467-019-11227-4

78. Kang R, Tang D, Lotze MT, Zeh I, Herbert J. AGER/RAGE-mediated autophagy promotes pancreatic tumorigenesis and bioenergetics through the IL6-pSTAT3 pathway. *Autophagy* (2012) 8(6):989–91. doi: 10.4161/auto.20258

79. Zhang Z-B, Xiong L-L, Xue L-L, Deng Y-P, Du R-L, Hu Q, et al. MiR-127-3p targeting CISD1 regulates autophagy in hypoxic–ischemic cortex. *Cell Death disease* (2021) 12(3):1–17. doi: 10.1038/s41419-021-03541-x

80. Tamir S, Rotem-Bamberger S, Katz C, Morcos F, Hailey KL, Zuris JA, et al. Integrated strategy reveals the protein interface between cancer targets bcl-2 and NAF-1. *Proc Natl Acad Sci* (2014) 111(14):5177–82. doi: 10.1073/pnas.1403770111

81. Sohn Y-S, Tamir S, Song L, Michaeli D, Matouk I, Conlan AR, et al. NAF-1 and mitoNEET are central to human breast cancer proliferation by maintaining mitochondrial homeostasis and promoting tumor growth. *Proc Natl Acad Sci* (2013) 110(36):14676–81. doi: 10.1073/pnas.1313198110

82. Yuan H, Li X, Zhang X, Kang R, Tang D. CISD1 inhibits ferroptosis by protection against mitochondrial lipid peroxidation. *Biochem Biophys Res Commun* (2016) 478(2):838–44. doi: 10.1016/j.bbrc.2016.08.034

83. Hou J, Rao M, Zheng W, Fan J, Law BYK. Advances on cell autophagy and its potential regulatory factors in renal ischemia-reperfusion injury. *DNA Cell Biol* (2019) 38(9):895–904. doi: 10.1089/dna.2019.4767

84. Shen L, Qi Z, Zhu Y, Song X, Xuan C, Ben P, et al. Phosphorylated heat shock protein 27 promotes lipid clearance in hepatic cells through interacting with STAT3 and activating autophagy. *Cell signalling* (2016) 28(8):1086–98. doi: 10.1016/j.cellsig.2016.05.008

85. Tang D, Kang R, Livesey KM, Kroemer G, Billiar TR, Van Houten B, et al. High-mobility group box 1 is essential for mitochondrial quality control. *Cell Metab* (2011) 13(6):701–11. doi: 10.1016/j.cmet.2011.04.008

86. Tang D, Kang R, Livesey KM, Cheh C-W, Farkas A, Loughran P, et al. Endogenous HMGB1 regulates autophagy. *J Cell Biol* (2010) 190(5):881–92. doi: 10.1083/jcb.200911078

87. Sun X, Ou Z, Xie M, Kang R, Fan Y, Niu X, et al. HSPB1 as a novel regulator of ferroptotic cancer cell death. *Oncogene* (2015) 34(45):5617–25. doi: 10.1038/onc.2015.32

88. Wang Z, Li Y, Wang D, Shen Y. Ferroptosis molecular inducers: A future direction for malignant tumor chemotherapy. *Biocell* (2022) 46(7):1599. doi: 10.32604/biocell.2022.018530

89. Song X, Xie Y, Kang R, Hou W, Sun X, Epperly MW, et al. FANCD2 protects against bone marrow injury from ferroptosis. *Biochem Biophys Res Commun* (2016) 480(3):443–9. doi: 10.1016/j.bbrc.2016.10.068

90. Sumpter R, Sirasanagandla S, Fernández ÁF, Wei Y, Dong X, Franco L, et al. Fanconi anemia proteins function in mitophagy and immunity. *Cell* (2016) 165(4):867–81. doi: 10.1016/j.cell.2016.04.006

91. Li Y, Zhang L, Zhou J, Luo S, Huang R, Zhao C, et al. Nedd4 E3 ubiquitin ligase promotes cell proliferation and autophagy. *Cell proliferation* (2015) 48(3):338–47. doi: 10.1111/cpr.12184

92. Yang Y, Luo M, Zhang K, Zhang J, Gao T, Connell DO, et al. Nedd4 ubiquitylates VDAC2/3 to suppress erastin-induced ferroptosis in melanoma. *Nat Commun* (2020) 11(1):1–14. doi: 10.1038/s41467-020-14324-x

93. Wang Y, Liu Y, Liu J, Kang R, Tang D. NEDD4L-mediated LTF protein degradation limits ferroptosis. *Biochem Biophys Res Commun* (2020) 531(4):581–7. doi: 10.1016/j.bbrc.2020.07.032

94. Halim TY, Steer CA, Mathä L, Gold MJ, Martinez-Gonzalez I, McNagny KM, et al. Group 2 innate lymphoid cells are critical for the initiation of adaptive T helper 2 cell-mediated allergic lung inflammation. *Immunity* (2014) 40(3):425–35. doi: 10.1016/j.immuni.2014.01.011

95. Willart MA, Deswarte K, Pouliot P, Braun H, Beyaert R, Lambrecht BN, et al. Interleukin-1α controls allergic sensitization to inhaled house dust mite *via* the epithelial release of GM-CSF and IL-33. *J Exp Med* (2012) 209(8):1505–17. doi: 10.1084/jem.20112691

96. Besnard AG, Togbe D, Guillou N, Erard F, Quesniaux V, Ryffel B. IL-33-activated dendritic cells are critical for allergic airway inflammation. *Eur J Immunol* (2011) 41(6):1675–86. doi: 10.1002/eji.201041033

97. Bell BD, Kitajima M, Larson RP, Stoklasek TA, Dang K, Sakamoto K, et al. The transcription factor STAT5 is critical in dendritic cells for the development of TH2 but not TH1 responses. *Nat Immunol* (2013) 14(4):364–71. doi: 10.1038/ni.2541

98. Chu DK, Llop-Guevara A, Walker TD, Flader K, Goncharova S, Boudreau JE, et al. IL-33, but not thymic stromal lymphopoietin or IL-25, is central to mite and peanut allergic sensitization. *J Allergy Clin Immunol* (2013) 131(1):187–200. e8. doi: 10.1016/j.jaci.2012.08.002

99. Fahy JV. Type 2 inflammation in asthma–present in most, absent in many. *Nat Rev Immunol* (2015) 15(1):57–65. doi: 10.1038/nri3786

100. Crosby LM, Waters CM. Epithelial repair mechanisms in the lung. *Am J Physiol-Lung Cell Mol Physiol* (2010) 298(6):L715–L31. doi: 10.1152/ajplung.00361.2009

101. Wenzel SE. Asthma phenotypes: the evolution from clinical to molecular approaches. *Nat Med* (2012) 18(5):716–25. doi: 10.1038/nm.2678

102. Dickinson JD, Alevy Y, Malvin NP, Patel KK, Gunsten SP, Holtzman MJ, et al. IL13 activates autophagy to regulate secretion in airway epithelial cells. *Autophagy* (2016) 12(2):397–409. doi: 10.1080/15548627.2015.1056967

103. Dickinson JD, Sweeter JM, Warren KJ, Ahmad IM, De Deken X, Zimmerman MC, et al. Autophagy regulates DUOX1 localization and superoxide production in airway epithelial cells during chronic IL-13 stimulation. *Redox Biol* (2018) 14:272–84. doi: 10.1016/j.redox.2017.09.013

104. Wong CK, Hu S, Leung KM-L, Dong J, He L, Chu YJ, et al. NOD-like receptors mediated activation of eosinophils interacting with bronchial epithelial cells: a link between innate immunity and allergic asthma. *Cell Mol Immunol* (2013) 10(4):317–29. doi: 10.1038/cmi.2012.77

105. Martinon F, Mayor A, Tschopp J. The inflammasomes: guardians of the body. *Annu Rev Immunol* (2009) 27:229–65. doi: 10.1146/annurev.immunol.021908.132715

106. Travassos LH, Carneiro LA, Ramjeet M, Hussey S, Kim Y-G, Magalhães JG, et al. Nod1 and Nod2 direct autophagy by recruiting ATG16L1 to the plasma membrane at the site of bacterial entry. *Nat Immunol* (2010) 11(1):55–62. doi: 10.1038/ni.1823

107. Fernández-García V, González-Ramos S, Avendaño-Ortiz J, Martín-Sanz P, Delgado C, Castrillo A, et al. NOD1 splenic activation confers ferroptosis protection and reduces macrophage recruitment under pro-atherogenic conditions. *Biomed Pharmacother* (2022) 148:112769. doi: 10.1016/j.biopha.2022.112769

108. Klöditz K, Fadeel B. Three cell deaths and a funeral: macrophage clearance of cells undergoing distinct modes of cell death. *Cell Death discovery* (2019) 5(1):1–9. doi: 10.1038/s41420-019-0146-x

109. Levine B, Mizushima N, Virgin HW. Autophagy in immunity and inflammation. *Nature* (2011) 469(7330):323–35. doi: 10.1038/nature09782

110. Murai H, Okazaki S, Hayashi H, Kawakita A, Hosoki K, Yasutomi M, et al. Alternaria extract activates autophagy that induces IL-18 release from airway epithelial cells. *Biochem Biophys Res Commun* (2015) 464(4):969–74. doi: 10.1016/j.bbrc.2015.05.076

111. Li W, Wu Y, Zhao Y, Li Z, Chen H, Dong L, et al. MTOR suppresses autophagy-mediated production of IL25 in allergic airway inflammation. *Thorax* (2020) 75(12):1047–57. doi: 10.1136/thoraxjnl-2019-213771

112. Holgate ST. Innate and adaptive immune responses in asthma. *Nat Med* (2012) 18(5):673–83. doi: 10.1038/nm.2731

113. Worbs T, Hammerschmidt SI, Förster R. Dendritic cell migration in health and disease. *Nat Rev Immunol* (2017) 17(1):30–48. doi: 10.1038/nri.2016.116

114. Izumi G, Nakano H, Nakano K, Whitehead GS, Grimm SA, Fessler MB, et al. CD11b+ lung dendritic cells at different stages of maturation induce Th17 or Th2 differentiation. *Nat Commun* (2021) 12(1):5029. doi: 10.1038/s41467-021-25307-x

115. Lambrecht BN, Hammad H. The immunology of asthma. *Nat Immunol* (2015) 16(1):45–56. doi: 10.1038/ni.3049

116. Ghislat G, Lawrence T. Autophagy in dendritic cells. *Cell Mol Immunol* (2018) 15(11):944–52. doi: 10.1038/cmi.2018.2

117. Chen X, Xu S, Zhao C, Liu B. Role of TLR4/NADPH oxidase 4 pathway in promoting cell death through autophagy and ferroptosis during heart failure. *Biochem Biophys Res Commun* (2019) 516(1):37–43. doi: 10.1016/j.bbrc.2019.06.015

118. Terawaki S, Camosseto V, Prete F, Wenger T, Papadopoulos A, Rondeau C, et al. RUN and FYVE domain–containing protein 4 enhances autophagy and lysosome tethering in response to interleukin-4. *J Cell Biol* (2015) 210(7):1133–52. doi: 10.1083/jcb.201501059

119. Khan N, Vidyarthi A, Pahari S, Negi S, Aqdas M, Nadeem S, et al. Signaling through NOD-2 and TLR-4 bolsters the T cell priming capability of dendritic cells by inducing autophagy. *Sci Rep* (2016) 6(1):1–8. doi: 10.1038/srep19084

120. Wildenberg M, Koelink P, Diederen K, Te Velde A, Wolfkamp S, Nuij V, et al. The ATG16L1 risk allele associated with crohn's disease results in a Rac1-dependent defect in dendritic cell migration that is corrected by thiopurines. *Mucosal Immunol* (2017) 10(2):352–60. doi: 10.1038/mi.2016.65

121. Ishikawa H, Barber GN. STING is an endoplasmic reticulum adaptor that facilitates innate immune signalling. *Nature* (2008) 455(7213):674–8. doi: 10.1038/nature07317

122. Barber GN. STING: infection, inflammation and cancer. *Nat Rev Immunol* (2015) 15(12):760–70. doi: 10.1038/nri3921

123. Motwani M, Pesiridis S, Fitzgerald KA. DNA Sensing by the cGAS–STING pathway in health and disease. *Nat Rev Genet* (2019) 20(11):657–74. doi: 10.1038/s41576-019-0151-1

124. Zhang R, Kang R, Tang D. The STING1 network regulates autophagy and cell death. *Signal Transduction Targeted Ther* (2021) 6(1):1–13. doi: 10.1038/s41392-021-00613-4

125. Zhou D, Li P, Lin Y, Lott JM, Hislop AD, Canaday DH, et al. Lamp-2a facilitates MHC class II presentation of cytoplasmic antigens. *Immunity* (2005) 22 (5):571–81. doi: 10.1016/j.immuni.2005.03.009

126. Wiernicki B, Maschalidi S, Pinney J, Adjemian S, Vanden Berghe T, Ravichandran KS, et al. Cancer cells dying from ferroptosis impede dendritic cell-mediated anti-tumor immunity. *Nat Commun* (2022) 13(1):1–15. doi: 10.1038/s41467-022-31218-2

127. Thurston TL, Wandel MP, von Muhlinen N, Foeglein Á, Randow F. Galectin 8 targets damaged vesicles for autophagy to defend cells against bacterial invasion. *Nature* (2012) 482(7385):414–8. doi: 10.1038/nature10744

128. Fujita N, Morita E, Itoh T, Tanaka A, Nakaoka M, Osada Y, et al. Recruitment of the autophagic machinery to endosomes during infection is mediated by ubiquitin. *J Cell Biol* (2013) 203(1):115–28. doi: 10.1083/jcb.201304188

129. Brooks CR, Yeung MY, Brooks YS, Chen H, Ichimura T, Henderson JM, et al. KIM-1-/TIM-1-mediated phagocytosis links ATG 5-/ULK 1-dependent clearance of apoptotic cells to antigen presentation. *EMBO J* (2015) 34(19):2441–64. doi: 10.15252/embj.201489838

130. MacMicking JD. Interferon-inducible effector mechanisms in cell-autonomous immunity. *Nat Rev Immunol* (2012) 12(5):367–82. doi: 10.1038/nri3210

131. Lee Y, Sasai M, Ma JS, Sakaguchi N, Ohshima J, Bando H, et al. p62 plays a specific role in interferon-γ-induced presentation of a toxoplasma vacuolar antigen. *Cell Rep* (2015) 13(2):223–33. doi: 10.1016/j.celrep.2015.09.005

132. Zang F, Chen Y, Lin Z, Cai Z, Yu L, Xu F, et al. Autophagy is involved in regulating the immune response of dendritic cells to influenza a (H1N1) pdm09 infection. *Immunology* (2016) 148(1):56–69. doi: 10.1111/imm.12587

133. Sato H, Fujiwara K, Sagara J-i, Bannai S. Induction of cystine transport activity in mouse peritoneal macrophages by bacterial lipopolysaccharide. *Biochem J* (1995) 310 (2):547–51. doi: 10.1042/bj3100547

134. Li G, Liang X, Lotze MT. HMGB1: the central cytokine for all lymphoid cells. *Front Immunol* (2013) 4:68. doi: 10.3389/fimmu.2013.00068

135. Gordon S, Taylor PR. Monocyte and macrophage heterogeneity. *Nat Rev Immunol* (2005) 5(12):953–64. doi: 10.1038/nri1733

136. Gordon S, Martinez FO. Alternative activation of macrophages: mechanism and functions. *Immunity* (2010) 32(5):593–604. doi: 10.1016/j.immuni.2010.05.007

137. Murray PJ, Allen JE, Biswas SK, Fisher EA, Gilroy DW, Goerdt S, et al. Macrophage activation and polarization: nomenclature and experimental guidelines. *Immunity* (2014) 41(1):14–20. doi: 10.1016/j.immuni.2014.06.008

138. Handa P, Thomas S, Morgan-Stevenson V, Maliken BD, Gochanour E, Boukhar S, et al. Iron alters macrophage polarization status and leads to steatohepatitis and fibrogenesis. *J Leukocyte Biol* (2019) 105(5):1015–26. doi: 10.1002/JLB.3A0318-108R

139. Zhou Y, Que KT, Zhang Z, Yi ZJ, Zhao PX, You Y, et al. Iron overloaded polarizes macrophage to proinflammation phenotype through ROS/acetyl-p53 pathway. *Cancer Med* (2018) 7(8):4012–22. doi: 10.1002/cam4.1670

140. Chen W, Ma T, Shen X-n, Xia X-f, Xu G-d, Bai X-l, et al. Macrophage-induced tumor angiogenesis is regulated by the TSC2–mTOR PathwayTSC2–mTOR regulates macrophage-induced tumor angiogenesis. *Cancer Res* (2012) 72(6):1363–72. doi: 10.1158/0008-5472.CAN-11-2684

141. Schlaepfer E, Rochat M-A, Duo L, Speck RF. Triggering TLR2,-3,-4,-5, and-8 reinforces the restrictive nature of M1-and M2-polarized macrophages to HIV. *J virol* (2014) 88(17):9769–81. doi: 10.1128/JVI.01053-14

142. Biswas SK, Lewis CE. NF-κB as a central regulator of macrophage function in tumors. *J leukocyte Biol* (2010) 88(5):877–84. doi: 10.1189/jlb.0310153

143. Chang C-P, Su Y-C, Lee P-H, Lei H-Y. Targeting NFKB by autophagy to polarize hepatoma-associated macrophage differentiation. *Autophagy* (2013) 9(4):619–21. doi: 10.4161/auto.23546

144. Chang C, Su Y, Hu C, Lei H. TLR2-dependent selective autophagy regulates NF-κB lysosomal degradation in hepatoma-derived M2 macrophage differentiation. *Cell Death Differentiation* (2013) 20(3):515–23. doi: 10.1038/cdd.2012.146

145. Roca H, Varsos ZS, Sud S, Craig MJ, Ying C, Pienta KJ. CCL2 and interleukin-6 promote survival of human CD11b+ peripheral blood mononuclear cells and induce M2-type macrophage polarization. *J Biol Chem* (2009) 284(49):34342–54. doi: 10.1074/jbc.M109.042671

146. Djudjaj S, Martin IV, Buhl EM, Nothofer NJ, Leng L, Piecychna M, et al. Macrophage migration inhibitory factor limits renal inflammation and fibrosis by counteracting tubular cell cycle arrest. *J Am Soc Nephrol* (2017) 28(12):3590–604. doi: 10.1681/ASN.2017020190

147. Lv L-L, Feng Y, Wen Y, Wu W-J, Ni H-F, Li Z-L, et al. Exosomal CCL2 from tubular epithelial cells is critical for albumin-induced tubulointerstitial inflammation. *J Am Soc Nephrol* (2018) 29(3):919–35. doi: 10.1681/ASN.2017050523

148. Wang Y, Quan F, Cao Q, Lin Y, Yue C, Bi R, et al. Quercetin alleviates acute kidney injury by inhibiting ferroptosis. *J advanced Res* (2021) 28:231–43. doi: 10.1016/j.jare.2020.07.007

149. Dai E, Han L, Liu J, Xie Y, Kroemer G, Klionsky DJ, et al. Autophagy-dependent ferroptosis drives tumor-associated macrophage polarization *via* release and uptake of oncogenic KRAS protein. *Autophagy* (2020) 16(11):2069–83. doi: 10.1080/15548627.2020.1714209

150. Kapralov AA, Yang Q, Dar HH, Tyurina YY, Anthonymuthu TS, Kim R, et al. Redox lipid reprogramming commands susceptibility of macrophages and microglia to ferroptotic death. *Nat Chem Biol* (2020) 16(3):278–90. doi: 10.1038/s41589-019-0462-8

151. Youssef LA, Rebbaa A, Pampou S, Weisberg SP, Stockwell BR, Hod EA, et al. Increased erythrophagocytosis induces ferroptosis in red pulp macrophages in a mouse model of transfusion. *Blood J Am Soc Hematol* (2018) 131(23):2581–93. doi: 10.1182/blood-2017-12-822619

152. Martinez J, Malireddi R, Lu Q, Cunha LD, Pelletier S, Gingras S, et al. Molecular characterization of LC3-associated phagocytosis reveals distinct roles for Rubicon, NOX2 and autophagy proteins. *Nat Cell Biol* (2015) 17(7):893–906. doi: 10.1038/ncb3192

153. Sanjuan MA, Dillon CP, Tait SW, Moshiach S, Dorsey F, Connell S, et al. Toll-like receptor signalling in macrophages links the autophagy pathway to phagocytosis. *Nature* (2007) 450(7173):1253–7. doi: 10.1038/nature06421

154. Romao S, Gasser N, Becker AC, Guhl B, Bajagic M, Vanoaica D, et al. Autophagy proteins stabilize pathogen-containing phagosomes for prolonged MHC II antigen processing. *J Cell Biol* (2013) 203(5):757–66. doi: 10.1083/jcb.201308173

155. Wu W, Bleecker E, Moore W, Busse WW, Castro M, Chung KF, et al. Unsupervised phenotyping of severe asthma research program participants using expanded lung data. *J Allergy Clin Immunol* (2014) 133(5):1280–8. doi: 10.1016/j.jaci.2013.11.042

156. Anderson GP. Endotyping asthma: new insights into key pathogenic mechanisms in a complex, heterogeneous disease. *Lancet* (2008) 372(9643):1107–19. doi: 10.1016/S0140-6736(08)61452-X

157. Woodruff PG, Modrek B, Choy DF, Jia G, Abbas AR, Ellwanger A, et al. T-Helper type 2–driven inflammation defines major subphenotypes of asthma. *Am J Respir Crit Care Med* (2009) 180(5):388–95. doi: 10.1164/rccm.200903-0392OC

158. Puleston DJ, Simon AK. Autophagy in the immune system. *Immunology* (2014) 141(1):1–8. doi: 10.1111/imm.12165

159. Kondylis V, Van Nispen Tot Pannerden HE, Van Dijk S, Ten Broeke T, Wubbolts R, Geerts WJ, et al. Endosome-mediated autophagy: an unconventional MIIC-driven autophagic pathway operational in dendritic cells. *Autophagy* (2013) 9 (6):861–80. doi: 10.4161/auto.24111

160. Kearley J, Barker JE, Robinson DS, Lloyd CM. Resolution of airway inflammation and hyperreactivity after *in vivo* transfer of CD4+ CD25+ regulatory T cells is interleukin 10 dependent. *J Exp Med* (2005) 202(11):1539–47. doi: 10.1084/jem.20051166

161. Hartl D, Koller B, Mehlhorn AT, Reinhardt D, Nicolai T, Schendel DJ, et al. Quantitative and functional impairment of pulmonary CD4+ CD25hi regulatory T cells in pediatric asthma. *J Allergy Clin Immunol* (2007) 119(5):1258–66. doi: 10.1016/j.jaci.2007.02.023

162. Garg SK, Yan Z, Vitvitsky V, Banerjee R. Differential dependence on cysteine from transsulfuration versus transport during T cell activation. *Antioxidants Redox Signaling* (2011) 15(1):39–47. doi: 10.1089/ars.2010.3496

163. Levring TB, Hansen AK, Nielsen BL, Kongsbak M, Von Essen MR, Woetmann A, et al. Activated human CD4+ T cells express transporters for both cysteine and cystine. *Sci Rep* (2012) 2(1):1–6. doi: 10.1038/srep00266

164. Pua HH, Dzhagalov I, Chuck M, Mizushima N, He Y-W. A critical role for the autophagy gene Atg5 in T cell survival and proliferation. *J Exp Med* (2007) 204(1):25–31. doi: 10.1084/jem.20061303

165. Jia W, He Y-W. Temporal regulation of intracellular organelle homeostasis in T lymphocytes by autophagy. *J Immunol* (2011) 186(9):5313–22. doi: 10.4049/jimmunol.1002404

166. Pua HH, Guo J, Komatsu M, He Y-W. Autophagy is essential for mitochondrial clearance in mature T lymphocytes. *J Immunol* (2009) 182(7):4046–55. doi: 10.4049/jimmunol.0801143

167. Willinger T, Flavell RA. Canonical autophagy dependent on the class III phosphoinositide-3 kinase Vps34 is required for naive T-cell homeostasis. *Proc Natl Acad Sci* (2012) 109(22):8670–5. doi: 10.1073/pnas.1205305109

168. Parekh VV, Wu L, Boyd KL, Williams JA, Gaddy JA, Olivares-Villagómez D, et al. Impaired autophagy, defective T cell homeostasis, and a wasting syndrome in mice with a T cell–specific deletion of Vps34. *J Immunol* (2013) 190(10):5086–101. doi: 10.4049/jimmunol.1202071

169. Reed M, Morris SH, Jang S, Mukherjee S, Yue Z, Lukacs NW. Autophagy-inducing protein beclin-1 in dendritic cells regulates CD4 T cell responses and disease severity during respiratory syncytial virus infection. *J Immunol* (2013) 191(5):2526–37. doi: 10.4049/jimmunol.1300477

170. Wang W, Green M, Choi JE, Gijón M, Kennedy PD, Johnson JK, et al. CD8+ T cells regulate tumour ferroptosis during cancer immunotherapy. *Nature* (2019) 569 (7755):270–4. doi: 10.1038/s41586-019-1170-y

171. Laberge S, Wu L, Olivenstein R, Xu L-J, Renzi PM, Martin JG. Depletion of CD8+ T cells enhances pulmonary inflammation but not airway responsiveness after antigen challenge in rats. *J Allergy Clin Immunol* (1996) 98(3):617–27. doi: 10.1016/S0091-6749(96)70096-9

172. Isogai S, Jedrzkiewicz S, Taha R, Hamid Q, Martin JG. Resident CD8+ T cells suppress CD4+ T cell–dependent late allergic airway responses. *J Allergy Clin Immunol* (2005) 115(3):521–6. doi: 10.1016/j.jaci.2004.11.036

173. Tsuchiya K, Isogai S, Tamaoka M, Inase N, Akashi T, Martin JG, et al. Depletion of CD8+ T cells enhances airway remodelling in a rodent model of asthma. *Immunology* (2009) 126(1):45–54. doi: 10.1111/j.1365-2567.2008.02876.x

174. Mahmutovic Persson I, Menzel M, Ramu S, Cerps S, Akbarshahi H, Uller L. IL-1β mediates lung neutrophilia and IL-33 expression in a mouse model of viral-induced asthma exacerbation. *Respir Res* (2018) 19(1):1–10. doi: 10.1186/s12931-018-0725-z

175. Xu C, Sun S, Johnson T, Qi R, Zhang S, Zhang J, et al. The glutathione peroxidase Gpx4 prevents lipid peroxidation and ferroptosis to sustain treg cell activation and suppression of antitumor immunity. *Cell Rep* (2021) 35(11):109235. doi: 10.1016/j.celrep.2021.109235

176. Xiong A, Duan L, Chen J, Fan Z, Zheng F, Tan Z, et al. Flt3L combined with rapamycin promotes cardiac allograft tolerance by inducing regulatory dendritic cells and allograft autophagy in mice. *Cell Reports* (2012) 35(11). doi: 10.1371/journal.pone.0046230

177. Hubbard-Lucey VM, Shono Y, Maurer K, West ML, Singer NV, Ziegler CG, et al. Autophagy gene Atg16L1 prevents lethal T cell alloreactivity mediated by dendritic cells. *Immunity* (2014) 41(4):579–91. doi: 10.1016/j.immuni.2014.09.011

178. Kim HY, DeKruyff RH, Umetsu DT. The many paths to asthma: phenotype shaped by innate and adaptive immunity. *Nat Immunol* (2010) 11(7):577–84. doi: 10.1038/ni.1892

179. De Vooght V, Carlier V, Devos FC, Haenen S, Verbeken E, Nemery B, et al. B-lymphocytes as key players in chemical-induced asthma. *PloS One* (2013) 8(12):e83228. doi: 10.1371/journal.pone.0083228

180. Miller BC, Zhao Z, Stephenson LM, Cadwell K, Pua HH, Lee HK, et al. The autophagy gene ATG5 plays an essential role in b lymphocyte development. *Autophagy* (2008) 4(3):309–14. doi: 10.4161/auto.5474

181. Muri J, Thut H, Bornkamm GW, Kopf M. B1 and marginal zone b cells but not follicular B2 cells require Gpx4 to prevent lipid peroxidation and ferroptosis. *Cell Rep* (2019) 29(9):2731–44. e4. doi: 10.1016/j.celrep.2019.10.070

182. Pengo N, Scolari M, Oliva L, Milan E, Mainoldi F, Raimondi A, et al. Plasma cells require autophagy for sustainable immunoglobulin production. *Nat Immunol* (2013) 14(3):298–305. doi: 10.1038/ni.2524

183. Yao Y, Chen Z, Zhang H, Chen C, Zeng M, Yunis J, et al. Selenium–GPX4 axis protects follicular helper T cells from ferroptosis. *Nat Immunol* (2021) 22(9):1127–39. doi: 10.1038/s41590-021-00996-0

184. Xia F, Deng C, Jiang Y, Qu Y, Deng J, Cai Z, et al. IL4 (interleukin 4) induces autophagy in b cells leading to exacerbated asthma. *Autophagy* (2018) 14(3):450–64. doi: 10.1080/15548627.2017.1421884

185. Wang D, Xie N, Gao W, Kang R, Tang D. The ferroptosis inducer erastin promotes proliferation and differentiation in human peripheral blood mononuclear cells. *Biochem Biophys Res Commun* (2018) 503(3):1689–95. doi: 10.1016/j.bbrc.2018.07.100

186. Liu J-N, Suh D-H, Trinh HKT, Chwae Y-J, Park H-S, Shin YS. The role of autophagy in allergic inflammation: a new target for severe asthma. *Exp Mol Med* (2016) 48(7):e243–e. doi: 10.1038/emm.2016.38

187. Wu Y, Chen H, Xuan N, Zhou L, Wu Y, Zhu C, et al. Induction of ferroptosis-like cell death of eosinophils exerts synergistic effects with glucocorticoids in allergic airway inflammation. *Thorax* (2020) 75(11):918–27. doi: 10.1136/thoraxjnl-2020-214764

188. Bianchi M, Hakkim A, Brinkmann V, Siler U, Seger RA, Zychlinsky A, et al. Restoration of NET formation by gene therapy in CGD controls aspergillosis. *Blood J Am Soc Hematol* (2009) 114(13):2619–22. doi: 10.1182/blood-2009-05-221606

189. Li P, Li M, Lindberg MR, Kennett MJ, Xiong N, Wang Y. PAD4 is essential for antibacterial innate immunity mediated by neutrophil extracellular traps. *J Exp Med* (2010) 207(9):1853–62. doi: 10.1084/jem.20100239

190. Xu F, Zhang C, Zou Z, Fan EK, Chen L, Li Y, et al. Aging-related Atg5 defect impairs neutrophil extracellular traps formation. *Immunol* (2017) 151(4):417–32. doi: 10.1111/imm.12740

191. Kambas K, Mitroulis I, Ritis K. The emerging role of neutrophils in thrombosis–the journey of TF through NETs. *Front Immunol* (2012) 3:385. doi: 10.3389/fimmu.2012.00385

192. Yotsumoto S, Muroi Y, Chiba T, Ohmura R, Yoneyama M, Magarisawa M, et al. Hyperoxidation of ether-linked phospholipids accelerates neutrophil extracellular trap formation. *Sci Rep* (2017) 7(1):1–18. doi: 10.1038/s41598-017-15668-z

193. Bhattacharya A, Wei Q, Shin JN, Fattah EA, Bonilla DL, Xiang Q, et al. Autophagy is required for neutrophil-mediated inflammation. *Cell Rep* (2015) 12 (11):1731–9. doi: 10.1016/j.celrep.2015.08.019

194. Li W, Feng G, Gauthier JM, Lokshina I, Higashikubo R, Evans S, et al. Ferroptotic cell death and TLR4/Trif signaling initiate neutrophil recruitment after heart transplantation. *J Clin Invest* (2019) 129(6):2293–304. doi: 10.1172/JCI126428

195. Ushio H, Ueno T, Kojima Y, Komatsu M, Tanaka S, Yamamoto A, et al. Crucial role for autophagy in degranulation of mast cells. *J Allergy Clin Immunol* (2011) 127 (5):1267–76. e6. doi: 10.1016/j.jaci.2010.12.1078

196. Yoo S-E, Chen L, Na R, Liu Y, Rios C, Van Remmen H, et al. Gpx4 ablation in adult mice results in a lethal phenotype accompanied by neuronal loss in brain. *Free Radical Biol Med* (2012) 52(9):1820–7. doi: 10.1016/j.freeradbiomed.2012.02.043

197. McAlinden KD, Deshpande DA, Ghavami S, Xenaki D, Sohal SS, Oliver BG, et al. Autophagy activation in asthma airways remodeling. *Am J Respir Cell Mol Biol* (2019) 60(5):541–53. doi: 10.1165/rcmb.2018-0169OC

198. Alizadeh J, Glogowska A, Thliveris J, Kalantari F, Shojaei S, Hombach-Klonisch S, et al. Autophagy modulates transforming growth factor beta 1 induced epithelial to mesenchymal transition in non-small cell lung cancer cells. *Biochim Biophys Acta (BBA)-Molecular Cell Res* (2018) 1865(5):749–68. doi: 10.1016/j.bbamcr.2018.02.007

199. Alizadeh J, Shojaei S, Sepanjnia A, Hashemi M, Eftekharpour E, Ghavami S. Simultaneous detection of autophagy and epithelial to mesenchymal transition in the non-small cell lung cancer cells. *Autophagy Differentiation Tissue Maintenance* (2017) 1854:87–103. doi: 10.1007/7651_2017_84

200. Wu Y, Zhang S, Gong X, Tam S, Xiao D, Liu S, et al. The epigenetic regulators and metabolic changes in ferroptosis-associated cancer progression. *Mol cancer* (2020) 19(1):1–17. doi: 10.1186/s12943-020-01157-x

201. Banerjee P, Balraj P, Ambhore NS, Wicher SA, Britt RD, Pabelick CM, et al. Network and co-expression analysis of airway smooth muscle cell transcriptome delineates potential gene signatures in asthma. *Sci Rep* (2021) 11(1):1–16. doi: 10.1038/s41598-021-93845-x

10.3389/fimmu.2023.1140791

Glossary

AP	autophagosome
ASM	airway smooth muscle
AHR	airway hyperresponsiveness
AMPK	5′-AMP-activated protein kinase
ARNTL/BMAL1	aryl hydrocarbon receptor nuclear translocator-like
Als	autolysosomes
ATG	autophagy-related gene
CMA	chaperon-mediated autophagy
cDCs	conventional dendritic cells
Cys	cysteine
HMOX1	heme oxygenase 1
GCL	glutamate-cysteine ligase
GPX4	glutathione peroxidase 4
GSS	glutathione synthetase
HAECs	human airway epithelial cells
HIF1	hypoxia-inducible factor 1
Hsp	heat shock protein
ILC2 cells	innate lymphoid type-2 cells
LDs	lipid droplets
LAMP2A	lysosome-associated membrane protein type 2A
mTORC1	mTOR complex 1
MZB lymphocytes	marginal zone B lymphocytes
NETs	neutrophil extracellular traps
NF-κb	nuclear factor-κB
NOD1	nucleotide-binding oligomerization domain-containing protein 1
NOX1	NADPH oxidase 1
NCOA4	nuclear receptor coactivator 4
NKT cells	natural killer T cells
PAMPs	pathogen-associated molecular patterns
PCBPs	poly (RC)- binding proteins (PCBPs) poly (RC)- binding proteins
PLOH	phospholipid alcohol
PUFAs	polyunsaturated fatty acids
RCD	regulated cell death
SQSTM1/P62	Sequestosome 1
SLC11A2	solute carrier family 11 member 2
ULK complex	unc-51-like kinase complex
VPS34	vacuolar protein sorting 34

Frontiers in Immunology

Explores novel approaches and diagnoses to treat immune disorders.

The official journal of the International Union of Immunological Societies (IUIS) and the most cited in its field, leading the way for research across basic, translational and clinical immunology.

Discover the latest Research Topics

See more →

Frontiers

Avenue du Tribunal-Fédéral 34
1005 Lausanne, Switzerland
frontiersin.org

Contact us

+41 (0)21 510 17 00
frontiersin.org/about/contact